THE
PHYSICAL REVIEW

A journal of experimental and theoretical physics established by E. L. Nichols in 1893

SECOND SERIES, VOL. 97, No. 5 MARCH 1, 1955

Electric Excitation of Heavy Nuclei by Protons*

CLYDE MCCLELLAND, HANS MARK, AND CLARK GOODMAN
Department of Physics and Laboratory for Nuclear Science, Massachusetts Institute of Technology, Cambridge, Massachusetts
(Received November 12, 1954)

Electric excitation of nuclei has been used to study the low-lying level structure in heavy nuclei. Experimental data for seventeen nuclides are presented, including isotopes of lutecium, hafnium, tantalum, wolfram, rhenium, and platinum. Excitation of twenty-five levels in these nuclei was observed. These data have been interpreted in terms of the hypothesis of nuclear rotational levels proposed by Bohr and Mottelson. Approximate intrinsic electric quadrupole moments of these nuclides determined in two ways from the experimental data are compared and interpreted as evidence for non-uniformity of the charge-mass distribution in nuclei.

I. INTRODUCTION

WITH the discovery of electric excitation[1,2] and its application to the collective model of nuclear structure of Bohr and Mottelson,[3] it became apparent that a study of this process in a series of neighboring nuclei would yield important information regarding the validity of this model. The collective model predicts that certain deformed nuclei should have low-lying "rotational" energy levels which have the following properties:

(1) A spectrum which is very similar to that of a rigid rotator with an effective moment of inertia which depends upon the ground-state deformation of the nucleus.

(2) An electric quadrupole transition probability which may be enhanced by as much as a factor of 100 over that which would be expected from a single particle transition.

All the nuclides which we have studied fulfill one or both of the above conditions and we have therefore interpreted our results as a strong confirmation of the applicability of the collective model in this region of the periodic table.

The collective model predicts a rotational level spectrum of the following form:

$$E=\frac{\hbar^2}{2\mathcal{I}}[I(I+1)-I_0(I_0+1)], \tag{1}$$

where I_0 is the ground-state angular momentum ($I_0\neq\frac{1}{2}$), I is the angular momentum of the excited level, and $\mathcal{I}$ is the effective moment of inertia. Knowledge of the excitation energy will therefore yield the value of the effective moment of inertia. This moment of inertia depends on the ground-state deformation of the nucleus and if the mass and the charge are uniformly distributed throughout the nuclear volume it can be related to the intrinsic electric quadrupole moment, Q_0, by[4]:

$$\mathcal{I}=\frac{5mA}{8R_0^2Z^2}Q_0^2, \tag{2}$$

where m is the nucleon mass, A the atomic number, R_0 the nuclear radius ($R_0=1.44A^{\frac{1}{3}}\times10^{-13}$ cm), and Z the nuclear charge. The value of Q_0 may therefore be determined from the excitation energy of a rotational level using (1) and (2).

The cross section for electric 2^n-pole excitation may be expressed as the product of three factors:

$$\sigma_{ex}=A_n(E,Z)B_e(n)g_n(\xi), \tag{3}$$

where

$$\xi=\frac{\Delta E}{2E}\frac{Zze^2}{\hbar v}.$$

* This work was supported by the joint program of the Office of Naval Research and the U. S. Atomic Energy Commission.

[1] T. Huus and C. Zupančič, Kgl. Danske Videnskab. Selskab, Mat. fys. Medd. **28**, No. 1 (1953).

[2] C. L. McClelland and Clark Goodman, Phys. Rev. **91**, 760 (1953).

[3] A. Bohr and B. R. Mottelson, Kgl. Danske Videnskab. Selskab, Mat. fys. Medd. **27**, No. 16 (1953).

[4] A. Bohr, *Rotational States of Atomic Nuclei* (Ejnar Munksgaards Forlag, Copenhagen, 1954). Eqs. (10) and (11).

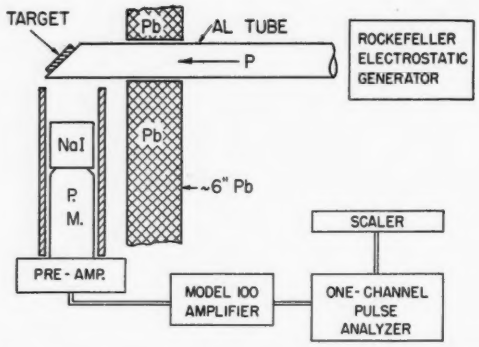

FIG. 1. Experimental equipment. This figure illustrates the simplicity of the experimental equipment. The NaI(Tl) crystal and the DuMont No. 6292 photomultiplier are shielded from the electrostatic generator by several inches of lead. This is necessary to reduce the gamma background from the acceleration tubes and generator slits. The aluminum tube is approximately 36 inches long. The crystal is about 9 feet from the exit slits of the generator, which are made of wolfram.

The function $g_n(\xi)$ has been evaluated for $n=1$, 2, and 3 and for a wide range of values of the parameter ξ by Alder and Winther.[5] The factor $A_n(E,Z)$ is a function of E, the energy of the incoming particle and Z, the charge of the target nucleus. $B_e(n)$ is the reduced electric 2^n-pole transition probability. For rotational levels, which always involve quadrupole ($n=2$) excitation, $B_e(2)$ can be written in a form which includes the square of the ground-state intrinsic quadrupole moment, Q_0, as a factor. The value of Q_0 may therefore also be determined from a knowledge of the electric excitation cross section.

The two methods of obtaining Q_0 outlined above differ in that the cross-section measurement is sensitive to the deformation of the nuclear charge distribution and hence Q_0 obtained from (3) is the actual intrinsic electric quadrupole moment whereas the energy measurement is sensitive to the deformation of the nuclear mass distribution and Q_0 obtained from (2) depends on some assumption about the relation between the charge and the mass distribution. (For instance, uniform distribution of charge and mass.) If the rotational model is correct, then a comparison of the value of Q_0 obtained from (2) and (3) for the same level is a test of the validity of this assumption.

II. EXPERIMENTAL TECHNIQUES

A schematic diagram of the experimental equipment is shown in Fig. 1. The Rockefeller electrostatic generator was used as the source of protons of known energy calibrated relative to the $Li^7(p,n)$ threshold taken as 1881.4 kev.[6]

The single-crystal scintillation spectrometer used for this work consisted of a DuMont 6292 photomultiplier and a Harshaw Chemical Company "canned" 2 inch×2 inch thallium-activated sodium-iodide crystal. The crystal was optically coupled to the photomultiplier with a thin film of Nujol. This unit was shielded from stray magnetic effects by a mu-metal shield and from the effects of gamma rays on the photomultiplier dynodes by a $\frac{3}{8}$-inch lead tube. Pulses from the photomultiplier were passed through a standard cathode-follower to a Model 100 amplifier and an A.I.C. single-channel pulse-height analyzer. A one percent window width was used in the pulse-height analyzer. This equipment could resolve the Cs^{137} 0.661 Mev[7] gamma photopeak with a half-width of approximately 8 percent. Other gammas of known energy used for calibration of the spectrometer included: Na^{22}, 511 kev and 1.277 Mev,[8] the gamma from electric excitation of the first state in tantalum −136.5 kev,[9] and the K x-ray series from wolfram, taken as 60.1 kev. The energy assigned this peak results from a graphical analysis of our experimental data combined with known relative intensities of the K x-ray series from wolfram.

The material to be bombarded, generally in the form of a powdered metal or metallic oxide, was compressed into a small circular depression in a lead target backing disk. Thick targets were obtained which withstood bombardment with reasonably heavy beam currents. Various absorbers were used between the crystal and target to reduce the characteristic x-ray background from the element bombarded.

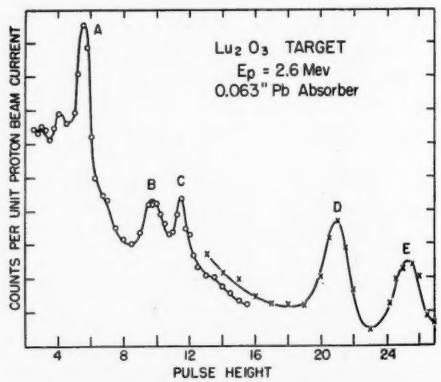

FIG. 2. Electric excitation of lutecium. Pulse spectrum observed from a target of Lu^{175} during bombardment with 2.6-Mev protons. Identification of the peaks is as follows: (A) 240-kev gamma from de-excitation of the second level in Lu^{175}. (B) 0.439-Mev gamma. Probable sodium impurity. (C) 490-kev gamma. $O^{16}(p,\gamma)F^{17}$ reaction. (D) 0.843-Mev gamma. $Al^{27}(p,p'\gamma)$ reaction. (E) 1.017-Mev gamma. $Al^{27}(p,p'\gamma)$ reaction. This target is contaminated with sufficient aluminum to be quite easily detectable, and a small quantity of sodium as well. Nominal purity of the sample was given as 99.9 percent. These data were obtained at two different amplifier gains, and plotted together for display. The discontinuity separating these two curves is produced by different relative bases in the electronic circuits for the different gain settings.

[5] K. Alder and A. Winther, Phys. Rev. **91**, 1578 (1953).
[6] Jones, Douglas, McEllistram, and Richards, Phys. Rev. **94**, 947 (1954).
[7] Muller, Hoyt, Kleim, and DuMond, Phys. Rev. **88**, 775 (1952).
[8] D. E. Alburger, Phys. Rev. **76**, 435 (1949).
[9] Cork, Nester, LeBlanc, and Brice, Phys. Rev. **92**, 119 (1953).

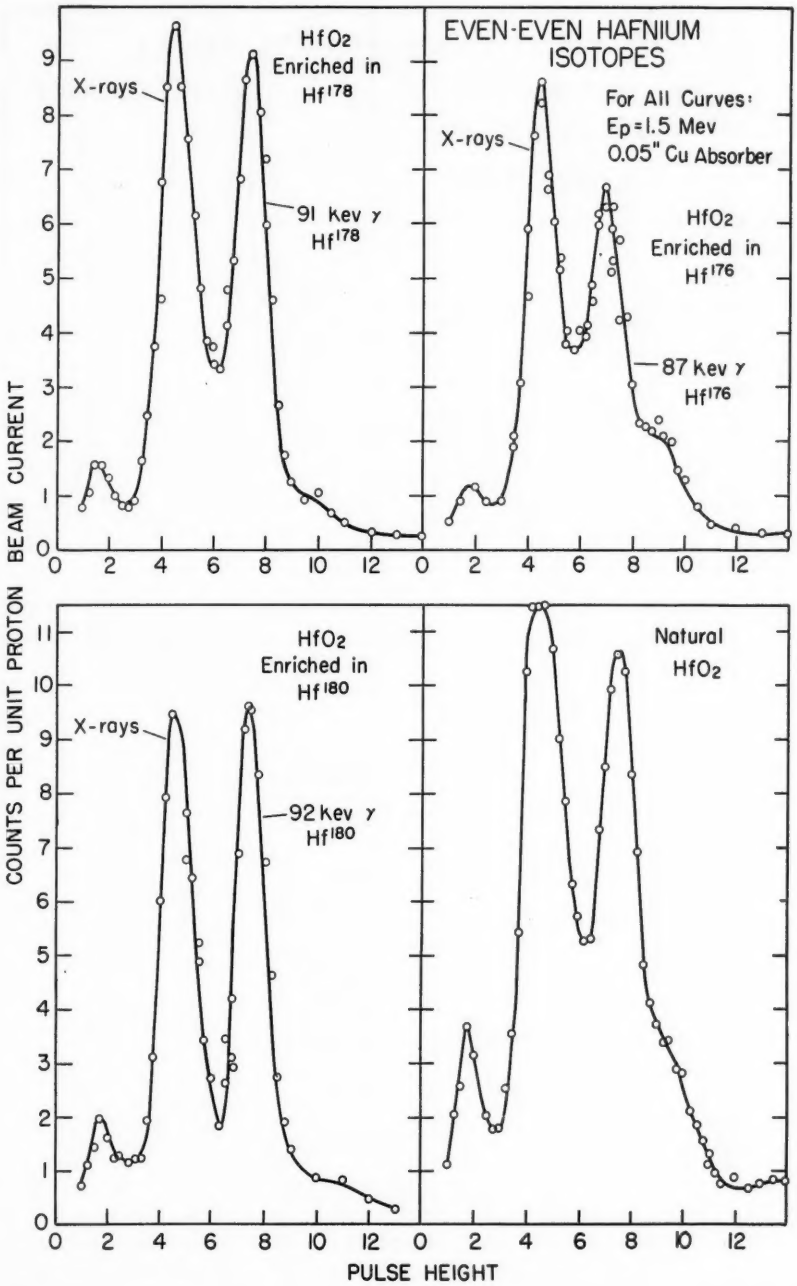

FIG. 3. Electric excitation of even-even hafnium isotopes. Pulse-height spectra observed during proton bombardment of four targets of HfO_2, three of which were enriched in the isotopes Hf^{176}, Hf^{178}, and Hf^{180}. In each case, an absorber of 0.05-in. Cu was used to reduce the x-ray background. None of the curves has been corrected for attenuation in this absorber.

An important background effect, represented by a broad, peaked, low-energy pulse distribution was present from all targets. This has been studied by Zupančič and Huus[10] who conclude that this effect is produced by proton bremsstrahlung. We have studied this process in some detail and our results, to be the subject of a separate paper, support this interpretation.

[10] C. Zupančič and T. Huus, Phys. Rev. **94**, 205 (1954).

The presence of extremely small quantities of light elements as impurities is easily detectable. Sodium, revealed by a 439-kev gamma from the $Na(p,p'\gamma)$ reaction and a 1.634-Mev gamma from the $Na(p,\alpha\gamma)$ reaction,[11] proved most troublesome. Aluminum was detected in the lutecium oxide target (see Fig. 2) by

[11] Donahue, Jones, McEllestrem, and Richards, Phys. Rev. **89**, 824 (1953).

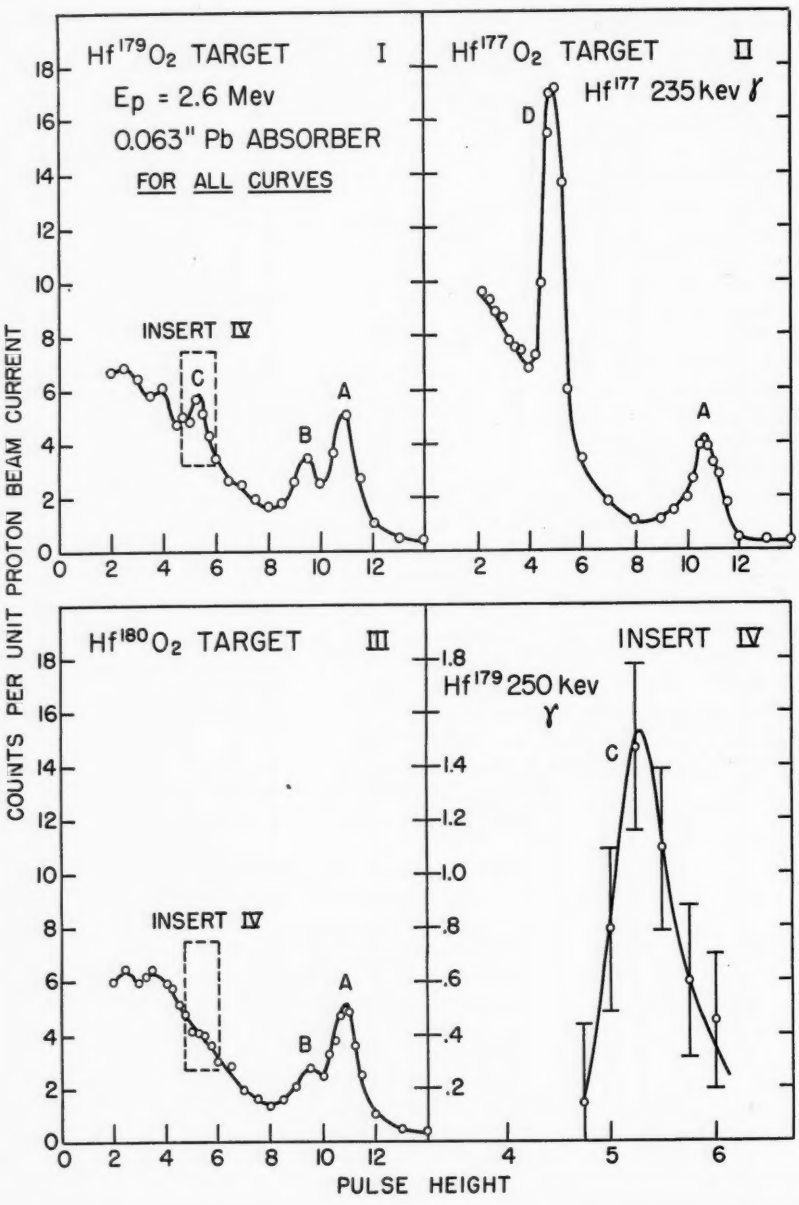

FIG. 4. Electric excitation of odd hafnium isotopes. Pulse-height spectra from targets of HfO_2 during bombardment with protons of 2.6-Mev energy. These targets were enriched in Hf^{177}, Hf^{179}, and Hf^{180}. In each case, peak *A* is produced by a 490-kev gamma attributed to the $O^{16}(p,\gamma)F^{17}$ reaction. Peak *B* is the 439-kev gamma from the $Na(p,p'\gamma)$ reaction. Peak *C* is produced by the 250-kev gamma from the de-excitation of the second level in Hf^{179}. The curve from Hf^{180} oxide in Sec. III was used as a background for the curve in Sec. I, and the resultant peak is displayed in insert IV. The yield of the 235-kev gamma from de-excitation of the second level in Hf^{177} is displayed in Sec. II.

the 0.843-Mev[12] and 1.017-Mev[13] gammas from the $Al(p,p'\gamma)$ reaction. Gammas from oxygen in the oxide targets distorted the experimental pulse-height spectra when using high-energy protons in attempts to excite higher levels in the target nuclei. It seems likely that the 0.49-Mev gamma observed under these conditions is the cascade decay between known levels at 4.35 and 3.86 Mev in F^{17} during de-excitation of the highly excited nucleus after the $O^{16}(p,\gamma)F^{17}$ reaction.[14] A broad low-energy pulse distribution is also attributed to the oxygen in the target.

The gamma energies reported in this work are considered reliable to ±3 percent, except when otherwise noted. This figure represents an estimate of the magnitude of the errors involved, most of which arise during the graphical analysis of the data.

Figures 3, 4, 5, and 6 are typical pulse-height spectra.

[12] P. M. Endt and J. C. Kluyver, Revs. Modern Phys. **26**, 116 (1954).
[13] C. P. Browne and S. F. Zimmerman (private communication).
[14] F. Ajzenberg and T. Lauritsen, Revs. Modern Phys. **24**, 321 (1952).

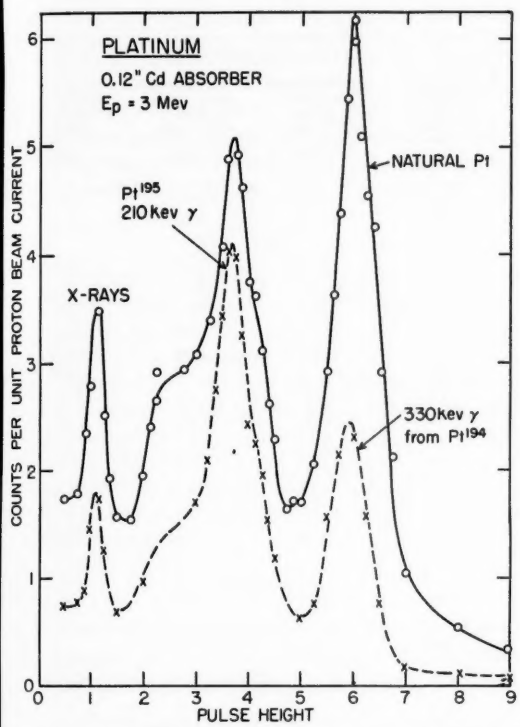

FIG. 5. Electric excitation of Pt^{195} and platinum. Superposition of the pulse-height spectra obtained during proton bombardment of targets of natural platinum metal and a target enriched in Pt^{195}. Gamma energies are considered reliable to ±3 percent. In each case, an absorber of 0.12-inch Cd was used between detector crystal and target to reduce x-ray background. Correction for attenuation in this absorber has not been made in the figure. Counting statistics in the photopeak for the Pt^{195} 210-kev gamma are approximately the size of the symbols used. The difference in the yield of platinum x-rays from these two targets is attributed to attentuation of these x-rays by the compressed metallic powder Pt^{195} target, which is not so dense as the natural metallic foil.

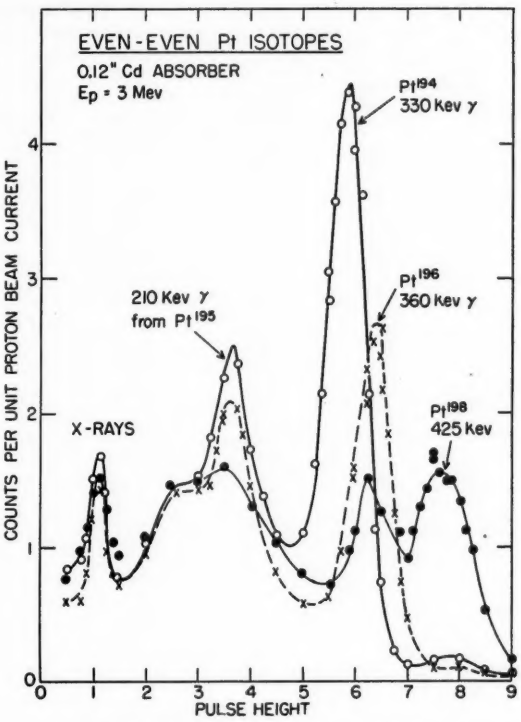

FIG. 6. Electric excitation of even-even platinum isotopes. Superposition of the pulse-height spectra obtained during proton bombardment of three thick platinum targets enriched in the even-even isotopes of platinum. Gamma energies are considered reliable to ±3 percent. In each case, an absorber of 0.12-inch cadmium was used to reduce the x-ray background. This figure does not include correction for absorption in the cadmium or for internal conversion. Relative cross sections for excitation are discussed in the text. Counting statistics at the Pt^{196}, 425-kev gamma photopeak are approximately the size of the symbols used. The presence of Pt^{198} in the targets enriched in Pt^{196} and Pt^{194} is quite obvious and traces of Pt^{198} in the Pt^{194} and Pt^{196} targets are detectable. The broad pulse distribution underlying the 210-kev photopeak from the Pt^{195} contaminant is attributed to the Compton peak in the crystal from the higher-energy gammas, and possible proton bremsstrahlung.

III. NUCLEAR LEVEL STRUCTURE

Table I gives the energy of the gammas observed during proton bombardment of the nuclei listed. These gammas result from de-excitation of levels in the target nucleus after electric excitation by the incident proton. The measured energy gives the position of the first or the first and second rotational levels in the nucleus.

For all the levels observed, the measured electric excitation cross section exceeds the cross section which would be expected from single particle excitation by a factor of ten or more. It is therefore assumed that all these levels are collective excitations. The rotational excitation hypothesis permits the assignment of spins for these excited levels which in some cases does not agree with the values determined earlier by other methods. In such cases further experimental work is required to resolve the disagreement.

We now consider the energy levels and spins of each nuclide studied in the order given in Table I.

Lu^{175}

Temmer and Heydenburg[15,16] have also studied the electric excitation of this nucleus with alpha particles. They report levels at 113 and 248 kev, and a lower level at 77 kev. Our data do not exclude the possibility of such a low-energy gamma since it may be hidden by the high yield of characteristic x-rays produced during proton bombardment. However, we have assumed that the level at 112 kev is the first rotational level in this nucleus, because the cross section for excitation of this level is large. The Bohr-Mottelson theory would then predict the second rotational level at 248 kev, in fairly good agreement with our measured value of 240 kev.

[15] G. M. Temmer and N. P. Heydenburg, Phys. Rev. **93**, 351 (1954).
[16] G. M. Temmer and N. P. Heydenburg, Phys. Rev. **94**, 1399 (1954).

TABLE I. Summary of results.

Nuclide	Measured excitation energy (kev)	Q_0(energy) from-excitation energy (units 10^{-24} cm^2)	$\frac{Q_0^2(\text{yield})}{\alpha\tau+1}$ (units 10^{-48} cm^4)	If $\alpha\tau$ were:	Then Q_0(yield) would be: (units 10^{-24} cm^2)	Known Q(spectroscopic) (units 10^{-24} cm^2)	Q_0(spectroscopic)-spec. value (units 10^{-24} cm^2)	Ratio Q_0(yield) Q_0(spectroscopic)
Lu^{175}	112 240	22.3 22.8	8.3	4.1	6.5	+5.9	12.66	0.51
Hf^{176}	87	20.8	17.4	9.0	13.2	...	...	...
Hf^{177}	112 235	16.8 17.9	21.4[a]	4.1	10.5	...	...	...
Hf^{178}	91	20.2	13.4	8.0	11.0	...	...	...
Hf^{179}	122 250[b]	16.3 17.5	9.5[a]	3.2	6.3	...	...	...
Hf^{180}	92	20.1	12.7	7.8	10.5	...	...	...
Ta^{181}	138 300	20.5 20.6	13.7 30.6[c]	2.3 0.11	6.7 5.8	+6.0	12.9	0.52 0.45
W^{182}	101	19.5	2.4	6.5	3.5	...	...	...
W^{183}	103[b]	17.8	1.5	3.9	2.7	...	...	...
W^{184}	112	18.7	3.2	5.4	4.5	...	...	...
W^{186}	124	17.9	3.9	3.4	4.1	...	...	...
Re^{185}	130 290[b]	19.1 19.4	4.3	2.8	4.7	+2.8	7.85	0.6
Re^{187}	139 320[b]	18.4 18.4	4.1	2.3	4.3	+2.6	7.28	0.59
Pt^{194}	330	11.4	5.1	0.084	2.4	...	...	...
Pt^{195}	210	13.1	5.7	0.8	3.2	...	...	...
Pt^{196}	360	10.9	2.6	0.065	1.7	...	...	...
Pt^{198}	425	10.0	2.0	0.039	1.4	...	...	...

[a] For ground-state spin $I_0=3/2$.
[b] Error ±6 percent.
[c] Branching ratio, cascade to crossover taken as 4.

Hf^{176}

Our value for the first rotational level in this nucleus, 87 kev, agrees well with the value, 89 kev, obtained by Arnold[17] in his study of radioactive Lu^{176}. We were unable to observe the excitation of the second rotational level in this or any other even-even nucleus because of the small cross section for a spin change of 4.

Hf^{177}

The energy of the first level in this nucleus as determined from electric excitation data, 112 kev, is in agreement with that determined from studies of radioactive Lu^{177} by several authors. The most recent study by McGowan *et al.*[18] contains references to most of the prior work. The ground state spin of Hf^{177} is either $\frac{1}{2}$ or $\frac{3}{2}$ as determined by Rasmussen.[19] If $\frac{3}{2}$ is assumed, the Bohr-Mottelson theory predicts the second rotational level at 269 kev. This does not agree well with our observed value of 235 kev, implying that the ground state spin of Hf^{177} is probably $\frac{1}{2}$. Level spectra predictions for a ground-state spin of $\frac{1}{2}$ are uncertain.[3] If the j of the last particle is a good quantum number, the first and second levels of the nucleus are degenerate. However, this assumption is probably invalid for these highly deformed nuclei and hence the first and second levels could have appreciably different energies.

Hf^{178}

Our value for the first rotational level in this nucleus, 91 kev, is reasonable based on the Bohr-Mottelson predictions that the energy of the first-excited state should be slightly greater than the corresponding level in Hf^{176}, which is 87 kev.

Hf^{179}

This nucleus has been studied by der Mateosian and Goldhaber.[20] These authors found a level at 215 kev and a 19-sec metastable level at 375 kev. We assume that the two levels, 122 and 250 kev, reported in Table I are new, and that they represent the first and second rotational states in this nucleus. The ground-state spin of Hf^{179} is either $\frac{1}{2}$ or $\frac{3}{2}$ and the comments made for Hf^{177} apply here as well. If the ground-state spin is assumed to be $\frac{3}{2}$, the energy of the second rotational level is predicted to be 293 kev. Agreement with our observed value of 250 kev is poor, and a ground-state spin of $\frac{1}{2}$ seems favored. Direct electric excitation of the 19-sec metastable level is very improbable, since the cross section for excitation decreases rapidly with increasing multipole order.

[17] J. R. Arnold, Phys. Rev. **93**, 743 (1954).
[18] McGowan, Klema, and Bell, Phys. Rev. **85**, 152 (1952).
[19] E. Rasmussen, Naturwiss. **23**, 69 (1935).
[20] E. der Mateosian and M. Goldhaber, Phys. Rev. **83**, 843 (1951).

Hf^{180}

The energy of the first rotational level in this nucleus, 92 kev, as determined from electric excitation data, agrees well with the known level reported as 93 kev. Other levels for this nucleus are known, and the energy-level diagram presents possibly the best illustration of a typical rotational spectrum[21] of an even-even nuclide.

Ta^{181}

The energy for the first-excited state obtained by Cork *et al.*[22] from studies of radioactive W^{181} agrees with the value, 138 kev, determined by electric excitation within our experimental error. These authors report a second level at 289 kev. Since Huus and Zupančič,[1] and others, have also observed the gamma from the second rotational level in tantalum after electric excitation and the energy obtained only ranges from our value of 300 kev to 303 kev, it seems unlikely that the second level given by Cork *et al.*, is identical with that observed in electric excitation.

Wolfram

This element was the subject of a previous report.[23] The results given in the next section of the present paper supplement the earlier data.

Re^{185}

Cork, Keller, and Stoddard[24] observed a 133.7-kev gamma in the radioactive decay of W^{185}. We have observed a gamma measured as 130 ± 4 kev during electric excitation of Re^{185}. These are probably identical, and correspond to the first-excited state in Re^{185}. The rotational nuclear excitation hypothesis predicts a second excited state at 295 kev. We observe a gamma of 290 ± 17 kev, corresponding to de-excitation of this state. The difference is well within the experimental error.

Re^{187}

Studies of radioactive W^{187} show a gamma of between 129 kev and 138 kev.[25] We have observed a gamma of 139 ± 4 kev during electric excitation of Re^{187}. These gammas are probably identical, and refer to the position of the first-excited state in the Re^{187} nucleus. Our observed energy for the second rotational state, 320 kev, agrees well with the value predicted from the theory, 318 kev. Additional study of radioactive W^{187} would be desirable, since our data are difficult to reconcile with the energy level diagram given by Goldhaber and Hill.[26]

[21] A. Bohr and B. R. Mottelson, Phys. Rev. **90**, 717 (1953).
[22] Cork, Nester, LeBlanc, and Brice, Phys. Rev. **92**, 119 (1953).
[23] McClelland, Mark, and Goodman, Phys. Rev. **93**, 904 (1954).
[24] Cork, Keller, and Stoddard, Phys. Rev. **76**, 575 (1949).
[25] National Bureau of Standards Circular 499 (U. S. Government Printing Office, Washington, D. C., 1950).
[26] M. Goldhaber and R. H. Hill, Revs. Modern Phys. **24**, 226 (1952).

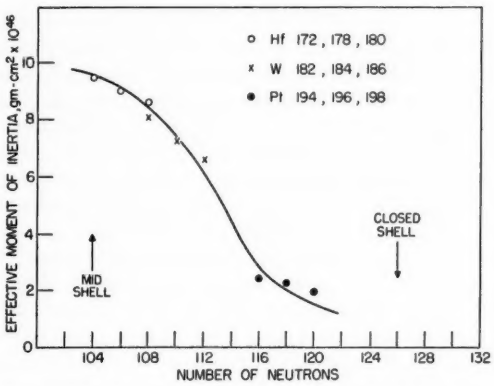

FIG. 7. Effective moments of inertia. A graph of the effective moment of inertia, $\mathcal{I}$, as a function of the number of neutrons in even-even nuclei. $\mathcal{I}$ is determined from the formula:

$$E=\frac{\hbar^2}{2\mathcal{I}}I(I+1),$$

for the energy spectrum of rotational levels. The curve is drawn primarily as a visual aid, but shows features somewhat similar to the quadrupole moment *versus* neutron number curves given by W. Gordy [Phys. Rev. **76**, 139 (1949)].

Pt^{194}

The 328-kev level reported for this nucleus from studies of radioactive Au^{194} by Steffen, Huber, and Hummel[27] agrees well with that determined from electric excitation, 330 kev.

Pt^{195}

We have observed a 210-kev gamma during electric excitation of this nucleus. Other lower energy gammas may be present, but the high yield of characteristic x-rays makes their identification uncertain. Since the ground-state spin of Pt^{195} is $\frac{1}{2}$, the rotational level spectrum cannot be predicted with certainty. For the calculations presented in the next section, we assumed the level at 210 kev to be the first rotational state.

Pt^{196}

The 358-kev level in this nucleus from studies of radioactive Au^{196} by Steffen *et al.*[27] agrees well with the energy, 360 kev, of the level from electric excitation studies.

Pt^{198}

No levels were previously known in this nucleus. The 425-kev level determined by this work is, as expected, higher than the first states of Pt^{194} and Pt^{196}. This is in accord with the rotational hypothesis since Pt^{198} is closer to the closed nuclear shells at 82 protons and 126 neutrons and is expected to be more nearly spherically symmetric.

[27] Steffen, Huber, and Hummel, Helv. Phys. Acta **22**, 167 (1949).

IV. NUCLEAR DEFORMATION

Figure 7 shows the effective moment of inertia, $\mathcal{I}$, for the even-even nuclei investigated in this work plotted as a function of the number of neutrons in the nucleus. Equation (1) has been used to calculate this quantity from the excitation energy of the first level. Since $\mathcal{I}$ is proportional to Q_0^2, this curve displays the well-known general features of the relationship between the quadrupole moment and the neutron number.

The intrinsic quadrupole moment, Q_0(energy) obtained from the excitation energy of the excited level by Eq. (2) is given in Table I, column 2. For W^{183} and Pt^{195} with a known ground-state spin $I_0=\frac{1}{2}$, the values presented include the assumption that the j of the last particle is a good quantum number.

In these heavy nuclei, and for the low excitation energies observed in this work, internal conversion of the gamma in the excited nucleus is an important effect. Therefore, the cross section for electric excitation determined from the number of gammas observed is not the excitation cross section but merely $\sigma_{ex}/(\alpha_T+1)$, where α_T is the total internal conversion coefficient. In column 3 of Table I, we have chosen to represent the experimental yield data in the form Q_0^2(yield)$/(\alpha_T+1)$ so that our evaluation of the experimental yield may be free of the uncertainty in the value of the total internal conversion coefficient.

The evaluation of Q_0^2(yield)$/(\alpha_T+1)$ involves more elaborate treatment of the experimental data. In general the following corrections were necessary:

(1) Gamma attenuation in absorbers.
(2) Gammas attenuation by target assembly and crystal can.
(3) Self-absorption in compressed powder targets.
(4) Relative detector efficiency for gammas of different energies.
(5) Lower yield from oxide targets.
(6) Anisotropy of gamma yield.
(7) Background effects in observed pulse-height spectra.
(8) Interpolation and extrapolation of known dE/dx data.
(9) Solid angle subtended by detector.

Corrections for attenuation in absorbers and detector efficiency were made from the data of Davisson and Evans,[28] and values of dE/dx for the target elements were estimated from Allison and Warshaw.[29] The tantalum nucleus was studied in detail. Isotropic distribution of the 138-kev gamma was assumed, and the value of the angular distribution function for the 300-kev gamma given by Eisinger, Cook, and Class[30] was used in the calculations for excitation of the second level. The crystal efficiency and solid angle factors were determined, and the absolute yield of gammas from tantalum was determined. Our results for the excitation cross section of the first level in tantalum agree with the value of approximately 0.5 mb at $E_p=2.0$ Mev quoted by Huus and Zupančič.[1] Thereafter, the yield of gammas from tantalum was used as a calibrated source for the measurement of the yield from all other targets. In this respect, it is encouraging to note that, after a value for the total internal conversion coefficient is assumed, the ratio, Q_0(yield)$/Q_0$(spectroscopic), for those nuclei for which a spectroscopic quadrupole moment has been determined, is approximately the same as the value of this ratio for the tantalum nucleus. These data are presented in the last column of Table I.

Some of the total internal conversion coefficients for the gammas in this work are given in the literature. However, for a consistent set of values of α_T, in all cases, an estimate of the magnitude of this quantity was made from the most recent theoretical data available, usually low-energy K-shell conversion coefficients calculated by Rose, Goertzel, and Swift[31] and L-shell conversion coefficients given by Gellman, Griffith, and Stanley.[32]

For the even-even nuclei, both excitation and radiation are electric quadrupole. Estimation of the magnitude of α_T in these nuclei includes only the errors of graphical interpolation and theoretical uncertainties in the value. For the odd A nuclei, however, while excitation is assumed to be electric quadrupole, the resultant radiation is a mixture of $E2$ and $M1$. Too few nuclei have been studied in detail to include an estimation of the relative proportions of $E2$ and $M1$ in the evaluation of α_T. Therefore, for every odd-A nucleus in Table I, pure magnetic dipole radiation was assumed. In the case of tantalum, Goldberg and Williamson[33] state that $E2$ radiation is less than 5 percent of the total radiation; for this nucleus, therefore, assumption of pure magnetic dipole radiation certainly does not introduce a large error.

Estimation of errors in data which required such extensive correction is difficult. For the quantity Q_0^2(yield)$/(\alpha_T+1)$, the probable error is 50 percent, while the final value of the intrinsic electric quadrupole moment from the cross section data must include errors in the estimation of α_T which range from a factor of two or more for the lowest-energy gammas studied to roughly 20 percent for the highest. The value of Q_0(yield) listed in Table I should therefore be considered as only semiquantitative.

Generally, the value of Q_0 as determined from the excitation energies is larger than that estimated from the yield data. A similar comparison between empirical Q_0 values and those obtained from the effective moment

[28] C. M. Davisson and R. D. Evans, Revs. Modern Phys. **24**, 79 (1952).
[29] S. K. Allison and S. D. Warshaw, Revs. Modern Phys. **25**, 779 (1953).
[30] Eisinger, Cook, and Class, Phys. Rev. **94**, 735 (1954).
[31] Rose, Goertzel, and Swift (private communication).
[32] Gellman, Griffith, and Stanley, Phys. Rev. **85**, 944 (1952).
[33] W. I. Goldberg and R. M. Williamson, Phys. Rev. **95**, 767 (1954).

of inertia was made by Bohr,[4] and other evidence for a similar conclusion was presented by Ford.[34] The values of Q_0(yield) and Q_0(energy) differ by roughly a factor of two for the even-even hafnium isotopes. These are the most highly deformed nuclei studied. The agreement between the values of Q_0 calculated from these two sources becomes worse as the nuclei become heavier and approach the closed proton shell at 82 protons and the closed neutron shell at 126 neutrons. For Pt^{198}, the least deformed nucleus studied, the ratio of the Q_0 from the excitation energy to that calculated from the yield data is about seven. This difference is much greater than the experimental error.

If the rotational model is valid, then in terms of the discussion in Sec. I, the most logical explanation for this phenomenon appears to be that the charge distribution within the nucleus becomes spherical more rapidly than the mass distribution as the closed shell at 82 protons and 126 neutrons is approached.

The authors are indebted to Dr. P. C. Aebersold and Dr. C. P. Keim for their assistance in obtaining the separated isotopes used in these experiments. Dr. J. A. Harvey assisted in obtaining the separated isotopes of hafnium and Dr. F. H. Spedding kindly supplied the sample of lutecium oxide used. We would like to thank Dr. M. E. Rose for supplying the tables of internal conversion coefficients prior to publication and Dr. K. Alder and Dr. A. Winther for sending a large scale graph of their calculation of $g_n(\xi)$. We are particularly grateful for helpful correspondence with Dr. Torben Huus and for interesting conversations with Dr. B. R. Mottelson and Professor V. F. Weisskopf.

[34] K. W. Ford, Phys. Rev. **95**, 1250 (1954).

PHYSICAL REVIEW VOLUME 97, NUMBER 5 MARCH 1, 1955

Concept of Parentage of Nuclear States and Its Importance in Nuclear Reaction Phenomena

A. M. LANE,* *Atomic Energy Research Establishment, Harwell, Berkshire, England*

AND

D. H. WILKINSON,† *Brookhaven National Laboratory, Upton, New York*

(Received November 9, 1954)

The concept of fractional parentage of nuclear states is invoked to point out that many dynamical properties of nuclear systems (transition rates and level widths) are controlled by products of the coefficients of fractional parentage for common parents (the "parentage overlap") between initial and final states. Illustrations are given from a range of nuclear reactions including radiative transitions, high- and low-energy stripping, pickup, and photonuclear processes. It is particularly to be emphasized that, because of the occurrence of the coefficients of fractional parentage and certain (vector coupling) weighting factors in the expression for the transition rate, one may find reduced and radiative widths very considerably less than the "single-particle" values even though the states concerned are wholly of an independent-particle character; enhanced transitions are also possible within the same scheme.

INTRODUCTION

IN recent years, many new types of nuclear reaction have been investigated experimentally with the new techniques and energy ranges available. Some of these reactions have received considerable theoretical attention of a sort in which an attempt is made to present *model-independent* formulas for cross sections by assuming only that certain general mechanisms are responsible for the transitions. As examples one can cite the theory of resonance reactions[1] (which did not, in fact, in its general form even assume a particular mechanism) and the theory of deuteron stripping.[2] It is not our purpose here to review the mass of detailed work that has been done, but rather we wish to show that there is often a considerable underlying similarity in the factors controlling the cross sections of apparently quite different types of reaction. If no nuclear model is assumed, this similarity is of only formal interest, but if a nuclear shell model is held to be valid, this unifying feature is of considerable practical interest and importance. It arises essentially from the fact that a whole range of nuclear reactions can be classified as "one-particle" reactions, by which we mean, not that only one particular particle in the nucleus can make a transition, but rather that a transition causes only a single particle (*any* single particle) to change its state. Since shell-model wave functions consist, rougly speaking, of products of single-particle wave functions, it follows that the differences between the formulas for the cross sections for different types of reactions can be separated out into certain multiplying single-particle

* Now on leave at the Massachusetts Institute of Technology, Cambridge, Massachusetts.

† On leave from the Cavendish Laboratory, Cambridge, England.

[1] E. P. Wigner and L. Eisenbud, Phys. Rev. **72**, 29 (1947).

[2] S. T. Butler, Proc. Roy. Soc. (London) **A208**, 559 (1951).

factors, which are the squares of single-particle matrix elements; the other factors, which only take account of the presence of other nucleons in the composition of the total initial and final states, are very similar for all varieties of one-particle reactions. It is this similarity between the formulas for the probabilities of various kinds of transition that we wish to stress here. The remainder of the paper is devoted to showing the usefulness of the fractional parentage concepts in representing this common factor, and to explicitly displaying the factor in a number of examples. In doing this, we shall not repeat the often lengthy formulas established by those workers who have studied the various reactions in detail, but rather we shall point out in each case the particular parameters containing the common factor. The realization of the presence of this factor will be seen to offer explanations of such diverse nuclear properties as the similarity of certain relative (n,γ) and (d,p) reaction yields, the spectra of high-energy inelastic proton scattering, and the variation in width of the "giant resonance" peaks of nuclear photodisintegration.

FRACTIONAL PARENTAGE

The concepts of "fractional parentage" and "parent states" were developed for the study of atomic spectroscopy by Racah.[3] He showed that any properly constructed (totally antisymmetric) shell-model state of n particles can be expanded in terms of the states of one particular particle vector-coupled to the "parent states" of the other $(n-1)$ particles. The coefficients in such an expansion are called the "coefficients of fractional parentage" or, in abbreviated form, the "c.f.p." Investigations into the nature of nuclear energy levels based on the quasi-atomic shell model have made direct use of Racah's methods and terminology, apart from changes arising from the existence of an extra quantum number (the isotopic spin). Jahn and Van Wieringen[4] have defined and evaluated the c.f.p. for states of equivalent particles in the L-S coupling approximation, and Flowers and Edmonds[5] have done this in j-j coupling.

The work of these authors has so far mainly been used to facilitate the calculation of nuclear energy level schemes and magnetic moments, i.e., the prediction of static nuclear properties. However the concept of parent states is also of fundamental importance for the understanding of certain dynamical nuclear properties such as transition rates and level widths. This we now discuss.

The types of transition that we have in mind are those for which the transition operator is either explicitly or effectively a "one-particle" one,[6] i.e., it can be expressed in the form

$$\Theta=\sum_k O(\mathbf{r}_k,\boldsymbol{\sigma}_k,\boldsymbol{\tau}_k), \tag{1}$$

where each term in the sum only operates on one particular particle k represented by the usual space, spin, and isotopic spin coordinates $\mathbf{r}_k$, $\boldsymbol{\sigma}_k$, and $\boldsymbol{\tau}_k$. The operator Θ must always be used when the states concerned possess detailed features; i.e., when they are not extreme "single particle" states. To find a transition probability, the matrix elements of the corresponding operator taken between the initial and final states must be evaluated. If there are present in the system n particles that are concerned in the transition (i.e., that are needed for the specification of the initial and final states), then, since the wave functions of these initial and final states are antisymmetric in all particles, the matrix element for a transition can be written in term of the matrix element of just one particular particle:

$$\langle i|\,\Theta\,|f\rangle=n\langle i|\,O(\mathbf{r}_n,\boldsymbol{\sigma}_n,\boldsymbol{\tau}_n)\,|f\rangle. \tag{2}$$

Here we have conventionally chosen the particular particle to be the nth one and put $k=n$ in the second matrix element. If now we assume that the fractional parentage expansions of the initial and final states are known, the evaluation of this quantity is quite straightforward. The total matrix element is expressible as a product of three factors:

$$\langle i|\,\Theta\,|f\rangle=n\times\begin{pmatrix}\text{single particle}\\ \text{matrix element}\end{pmatrix}\times(\text{parentage overlap}). \tag{3}$$

This last quantity is a sum of weighted products of the c.f.p. of the initial and final states. The sum is over all the parent states that the initial and final states have in common (the "common parents") and the weighting factors are usually Racah coefficients which take account of the recoupling of the various spins involved in the transition. It is to be noted that these weighting factors depend on the type of transition, so that the definition of parentage overlap is not quite the same for different kinds of transitions. However, we can make some remarks about the values of the parentage overlap which are quite generally true: for instance, its value cannot exceed unity, and can only equal unity in those exceptional cases when the initial and final states are very similar (in the sense of having the same parentage characteristics). In such cases, the

[3] G. Racah, Phys. Rev. **63**, 367 (1943). See earlier R. F. Bacher and S. Goudsmit, Phys. Rev. **46**, 948 (1934).

[4] H. A. Jahn and H. Van Wieringen, Proc. Roy. Soc. (London) **A209**, 502 (1951).

[5] A. R. Edmonds and B. H. Flowers, Proc. Roy. Soc. (London) **A214**, 515 (1952).

[6] It should be noted that we are confining ourselves to one-particle operators in the interests of simplicity and practical importance. One can develop a fractional parentage theory for the expansion of a state of n particles into states of $n-m$ and m particles where m is *any* number less than n. Such an expansion would be appropriate for the evaluation of m-particle operators. For instance, expansion with $m=2,4$ are appropriate for dealing with deuteron and alpha-particle transitions.

transition rates are larger than the single-particle values by the factor n^2. In most instances, the parentage overlap will be less than unity, and often less than n^{-1} so that the transition probability is usually reduced to less than the single-particle value. This happens when the two sets of parent states are different and there are only a few common parents. Since the c.f.p. of any given state satisfy a normalization condition (the sum of the squares is unity), the smaller the number of common parents relative to the total number, the smaller the value of the parentage overlap. It sometimes happens that there are no common parents at all, in which case the parentage overlap is zero and the transition is forbidden. Thus there are selection rules associated with the parentage overlap. We shall later see that these can be quite powerful. It is of great importance to realize that, because of the first and third factors in expression (3), the rate of a transition between pure shell model states needing several particles for their specification may be very different from that of an isolated single particle. Thus the fact that an observed transition rate is very much less than (or, for that matter, greater than) the single-particle value does not imply that other than pure shell-model states are involved.

It is tempting to try to give a simple semiclassical interpretation of the parentage overlap and the associated selection rules. The surface oscillation model of the nucleus[7] seems especially appropriate in this connection. Qualitatively, on this model, one imagines the initial state as consisting of one particle that can make a one-particle transition plus the rest of the nucleus (the core) acting as a hydrodynamical fluid behaving in a certain way (having a certain shape and rotating with a certain angular momentum). The only final states that are accessible by one-particle transitions are those in which the core has the same angular momentum. Even for these states the transition rates may be severely inhibited if a change in shape of the core is implied in the transition. Quantitatively, in the formulas for transition matrix elements, this inhibition factor appears in the form of a shape overlap integral, $\int\varphi_i\varphi_f dV$, between the initial and final core states.[8] This integral, in fact, occurs in the place of the parentage overlap factor (times n) in (3). One may associate the two factors, but should not take the analogy too seriously because an essential feature of fractional parentage and the evaluation of the parentage overlap is the antisymmetrization of the wave functions. There is no real classical analog of antisymmetrization and, in particular, its role in the surface oscillation model that we have used in illustration is obscure.

To some extent in the discussion so far, a nuclear shell model has been assumed. However our remarks are relevant to any model provided that the initial and final states are expanded in terms of shell-model states of various configurations, and that the c.f.p. are defined and evaluated. In such cases formula (3) must include a sum over the component configurations of the two states.

If we do indeed assume a shell model with pure configurations for the two states, an interesting situation exists near closed shells. In this region, low-lying states tend to have only few parent states, often only one or two, in contrast to the situation in between shells where there may be several dozen parents or more. Consequently transitions in the closed-shell region are liable either to be very strong (when there are common parents) or very weak (when there are no common parents).

SOME PRACTICAL ILLUSTRATIONS

To illustrate these rather formal remarks, we briefly consider a number of specific reactions which are of the one-particle type and in which the parentage overlap between the initial and final states therefore plays a dominant role.

(1) Nucleon Emission from a Compound Nucleus

In this type of transition, the final state is the system "residual nucleus+separating nucleon." By its nature, this total state has only one parent, *viz.* the state of the residual nucleus, and the corresponding c.f.p. is $n^{-\frac{1}{2}}$ where n is the number of nucleons concerned in the specification of the total state. From our general remarks above, the transition rate or reduced width is the single-particle value times n^2, times the square of the parentage overlap which now has the form:

$$n^{-\frac{1}{2}}\times(\text{the appropriate c.f.p. of the initial state})\times\left[\begin{array}{c}\text{a weighting factor}\\ \text{consisting of Racah}\\ \text{coefficients}\end{array}\right].$$

The explicit formula has been given in a previous publication,[9] where four experimentally known reduced widths of C^{13} and N^{13} were cited as examples of its application. Two of the compound states involved belonged to the configuration $1p^9$, and the other two belonged to $1p^8\,2s$ and $1p^8\,1d$. For the first two, the above formula could be applied directly using the previously mentioned work[4,5] on the parentage of states of equivalent particles. For the last two states, this could not be done because the compound states belong to mixed configurations of the type $l^{n-1}l'$ and there is considerable choice in the precise way such states may be constructed. Usually, for formal mathematical purposes, states of such mixed configurations are constructed by simply vector-coupling the l'

[7] A. Bohr and B. Mottelson, Kgl. Danske Videnskab. Selskab, Mat.-fys. Medd. **27**, No. 16 (1953).

[8] E.g., this factor appears in formulas (VIII. 14) and (VII. 14) of reference 8; these apply to beta and gamma transitions, respectively.

[9] A. M. Lane, Phys. Rev. **92**, 839 (1953).

particle on to definite proper states of l^{n-1} and then antisymmetrizing. Such states are said to be defined "genealogically." As far as a particle being in the l' orbit is concerned, each total state has only one parent state of l^{n-1} and the corresponding c.f.p. for this state is $n^{-\frac{1}{2}}$. If the actual physical states of mixed configurations are approximated by these simply-constructed states, the reduced width for nucleon emission to the "unique parent" state is then seen to be just the single-particle one (apart from possible Racah coefficients in the weighting factor).

It has been pointed out[10] that there is considerable experimental evidence that states of mixed configurations have single-particle reduced widths, at least in light nuclei. Thus one gathers that the "unique parent" approximation to these states is a good one. The theoretical reason for this is certainly not obvious, but detailed investigation[10] provides some justification for the approximation in particular cases. We do not propose to discuss this matter here, but merely to point out that the experimental facts give support to the approximation. Assuming the approximation enables us to evaluate the parentage overlap for states of mixed configurations.

(2) Beta Decay

Since the beta-decay operator is a one-particle operator, this comes into the class of one-particle reactions. However, since beta decay usually takes place between low-lying states of nuclei (which almost always have common parents), the *selection rules* arising from parentage are of little practical use, although the parentage overlap directly controls the ft value. Explicit expressions for the beta-decay matrix elements in L-S and j-j coupling have been given,[11] and can be seen to be of the form (3).

(3) Radiative Transitions

These are one-particle transitions as an immediate consequence of the one-particle nature of the electromagnetic transition operators. The precise manner in which a transition probability is controlled by the parentage overlap between the initial and final states has been shown already.[12] The formulas for $E1$, $M1$, and $E2$ transition matrix elements all have a form identical to (3).

An interesting situation exists when one state (say the emitting state) has a mixed configuration of the type $l^{n-1}l'$ discussed in example (1). If the 'unique parent' state is the ground state of l^{n-1}, it follows that the intrinsically strongest transitions will be to those states of l^n which also have this ground state as a parent. Such states will be those near the ground state of l^n, and consequently one expects radiative transitions from the upper state to favor high-energy transitions more strongly than is suggested by their greater energy alone.

The preference for ground-state transitions has been noted[13] in the capture of thermal neutrons in a number of cases: F^{20}, Al^{28}, Pb^{207}, Pb^{208} (final nuclei). Considerations similar to those above indicate a possible simple explanation for these phenomena.

The recent unpublished work of P. C. Gugelot on the radiative capture of 18-Mev protons by copper also shows a rather considerable favoring of transitions to the lower-lying excited states (an apparently too-slowly increasing level density with excitation energy), suggesting that the target nucleus may not be too violently disturbed even by the addition of so fast a particle.

Of course, the electric excitation of nuclei under charged particle bombardment (Coulomb excitation) is directly governed by the radiative transition probabilities from the ground state, and so, to this extent, is included in the present considerations. Detailed theoretical studies revealing the relation between cross section and transition probability have been reported for both positive[14,15] and negative[16] particle bombardment. Experimentally the (e,e') reaction on C^{12} has been recently investigated with high-energy electrons.[17] It is found that the 7.68-Mev level is excited only relatively weakly compared with the 4.45-Mev level. The latter state is $2+$ and, on any shell model, has a strong parentage overlap with the ground state. The 7.68-Mev state is believed to be $0+$ and does not appear in the shell-model spectrum.[18] Its parentage overlap with the ground state is thus presumably small since it differs from it by the excitation of more than one nucleon (though note that it is incorrect to attribute the observed difference in excitation probability to overlap factors alone since the single particle probabilities are different for the two excitations).

(4) High-Energy Stripping and Pickup Reactions

In high-energy pickup reactions (for example) one imagines that the incident particle "snatches" a nucleon from the target nucleus. A treatment of this phenomenon in the impulse approximation essentially assumes that the condition of all the other nucleons is unchanged. Since the squares of the c.f.p. of the target nucleus determine the relative times that these other nucleons spend in their various parent states,

[10] A. M. Lane, Proc. Phys. Soc. (London) (to be published), and Atomic Research Establishment, Harwell Report T/R 1289, 1954 (unpublished).
[11] A. M. Lane, Proc. Phys. Soc. (London) (to be published).
[12] A. M. Lane and L. A. Radicati, Proc. Phys. Soc. (London) **A67**, 167 (1954).
[13] B. B. Kinsey and G. A. Bartholomew, Phys. Rev. **93**, 1260 (1954).
[14] K. A. Ter-Martirosyan, J. Exptl. Theoret. Phys. (U.S.S.R.) **22**, 284 (1952).
[15] K. Alder and A. Winther, Phys. Rev. **91**, 1578 (1953).
[16] Thie, Mullin, and Guth, Phys. Rev. **87**, 962 (1952); L. I. Schiff, Phys. Rev. **96**, 765 (1954).
[17] R. Hofstadter (private communication).
[18] D. R. Inglis, Revs. Modern Phys. **25**, 390 (1953).

it is clear that these quantities determine the relative cross sections for the pickup production of the various possible residual (parent) states. When the target nucleus is a closed shell, since any component (lj) shell has only one parent state (the state of one hole in jj coupling), if a nucleon is removed from the last shell only one final state (the ground state) of the residual nucleus is allowed. When the target is not a closed shell, there are, in general, several parent states and so several final states that are open to the residual nucleus. This means that when individual product groups are not resolved, one expects the spectrum of product particles to be sharp at closed shells and to broaden on going away from closed shells. The results of Selove[19] with 90-Mev protons on $Si^{28}(p,d)Si^{27}$ (closed $1d_{5/2}$ shell, spectrum width $\sim$5 Mev) and $Al^{27}(p,d)Al^{26}$ (nonclosed shell, spectrum width $\sim$10 Mev) exemplify this idea. It should be mentioned that in the discussion of such work, Selove concludes that the shell model is not a satisfactory model on the grounds that no resolved product groups are observed to correspond to the removal of nucleons from the inner closed shells; Selove expects such a group to occur at about 8 Mev (the presumptive single-particle spacing) from the observed group due to pickup from the outer shell. However, apart from the fact that this energy should be increased to allow for the excess pairing energies of the last nucleons in the inner shells, one may expect considerable configuration interaction at such high excitations in the residual nuclei. For instance, if a $1s_{\frac{1}{2}}$ neutron is "snatched" from Si^{28}, the simple $1s_{\frac{1}{2}}$ hole state of Si^{27} is probably immediately "dissolved" and shared amongst proper eigenstates perhaps over a wide energy range. Thus no sharp product groups should necessarily be expected for the removal of nucleons from the inner shells. In contrast to the one-peak spectra from Si^{28} and Al^{27} that we have mentioned, Selove (private communication) finds that the spectrum of deuterons in the $Be^9(pd)Be^8$ reaction has two well-defined peaks separated by about 15 Mev. On an alpha-particle model of Be^9 these two peaks would be said to correspond to the removed neutron being in the one case the odd neutron and in the other a neutron from an alpha particle. However we again find that a shell model gives an equally good explanation because, for instance, in L-S coupling, the ground state of Be^9, which has partition [441] has parent states in Be^8 in two distinct groups, namely [44] and [431] which are known to be separated by about 17 Mev. The difference behavior that Selove finds for target nuclei of the $4n$, $4n+1$, and $4n+3$ types certainly reflects the existence of 4-groups in the nucleus of the "saturated spin-isotopic spin" type. However it seems to us that there is no evidence for any actual spatial separation between such saturated groups of four particles as is implied in the alpha-particle model.

[19] W. Selove, Phys. Rev. **92**, 1328 (1953).

(5) Low-Energy ($\leq$15 Mev) Stripping and Pickup Reactions

According to the stripping theory,[2] one imagines stripping and pickup reactions simply to involve the exchange of a nucleon between the colliding nuclei outside the surface of the target nucleus. In this region, the exchanged nucleon is temporarily dissociated from the others in the target, and so the latter cannot change their state. This means that just as in the example (1), the transition rate (for the case of pickup) is determined by the reduced-width of the initial (target) state for dissociation into a nucleon and the final (residual) state. This reduced width is, in turn, simply proportional to the square of the corresponding c.f.p. The explicit relation between stripping cross section and reduced width has been demonstrated and used[20] to extract values of the latter from experimental data.

It has been remarked[21] that one sometimes finds considerable similarity between the relative intensities of gamma rays (of given multipolarity and parity change) emitted in the radiative capture of thermal neutrons to various states of the residual nucleus and the relative intensities of the proton groups that give the same residual states by (d,p) stripping. This seemingly curious relationship follows immediately from the present considerations and those of item (3) above if we may assume that the ground state of the target nucleus for the (n,γ) reaction is the chief parent of the radiating state—for then the radiative widths of the gamma transitions will be proportional to the squares of the c.f.p. of the residual states for the target nucleus and so will the intensities of the proton groups. The fact that the intermediate systems are wholly different for the two processes is irrelevant.

One interesting experimental result[22] is the absence of a proton group to the 7.68-Mev state in C^{12} in the reaction $B^{11}(d,n)C^{12}$ using deuterons of 8 Mev. This suggests that (since this is presumably a stripping reaction) the ground state of B^{11} is not a parent of the 7.68-Mev state of C^{12}. Since the ground state of B^{11} is the only parent of the ground state of C^{12} (strictly true in j-j coupling and approximately so in L-S coupling), it follows that the parentage overlap of the 7.68-Mev and ground states of C^{12} must be small or zero. We saw in example (3) that the fact that the inelastic electron scattering to the 7.68-Mev state was so small could be explained on these same grounds.

(6) Moderate and High-Energy ($\geq$10 Mev) (n,p) and (p,p') Reactions

Arguments for treating these reactions in the impulse approximation have been put forward in a paper[23]

[20] Fuyimoto, Kikuchi, and Yoshida, Proc. Theoret. Phys. (Japan) **11**, 264 (1954).
[21] B. B. Kinsey (unpublished).
[22] V. R. Johnson, Phys. Rev. **86**, 302 (1952).
[23] Austern, Butler, and McManus, Phys. Rev. **92**, 350 (1953).

mainly concerned with their angular distributions. Acceptance of this approximation places these reactions in the "one-particle" category; one imagines the incident particle to collide with just one target nucleon. In inelastic scattering, the struck nucleon may receive energy which is eventually shared, but, during the time of collision, the other target nucleons are not disturbed. Thus, as in the other examples we have given, the cross sections for such reactions are determined by the squares of the parentage overlaps, which are defined with weighting factors peculiar to the process. (The parentage overlaps can be written as sums over products of reduced-width amplitudes). Explicit demonstration of this has been given by Austern *et al.*,[23] in their formula (14), in which their quantity $\sum_s A_{st}(j_s,m_s,j_p,\mu_p) \times B_{st'}(j_s,m_s,j_n,\mu_n)$ our parentage overlap. In inelastic scattering reactions on closed-shell nuclei, this result implies that only those states sharing the (unique) parent of the ground state can be excited. In the $C^{12}(p,p')C^{12}$ reaction with 90-Mev protons,[24] the 7.68-Mev level appears to be less readily excited than the 4.45-Mev level. This is precisely the same result as that obtained with inelastic electron scattering mentioned in example (3) and with stripping in example (5). Again we see that apparently very different reaction mechanisms can yield very similar results and that the parentage overlap factors may well provide the correct explanation of these similarities.

There is some evidence from the unpublished results of P. C. Gugelot on the inelastic scattering of 18-Mev protons that the impulse approximation[23] may have some validity in this energy range. He finds an apparent rate of increase of level density with excitation that is somewhat less than expected, on the basis of the usual thermodynamic expressions; this reflects the worsening parentage overlap between ground and excited states as the excitation increases and is just the result to be expected on the basis of the present considerations. Of course, a direct inelastic scattering process such as that which we have in mind will, in general, give an entirely different spectrum of product particles from that predicted by the compound nucleus theory where most particles emerge with low energies. Especially when the target nucleus is well approximated by a shell-model description, the parentage overlap factor implies that the direct process favors high-energy particle groups leaving behind those residual states whose overlap with the ground state is appreciable. If no allowance is made for the presence of the direct process in interpreting a spectrum of inelastically scattered particles, there will be an apparently anomalously low rate of increase of level density with energy for excitations of up to 5 Mev or more in the residual nucleus.

[24] K. Strauch and W. F. Titus, Phys. Rev. **95**, 854 (1954).

(7) Photonuclear Reactions

The present ideas have one of their most interesting applications in the study of photonuclear reactions, where they offer a possible explanation of the sharpness of the giant electric dipole photonuclear peaks at closed shells.[25] Owing to the one-particle nature of the electric dipole operator, provided that the ground state of the target nucleus is a reasonably good shell-model state, photoexcitation can take place solely to a few shell-model component states differing in configuration by one particle from the ground state, and having at least one parent state in common with it. Of course, since they occur at such high energies, these states are almost never good eigenstates, but are dissolved by configuration interaction over some energy range. Nevertheless, unless this interaction is strong (and the complex potential model[26] suggests that it is not), one expects that the width of the photonuclear peak is roughly equal to the energy spread of the contributing shell-model states. At closed shells, there are only very few such states because the ground state of a closed shell has only one parent state (in j-j coupling); on the other hand, the matrix elements are especially strong[27] [essentially due to the factor n in expression (3)]. Thus the photonuclear peaks are expected to be considerably sharper at closed shells than in between shells, where there are many more (and widely-spread) contributing states with weaker matrix elements. Details of quantitative calculations will be published elsewhere.[27]

CONCLUSIONS

Several of the types of one-particle reactions mentioned above have in the past been discussed from a purely single-particle viewpoint in which the initial and final wave functions are represented by the wave functions of a single particle. We have indicated that, in general, this approach is invalid and that one must take into account in a nuclear reaction the presence of all nucleons needed to specify the states concerned: this leads to a factor in the transition matrix elements that we have called the parentage overlap. The parentage overlap appears in the cross sections for all reactions in the one-particle category, and consequently provides an explicit unifying feature of these reactions. In the examples, the factor has been shown to be able to explain a number of phenomena that cannot be understood from the elementary single-particle viewpoint.

[25] D. H. Wilkinson, Philadelphia Conference on Photonuclear Reactions, 1954 (unpublished), p. 5.
[26] Feshbach, Porter, and Weisskopf, Phys. Rev. **96**, 448 (1954).
[27] D. H. Wilkinson, Phil. Mag. (to be published).

Cross Sections for Nonelastic Interactions of 14-Mev Neutrons with Various Elements*

ELIZABETH R. GRAVES AND ROLAND W. DAVIS
Los Alamos Scientific Laboratory, University of California, Los Alamos, New Mexico
(Received October 18, 1954)

The multiplication of neutrons by thin spherical shells of various materials surrounding a point source of 14-Mev neutrons has been measured. A special long counter was used whose energy response is independent of neutron energy over a range of energies from about 1 Mev to 14 Mev. The transmission of primary energy neutrons through the shells has been measured with a trans-stilbene detector and values of the inelastic collision cross sections have been derived. The quantity $\sigma_{n,2n}+2\sigma_{n,3n}-\sigma_c$ is calculated, where $\sigma_{n,2n}$ and $\sigma_{n,3n}$ are the cross sections for $(n,2n)$ and $(n,3n)$ reactions and σ_c is the sum of the cross sections of all processes which destroy a neutron. Upper and lower limits are derived for $\sigma_{n,2n}$, σ_c, and σ_{is} (inelastic scattering) for all materials investigated. For a number of materials specific values for the cross sections are obtained.

INTRODUCTION

USUALLY the cross sections for $(n,2n)$, (n,p), (n,α), etc., reactions are measured by utilizing induced activities.[1,2] However, where stable isotopes result, this method is not applicable and in many other cases it is impractical. However, the existence of $(n,2n)$ reactions is manifest in a material under neutron bombardment by an increase in the number of neutrons, while the effect of capture, (n,p), (n,d), (n,α) reactions etc., is to reduce the number of neutrons. The concept of neutron multiplication is thus introduced which is not dependent upon the characteristics of the end products of the reactions but only upon the balance between those processes which increase, those which leave unchanged, and those which decrease the number of neutrons, and upon the number of events of the three kinds which occur in the material. The neutron multiplication of a layer of material is then defined as the total number of neutrons emerging divided by the number of primary neutrons incident upon the layer.

It is clear that a primary neutron incident upon the layer either will suffer a collision while traversing the layer or will be transmitted without suffering a collision. The concept of the transmission of primary neutrons is thereby established, namely that fraction of the primaries which is transmitted without collision. For further ease in handling the problem this concept is in the present analysis extended to mean the transmission of *primary energy* neutrons, since collisions of the kind in which we are interested result in secondary neutrons of energy much lower than the primary energy. For intermediate and heavy nuclei, and to a lesser extent for light nuclei, the energy change of a neutron upon elastic scattering is so small that elastically scattered neutrons are classed as primary energy neutrons. The transmission of primary energy neutrons is thus defined as that fraction of the primary neutrons which, during traversal through the material, do not suffer a collision at all or suffer only elastic collisions. Hence, one minus the transmission represents that fraction of the source or primary neutrons which, during traversal of the material, suffer collisions wherein (1) the neutron is lost, (2) the neutron merely suffers appreciable energy loss, or (3) more than one neutron results from the interaction. These collisions are called inelastic collisions and are associated with the cross section for inelastic collision, σ_i. For brevity, neutrons resulting from such collisions, as distinguished from elastic scattering collisions, will be called inelastic-collision neutrons.

Having established the concepts of neutron multiplication and transmission, it is proposed firstly to establish the relationship between these quantities and certain cross sections; secondly to describe the measurement of these quantities for 14-Mev primary neutrons; and thirdly to derive, from these measurements, values of inelastic collision cross section, and limits of permissible values for, and in many cases specific values for, cross sections for the three kinds of inelastic events (1), (2), and (3) as described above.

OUTLINE OF METHOD

As has been stated by a number of investigators,[3] if a thin shell of material surrounds an isotropic point source of neutrons and all cross sections for neutron interaction in the material are zero except for elastic scattering, a neutron detector placed at sufficient distance from the shell will not detect the presence of the shell of material. That is, the neutrons per cm^2 per second passing through any imaginary surface for a fixed source strength will be unchanged by introducing the shell around the source. It follows that even if the cross sections for processes other than elastic scattering are not zero, the elastic scattering may still be ignored except insofar as it increases the average path length of neutrons emerging through the sphere. It is generally accepted that for 14-Mev neutrons the elastic scattering should be diffraction type scattering, and, except perhaps for very light elements, will be confined primarily to small angles. Consequently the path length of an elastically scattered neutron emerging through the shell

* Work done under the auspices of the U. S. Atomic Energy Commission.
[1] Stuart G. Forbes, Phys. Rev. **88**, 1309 (1952).
[2] E. B. Paul and R. L. Clarke, Can. J. Phys. **31**, 267 (1953).
[3] H. H. Barschall, Revs. Modern Phys. **24**, 120 (1952), see p. 128.

differs only very slightly from an unscattered neutron and the effect may be neglected.

Let a thin spherical shell of material surround an isotropic source of 14-Mev neutrons. Then the following equation relating multiplication and transmission may be stated for nonfissioning materials:

$$M=T+(1-T)\left\{\frac{\sigma_{is}}{\sigma_i}+\frac{2\sigma_{n,2n}}{\sigma_i}+\frac{3\sigma_{n,3n}}{\sigma_i}\right\}, \quad (1)$$

where M, the multiplication, is the total number of neutrons emerging per source neutron, T, the transmission of primary energy neutrons is that fraction of the source neutrons which emerges from the shell having suffered no inelastic collisions, and σ_i is the inelastic collision cross section defined by

$$\sigma_i\equiv\sigma_{\text{total}}-\sigma_{\text{elastic}}=\sigma_{is}+\sigma_{n,2n}+\sigma_{n,3n}+\sigma_c, \quad (1a)$$

where σ_{is} = cross section for inelastic scattering, i.e., any $(n,1n)$ inelastic reaction, $\sigma_{n,2n}$ and $\sigma_{n,3n}$ = cross section for $(n,2n)$ and $(n,3n)$ reactions [for higher-energy primary neutrons similar terms for $(n,4n)$, etc. should be included], and

$$\sigma_c=\sigma_{n,p}+\sigma_{n,\alpha}+\sigma_{n,\gamma}, \text{ etc.}, \quad (1b)$$

is the sum of the cross sections for all processes which destroy a neutron. Substitution for σ_{is} and collection of terms leads to

$$\frac{M-T}{1-T}=\left\{1+\frac{\sigma_{n,2n}}{\sigma_i}+2\frac{\sigma_{n,3n}}{\sigma_i}-\frac{\sigma_c}{\sigma_i}\right\}\equiv 1+k. \quad (2)$$

The left side of this equation combines the observable quantities M and T, each of which is a function of the thickness of the material while the right side involves only nuclear constants. The quantity in brackets in Eq. (2) is the number of neutrons per inelastic collision, and defines the quantity k as shown.

If a neutron detector whose sensitivity is entirely independent of neutron energy is placed at a sufficiently large distance from the shell surrounding the source, the counting rate of this detector per source neutron for the source surrounded by a shell divided by the counting rate per source neutron for the bare source is equal to the neutron multiplication M. However, if the detector sensitivity is not independent of neutron energy, the measured multiplication M', that is, the ratio of the counting rates just described, will be related to the true multiplication, M, in some manner which must be determined. It has been found by the photographic plate method[4–6] that the neutrons resulting from inelastic interaction of 14-Mev neutrons with intermediate and heavy nuclei are almost entirely of low energy, that is, below about 3 or 4 Mev. Hence neutrons emerging from the shell are in one of two energy groups, either 14 Mev or degraded to less than 3 or 4 Mev. If a detector such as the Hanson-McKibben[7] type long counter whose sensitivity is independent of neutron energy from approximately zero to 5 Mev be used, the equation for M', the measured multiplication, may be written

$$M'=T+(1-T)(1+k)(\epsilon'/\epsilon_0), \quad (3)$$

where ϵ'/ϵ_0 = efficiency for detecting the inelastic neutrons divided by the efficiency for detecting the primary neutrons.

The equation as derived so far assumes thin shells and ignores second-order effects, i.e., multiplication or capture of the inelastic-collision neutrons from the primary interaction before escape from the material. This effect may be introduced by defining M'', the apparent multiplication including this effect as well as detector sensitivity, as

$$M''=T+(1-T)(1+k)(\epsilon'/\epsilon_0)(1+\delta), \quad (4)$$

where δ may be either positive or negative and will be a function of the shell thickness for any given material. For the majority of materials, δ will be negative (if not zero) because of capture before escape. Experimentally, δ is shown to be either zero or negligible by establishing the invariance of $(M''-T)/(1-T)(\epsilon'/\epsilon_0)$ with respect to change of shell thickness.

NEUTRON DETECTORS

1. For the Measurement of M

A shielded Hanson-McKibben type long counter built as described by the originators[7] has a sensitivity to 14-Mev neutrons which is approximately 60 percent of the sensitivity to Ra-α-Be neutrons. The sensitivity of such a long counter was modified by changing the proportional counter in the central tube. A shorter counter (5-in. active length) was substituted which was located farther back in the paraffin such that its active volume began approximately at the base of the 1-in. holes which are drilled in the paraffin face, although the exact boundaries of the active volume within the counter tube were not determined. This served to reduce the absolute sensitivity to neutrons of all energies but reduced the sensitivity to faster ones less than to slower ones. The relative sensitivity depended strongly on the counter location.

A calibration of the sensitivity of the counter as a function of neutron energy was made with the 14-Mev neutron source whose strength was accurately determined by counting alpha particles from the reaction, with a standard Ra-α-Be source, and with mock fission,[8] Na-γ-D, and Sb-γ-Be sources whose strengths were determined by comparison of the flux produced in a

[4] E. R. Graves and Louis Rosen, Phys. Rev. **89**, 343 (1953).
[5] P. H. Stelson and C. Goodman, Phys. Rev. **82**, 69 (1951).
[6] B. G. Whitmore and G. E. Dennis, Phys. Rev. **84**, 296 (1951).
[7] A. O. Hanson and J. L. McKibben, Phys. Rev. **72**, 673 (1947).
[8] D. S. Martin, Atomic Energy Commission Document No. 3077 (unpublished).

graphite pile[9] with that produced by the standard RaBe source. The thermal fluxes were compared and the source strengths calculated making use of the age theory with refinements indicated by Marshak.[10] It was assumed that because of the growing in of RaD+E +F the standard neutron source strength had increased by 2.0 percent between the standardization by Walker[11] in 1944 and this calibration which was made in February 1952.

The relative sensitivity values of the long counter are given in Table I for two locations of the counter such that position B was 0.75 in. farther back from the front face of the paraffin than position A. Position A was used for the multiplication measurements. The accuracy of the relative sensitivity is about 2 percent for the energy range up to Ra-α-Be neutrons. The accuracy of the comparison of this range with 14-Mev is limited by the uncertainty of 5 percent in the primary Ra-α-Be source standardization. It may be seen that the sensitivity drops off for neutron energies of a few hundred kilovolts. This means that the measured multiplications may fall slightly below the true values depending on the fraction of the neutrons which fall in this energy region. It is felt that the error is not large, however, and that the advantage of energy independence at the higher energies outweighs this disadvantage. (ϵ'/ϵ_0) as defined in Eq. (3) is taken to be equal to 1.00. It may be seen that an error in ϵ'/ϵ_0 will reflect in a systematic error of the same magnitude in $(M-T)/(1-T)$. This has not been included in the errors given for the measurements. The change in k and hence in $k\sigma_i$ induced by a 5 percent change in ϵ'/ϵ_0 is about equal to the experimental errors quoted for the light and intermediate elements and up to 4 or 5 times the quoted errors for the heavy elements.

The long-counter detector was placed at a distance of 180 cm from the neutron source. The background counting rate measured with a thick iron shadow cone between the source and long counter was about 14 percent for both 14-Mev neutrons and Ra-α-Be neutrons. Since the multiplications are close to unity and the background appeared not to vary appreciably with neutron energy, no correction was made for background in the measurement of M.

TABLE I. Sensitivity of the modified long counter as a function of neutron energy for two positions of the proportional counter in the center tube.

Neutron source	Neutron energy	Sensitivity = counts per neutron (arbitrary units) Position A	Position B
Sb-γ-Be	25 kev	0.57	0.45
Na-γ-Be	220 kev	0.63	0.56
M.F.	fission spectrum	1.01	...
Ra-α-Be	Average 5 Mev	1.00	1.00
$d-T$	14 Mev	1.00	1.00

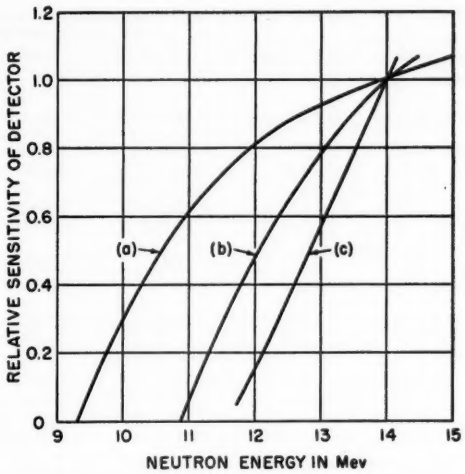

FIG. 1. Sensitivity of detectors. (a) Ideal hydrogen recoil detector biased such that all protons of energy greater than two-thirds of 14 Mev are counted. (b) Stilbene scintillator used in this experiment biased such that all pulses greater than two-thirds of the pulse height produced by a 14-Mev proton are counted. (c) $Cu^{63}(n,2n)$ detector from references 16 and 17.

2. For the Measurement of T

A trans-stilbene crystal mounted on a photomultiplier tube served to detect high-energy neutrons. The detector was biased so that all pulses larger than $\frac{2}{3}$ of the maximum pulse height were counted. The background counting rate determined with a shadow bar was approximately 1 percent. Curve (a) of Fig. 1 shows the calculated sensitivity of an ideal hydrogen recoil detector biased at $\frac{2}{3}$ of incident neutron energy. The curve of pulse height *vs* proton energy measured for another trans-stilbene detector was used to convert the ideal sensitivity curve to that of the actual detector used. Curve (b) portrays the result of this calculation. Since, for all but the lightest elements, degradation of neutron energy by elastic scattering is negligible, the counting rate of this detector with and without the sphere of scattering material surrounding the source gave the transmission, T, desired. Small deviations introduced by the detector sensitivity will be discussed later.

The assumption must be justified that the detector as used is sufficiently insensitive to γ rays. Inelastic scattering in the sphere material and in the target material both produce γ rays. Hence if the detector responds to γ rays, the observed transmission may be either too large or too small, depending on the properties of the sphere material. Calibration of the detector showed the pulse height of a 14-Mev proton to be 6.5 times the maximum height of the pulse from a 1.28-Mev γ ray. Hence the bias of two-thirds of the 14-Mev proton pulse height was still about $4\frac{1}{2}$ times the γ-ray

[9] A. C. Graves *et al.*, *Neutron Sources* (McGraw-Hill Book Company, Inc., New York, 1952); National Nuclear Energy Series, Plutonium Project Record, Vol. 3, Div. V, Chap. 2, Sec. 5.
[10] R. E. Marshak, Revs. Modern Phys. **19**, 185 (1947).
[11] R. L. Walker, Atomic Energy Commission Document MDDC-414 (unpublished).

TABLE II. Summary of measurements of transmissions and multiplication of spherical shells of various materials. Symbols are defined in Eqs. (1) through (4) and text.

Element	N (atoms/cm²) $\times 10^{-24}$	M''	T	$\left(\frac{M-T}{1-T}\right)$	$\left(\frac{M-T}{1-T}\right)-1$ $=k$	σ_i (barns) from $T=e^{-N\sigma_i}$	$k\sigma_i$ (barns)
C	0.299	0.9831	0.8364	0.897	−0.103	0.597	−0.062
	0.597	0.9507	0.695	0.839	−0.161	0.609	−0.098
Al	0.218	0.9590	0.7962	0.799	−0.201	1.01[a]	−0.20
	0.435	0.9194	0.6409	0.776	−0.224	0.994[a]	−0.22
Fe	0.174	1.012	0.8052	1.062	0.062	1.24	0.077
	0.349	1.009	0.6325	1.026	0.026	1.31	0.034
Cu	0.175	1.040	0.7851	1.187	0.187	1.38	0.266
	0.349	1.056	0.5997	1.139	0.139	1.47	0.197
Zn	0.169	1.021	0.7851	1.098	0.098	1.43	0.143
	0.340	1.014	0.6014	1.036	0.036	1.50	0.053
Ag	0.151	1.095	0.7596	1.394	0.394	1.82	0.717
Cd	0.139	1.113	0.7573	1.467	0.467	2.00	0.911
	0.279	1.175	0.5914	1.429	0.429	1.88	0.837
Sn	0.130	1.123	0.7669	1.527	0.527	2.04	1.03
	0.259	1.208	0.6142	1.539	0.539	1.88	1.06
Au	0.130	1.136	0.7282	1.501	0.501	2.44	1.22
Pb	0.105	1.166	0.7699	1.721	0.721	2.49	1.80
	0.210	1.280	0.5929	1.688	0.688	2.49	1.71
Bi	0.0985	1.165	0.7789	1.746	0.746	2.54	1.88
	0.1970	1.285	0.6099	1.730	0.730	2.51	1.84

[a] Correction has been made for copper content of alloy used.

pulse quoted. For most materials the γ-ray energy emitted is predominately lower than 6 or 7 Mev,[12] and hence would not be detected with appreciable efficiency. However, iron emits some γ rays of ≈ 7 Mev and 9 Mev with a cross section of ≈ 0.1 barn.[13,14] The neutrons emitted from the target in the present experiment pass through a thin stainless steel shell and it may be calculated that about 0.03 percent of them produce these γ rays. The number of γ rays per source neutron produced in the tungsten target backing is estimated to be 0.5 percent per barn of cross section for their production. Since it may be shown that the stilbene detector is somewhat less sensitive to γ rays of this energy than it is to 14-Mev neutrons, the effect of γ rays from the target is considered negligible.

Of the materials investigated, the only one for which γ rays from the sphere itself might be detected is iron. It has been calculated that, if they all emerged from the sphere and the pulses generated in the detector were recorded with the same efficiency as the 14-Mev neutron pulses, the measured transmission of the $\frac{1}{2}\lambda$ sphere should be multiplied by a factor 0.96 and of that of the $\frac{1}{4}\lambda$ sphere by a factor 0.98. Since the bias of the detector is relatively higher for the γ rays than for the neutrons, and since there is considerable attenuation of the γ rays by the sphere, it is felt that this correction should not be made and it has therefore been omitted.

[12] M. E. Battat (private communication).
[13] Sherrer, Theus, and Faust, Phys. Rev. **89**, 1268 (1953).
[14] Sherrer, Theus, and Faust, Phys. Rev. **91**, 1476 (1953).

NEUTRON SOURCE AND SCATTERERS

A thick Zr-T target was bombarded by a collimated $\frac{3}{16}$-inch diameter beam of 220-kev diatomic deuterium ions to produce neutrons. The strength of the source was measured by counting alpha particles in a proportional counter in a known geometry. The emission of neutrons was only slightly different from isotropic. The forward yield was calculated to be four percent greater and the backward yield four percent lower than the yield at 90°. Both neutron detectors were very nearly at 90°. It is felt that the yield variation is not important for the spherical shell experiments reported here. The neutron energy varied somewhat with angle of emission. Neutrons emitted at 90° to the incident beam had an average energy of 14.1 Mev while at 0° and 180° the averages were, respectively, 0.6 Mev higher and 0.6 Mev lower than the 90° value.

The scatterers were interlocking hemispherical shells through which two holes three-quarters of an inch in diameter and one hole one-half inch in diameter passed to accomodate the beam tube, target tube, and alpha monitor tube. The shells were hung by means of screw eyes which threaded into them. The outer diameter of all the shells was 8.00 inches, and the wall thickness of any shell was uniform to within ± 0.001 inch. Thick-

TABLE III. Summary of cross sections in barns derived from transmission and multiplication measurements. Columns 2 and 3 give values of σ_i and $k\sigma_i$ as measured in the present experiment. For comparison, σ_i from Phillips, Davis, and Graves[a] is given in parenthesis under σ_i from this experiment in Column 2. Columns 4, 5, and 6 give limits of σ_c, $\sigma_{n,2n}$, and σ_{is} as defined in Eqs. (1a) and (1b). For elements Al through Ag values for one of the three cross sections are taken from Forbes[b] or Paul and Clarke[c] and the other two calculated from Eqs. (5a) and (6).

Element	σ_i, this expt. (σ_i, reference a)	$k\sigma_i$	σ_c	$\sigma_{n,2n}$	σ_{is}
C	0.601±0.006 (0.76±0.04)	−0.08±0.02	0.08±0.02 (=C(n,α)Be[8] grnd. state)	0.00 (below threshold)	0.52±0.02 (See text for components)
Al	1.00±0.01 (1.06±0.05)	−0.21±0.01	0.214±0.015[b] [0.13±0.03][b]	0.00±0.02 [−0.08±0.03]	0.79±0.03
Fe	1.27±0.04 (1.45±0.02)	0.07±0.03	$0.114 \leqq \sigma_c \leqq 0.60$ ±0.01 ±0.03[b]	$0.18 \leqq \sigma_{n,2n} \leqq 0.67$ ±0.03 ±0.04	$0.97 \geqq \sigma_{is} \geqq 0.00$ ±0.06
Cu	1.42±0.04 (1.51±0.06)	0.24±0.02	0.41±0.06 (See text)	0.65±0.05[b]	0.36±0.09
Zn	1.46±0.03	0.11±0.04	$0.22 \leqq \sigma_c \leqq 0.68$[c] ±0.04 ±0.03	$0.33 \leqq \sigma_{n,2n} \leqq 0.79$ ±0.06 ±0.05 (See text)	$0.91 \geqq \sigma_{is} \geqq 0.00$ ±0.09
Ag	1.82±0.02	0.72±0.03	0.06±0.09	0.77±0.08[b]	1.0±0.2
Cd	1.95±0.05 (1.89±0.06)	0.89±0.02	$0.00 \leqq \sigma_c \leqq 0.53$ ±0.03	$0.89 \leqq \sigma_{n,2n} \leqq 1.42$ ±0.02 ±0.04	$1.06 \geqq \sigma_{is} \geqq 0.00$ ±0.06
Sn	1.96±0.05	1.04±0.02	$0.00 \leqq \sigma_c \leqq 0.46$ ±0.03	$1.04 \leqq \sigma_{n,2n} \leqq 1.50$ ±0.02 ±0.04	$0.92 \geqq \sigma_{is} \geqq 0.00$ ±0.06
Au	2.44±0.02 (2.51±0.04)	1.22±0.02	$0.00 \leqq \sigma_c \leqq 0.61$ ±0.02	$1.22 \leqq \sigma_{n,2n} \leqq 1.83$ ±0.02 ±0.03	$1.22 \geqq \sigma_{is} \geqq 0.00$ ±0.04
Pb	2.49±0.02 (2.56±0.05)	1.76±0.04	$0.00 \leqq \sigma_c \leqq 0.36$ ±0.03	$1.76 \leqq \sigma_{n,2n} \leqq 2.12$ ±0.04 ±0.05	$0.73 \geqq \sigma_{is} \geqq 0.00$ ±0.06
Bi	2.53±0.02 (2.56±0.05)	1.86±0.02	$0.00 \leqq \sigma_c \leqq 0.33$ ±0.02	$1.86 \leqq \sigma_{n,2n} \leqq 2.19$ ±0.02 ±0.03	$0.67 \geqq \sigma_{is} \geqq 0.00$ ±0.04

[a] See reference 15.
[b] See reference 1.
[c] See reference 2.

nesses in atoms per cm² were calculated from accurate weights and dimensions and are thought to be accurate to about ±1 percent. Two shells of approximately one-quarter and one-half mean free path thickness for inelastic collisions were measured for each element except gold and silver.

RESULTS

Table II summarizes the measurement of M and T and the resulting inelastic-collision cross sections and number of neutrons per inelastic collision. Column 5 lists measured values of $(M''-T)/(1-T)$ which should be equal to $(M-T)/(1-T)$, the number of neutrons per inelastic collision, if δ as defined in Eq. (4) is zero. It may be seen that $(M''-T)/(1-T)$ for the thinner shells tends to be around two to four percent higher than for the thicker shells. Not only true capture, i.e., $\delta<0$, could cause this effect but a degradation of neutron energy by multiple scattering into the few-hundred-kilovolt energy region where the sensitivity of the long counter is reduced. The effect, if real, is so small that the thin-shell values are interpreted as good values of the number of neutrons per inelastic collision. The statistical errors in the data are negligible.

The inelastic-collision cross sections, σ_i, given in Column 7 have been calculated from the formula $T=e^{-N\sigma_i}$, where N is the number of atoms per cm² in the shell. This method ignores elastic scattering effects which tend to increase the average path length of the emerging neutrons. However, for 14-Mev neutrons the elastic scattering is concentrated in a forward cone so that the increase of path length is not very large. It is estimated that for the 60 percent transmission shells the error in the calculated value of σ_i will be less than 3 percent. This correction has not been made. For the thinner shells the error is negligible.

A second source of possible error in the σ_i values is the variation of sensitivity of the scintillation detector with energy of elastically scattered neutrons. Only in the lightest elements will there be sufficient energy loss accompanying elastic scattering to cause any possibility of error. A neutron scattered from carbon at an angle of 40° has an energy of 0.96 times the primary energy. It may be seen from Fig. 1 that for this energy the detector sensitivity has dropped to 89 percent of its value for the primary energy, while for 70° scattered neutrons the detector sensitivity is reduced to 65 percent of the pri-

mary value. A rough estimate of the contribution of elastic scattering to the measured σ_i is 0.05 barn. The $Cu^{63}(n,2n)$ threshold detector was used to measure inelastic-collision cross sections by Phillips *et al.*[15] and their values appear in parenthesis in Table III Column 2 for comparison. Curve (c) of Fig. 1 gives the normalized sensitivity of the $Cu^{63}(n,2n)$ detector from measurements of Fowler and Slye,[16] and Brolley *et al.*[17] The same assumptions concerning elastic scattering as made above lead to the conclusion that as much as 0.1 barn of elastic scattering cross section might be included in the σ_i value measured with the copper detector. The difference between the values for carbon is thus fairly well accounted for by the estimate of the difference in detector sensitivity. Measurements of angular distribution of elastic scattering now being completed by J. H. Coon of this laboratory will allow more precise evaluation of this effect on σ_i as measured. Except for iron, the inelastic-collision cross section measurements are in reasonably good agreement for the various materials. No explanation is offered here for the discrepancy between the iron values.

From Eq. (2) it may be seen that

$$\left(\frac{M-T}{1-T}-1\right)\sigma_i=k\sigma_i\equiv\sigma_{n,2n}+2\sigma_{n,3n}-\sigma_c. \quad (5)$$

Rewriting Eq. (1a) in more convenient form, one has

$$\sigma_i=k\sigma_i+2\sigma_c+\sigma_{is}-\sigma_{n,3n}. \quad (6)$$

Provided that $\sigma_{n,3n}$ be zero, which must be true for 14-Mev neutrons on almost all elements, Eqs. (5) and (6) used with the measured values of $k\sigma_i$ and σ_i serve to establish upper and lower limits on the allowed values of $\sigma_{n,2n}$, σ_c, and σ_{is}. From Eq. (5) it is seen that lower limits for σ_c and $\sigma_{n,2n}$ are $\sigma_c\geqq 0$ and $\sigma_{n,2n}\geqq k\sigma_i$ corresponding to the upper limit $\sigma_{is}\leqq\sigma_i-k\sigma_i$ for σ_{is} from Eq. (6). The lower limit for σ_{is} is obviously zero and leads to upper limits of $\sigma_c\leqq\frac{1}{2}(\sigma_i-k\sigma_i)$ and $\sigma_{n,2n}\leqq[k\sigma_i+\frac{1}{2}(\sigma_i-k\sigma_i)]$. The limits derived thusly define the range of possible values for the cross sections $\sigma_{n,2n}$, σ_c, and σ_{is}. Selection of any particular allowed value for one of them fixes the values of the other two. Various information available in the literature allows determination for some elements of values of the cross sections. For elements where such is not the case, limits of possible cross section values are derived. Table III summarizes the values of σ_i and $k\sigma_i$ from this experiment, and the resulting limits of values for $\sigma_{n,2n}$, σ_c, and σ_{is} or the specific values for each in cases where one is available from the literature.

Carbon

Since $(n,2n)$ reaction is impossible for 14-Mev incident neutrons, $k\sigma_i$ is equal to $-\sigma_c$. An average cross section from the two shells for σ_c is 0.08 ± 0.02 barn. Since the reactions $C^{12}(n,p)B^{12}$ and $C^{12}(n,d)B^{11}$ with Q values of -12.6 Mev and -13.7 Mev are not likely to occur, this cross section is assigned, at least as an upper limit, to the reaction $C(n,\alpha)Be^9$ where the Be^9 is formed in the ground state. Formation of Be^{9*} in the 2.43-Mev level which decays mainly by neutron emission[18,19] would not be included in this cross section. The difference between $\sigma_i=0.601\pm0.006$ barn and 0.08 ± 0.02 barn must represent the cross section for all reactions which do not result in the disappearance of a neutron. Two different reactions may contribute to this cross section:

(1) $C+n\rightarrow C^{13*}\rightarrow C^{12*}+n$,

(2) $C+n\rightarrow C^{13*}\rightarrow Be^{9*}+\alpha\rightarrow Be^8+n+\alpha$.

The nucleus C^{12} in (1) may be left in a number of different states. Decay to the ground state of C^{12} by gamma emission has been measured by a number of observers.[14,20–22] Values range from 0.1 to 0.3 barn for the cross section for production for the 4.4-Mev line. Green and Gibson[23] have measured the cross section for $C^{12}(n,n)C^{12*}\rightarrow 3\alpha+n$ by the photographic emulsion technique to be 0.16 barn for 14.5-Mev neutrons. If 0.20 barn be taken for the decay by gamma-ray emission and 0.16 barn for decay by alpha emission there remains 0.15 barn of cross section for other processes in which a neutron does not disappear. Within the errors this value could be as low as 0.05 barn.

Reaction (2) leads to the same end products as those reached from C^{12*} levels decaying by alpha emission. The Q for reaction (2) going to the first excited state of Be^{9*} is -8.1 Mev and hence the alpha particles emitted should have about 4 Mev of energy. These should be easily observable as should the ground-state alphas.

Since the 7.5-Mev level of C^{12} cannot decay to the ground state by gamma emission ($J=0\rightarrow J=0$) it must decay by cascade gamma emission, by internal pair formation, or by alpha emission. The energy available for alpha emission is very small, only about 0.2 Mev and such disintegration would be most difficult to observe. Internal pair formation of this level has been observed by Harris and Davis[24] along with similar decay of the 4.4-Mev level. However, as expected theoretically, the probability was extremely small. Sherrer, Theus, and Faust[14] have reported a 2.8-Mev gamma-ray line which might be a cascade line with a production cross section approximately one-third of that for the 4.4-Mev line, but this was not observed by Battat and Graves.[21] One is forced to conclude that the 7.5-Mev level is not

[15] Phillips, Davis, and Graves, Phys. Rev. **88**, 600 (1952).
[16] J. L. Fowler and J. M. Slye, Phys. Rev. **77**, 787 (1950).
[17] Brolley, Fowler, and Schlacks, Phys. Rev. **88**, 618 (1952).
[18] G. A. Dissanaike and J. O. Newton, Proc. Phys. Soc. (London) **A65**, 675 (1952).
[19] F. Ajzenberg and T. Lauritsen, Revs. Modern Phys. **24**, 321 (1952), see p. 343.
[20] M. E. Battat, Phys. Rev. **91**, 441 (1953).
[21] M. E. Battat and E. R. Graves, Phys. Rev. **97**, 1266 (1955).
[22] L. C. Thompson and J. R. Risser, Phys. Rev. **94**, 941 (1954).
[23] L. L. Green and W. M. Gibson, Proc. Phys. Soc. (London) **62**, 296 (1949).
[24] G. Harries and W. T. Davis, Proc. Phys. Soc. (London) **A65**, 564 (1952).

formed with any degree of abundance or that it decays by alpha emission of such low energy as to be unobservable. More precise determinations of the 4.4-Mev gamma-production cross section and of the $C^{12}(n,\alpha)Be^{9*}$ reaction cross section should be useful in this connection.† It is suggested then that the component parts of $\sigma_i=0.60$ barn are as follows:

$C^{12}(n,\alpha)Be^{9}$, $\sigma=0.08\pm0.02$ barn;

$C^{12}(n,n)C^{12*}$ levels 9.6 Mev to $\approx$13 Mev, $\sigma=0.16$ barn, (these levels go to 3 alphas);

$C^{12}(n,n)C^{12*}$ levels 7.5 Mev and 4.4 Mev, $\sigma\approx0.10$ to 0.30 barn;

$C^{12}(n,\alpha)Be^{9*}$, $\sigma=0.31$ barn minus σ for $C^{12}(n,n)C^{12*}$ for 7.5-Mev and 4.4-Mev levels;

$C^{12}(n,n)C^{12}$ elastic scattering included in σ_i, $\sigma_{es}\approx0.05$ barn.

Aluminum

The average value of $k\sigma_i$ from the two shells is -0.21 ± 0.01 barn. Forbes[1] has measured the cross sections for (n,p) and (n,α) reactions, the sum of which equals σ_c for aluminum. This sum is 0.214 barn and substituting in the equation $k\sigma_i=\sigma_{n,2n}-\sigma_c$ we find that $\sigma_{n,2n}=0.00$ barn which checks expectation from measurements of the (γ,n) reaction,[25,26] and with measurements in this Laboratory. Paul and Clarke[2] find a value for the sum of (n,p) and (n,α) reactions equal to 0.13 barn which, combined with the present experiment would lead to an $(n,2n)$ cross section of -0.08 ± 0.01 barn. The more consistent results are hence obtained using the values of Forbes. The difference $(\sigma_i-\sigma_c)=0.79\pm0.02$ barn hence represents inelastic scattering to be compared with 0.65 ± 0.17 barn from nuclear plate measurements.[4]

Iron

If a value of $\sigma_c\geqq0.114$ barn is taken for the normal isotopic mixture derived from Forbes' cross-section value of 0.124 barn for the $Fe^{56}(n,p)Mn^{56}$ reaction, Eq. (5) leads to $\sigma_{n,2n}\geqq0.18\pm0.02$ barn for the normal isotopic mixture. Because the Q-value for $Fe^{54}(n,2n)Fe^{53}$ is -13.8 Mev, all of this is probably due to $Fe^{56}(n,2n)Fe^{55}$ which would then have an isotopic cross section of $\geqq0.36\pm0.04$ barn.

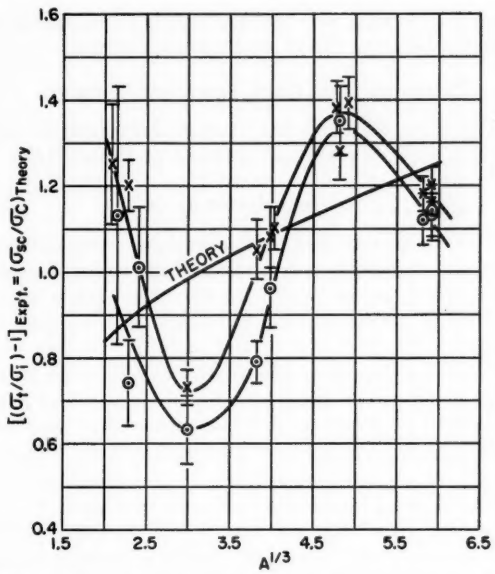

FIG. 2. Experimental values of $[(\sigma_i/\sigma_i)-1]$ are plotted as a function of the cube root of the mass. Values of σ_i are taken from reference 29. × points are from σ_i reported here (with the exception of beryllium for which a preliminary unreported value is included), whereas circles are from σ_i values from reference 15. The solid line marked "THEORY" shows the prediction of Weisskopf and his associates (see references 27 and 28) for σ_{sc}/σ_C which is identified with the experimental quantity plotted.

Copper

From Forbes,[1] $\sigma_{n,2n}$ for the normal mixture is 0.65 ± 0.05 barn. Solving Eq. (5) one finds $\sigma_c=0.41\pm0.06$ barn. The contribution[1] to σ_c of $Cu^{65}(n,p)Ni^{65}$ is 0.006 barn, leaving 0.40 ± 0.06 barn for the normal isotopic mixture to be accounted for by some other reaction which destroys a neutron. The reaction $Cu(n,np)Ni$ does not result in the destruction of a neutron and hence, in this kind of measurement, is not included in σ_c but is included in σ_{is}. Substituting in Eq. (1a) one derives for the normal isotopic mixture $\sigma_{is}=0.36\pm0.09$ barn.

Zinc

From Paul and Clarke's[2] measurements of $Zn^{64}(n,p)Cu^{64}$ and $Zn^{66}(n,p)Cu^{66}$ reaction cross sections, a value for σ_c is calculated of $\geqq0.22\pm0.04$ barn for the normal isotopic mixture. The value for $\sigma_{n,2n}$ derived from Eq. (5) is then $\sigma_{n,2n}\geqq0.33\pm0.06$ barn and for σ_{is} is $\leqq0.91\pm0.09$ barn. Paul and Clarke also measured $\sigma_{n,2n}$ for Zn^{64}. Their value would give a contribution of 0.11 ± 0.02 barn to the normal isotopic mixture value leaving 0.22 ± 0.07 barn to be accounted for by the other isotopes. This would imply that the isotopic cross section for $Zn^{66}(n,2n)Zn^{65}$ must be from 0.4 to 0.5 barn.

Silver

Combining $k\sigma_i=0.72\pm0.03$ barn with $\sigma_{n,2n}=0.774\pm0.08$ barn for the normal isotopic mixture as derived

† *Note added in proof.*—Recently completed work by Frye, Rosen, and Stewart of this Laboratory [G. M. Frye, Jr., L. Rosen, and L. Stewart (to be published)] utilizes the nuclear emulsion technique to investigate three-alpha-decay processes following neutron bombardment of carbon. For 14-Mev primary neutron energy, only a small fraction of the observed events could be attributed to decay through Be^{9*}. The observed events are examined carefully according to momentum considerations and various modes of disintegration are assigned. A correction for "missed" events is applied leading to a cross section of 230 ± 50 mb for three-alpha decay through C^{12*} excited to 9.6 Mev and higher.

[25] McElhinney, Hanson, Becker, Duffield, and Diven, Phys. Rev. **75**, 542 (1949).

[26] L. Katz and A. G. W. Cameron, Phys. Rev. **83**, 892 (1951).

from Forbes leads to $\sigma_c = 0.06 \pm 0.09$ barn. σ_{is} becomes 1.0 ± 0.2 barns for the normal isotopic mixture.

Cadmium, Tin, Gold, Lead, and Bismuth

For these materials only permissible limits of the cross section are presented as shown in Table III.

Behavior of σ_i

The inelastic-collision cross sections reported here increase somewhat the precision with which a comparison may be made with the theory of nuclear interactions of Weisskopf and his associates.[27,28] Figure 2 portrays the behavior of the quantity $[(\sigma_t/\sigma_i)-1]$ where the values of σ_t, the total cross section for 14.1-Mev neutrons are taken from Coon, Graves, and Barschall.[29] The × points refer to values of σ_i reported here and the circles to values obtained by Phillips *et al.*[15] Although the measurements on beryllium are not reported here, a preliminary value is included in the curve. A curve through the × points and another through the circles are drawn to indicate a band which portrays the general behavior of the experimental quantity. The inelastic collision cross section σ_i experimentally determined is identified with σ_C for compound nucleus formation from the theory where

$$\sigma_t = \sigma_C + \sigma_{sc}.$$

Hence $[(\sigma_t/\sigma_i)-1]$ is equivalent to (σ_{sc}/σ_C) from the theory. The curve marked "THEORY" shows (σ_{sc}/σ_C) upon the assumption that the nuclear radius $= 1.5 \times 10^{-13} A^{\frac{1}{3}}$ cm. Although this theory is undergoing revision, it is felt that the comparison as shown is a useful one since it deals with a fairly fundamental concept. It also shows clearly the regions of atomic mass which need further investigation to better establish the empirical curve.‡

[27] H. Feshbach and V. F. Weisskopf, Phys. Rev. **76**, 1550 (1949).
[28] J. M. Blatt and V. F. Weisskopf, *Theoretical Nuclear Physics* (John Wiley and Sons, Inc., New York, 1952), Chap. VIII, Sec. 4.
[29] Coon, Graves, and Barschall, Phys. Rev. **88**, 562 (1952).

‡ *Note added in proof.*—Further investigation of the region between carbon and iron has been made. Preliminary values of the inelastic collision cross section, σ_i, have been obtained for F, S, KCl, Ca, Sc, Ti, and V. These show a discontinuity in the curve of σ_i *vs* $A^{1/3}$ between Ca and Sc, preceded by a smooth rise of σ_i to 1.5 ± 0.1 barn for Ca. Beginning with Sc the values fall on a new smooth curve which extrapolated to lower masses would join the lower branch between F and Al. The preliminary value of σ_i for Ti is 1.23 ± 0.04 barns and for V is 1.32 ± 0.08 barns. These results in conjunction with total cross sections (see reference 29) give additional experimental points for $[(\sigma_t/\sigma_i)-1]$ as a function of $A^{1/3}$ as shown in Fig. 2. From $A^{1/3}=3.00$ the points continue to drop through 0.58 ± 0.07 for $A^{1/3}=3.3 \pm 0.1$ (KCl) to 0.43 ± 0.10 for $A^{1/3}=3.42$ (Ca). For the next higher $A^{1/3}$ values, Sc and Ti, the values are on a rising curve. For $A^{1/3}=3.63$ (Ti) the preliminary value is 0.85 ± 0.10. Further measurements are in progress.

PHYSICAL REVIEW VOLUME 97, NUMBER 5 MARCH 1, 1955

Alignment of Cerium-141 and Neodymium-147 Nuclei*†

E. Ambler and R. P. Hudson, *National Bureau of Standards, Washington, D. C.*

and

G. M. Temmer, *Department of Terrestrial Magnetism, Carnegie Institution of Washington, Washington, D. C.*

(Received November 1, 1954)

The radioactive nuclei Ce^{141} and Nd^{147} have been aligned by the magnetic hfs method (Bleaney) using single crystals of cerium magnesium nitrate. The cerium site is characterized by $B \gg A$, i.e., the "alignment" occurs in a plane. The anisotropies for the 142-kev gamma ray of Ce^{141}, and the 92-kev and 530-kev gamma rays of Nd^{147}, at the lowest temperature (0.00308°K) were found to be +0.12, 0, and −0.39, respectively. These values coupled with the rate of change of anisotropy with temperature identify the transitions as $M1$, $M1+E2$, and $E2$, respectively. The decay schemes supported by these experiments are as follows: Ce^{141} (142 kev), $7/2^- \xrightarrow{0} 7/2^+ \xrightarrow{1} 5/2^+$; Nd^{147} (92 kev), $9/2^- \xrightarrow{1} 7/2^+ \xrightarrow{1,2} 5/2^+$; Nd^{147} (530 kev), $9/2^- \xrightarrow{0} 9/2^+ \xrightarrow{2} 5/2^+$. From the temperature dependence of the anisotropies we can deduce values for the magnetic moments as follows: Ce^{141}, 0.16 ± 0.06 nm; Nd^{147}, 0.22 ± 0.05 nm. These rather small values for odd-neutron nuclei may not be meaningful because of possible internal magnetic field effects in the crystal which are not taken into account in the treatment of the hyperfine interaction.

1. INTRODUCTION

TO date, two of the methods which have been proposed for producing oriented nuclear systems at low temperatures have been carried out successfully. Both methods rely on the fact that at the nucleus of certain paramagnetic ions there exists a very large magnetic field (10^5-10^6 oersteds, produced by the unpaired electrons in the unfilled shell) which couples together the electron and nuclear magnetic moments, and produces a considerable hyperfine splitting.

In one method, suggested independently by Gorter[1]

* Supported in part by the Office of Naval Research, under contract with the National Bureau of Standards.

† A preliminary account of the work on cerium-141 was given at the Spring Meeting of the American Physical Society, April 29–May 1, 1954 [Ambler, Hudson, and Temmer, Phys. Rev. **95**, 625 (1954)].

[1] C. J. Gorter, Physica **14**, 504 (1948).

and by Rose,[2] the proposal was to apply a fairly small magnetic field (100–1000 oersteds) to a suitable paramagnetic salt at a very low temperature, so that the electron moments would be polarized almost to saturation. The temperature, T, should be sufficiently low ($\sim$0.01°K) so that kT is of the order of the hyperfine splitting; under these circumstances only the lowest of the hyperfine levels would be populated, corresponding to a nuclear polarization along the direction of the magnetic field. This principle has been applied to polarize assemblies of the nuclei Co^{60},[3] Mn^{55},[4] and Sm^{149}.[5]

The other method, which was proposed by Bleaney,[6,7] produces an *alignment* of the nuclei rather than a *polarization* and there is preferential orientation, both parallel and antiparallel to a certain direction in space; in other words, states with positive and negative values of the magnetic quantum number have the same energy. This, however, is of no consequence if the aim is to orient radioactive nuclei and to observe the polar diagram of the emission of gamma rays, since the pattern of the radiation is symmetrical with respect to a plane perpendicular to the axis of quantization of the nucleus.[8] No external magnetic field is necessary in this method. It relies entirely on the fact that in certain paramagnetic salts, the crystalline electric field produces anisotropic hyperfine splitting, so that the energy of interaction between nuclear and electron magnetic moments depends not only upon their relative orientation, but also upon their orientation with respect to some preferred axis within the crystal. In other words, the magnitude of the magnetic field at the nucleus depends upon the direction of the electron moment relative to this axis.

The problem of nuclear orientation has been discussed by Bleaney in terms of the spin-Hamiltonian. In many paramagnetic crystals the hyperfine structure is symmetrical with respect to a particular axis, and if the axis is taken to be the z-axis, the magnetic interaction can be written

$$\mathcal{H}=AS_zI_z+B(S_xI_x+S_yI_y),$$

where S_x, S_y, and S_z are the components of the electron spin operator, and I_x, I_y, and I_z the components of the nuclear spin operator. A and B are constants which can be determined from paramagnetic resonance experiments. When the lowest electronic level is a doublet, S is set equal to $1/2$ and the two extreme cases (i) $A\gg B$, and (ii) $B\gg A$, are favorable for producing alignment.

(i) When $A\gg B$, the levels consist of a set of $(2I+1)$ doublets spaced by an energy interval $A/2$; the lowest level is characterized by $I_z=\pm I$, the next by $I_z=\pm(I-1)$ and so on, as shown in Fig. 1(a) for the particular case $I=7/2$. At a sufficiently low temperature, therefore, the nuclear spins will become aligned along the direction of the z-axis. This method has been used for aligning various radioactive cobalt nuclei.[9–17]

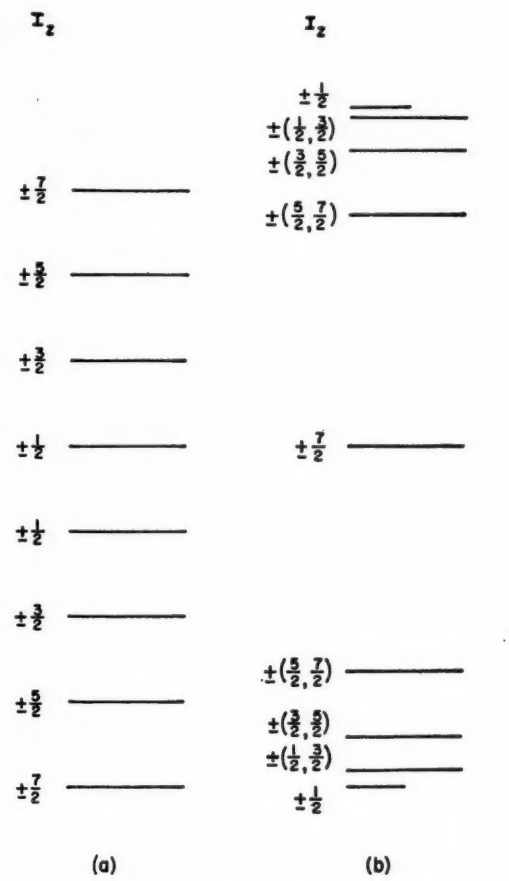

FIG. 1. Hyperfine energy levels for the case of nuclear spin $I=7/2$. (a) $A\gg B$, favorable for axial alignment; (b) $B\gg A$, favorable for "alignment" in a plane. A and B are hyperfine splitting constants in the spin-Hamiltonian.

[2] M. E. Rose, Phys. Rev. **75**, 213 (1949).
[3] Ambler, Grace, Halban, Kurti, Durand, Johnson, and Lemmer, Phil. Mag. **44**, 216 (1953).
[4] Bernstein, Roberts, Stanford, Dabbs, and Stevenson, Phys. Rev. **94**, 1243 (1954).
[5] Roberts, Bernstein, Dabbs, and Stanford, Phys. Rev. **95**, 105 (1954).
[6] B. Bleaney, Proc. Phys. Soc. (London) **A64**, 315 (1951).
[7] B. Bleaney, Phil. Mag. **42**, 441 (1951).
[8] J. A. Spiers, Nature **161**, 807 (1948).
[9] Daniels, Grace, and Robinson, Nature **168**, 780 (1951).
[10] Gorter, Poppema, Steenland, and Beun, Physica **17**, 1050 (1951).
[11] Bleaney, Daniels, Grace, Halban, Kurti, and Robinson, Phys. Rev. **85**, 688 (1952).
[12] Bleaney, Daniels, Grace, Halban, Kurti, Robinson, and Simon, Proc. Roy. Soc. **A221**, 170 (1954).
[13] Poppema, Beun, Steenland, and Gorter, Physica **18**, 1235 (1952).
[14] Gorter, Tolhoek, Poppema, Steenland, and Beun, Physica **18**, 135 (1952).
[15] Bishop, Daniels, Goldschmidt, Halban, Kurti, and Robinson, Phys. Rev. **88**, 1432 (1952).
[16] Daniels, Grace, Halban, Kurti, and Robinson, Phil. Mag. **43**, 1297 (1952).
[17] M. A. Grace and H. Halban, Physica **18**, 1227 (1952).

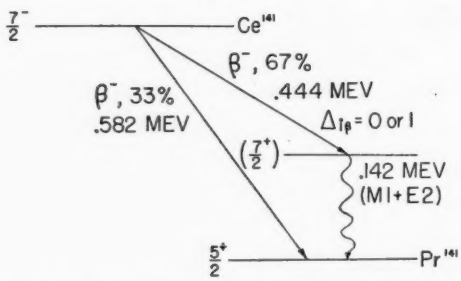

FIG. 2. Decay scheme of Ce^{141}, according to Kondaiah (see reference 18).

(ii) When $B \gg A$, the energy levels are as shown in Fig. 1(b), again drawn for $I=7/2$; in this case it is necessary to go to a much lower temperature to produce a high degree of alignment, partly on account of the crowding together of the lower energy levels, and partly because the lowest level has only half the degeneracy of the others. The lowest and highest levels are characterized by $I_z=\pm 1/2$, and the others, apart from the $I_z=\pm 7/2$ level, contain equal amounts of two adjacent nuclear magnetic substates, as shown in Fig. 1(b). At a low enough temperature the nuclei will precess about the z-axis in the $I_z=\pm 1/2$ state and we have, effectively, "alignment" in a plane perpendicular to the z-axis. It is this type of alignment which occurred in the experiments on Ce^{141} and Nd^{147} to be described.

2. NUCLEAR PROPERTIES

(a) Ce^{141}

The decay scheme of 30-day Ce^{141} as given, for example, by Kondaiah,[18] is shown in Fig. 2. The beta ray to the excited state of Pr^{141} has an upper energy limit of 0.444 Mev, the one to the ground state of Pr^{141} has an upper energy limit of 0.582 Mev. The gamma ray connecting these two states, which is the one observed in the experiments, has an energy of 142 kev and occurs in 67 percent of the disintegrations. The experimental values of the internal conversion coefficient and K to L conversion ratio[19] are given in Table I, together with the predicted values[20,21] for electric dipole ($E1$), electric quadrupole ($E2$), and magnetic dipole ($M1$) radiation. Internal conversion data do not permit distinction between $M1$ and $E2$ radiation, although they certainly eliminate $E1$; the K to L ratio favors $M1$ over $E2$ though not as decisively as Table I would indicate, since the experimental value is uncertain by about 20 percent. As we shall explain later, it is just this sort of problem that can often be settled rather easily by the method of nuclear alignment. The ground-state spin of Pr^{141} is known to be 5/2 and is classified as a $d_{5/2}$ state by the shell model, i.e., its parity is even. The logft value of the ground-state beta transition is 7.75 and that for the excited-state transition is 7.00.[18] According to Nordheim,[22] both of these transitions can be classified as first-forbidden with a parity change, and spin change $\Delta i_\beta=0$ or 1 (angular momentum carried away by the electron-neutrino field). Hence Ce^{141} should have odd parity and spin 3/2, 5/2, or 7/2. According to the spin-orbit coupling scheme, the 83rd neutron outside the closed 82-neutron shell should be in an $h_{9/2}$ orbit, but an $f_{7/2}$ configuration occurs in the same shell and is not unlikely.

We shall therefore assume a spin of 7/2 for Ce^{141}.

TABLE I. Comparison of experimental and theoretical internal conversion coefficients for the 142-kev gamma ray of Ce^{141} (see references 19, 20, and 21).

K-shell internal conversion coefficients				K/L ratio			
	Theoretical				Theoretical		
Experimental	$E1$	$E2$	$M1$	Experimental	$E1$	$E2$	$M1$
0.48	0.08	0.42	0.43	6.5	9.5	4.6	6.3

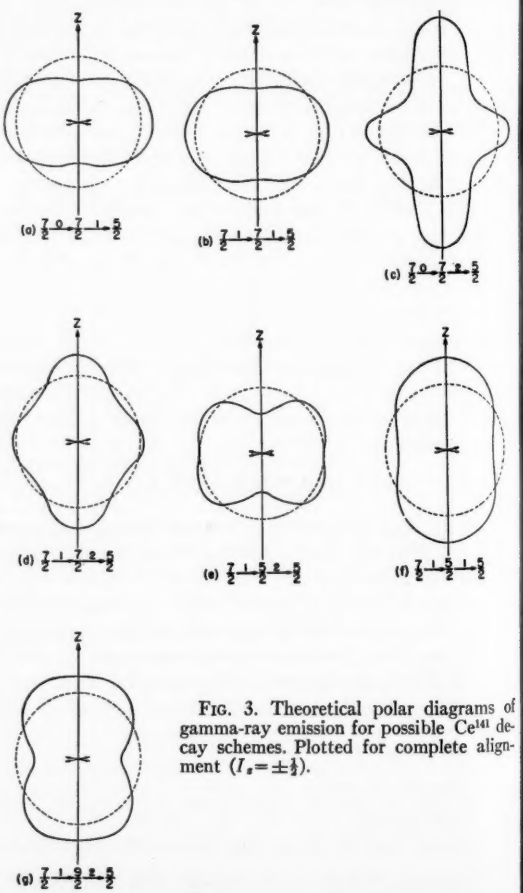

FIG. 3. Theoretical polar diagrams of gamma-ray emission for possible Ce^{141} decay schemes. Plotted for complete alignment ($I_z=\pm\frac{1}{2}$).

[18] E. Kondaiah, Arkiv Fysik 4, 81 (1951).
[19] S. Johansson, Arkiv Fysik 3, 533 (1952).
[20] Rose, Goertzel, Harr, Spinrad, and Strong, Phys. Rev. 76, 184 (1949).
[21] M. Goldhaber and A. W. Sunyar, Phys. Rev. 83, 906 (1951).
[22] L. W. Nordheim, Revs. Modern Phys. 23, 322 (1951).

The 142-kev level of Pr^{141} has even parity because of the $M1$ or $E2$ character of the gamma radiation. The first-forbidden beta decay allows its spin to be $5/2^+$, $7/2^+$, or $9/2^+$, unless the gamma radiation is at least partly $M1$ in which case $9/2^+$ is ruled out.

From what has been said above, the following decay schemes are possible:

$$7/2 \xrightarrow{1} 5/2 \xrightarrow{1,2} 5/2; \quad 7/2 \xrightarrow{0,1} 7/2 \xrightarrow{1,2} 5/2;$$
$$7/2 \xrightarrow{1} 9/2 \xrightarrow{2} 5/2.$$

In Fig. 3, we have plotted the corresponding polar diagrams to be expected for complete alignment in a plane (i.e., at $T=0$), using formulas given by Steenberg.[23] As an example we quote the expression for the angular distribution of gamma radiation for the decay scheme $7/2 \xrightarrow{0} 7/2 \xrightarrow{1} 5/2$ at $T=0$:

$$I(\theta)=1-(5/14)P_2(\cos\theta).$$

We thought it worth while, therefore, to carry out an experiment on the alignment of Ce^{141}, with the primary objective of establishing the type of gamma transition involved.

(b) Nd^{147}

The decay scheme of 11-day Nd^{147} has been studied by a number of authors.[18,24,25] The gamma spectrum is believed to be rather complex[25] but there are only two gamma rays intense enough to be of interest in an alignment experiment, having energies 92 kev and 530 kev. Our scintillation spectrum of the gamma radiation emitted from our sample of Nd^{147} [26] is shown in Fig. 4. The 92-kev gamma ray is most intense and is known to be in coincidence with the most energetic beta-ray branch[24]; it undoubtedly represents a ground-state transition. A comparison of its K/L conversion ratio (~ 7)[18,27,28] with empirical curves of this ratio[21] indicates either an $M1$ transition, or an $M1+E2$ transition, the $M1$ component being predominant. The 530-kev gamma ray is known to be in coincidence with the 384-kev beta component; its K/L conversion ratio (5.7) points to an $E2$ transition.[25]

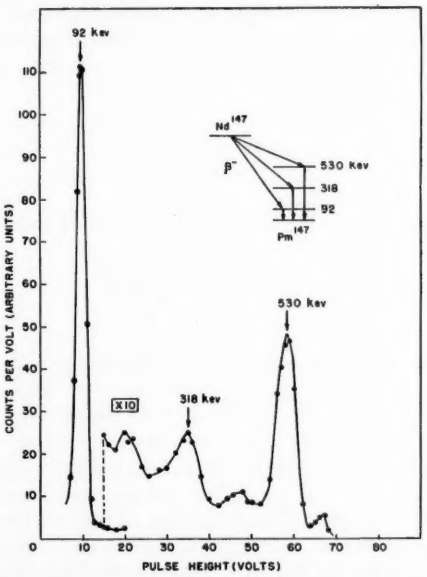

FIG. 4. Gamma-ray spectrum of Nd^{147} obtained with $1\frac{3}{4}$ in. X2 in. NaI(Tl) scintillation crystal. Insert shows main portion of decay scheme.

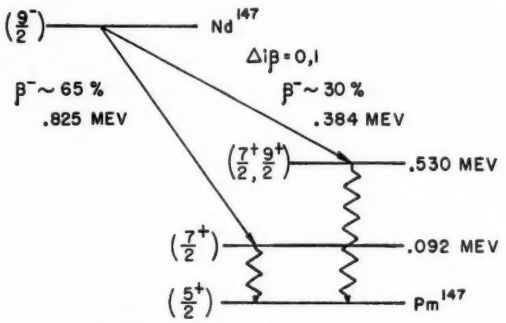

FIG. 5. Portion of decay scheme of Nd^{147} of interest in this experiment.

Figure 5 summarizes the portion of the decay scheme which is of interest here. The ground state of Pm^{147} probably has spin $5/2^+$ ($d_{5/2}$ configuration); this is in keeping with the character of the first-forbidden beta transition ($\Delta i_\beta=1$) from this state to the ground state of Sm^{147} whose spin has been measured to be $7/2$.[29] The beta transitions to both the 92-kev and 530-kev levels in Pm^{147} have $\log ft$ values indicating first-forbidden character with spin change 0 or 1 and a change in parity. Since these two levels are connected to the ground state by $M1$ or $E2$ transitions, their parities must be even, and Nd^{147} must have odd parity. Nd^{147} with 60 protons and 87 neutrons, is expected to have a $h_{9/2}$ configuration. This is corroborated by the fact that no direct beta ray to the ground state is observed, indicating a higher order of forbiddenness. Assuming this, we would predict:

(i) spin $7/2$ for the 92-kev state in order to allow both a first-forbidden beta transition and $M1$ gamma transition,

(ii) spin $7/2$ or $9/2$ for the 530-kev state in order to allow both a first-forbidden beta transition and either an $M1$ or $E2$ gamma transition. The possible decay schemes would then be: $9/2 \xrightarrow{0,1} 9/2 \xrightarrow{2} 5/2$; $9/2 \xrightarrow{1} 7/2 \xrightarrow{2} 5/2$; $9/2 \xrightarrow{1} 7/2 \xrightarrow{1} 5/2$. The

[23] N. R. Steenberg, Proc. Phys. Soc. (London) **A65**, 791 (1952).
[24] W. S. Emmerich and J. D. Kurbatov, Phys. Rev. **83**, 40 (1951).
[25] Rutledge, Cork, and Burson, Phys. Rev. **86**, 775 (1952).
[26] Both Ce^{141} and Nd^{147} were obtained from the Oak Ridge National Laboratory, Oak Ridge, Tennessee.
[27] J. W. Mihelich and E. L. Church, Phys. Rev. **85**, 690 (1952).
[28] A. B. Smith and A. C. G. Mitchell, Phys. Rev. **87**, 1128 (1952).
[29] K. Murakawa, Phys. Rev. **93**, 1232 (1954).

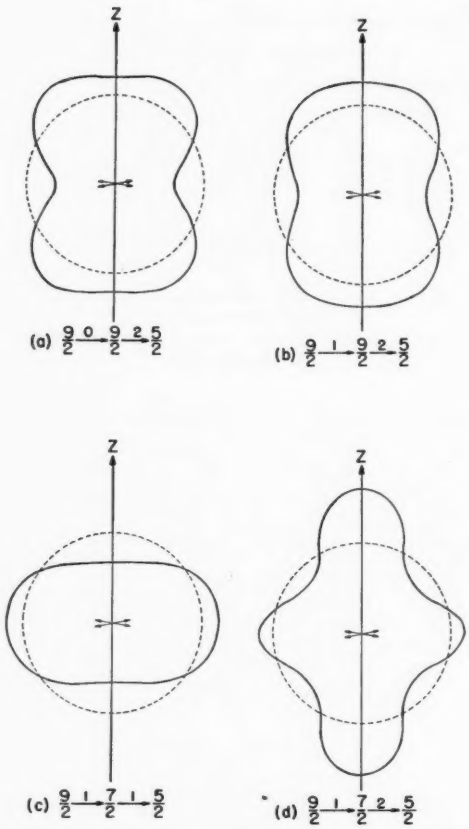

FIG. 6. Theoretical polar diagrams of gamma-ray emission for possible Nd^{147} (530 kev) decay schemes. Plotted for complete alignment ($I_z=\pm\frac{1}{2}$).

theoretical polar diagrams of emission of the gamma rays in these cases are shown in Fig. 6, for alignment in a plane at $T=0$. The angular distribution for the most likely case $9/2 \xrightarrow{0} 9/2 \xrightarrow{2} 5/2$ is given by:

$$I(\theta)=1+(10/21)P_2(\cos\theta)-(2/7)P_4(\cos\theta).$$

3. SOLID STATE PROPERTIES

(a) Cerium

In searching for a paramagnetic salt suitable for a nuclear alignment experiment it is usual to examine hyperfine splitting as determined by paramagnetic resonance experiments. Unfortunately, the naturally occurring isotopes of cerium are all even-even nuclei, hence have zero spin, and the paramagnetic resonance spectrum of the element shows no hyperfine structure. We are therefore entirely dependent upon theoretical predictions for the values of A and B. The theory of the Ce^{+++} ion has been given by Elliott and Stevens[30] with special reference to the salt cerium ethyl sulfate. This salt is not particularly useful for adiabatic demagnetization work, but cerium magnesium nitrate, to which one thought the theory would also apply, is in many respects an ideal substance. Daniels and Robinson[31] investigated the thermal and magnetic properties below 1°K and showed that it is possible, by demagnetizing from 1°K and 14 kilo-oersteds, to reach a temperature of 0.00308°K. Here the salt has an appreciable specific heat so that it is possible to maintain this temperature for a usefully long period of time. Alignment would then depend upon the hyperfine splitting being of the order of 0.003°K, and markedly anisotropic.

The results of paramagnetic resonance experiments[32] show that in the liquid-helium range of temperature the magnetic properties of the Ce^{+++} ion in cerium magnesium nitrate can be described by an effective spin $S=1/2$, with an anisotropic g-factor: $g_{\parallel}=0.25$ (along the z-axis) and $g_{\perp}=1.84$. It is possible to combine these results with theory to obtain the matrix elements needed in computing the values of A and B through the formulas[33]:

$$A=\frac{4\beta\beta_n\mu_n}{I}\left\langle\frac{1}{r^3}\right\rangle_{Av}\langle+\tfrac{1}{2}|N_z|+\tfrac{1}{2}\rangle, \quad (1)$$

$$B=\frac{4\beta\beta_n\mu_n}{I}\left\langle\frac{1}{r^3}\right\rangle_{Av}\langle+\tfrac{1}{2}|N_z|-\tfrac{1}{2}\rangle, \quad (2)$$

where β is the Bohr magneton, β_n the nuclear magneton, μ_n the nuclear magnetic moment in nuclear magnetons, r the radial distance of the $4f$ electron from the nucleus, and $\mathbf{N}$ a vector,

$$\mathbf{N}=\left\{\mathbf{l}-\mathbf{s}+\frac{3(\mathbf{r}\cdot\mathbf{s})\mathbf{r}}{r^2}\right\},$$

which appears in the hyperfine interaction Hamiltonian,

$$\mathcal{H}_n=\frac{2\beta\beta_n\mu_n}{I}\left\langle\frac{1}{r^3}\right\rangle_{Av}\mathbf{N}\cdot\mathbf{I}.$$

We can see that the ratio of A to B is determined solely by the ratio of two matrix elements.

More recent calculations of Judd and Pryce[34] have shown that better agreement between theory and experiment is obtained if one assumes a slightly different symmetry for the crystalline electric field from that assumed by Elliott and Stevens. Their preliminary numerical values for the matrix elements in Eqs. (1) and (2) are 0.10 and 1.62, respectively. Thus if radioactive cerium nuclei possessing a magnetic moment are

[30] R. J. Elliott and K. W. H. Stevens, Proc. Roy. Soc. (London) **A215**, 437 (1952).

[31] J. M. Daniels and F. N. H. Robinson, Phil. Mag. **44**, 630 (1953).

[32] Cooke, Duffus, and Wolf, Phil. Mag. **44**, 623 (1953).

[33] R. J. Elliott and K. W. H. Stevens, Proc. Roy. Soc. (London) **A218**, 553 (1953).

[34] B. R. Judd (private communication).

included in the double nitrate salt they will approximate closely to the case of $B \gg A$, and at a sufficiently low temperature there will result alignment in a plane.

(b) Neodymium

Hyperfine splittings have been observed in paramagnetic resonance spectra of the Nd^{+++} ion in neodymium magnesium nitrate[35] for the stable isotopes of mass numbers 143 and 145. The experiments show that at liquid helium temperatures the magnetic behavior can be described by a spin-Hamiltonian with $S=1/2$, $g_{\parallel}=0.45$, and $g_{\perp}=2.73$. The hyperfine splitting constants are:

$$A_{143}=0.005 \text{ cm}^{-1}, \quad B_{143}=0.0312 \text{ cm}^{-1};$$
$$A_{145}=0.003_3 \text{ cm}^{-1}, \quad B_{145}=0.0194 \text{ cm}^{-1}.$$

Once again, therefore, we have the case of $B \gg A$, with alignment in a plane at sufficiently low temperatures. The ratio of the constants A and B for the radioactive isotope 147 to the corresponding constants for the stable isotopes will, of course, just equal the ratio of the respective nuclear gyromagnetic ratios.

4. EXPERIMENTAL METHOD

Cerium magnesium nitrate crystallizes in flat hexagonal plates with a width-to-thickness ratio of about 8:1; the axis perpendicular to the plate is the axis of low susceptibility, i.e., the z-axis. For each of the experiments, three such crystals were grown weighing altogether about 5 g and containing, at the beginning of the experiments, about 60 microcuries of activity. In the second series of experiments the neodymium replaced a very small fraction of cerium in the crystals. The latter, X, were mounted with the direction of their z-axes coincident and horizontal, inside a glass demagnetization cryostat as shown in Fig. 7. The support is a glass tube, T, 1.5 mm diameter and 0.2 mm wall thickness, which is attached to the ground-glass plug P. A vacuum-tight seal is made at the ground joint by means of a mixture described elsewhere.[36] The general arrangement of the pickup coils and ac bridge for measuring the susceptibility have also been described.[37] The whole cryostat was immersed in a Dewar of liquid helium jacketed by liquid nitrogen.

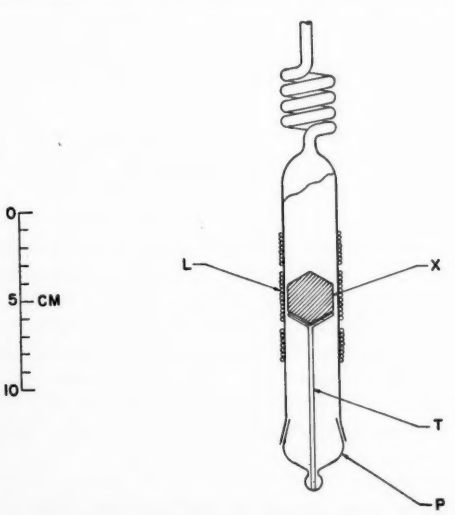

FIG. 7. Schematic diagram of demagnetization cryostat. X, radioactive crystal specimen; T, thin glass support; P, ground glass plug; L, mutual inductance secondary coil for susceptibility measurements.

[35] A. H. Cooke and H. J. Duffus, Proc. Roy. Soc. (London) (to be published).

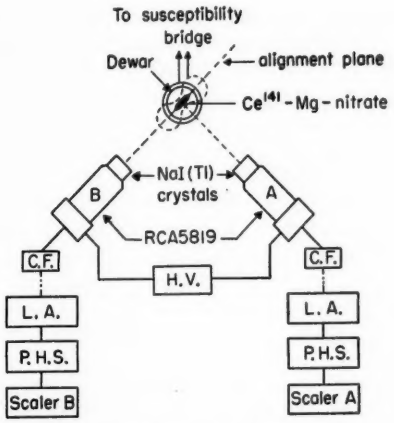

FIG. 8. Block diagram of counter array (plan view). A and B are scintillation counters; C.F., cathode followers; L.A., linear amplifiers; P.H.S., single-channel pulse-height selectors.

The salt was magnetized in a field of about 22 kilooersteds at 1.1°K along a direction of large magnetic susceptibility, i.e., along a direction in the plane of the crystals. This corresponded to an entropy given by $S/R=0.22$, and, as can be deduced from the table of results given in reference 31, this is well within the region of the large specific heat of the salt. After adiabatic demagnetization the apparatus was swung from the magnet into the counter array shown schematically in Fig. 8.

Two scintillation counter systems A and B were used, each consisting of a 1 in.×1 in. cylindrical sodium iodide crystal mounted on a RCA 5819 photomultiplier tube, followed by a conventional sequence of cathode follower, linear amplifier, single-channel pulse-height selector, and a scaling unit. A window of 2 volts was used which was sufficient to discriminate against a small amount of impurity radiation present, as well as wide-angle scattered (and hence energy-degraded) radiation. The latter point was checked by verifying the inverse-square dependence of counting rate upon distance. Counts were collected in both channels A and B over ten-second or twenty-second intervals starting about 30 seconds after de-

[36] R. P. Hudson and C. K. McLane, Rev. Sci. Instr. **25**, 190 (1954).

[37] D. de Klerk and R. P. Hudson, J. Research Natl. Bur. Standards **53**, 173 (1954).

magnetization, there being about ten seconds recording time between these intervals. Some 10 000 counts were recorded in each counter during each 10-second period for the 142-kev gamma ray in the Ce^{141} experiment. The counters were at a distance of 35 cm from the sample. Some 1000 and 5000 counts were recorded during each 20-second period for the 530-kev and 92-kev gamma rays, respectively, in the neodymium experiment. Because of lower gamma-ray intensities the counters were moved in to a distance 15 cm from the sample. Finite solid angle corrections to the anisotropy never exceeded 3 percent of the observed value (small compared to the statistical errors) and were not applied.

During each run the magnetic susceptibility of the specimen was monitored in order to determine its temperature. When too high an ac measuring field was used, we found that significant heating was produced in the specimen which rapidly warmed it to the helium bath temperature. Upon reducing this field to 0.1 oersted, the ac heating became negligible compared to that due to other sources, estimated to be about 100 erg/min. About half of this is accounted for by the heating due to radioactivity. The warmup time, during which there was a detectable anisotropy, was about eight minutes from the time of demagnetization.

5. RESULTS

(a) Ce^{141}

The results of a typical run are shown in Fig. 9, where we have plotted, as functions of time, the individual counting rates of counters A and B, with B situated along the z-axis of the crystal and A perpendicular to it; $1/T$, the reciprocal of the absolute temperature; and the anisotropy $\epsilon=[I(\frac{1}{2}\pi)-I(0)]/I(\frac{1}{2}\pi)$, where $I(\theta)$ is the intensity measured in a direction making an angle θ with the z-axis of the crystal. It will be seen that, as the temperature increases, counting rate A decreases while B increases, and that ϵ is positive. The scatter of the points of the individual counting rates is mainly due to inaccuracies in timing the ten-second counting interval, a factor which does not affect the value of ϵ; the limits shown for the values of ϵ are due to counting statistics only.

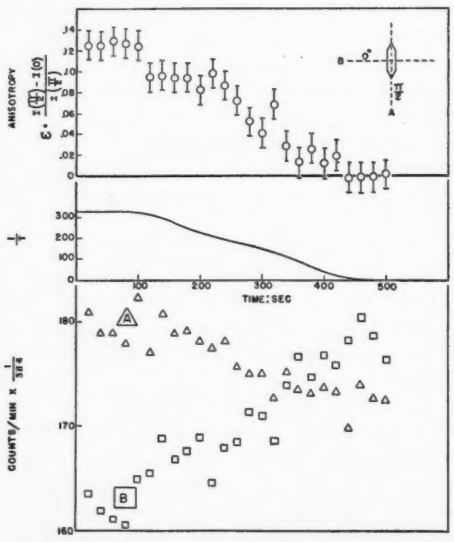

FIG. 9. Results of a single demagnetization in Ce^{141} experiment. Plotted against time are anisotropy (top), reciprocal of absolute temperature (center), and individual counting rates (unnormalized) of counters A(△) and B(⊡). Each point represents a ten-second counting interval. Insert shows counter positions with respect to crystal axes.

The average value of ϵ for a number of runs is plotted against $1/T$ in Fig. 10. Counters A and B were interchanged for about half of the runs and no difference could be noted in the results. The point at the lowest temperature ($T=0.00308$°K, $\epsilon=0.12$) has a much smaller standard deviation than the others. This is because the salt remained at the lowest temperature for about 100 seconds during each of ten demagnetizations, allowing a greater number of counting periods than at any other temperature. Another reason why this point is most reliable is that the value of the absolute temperature is more accurately known. Since with cerium magnesium nitrate the absolute temperature remains substantially constant at 0.00308°K[31] over the wide entropy range $S/R=0.100$ to 0.425, the absolute temperature of our specimen immediately after demagnetization ($S/R\simeq 0.22$) is well known. However, when the temperature of the specimen rises above 0.00308°K due to unavoidable heat leaks, it must be determined from susceptibility measurements through the familiar $T^* \rightarrow T^{\otimes} \rightarrow T$ correlations.[31,38] Because of the very small thermal conductivity of paramagnetic

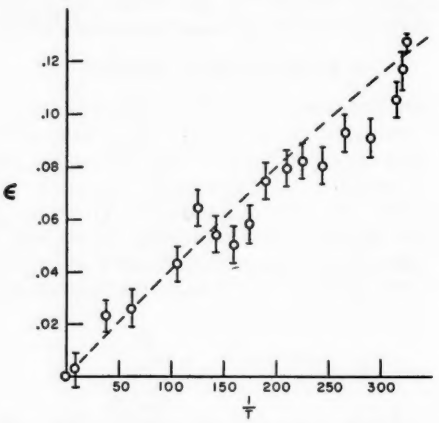

FIG. 10. Anisotropy (ϵ) *vs* reciprocal of absolute temperature ($1/T$) for Ce^{141} experiment. Points represent averages of ten demagnetizations. Note smaller statistical error at lowest temperature (see text).

[38] N. Kurti and F. E. Simon, Phil. Mag. **26**, 849 (1938).

alts at very low temperatures, extraneous heat leaks ause inhomogeneous heating of the specimen and any easured susceptibility represents an average value. onsequently the value of T^* obtained is an average alue. In addition to this, it should be remembered hat the conversion of T^* to $T^{\otimes}$ is strictly permissible nly in the case of an ellipsoidal specimen.[38]

The general symmetry of the polar diagram of emission was verified by placing both counters in the alignment plane and perpendicular to each other (no anisotropy was observed) and also by placing both counters at 45° to the z-axis (again no anisotropy was detected).

(b) Nd^{147}

The results of a typical run are shown in Fig. 11 where we have plotted for the 530-kev gamma ray similar quantities to those shown in Fig. 8 for the gamma ray from Ce^{141}. It will be seen that in this case, as the temperature increases, counting rate A increases while B decreases (B again being on the z-axis) and that the relative changes in the counting rates are very nearly equal. The average value of the anisotropy ϵ for a number of runs is plotted against $1/T$ in Fig. 12; at the lowest temperature, $T=0.00308°K$, $\epsilon=-0.39$. Measurements were also made with counter A at

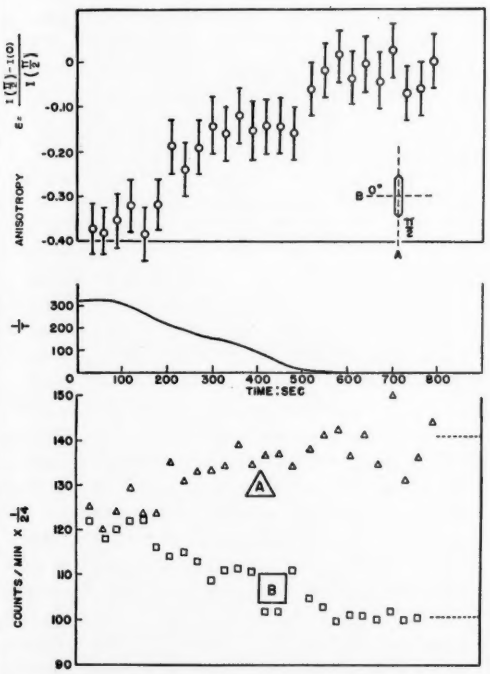

FIG. 11. Results of a single demagnetization in Nd^{147} experiment (530-kev gamma ray). Plotted against time are anisotropy (top), reciprocal of absolute temperature (center), and individual counting rates (unnormalized) of counter A(△) and B(□). Each point represents a twenty-second counting interval. Insert shows counter positions with respect to crystal axis. Dotted horizontal lines indicate "warm" (isotropic) counting rates.

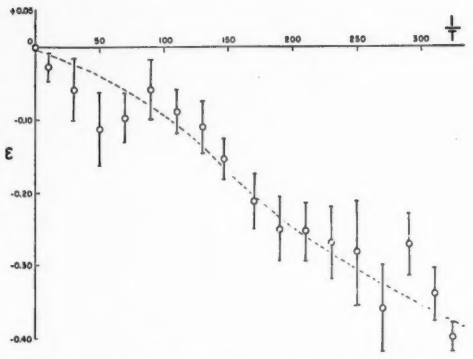

FIG. 12. Anisotropy (ϵ) *vs* reciprocal of absolute temperature ($1/T$) for Nd^{147} experiment (530-kev gamma ray). Points represent averages of fifteen demagnetizations. Note smaller statistical error at lowest temperature.

$\theta=50°$, counter B remaining along the z-axis of the crystal. An anisotropy of 0.16 was observed.

No anisotropy greater than 0.05 was detected in the angular distribution of the 92-kev gamma ray.

6. DISCUSSION

The observed gamma-ray anisotropy in the case of the Ce^{141} experiment establishes the gamma transition as being predominantly dipole, and the excited state of Pr^{141} as a $7/2^+$ level.[39] This is deduced from the following salient features of our results:

(i) the sign of ϵ is positive; referring to Fig. 3 this eliminates all decay schemes except

$$7/2 \xrightarrow{1} 5/2 \xrightarrow{2} 5/2 \text{ and, } 7/2 \xrightarrow{0,1} 7/2 \xrightarrow{1} 5/2;$$

(ii) during warmup the fractional change in the number of counts registered by A was about half that of B. It will be noted from Fig. 3 that if the decay scheme $7/2 \xrightarrow{1} 5/2 \xrightarrow{2} 5/2$ were correct, counting rate A would change very little during warmup, whereas with a decay scheme $7/2 \xrightarrow{0,1} 7/2 \xrightarrow{1} 5/2$ the theoretically predicted relative changes of A and B would be close to those observed. This is illustrated in Fig. 13 where we have shown how the theoretical polar diagrams in the two cases change during warmup.

Our results do not permit us to determine whether $\Delta i_\beta=0$ or 1 because of the relatively small difference between the polar diagrams of emission of the succeeding gamma ray in the two cases. Referring to Fig. 3 we see that, even at $T=0$, the values of ϵ in the two cases are very little different (0.46 and 0.38).

[39] It is interesting to note that this 142-kev level of Pr^{141} has been weakly Coulomb excited with low-energy alpha particles [G. M. Temmer and N. P. Heydenburg, Phys. Rev. **93**, 351 (1954)]. Since Coulomb excitation takes place almost entirely by $E2$ transitions, this weak excitation implies a very small electric quadrupole transition matrix element as compared with most other low-lying excited states in neighboring nuclei. Although this argument cannot be made complete until the lifetime (i.e., sum of $M1$ and $E2$ matrix elements) has been determined by delayed-coincidence measurements, the facts seem to support our finding of predominant $M1$ radiation.

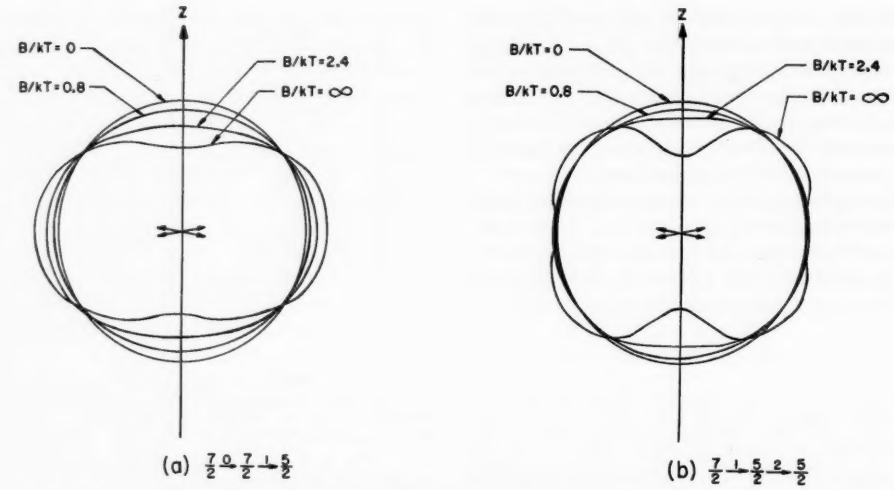

FIG. 13. Theoretical polar diagrams of gamma-ray emission for possible Ce^{141} decay schemes for several values of B/kT (B is hyperfine splitting constant; T, absolute temperature, and k, the Boltzmann constant).

From the sign of ϵ observed for the 530-kev gamma ray in the Nd^{147} experiment we can see, referring to Fig. 6, that the decay scheme $9/2 \xrightarrow{1} 7/2 \xrightarrow{1} 5/2$ can be eliminated. Since, during warmup, counting rate A increased while B decreased, and the fractional changes in the counting rates were about equal, we can eliminate the decay scheme $9/2 \xrightarrow{1} 7/2 \xrightarrow{2} 5/2$ (see Fig. 6). Thus we are left with the possibility $9/2 \xrightarrow{0,1} 9/2 \xrightarrow{2} 5/2$ with Δi_β undetermined, as in the case of Ce^{141}.

Since a significant anisotropy was obtained with the 530-kev gamma ray, the existence of nuclear alignment is established, and hence the absence of an anisotropy for the 92-kev gamma ray implies that this transition is a mixture of $M1$ and $E2$ radiation.‡ We can then deduce that the decay path including the 92-kev gamma ray must be $9/2 \xrightarrow{1} 7/2 \xrightarrow{1,2} 5/2$. Spin 7/2 for the 92-kev excited state of Pm^{147} is assured since it is the only one which allows a mixture of $M1$ and $E2$ gamma radiation, and a first-forbidden beta transition.

Now the magnitude of the gamma-ray anisotropy, once the decay scheme is established, depends only upon the relative populations of the various magnetic substates, i.e., upon the temperature and the hfs constant, B. By fitting a theoretical ϵ *vs* $1/T$ curve to the experimental points it is thus possible to obtain a value for B. In both of our cases we do not know whether $\Delta i_\beta = 0$, or a mixture of 0 and 1; assuming it to be zero[40] we obtain for Nd^{147}, $B = 0.004 \pm 0.001$ cm^{-1}; and for Ce^{141}, assuming a pure $M1$ transition, $B = 0.0022 \pm 0.0002$ cm^{-1}.

We may proceed to obtain estimates of the nuclear magnetic moments. For neodymium, the ratio of B for the radioactive isotope to that for a stable isotope is just the ratio of the nuclear gyromagnetic ratios [see Eq. (2)]. Using the value of $B_{145} = 0.0194$ cm^{-1} quoted in Sec. 3(b), taking $I_{147} = 9/2$, $I_{145} = 7/2$,[41] and $\mu_{145} = 0.85$[42] nuclear magnetons, we obtain $\mu_{147} = 0.22 \pm 0.05$ nm. To obtain a value for the nuclear moment of Ce^{141} we have to make use of theory. Inserting in Eq. (2) the values[34] $\langle +\frac{1}{2}|N_x|-\frac{1}{2}\rangle = 1.62$, $\langle 1/r^3\rangle_{Av} = 27 \pm 7$ A^{-3},[33] and $I = 7/2$, we obtain $\mu_{141} = 0.16 \pm 0.06$ nm.

The values of the magnetic moments estimated for both Nd^{147} and Ce^{141} are much smaller than those usually observed for odd-neutron nuclei. A possible explanation for this may lie in the method of deriving the theoretical values of the anisotropy. In calculating the population distribution over the various magnetic substates we have taken into account only the hyperfine splitting as obtained from the results of paramagnetic resonance, where it is normal to work with very dilute salts. In adiabatic demagnetization work, however, it is desirable to have a high concentration of magnetic ions to ensure a large heat capacity, but this causes stronger interaction magnetic fields within the crystal. The effect of these internal fields is to broaden the hyperfine energy levels of the assembly. Unfortunately there is no simple way of taking this effect into account, especially at low temperatures where a cooperative transition among the electron spins takes place. It is conceivable that they might significantly alter the population distributions

‡ *Note added in proof.*—After completion of this paper we discovered that the lifetime of the 92-kev transition in Pm^{147} had been accurately measured some time ago [R. L. Graham and R. E. Bell, Can. J. Phys. **31**, 377 (1953)], and was found to be 2.44×10^{-9} second. This would account for the lack of anisotropy observed (see reference 45).

[40] In the extreme case of $\Delta i_\beta = 1$, the above estimates of B must be increased by about 20 percent. Actually, from the systematics of $\Delta I = 0$ beta transitions with parity change, the $\Delta i_\beta = 1$ admixture is expected to be negligible [R. W. King (private communication)].

[41] B. Bleaney and H. E. D. Scovil, Proc. Phys. Soc. (London) **A63**, 1369 (1950).

[42] Bleaney, Scovil, and Trenam, Phil. Mag. **43**, 995 (1952).

and provide an explanation for the above discrepancies. Similar effects have been observed with Co^{60} nuclei[43] and Mn^{54} nuclei[44] in the same salt as used in our experiments, and some evidence has been obtained for the essential correctness of this explanation. We have computed the interference term due to $M1$–$E2$ mixture in the case of Ce^{141}. For reasonable values of the intensity ratio $E2/(M1+E2)$ (<15 percent) the anisotropy would not be altered significantly.

7. SUMMARY

In view of the many aspects of both solid state and nuclear physics which enter into this type of experiment, we think it worth while to emphasize here the main results:

(a) The type of nuclear alignment achieved is novel in that it is characterized by the condition that $B \gg A$, i.e., it represents "alignment" in a plane.

(b) The sign of the anisotropies, coupled with the relative change in individual counting rates between the lowest temperature reached (0.00308°K) and temperatures of essential isotropy ($\sim$0.1°K), definitely tell us the type of gamma radiation emitted; the data also permit us to eliminate most of the *a priori* possible spin and parity assignments for the initial, intermediate and final states involved in the decay chains. These conclusions are summarized in Table II. In the Nd^{147} experiment the lack of anisotropy of the 92-kev radiation is proved to be meaningful by the simultaneous occurrence of a comparatively large anisotropy in the 530-kev radiation.

(c) Some limits can be set on the lifetimes of the gamma-ray transitions studied here. The 142-kev transition in Ce^{141} as well as the 530-kev transition in Nd^{147} cannot have lifetimes much in excess of 10^{-10} second, simply because sizeable anisotropies were observed, and nuclear reorientation effects could not have been important.[45] The limit is in keeping with theoretical expectations for $M1$ and $E2$ transitions of these energies. On the other hand, it may be argued that the 92-kev transition in Nd^{147}, showing no anisotropy, might well have a long lifetime. However, Weisskopf's formula[46] for $M1$ radiation (which seems to be predominant from internal conversion data) of 92 kev yields a mean life $\tau_\gamma \simeq 5\times10^{-11}$ second, which is definitely too short to permit appreciable reorientation.§

(d) From the observed anisotropy-absolute temperature relationship, we arrive at an experimental value for the coefficient B in the spin-Hamiltonian, and hence a value for the nuclear magnetic moment. The unusually low values obtained in this manner when compared with other odd-neutron nuclei in general, and the stable isotopes of neodymium in particular, however, lead us to suspect the correctness of the assumptions made to obtain the values of B. A phenomenon produced by internal magnetic fields (not included in the spin-Hamiltonian) may well be responsible for this fact. The values of the nuclear magnetic moments are therefore in a category of much lower reliability.

TABLE II. Summary of experimental results on Ce^{141} and Nd^{147}. Λ_γ: multipolarity of gamma transition.

Nucleus	E_γ (kev)	Λ_γ	Spin and parity Initial	Intermediate	Final
Ce^{141}	142	$M1$[a]	$7/2^-$	$7/2^+$	$5/2^+$
Nd^{147}	92	$(M1+E2)$	$9/2^-$	$7/2^+$	$5/2^+$
Nd^{147}	530	$E2$	$9/2^-$	$9/2^+$	$5/2^+$

[a] See footnote 39.

8. ACKNOWLEDGMENT

We wish to thank Mr. R. Fessel for his valuable assistance with the work on Nd^{147}.

[43] E. Ambler and N. Kurti, Third International Conference on Low Temperature Physics and Chemistry (Rice Institute, Houston, 1953).

[44] J. M. Daniels and N. Kurti, Third International Conference on Low Temperature Physics and Chemistry (Rice Institute, Houston, 1953).

[45] N. R. Steenberg, Phys. Rev. **95**, 982 (1954).

[46] J. M. Blatt and V. F. Weisskopf, *Theoretical Nuclear Physics* (John Wiley and Sons, Inc., New York, 1952), p. 627.

§ *Note added in proof.*—However, as pointed out in the aforementioned note, the measured lifetime for this transition is 2.44×10^{-9} second, which is long enough to wipe out any intrinsic anisotropy through coupling with crystalline electric and/or magnetic fields; no conclusions can therefore be drawn concerning the $E2$ to $M1$ mixing ratio.

Cross Section for Excitation of Pb^{207m} by Inelastic Scattering of Neutrons

P. H. STELSON AND E. C. CAMPBELL
Oak Ridge National Laboratory, Oak Ridge, Tennessee
(Received November 26, 1954)

The cross section for the excitation of the 0.8-sec metastable state of Pb^{207} by inelastic neutron scattering has been measured for neutron energies up to 3.1 Mev. Neutrons were produced by the Li(p,n) reaction. The lowest neutron energy for which excitation is observed is 1.6 Mev. This is in agreement with the level scheme for Pb^{207} based on other information. For the first 800 kev above threshold, the cross section rises approximately linearly, attaining a value of 75 millibarns at 2.4 Mev. After leveling off, it abruptly increases at 2.75 Mev and has a value of 190 millibarns at 3.1 Mev. It is judged that the absolute values of the cross section are accurate to ±40 percent. The absolute cross section for excitation of the metastable state as a function of neutron energy is calculated by the use of the strong interaction theory of nuclear reactions. The theoretical predictions agree well with the measured curve.

I. INTRODUCTION

SEVERAL investigations of the excitation of metastable nuclear states by the inelastic scattering of an incident beam of monoenergetic neutrons have now been reported.[1–3] In contrast to states with prompt decay, the study of metastable states obviates the problem of observing the inelastic scattering event with detectors in which there are high background counting rates associated with proximity to the fast neutron source. Consequently, the inelastic neutron scattering process may be studied with a considerable increase in sensitivity for those few cases in which the residual state is metastable. One such case is the 0.8-sec metastable state of Pb^{207}.[4,5] We wish to report the absolute cross section for the excitation of this state as a function of neutron energy.

Hauser and Feshbach,[6] have discussed the application of the strong interaction theory of nuclear reactions to the case of inelastic neutron scattering. They point out that just above threshold, the cross section for the production of an excited state is sensitive to energy, angular momentum, and parity differences which exist between the ground state and the excited states of the target nucleus. Margolis[7] has investigated the prediction of this theory for the experimental cases cited above.[1–3] He finds agreement of experiment with theory is good and remarks that this is notable because of the rather simple assumptions of the strong interaction theory and because recent calculations by Feshbach, Porter, and Weisskopf[8,9] have shown that for total neutron cross sections better agreement with experiment is obtained if one does not assume immediate compound nucleus formation.

The positions, spins, and parities of the low-lying excited states of Pb^{207} are rather well established. According to shell theory, the level scheme is one of the simplest to interpret since the nucleus differs from Pb^{208} by one neutron. The low-lying excited states are expected to be single particle states of the type that are available in the 82 to 126 neutron shell. Experimental information is in agreement with this conclusion.[10] Therefore, the energies, spins, and parities of the isomeric state and the levels below it may be taken as known and one has sufficient information to carry out an effective comparison of the strong interaction theory with the experimentally determined cross section. Using the information on the levels in the lead isotopes, Oleksa[11] has applied the strong interaction theory to predict the inelastic neutron scattering properties of lead.

II. EXPERIMENTAL METHOD

A schematic diagram of the experimental setup is given in Fig. 1. Monoenergetic neutrons were produced by bombarding thin lithium targets by protons from the 5.5-Mev ORNL electrostatic generator. The lead cylinder was irradiated by neutrons emerging from the target in the forward direction. After a suitable bombardment period, the proton beam was deflected off the target and the γ-ray activity induced

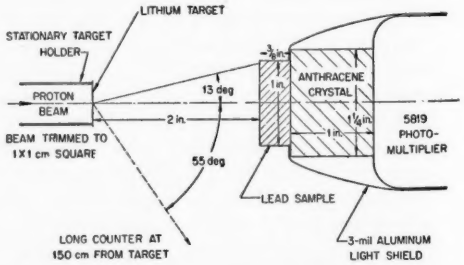

FIG. 1. Schematic diagram of the experimental set-up.

[1] Francis, McCue, and Goodman, Phys. Rev. **89**, 1232 (1953).
[2] A. A. Ebel and C. Goodman, Phys. Rev. **93**, 197 (1954).
[3] Martin, Diven, and Taschek, Phys. Rev. **93**, 199 (1954).
[4] E. C. Campbell and M. Goodrich, Phys. Rev. **78**, 640(A) (1950).
[5] G. Vendryes, Ann. phys. **7**, 655 (1952).
[6] W. Hauser and H. Feshbach, Phys. Rev. **87**, 366 (1952).
[7] B. Margolis, Phys. Rev. **93**, 204 (1953).
[8] Feshbach, Porter, and Weisskopf, Phys. Rev. **90**, 166 (1953).
[9] Feshbach, Porter, and Weisskopf, Phys. Rev. **96**, 448 (1954).
[10] See M. H. L. Pryce, Proc. Phys. Soc. (London) **A65**, 773 (1952).
[11] Sophie Oleksa, Brookhaven National Laboratory Report BNL-273 (T-45), December, 1953 (unpublished).

in the lead sample was detected by an anthracene scintillation counter.

The energy homogeneity of the neutrons passing through the lead sample was limited mainly by the target thickness which varied from 70 to 80 kev. The spread in neutron energy caused by the finite solid angle subtended by the sample varied from 15 to 30 kev. Measured cross sections are plotted at mean neutron energies.

An electrostatic deflector, located in the beam tube on the exit side of the analyzing magnet at a distance of 5 meters from the target, was used to remove the proton beam from the target. The deflected protons were caught in a lead plug placed about 1 meter from the deflector. With this arrangement, the neutron flux could be turned off or on in less than 1/100 of a second.

The timing sequence was carried out automatically by the use of a electronic timing device. The proton beam was held on the target for 2.1 second (about $2\frac{1}{2}$ half-lives) to build up the induced activity. The anthracene counter was turned on 0.2 second after the proton beam was cut off the target and held on for 1.3 sec (about $1\frac{1}{2}$ half-lives). A delay of 10 seconds followed and the sequence was then repeated. Fifty to 100 repetitions of the sequence were carried out at each neutron energy. The time interval between the cutoff of the proton beam at the start of the counting interval was variable so that the decay curve of the induced activity could be studied.

To determine the absolute cross section it was necessary to know both the neutron flux incident on the lead sample and the efficiency with which the decay of the metastable state was detected. During the experiment, the neutron flux was monitored by a long counter placed 55° to the forward direction and 1.5 meters from the target. An auxiliary experiment was performed to determine the ratio of the neutron yields at 55° and 0° from the $Li(p,n)$ reaction as a function of the proton energy. The counts recorded by the long counter were converted to absolute neutron flux by calibrating the long counter with a standard Po-Be source. A small percentage of the neutrons from the $Li^7(p,n)$ reaction leave the residual nucleus Be^7 in the first excited state. No correction has been made for the effect of this second group of neutrons because of the lack of data on the yield and angular distribution as a function of proton energy. It is judged that the neutron flux (primary group+small admixture of the second group) incident on the lead sample was determined to an accuracy of 15 percent.

The incident neutron flux is attenuated to some extent in traversing the lead. Taking the total cross section of lead as 7 barns it is calculated that 20 percent of the incident neutrons undergo a primary collision so that the average primary flux throughout the sample is about 90 percent of the incident flux. However, roughly half of the primary collisions are diffraction scattering in which the neutron energy is not appreciably changed, and this part of the secondary flux is as effective as the primary flux for excitation of the metastable state. On the other hand, the efficiency with which the decay of the metastable state is detected is considerably larger for that part of the lead sample adjacent to the anthracene crystal which is the region of minimum neutron flux. After considering these effects, we decided to take the effective neutron flux as 90 percent of the incident flux.

The efficiency of the anthracene scintillation counter for the detection of the decay of the metastable state excited in the lead sample was determined as follows. The long-lived radioactive nucleus Bi^{207} decays primarily[12,13] to the metastable state of Pb^{207} and is, therefore, a convenient source of γ rays with energies identical to those detected in the experiment. A source of Bi^{207} of small lateral dimensions ($\frac{1}{8}$ in. diameter) was prepared by evaporation to dryness of a solution of bismuth nitrate deposited on a thin polystyrene film. The strength of this source was established to 10 percent. Next, the lead sample (a cylinder 1 inch in diameter and $\frac{3}{8}$ in. thick) was replaced by three lead disks of 1 inch diameter and $\frac{1}{8}$ in. thickness. The source was placed at different points in the lead sample by sandwiching it between the lead disks and the efficiency for detection of the decay of the metastable state systematically determined at various points throughout the lead sample. The bias on the counter was set so that only the higher energy 1.07-Mev γ ray was detected because large background rates (in part due to the 479-kev γ ray from Be^7 build-up in target) were encountered at lower bias setting during the actual experiment. The overall efficiency for detection of the γ rays excited in the lead sample was (1.20 ± 0.25) percent.

The total internal conversion coefficient of the 1.07-Mev γ ray is taken to be 0.12 ± 0.01.[14] The range in the lead of the fast electrons from internal conversion is so short that the metastable states which decay by internal conversion are detected with a rather poor efficiency. It is estimated that 0.5 percent of the decays by internal conversion are detected. Consequently, the counts registered by the detector are 95 percent the result of gamma-ray detection and 5 percent the result of fast electron detection.

III. RESULTS

The cross section for the excitation of the metastable state of Pb^{207} as a function of neutron energy is given in Fig. 2(a). The experimentally observed cross section for normal lead has been multiplied by 4.76 to obtain

[12] Friedlander, Wilson, Ghiorso, and Perlman, Phys. Rev. **91**, 498(A) (1953).
[13] E. C. Campbell and F. Nelson, Phys. Rev. **91**, 499(A) (1953).
[14] F. K. McGowan and E. C. Campbell, Phys. Rev. **92**, 523 (1953).

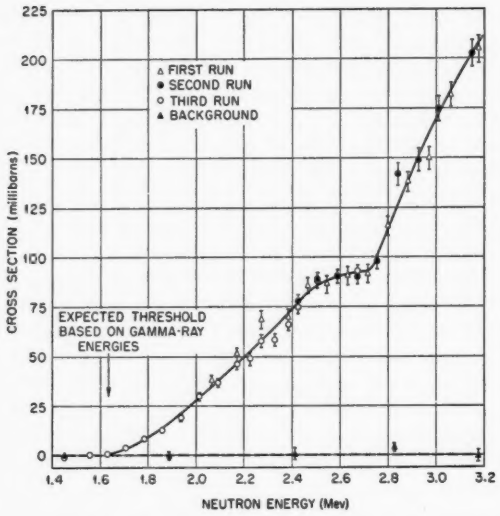

FIG. 2(a). Cross section for the excitation of the metastable state of Pb^{207}. The observed cross section for normal lead has been multiplied by 4.76 to obtain the cross section for Pb^{207} (isotopic abundance 21 percent). The errors shown are the statistical errors. The absolute cross section is judged to be accurate to ±40 percent.

the cross section for Pb^{207} (isotopic abundance 21 percent). Three different runs were made. The first run gave absolute cross sections about 8 percent higher on the average than those of the other two runs. To present a less confused picture of the shape of the curve, the points for the first run have been lowered by 8 percent.

Since the anthracene detector was periodically subject to a high flux of fast neutrons, it was necessary to investigate the possibility of activities, other than that of the lead, contributing to the counting rate of the detector. The lead cylinder was replaced by a tantalum cylinder of equal thickness in grams/cm². The resulting points are shown in Fig. 2(a) as background points. It is seen that counts caused by activities other than that in lead are relatively unimportant, being the equivalent of about 6 millibarns of cross section. The level given by the background points is taken as the zero of the ordinate scale.

To make certain that the activity in the lead itself was the 0.8-sec decay of the metastable state, a half-life determination at the highest neutron bombarding energy was carried out by varying the time interval between the cutoff of the neutron flux and the start of the counting time. These data are presented in Fig. 3. The decay follows a straight line on semilog plot (half-life of 0.8 sec) down to an intensity which is a few percent of the initial intensity.

From the consideration of the sources of errors it is judged that the determination of the absolute cross section is accurate to ±40 percent.

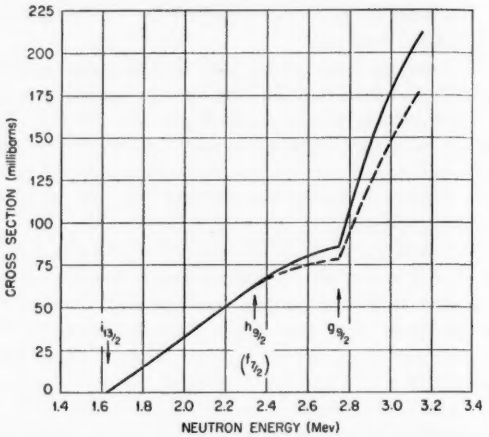

FIG. 2(b). Theoretical cross section calculated by the use of the strong interaction theory of nuclear reactions. The solid curve is based on the assumption of $h_{9/2}$ and $g_{9/2}$ states and the dashed curve is based on the assumption of $h_{9/2}$, $f_{7/2}$, and $g_{9/2}$ states.

IV. DISCUSSION

As previously mentioned, Pb^{207} differs from doubly magic Pb^{208} by one neutron and, therefore, the low-lying states are expected to be of the simple, single particle type which are available to a neutron hole in the 82–126 shell, viz., $p_{1/2}$, $p_{3/2}$, $f_{5/2}$, $f_{7/2}$, $h_{9/2}$, and $i_{13/2}$. Experimental information and assignments are shown in Fig. 4. The $p_{1/2}$, $f_{5/2}$, and $i_{13/2}$ states are well established. The location of the $f_{7/2}$ state is not known. One would expect electron capture in Bi^{207} to decay to the $f_{7/2}$ state if this were energetically possible since the reasonable assignment of $h_{9/2}$ for the ground state of Bi^{207} makes this an allowed transition. It is therefore likely that the $f_{7/2}$ level is a little above the 2.34-Mev level.

In addition to the information given by the study of the decay of Tl^{207}, Bi^{207}, and Po^{211}, we have the work of

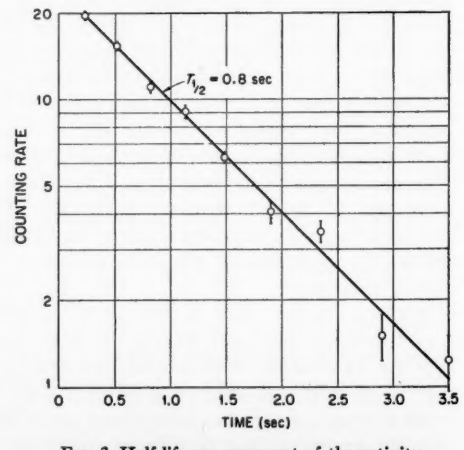

FIG. 3. Half-life measurement of the activity induced in the lead sample. E_n=3.17 Mev.

Harvey[15] on the reactions $Pb^{206}(d,p)Pb^{207}$ and $Pb^{208}(d,t)Pb^{207}$. The levels identified from this study are indicated by the symbols (d,p) and (d,t). New states were found at higher excitation energies. Harvey suggested the assignment $g_{9/2}$ and $i_{11/2}$ for the states at 2.75 and 3.60 Mev. The $g_{9/2}$ and $i_{11/2}$ states are of the type expected in the shell beyond 126 nucleons and are expected to be located at higher excitation energies than those corresponding to a hole in the 82 to 126 shell.

The region of several hundred kev above the threshold for excitation of the metastable state is probably free of levels. In this region we can compare the experimental cross section with the theoretical cross section for direct excitation of the metastable state by inelastic neutron scattering. Direct excitation requires the transfer of 6 units of angular momentum and a change of parity. Taking the locations and assignments for the levels given in Fig. 4, we have calculated the cross section predicted by the strong interaction theory. The nuclear radius for lead was taken to be 8.0×10^{-13} cm (8.0 for the parameter X_0).

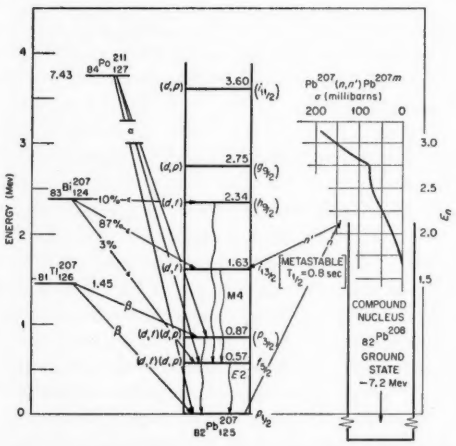

FIG. 4. Energy level diagram summarizing the formation on the low-lying levels of Pb^{207}. Note: The schematic curve of the excitation cross should be increased by 10 percent to agree with curve presented in Fig. 2(a).

Figure 5 shows the calculated cross section together with two runs of the experimental cross section near threshold. The general agreement with respect to shape and absolute cross section is good. The experimental points suggest more curvature near threshold but this may be at least in part attributed to the finite energy spread used to measure the cross section. The agreement in absolute cross section is well within the errors of the experimental determination. It might be mentioned that the inclusion in the calculation of the competition offered by the other low-lying states (0.57 and 0.87 Mev) is quite important. If these states had been

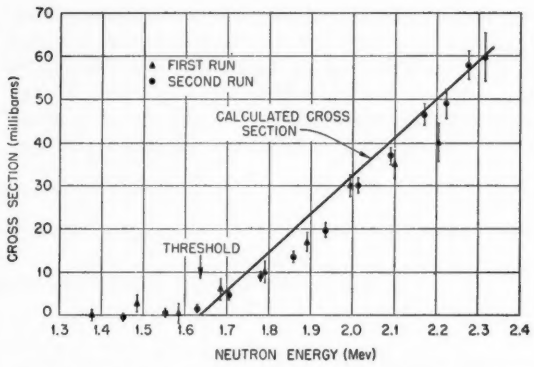

FIG. 5. Calculated cross section based on the strong interaction theory of nuclear reactions together with two runs of the experimental cross section near threshold.

omitted, the calculated cross section would have been, on the average, about a factor of 3 larger.

At higher neutron energies, states above the metastable state will be excited by inelastic scattering. As the incident neutron energy is raised above the threshold for excitation of a new state the cross section for excitation of the metastable state is modified. The cross section for direct excitation is always adversely affected by the onset of inelastic scattering to a new level because of the increased competition. However, since the measured cross section includes indirect as well as direct excitation, the cross section actually may show a rather abrupt increase with the advent of a new state if this state subsequently decays to the metastable state.

After the initial almost linear increase with neutron energy, the experimental cross section levels off at about 2.5 Mev. Now, the existence of a state of 2.34 Mev is well established and its character is quite likely $h_{9/2}$. It is known that this state by-passes the metastable states in the subsequent decay to the ground state.[16] Therefore the excitation of this state would tend to decrease the cross section for excitation of the metastable state.

At 2.75 Mev, the experimental curve shows an abrupt rise and the natural inference is that a new state is excited which feeds the metastable state. Such a state must have a fairly high spin to ensure at least partial decay to the metastable state ($i_{13/2}$) instead of completely by-passing it in favor of the other low-lying states. Harvey found a level at 2.75 Mev and suggested the assignment $g_{9/2}$. A state of the type $g_{9/2}$ can decay to the metastable state by an $E2$ transition whereas decay to the $p_{1/2}$, $p_{3/2}$, or $f_{5/2}$ states requires less favorable types of transitions. However, it is difficult to decide to what extent decay to the $h_{9/2}$ and $f_{7/2}$ states ($E1$ transitions) would compete with the $E2$ transition.

We have extended the calculated cross section to higher neutron energies on the assumption that there

[15] John A. Harvey, Can. J. Phys. **31**, 278 (1953).

[16] N. Lazar (private communication).

is a level at 2.34 Mev of the type $h_{9/2}$ which completely by-passes the metastable state and that there is a level at 2.75 Mev of the type $g_{9/2}$ which decays predominantly to the metastable state. The calculated curve is given in Fig. 2(b) as the solid line. The dashed curve shows the calculated cross section with the assumption that there is also an $f_{7/2}$ level (taken to be superimposed on the $h_{9/2}$ level for calculational simplicity since its exact location is not known) which by-passes the metastable state in its subsequent decay. It is seen that the experimental cross section is reasonably well represented by the calculated curves.

PHYSICAL REVIEW VOLUME 97, NUMBER 5 MARCH 1, 1955

Gamma Radiation from the Inelastic Scattering of Protons by F^{19}†

C. A. BARNES*
Kellogg Radiation Laboratory, California Institute of Technology, Pasadena, California
(Received November 4, 1954)

The absolute cross section for the excitation of the 109-kev and 197-kev excited states of F^{19}, by the inelastic scattering of protons, has been studied as a function of bombarding energy up to 1750 kev by detecting the resultant gamma radiation in scintillation counters. Most of the resonances for the various $F^{19}(p,\alpha)O^{16}$ reactions appear as resonances for the excitation of one or both of these low-lying states. A detailed study of the angular distributions of the two gamma rays, together with the direct measurements of the lifetimes of these states by Thirion, Barnes, and Lauritsen, and the Coulomb excitation work of Sherr, Li, and Christy, leads to the assignments: 109-kev state, $J=\frac{1}{2}$, odd parity; 197-kev state, $J=5/2$, even parity. The nonresonant yield of 197-kev gamma rays is approximately that expected from Coulomb excitation at low incident proton energies. The nonresonant yield of 109-kev gamma rays exceeds the expected Coulomb excitation. In conjunction with the recent measurements of the elastic scattering of protons by F^{19} made by Peterson, Webb, Hagedorn, and Fowler, in this laboratory, and older measurements of the $F^{19}(p,\alpha)O^{16}$ reactions, the resonant inelastic cross sections allow a new determination of the partial widths for the various modes of decay of the Ne^{20} compound nuclear states.

I. INTRODUCTION

THE bombardment of F^{19} by protons up to energies ~2 Mev can lead to the following reactions:

$$F^{19}+p\rightarrow Ne^{20*}\rightarrow\alpha_{0,\pi,1,2,3}+O^{16} \quad (1)$$

$$\rightarrow\gamma+Ne^{20} \quad (2)$$

$$\rightarrow p_0+F^{19} \quad \text{(elastic scattering)} \quad (3)$$

$$\rightarrow p_{1,2}+F^{19*} \quad \text{(inelastic scattering to first and second excited states of } F^{19}\text{)}. \quad (4)$$

The first of these reactions[1,2] can leave O^{16} in its ground state, in a pair-emitting state at 6.05-Mev excitation, or in gamma-ray emitting states at 6.13, 6.9, and 7.1 Mev. The detailed study of this reaction has made possible the assignment[2,3] of spin and parity to many of the levels in Ne^{20} and O^{16} involved in the reactions.

Reaction (2) shows resonances at proton energies of 669, 874, 935, 980, 1092, 1290, 1324, 1346, 1372, and 1422 kev.[2,4]‡ Elastic scattering of protons (reaction 3) has recently been investigated[5,6] up to 1.8 Mev and gives directly or confirms the spin and parity of many of the Ne^{20} states.

Prior to the present investigation, the inelastic scattering of protons by fluorine has been studied at 7.17-Mev and 8-Mev incident proton energy.[7] Several levels at energies >1.37 Mev in F^{19} were excited, but the resolution in these experiments was insufficient to resolve proton groups to the low-lying levels first reported by Mileikowsky and Whaling.[8] These levels have recently been excited by inelastic scattering of neutrons[9] and by inelastic scattering of α particles.[10,11]

† Assisted by the joint program of the U. S. Office of Naval Research and the U. S. Atomic Energy Commission.
* On leave of absence from the University of British Columbia.
[1] Streib, Fowler, and Lauritsen, Phys. Rev. **59**, 253 (1941); Bennett, Bonner, Mandeville, and Watt, Phys. Rev. **70**, 882 (1946); Chao, Tollestrup, Fowler, and Lauritsen, Phys. Rev. **79**, 108 (1950).
[2] F. Ajzenberg and T. Lauritsen, Revs. Modern Phys. **24**, 321 (1952).
[3] W. A. Fowler and C. C. Lauritsen, Phys. Rev. **56**, 840 (1939); J. R. Oppenheimer and J. S. Schwinger, Phys. Rev. **56**, 1066 (1939); W. R. Arnold, Phys. Rev. **79**, 170 (1950); **80**, 34 (1950); Barnes, French, and Devons, Nature **166**, 145 (1950); C. Y. Chao, Phys. Rev. **80**, 1035 (1950); J. Seed and A. P. French, Phys. Rev. **88**, 1007 (1952); Rasmussen, Hornyak, Lauritsen, and Lauritsen, Phys. Rev. **77**, 617 (1950); Devons, Goldring, and Lindsey, Proc. Phys. Soc. (London) **A67**, 134 (1954).
[4] S. Devons and H. G. Hereward, Nature **162**, 331 (1948); R. M. Sinclair, Phys. Rev. **93**, 1083 (1954); T. M. Hahn and B. D. Kern, University of Kentucky report, August 31, 1954 (unpublished).
‡ See note added in proof in the caption of Fig. 1.
[5] Peterson, Barnes, Fowler, and Lauritsen, Phys. Rev. **94**, 1075 (1954).
[6] Webb, Hagedorn, Fowler, and Lauritsen, Phys. Rev. **96**, 851(A) (1954).
[7] Cowie, Heydenburg, and Phillips, Phys. Rev. **87**, 304 (1952); Arthur, Allen, Bender, Hausman, and McDole, Phys. Rev. **88**, 1291 (1952).
[8] C. Mileikowsky and W. Whaling, Phys. Rev. **88**, 1254 (1952).
[9] R. B. Day, Phys. Rev. **89**, 908(A) (1953).
[10] Sherr, Li, and Christy, Phys. Rev. **94**, 1076 (1954); **96**, 1258 (1954).
[11] N. P. Heydenburg and G. M. Temmer, Phys. Rev. **94**, 748(A) (1954) and Phys. Rev. **94**, 1232 (1954); G. A. Jones and D. H. Wilkinson (private communication).

A preliminary account of the excitation of these low-lying levels by protons has been published,[5] together with measurements of the lifetime of the states,[12] the α-particle Coulomb excitation cross section,[10] and a theoretical study of the various angular distributions.[13] On the basis of these results, the 109-kev state in F^{19} was assigned spin and parity $\frac{1}{2}^-$ and the 197-kev state $5/2^+$. The present paper contains a more detailed account of the studies of the 109-kev and 197-kev gamma rays excited by inelastic scattering of protons up to 1750-kev incident energy.

II. EXPERIMENTAL DETAILS

Protons were accelerated by the Kellogg Radiation Laboratory 2-Mv electrostatic accelerator and resolved in energy with a resolution of about one or two kev, in either electrostatic or magnetic analyzers. Proton beams of the order of $\frac{1}{2}$ μa bombarded thin evaporated targets of CaF_2 on 0.004-inch copper backings. The target chamber was a $2\frac{1}{2}$-inch o.d. Lucite cylinder of $\frac{1}{8}$ in. wall thickness with the proton beam entering normal to the axis of the chamber. The spot where the beam hit the target was accurately located on the chamber axis. It was possible to carry out angular distribution measurements of the emitted γ radiation by rotating a scintillation counter around the target at a fixed distance from the axis of the target chamber.

The scintillation counter employed a 1-in. diam $\times\frac{1}{2}$-in. thick NaI(Tl) crystal, drymounted in a thin aluminum housing coated on the inside with MgO. A $\frac{1}{4}$-inch thick quartz window let out the light from the scintillations. The mounted crystal was then cemented to a Dumont 6292 photomultiplier tube with Dow Corning high-viscosity silicone oil. The photomultiplier tube was magnetically shielded with a mumetal shield, and the crystal and photomultiplier were enclosed in an inner shield of mild steel, $\frac{1}{4}$ in. thick, and an outer lead shield, $\frac{1}{2}$ in. thick. The lead shield was found to be necessary to shield out x-radiation from the accelerator while the inner steel shield served the double purpose of supplying additional magnetic shielding for the photomultiplier tube, and of eliminating the fluorescent x-rays excited in the lead by γ radiation. The opening of the shielding towards the target was a collimator consisting of a $\frac{1}{4}$ in. thick lead ring backed by 2 mm of cadmium to remove the lead x-rays. The aperture of the collimator, $\frac{3}{4}$ in. diameter, defined the solid angle of the scintillation counter.

Typical differential bias curves taken with the arrangement are shown in Figs. 1(a), (b), and (c). The differences in the bias curves show clearly the variations in relative yield of the low-energy gamma rays and the 6- and 7-Mev gamma rays from one resonance to another. The small peak to the left of the main peak in Fig. 1(a) is probably the "escape" peak from the 109-kev peak,

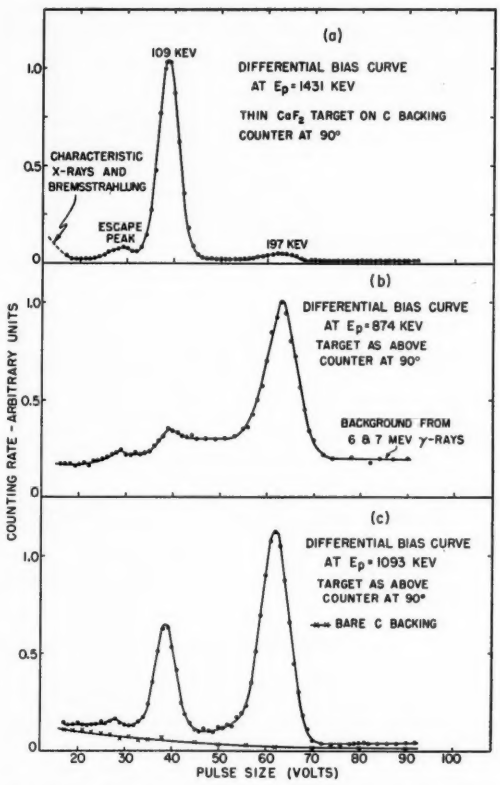

FIG. 1. Typical differential bias curves at the 1431, 873, and 1092-kev resonances in the $F^{19}+p$ reactions, showing the wide variations in relative yield of the various gamma radiations. *Note added in proof.*—The previously accepted resonance energies 1355, 1381, and 1431 have been changed to 1346, 1372, and 1422 kev on the basis of measurements made by the author during the past year. These measurements employed the 873.5-kev resonance in $F^{19}+p$ and the 1881.6 kev $Li^7(p,n)$ threshold as standards, and have an uncertainty of about 0.1 percent. The author is indebted to Mr. F. Mozer of this laboratory, and Dr. H. B. Willard of the Oak Ridge National Laboratory, for communicating their unpublished measurements of some of these resonance energies, which are in agreement with the results quoted here.

i.e., the peak due to photoelectric interactions in the NaI crystal in which the iodine *K*-x-ray escapes from the crystal. In some cases, the peak in this energy region may also contain a small contribution from residual fluorescence radiation from lead, and from the Compton collisions of the 197-kev radiation in the NaI crystal, in which the scattered quantum is scattered through angles near 180°. Similarly, a spurious contribution may appear near the 109-kev peak produced by back-scattering of the 197-kev radiation in the vicinity of the target. These effects determine the lower limit of detection for γ radiation near 109 kev and near 88 kev. The instrumental width at half-maximum of the 109-kev peak in Fig. 1(a) is about 14 percent in energy.

In most of the runs during these experiments, the number of counts was determined for a fixed quantity of proton charge collected by the target, as measured by a

[12] Thirion, Barnes, and Lauritsen, Phys. Rev. **94**, 1076 (1954).
[13] R. F. Christy, Phys. Rev. **94**, 1077 (1954).

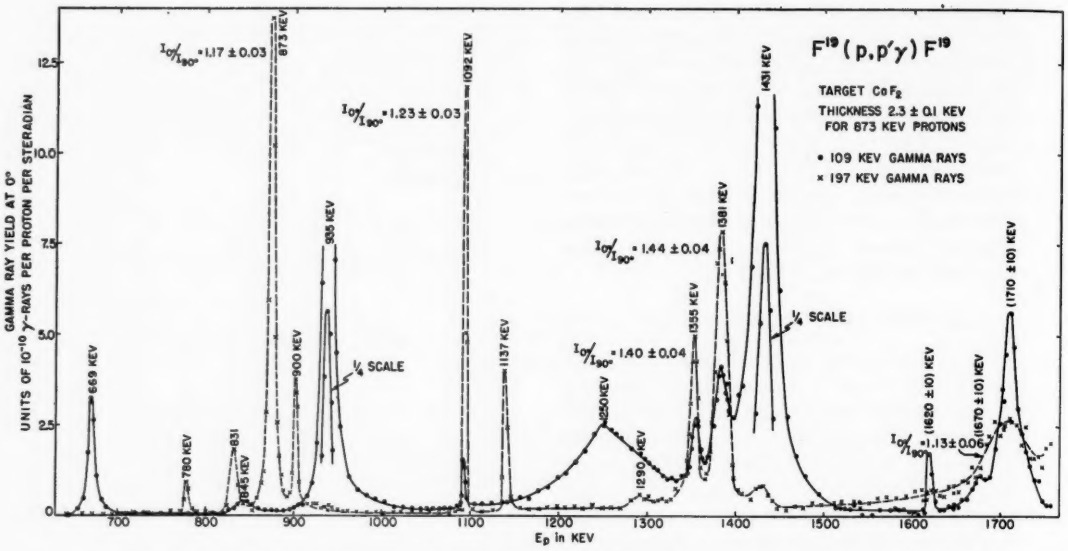

FIG. 2. Excitation curve for the 109-kev and 197-kev gamma rays from the inelastic scattering of protons by F^{19}. (See note added in proof, Fig. 1.)

calibrated current integrator. An electron suppressor was employed to remove extraneous electrons from the slits defining the incoming proton beam and the target was biassed at +300 volts with respect to its surroundings to prevent loss of secondary electrons.

III. EXCITATION ENERGY OF THE LOW-LYING F^{19} STATES

The energy scale of the scintillation counter was calibrated by observing the "photopeaks" from the Lu^{177} gamma rays at energies of (112.97±0.02) kev and (208.36±0.02) kev.[14] With this calibration, the quantum energies of the γ radiations were measured as (110±1) kev and (197.5±1.5) kev.[15] By the same method, Day has obtained the values (110±1) kev and (197±2) kev.[16]

Measurements of the excitation energies of these states in F^{19} have also been made by Peterson, Fowler, and Lauritsen,[3] by observing the difference in energy between the elastically and inelastically scattered protons from fluorine. These authors quote (108.8±0.8) kev and (196.0±1.4) kev.[17] Recently, Mills, Hilton, and Barnes[18] have observed the internal conversion electrons from these two states, and quote (109.1±1.0) kev and (196.8±1.5) kev. We take the weighted mean of these results as (109.2±0.6) kev and (196.8±0.7) kev. These values are in satisfactory agreement with determinations in other laboratories.[11,19]

From a comparison of many bias curves such as Fig. 1(a) and 1(c), we feel that the peak present at about 88 kev in Fig. 1(c) can be ascribed to the "escape" peak associated with the 109-kev peak. We estimate that the cascade transition through the 109-kev state occurs with less than 1 percent of the intensity of the 197-kev cross-over transition. Heydenburg and Temmer[11] estimate that the cascade transition occurs with <2 percent of the intensity of the 197-kev transition, while Jones *et al.*[19] estimate <½ percent.

Recently, Cook, Marion, and Bonner[20] have reported two levels in Ne^{19} at 255 and 289 kev respectively. It would be of special interest to ascertain the spin and parity of these Ne^{19} states to see if they correspond to the levels at 109 and 197 kev in F^{19}. No other gamma rays below 1.3 Mev have been observed in the $F^{19}(p,p')F^{19}$ reaction. It should be stated however, that the detection of weak low-energy radiation is made difficult by the x-rays and bremsstrahlung[21] from the target, and the presence of other, weakly-excited, states cannot be absolutely ruled out.

IV. EXCITATION CURVE OF THE 109-KEV AND 197-KEV γ RADIATION

The excitation curves of the radiations, following the inelastic proton scattering, are shown in Fig. 2. The most striking feature of these curves is the pronounced resonant character of the excitation. Most of the resonances which appear in Fig. 2 have been identified previously as resonances for the production of capture gamma radiation or for the emission of alpha particles to the ground state (α_0), to the pair-emitting state at 6.05

[14] P. Marmier and F. Boehm, Phys. Rev. **97**, 103 (1955). The writer is indebted to these authors for the loan of a Lu^{177} source.
[15] The slightly higher values quoted in reference 5 appear to be in error because of a nonlinear amplifier gain characteristic curve.
[16] R. B. Day, (private communication).
[17] Peterson, Fowler, and Lauritsen, Phys. Rev. **96**, 1250 (1954).
[18] Mills, Hilton, and Barnes, Phys. Rev. (to be published).
[19] Jones, Phillips, Johnson, and Wilkinson (to be published).
[20] Cook, Marion, and Bonner (private communication to T. Lauritsen).
[21] Č. Zupančič and T. Huus, Phys. Rev. **94**, 205 (1954).

TABLE I. Cross sections and angular distributions for the gamma rays following inelastic scattering of protons by F^{19}. Cross sections quoted without parentheses are the sum of resonant and nonresonant values. Cross sections in parentheses are resonant portions only, when these are significantly different from the summed values.

Res. E (kev)	Γ (kev)	σ (109-kev γ's) mb	$I_0°/I_{90°}$ (109 kev γ's)	σ (197-kev γ's) mb	$I_0°/I_{90°}$ 197 kev γ's
669	7.5	20 ±3	0.98 ±0.02	(<0.2)	···
780	∼10[a]	(<0.2)	···	∼5	···
831	8.3	(<0.2)	···	∼8	···
845	23[a]	∼2	···	(<0.3)	···
873	5.2	(<0.3)	···	87 ±20	1.17±0.03
900	4.8	(<0.3)	···	∼20	···
935	8.0	147 ±22	0.98 ±0.02	(<1)	···
1092	<1.2	>13	0.98 ±0.03	>100	1.23±0.03
1137	3.7	(<0.4)	···	∼20	···
∼1250[a]	∼80[a]	17 ±3	1.01 ±0.03	1.7 ±0.5 (<1)	···
1290	19	(<1)	···	3 ±1 (1.5)	···
1346[a]	4.5[b]	17 ±4 (12)	0.99 ±0.03	27 ±7 (22)	1.40±0.04
1372[a]	15	26 ±4 (20)	1.00 ±0.03	40 ±6	1.44±0.04
1422[a]	14.6±1[a]	189 ±30	1.005±0.010	7 ±2 (≤3)	1.01±0.01
1610±10[a]	∼5[a]	12 ±3	···	(<2)	···
1660±10[a]	···	3	···	(≤2)	···
1700±10[a]	···	36 ±7	0.96 ±0.05	17 ±5	1.13±0.06
740	non-res. yield	0.1±0.04	1.01 ±0.05	0.14±0.05	1.4 ±0.2
1045	non-res. yield	1.0±0.04	0.96 ±0.05	0.3 ±0.1	1.2 ±0.1

[a] New measurements of widths or resonance energies in this investigation.
[b] D. Aaronson, Ph.D. thesis, University of British Columbia, 1952 (unpublished). T. Bonner and J. Evans, Phys. Rev. **73**, 666 (1948) quote 4.4 kev; Chao *et al.* (see reference 1) quote 8.6 kev.

Mev (α_π), or to the gamma-ray-emitting states of O^{16} at 6.13, 6.9, and 7.1 Mev (α_1, α_2, α_3, respectively).

The states of Ne^{20} which are believed to be of the type $J=1$, even (+) parity, formed by s-wave protons, decay predominantly to the 109-kev state of F^{19}. These states include the resonances at 669-kev, 935-kev,[3] and 1422-kev[5] proton energy. The 2^- (p-wave formation) state of Ne^{20}, corresponding to the 873.5-kev resonance, decays almost entirely to the 197-kev state of F^{19}, while the other 2^- states at resonance energies of 1346-kev and 1372-kev decay in comparable amounts to both low states of F^{19}. The very sharp 1092-kev resonance seems also to lead to comparable yields of the two excited states.

The structure of the excitation curve for the low-energy γ rays differs considerably from the excitation curve for the (p,α_{123}) reaction in the region of 1700 kev. The resonance at ∼845 kev is probably the same resonance as previously reported for emission of long-range α particles (α_0), and short range alphas (α_π). The small resonance at 780 kev is likely the same as that reported by Devons *et al.*[3] for nuclear pairs, and as observed in this laboratory,[22] for long-range α particles.

Table I gives a list of the resonances appearing in Fig. 2 with their cross sections. (See Sec. VI.) Except where noted, the resonance energies and widths are taken from Chao *et al.*[1] since no differences greater than the experimental resolution (∼1–2 kev) were observed between the widths and resonant energies of the low-energy and high-energy gamma rays.

[22] A. W. Schardt and W. A. Fowler (unpublished).

V. ANGULAR DISTRIBUTIONS

During the study of the excitation curves, readings of the yield were taken at both 0° and 90° with respect to the incident beam direction. At most resonances 45° and 135° intensities were also measured. At no energy was the 109-kev gamma radiation observed to be significantly anisotropic, whereas the 197-kev gamma radiation showed a distribution of the form $1+A\cos^2\theta$ with $A\geq 0$ at all energies covered in this investigation. The ratios $I_0°/I_{90°}$ are given in Table I for energies where angular distributions were measured.

The angular distribution of the gamma radiation may be readily evaluated from published formulas[23] if the distributions are calculated for separate j-values of the outgoing inelastic protons, and then combined incoherently.[13]

We assume $J=\frac{1}{2}$, even parity for F^{19} in its ground state.[24] If we assign $J=\frac{1}{2}$ to the F^{19} excited state, isotropy of the subsequent gamma radiation follows irrespective of the orbital and spin angular momenta in the earlier stages of the reaction. The consistent isotropy of the 109-kev radiation strongly suggests the assignment of $J=\frac{1}{2}$ for the 109-kev state, though isotropy of the radiation may also be caused in one of the earlier stages of the reaction.

For states of Ne^{20} with $J=2^-$, which can be formed by incoming p-wave protons with channel spin=1, we can calculate the expected angular distributions of the outgoing 197-kev radiation. If the F^{19} excited state has

[23] E.g., L. C. Biedenharn and M. E. Rose, Revs. Modern Phys. **25**, 729 (1953); or Sharp, Kennedy, Sears, and Hoyle, Chalk River Report CRT-556, 1953 (unpublished).
[24] A. P. French and J. O. Newton, Phys. Rev. **85**, 1041 (1952).

the assignment $J=5/2^+$, the radiation is of the $E2$ type, and is distributed as $(1+A\cos^2\theta)$ where $0.23\leq A\leq 0.75$, the limits corresponding to j-values of the outgoing proton of $\frac{3}{2}$ or $\frac{1}{2}$ respectively. $J=5/2^-$ for the F^{19} state would lead to isotropy of the inelastic protons since the F^{19} state could be reached from Ne^{20*} (2^-) by s-wave outgoing protons.[5] If the F^{19} excited state had the assignment $J=\frac{3}{2}^+$, it would be expected to decay by $M1$ radiation with a distribution of the form $(1+A\cos^2\theta)$ where $-0.45\leq A\leq 0$ which is clearly inconsistent with observation. It should be noted that $J=\frac{3}{2}^+$ for the F^{19} state, followed by $E2$ radiation, could give $0\leq A\leq 0.6$. This possibility is discussed later in Sec. VII. $J=\frac{3}{2}^-$, and $J\geq 7/2$ for the 197-kev state are not considered here because of lifetime considerations (discussed in Sec. VII).

It is interesting to note that the long lifetime of the 197-kev state, $\sim 10^{-7}$ sec, allows an appreciable decrease of the initial anisotropy of this state due to magnetic or electric interactions of extra-nuclear fields on the excited F^{19} nucleus. If the minimum value of A observed, 0.17, corresponds to the minimum A allowed for $J=5/2^+$ in the excited state, namely 0.23, it would appear that the anisotropy has been reduced to $\sim 7/10$ of the predicted value. This attenuation of the anisotropy is consistent with that obtained in the Coulomb excitation work,[10] and in the γ–γ correlation[19] following the β decay of O^{19}.

VI. ABSOLUTE CROSS SECTIONS

In addition to the gamma-ray yield, and the geometrical and intrinsic efficiency of the scintillation counter, the calculation of absolute cross sections requires a knowledge of the stopping cross section, ϵ, of the target material per fluorine nucleus. The value of ϵ for calcium was estimated from the known ϵ for argon as a function of energy.[25] ϵ for fluorine was interpolated from the values for oxygen and neon. Values of ϵ for fluorine determined experimentally by T. Webb and W. A. Fowler in this laboratory differ from this interpolation by only a few percent over the range of energies of the present experiment. We therefore estimate the uncertainty in ϵ for CaF_2 as less than 10 percent.

The target thickness was determined in a separate experiment on the 6- and 7-Mev gamma rays by comparing the area under the thin-target yield curve at the 873-kev resonance with the yield of a thick target. This method[26] is independent of the energy inhomogeneity of the incoming proton beam. The target employed was found to be (2.3 ± 0.1) kev thick for 873-kev protons.

The calculation of the intrinsic efficiency of the scintillation counter involves only the well-known cross sections for the photoelectric and Compton interactions of the gamma rays in the NaI crystal. Small corrections of the order of 2–6 percent were made for the "escape peaks" and for the absorption of Compton scattered quanta in the crystal which gave pulses in the full energy peak of the bias curve.

The geometrical efficiency, or solid angle calculation, involves the absorption cross section of the two gamma rays in the lead and cadmium of the collimator. We consider the resulting efficiency of the counter is accurate to better than 10 percent.

The absolute cross section for the 109-kev radiation was obtained at the 669-kev resonance from the height of the step in the excitation curve for a thick CaF_2 target of compressed powder. The cross sections at other resonances were then determined by comparing the maximum resonant yields at the peaks of the resonances using the thin target. Small corrections were made for the fact that at some narrow resonances the target thickness was an appreciable fraction of the natural width of the resonance. Corrections were also made for the change in ϵ with bombarding energy

The ratio of the peak yields of resonances will vary if the energy inhomogeneity of the beam is an appreciable fraction of the natural width of the resonance and is variable. In these measurements the ratios of peak yields were reproducible to ± 10 percent or better for varying conditions of beam resolution, focussing, etc. We conclude that our beam resolution is sufficient that it contributes little to the error in peak yield ratios except perhaps for the sharpest resonances listed. Considering all the sources of error, we have assigned probable errors to the absolute cross sections varying from 15 to 25 percent depending on the reproducibility of the experimental data and the accuracy with which the "photopeaks" in the bias curve could be separated from the continuum of pulse sizes due to background effects in the crystal.

Peterson, Fowler, and Lauritsen[17] have measured the absolute cross sections for the inelastic scattering by detecting the inelastically scattered protons in a magnetic spectrometer. These authors calibrated their spectrometer solid angle by observing Rutherford-scattered protons from copper. At $E_p=1422$ kev they give $\sigma(109\text{-kev state})=(187\pm 15)$ mb, and $\sigma(197\text{-kev state})=(7\pm 2)$ mb. These values are to be compared with the values, $\sigma(109\text{-kev state})=(189\pm 30)$ mb and $\sigma(197\text{-kev state})=(7\pm 2)$ mb, from the present investigation. Similarly, their value $\sigma(197\text{-kev state})=(42.7\pm 4.0)$ mb at the 1372-kev resonance is in good agreement with the value $\sigma(197\text{-kev state})=(40\pm 6)$ mb of the present investigation.

It is of interest to compare the nonresonant cross sections listed in Table I at 740- and 1045-kev proton energy with the values expected from Coulomb excitation of these states by protons. As we show in Sec. VII, we take the assignments of the two excited states to be: 109 kev, $\frac{1}{2}^-$; 197 kev, $5/2^+$.

Employing the terminology of Bohr and Mottelson,[27]

[25] Reynolds, Dunbar, Wenzel, and Whaling, Phys. Rev. **92**, 742 (1953); Chilton, Cooper, and Harris, Phys. Rev. **93**, 413 (1954).

[26] Bernet, Herb, and Parkinson, Phys. Rev. **54**, 398 (1938); Fowler, Lauritsen, and Lauritsen, Revs. Modern Phys. **20**, 236 (1948).

[27] A. Bohr and B. R. Mottelson, Kgl. Videnskab. Selskab, Matfys. Medd. **27**, No. 16, (1953).

we can express the cross section for $E2$ excitation of a 5/2 level as

$$\sigma=\frac{2\pi^2}{25}\frac{1}{Z_2^2e^2}\left(\frac{Mv_f}{\hbar}\right)^2 B_{E2(\frac{1}{2}\to\frac{5}{2})}g_{E2}(\xi),$$

where $Z_2=9$ for F^{19}, M is the proton mass, v_f is the velocity of the outgoing proton, and $g(\xi)$ is a function of the velocities and charges of the nuclei involved which has been calculated by Alder and Winther.[28] We have taken $\xi=n_2-n_1$ where $n_1=Z_1Z_2e^2/\hbar v_i$ and $n_2=Z_1Z_2e^2/\hbar v_f$.

If we take the value of $B_{E2(\frac{1}{2}\to\frac{5}{2})}$ from the directly measured lifetime of $\sim10^{-7}$ sec for the 5/2 state of F^{19}, we have $B_{E2(\frac{1}{2}\to\frac{5}{2})}=3B_{E2(\frac{5}{2}\to\frac{1}{2})}=2.0\times10^{-69}$. The calculated cross sections are 1.4×10^{-28} cm² at 740-kev incident energy, and 2.9×10^{-28} cm² at 1045-kev proton energy. These are in good agreement with the observed values, namely $(1.4\pm0.5)\times10^{-28}$ cm² and $(3\pm1)\times10^{-28}$ cm².

Similarly we calculate the cross sections for $E1$ excitation of a $\frac{1}{2}^-$ state from the formula[28]

$$\sigma=\frac{2\pi^2}{9\hbar^2}\frac{Z_1^2e^2}{v_i^2}B_{E1(\frac{1}{2}\to\frac{1}{2})}g_{E1}(\xi).$$

Employing the B calculated from the observed lifetime of $\sim10^{-9}$ sec, we have $\sigma=7\times10^{-30}$ cm² at 740 kev, and $\sigma=9\times10^{-30}$ cm² at 1045 kev. These values are clearly much smaller than the experimentally observed values of $(1\pm0.4)\times10^{-28}$ cm² and $(1\pm0.4)\times10^{-27}$ cm² respectively.

These large values observed for the excitation cross section of the 109-kev state, may be attributed to the formation of very broad 0^+ states of Ne^{20}, which can decay by p-wave proton emission to the $\frac{1}{2}^-$ state but would require d-wave proton emission to decay to the 197-kev state.

If the excitation of the 197-kev state at 740 kev, and 1045-kev proton energy proceeds mainly by Coulomb excitation, the angular distribution of the gamma radiation may be predicted. The $I_{0°}/I_{90°}$ ratios calculated for the 197-kev excitation are 1.28 and 1.25 respectively. If there is some attenuation of the anisotropy due to lifetime effects (see Sec. V), these ratios should be reduced to about 1.19 and 1.17. While these values are not inconsistent with those of Table I, the experimental ratios are not sufficiently accurate to justify any conclusions.

The isotropy of the 109-kev radiation at 740 and 1045 kev is consistent with the suggested assignment of $J=\frac{1}{2}$ to this state. Further work is in progress to measure the cross sections and angular distributions of the nonresonant gamma radiation as a function of energy.

[28] K. Alder and A. Winther, Phys. Rev. **91**, 1578 (1953); **96**, 237 (1954).

VII. SPIN AND PARITY OF THE LOW LYING STATES OF F^{19}

In our earlier series of papers on the assignment of spin and parity to the F^{19} states[5,10,12,13] we suggested the assignments of spin $\frac{1}{2}^-$ and $5/2^+$ for the 109-kev and 197-kev states, respectively. In this section of the present paper we shall merely review the arguments for the sake of completeness. A similar discussion is given in a paper by Sherr, Li, and Christy.[10]

The experimental data on which the assignments were based include:

(a) The excitation function of the radiation from inelastic proton scattering.

(b) The angular distribution of the inelastically scattered protons.

(c) The angular distribution of the 109 and 197 kev gamma radiation.

(d) The mean lifetime[12] of the gamma rays: 109 kev, $\sim10^{-9}$ sec; 197 kev, $\sim10^{-7}$ sec; 88 kev, $\geqslant10^{-5}$ sec.

(e) The transition probability for the 109-kev and 197-kev transition as determined from Coulomb excitation by α particles.[10]

(f) The angular distribution of the Coulomb-excited gamma radiation.[10]

The directly measured lifetimes immediately suggest that the multipolarities of the gamma-ray transitions are limited as follows:

197 kev—not higher than $E2$;

109 kev—not higher than $M1$ or $E1$;

88 kev—not lower than $E2$.

Taking the ground state of F^{19} as $\frac{1}{2}^+$, we are then lead to the possible assignments: 197-kev state, $5/2^+$, $\frac{3}{2}^\pm$, $\frac{1}{2}^\pm$; 109-kev state, $\frac{3}{2}^\pm$, $\frac{1}{2}^\pm$. The $\frac{1}{2}^\pm$ and $\frac{3}{2}^\pm$ assignments for the 197-kev state would be expected to lead to $M1$ or $E1$ radiation which would be several orders of magnitude faster than the observed transition and would thus require to be forbidden by an improbably large factor, $\geq10^4$. In addition, the angular distribution of the 197-kev gamma radiation requires $E2$ de-excitation in both the proton and α particle experiments. Furthermore $\frac{1}{2}^\pm$, $\frac{3}{2}^\pm$ assignments to the 197-kev state would allow the 88-kev transition to a $\frac{1}{2}$ or $\frac{3}{2}$ state at 109 kev to be $E1$ or $M1$, requiring that the 88-kev gamma-ray transition probability also be reduced by a factor $\geq10^4$. In view of these limitations, we consider the assignment $5/2^+$ to be the only reasonable assignment to the 197-kev state. A comparison of the observed lifetime and the cross section for Coulomb excitation by α particles,[10] also leads directly to an $E2$ assignment for both excitation and de-excitation of this level, further strengthening the $5/2^+$ assignment.

Of the possible assignments for the 109-kev state, the $\frac{1}{2}$ assignment is suggested by the isotropy of the 109-kev gamma ray in both the proton and α particle work. $\frac{3}{2}^\pm$ would require the reduction of the $M1$ or $E1$ 88-kev transition probability from the $5/2^+$ state by an im-

TABLE II. Partial widths of certain $F^{19}+p$ resonances below 1650-kev proton energy. All Γ's in laboratory coordinates. [$\Gamma_{c.m.}=(19/20)\Gamma_{lab}$]. A dash indicates not observed—no upper limit available. An x indicates not observed—forbidden by J and π considerations.

E_{res} (kev)[a]	Ne^{20} J,π	Γ (kev)[a]	Γ_{p_0} (ev)	Γ_{p_1} (ev)	Γ_{p_2} (ev)	Γ_{α_0} (ev)	Γ_{α_π} (ev)	Γ_{α_1} (ev)	Γ_{α_2} (ev)	Γ_{α_3} (ev)	Γ_{α} 12 Mev γ's (ev)
340	1, +[b]	2.9[j]	45	<0.5	<0.1	x	x	2800	16	75	≤1.6[e]
669	1, +[d]	7.5	7300	46	<0.5	x	x	110	0.4	25	2.4[e]
935	1, +[d]	8.0	1400	3000	<20	x	x	2800	100	780	~1,[f] ≤1.8[e]
1422	1, +[g]	14.6	12 400	2200	≤35	x	x		total <40		4.5[e]
598	2, −[h]	37	43	<500	<500	x	x	37 000	<100	<100	<21[e]
873	2, −[d]	5.2	1100	<2	570	x	x	2400	850	300	~1,[f] ≤1.9[e]
1346	2, −[g]	4.5	300	300	600	x	x	1800[i]	450[i]	1050[i]	≤2[e]
1372	2, −[g]	15	2500	700	1400	x	x	9100	840	520	~3,[f] ≤8[e]
483[j]		2.2[j]	~11/ω	<1.5	<1.5	—	—	~1700	~30	~450	—
720[k]		~30	~2/ω	<10 000	<10 000	~20 000	~10 000	—	—	—	—
780[k]		~10	~14/ω	<400	~9000	~400	~50	—	—	—	—
831		8.3	~65/ω	<6	~2300	—	—		total ~5400		—
843	(0, +)[l]	23	~23 000	~50	<10	~5	~33	—	—	—	—
900		4.8	~65/ω	<30	~2200	—	—	~2500	<130		—
1137		3.7	~50/ω	<40	~2100	—	—		total ~1600		—
~1250		~80	~700/ω	~70 000	<4000	—	~10 000	—	—	—	—
1290	(3, +)[m]	19	~150	<600	~900	—	—	~13 000	~1300	~3200	—

[a] Resonance widths, energies, from Table I. α_1, α_2, α_3 data from Chao *et al.*, reference 1; J. M. Freeman, Phil. Mag. 41, 1225 (1950); Seed and French, reference 3; and Peterson *et al.*, reference 17.
[b] Barnes *et al.*, Arnold, reference 3.
[c] A. B. Clegg (private communication).
[d] Seed and French, reference 3.
[e] Sinclair, reference 4, cross sections corrected to $(p,\alpha\gamma)$ cross sections of Chao *et al.*[1]
[f] Hahn and Kern, reference 4.
[g] References 5, 6, 2.
[h] Seed and Dearnley, quoted by D. H. Wilkinson and A. B. Clegg (private communication).
[i] (p,α) cross section measured by comparison with 1372-kev resonance cross section.
[j] S. E. Hunt, Proc. Phys. Soc. (London) A65, 982 (1952).
[k] $(p,\alpha\gamma)$ cross sections estimated from 843-kev cross section of Chao *et al.*[1] and excitation function of Devons *et al.*, reference 3. (p,α_0) from unpublished work of A. W. Schardt and W. A. Fowler.
[l] From elastic scattering.
[m] Chao, reference 3.

probably large factor, $\geq 10^4$. An assignment of $\frac{1}{2}^+$ to the 109-kev state would mean that the $E2$ transition from the 197- to the 109-kev state would be expected to have a lifetime $\approx (197/88)^5\times 10^{-7}\approx 5\times 10^{-6}$ sec. While this is below the lower limit observed experimentally for the 88-kev transition lifetime, a stronger argument against the $\frac{1}{2}^+$ assignment comes from combining the knowledge of the lifetime of the 109-kev state with the Coulomb excitation cross section of Sherr, Li, and Christy.[10] If the Coulomb excitation is assumed to be $M1$, then the observed absolute cross section predicts a lifetime of the order of 10^{-12} sec, as compared with the observed lifetime of 10^{-9} sec. $E1$ excitation, on the other hand, yields good agreement between the measured and predicted lifetimes.

We therefore conclude that the most reasonable explanation of the experimental results cited, is the assignment, 109-kev state, $\frac{1}{2}^-$; 197-kev state, $5/2^+$. Since the publication of our earlier papers, an independent check of these assignments has been made.

Jones, Phillips, Johnson, and Wilkinson[19] have reexamined the β decay of Ne^{19} and O^{19} in detail, and they have also studied the α-particle Coulomb excitation of F^{19}. The F^{19} assignments which they conclude are necessary to explain their results, are in agreement with our work.

The occurrence of a $5/2^+$ state is not too surprising for this nucleus as some, or all, of the nucleons outside the O^{16} core are probably in $d_{\frac{5}{2}}$ orbits. It has been pointed out that the ground state magnetic moment may be explained as well by the $(d_{\frac{5}{2}}{}^3)_{\frac{1}{2}}$ assignment as by the more usual assignment $2s_{\frac{1}{2}}$.

At first sight the occurrence of an odd parity state, so close as 109 kev to the ground state, might seem a little surprising. It has been pointed out by Christy and Fowler[29] that the $\frac{1}{2}^-$ state may be considered as a hole in the $p_{\frac{1}{2}}$ shell with the four nucleons outside the p-shell being coupled to give $T=J=0$. From empirical mass considerations it can be shown that the strong binding of the four outside nucleons compensates in large measure for the energy required to make a hole in the p shell.

VIII. COMPETING MODES OF DECAY OF THE Ne^{20} COMPOUND NUCLEUS

On the basis of the known (p,α) cross sections, Chao *et al.*[1] made an analysis of the $F^{19}+p$ resonances into partial widths. Since their analysis, the following new data have become available: (i) the inelastic scattering cross sections of the present paper; (ii) J and parity values for many of the resonances; (iii) radiative capture cross sections; (iv) elastic scattering studies.[30] A recalculation of partial widths incorporating the new

[29] R. F. Christy and W. A. Fowler, Phys. Rev. 96, 851(A) (1954).
[30] The writer is indebted to Webb, Hagedorn, Fowler, and Lauritsen, for communicating their experimental results to him before publication. The writer is also indebted to E. Baranger for discussions of her calculations based on the elastic scattering data.

data is presented in Table II. The (p,α) reaction data is taken from Chao *et al.*[1] except where noted.

If Γ_R is the total partial width for all reactions except elastic scattering, and Γ_{p0} is the partial width for re-emission of the incident proton, we can write the Breit-Wigner dispersion formula for the cross section at resonance in the form

$$\sigma_{\text{Reaction}}=4\pi\lambda^2\omega\Gamma_{p0}\Gamma_R/\Gamma^2,$$

where

$$\omega=(2J+1)/(2s+1)(2i+1).$$

J is the total angular momentum of the compound nucleus, and s and i are the intrinsic spin of the incoming particle (proton), and the total angular momentum of the target nucleus respectively. $\Gamma(=\Gamma_{p0}+\Gamma_R)$ is the resonance width, a directly measured quantity. If ω is known, the measurement of σ_{Reaction} and Γ leads to two sets of values of Γ_{p0} and Γ_R. The study of the elastic scattering will remove the ambiguity, in general, since the magnitude of the scattering anomaly, due to the interference of resonant and Rutherford scattering, depends on Γ_{p0}/Γ. Where the elastic scattering does not show an appreciable anomaly, we have taken the smaller of the two possible values of Γ_{p0}/Γ as being correct. In the case of narrow resonances such as the 1092-kev resonance, it is possible that an elastic scattering interference anomaly might have been missed due to the averaging produced by the finite experimental resolution. On the other hand, resonances several hundred kev wide would give rise to such broad elastic scattering anomalies that the identification of the anomalies would become difficult.

It should be pointed out that there is considerable divergence in the published literature on the cross-section values for the (p,α) reactions, particularly for the (p,α_π) and (p,α_0) resonances. The partial widths for these processes in Table II are subject to corresponding uncertainties, which may be as high as a factor 3 for the (p,α_π) and (p,α_0) partial widths.

Known $(p,\alpha_{1,2,3})$ resonances at 222, 486, 1092, and 1176 kev, (p,α_π) resonances at 1130 and 1367 kev, (p,α_0) resonances at 1100 and 1380, and (p,γ) resonances at 980, and 1324 have been omitted from Table II, due to lack of knowledge regarding widths, cross sections, and competing modes of decay. In addition we have not included the region near 1700 kev as there are several $(p,\alpha_{1,2,3})$, (p,α_0), and (p,α_π) resonances close together in energy, and the inelastic scattering and elastic scattering data are not subject to clear interpretation.

The resonance at 1610 kev appears to decay entirely by emitting inelastic protons to the 109-kev state. If it is true that no other reaction takes place at this resonance, an assignment of $J=0$, odd parity, would seem to be indicated for the state of Ne involved. Further investigation of this region, for the emission of alpha particles, is in progress.

Little can be said at our present stage of knowledge regarding the observed partial widths listed in Table II. The first half of the table concerns the resonances for which J and parity (π) are known, and these resonances form a reasonably consistent set.

The earlier failure to observe capture radiation at 935 kev and 340 kev finds a natural explanation in the small value of Γ_{p0}/Γ, which enters the expression for the resonant cross section for radiative capture. The close spacing of levels in F^{20} in the energy region corresponding to the present energy region in Ne^{20}, indicates that there are many $T=1$ states present. It may be that the small widths for α emission of the 1422-kev $(1,^+)$ and the 843-kev $(0,^+)$ states are due to this cause. Wilkinson and Clegg (Table II, reference h) have suggested that the low yield of $E1$ capture gamma rays at 598 kev and 873 kev, brands these as $T=0$ levels. The same argument applies to the 1346- and 1372-kev (2^-) levels, although small radiative widths for these four levels can arise from other causes. The small α_0 and α_π width of the 780-kev resonance would be consistent with either a $T=1$ assignment or a high value of J. The preference of this state for inelastic scattering to the $5/2^+$ state of F^{19} indicates that the latter alternative is probably correct. It seems probable that all the observed (p,α_0) resonances have $T=1$ and/or high J values, since the resonances would probably be so broad as to be unobserved in the absence of some inhibiting factor.

E. Baranger has computed reduced widths for the resonances with known J-values, and these will be included in a forthcoming publication.

IX. ACKNOWLEDGMENTS

It is a pleasure to acknowledge my indebtedness to C. C. Lauritsen, W. A. Fowler, R. F. Christy, R. Sherr, and T. Lauritsen for assistance in the experimental work and many helpful discussions of the data. The writer is also indebted to the California Institute of Technology for the award of a Research Fellowship, and to the University of British Columbia for granting leave of absence.

Search for Double Beta Decay in Ca^{48}†

JOHN A. MCCARTHY*
Massachusetts Institute of Technology, Cambridge, Massachusetts
(Received June 11, 1954; revised manuscript received November 29, 1954)

If double beta decay occurs without the emission of neutrinos, the total kinetic energy of the two emitted electrons is constant. An experiment has been performed using this constancy of energy and the coincidence nature of the activity in an attempt to observe and identify this process in Ca^{48}.

The results show a peak in the total energy spectrum at 4.1±0.3 Mev. Mass spectrographic data gives 4.3±0.1 Mev as the available energy for double beta decay. The author believes this to be evidence for double beta decay without neutrino emission unless the observed counts are due to an unusual phenomenon of unknown origin.

INTRODUCTION

DOUBLE beta decay (hereafter referred to as $\beta\beta$ decay) is a process which can be important as a mode of decay only in the even-A, even-Z isotopes, and then only when an isotope (which does not have the minimum atomic mass in its isobaric series) cannot go to its neighboring odd-Z isobar by simple beta decay or K capture with a lifetime shorter than about 10^{17} years. This situation occurs in the cases of the "stable" isobaric triplets ($A=96$, 124, 130, and 136) and in most of the isobaric doublets (some probable cases are $A=48$, 110, 116, and 150).

The process is the simultaneous emission of two electrons (or positrons) which may or may not be accompanied by two neutrinos. The question of whether or not neutrinos are emitted is an important one since the answer would afford an indirect method of study of that particle, and particularly since it allows an experimental choice between two theories regarding the nature of the neutrino.

The first theory[1] requires that the neutrino (ν) and the antineutrino (ν') are distinctly different particles, one of which is emitted with the electron and the other with the positron. We shall only consider electron emission here, so that the process could be written $n\rightarrow p+e^-+\nu'$, where n is the neutron in the nucleus which changes to the proton p, e^- is the emitted electron and ν' is the antineutrino. Since the emission of an anti-neutrino would be equivalent to the absorption of a neutrino, we might also have the process $\nu+n\rightarrow p+e^-$, but the process $\nu'+n\rightarrow p+e^-$ is forbidden.

In $\beta\beta$ decay involving the emission of two electrons, two neutrons in the nucleus change to two protons. Considering this as a two-step process, the first step would be $n\rightarrow p+e^-+\nu'$ and the second must also be $n\rightarrow p+e^-+\nu'$, since the antineutrino emitted in the first step cannot be absorbed in the second. Thus the overall process becomes $2n\rightarrow 2p+2e^-+2\nu'$. This has two experimental consequences:

(1) The electrons would carry off only part of the available energy of the transition and would therefore have a continuous energy spectrum.

(2) The lifetime of the process would be of the order of 10^{24} years, which is not detectable with currently available experimental equipment.

The second theory[2,3] postulates the existence of only one type of neutrino, which can be either emitted or absorbed in any beta decay process. $\beta\beta$ decay can then take place according to the following scheme: $n\rightarrow p+e^-+\nu$ first, followed by $\nu+n\rightarrow p+e^-$. In this case the neutrino is virtual. For the entire process we may write $2n\rightarrow 2p+2e^-$. We have the following experimental predictions for this reaction:

(1) The two electrons would carry off all of the energy available for the transition (neglecting the recoil energy of the nucleus), so that the total kinetic energy of the electrons would be constant.

(2) The lifetime of the process would be of the order of 10^{17} years for a total available energy of about 5 Mev. (A correction of the order of 10^3 has been made to compensate for the fact that the process is more analogous to allowed beta decay than to superallowed decay.)

In spite of the long lifetime, this latter type of activity should be detectable if we take advantage of the first experimental property. This property was used in an earlier experiment[4] in an attempt to investigate the possible decay of Zr^{96}. The experiment reported herein used the coincidence nature of the activity in combination with the constancy of the energy in an attempt to observe and identify $\beta\beta$ decay in Ca^{48}. Ca^{48} was chosen for its large available energy for the transition (4.3±0.1 Mev plus the rest mass energy of the electrons)[5] and because of the availability of the separated isotope.

THE EXPERIMENT

Although the geometry and over-all method used in this experiment were similar to the earlier experiment,[4]

† Work performed under the auspices of the joint program of the U. S. Office of Naval Research and the U. S. Atomic Energy Commission.
* Now at Bell Telephone Laboratories, Murray Hill, New Jersey.
[1] M. Goeppert-Mayer, Phys. Rev. **48**, 512 (1935).
[2] W. H. Furry, Phys. Rev. **56**, 1184 (1939).
[3] H. Primakoff, Phys. Rev. **85**, 888 (1952).
[4] J. A. McCarthy, Phys. Rev. **90**, 853 (1953).
[5] Collins, Nier, and Johnson, Phys. Rev. **86**, 408 (1952).

the equipment was considerably different, hence a brief description will be given.

Two scintillation counters (consisting of plastic phosphors mounted on RCA 5819 photomultipliers), each subtending a solid angle, averaged over the source, of 1.8π, were placed on opposite sides of the source. The outputs of these counters were amplified and added electronically. The resultant pulse height was recorded on an Esterline Angus chart recorder whenever a coincidence occurred. Provision was also made for simultaneous recording of all activity without regard to its coincidence or noncoincidence nature.

The equipment was shielded by 1 in. of steel and 3 in. of lead during the early part of the experiment, and during the later part of the experiment was shielded by $\frac{1}{8}$ in. of steel, 3 in. of lead and the mass of the John Hancock Life Insurance Company building, a 571 foot office building. (The later part of the experiment was performed in the sub-basement of the building, 35 feet below ground level.) Further background reduction was accomplished by an arrangement of Geiger tubes in anticoincidence with the scintillation counters.

78 milligrams of Ca in the form of $CaCO_3$ enriched to 84.3 percent Ca^{48} was used.[6] The background measurements were made with a similar sample of Ca containing 97.9 percent Ca^{44} and 0.01 percent Ca^{48}.[7] The samples were mounted between pieces of 1-mil (0.001-in.) aluminum foil. A small amount (about 5 milligrams per square centimeter) of Polyweld, a polystyrene in Xylene organic compound, was used as a binder for the $CaCO_3$. Each sample covered an area of 4.3 cm^2. They were mounted on a wheel so that they could be alternately placed in the counting position without otherwise disturbing the equipment. Such alternation was performed at intervals of approximately 20 hours.

During the portion of the experiment performed in the John Hancock building, the sample identifications were coded by Professor J. W. Rosengren and the key to the code was withheld from the author until the conclusion of the experiment to eliminate possible (but carefully guarded against) "bias effects."

Although the total activity background was too high for the use of total activity data as a significant part of the results of this experiment, such data were taken during part of the experiment and are included as additional evidence against some types of possible contamination.

RESULTS

The results of the portion of the experiment performed in the John Hancock building are presented in Fig. 1 to illustrate the energy spectrum of the background coincidence activity and the method of treatment of the data. The background (Ca^{44}) activity measurements are identified by the dashed line which connects the experimental points. The total number of coincidence events during 230 hours whose total energy lies within an energy interval is plotted at the midpoint of the energy interval. Standard deviations are given for purposes of illustration on two representative points.

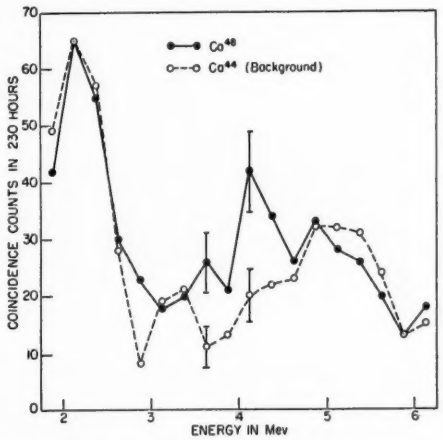

FIG. 1. Coincidence activity observed in the John Hancock Building with Ca^{48} and with Ca^{44} samples. The dashed line identifies the activity with the Ca^{44} sample in position and the solid line identifies the activity with the Ca^{48} sample in counting position.

The low-energy activity is due primarily to natural activity in the surroundings. The broad peak in the neighborhood of 5.5 Mev is primarily due to high-energy particles (probably cosmic in origin) crossing the equipment.

The coincidence activity with the Ca^{48} sample in the counting position is identified by a solid line connecting the experimental points. This activity is, in general, similar to the background activity except in the region near 4 Mev, where the activity is considerably higher than the background. The earlier portions of the experiment showed a similar effect at about 4 Mev but in the earlier runs the background was higher than that shown in Fig. 1 by a factor of 4.

All of the coincidence data were collected and the background, as measured with the Ca^{44} sample, was subtracted from the activity measured with the Ca^{48} sample. Any significant difference, then, is presumably due to activity originating in the Ca^{48}, since the chemical combination, masses and positions of the samples were similar. The difference is presented in Fig. 2, with standard deviations given for each point. This figure represents the difference between the coincidence activity observed in 755 hours with the Ca^{48} sample and that observed in 755 hours with the Ca^{44} sample (in alternating runs, as explained above). The actual number of counts is given. Between 3.75 and 4.5 Mev, for example, there were 595 coincidences in 755 hours with the Ca^{48} sample in counting position and 455 coinci-

[6] This sample was obtained from Professor H. W. Fulbright of the University of Rochester with the consent of the Isotope Division, Oak Ridge National Laboratory, which had performed the isotopic separation and loaned the sample to Professor Fulbright.

[7] This sample was obtained from the Isotope Division, Oak Ridge National Laboratory.

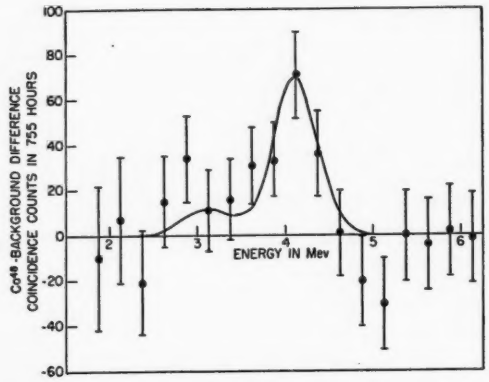

FIG. 2. Difference between coincidence activity with the Ca^{48} sample in position and with the Ca^{44} sample in position in 755 hours of counting with each sample. The curve drawn in indicates the predicted curve if $\beta\beta$ decay occurs with a lifetime of 1.6×10^{17} years.

dences with the Ca^{44} sample in position; the total difference in these three points is therefore 140 counts as shown (33+71+36).

A smooth curve has been drawn in the figure to indicate the predicted energy spectrum if $\beta\beta$ decay occurs in Ca^{48} with a lifetime of 1.6×10^{17} years and an energy release (excluding the rest masses of the electrons) of 4.1 Mev. In calculating this curve, the coincidence efficiency of the equipment was calculated to be $\frac{1}{3}$ (0.4 over-all geometric efficiency assuming isotropy and 0.8 transmission efficiency). In constructing the smaller peak at 3.1 Mev, the assumption was used that the nuclear matrix element in $\beta\beta$ decay of Ca^{48} to the first excited state of Ti^{48} was the same as that to the ground state. This assumption is good only to within a factor of 4 at best in predicting the proper area under the peak (and therefore, of course, the proper height of the peak).

Figure 3 is a similar difference graph for the total

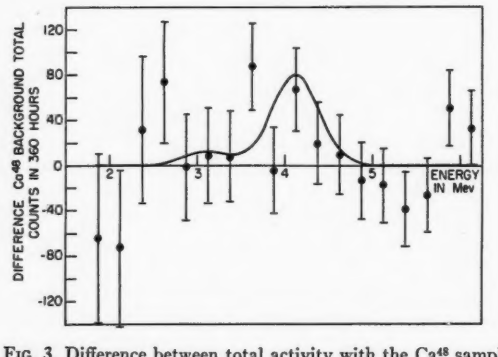

FIG. 3. Difference between total activity with the Ca^{48} sample in position and with the Ca^{44} sample in position in 360 hours of counting with each sample. The curve drawn in indicates the predicted curve if $\beta\beta$ decay occurs with a lifetime of 1.6×10^{17} years.

activities observed with the samples in 360 hours each without regard to their coincidence or noncoincidence nature. This is included not to indicate any evidence for or against $\beta\beta$ decay, but as evidence against some possible types of activity other than $\beta\beta$ decay.

DISCUSSION

The only known type of activity, other than $\beta\beta$ decay, which would result in a coincidence activity with a peaked energy spectrum when investigated with this experimental equipment is internal pair production. This seems a rather unlikely alternative, since it requires an unusual type of activity produced presumably by an unknown and otherwise undetected contaminant, but it must be admitted as a remote possibility. Another possibility is of course experimental error.

If this is $\beta\beta$ decay, the lifetime is $(1.6 \pm 0.7) \times 10^{17}$ years. The large uncertainty in the lifetime reflects our lack of knowledge of the exact individual electron energy spectrum and of the angular distribution, although the effect of the latter is largely eliminated by multiple scattering in the source. The efficiency of the coincidence equipment is sensitive to these two factors.

The peak is observed at an energy of 4.1 ± 0.3 Mev, which is in good agreement with the mass spectrographic data[5] (as stated above, these data give 4.3 ± 0.1 Mev as the proper energy for $\beta\beta$ decay of Ca^{48}). The statistical probability of observing the peak shown in Fig. 2 purely by chance in the proper energy region if it is not actually present is less than 1 chance in 10^6.

CONCLUSION

The results presented here, particularly if considered in conjunction with the Zr^{96} evidence,[4] seem to the author to furnish significant evidence that $\beta\beta$ decay can occur without the emission of neutrinos. However, it should be noted here that the experimental results of Inghram and Reynolds[8] do not seem to be compatible with this viewpoint, so that an area of disagreement exists. These latter results[8] do not agree with the theory requiring the emission of neutrinos either, but give a value for the lifetime lying approximately halfway between the predictions of the two theories.

The author would like to take this opportunity to thank Professor Martin Deutsch, whose advice, suggestions, and criticism were invaluable in the performance of this experiment. He is also indebted to Professor H. W. Fulbright of the University of Rochester for his generous cooperation in the loan of the Ca^{48} sample, to the officials of the John Hancock Mutual Life Insurance Company, to Professor J. W. Rosengren, and to the many others who helped and advised him in the course of the experiment.

[8] M. G. Inghram and J. H. Reynolds, Phys. Rev. **78**, 822 (1950).

Nuclear Reactions in Stars. II. Protons on Light Nuclei*†

E. E. SALPETER
Newman Laboratory of Nuclear Studies, Cornell University, Ithaca, New York
(Received October 11, 1954)

The rates are calculated for thermonuclear reactions involving the collision of a proton with various light nuclei. These calculations are based directly on low-energy experiments for deuterium, Li, Be, and B, partly on experiments for O^{16}, and purely on theoretical estimates for the other isotopes of O, F, Ne, and Na.

Temperatures are calculated at which D, Li, Be, and B are effectively destroyed by these reactions, both in the interior of young and cool stars which are still contracting gravitationally and in the outer layers of main sequence stars. It is shown that in the interior of even a hot main sequence star only O^{18} and F^{19} (and possibly O^{17}) are destroyed of all the isotopes heavier than nitrogen.

1. INTRODUCTION

THE present paper is a continuation of a previous one[1] (hereafter referred to as I), forming part of a series on the various thermonuclear reactions which might take place in the interior of various stars. We shall deal mainly with the calculation of reaction rates as a function of temperature, density and chemical composition, but a short explanation of their astrophysical significance may be in order.

Hydrogen is the main constituent of most stars and of the gas from which they were presumably formed. Consequently, nuclear reactions involving the capture of protons by various nuclei are most important for stars. The main source of energy in the less luminous main sequence stars (sun and cooler) is the proton-proton chain, involving as its initial step the collision between two protons. This chain of reactions was discussed in detail in I. The main energy source of the more luminous (hotter than sun) main sequence stars is the carbon cycle, involving the capture of protons by the stable isotopes of carbon and nitrogen. A discussion of this reaction cycle should follow I, logically, but Fowler[2] has recently given a detailed discussion of our present knowledge of these reaction rates. We shall only quote Fowler's results briefly in Sec. 4.

The reaction rate for the capture of protons by nuclei of charge Z depends very strongly on Z. This rate is of the right order of magnitude to explain the energy production and lifetime of main sequence stars for $Z=6$ or 7 (carbon-nitrogen cycle). Bethe[3] pointed out long ago that for $Z<6$ the reaction rate is so fast that these elements are burned out in a main sequence star in a time very much shorter than the age of our galaxy[4] (several billion years). For $Z>7$, on the other hand, the rate is so slow that the corresponding rate of energy production is negligible. These conclusions are still essentially correct, but it is nevertheless of some interest to investigate reactions for $Z<6$ and $Z>7$, for the following reasons.

(*a*) $Z<6$: Many astrophysical observations are and will be carried out on star associations and other regions which contain stars formed extremely recently (on an astronomical scale), some as young as a million years. Many such stars have not yet had time for their gravitational contraction from a cold gas cloud to the main sequence, and may have low enough density and temperature for reactions involving D, Li, Be, and B to go on. These reactions would be an important energy source in such stars and, conversely, astrophysical observations may lead to information on the original abundance of these light elements in the gas clouds from which these stars were formed. At present there is some direct data on chemical abundances in stellar atmospheres, but rather little on abundances in interstellar gas.

(*b*) $Z>7$: Since the abundance of oxygen in stars is only of order 1 percent (and the abundance of heavier nuclei much smaller still) and since the reaction rates are very slow, these reactions are certainly negligible as sources of energy production in most stars. But, in connection with detailed theories on the origin of the chemical elements, it may be important to know whether an appreciable fraction of the original content of these elements is burned up in the interior of a hot main sequence star or not. We shall discuss reactions on O, F, Ne, and Na in Secs. 4 and 5.

We shall use the notation of I. Most of this paper will be concerned with the derivation from experiments (or theoretical estimates) of the cross-section factor S, defined by (S and E in laboratory system of measurement)

$$S=\sigma(E)E\exp(2\pi e^2Z_1Z_2/\hbar v), \tag{1}$$

extrapolated to the very low energies E of the "stellar energy region" (a few to 50 kev). Once S is known, the mean reaction rate p is obtained very simply (I, Sec. 1) from

$$p=430(\rho x_1)S(A_1^2Z_1Z_2)^{-1}\tau^2e^{-\tau}\ \text{sec}^{-1},$$
$$\tau=42.48[Z_1^2Z_2^2A_1A_2/(A_1+A_2)]^{\frac{1}{3}}T^{-\frac{1}{3}}. \tag{2}$$

* Supported in part by the joint program of the Office of Naval Research and the U. S. Atomic Energy Commission.

† This work was done partly at the Australian National University, Canberra, Australia.

[1] E. E. Salpeter, Phys. Rev. 88, 547 (1952).

[2] W. A. Fowler, Mem. Soc. Roy. Sci. Liège 13, 88 (1954).

[3] H. A. Bethe, Phys. Rev. 55, 434 (1939).

[4] The p-p reaction is slow enough, even though $Z=1$, because it involves a beta decay instead of γ or α emission.

The cross-section factor S is in units of ev-barns and the temperature T in 10^6 °K.

2. REACTIONS INVOLVING DEUTERONS

In I, Sec. 4, we have already discussed reactions involving deuterons going on in the interior of main sequence stars. Here we are concerned with the interior of young stars, with lower density and temperatures only of the order of 10^6 °K. In such cases, there has not been time to reach the dynamic equilibrium, discussed in I, and the abundance of deuterium may still be appreciable. There are a number of competing reactions and the end result, at these temperatures, of each reaction is the conversion of D into He^3. But the energy release per deuteron is different for the various reactions, discussed below.

(*A*) The direct conversion of D into He^3 by proton capture,

$$H^1+D^2\rightarrow He^3+\gamma+5.51 \text{ Mev}, \tag{3}$$

has already been discussed in I, Sec. 5. The cross-section factor derived there (including the correction mentioned in a footnote) is

$$S_p=(11.7\pm4.0)\times10^{-2} \text{ ev barns}. \tag{4}$$

(*B*) If the abundance of deuterium is at all appreciable we also have to consider reactions involving two deuterons,

$$D^2+D^2\rightarrow T^3+H^1+4.03 \text{ Mev}, \tag{5a}$$

$$D^2+D^2\rightarrow He^3+n+3.27 \text{ Mev}. \tag{5b}$$

These reactions have been investigated[5,6] carefully for deuteron energies between 20 and 250 kev. The rates of the two reactions (5a) and (5b) are very nearly the same. The total experimental cross-section factor S, Eq. (1), increases very slowly with energy, being about 2.2 and 2.6 ($\times10^5$ ev barn), respectively, at 25 and 150 kev. We adopt as cross-section factor, for reactions (5a) and (5b) combined,

$$S_D=(2.1\pm0.5)\times10^5 \text{ ev barns}. \tag{6}$$

Substituting the values for S, Eqs. (4) and (6), into Eq. (2) we find for the mean reaction rates for reactions (3) and (4), respectively (with T in 10^6 °K)

$$p_p=(7.0\pm2.5)\times10^4(\rho x_H)\exp(-37.2/T^{\frac{1}{3}})T^{-\frac{2}{3}}, \tag{7}$$

$$p_d=(4.0\pm0.7)\times10^{10}(\rho x_D)\exp(-42.6/T^{\frac{1}{3}})T^{-\frac{2}{3}}. \tag{8}$$

$$p_d=(4.0\pm0.7)\times10^{10}(\rho x_D)\exp(-42.6/T^{\frac{1}{3}})T^{-\frac{2}{3}}$$

Since the value of S is very much larger for the D−D reaction (involving particle emission instead of γ-ray emission), the D−D reaction predominates if the abundance (by mass) of deuterium, x_D, is larger than a small fraction of a percent. The values of (x_D/x_H), for which the reaction rates, Eqs. (7) and (8), are equal, are 2×10^{-3}, 5×10^{-4}, and 2×10^{-4}, respectively, for $T=0.5$, 1, and 2. The value of (x_D/x_H) both in sea water and in meteorites[7] is 1.5×10^{-4}, but could be larger (or smaller) in interstellar gas.

At temperatures T between 0.5 and 2, the He^3 produced in reaction (3) is essentially stable, being converted into He^4 at an appreciable rate only for $T>5$. The tritons produced in reaction (5a) decay into He^3 with a half-life of 12 years. At the low stellar temperatures, we are considering here, all nuclear reactions involving tritons are too slow to compete successfully with the beta decay. We finally have to consider the fate of the neutrons produced in reaction (5b).

The fast neutrons produced in reaction (5b) are quickly slowed down to thermal energies in scattering processes in the stellar gas, mainly by elastic collisions with protons. At a temperature of 10^6 °K the mean thermal energy kT is slightly less than 100 ev. These "thermal" neutrons are finally captured by some of the nuclei present. If the gas consists essentially of pure hydrogen, the only possible process is n-p capture,

$$n+H^1\rightarrow D^2+\gamma+2.23 \text{ Mev}. \tag{9}$$

Since the branching ratio between reactions (5a) and (5b) is approximately unity, for four deuterons originally taking part in a D−D reaction two He^3-nuclei will be formed and one deuteron reproduced.

If, on the other hand, the stellar interior contains an appreciable abundance of elements other than hydrogen, the neutrons may be absorbed by some isotope with a large capture cross section, instead of by a proton. In particular, if an appreciable amount of He^3 has built up by means of reactions (3) and (5) in the stellar interior, a competing reaction is

$$n+He^3\rightarrow H^1+T^3+0.76 \text{ Mev}. \tag{10}$$

In this case, the triton again beta-decays to He^3 and for two deuterons taking part in a D−D reaction only one He^3 nucleus and a proton are formed. The cross sections for reactions (9) and (10) are known for thermal neutrons at 300°K (energy of 0.025 ev). Both these cross sections should obey the $(1/v)$ law up to energies of about 50 kev and hence the ratio of their cross sections should be the same at neutron energies of about 100 ev and 0.025 ev. At 100 ev, these two cross sections are 5.2 millibarns and 81 barns, respectively. Thus, reaction (10) will predominate over (11) if the ratio of the abundance (by mass) of He^3 to that of hydrogen is larger than about 2×10^{-4}.

Apart from He^3 there are a large number of isotopes which have neutron-capture cross sections large compared with that of the proton. Amongst the light elements (n,α) reactions take place on Li^6 and B^{10}. At a neutron energy of 100 ev these reaction cross sections should be about 15 and 60 barns, respectively. Amongst the heavy and medium-heavy nuclei, many will have neutron capture resonances at energies comparable with our thermal energy of about 100 ev. We take,

[5] W. A. Wenzel and W. Whaling, Phys. Rev. **88**, 1149 (1952).
[6] W. R. Arnold *et al.*, Phys. Rev. **93**, 483 (1954).
[7] G. Boato, Phys. Rev. **93**, 640 (1954).

merely as an example, the well-known resonance[8] at 120 ev for Co^{59}. The total width of this resonance, Γ, is about 5 ev and the neutron capture cross section (about one tenth the scattering cross section) at resonance is about 1000 barns. The capture cross section, averaged over a Maxwell energy distribution for 10^6 °K, is then about 25 barns. The energy released in the absorption of one neutron by Li^6, B^{10}, and Co^{59} is 4.8, 2.8, and about 7 Mev, respectively. The absorption rate by each of these isotopes equals that by hydrogen when the ratio of its abundance (by mass) to that of hydrogen is about 2×10^{-3}, 8×10^{-4} and 12×10^{-3}, respectively. These abundance ratios are considerably larger than the ones usually found in stellar atmospheres.

The net result of the various reaction chains is then as follows. If the deuterium abundance is low enough (e.g., $x_D/x_H<5\times10^{-4}$ for $T=10^6$ °K) each deuteron results in one He^3 nucleus and releases 5.5 Mev energy, which is 3×10^{-3} of the deuterium restmass energy. If the deuterium abundance is larger than this critical value then (*a*) if the abundance of isotopes other than hydrogen and deuterium is negligible each deuteron results in two thirds of a He^3 nucleus, releasing 3.2 Mev; (*b*) if $x_{He^3}/x_H>2\times10^{-4}$ and heavier elements are negligible, each deuteron results in one half of a He^3 nucleus, releasing 2.0 Mev; (*c*) if the abundance of some heavier isotopes is large enough, each deuteron results in one half a He^3 nucleus, releasing from 3.4 to 5.5 Mev. At much higher temperatures ($T>8$, say) each He^3 nucleus, produced in any of the above reactions, results in one half of a He^4 nucleus and releases an additional energy of 6.4 Mev.

In Table I, we give the mean life of deuterium, and the rate of energy production (proportional to $\rho x_H x_D$) for reaction (3) at various temperatures. The reaction rates given in Eqs. (7) and (8) should be multiplied by a correction factor for the effect of electron screening. This factor[9] is approximately given by $\exp(0.26\rho^{\frac{1}{2}}T^{-\frac{3}{2}})$. For the low densities normally expected in the interior of such cool stars, this correction factor should be unimportant.

3. REACTIONS ON Li, Be, AND B

The proton reactions on the five stable isotopes of these light p-shell nuclei have already been discussed briefly by Fowler,[2] but some more recent data is now available and we will discuss the present situation in some detail.

The cross sections for the (p,α) reactions on the two isotopes of lithium,

$$H^1+Li^6\rightarrow He^4+He^3+4.02 \text{ Mev}, \quad (11a)$$

$$H^1+Li^7\rightarrow He^4+He^4+17.34 \text{ Mev}, \quad (11b)$$

TABLE I. The mean life of deuterium, t (in years), and the rate of energy production, ϵ (in ergs g^{-1} sec^{-1}), for $\rho x_H=0.1$ and $x_D=10^{-4}$ for various temperatures T (in 10^6 °K).

T	0.35	0.5	0.75	1	1.5
t	2×10^{11}	6×10^8	2×10^6	6×10^4	700
ϵ	5×10^{-5}	1.5×10^{-2}	4	140	1.2×10^4

have been measured recently by Phillips and Sawyer[10] for proton energies of 40 to 250 kev. The cross sections for Li^7 are somewhat low and this reaction is suspected to be due to P-state protons, proceeding through a (0+)-state in Be^8 of several Mev width. The measurements of Phillips and Sawyer give cross sections larger by a factor of almost two than some prewar data, but give a cross section factor S, Eq. (1), practically constant between 40 and 240 kev. For these two reactions we adopt the values

$$S_6=(6\pm3)\times10^6 \text{ ev barns},$$
$$S_7=(1.2\pm0.5)\times10^5 \text{ ev barns}. \quad (12)$$

The proton absorption on Be^9 can proceed in two different ways,

$$H^1+Be^9\rightarrow D^2+Be^8+0.56 \text{ Mev}, \quad (13a)$$

$$H^1+Be^9\rightarrow He^4+Li^6+2.13 \text{ Mev}. \quad (13b)$$

After reaction (13a), the Be^8 nucleus immediately breaks up into two alpha particles and the deuteron very quickly absorbs a proton. After reaction (13b), the Li^6-nucleus quickly absorbs a proton, reaction (11a). The end result of both reactions (13a) and (13b) is the formation of two alpha particles and one He^3 nucleus from one Be^9 nucleus. For reaction (13), there are two resonances near the stellar energy region, one for a proton energy of 300 kev (width about 150 kev) and one just below threshold (proton energy about -50 kev). Milne[11] has recently measured the cross section for reactions (13a) and (13b) combined for proton energies of 50 to 350 kev. This measured cross section factor, S, is practically constant from 50 to 100 kev. We adopt this value of $S=3\times10^7$ ev barns for S in the stellar energy region. This value may be in error by a factor of two or more, since the position and width of the negative energy resonance is not known very accurately.

The proton reactions on the two isotopes of boron are

$$H^1+B^{10}\rightarrow He^4+Be^7+1.15 \text{ Mev}, \quad (14a)$$

$$H^1+B^{11}\rightarrow He^4+Be^8+8.58 \text{ Mev}. \quad (14b)$$

After reaction (14a), the Be^7 nucleus decays to Li^7 in a few weeks and Li^7 quickly absorbs a proton, reaction (11b). The Be^8 nucleus formed in reaction (14b) quickly decays into two alpha particles. The cross

[8] Serge, Morrison, and Feld, *Experimental Nuclear Physics*, pages 291 and 329 (John Wiley and Sons, Inc., New York, 1953).
[9] E. E. Salpeter, Australian J. Phys. 7, 373 (1954).
[10] J. A. Phillips and G. A. Sawyer, Los Alamos Report 1578, 1953 (unpublished).
[11] E. A. Milne, California Institute of Technology report (unpublished).

TABLE II. Proton-reactions on Li, Be, and B. Q is the net energy release, A and B are the coefficients for Eq. (15). The last four columns give the mean lifetime p^{-1}, in years, for $\rho x_H = 10$ and for temperatures of 2, 3, 5, and 8.

Net reaction	Q (Mev)	A	B	$T=$ 2	3	5	8
$Li^6+H^1\rightarrow He^4+He^3$	4.0	6×10^{12}	84.1	1.7×10^{8}	5×10^{4}	3	
$Li^7+H^1\rightarrow 2He^4$	17.3	1.2×10^{11}	84.7	1.5×10^{10}	4×10^{6}	250	
$Be^9+2H^1\rightarrow 2He^4+He^3$	6.2	3×10^{13}	103.6		7×10^{9}	6×10^{4}	10
$B^{10}+2H^1\rightarrow 3He^4$	19.3	2.5×10^{13}	120.6			1.5×10^{9}	5×10^{4}
$B^{11}+H^1\rightarrow 3He^4$	8.7	1.2×10^{14}	121.0			4×10^{8}	1×10^{4}

section for reaction (14a) has been measured by Burcham and Freeman[12] for proton energies of 200 to 500 kev. In this region, the cross-section factor S decreases slowly with increasing energy, being about 1.2×10^7 ev barns at 200 kev. We adopt a value of $S=2\times10^7$ ev barns for the stellar energy region, but this value could possibly be in error by quite a large factor, since little is known about possible resonances below 200 kev. The cross section for reaction (14b) has been measured by Schardt[13] in the 100-kev region and gives a value of $S=10^8$ ev barns, which is probably accurate to within a factor of three or four.

The results of this section are summarized in Table II. We can write the mean reaction rate p in the form

$$p=A(\rho x_H)T^{-\frac{2}{3}}\exp(-B/T^{\frac{1}{3}})\ \text{sec}^{-1}, \qquad (15)$$

with T in 10^6 °K and ρ in g/cc. The coefficients A and B are given in Table II, as are also the mean reaction times (p^{-1}) for a few typical temperatures.

4. REACTIONS ON O^{16}

We have so far discussed proton reactions on nuclei of $Z<6$. We should discuss next reactions on the stable isotopes of carbon and nitrogen. It was pointed out long ago by Bethe[3] and others that these reactions form the so-called carbon-nitrogen cycle, the net result of the cycle being the conversion of four hydrogen atoms into one helium atom without changing the total abundance of carbon and nitrogen. The individual steps in the cycle are:

$$C^{12}(p,\gamma)N^{13};\quad N^{13}(\beta^+\nu)C^{13};\quad C^{13}(p,\gamma)N^{14};$$
$$N^{14}(p,\gamma)O^{15};\quad O^{15}(\beta^+\nu)N^{15};\quad N^{15}(p,\alpha)C^{12}.$$

This cycle has been discussed quantitatively by Fowler[2] in the light of the most recent experimental information and we shall merely quote some of his results:

The reaction $N^{15}(p,\gamma)O^{16}$ competes, in principle, with the last reaction of the cycle, but its cross section is smaller by a factor of about 10^4 and hence only one part in 10^4 of the carbon and nitrogen is converted into oxygen in one complete cycle. It is now very probable (but by no means certain) that there is no resonance in the stellar energy region for the reaction $N^{14}(p,\gamma)O^{15}$. This reaction is then the slowest of the cycle reactions and determines the over-all rate of the cycle, at least for temperatures well below $40(\times10^6$ °K). The extrapolated cross-section factor for this reaction is $(3.3\pm1.5)\times10^4$ ev barns. If we write the mean rate p of this reaction (and hence of the cycle) in the form of Eq. (15), we have

$$A=(5\pm2)\times10^{10},\quad B=152.3. \qquad (16)$$

This rate p has to be multiplied by a factor correcting for the effect of electron shielding, which is about 1.5 for the central conditions in the sun. When dynamic equilibrium has been established, the abundance ratios of the four carbon and nitrogen isotopes are then given by the rates of the various reactions. These ratios are

$$x_{12}/x_{13}\approx4,\quad x_N/x_C\approx20(13/T)^2,\quad x_{14}/x_{15}\approx3000. \qquad (17)$$

We discuss next proton reactions on the various isotopes of oxygen, fluorine, neon, and sodium. Of these, by far the most important is O^{16}, which is likely to be much more abundant than any other isotope heavier than nitrogen (of the order of a percent, by mass, for the sun). The situation regarding the absorption of low energy protons by O^{16} is somewhat unclear at the moment and we discuss it in detail.

Rough measurements of the absolute total cross section for a proton energy $E_p=2$ Mev have been made by various authors for the reaction

$$H^1+O^{16}\rightarrow F^{17}+\gamma+0.59\ \text{Mev}. \qquad (18)$$

The values for this cross section[14] range from 3×10^{-6} barn to 3×10^{-5} barn. We adopt for this cross section, and hence for the factor S,

$$\sigma(2\ \text{Mev})\approx1\times10^{-5}\ \text{barn},$$
$$S(2\ \text{Mev})\approx6\times10^{8}\ \text{ev barns}. \qquad (19)$$

These values should be accurate to within a factor of about 5. The relative cross section as a function of proton energy has been measured[15] in the range of $E_p=1.4$ to 4 Mev. This cross section is a smoothly increasing function of E_p in this range, except for a sharp resonance at 3.5 Mev.

To extrapolate the cross section factor S, Eq. (19), to zero proton energy, we have to know the energy position, angular momentum, etc. of the resonance levels contributing most to this reaction. A resonance

[12] W. E. Burcham and J. M. Freeman, Phil. Mag. 41, 337 (1950).
[13] A. W. Schardt, Ph.D. thesis, California Institute of Technology, 1951 (unpublished).
[14] F. J. Eppling (private communication).
[15] R. A. Laubenstein *et al.*, Phys. Rev. 84, 12 (1951).

level in F^{17}, for which the proton is only just bound with $E_p \approx -60$ kev, has been observed[16] in a $O^{16}(d,n)F^{17}$ reaction. The effect of this level was also found in an experiment[15] on the elastic scattering of low-energy protons from O^{16}. An analysis[17] of the scattering data indicates a rather large nuclear radius $R(\sim 6\times 10^{-13}$ cm), a very large reduced width $\gamma^2(\sim 6\times 10^{-13}$ cm Mev) and $J=\frac{1}{2}$, even parity (S-state proton) for this level. The quantitative features of this analysis are not very accurate, since the experimental data do not extend to very low proton energies and since the variation with energy of the level shift is quite appreciable for such a large reduced width.

If we assume that the entire experimental cross section[15] for the $O^{16}(p,\gamma)F^{17}$ reaction for $E_p=1.4$ to 4 Mev is due to this low-lying resonance level, we can calculate Γ_γ, the partial width for the gamma ray transition to the F^{17} ground state, as a function of energy. Using a single-level Breit-Wigner formula and the values for γ^2 and R given by the scattering data, one finds[17] that Γ_γ is approximately proportional to E_γ^5, where $E_\gamma=(E_p+0.6$ Mev) is the energy of the γ ray. This is consistent with the theoretical energy variation of Γ_γ for electric quadrupole radiation, rather than electric dipole ($\Gamma_\gamma \propto E_\gamma^3$). Electric quadrupole radiation, in turn, is consistent with the assumption that the F^{17} ground state is $[(5/2)+]$, as is suggested by the shell model and by the mirror nucleus O^{17}. Under these assumptions we can then calculate the cross-section factor S for the stellar energy region, $E_p^{st}\approx 40$ kev, from Eq. (19) and dispersion theory. Using $\gamma^2=6\times 10^{-13}$ cm Mev and $R=6\times 10^{-13}$ cm, the level shift can be calculated as a function of energy.[18] For the stellar energy region the apparent position of the resonance level is shifted from -60 kev to $E_r\approx -140$ kev. Assuming $\Gamma_\gamma \propto E_\gamma^5$, we then find for S in the stellar energy region approximately 2×10^3 ev barns.

However, the above analysis is made very doubtful by the following fact. From the above assumptions and the experimental cross section, Eq. (19) it follows that, for $E_p=2$ Mev, the gamma-ray partial width Γ_γ is about 5 ev. This value is orders of magnitude larger than any theoretically expected value for quadrupole radiation, but of the right order of magnitude for dipole radiation. The suspicion that the (p,γ) cross section for $E_p=1.4$ to 3 Mev cannot largely be due to quadrupole radiation is also strengthened by the following fact. The very marked resonance for S-state protons[15] found for elastic proton scattering from O^{16} at $E_p=2.66$ Mev is missing completely in the $O^{16}(p,\gamma)$ cross section,[15] this resonance also requiring electric quadrupole radiation. On the other hand, the evidence for the resonance level at -60 kev being $(\frac{1}{2}+)$ seems very good and the evidence for the F^{17} ground state being $[(5/2)+]$ at least fairly good (apart from the shell model and the analogy with O^{17}, the strong γ-ray transition to the ground state from the $[(7/2)+]$ level at $E_p=3.47$ Mev favors $[(5/2)+]$ for the ground state). These arguments make it seem unlikely that the proton capture is due to S-state protons, which require an angular momentum change $\Delta J=2$.

We shall now investigate the possibility that the bulk of the proton capture cross section is due to P-state protons on O^{16} which form a $(\frac{3}{2}-)$ state in F^{17} and hence give rise to electric dipole radiation to the groundstate. The ratio of nuclear radius R to "effective Bohr radius" is reasonably large for the $(O^{16}+p)$ system, about 2.7 for $R=5\times 10^{-13}$ cm. In this case the barrier penetration factor for P-state protons is comparable with that for S-state protons for $E_p \gtrsim 2$ Mev and is smaller by a factor of only about 5 even for very low values of E_p. Let us assume the existence of a $(\frac{3}{2}+)$ resonance level for E_p of the order of magnitude of 4 Mev. If this level has a very large reduced width γ^2, comparable with Wigner's upper limit of $(3\hbar^2/2_m R) = 10^{-12}$ cm Mev, its proton width at resonance will be several Mev. Such a broad resonance level would not necessarily have been noticed in $O^{16}(p,p)$ and other reactions to date. The resonance denominator in the Breit-Wigner formula for such a state varies very little from $E_p=1.4$ to 4 Mev. One can then calculate the $O^{16}(p,\gamma)F^{17}$ cross section σ in this energy range due to such a state, assuming $\Gamma_\gamma \propto E_\gamma^3$. An approximate calculation of σ gave a function of energy which was at least not in bad disagreement with the experimental data. The partial γ-ray width required for $E_p=2$ Mev was about 10 ev, which is not unreasonable for electric dipole radiation. Under the assumption of such a broad P-state resonance, S was again calculated for the stellar energy region and found to be about 100-ev barns.‡

We provisionally adopt this value of $S=100$-ev barns, which should be accurate to within a factor of about 10 or 20, if the above assumptions are correct. More accurate experiments on the elastic scattering of low-energy protons from O^{16} are now in progress.[14] An analysis of these experiments should clarify the situation somewhat and more accurate measurements of the $O^{16}(p,\gamma)F^{17}$ cross section, especially at proton energies well below 2 Mev and above 4 Mev, would be very useful. Expressing the reaction rate in the form of Eq. (15), we have

$$A\sim 1.5\times 10^8, \quad B=166.7. \tag{20}$$

[16] F. Ajzenberg, Phys. Rev. **83**, 875 (1951).
[17] R. A. Laubenstein and M. J. Laubenstein, Phys. Rev. **83**, 18 (1951).
[18] R. G. Thomas, Phys. Rev. **88**, 1109 (1952).

‡ *Note added in proof.*—Recent work [Warren *et al.*, Can. J. Phys. **32**, 563 (1954)] indicates that the $O^{16}(p,\gamma)F^{17}$ reaction for $E_p=0.8$ to 2 Mev proceeds mainly by radiative capture into the state of $E_p\sim -60$ kev of F^{17}, followed by a gamma-ray transition to the ground state. This also seems to indicate capture of P-state protons (if the -60-kev state is really $J=\frac{1}{2}+$), but the reasons for the small probability of transitions directly to the ground state and for the energy dependence of the cross section are not at all clear. Our adopted value for S is thus highly tentative.

The F^{17} produced in reaction (18) beta decays to O^{17} with the emission of a positron of end-point energy 1.72 Mev with a half-life of about 1 minute.

5. REACTIONS ON O, F AND THE NE-NA CYCLE

For the three remaining isotopes of oxygen and fluorine, (p,α) reactions are energetically allowed. The energy releases per reaction for $O^{17}(p,\alpha)N^{14}$, $O^{18}(p,\alpha)N^{15}$, and $F^{19}(p,\alpha)O^{16}$ are 1.20, 3.97, and 8.12 Mev, respectively. No cross sections for these reactions have as yet been measured for reasonably low-proton energies and we have to estimate them theoretically.

In the $O^{17}(p,\alpha)$ reaction (for protons of about 40 kev, the "stellar energy region") the energy of the emerging alpha particles is low and their barrier penetration factor P quite small. Assuming a radius of the compound nucleus of about 5×10^{-13} cm, P is of the order of 10^{-4} for S-state alpha particles, slightly smaller for P state and about 10 times smaller for D state. If we assume resonance levels of reduced widths of about 10^{-13} cm Mev, the alpha-particle widths will be of the order of 100 ev. A resonance level in F^{18} has been observed[19] corresponding to a proton energy of (zero ±100 kev). The spin and parity of this state is not yet known, but any spin and parity can be reached from both the $(O^{17}+p)$ and from the $(N^{14}+\alpha)$ channel. Thus a (2 or 3+) state can be reached by S-state protons and D-state α particles, a (1, 2, 3 or 4−) state by P-state proton and P or F α particles, etc. If we assume the exact position of the resonance level to be 50 kev away from the stellar energy, its spin and parity to be (2 or 3+) or (1 or 2−) and the above-mentioned values for values for reduced width and nuclear radius, then the Breit-Wigner single-level formula gives a value of 2×10^5 ev barns for the cross section factor S. We adopt this value for S, but the correct value could be smaller by a factor of up to 100, if the spin and parity of the level is less favorable, larger by a factor of up to 10^4 if the level is right in the stellar energy region.

Little is known of resonance levels in F^{19} and Ne^{20} in the energy region relevant to the $O^{18}(p,\alpha)N^{15}$ and $F^{19}(p,\alpha)O^{16}$ reactions for low energy protons. But the energy of the emerging alpha particle is high enough so that its barrier penetration factor is about unity for $(O^{16}+\alpha)$ and not very much smaller for $(N^{15}+\alpha)$. The widths of resonance levels in the compound nucleus which can be reached by the alpha particles should therefore be quite large, the levels almost overlapping and the exact positions of the resonance levels should therefore not affect the reaction rates extremely strongly. We adopt for the cross section factor S the following estimates, based on barrier penetration factors and density of resonance levels in the relevant energy region: $S=10^8$ and 10^9 ev barns, respectively, for $O^{18}(p,\alpha)$ and $F^{19}(p,\alpha)$.

Neon-sodium cycle. The proton reactions on the four stable isotopes of neon and sodium form a cycle somewhat similar to the carbon cycle. For all except the heaviest of the four isotopes only (p,γ) reactions are energetically possible, followed by beta-decays in two of the three cases. For Na^{23} the (p,α) reaction is energetically possible, leading back to Ne^{20}. The net result of this cycle would again be the conversion of four protons into one alpha particle without destroying Ne or Na. We shall see however that $Na^{23}(p,\gamma)Mg^{24}$ is probably not much slower than the (p,α) reaction. The detailed steps in this "cycle" are[19,20]:

$$H^1+Ne^{20}\rightarrow Na^{21}+\gamma+2.45\text{ Mev},$$
$$Na^{21}\xrightarrow{23\text{ sec}}Ne^{21}+e^{+}+\nu+2.50\text{ Mev}, \tag{21}$$

$$H^1+Ne^{21}\rightarrow Na^{22}+\gamma+6.74\text{ Mev},$$
$$Na^{22}\xrightarrow{3\text{ yr}}Ne^{22}+e^{+}+\nu+\gamma+2.84\text{ Mev}, \tag{22}$$

$$H^1+Ne^{22}\rightarrow Na^{23}+\gamma+8.80\text{ Mev}, \tag{23}$$

$$H^1+Na^{23}\begin{cases}\rightarrow Ne^{20}+\alpha+2.37\text{ Mev},\\ \rightarrow Mg^{24}+\gamma+11.70\text{ Mev}.\end{cases} \tag{24}$$

No cross sections are known for these reactions and very little about the relevant resonance levels in the compound nuclei, except the order of magnitude of the level density. To get (p,γ) transitions to the ground state of the final nucleus by means of electric dipole radiation, an incident proton in a P-state is required in all four cases (parity of all initial and final nuclei positive). We estimate the cross-section factors S by making the following (very crude) approximations and assumptions: (i) The reduced particle widths of the resonance levels, in energy units (γ^2/R), are of the order of the level spacing, as is the energy distance of the nearest level to the stellar energy region. (ii) The gamma-ray widths are given by Weisskopf's estimate,[21] for nuclear radii of about $\sigma\times10^{-13}$ cm, $\Gamma_\gamma\sim(E_\gamma^3)$ ev, where E_γ is the gamma-ray energy in Mev.

For $Ne^{20}(p,\gamma)$ the calculated value for S is rather small, $S\sim2\times10^3$ ev barns, due to the low Q-value of the reaction which leads to wide level spacing (of order 1 Mev) and small gamma-ray width (order 10 ev). For the other two isotopes of neon, the level spacing is appreciably smaller and Γ_γ larger and we estimate $S\sim1\times10^5$ and 3×10^5 ev barns, respectively, for Ne^{21} and Ne^{22}. For $Na^{23}(p,\alpha)$, the barrier penetration factor for the emerging alpha particle is less than 10^{-2} and the estimated α width of the order of 1 kev, giving $S\sim10^7$ ev barns. For $Na^{23}(p,\gamma)$ the estimated Γ_γ is a few hundred ev and this reaction is not very much slower than the (p,α) reactions.

The above estimates are of course very crude. The correct values of S could be smaller than the estimates

[19] F. Ajzenberg and T. Lauritsen, Revs. Modern Phys. **24**, 321 (1952).

[20] P. M. Endt and J. C. Kluyver, Revs. Modern Phys. **26**, 95 (1954).

[21] J. M. Blatt and V. F. Weisskopf, *Theoretical Nuclear Physics* (John Wiley and Sons, Inc., New York, 1952), Chap. XII.

by factors of 10 or 100 and they could be very much larger still if some resonances fall in or very near the stellar energy region. It should also be pointed out that resonance levels in Mg^{24} of different spin and parity are required for the two different modes of decay, $(Mg^{24}+\gamma)$ and $(Ne^{20}+\alpha)$. Hence the branching ratio of these two modes will also depend quite strongly on the details of the nearest levels.

We can again express the reaction rate p in the form of Eq. (15). The coefficients A and B for this equation are given in Table III. The mean life (p^{-1}) of the various nuclei is given in Table IV, together with the reaction time for the conversion of hydrogen into helium.

6. DISCUSSION

We shall now summarize the significance of the reaction rates, calculated in this paper, to two problems. First, the possible sources of energy production in various stars. Second, the extent to which the nuclear reactions which have taken place in the interior of various stars have altered the relative abundance of the chemical elements and their isotopes. The most important variable for these considerations is the temperature in the stellar interior. For most of the stars which lie on the main sequence (referred to as *MS*) the central temperature, T_c (in 10^6 °K), lies in the range of about 6 to 25. A star with T_c less than about 15 lives mainly on the proton-proton chain, with $T_c>15$ mainly on the carbon cycle. For *Castor C*, the sun, and *Sirius A*, T_c is about 8, 13, and 20, respectively. For the very brightest *MS* stars and some stars which have a "burned out core" (all He) and are burning hydrogen only in a thin shell, T_c may be about 30 or even slightly larger.

$Z<6$.—Astrophysical observations are now becoming available on very young star groups. One famous example is the star aggregate in *ζ-Perseus* which is known to be only about 1.3 million years old.[22] An open star cluster which may be even younger is at present being investigated by Walker.[23] He finds that most of the fainter stars in this cluster have appreciably lower surface temperature, and hence larger radii, than *MS* stars of the same luminosity. These stars probably are still contracting gravitationally and have much lower central temperatures than equivalent *MS* stars. Some of these stars are probably still burning whatever D, Li, Be, and B they contained initially. For such special stars the burning of these elements may be an important source of energy production.[24] For instance, if the original abundance ratio of D/H had the terrestrial value, then the total energy content of deuterium burning is about the same as that of the gravitational contraction. The observations and calculations on the interior of such stars are too incomplete to draw any conclusions about the original abundance of such light elements.

TABLE III. The coefficients A and B for Eq. (15) for the reaction rate of the absorption of protons on the following nuclei.

	O^{17}	O^{18}	F^{19}	Ne^{20}	$Ne^{21,22}$	Na^{23}
A	3×10^{11}	1.5×10^{14}	1.5×10^{15}	3×10^{9}	3×10^{11}	2×10^{13}
B		167	181		194	208

TABLE IV. $\log_{10}$ of the mean reaction times (in years) for $\rho x_H=100$ for the absorption of protons on various nuclei for various temperatures T (in 10^6 °K). The first two columns give $\log_{10}$ of the mean life of hydrogen for (i) proton-proton chain alone, (ii) for p-p chain plus C,N-cycle for $x_{C,N}=0.01$.

T	"H" with $x_{C,N}=0$	"H" with $x_{C,N}=0.01$	O^{16}	O^{17}	O^{18}	F^{19}	Ne^{20}	$Ne^{21,22}$	Na^{23}
10	10.4	10.4	17	14	11	13	21	19	20
15	9.6	9.4	12.5	9.5	6.5	8	16	14	15
30	8.6	4.7	7.5	4.5	1.5	1.5	9	7	7.5
100	7.3	−1.5	0	−3	−6	−7	0	−2	−2

As Tables I and II show, the central temperatures of almost all *MS* stars are sufficiently high so that all of the original D, Li, Be, and B will have absorbed protons long ago. It should be noted that these light elements do not undergo any cycles, but are irrevocably destroyed, the end products consisting entirely of He^3 and He^4. Hence, in the interior of *MS* stars there can exist no isotopes lighter than carbon, except H^1, He^3, and He^4. In the hotter *MS* stars ($T_c>10$) the He^3 is further converted into He^4. It is of some interest, however, to discuss the abundance of these light elements in the outer parts of a *MS* star, where the temperatures are appreciably lower than T_c.

The age of the sun, and of many other *MS* stars, is known to be about 5×10^9 years. Fairly reliable calculations of the temperature and density, as a function of distance from the center r, are now available for *MS* stars and especially for the sun. We can then calculate the radial distance r and temperature T_r of the shell in a *MS* star, where the mean lifetime of a light element is equal to 5×10^9 years. The results of such a calculation for the sun are given in Table V, based on the reaction rates of Secs. 2 and 3 and on a calculation by Naur[25] giving temperature and density as a function of r ("Model 1," $T_c=13.5$). The fraction M_r/M of the solar mass contained inside radius r is also given in Table V.

If there is no mixing between various layers in the sun, then each element will be essentially absent in the solar matter inside the appropriate radial distance r, since the temperature increases with decreasing r and since the reaction rates increase very rapidly with temperature. Conversely, the element would have essentially its original abundance in the layers outside the radius r. In reality the sun most probably contains a fairly thick outer layer which is under convection and

[22] A. Blaauw, Bull. Astron. Netherlands **11**, 405 (1952).
[23] R. Walker (private communication).
[24] E. E. Salpeter, Mem. Roy. Soc. Liège **13**, 116 (1954).
[25] P. Naur, Astrophys. J. **119**, 365 (1954).

TABLE V. Position in the sun for which the mean life of various nuclei is 5×10^9 years. r is distance from the center, R the solar radius, T_r, the temperature in 10^6 °K, M_r the mass contained inside radius r and M the total solar mass.

	D	Li^6	Li^7	Be^9	B^{10}	B^{11}
r/R	0.86	0.62	0.57	0.49	0.37	0.39
T_r	0.54	2.0	2.4	3.2	4.9	4.7
M_r/M	1.00	0.98	0.97	0.93	0.79	0.83

hence thoroughly mixed. If the lower boundary of this convective zone lies deeper than the critical radius r for an element, then atoms of this element will be destroyed when convection carried them though the lower parts of the zone. Hence, the abundance of such an element should be very low even in the solar atmosphere at the top of the zone.[26]

The abundance of lithium (normally consisting mainly of Li^7) and of beryllium in the solar atmosphere has been observed spectroscopically.[26] The abundance of Be is about the same as on the earth, whereas that of Li is lower by a factor of about 50. One is tempted to assume that the lower boundary of the outer convective zone lies between the critical values of r for Li and Be, say, at a temperature of 2.6 to 3. No conclusive observations on the abundance of D and B in the solar atmosphere are as yet available. If the above assumptions on the convective zone are correct, B should have its original abundance in the atmosphere and D should be completely missing (unless it is produced continuously by some process taking place in the atmosphere). Note that, even for B, the fractional mass of the sun which can still contain this element is only about 0.2.

We finally should keep in mind the fact that, if the original abundance of D was high enough, some neutrons were produced in the D−D reaction. The number of neutrons produced was probably not very large and (see Sec. 2) most of them probably were absorbed by H^1 or He^3. But it is possible that the abundance of some very rare heavy elements with suitable resonances was altered by neutron absorption during the deuterium burning.

$Z>7$.—If temperatures were high enough for proton absorption on all isotopes of O, F, Ne, and Na to go on, the net result would be as follows. All oxygen and fluorine would eventually be converted into He^4 and into nitrogen. The neon and sodium isotopes would not be destroyed at all (but "catalyze" the H−He conversion) if the (p,γ) reaction on Na^{23} is very much slower than (p,α). If (p,γ) can compete, sodium, and neon would eventually be converted into magnesium. But under most stellar conditions temperatures are not high enough for any but a few of these reactions to go on.

Central temperatures of *MS* stars may vary over a wide range of temperatures (from 5 to 30, say), depending on the luminosity and other factors. Whether a particular isotope will absorb protons to an appreciable extent or not at a particular temperature depends on whether the mean reaction time is shorter or longer than the corresponding reaction time for the conversion of H into He. Such a comparison of reaction rates is given in Table IV.

For stars appreciably cooler than the sun ($T_c<10$), all the isotopes heavier than nitrogen are essentially unaffected. In the hotter *MS* stars which burn hydrogen on the carbon-cycle ($T_c>15$), both O^{18} and F^{19} (and possibly, but not certainly, O^{17}) are destroyed much more rapidly than hydrogen, forming nitrogen and O^{16}. Unless the assumptions of Sec. 4 are violently wrong or the abundance of C and N orders of magnitude less than the expected percent or so, O^{16} will not be depleted appreciably during the mean life of hydrogen. Since the original abundance in stars of O^{17}, O^{18}, and F^{19} most probably was rather low, the depletion of these isotopes in the hotter *MS* stars is not likely to be a very important source of energy.

Unless resonances increase the cross sections for the Ne−Na cycle greatly, these isotopes are unaffected during the lifetime of hydrogen. If a star happened to contain Ne or Na, but no carbon or nitrogen at all ($x_{C,N}<10^{-6}$) and had central temperatures higher than 30, the Ne−Na cycle would be a more important energy source than the proton chain, but such abnormal abundances are extremely unlikely. Proton reactions on Mg, Al, and heavier nuclei can be neglected completely. The cross-section factors S for reactions on Mg and Al are comparable with those for Ne and Na, but the barrier penetration factors for the proton very much smaller.

To summarize: Hydrogen in the core of main sequence stars will be converted into He^4 at temperatures below 30×10^6 °K. When this conversion has practically gone to completion, neon and all heavier elements will still have their original abundance. Of the lighter elements, besides He^4 which comprises most of the matter, only carbon, nitrogen and O^{16} (and possibly O^{17}) remain. After the H−He conversion, the stellar core may contract again and the temperature may rise to very much more than 30×10^6 °K. At these high temperatures the reaction rates for proton absorption from heavier nuclei would be quite high, but there simply is not any hydrogen left. Nuclear reactions will set in again when temperatures are high enough for alpha particles to be captured. These reactions will be discussed in a sequel to this paper.

I would like to thank Mr. S. Lapointe for help with the numerical calculations, Dr. F. J. Eppling for communicating unpublished results and Professors W. Fowler and P. Morrison for stimulating discussions. I am also indebted to the Australian National University where part of this work was carried out, for their hospitality.

[26] J. L. Greenstein and E. Tandberg-Hannsen, Astrophys. J. 119, 113 (1954).

Gamma Rays from Proton Bombardment of Li^6†

S. Bashkin and R. R. Carlson
State University of Iowa, Iowa City, Iowa
(Received November 8, 1954)

A NaI(Tl) scintillation spectrometer, limited to 1.5-Mev gamma rays, detected 430±20 kev radiation when separated Li^6 was bombarded with monochromatic protons from 180 kev to 415 kev. Spectrometer efficiency was measured using an Au^{198} source of beta-gamma coincidences. The thick target yield was $(7\pm4)\times10^{-13}$ gamma per proton at 180 kev and $(170\pm35)\times10^{-13}$ at 415 kev. The 430-kev gamma ray was interpreted as part of the cascade decay of the broad 6.35-Mev state of Be^7. Assuming *s*-wave capture, the experimental yield has been fitted with a Breit-Wigner resonance curve. At 415 kev, a cross section of 0.7 ± 0.2 μb is obtained for the decay of the capture state through the 430-kev state. This gives $(2J+1)\Gamma_\gamma$ a value of 1.0 ± 0.3 ev for this cascade process. The spectrometer, when unlimited, detected gamma rays corresponding to transitions from the capture level to the ground and 430-kev states. The number of transitions from the capture state to the 430-kev state of Be^7 is 35±5 percent of the total radiative decays. Transitions through the 4.65-Mev state of Be^7 occur in less than 4 percent of the total radiative decays.

INTRODUCTION

THE level structure of the nucleus Be^7 has been studied in a number of nuclear reactions.[1] These investigations have located the four excited states shown in Fig. 1. The evidence for the spin and parity assignments indicated in Fig. 1 is discussed in the review article by Ajzenberg and Lauritsen.[1] These assignments are consistent with the interpretation that each of the Be^7 levels is mirror to a state of approximately the same energy in Li^7.

An energetically possible alternative to particle emission from Be^7 as formed in the proton bombardment of Li^6 is de-excitation to lower states by electromagnetic radiation. The first search[2] for the $Li^6(p,\gamma)Be^7$ reaction had a negative result, from which an upper limit of 2.5×10^{-10} gamma per proton was deduced for 950-kev protons incident on a thick target. However, it has recently been reported[3] that a complicated pattern of direct and cascade gamma rays has been observed for bombarding energies from 400 kev to 2.2 Mev.

In the present experiment, the absolute, thick target yield curve for gamma radiation from the $Li^6(p,\gamma)Be^7$ reaction was measured for bombarding energies between 180 kev and 415 kev. The relative intensities of the gamma rays leading from the capture state to the ground state directly and in cascade through the first excited state were also studied. These measurements were made in the hope of clarifying the nature of the gamma-ray transitions.

EXPERIMENTAL METHOD

A 500-kev Cockcroft-Walton voltage multiplier was used to accelerate protons to well-defined energies between 180 kev and 415 kev. Proton energies were measured in terms of the current needed for an electromagnet to deflect the beam 90° and, through a slit system, into the target chamber. Resonances at 163 kev in the $B^{11}(p,\gamma)C^{12}$ reaction, at 224 kev and 340 kev in the $F^{19}(p,\alpha\gamma)O^{16}$ reaction, and at 440 kev in the $Li^7(p,\gamma)Be^8$ reaction, were used to calibrate the magnet current against proton energy. The reproducibility of the resonance points indicated that proton energies were known to ±5 kev over the range of this experiment.

Thick targets of elemental, separated[4] Li^6 (93 percent Li^6, 7 percent Li^7) were evaporated *in situ* on a $\frac{1}{8}$-in. thick aluminum plate. The accumulation of carbon on the target surface was reduced to a negligible amount by the installation of a dry ice and acetone cold trap immediately in front of the target chamber. The cleanliness of the target was attested by the absence of any ten minute period annihilation radiation from N^{13}, which would have resulted from the $C^{12}(p,\gamma)N^{13}$ reaction, and by the constancy of the $Li^6(p,\gamma)Be^7$ yield during lengthy bombardments at a fixed incident energy.

The target chamber served as a Faraday cage, and the cold trap, biased at 300 volts below ground, served as a secondary electron repeller. Charge measurements were made with a condenser-discharge type of current integrator. Beam currents of about 5 μa were used.

Gamma rays ranging in energy from 430 kev to $(5.60\ \text{Mev}+6E_p/7)$ are possible when Li^6 is struck by protons whose energy in the laboratory system is E_p. The energetic photons due to decays from the capture state to the ground and first excited states of Be^7 were studied at a bombarding energy of 300 kev, but they were not well resolved. They were also obscured, for incident energies above 340 kev, by the 6.13-Mev gamma rays from the $F^{19}(p,\alpha\gamma)O^{16}$ reaction in fluorine contamination on the slit system at the target end of

† Supported in part by the U. S. Atomic Energy Commission.
[1] F. Ajzenberg and T. Lauritsen, Revs. Modern Phys. **24**, 321 (1952). See also forthcoming supplement in the *Reviews of Modern Physics*. We wish to thank Professor Lauritsen for a preprint of the supplement.
[2] S. C. Curran and J. E. Strothers, Proc. Roy. Soc. (London) **A172**, 72 (1939).
[3] Erdman, Warren, James, and Alexander, Phys. Rev. **96**, 858(A) (1954).
[4] The enriched Li^6 was kindly supplied by the Oak Ridge National Laboratory.

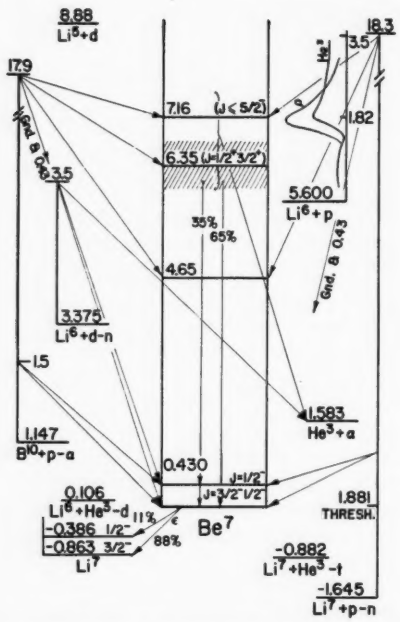

FIG. 1. Energy level diagram of Be^7 [after Ajzenberg and Lauritsen (see reference 1)].

the accelerator. The 430-kev cascade gamma rays appeared in the presence of pile-up x-rays from the accelerator, degraded photons, and annihilation radiation due principally to pair formation in materials near the detector. Comparing the factors involved, it was clear that more precise studies were possible with the 430-kev gamma rays than with the higher-energy gamma rays.

Gamma radiation was detected with a NaI(Tl) crystal $1\frac{1}{2}$ in. in diameter and 2 in. long, mounted on an RCA5819 photomultiplier tube. The photomultiplier output was fed into a limiter of Elmore's design[5] adjusted so that all radiation above 1.5 Mev gave the same size output pulse. An Atomic Instruments Company Model 204B linear amplifier followed the limiter and delivered pulses to a ten-channel pulse-height analyzer of Johnstone's design.[6] Below the limiting region, the detecting system was found to be linear within the accuracy of measurement. Sources of Au^{198} (411-kev gamma rays), Na^{22} (annihilation radiation), Cs^{137} (667-kev gamma rays) and Co^{60} (1.17-Mev and 1.33-Mev gamma rays) were used to calibrate the energy scale of the detector to ± 20 kev.

The absolute efficiency of the detector was measured by counting coincidences between the Au^{198} betas and the subsequent 411-kev gamma rays. A source of Au^{198} was painted on a thin anthracene crystal which, optically coupled to an RCA5819 photomultiplier tube, was used to detect the betas. The NaI(Tl) crystal was placed the same distance from the source as it was from the lithium target, and the aluminum target-backing plate was placed between the source and crystal. Only the total absorption peak of the 411-kev gamma ray in the NaI(Tl) crystal was counted. After correcting for geometry, the absolute efficiency of the present crystal was found to be the same as that reported by Hornyak and Coor[7] for a somewhat smaller crystal. Hence Hornyak and Coor's empirical relation for the energy dependence of their crystal's detection efficiency was used to correct the measured efficiency of our crystal at 411 kev for the 430-kev gamma radiation studied in this experiment. The correction was a 9 percent reduction. The uncertainty in the absolute efficiency is estimated at 10 percent.

ABSOLUTE THICK TARGET YIELD

The limited pulse-height distribution obtained at an incident proton energy of 215 kev is shown in Fig. 2. A single gamma ray of energy 430 ± 20 kev appears in the range up to 1.5 Mev. The arrow at a pulse height corresponding to 1.13 Mev indicates where the total absorption peak of a gamma ray from the capture state to the 4.65-Mev state should show up. The 430-kev gamma ray was taken to be the lower element of the cascade decay of the capture state through the first excited state of Be^7. The yield of the cascade gamma ray was measured at six different energies using a freshly evaporated target which showed no signs of deterioration or carbon accumulation during the bombardment. The uppermost curve in Fig. 3 shows the pulse-height distribution for the 430-kev gamma ray obtained at a proton energy of 365 kev. Background was approximated over the width of each total absorption peak by a straight line, as illustrated in Fig. 3,

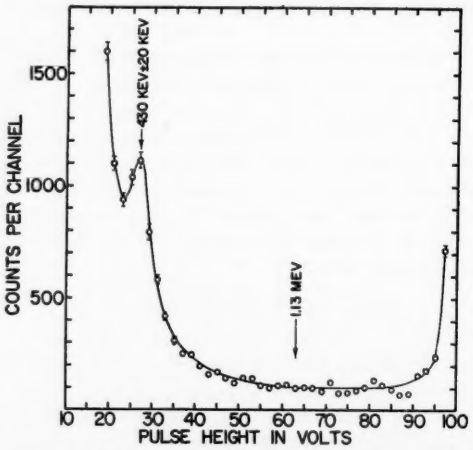

FIG. 2. Limited, single-crystal spectrometer, pulse-height analysis of gamma rays from capture by Li^6 of protons having energy of 215 kev. Arrows indicate where the total absorption peaks of gamma rays of the energies specified should appear.

[5] W. C. Elmore, Rev. Sci. Instr. **20**, 963 (1949).
[6] W. C. Johnstone, Nucleonics **11**, No. 1, 36 (1953).
[7] W. F. Hornyak and T. Coor, Phys. Rev. **92**, 675 (1953).

drawn roughly tangent to the high-energy tail of the pulse-height distribution and giving the same peak-to-valley ratio as measured with the Au^{198} source. The area, shown shaded in Fig. 3, under the total absorption peak in the net curve was then measured. The six areas so obtained, together with the detection efficiency, the charge collected, and the isotopic content of the target, gave the absolute thick target yield points shown in Fig. 4. Statistical and subtraction uncertainties are indicated by vertical lines. There is an additional 10 percent uncertainty in the absolute yield from the detection efficiency measurement.

The thick target yield, Y, is related to the cross section, σ, by

$$Y=\int_0^E \frac{\sigma}{\epsilon}\,dE,$$

where E is the bombarding energy in the center-of-mass system and ϵ is the stopping power[8] of the target. Over the energy range of this experiment, the $Li^6(p,\gamma)Be^7$ excitation function is resonant in nature, being influenced primarily by the broad level at 6.35 Mev[1] in Be^7. Assuming single-level Breit-Wigner resonance theory to be adequate, the above expression can be numerically integrated. For a total width at resonance of 1.5 Mev and s-wave proton capture, both obtained from the

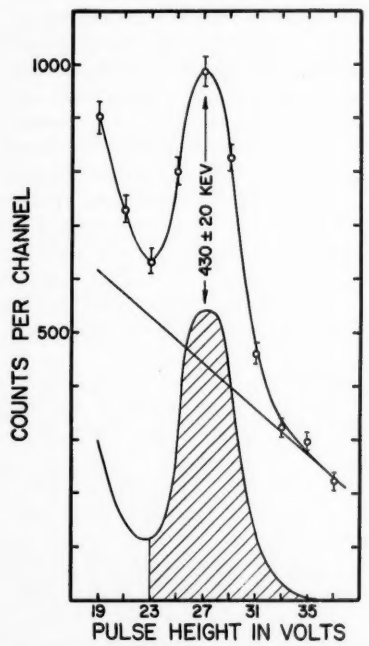

FIG. 3. Total absorption peak of the $Li^6(p,\gamma)Be^7$ 430-kev cascade gamma ray at a proton bombarding energy of 365 kev. Top curve shows the raw data. The slanting straight line is the background correction. Bottom curve shows the net data. The absolute efficiency of the detector was measured for gamma-ray pulses in the shaded region.

[8] Warters, Fowler, and Lauritsen, Phys. Rev. 91, 917 (1953).

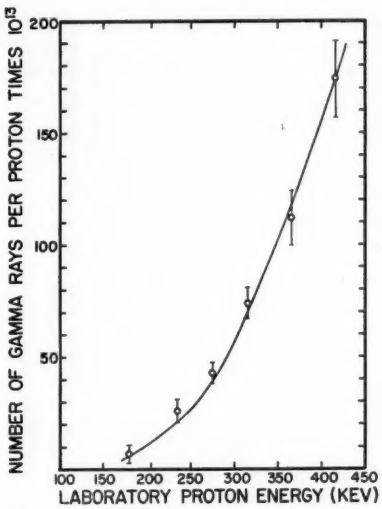

FIG. 4. Thick target yield curve for the $Li^6(p,\gamma)Be^7$ 430-kev cascade gamma ray. Points are experimental. The curve was calculated from Breit-Wigner resonance theory.

$Li^6(p,\alpha)He^3$ experiment,[9] the theoretical thick target yield of 430-kev cascade gamma rays was computed. It was assumed that the gamma width varied as the cube of the gamma-ray energy. The curve, shown in Fig. 4, was normalized to the data at an incident proton energy of 415 kev. The agreement of the calculated curve and the data makes unnecessary the use of Thomas' more complete expression for the energy dependence of the gamma width.[10] To within an uncertainty of 30 percent, a cross section of 0.7 μb at a bombarding energy of 415 kev results for the cascade process. As discussed below, direct transitions to the ground state are expected to have a somewhat larger probability. The total radiative capture cross section is estimated as 2 ± 1 μb for an incident energy of 400 kev, in comparison with the 10^{-30} cm^2 obtained by Erdman *et al.*[3] at the same energy. For reasons given below, the present estimate does not include any contributions from decays through the second excited state of Be^7.

The cross section at an energy E is given by the relation

$$\sigma=\pi\lambda^2\omega\frac{\Gamma_p\Gamma_\gamma}{(E-E_r)^2+\frac{1}{4}\Gamma^2},$$

where $2\pi\lambda$ is the deBroglie wavelength of the proton, ω is a statistical weight factor equal to $(2J+1)/6$, J is the spin of the compound nucleus, E_r is the resonance energy, Γ is the total width of the state, Γ_p is the proton width, and Γ_γ is the radiative width, where all quantities refer to the center-of-mass system. The quantity $(2J+1)\Gamma_\gamma$ is 1.0 ± 0.3 ev for cascade decay at an excitation of 5.95 Mev in Be^7. Weisskopf[11] has given

[9] S. Bashkin and H. T. Richards, Phys. Rev. 84, 1124 (1951).
[10] R. G. Thomas, Phys. Rev. 88, 1109 (1952).
[11] V. F. Weisskopf, Phys. Rev. 83, 1073 (1951).

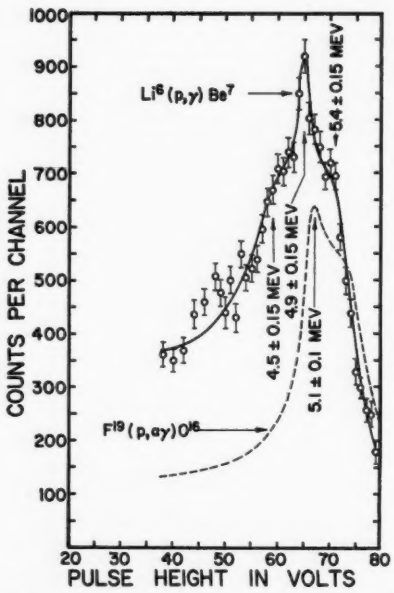

FIG. 5. Single-crystal spectrometer pulse-height analysis (solid curve) of high-energy gamma rays from capture by Li^6 of protons having energy of 300 kev. Dashed curve shows one- and two-escape peaks of 6.13-Mev gamma from $F^{19}(p,\alpha\gamma)O^{16}$ reaction.

formulas for calculating radiation widths of various multipole orders and types. The calculated values are expected to be too large by perhaps as much as 10^3, although a survey of the light elements[12] suggests somewhat better agreement. An electric dipole calculation for the high-energy component of the cascade decay in Be^7 gives 60 ev for the radiative width.

RELATIVE INTENSITIES

The relative intensities of the gamma rays leading from the capture state to the ground and first excited states can be predicted[11] rather crudely on the basis of the spins and parities of these states. The commonly accepted assignments[1] of $1/2^-$ or $3/2^-$ for the Be^7 ground state and $1/2^-$ for the 430-kev state mean that the cascade transition cannot predominate over the direct decay, no matter what the spin of the third excited state may be. If that state has even parity and a spin of 1/2 or 3/2, as implied in the assumption of *s*-wave proton capture, the two gamma rays should have comparable intensities. Erdman *et al.*[3] have found that an appreciable fraction of the decays proceed through the first excited state. This is substantiated by two measurements made in the present experiment.

The first of these measurements was a single-crystal pulse-height analysis of the high-energy gamma-ray spectrum, obtained at a bombarding energy of 300 kev. For this work, the spectrometer was calibrated with the 2.62-Mev gamma ray from *ThC''* and the 6.13-Mev gamma ray from the $F^{19}(p,\alpha\gamma)O^{16}$ reaction. As shown in Fig. 5, the one- and two-annihilation photon escape peaks of the ground state-gamma ray from the $Li^6(p,\gamma)Be^7$ reaction are clearly seen in the pulse-height distribution, along with the two-escape peak of the more energetic component of the cascade. The one-escape peak of the latter is submerged in the two-escape yield of the direct gamma ray. The pulse-height analysis of the spectrum obtained in the same crystal with the single 6.13-Mev gamma ray from $F^{19}(p,\alpha\gamma)O^{16}$ is included for comparison. From Fig. 5, it is deduced that the direct transition is about two times as intense as the cascade transition.

The second measurement establishes a poorer, but still significant, upper limit to the ratio of the number of direct to cascade transitions. If there were appreciably more ground-state transitions than cascade transitions, the number of Be^7 nuclei formed should be correspondingly greater than the measured number of 430-kev gamma rays. However, Be^7 decays to Li^7 by *K*-capture, with 11 percent[13] of the Li^7 nuclei being formed in the first excited state. This state de-excites by emitting a 480-kev gamma ray. Hence the ratio of the number of 430-kev gamma rays counted in a lengthy bombardment to the number of delayed 480-kev gamma rays should be a measure of the relative intensities of the cascade and direct transitions.

This measurement was made with a 4 μa-hour bombardment at a proton energy of 365 kev, the limitations on the bombardment being the stability of the target under the beam and the rate of growth of carbon on the target surface. The accelerator was turned off at the end of the bombardment and the target was counted for one hour, during which time the decay rate rate of the Be^7 (half-life 53 days[14]) was constant. No delayed 480-kev gamma rays were seen. From the efficiency, background, resolution, and statistics, it is estimated that the cascade transition occurs at least 1 percent as often as the direct transition. The spin assignments discussed above are consistent with these measurements.

Gamma decay by cascade through the second excited state is not expected to compete with the transitions discussed above since no spin assignment to this level can overcome the discouragement resulting from the reduced energy available.[11] The arrow at 1.13 Mev in Fig. 2 indicates where the total absorption peak of the gamma ray from the capture level to the 4.65-Mev level should appear for an incident energy of 215 kev. If we assume that the efficiency of detection in the total absorption peak varies inversely as the 1.31 power of the gamma-ray energy,[7] the results shown in Fig. 2 allow a limit to be placed on the number of transitions from the capture level to the second excited state. At a bombarding energy of 215 kev the number of transi-

[12] D. H. Wilkinson, Phil. Mag. **44**, 450 (1953).

[13] R. M. Williamson and H. T. Richards, Phys. Rev. **76**, 614 (1949).

[14] E. Segrè and C. E. Wiegand, Phys. Rev. **75**, 39 (1949).

tions through the second excited state is less than 10 percent of those through the first excited state, as expected.

The results on intensity measurements may be summarized by saying that 35±5 percent of the gamma decays of the capture state proceed by cascade through the first excited state and 65±5 percent by direct transition to the ground state. Less than 4 percent of the gamma decays of the capture state proceed by cascade through the second excited state.

PHYSICAL REVIEW VOLUME 97, NUMBER 5 MARCH 1, 1955

Angular Distributions of Deuteron-Induced Reactions in Lithium*

S. H. LEVINE,† R. S. BENDER, AND J. N. MCGRUER
University of Pittsburgh, Pittsburgh, Pennsylvania
(Received October 25, 1954)

Angular distributions of (d,t), (d,He^3), (d,p), and (d,d') reactions have been obtained using a natural lithium target. Butler type calculations for $l=1$ transfer fit all of the above data except for the (d,d') reactions. A Q-value of 0.974±0.015 Mev has been assigned to the first excited level in Li^8. The He^5 ground state was observed with the two reactions $Li^7(d,\alpha)He^5$ and $Li^6(d,He^3)He^5$ for which the Q values were 14.26±0.09 Mev and 0.91±0.09 Mev, respectively.

I. INTRODUCTION

A STUDY of the angular distributions of some of the reaction particles resulting from the bombardment of Li^6 and Li^7 with 14.4-Mev deuterons has been made here. The observed angular distributions of the (d,t), (d,He^3), (d,p), and (d,d') reactions are shown. Butler-type calculations[1–3] are used, where possible, to determine the angular momentum transfer and parity change of the reaction. Information about the He^5 ground state is obtained from the two reactions $Li^7(d,\alpha)He^5$ and $Li^6(d,He^3)He^5$.

II. APPARATUS

The scattering project at the University of Pittsburgh[4] uses an incident beam of 14.4-Mev deuterons. The angular spread of the incident beam and of the outgoing particles accepted by the particle analyzer were each 1.8°. A new scattering chamber was installed which could rotate 60° under vacuum. The particle analyzer could be made to cover a continuous range of 120° by changing ports on the scattering chamber. The detector was a CsI crystal cemented to a Type 6292 Dumont photomultiplier tube. The pulse-height resolution was between 4 percent and 6 percent for all charged particles observed. Various aluminum foils could be rotated in front of the crystal to aid in identifying the particles by their pulse height and their energy loss in the foils. Foils also separated pulses of different particles so that they could be resolved and counted simultaneously with a six-channel pulse-height analyzer.

III. TARGET PREPARATION

The target was prepared by evaporating natural lithium, which contains 92.5 percent Li^7 and 7.5 percent Li^6, on a thin silver foil (0.01 mg/cm²) in the scattering chamber. Two targets, No. 1 and No. 2, were used during the experiment. The absolute thickness of the targets was measured with a Beckman spectrophotometer, yielding values of 0.16 mg/cm² for target No. 1 and 0.10 mg/cm² for target No. 2. The relative thicknesses as obtained from the magnet spectrometer were in the ratio of 2.1/1.

IV. RESULTS

A. Magnetic Analysis

Table I lists the energy levels observed whose assignments have been uniquely determined by the variation in recoil energy of the outgoing particles with angle except for the $(d,\alpha)He^5$ and $(d,He^3)He^5$ reactions. Data for these two reactions were taken at only one angle; however, the Q-values were such that the detected particles could not have come from any of

TABLE I. List of energy levels and reactions observed. (g.s. ≡ ground state.)

Reaction	Levels (Mev)
$Li^7(d,t)Li^6$	g.s., 2.187
$Li^7(d,d')Li^7$	g.s.,[a] 0.478, 4.61
$Li^7(d,p)Li^8$	g.s., 0.97, 2.28[a]
$Li^7(d,He^3)He^6$	g.s., 1.71
$Li^7(d,\alpha)He^5$	g.s.[a]
$Li^6(d,p)Li^7$	g.s., 0.478, 6.56[a]
$LI^6(d,He^3)He^5$	g.s.[a]

[a] Levels observed but angular distribution data not taken.

* This work was done in the Sarah Mellon Scaife Radiation Laboratory and was assisted by the joint program of the Office of Naval Research and the U. S. Atomic Energy Commission.
† Now at Westinghouse Atomic Power Division Laboratory.
[1] H. C. Newns, Proc. Phys. Soc. (London) A65, 916 (1952).
[2] S. T. Butler, Proc. Roy. Soc. (London) A208, 559 (1951).
[3] R. Huby and H. C. Newns, Phil. Mag. 42, 1442 (1952).
[4] Bender, Reilley, Allen, Ely, Arthur, and Hausman, Rev. Sci. Instr. 23, 542 (1952).

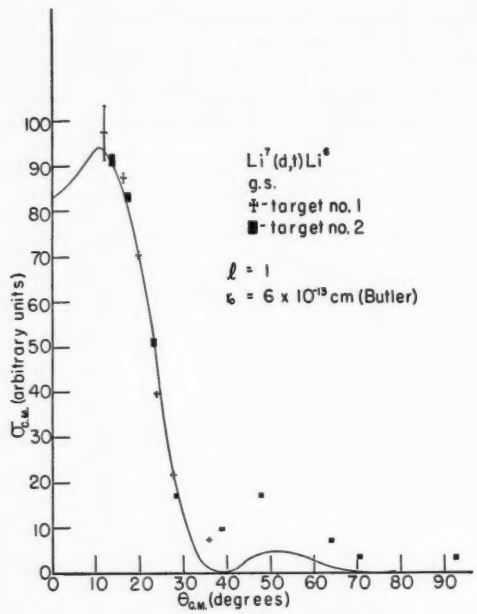

FIG. 1. Angular distribution of the $Li^7(d,t)Li^6$ ground-state reaction.

the contaminants. All levels listed have been reported previously.[5]

Data taken at the laboratory angle of 8.6° had to be corrected, since at this angle the Faraday cage was partially blocking the used sector of No. 3 magnet. A correction of 12 percent was made from the geometry of the system; the uncertainty of this correction introduced an error of ±6 percent. This accounts for the large error at the most forward points of each angular distribution.

The solid angle Ω of the particle analyzer was measured experimentally by observing the ratio of Po α particles counted by a known solid angle to that counted by the analyzer. The measured solid angle $\Omega = 1.77 \times 10^{-4}$ steradian agreed with the geometric solid angle of 1.8×10^{-4} steradian. The absolute cross section of the elastically scattered deuterons was compared with the Rutherford scattering cross section at an angle of 36° in the center-of-mass system. The Rutherford scattering cross section was found to be smaller by a factor of four.

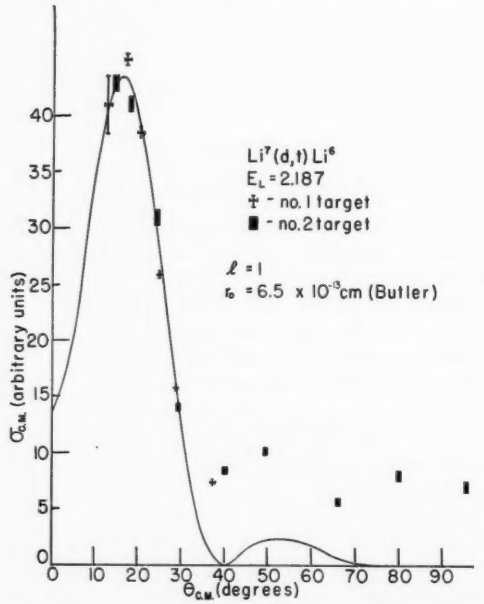

FIG. 2. Angular distribution of the $Li^7(d,t)Li^6$ 2.187 level.

[5] F. Ajzenberg and T. Lauritsen, Revs. Modern Phys. **24**, 321 (1952).

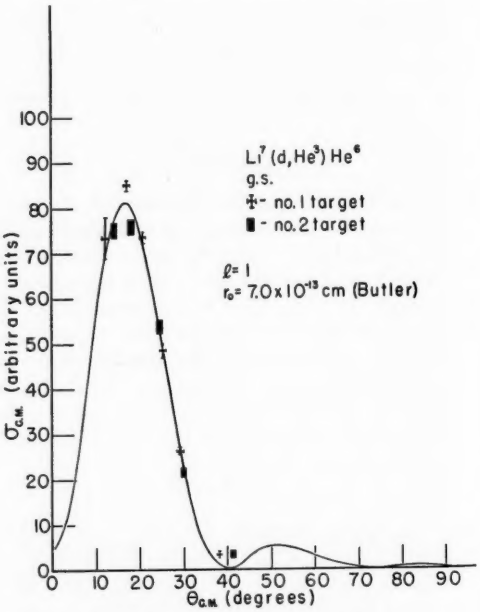

FIG. 3. Angular distribution of the $Li^7(d,He^3)He^6$ ground-state level.

Using the silver backing material as a target, a survey run at an angle of 16° showed that the silver made no contribution to the lithium cross sections.

B. $Li^7(d,t)Li^6$

The two triton groups observed correspond to the Li^6 ground state and the 2.187-Mev level. At the most forward angles the magnetic field required to focus the tritons was so great as to be out of range of the proton resonance equipment. For these cases, the proton resonance frequency was obtained in the following manner. Since the current in the magnet coils could also be measured using a potentiometer dial reading, a

graph of potentiometer dial reading *versus* proton resonance frequency was drawn. This graph was then extended beyond the range of the proton resonance frequency, 61 Mc/sec, to 66 Mc/sec from which all the necessary data could be obtained. Tritons from the Li^6 3.58-Mev level were not observed. This might be attributed to the fact that at the most forward angles where the cross sections are relatively greater, the elastic peak appeared at the same value of the magnetic field as would tritons from the Li^6 3.58-Mev level; the intensity of the elastic peak made such observations impossible.

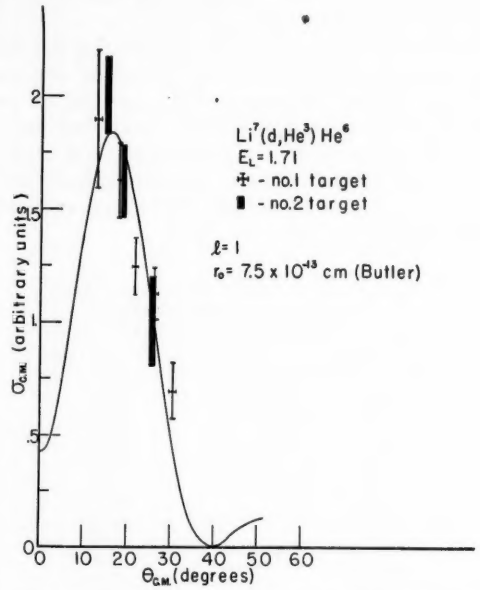

FIG. 4. Angular distribution of the $Li^7(d,He^3)He^6$ 1.71 level.

1. Li^6 Ground State

The angular distribution in the center-of-mass system for the triton group corresponding to the ground state of Li^6 is shown in Fig. 1. The solid line is the Butler curve for $l=1$ and radius $r_0=6\times10^{-13}$ cm. Holt and Marsham[6] have previously reported the angular distribution of this reaction using an incident deuteron energy of approximately 7.7 Mev. Normalizing their peak to the peak of the data presented here produces a similar distribution displaced toward the larger angles. A larger radius, however, is needed to fit their data.

2. Li^6 2.187-Mev Level

The solid line in Fig. 2 is the Butler curve for $l=1$ and $r_0=6.5\times10^{-13}$ cm.

[6] J. R. Holt and T. N. Marsham, Proc. Phys. Soc. (London) 66A, 1032 (1953).

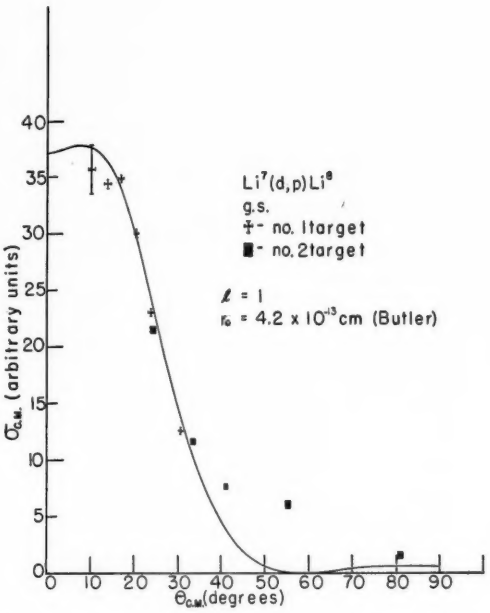

FIG. 5. Angular distribution of the $Li^7(d,p)Li^8$ ground state.

C. $Li^7(d,He^3)He^6$

1. He^6 Ground State

The angular distribution of this reaction is shown in Fig. 3. The best fit is obtained with a radius of 7×10^{-13} cm and $l=1$.

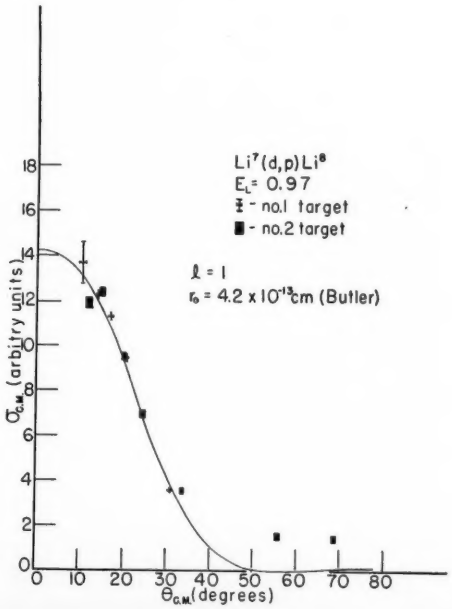

FIG. 6. Angular distribution of the $Li^7(d,p)Li^8$ 0.97 level.

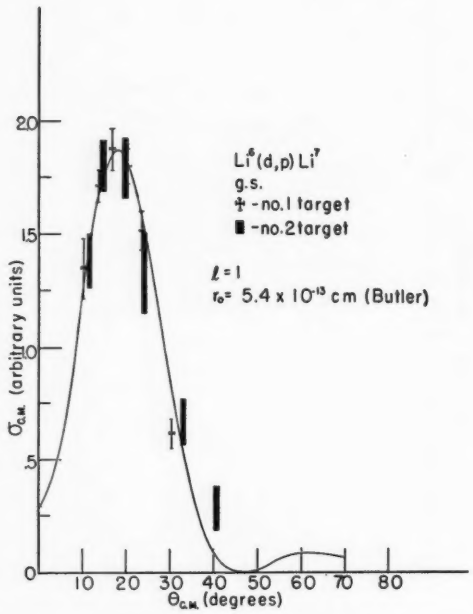

FIG. 7. Angular distribution of the $Li^6(d,p)Li^7$ ground state.

2. He^6 1.71-Mev Level

The angular distribution of this reaction is shown in Fig. 4. A Butler curve of $l=1$ and $r_0=7.5\times10^{-13}$ cm gives a fit to the data.

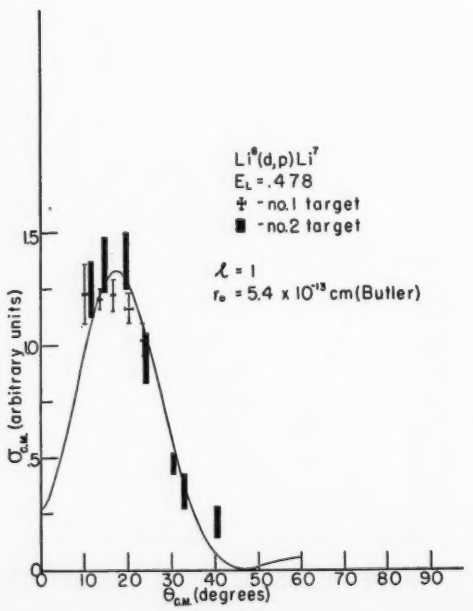

FIG. 8. Angular distribution of the $Li^6(d,p)Li^7$ 0.478 level.

D. $Li^7(d,p)Li^8$

1. Li^8 Ground State

For this reaction a correction for the contaminant peak, C^{13} 3.08-Mev level, underneath the Li^8 ground state had to be made at the most forward angles. The two targets had different amounts of carbon deposits giving two different angular distributions for the Li^8 ground-state reaction. The difference between the two curves yielded the angular distribution of the contaminant peak. A correction could therefore be made for the contaminant peak contribution. The Butler curve for $l=1$ and $r_0=4.2\times10^{-13}$ cm gave the best fit to the experimental data as shown in Fig. 5.

The angular distribution of this reaction has been previously reported by Holt and Marsham[6] who used 7.7-Mev incident deuterons. They ascribed an $l=1$ transfer to this reaction; however, they were unable to fit the data exactly with a Butler curve. The shape of their distribution was such that two different radii, $r_0=5.3\times10^{-13}$ cm and $r_0=4.0\times10^{-13}$ cm, gave equally good results.

TABLE II. Energy values observed for the Li^8 0.97-Mev level at various angles.

θ_{lab} (degrees)	Level values (Mev)
15	0.973
22.3	0.974
11	0.965
12.1	0.974
11.6	0.970
8.6	0.971
14.1	0.974
17.1	0.977
17.1	0.975
19.9	0.980
25.9	0.976
12.4	0.976

2. Li^8 0.97-Mev Level

Data for this reaction were taken at 11 different angles; the possibility that this level could have been a contaminant level was ruled out by the angular dependence of the level spacing from the Li^8 ground state which is a sensitive function of the assumed target nucleus. Data for this level are presented in Table II. The average of the values in Table II assign to this level a value of 0.974 ± 0.015 Mev.

The Butler curve for $l=1$ and $r_0=4.2\times10^{-13}$ cm gave the best fit to the data taken for this reaction as shown in Fig. 6.

E. $Li^6(d,p)Li^7$

Holt and Marsham[6] have obtained angular distributions of the $Li^6(d,p)Li^7$ ground state and 0.478-Mev levels as far forward as 0°. They used values of $l=1$ and $r_0=4.9\times10^{-13}$ cm for the Butler curve.

1. Li^7 Ground State

Figure 7 shows that a Butler curve for $l=1$ and $r_0=5.4\times10^{-13}$ cm fits the data.

2. Li^7 0.478-Mev Level

Figure 8 shows the fit obtained with a Butler curve using values $l=1$ and $r_0=5.4\times10^{-13}$ cm.

F. $Li^7(d,d')Li^7$

1. Li^7 0.478-Mev Level

Figure 9 shows the Huby and Newns[8] theory for $l=2$ and $r_0=6.5\times10^{-13}$ cm and the experimental data.

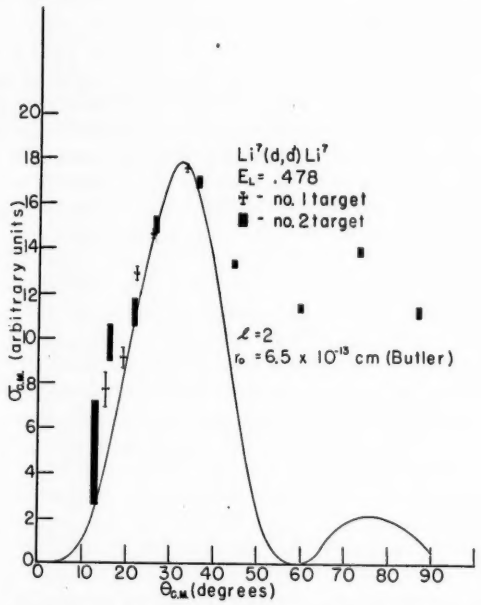

FIG. 9. Angular distribution of the $Li^7(d,d')Li^7$ 0.478 level.

This value of l is consistent with the results obtained from the $Li^6(d,p)Li^7$ 0.478-Mev reaction. Slit edge scattering increased rapidly toward smaller angles and at the same time the cross section decreased producing large errors for this reaction at the forward angles.

2. Li^7 4.61-Mev Level

Figure 10 shows only the experimental points since no values of the parameters in the Huby and Newns theory produced a reasonable fit to the data.

A search for the $Li^6(d,p)Li^7$ 4.61-Mev level was made only at angles less than 20° in the laboratory system, because at angles greater than 20°, proton groups from other elements appeared at the same magnetic field setting. This reaction was not observed although a differential cross section greater than 3 mb would have permitted its observation.

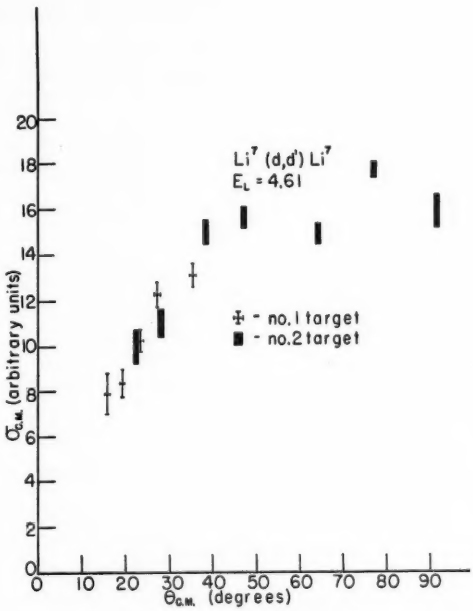

FIG. 10. Angular distribution of the $Li^7(d,d')Li^7$ 4.61 level.

Three values of the Q of the $Li^7(d,d')Li^7$ 4.61-Mev reaction were -4.60, -4.62, and -4.63 Mev yielding an average Q-value $=-4.62\pm0.04$ Mev. The width of the peak, ΔE, at half-maximum in the laboratory

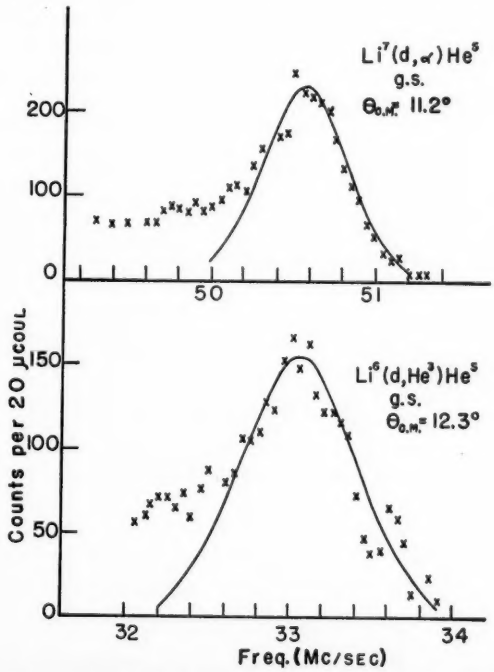

FIG. 11. Counts per 20 microcoulombs as a function of analyzing magnet field for the $Li^7(d,\alpha)He^5$ ground state and the $Li^6(d,He^3)He^5$ ground state.

TABLE III. Summary of results obtained. (g.s.≡ground state.)

Reaction	l	Spin(parity)	$r_0\times10^{-13}$ cm	Q(Mev)	$\sigma(\theta)$ mb/sterad	θ(c.m.)	ΔQ(Mev)
$Li^7(d,t)Li^6$ g.s.	1	1^+	6.0		32.4	11°	
$Li^7(d,t)Li^6$ 2.187 Mev	1	3^+	6.5		16.0	16°	
$Li^7(d,p)Li^8$ g.s.	1	0^+, 1^+, 2^+, 3^+	4.2		26.1	8°	
$Li^7(d,p)Li^8$ 0.97 Mev	1	0^+, 1^+, 2^+, 3^+	4.2	− 1.162	10.2	2°	
$Li^7(d,He^3)He^6$ g.s.	1	0^+	7.0		8.0	17°	
$Li^7(d,He^3)He^6$ 1.71 Mev	1	0^+, 1^+, 2^+, 3^+	7.5		2.0	16.5°	
$Li^7(d,\alpha)He^5$ g.s.[a]				14.26	2.1	11.2°	0.66
$Li^6(d,He^3)He^5$ g.s.[a]				0.91	32.0	12.3°	0.69
$Li^6(d,p)Li^7$ g.s.	1	$\frac{3}{2}^-$	5.4		12.8	18°	
$Li^6(d,p)Li^7$ 0.478 Mev	1	$\frac{1}{2}^-$	5.4		9.2	17.5°	
$Li^6(d,p)Li^7$ 6.56 Mev[a]				0.91	32.0	12.3°	0.67
$Li^7(d,d')Li^7$ g.s.[a]							
$Li^7(d,d')Li^7$ 0.478 Mev					7.7	32°	
$Li^7(d,d')Li^7$ 4.61 Mev				− 4.62	8.8	47°	0.3

[a] Levels observed but angular distribution data not taken.

system was found to be 0.3±0.1 Mev corresponding to a ΔQ of 0.3±0.1 Mev.

G. Ground State of He^5

The $Li^7(d,\alpha)He^5$ and the $Li^6(d,He^3)He^5$ reactions were observed to lead to the He^5 ground state. Figure 11 shows the observed counting rate as a function of proton resonance frequency, the high-energy part of the data having been fitted with a Gaussian curve. The (d,He^3) reaction data have been plotted with a gamma-ray background of 31 counts subtracted from each point. Both levels are very broad having asymmetrical shapes that indicate three-body disintegration.[7] By correcting the observed level widths for the instrumental contributions, the resulting widths of the fitted Gaussian at half-maximum of the $Li^7(d,\alpha)He^5$ and the $Li^6(d,He^3)He^5$ reactions in the laboratory system were 0.48 Mev and 0.62 Mev respectively. The corresponding ΔQ's are 0.66±0.20 Mev and 0.69±0.20 Mev. The Q-values obtained for these reactions were 14.26±0.09 Mev for the (d,α) reaction and 0.91±0.09 Mev for the (d,He^3) reaction, corresponding to mass defects of 12.82 Mev and 12.86 Mev.

The absolute differential cross sections obtained at center-of-mass angles of 11.2° for the (d,α) reaction and 12.3° for the (d,He^3) reaction were

$$\sigma(\theta)_\alpha = 2.1\pm0.7 \text{ mb/sterad},$$

and

$$\sigma(\theta)_{He^3} = 32\pm13 \text{ mb/sterad}.$$

V. DISCUSSION

The errors in the relative cross section were computed for each point. Statistical variation in counts and errors in background subtraction accounted for most of the errors. An additional error of 2 percent was introduced for those triton peaks which were focused by magnetic fields too large to be measured with the proton resonance equipment. The error in the absolute cross section was due almost entirely to an estimated uncertainty of 25 percent in the target thickness.

Either Born or Butler type calculations provide satisfactory fits to the observed angular distributions resulting from pickup reactions at angles smaller than 35° (c.m.). In the pickup calculations a Gaussian wave function was used for the internal wave function of the triton or He^3 particle. A single radius was employed to fit the Butler curves to the angular distributions of the (d,p) reactions involving the same final nucleus. The radius $r_0=4.2\times10^{-13}$ cm used with the Li^8 angular distributions comes close to the value 4.1×10^{-13} cm obtained using the Gamow and Critchfield formula. Butler type calculations for $l=1$ transfer provide the best fit to all the above data. Neither $l=0$ or $l=2$ transfer provided a satisfactory fit. In all cases the l values are consistent with the known data.

Table III summarizes the majority of the results obtained from this experiment. The article of Ajzenberg and Lauritsen[5] was used in preparing the column listing spin and parity. It lists the reactions observed, the l transfer for each reaction, the parity and possible spin values of the final state, the radius r_0, the measured Q-values for the particular reaction, the absolute differential cross section $\sigma(\theta)$ with the corresponding angle in the center-of-mass system, and the width at half-maximum ΔQ.

We wish to acknowledge the help received from Dr. A. J. Allen, Dr. E. Gerjuoy, Mr. W. F. Vogelsang, and Mr. E. K. Warburton, as well as from the many other members of the Laboratory who have taken interest in this project.

[7] C. D. Moak, Phys. Rev. **92**, 383 (1953).

Isomeric State of Y^{88} in the Decay of Zr^{88}†

E. K. Hyde, M. G. Florence, and A. E. Larsh
Radiation Laboratory, University of California, Berkeley, California
(Received November 29, 1954)

The 85-day activity Zr^{88} decays by electron capture to Y^{88m} which de-excites by emission of 395-kev gamma radiation with a half-life of 0.37 ± 0.03 millisecond. From the half-life and the conversion coefficient the transition is characterized as $E3$.

I. INTRODUCTION

A PRELIMINARY report on the nuclide Zr^{88} by Hyde and O'Kelley[1] showed that it decayed by electron capture with a half-life of many months into the well-known 105-day isotope Y^{88}. An accurate value of 85 days was given later.[2] Prominent in the decay was a single gamma ray of 406 kev as determined in a beta-ray spectrometer. No positrons were detected nor were any other gamma radiations observed.

Recently we have restudied the gamma radiation of this isotope in a scintillation spectrometer. The activity was prepared by bombarding 0.005-inch thick foils of pure niobium metal with 100-Mev protons in the 184-inch cyclotron, whereby Zr^{88} is produced by the $Nb^{93}(p,2p4n)Zr^{88}$ reaction. The target was set aside for two months to allow complete decay of all interfering zirconium activities, principally 80-hour Zr^{89}. At the end of this time a pure sample of Zr^{88} was isolated by the radiochemical procedures previously described.[1]

The gamma radiation was studied in a sodium iodide crystal-photomultiplier tube combination coupled, after suitable amplification, to a 50-channel electronic pulse-height analyzer. As shown in Fig. 1, a single gamma ray was detected. By repeated calibration against the gamma standards U^{235}(184 kev), Cs^{137}(662 kev), Am^{241}(59.8 kev), Cd^{109}(87 kev), Na^{22}(510 kev), Hg^{203}(279 kev), and Nb^{95}(745 kev), the energy was determined to be 395 kev. This is believed to be more accurate than the previous beta-ray spectrometer value of 406 kev. No other gamma radiation was detected nor was there any evidence of annihilation radiation from positron decay.

Isomerism in the Y^{88} daughter was established by an x-ray—gamma-ray coincidence experiment carried out with the assistance of Frank S. Stephens. A set-up was used in which the sample was placed between two sodium iodide-photomultiplier combinations facing each other. The gate crystal was encased in beryllium rather than aluminum to increase the transition of 15-kev x-rays. The output of this crystal-photomultiplier assembly was applied to a single-channel pulse-height analyzer to allow selection of pulses corresponding to the x-rays and these were used to gate the coincidence circuit. The output of the second crystal-photomultiplier combination was applied to the signal side of the coincidence circuit. Those pulses arriving in coincidence with the gate pulses within the rather slow resolving time of 5×10^{-6} second were displayed on the 50-channel pulse-height analyzer. Experiments performed in this apparatus with pure samples of Zr^{88} showed conclusively that the 395-kev gamma ray was not in coincidence with the x-rays, indicating a delayed state in Y^{88} with a half-life longer than 5×10^{-6} second.

Application of the Montalbetti[3] nomogram of the Weisskopf[4,5] formula for half-lives of isomers indicated the following predicted mean lives for various transition types: 2×10^{-9} second for $E2$, 2×10^{-7} second for $M2$, 8×10^{-4} second for $E3$, 0.8 second for $M3$, 13 minutes for $E4$, and 2 hours for $M4$. Conversion would affect these values but little.[6] Chemical experiments in which yttrium daughter activity was rapidly separated from the Zr^{88} parent activity and examined for the 395-kev gamma radiation were negative, indicating a half-life shorter than a few seconds. Hence it seemed apparent that the transition was $E3$ or $M3$ in nature and that the half-life might be expected to lie in the region of 10^{-2} to 10^{-4} second. A delayed-coincidence technique was applied to this problem with success.

II. MEASUREMENT OF THE HALF-LIFE

A weak sample of Zr^{88} with a disintegration rate of a few hundreds per minute and mounted on aluminum foil was placed between the two sodium iodide crystals mentioned above. The side of the aluminum foil on which the activity had been evaporated faced the beryllium covered crystal. As before, pulses corresponding to 15-kev x-radiation intercepted by the gate crystal were selected by a single-channel analyzer. The output of the analyzer was fed to the trigger input of a Tektronix-514D oscilloscope to start a trace across the oscilloscope face. The speed of this trace could be adjusted with the standard controls of the oscilloscope. The pulses from the signal crystal were fed to the vertical deflecting system of the oscilloscope. Signal pulses arriving in prompt coincidence with the 15-kev

† This research was carried out under the auspices of the U. S. Atomic Energy Commission.

[1] E. K. Hyde and G. D. O'Kelley, Phys. Rev. 82, 944 (1951).
[2] E. K. Hyde, Phys. Rev. 92, 927 (1953).
[3] R. Montalbetti, Can. J. Phys. 30, 660 (1952).
[4] V. F. Weisskopf and J. M. Blatt, *Theoretical Nuclear Physics* (John Wiley and Sons, Inc., New York, 1952).
[5] V. F. Weisskopf, Phys. Rev. 83, 1073 (1951).
[6] Rose, Goertzel, Spinrad, Harr, and Strong, Phys. Rev. 83, 79 (1951).

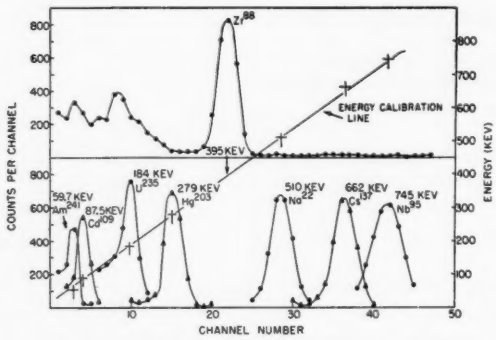

FIG. 1. Gamma spectrum of pure sample of Zr^{88}.

trigger pulses were displayed as dots at the start of the trace. The height of the dots above the base line was proportional to the energy of the detected gamma radiation. These signal pulses appeared as dots for the usual reason that the duration of the flat-topped pulse (7 microseconds) was greater than the rise and decay time. Any delayed gamma-ray signal pulses or randomly occurring chance pulses which arrived during the sweep appeared as dots at a corresponding distance from the start of the trace.

A Poloroid Land camera was used to take exposures of 4-minute duration of the scope face. When the sweep speed was set at 0.3 millisecond per centimeter a finished photograph showed a band of dots at a height corresponding to the 395-kev gamma ray decreasing in intensity across the horizontal time scale. Dots at lower energies corresponding to the Compton scattered radiation were also observed. An exact time scale was printed on the photographs by impressing a sine wave of 1200 cycles per second from a calibrated signal generator on the vertical deflection plates of the oscilloscope.

To extract the data recorded on the photographs the 395 ± 20-kev energy band was marked off by penciled lines and the horizontal time scale was marked off in units of 333 microseconds ($\frac{1}{2}$ the period of the 1200-cycle sine wave). The dots in each square were then counted under a low-power microscope. The number of dots per square were plotted on semi-logarithmic graph paper as a function of the distance (time). Figure 2 is a composite plot of the data from 17 photographs. The half-life of 0.37 millisecond is believed to be good to ±0.03 millisecond.

A common difficulty in this type of experiment is that halation from the base line on the oscilloscope screen fogs the photograph during the necessarily long exposure times. This difficulty was avoided by not using the normal unblanking circuit of the Tektronix-514D oscilloscope. Instead, when the positive signal pulse from the crystal-photomultiplier amplifier combination was fed to the vertical deflection system as mentioned above, it was simultaneously fed to an inverter circuit which inverted and amplified the pulse. The resulting negative pulse was fed to the cathode input post on the oscilloscope to unblank the trace at the instant a signal appeared on the vertical deflector.

The Zr^{88} is an almost ideal case for the application of this delayed coincidence method inasmuch as no extraneous radiations are present, although we have applied the method successfully to the measurement of a 10-millisecond delay in a gamma ray associated with Mo^{90} where an appreciable chance background had to be considered.[7]

The 0.37-millisecond half-life corresponds most closely to the $E3$ half-life prediction, although $M3$ probably cannot be ruled out. The conversion electron spectrum of the 395-kev gamma transition is shown in Fig. 3. The observed K/L ratio is 8.4. With presently available empirical data on K/L ratios[8] or theoretical calculations of L-shell conversion coefficients no clear choice between $E3$ and $M3$ can be made on the basis of this K/L ratio although $M3$ appears to be favored.

III. MEASUREMENT OF THE CONVERSION COEFFICIENT

A sensitive test of transition type is the K-shell conversion coefficient. Exact theoretical value for the transition under discussion can be taken from the theoretical curves of Rose *et al.*[6] The expected K conversion coefficients are 0.03 for $E3$ and 0.065 for $M3$.

An experimental measurement of the total conversion coefficient (which, within the experimental error, can be equated to the K-shell conversion coefficient inasmuch as the K/L ratio is large) was made in the following way.

A sample of freshly purified Zr^{88} was mounted on aluminum and counted in a GM counter which had been calibrated with a Bureau of Standard's RaDEF beta standard. Beryllium and aluminum absorption curves were run to determine that 55 percent of the activity detected through no absorber was assignable

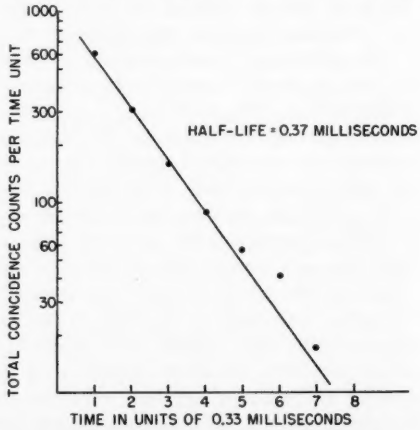

FIG. 2. Decay curve for Y^{88m}. Data compiled from 17 photographs as described in text.

[7] H. B. Mathur and E. K. Hyde, Phys. Rev. (to be published).
[8] M. Goldhaber and A. W. Sunyar, Phys. Rev. **83**, 906 (1951).

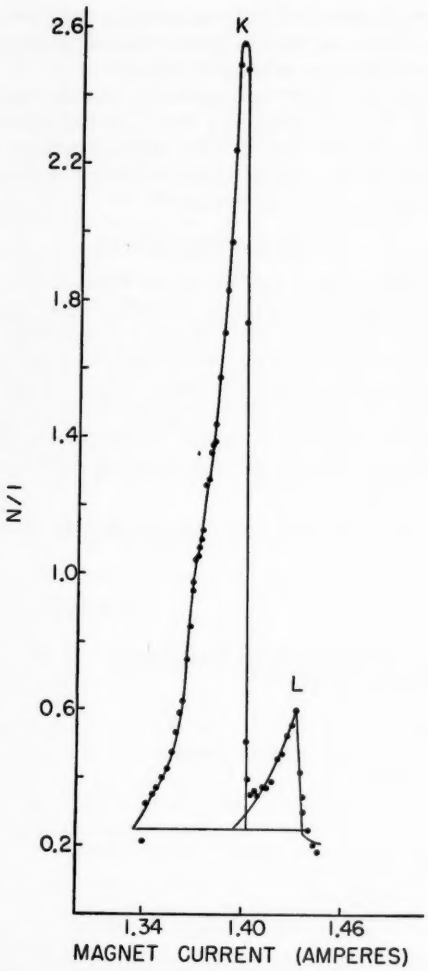

FIG. 3. Conversion electrons of 395-kev transition in Y^{88m}. Data taken by J. Schooley and J. Juliano. *Note added in proof.*—Recent recalibration of the beta-ray spectrometer shows that the best value of the γ-ray energy is 387 rather than 395 kev.

to conversion electrons, the remaining 45 percent being due to the much less efficiently counted x-ray and 395-kev gamma-ray photons. The electron counting rate was corrected for geometry and a backscattering to 10 percent, which yielded a value of 6350 electrons per minute for the sample.

The gamma-ray emission rate was measured by duplicating Fig. 1 with this particular sample, using a sample position about 4.5 cm away from the 1-inch $\times 1\frac{1}{2}$-inch sodium iodide crystal. The geometry factor of this position was known to be 3.8 percent from measurements of the photopeak of the 59.8-kev gamma ray emitted by an Am^{241} sample of known alpha disintegration rate. The area under the photopeak of the 395-kev gamma ray was corrected for this geometry factor and for a 27 percent photopeak efficiency to calculate an absolute gamma emission rate of 261,000 per minute.

The ratio of conversion electrons to gamma-ray photons was 0.024. The number of conversion electrons was checked by counting the same Zr^{88} sample in an anthracene crystal-photomultiplier combination coupled to the 50-channel pulse-height analyzer. Because of the low conversion coefficient the conversion electron peak was obscured somewhat by Compton scattered electrons, but the contribution to the observed electron spectrum from this source was easily found by rerunning the spectrum with a 120 mg/cm^2 aluminum absorber between the sample and the crystal to absorb the electrons.

The counting yield of the geometrical arrangement used in this measurement was calibrated by counting a sample of Cs^{137} under identical conditions. The conversion electron line at 625 kev was easily resolved from the β^- spectrum. The conversion coefficient of the 662-kev transition in the Cs^{137} decay is 0.1.[8] By counting the gamma-ray photons in the sodium iodide spectrometer, integrating under the photopeak, correcting for a crystal efficiency of 12 percent and correcting for geometry, the absolute number of conversion electrons expected from the sample was calculated and compared with the observed electron counting rate. The counting yield figure so obtained was 23 percent.

This number was used to convert the observed electron counting rate for the Zr^{88} sample to an absolute disintegration rate. This number was 17 percent higher than that found in the GM counter, yielding a conversion coefficient of 0.027.

Considering the errors in the measurements, the final value for the total conversion coefficient can be given within the limits $0.02_5 \pm 0.01$. Hence the conversion coefficient clearly favors $E3$ rather than $M3$ for the transition type.

IV. DISCUSSION

The 0.37-millisecond activity decays into and is isomeric with the 105-day Y^{88} whose decay scheme is well established.[9] The great majority of nuclear isomers can be related to the nuclear shell model as has been shown conclusively in the review of Goldhaber and Hill.[10] Even in the case of odd-odd nuclei the configurations of the individual odd particles correspond to the predictions of the single-particle model and isomers can occur when the odd neutron or proton lies just beneath a completed shell. In this new example the odd-proton and odd-neutron numbers are 39 and 49, respectively, and the isomerism can be attributed to the closed shell at 50 particles.

Empirical data from many nuclides show that $f_{5/2}$, $p_{3/2}$, $p_{1/2}$, and even $g_{9/2}$ levels are available to the 39th particle. The 49th particle may be either $g_{9/2}$ or $p_{1/2}$.

[9] For references see Hollander, Perlman, and Seaborg, Revs. Modern Phys. **25**, 469 (1953).

[10] M. Goldhaber and R. D. Hill, Revs. Modern Phys. **24**, 179 (1952).

It cannot be predicted with certainty which of these possible orbitals will be occupied or how the odd neutron-odd proton orbitals will couple. Nordheim's rule[11] is useful for ground state predictions, but it has many exceptions.[12] In the case of the 105-day ground state of Y^{88} the spin is 4 with odd parity resulting from a $p_{1/2}$ proton and a $g_{9/2}$ neutron. Inasmuch as the 0.37-millisecond gamma transition is $E3(\Delta I=3$, yes), the isomeric level must be $+1$ or $+7$. Using the orbitals just mentioned, the only likely choice is $+1$ resulting from a $p_{1/2}$ proton and a $p_{1/2}$ neutron. An additional reason excluding $+7$ is that the even-even Zr^{88}, presumably with spin 0, would not be expected to show prominent electron capture decay to a $+7$ state.

There are several other examples of odd-odd isomerism in this mass region. The most closely related examples are $_{37}Rb_{49}^{86}$ (2 isomeric forms)[10,13,14] and $_{41}Nb_{49}^{90}$ (3 isomeric forms)[7] which differ from Y^{88} only in the subtraction or addition of 2 protons. In addition, Rb^{84} and Nb^{94} exist in isomeric forms.[10]

It perhaps should be mentioned that an isomeric form of Y^{88} with properties distinctly different from the one reported here (2-hour positron emitter) was published many years ago[9] but that later workers have shown this report to be in error.[15]

V. ACKNOWLEDGMENTS

We wish to thank the crew of the 184-inch cyclotron for the proton bombardments of niobium foil required in this research. One of us (M.G.F.) acknowledges the support of the U. S. Air Force Institute of Technology, Wright-Patterson Air Force Base, Dayton, Ohio. We also wish to thank Frank S. Stephens for considerable help on the scintillation counter measurements. James Schooley and Jose Juliano determined the electron spectrum of Fig. 3.

[11] L. W. Nordheim, Revs. Modern Phys. **23**, 322 (1951).
[12] M. H. L. Pryce, Repts. Progr. Phys. **17**, 26 (1954).
[13] A. Flammersfeld, Z. Naturforsch. **6a**, 559 (1951).
[14] Schwartz, Perlman, and Bernstein, Phys. Rev. **91**, 883 (1953).
[15] Robertson, Scott, and Pool, Phys. Rev. **76**, 1649 (1949).

PHYSICAL REVIEW VOLUME 97, NUMBER 5 MARCH 1, 1955

Angular Distribution of the Resonance Fluorescence Radiation from the 411-kev Excited State of Hg^{198}*

FRANZ R. METZGER
Bartol Research Foundation of The Franklin Institute, Swarthmore, Pennsylvania
(Received November 16, 1954)

By using the Doppler broadening due to thermal agitation at elevated temperatures as a means of restoring the resonance condition, the angular distribution of the resonance fluorescence radiation from the 411-kev excited state in Hg^{198} has been measured. The observed distribution has the form

$$1+(0.37\pm0.06)P_2(\cos\theta)+(1.07\pm0.08)P_4(\cos\theta),$$

which agrees very well with the theoretical expectation for the excitation of a state with spin 2 from a ground state with spin 0.

INTRODUCTION

IN his paper on the directional correlation of successive quanta, Hamilton[1] pointed out that the correlation functions $W(\theta)$ should also apply if one or both transitions are absorptions rather than emissions. Thus $W(\theta)$ should give the angular distribution of resonance radiation excited by a unidirectional, unpolarized beam of gamma rays.

Over the past few years the investigation of the angular correlation of successive gamma rays has provided very valuable information on the excited states of nuclei. The success has been especially good for even-even nuclei because the value 0 of the spin of the ground state reduces the number of possible complications due to mixtures of multipoles to a minimum. For odd-A nuclei the interpretation of angular correlation data is sometimes rather ambiguous due to the many parameters determining $W(\theta)$. In this respect the study of the angular distribution of resonance fluorescence radiation offers considerable advantages: If the spin of the ground state is known, the only parameters entering into the calculation of $W(\theta)$ for resonance radiation are the J-value of the excited state and the multipole character of the transition. In the angular correlation case the J-values of two different excited states and the multipole character of the two gamma rays define $W(\theta)$. The number of parameters involved in the angular correlation case is thus in general considerably greater than the number involved in the angular distribution of resonance radiation.

With an ingenious experiment on Hg^{198}, Moon[2] and co-workers have recently demonstrated that under suitable conditions resonance fluorescence becomes a very prominent phenomenon which can be studied in detail. Moon[2] used the large peripheral speed of a centrifuge to compensate via Doppler shift for the small energy

* Assisted by the joint program of the Office of Naval Research and the U. S. Atomic Energy Commission.
[1] D. R. Hamilton, Phys. Rev. **58**, 122 (1940).
[2] P. B. Moon, Proc. Phys. Soc. (London) **A64**, 76 (1951); P. B. Moon and A. Storruste, Proc. Phys. Soc. (London) **A66**, 585 (1953); W. G. Davey and P. B. Moon, Proc. Phys. Soc. (London) **A66**, 956 (1953).

losses suffered by the gamma radiation in the emission and absorption processes.[3] Malmfors[4] later demonstrated, again with Hg^{198}, that the Doppler broadening from the thermal agitation at elevated temperatures is sufficient to produce an observable resonance fluorescence. Further studies[5] indicated that this less elaborate method is capable of an accuracy comparable to the one obtained with the rotor method.

Measurements of the internal conversion[6] of the 411-kev transition in Hg^{198} and studies of the angular correlation[7] between the 680 kev and the 411-kev gamma rays unambiguously assign spin 2, even parity to the 411-kev level in Hg^{198}. Although no new information concerning the 411-kev level was expected from a measurement of the angular distribution of the resonance radiation, Hg^{198} appeared to be a good case on which to test the feasibility of angular distribution measurements and on which to demonstrate how straightforward the interpretation of this type of experiment is.

EXPERIMENTAL PROCEDURE

The experimental arrangement is sketched in Fig. 1. The gamma radiation from the Au^{198} source was scattered by a mercury ring 1 foot in diameter, $2\frac{1}{2}$ inches high, and $\frac{1}{4}$ inch wide. The elastically scattered radiation was detected with a sodium iodide crystal connected to a scintillation spectrometer. A gold cone shielded the detector from the direct radiation. For the measurements at scattering angles smaller than 120 degrees, the gold cone had to be surrounded by an additional lead cone in order to eliminate small angle Compton scattering into the crystal from the air surrounding the gold cone. Lead and cadmium absorbers around the detector reduced the counting rate due to the Compton scattered radiation and thus prevented serious pileup.

By changing the position of the detector relative to the source and to the ring scatterer, the average scattering angle could be changed from 90 degrees up to 150 degrees. In order to measure at 150 degrees, however, the gold cone had to be raised and the surrounding lead cone had to be removed. For scattering angles larger than 150 degrees a set of larger ring scatterers was used.

The thermal agitation at room temperature gives rise, through resonance fluorescence, to less than one-tenth of one percent of the elastically scattered radiation which is mainly Rayleigh scattering.[8] As the temperature of the source is increased, the contribution from resonance fluorescence increases rapidly and reaches several percent at temperatures around the melting point of gold (1063°C). But even at these high

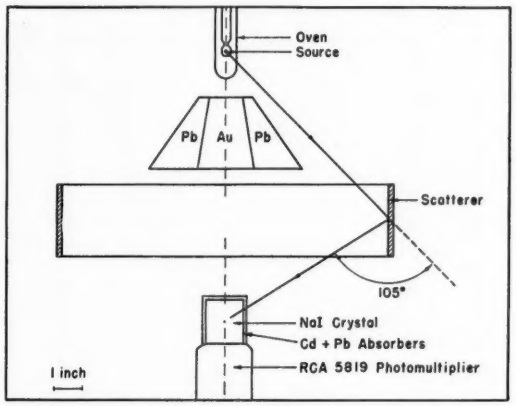

FIG. 1. Experimental arrangement. The relative position of source, scatterer and detector depicted is the one corresponding to a mean scattering angle of 105 degrees.

temperatures Rayleigh scattering is at least ten times larger than resonance scattering. Thus any small change in geometry or in the self-absorption in the source, which might accompany the heating of the source, could simulate a temperature dependence which could be even larger than the effect one is interested in. It is, therefore, necessary to monitor the elastic scattering exclusive of resonance fluorescence by using alternately with the mercury scatterer a lead ring scatterer of identical dimensions. The temperature dependence of the difference in the counting rates of the two scatterers should then be essentially free of any simulated effect and should truly represent the resonance fluorescence contribution.

Ultimately the following procedure was adopted: For every scattering angle the lead and mercury rings were compared at room temperature and the amount of mismatch was determined. Then the source was heated to 1125°C and the two scatterers were compared again. The excess of the difference at 1125°C over the mismatch at room temperature was then attributed to resonance fluorescence in mercury. In order to eliminate drift effects, readings were taken every five minutes alternately with the mercury scatterer and with the lead scatterer. After the measurement at 1125°C another comparison of the scatterers was carried out at room temperature.

As described earlier, the scattering angle was changed by moving the detector with respect to the source and the scatterer. The relative position of source and scatterer was not changed at all. Thus only the solid angle subtended by the detector at the position of the scatterer was changed as one proceeded from one scattering angle to another. The counting rates due to a point source of Au^{198} at the position of the scatterer were measured for the different positions of the detector and were taken as representative of the relative solid angles.

The temperature of the source was measured with a chromel *P*-alumel thermocouple in contact with the

[3] E. Pollard and D. E. Alburger, Phys. Rev. **74**, 926 (1948).
[4] K. G. Malmfors, Arkiv Fysik **6**, 49 (1953).
[5] F. R. Metzger and W. B. Todd, Phys. Rev. **95**, 853 (1954).
[6] P. Hubert, Compt. rend. **232**, 2201 (1951); L. Simons, Phys. Rev. **86**, 570 (1952).
[7] D. Schiff and F. R. Metzger, Phys. Rev. **90**, 849 (1953); C. D. Schrader, Phys. Rev. **92**, 928 (1953).
[8] For a discussion of the hard component of scattered gamma rays, see, e.g., P. B. Moon, Proc. Phys. Soc. (London) **A63**, 1189 (1950).

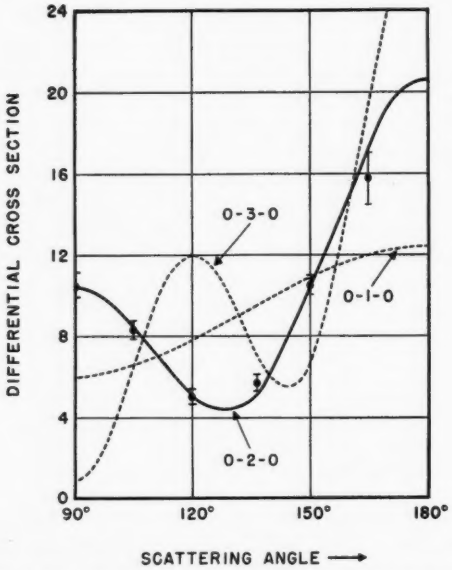

FIG. 2. Angular distribution of the resonance radiation from the 411-kev level of Hg^{198}. The solid line represents the theoretical angular distribution for an excited state with spin 2 and a ground state with spin 0. The dashed lines represent the theoretical distributions for other J-values of the 411-kev state. The differential cross section (in millibarns per steradian) for resonance scattering of the radiation of a Au^{198} source at 1125°C from the 411-kev state in Hg^{198} is plotted as the ordinate.

quartz bulb containing the source. The reliability of the temperature measurements was checked with every new source by observing the sharp change in counting rate occurring at the melting point of gold. This change takes place because the source, which is put into the quartz bulb as a folded piece of gold foil, melts to one gold globule, increasing in this way appreciably the self-absorption.

All the experiments for the angular distribution of the Hg^{198} resonance radiation were carried out at an average room temperature of 25°C and at an average high temperature of 1125°±15°C.

The Au^{198} sources were obtained from Oak Ridge National Laboratory. Sources up to 80 millicuries were used with the large ring scatterers. With the 1-ft diameter rings, sources up to 50 millicuries could be used without causing excessive counting rates.

The single channel of the scintillation spectrometer comprised approximately one full width at half-maximum of the 411-kev photopeak.

RESULTS AND DISCUSSION

Table I represents the results of a typical run with the 1-ft diameter ring scatterers at a mean scattering angle of 150 degrees. The run lasted for three hours. The difference in the counting rates for the lead ring at 23°C and at 1125°C is of the order of magnitude expected on the basis of thermal expansion plus volume change upon melting of the gold source.[4]

The difference in the counting rates of the two scatterers at room temperature showed a variation with scattering angle similar to the angular distribution of the resonance radiation. Although this observation needs further investigation, such a behavior would be expected if a small percentage of the gamma rays were emitted while the beta recoil was still effective, i.e., before the recoiling nucleus had again reached thermal equilibrium with the source. The existence of this effect does not have any influence on the angular distribution, but it is important for an accurate determination of the absolute cross section and consequently of the lifetime of the 411-kev transition.

The results of all the runs with both sets of ring scatterers are summarized in Fig. 2. The differential cross section plotted as a function of the scattering angle has a very specialized meaning: It is the differential cross section of Hg^{198} for resonance scattering of the gamma radiation emitted by an Au^{198} source at 1125°C. It was obtained by normalizing the relative cross sections with the help of a previous absolute measurement.[5] The least squares fit of the form $A_0+A_2P_2(\cos\theta)+A_4P_4(\cos\theta)$ to the experimental points leads to the constants $A_0=8.28\pm0.20$; $A_2=3.04\pm0.48$ and $A_4=8.81\pm0.66$ in units 10^{-27} cm²/steradian. Dividing by A_0, we obtain $W(\theta)=1+(0.37\pm0.06)P_2(\cos\theta)+(1.07\pm0.08)P_4(\cos\theta)$.

TABLE I. Experimental data obtained in a typical run at a mean scattering angle of 150°.

	Counts per minute	
	Pb ring	Hg ring
Source at 23°C	3623.0±11.0	3656.2±11.1
Source at 1125°C	3664.7±11.1	3988.6±11.5
Nonresonance increase	41.7±15.6	42.1±15.8
Resonance fluorescence	...	290.3±22.4

The theoretical coefficients[9] for the angular distribution of the resonance radiation involving a ground state with spin 0 and an excited state with spin 2 are identical with the coefficients for an 0–2–0 gamma-gamma cascade: $A_2/A_0=0.357$; $A_4/A_0=1.143$. The agreement with the observed coefficients is good, and is still improved by correcting for the finite angular spread.

A comparison (Fig. 2) of the observed angular distribution with the angular distributions for other spin assignments to the 411-kev level leaves no doubt as to the correctness of the assignment of spin 2 to this level.

The close agreement between the experimental angular distribution of the resonance radiation and the distribution expected for a level with spin 2 indicates that the lifetime of the 411-kev level is too short for any extranuclear field to affect the angular distribution.

ACKNOWLEDGMENT

The author wishes to thank Mr. W. B. Todd for his help in assembling the equipment and in taking the data, Mr. R. C. Pfeiffer for his assistance in the design and construction of the apparatus, and Dr. L. Eisenbud for valuable discussions.

[9] S. P. Lloyd, Phys. Rev. 83, 716 (1951).

Effects of Perturbing Radiofrequency Fields on Nuclear Spin Coupling

ARNOLD L. BLOOM AND JAMES N. SHOOLERY
Varian Associates, Palo Alto, California

(Received October 8, 1954; revised manuscript received November 24, 1954)

An analysis is made of double resonance experiments in which the $\mathbf{I}_1\cdot\mathbf{I}_2$ interaction observable in certain nuclear magnetic resonance spectra is perturbed by a strong radiofrequency field. The problem is treated by transforming to a rotating coordinate system in which all terms in the Hamiltonian are stationary except for the weak rf field used to investigate the spectrum. Transition energies and intensities are computed in the rotating frame and the spectrum transformed back to the laboratory frame by adding a constant factor to the energy. A double-resonance experiment involving the nuclei F^{19} and P^{31} is described and the experimental results compared with those computed from the theory.

I. INTRODUCTION

WHEN a molecule in a liquid contains several nuclei that have different Larmor frequencies in a given magnetic field, it is often found that the magnetic resonance line for a given nucleus is split into a multiplet whose separation is independent of the applied field.[1] The origin of this line splitting has been discussed by Ramsey,[2] and by Ramsey and Purcell,[3] who show that a coupling between nuclei transmitted via the surrounding electron cloud produces an $\mathbf{I}_1\cdot\mathbf{I}_2$ type of interaction. Recently, experiments have been performed in this laboratory and at Stanford University in which the spin-spin interaction has been disturbed by the application of a strong rf in the vicinity of resonance of one of the nuclei.[4-6] If the rf is strong enough, the spin-spin coupling can be completely destroyed, but for intermediate rf amplitudes the multiplet structure of the spectrum from the undisturbed nucleus often increases in complexity. The purpose of this paper is to discuss the more complex multiplet structure and its behavior as a function of the disturbing rf.

II. THEORY

We shall consider the simplest possible case, that of a system of two nuclei with different gyromagnetic ratios γ_1 and γ_2 respectively. A steady magnetic field H_0 is applied in the z direction which, in the absence of any spin-spin interaction, would provide Larmor angular frequencies $\gamma_1 H_0$ and $\gamma_2 H_0$ for the respective nuclei. The γ's are here defined to be observed gyromagnetic ratios and thus include the effects of any chemical shifts (i.e., induced local fields) that may be present. With the spin-spin interaction, the Hamiltonian for the system is

$$\mathcal{H}=-\hbar[\gamma_1(\mathbf{I}_1\cdot\mathbf{H})+\gamma_2(\mathbf{I}_2\cdot\mathbf{H})+J(\mathbf{I}_1\cdot\mathbf{I}_2)]. \quad (1)$$

We are concerned with the usual experimental conditions of nuclear magnetic resonance where H is predominantly in the z direction, the Larmor frequencies and their difference are of the order of megacycles/second, and $J/2\pi$ is a kilocycle/second or less. Under these conditions only the expectation values for spin in the z direction are effective in the spin-spin interaction, and the allowed transitions between energy levels of Eq. (1) occur at $\gamma_1 H_0+m_2 J, \gamma_2 H_0+m_1 J$, $(m=I, I-1, \cdots, -I)$; thus each of the original Larmor frequencies is split into a field-independent multiplet. We now propose to do the following experiment: A strong rf magnetic field H_2, rotating in the xy plane with angular frequency ω_2 in the vicinity of $\gamma_2 H_0$ is impressed on nucleus 2; simultaneously the transitions in the vicinity of $\gamma_1 H_0$ are investigated by producing resonance with a weak rf field H_1 whose angular frequency is ω_1. The field H_1 is to be weak enough so that it does not appreciably affect the line width of the observed transitions.

The problem is most easily solved by transforming to a coordinate system rotating with H_2. In the rotating frame of reference, terms in the Hamiltonian including H_2, H_0, and $\mathbf{I}_1\cdot\mathbf{I}_2$ are time-independent and the effect of H_1 can be considered as a perturbation inducing transitions between otherwise well-defined energy levels. Since the effect of H_2 and the spin-spin coupling term is at best only a small perturbation on the precession of the spin of nucleus 1, the resonance radiation will be predominantly polarized in the xy plane and spectrum frequencies calculated in the rotating frame can be transferred to the laboratory frame merely by adding to them the factor $\omega_2/2\pi$.

The dynamics of magnetic resonance problems in a rotating coordinate system has been discussed by Rabi, Ramsey, and Schwinger,[7] and by others. For a nucleus with gyromagnetic ratio γ_i, the H_0 field in the z direction must be replaced by the "effective" z component $(H_0-\omega/\gamma_i)$. Thus, the Hamiltonian for our problem, including only stationary terms, can be described in the

[1] Gutowsky, McCall, and Slichter, J. Chem. Phys. **21**, 279 (1953). References to earlier experimental work are given here.
[2] N. F. Ramsey, Phys. Rev. **91**, 303 (1953).
[3] N. F. Ramsey and E. M. Purcell, Phys. Rev. **85**, 143 (1952).
[4] F. Bloch, Phys. Rev. **93**, 944 (1954).
[5] V. Royden, Phys. Rev. **96**, 543 (1954).
[6] For other experiments involving double resonance see J. Brossel and F. Bitter, Phys. Rev. **86**, 308 (1952); T. R. Carver and C. P. Slichter, Phys. Rev. **92**, 212 (1953).
[7] Rabi, Ramsey, and Schwinger, Revs. Modern Phys. **26**, 167 (1954).

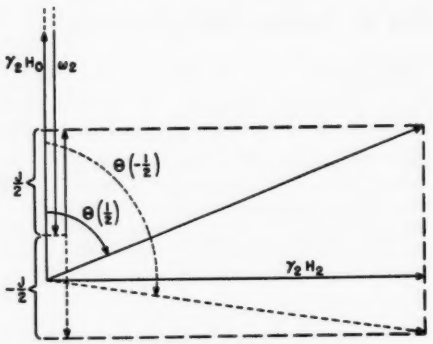

FIG. 1. Vector diagram of forces acting on I_2 in the rotating coordinate system, showing the effect of different orientations of I_1. The special case shown is $I_1=I_2=\frac{1}{2}$.

rotating frame as

$$\mathcal{H}'=-\hbar[\mathbf{I}_1\cdot\mathbf{k}(\gamma_1H_0-\omega_2)+\mathbf{I}_2\cdot\mathbf{k}(\gamma_2H_0-\omega_2)+\mathbf{I}_1\cdot\mathbf{i}(\gamma_1H_2)+\mathbf{I}_2\cdot\mathbf{i}(\gamma_2H_2)+J\mathbf{I}_1\cdot\mathbf{I}_2]. \quad (2)$$

For simplicity, and because it is obviously valid in the experimental case considered here, we shall assume the first term large compared to the others involving $\mathbf{I}_1$. This is equivalent to saying that the nucleus 1 spin is quantized only in the z direction. Spin 2, on the other hand, is quantized in the direction of its effective field, at an angle Θ from the z axis. To determine Θ we consider $J\mathbf{I}_1\cdot\mathbf{I}_2$ in terms of an equivalent magnetic field acting at the site of the nucleus. Refer to Fig. 1. We have

$$a(m_1)=[(\gamma_2H_0+Jm_1-\omega_2)^2+\gamma_2^2H_2^2]^{\frac{1}{2}}, \quad (3)$$

$$\cos\Theta(m_1)=(\gamma_2H_0+Jm_1-\omega_2)/a(m_1), \quad (4)$$

$$\sin\Theta(m_1)=\gamma_2H_2/a(m_1); \quad (5)$$

then the energy levels in the rotating frame are

$$W(m_1,m_2)=\hbar[m_1(\gamma_1H_0-\omega_2)+m_2(\gamma_2H_0-\omega_2+m_1J)\times\cos\Theta(m_1)+m_2\gamma_2H_2\sin\Theta(m_1)], \quad (6)$$

where m_1 is the z component of spin of nucleus 1 and m_2 is now the nucleus 2 spin component in the direction of the effective field.

Restricting ourselves for the time being to $I_1=I_2=\frac{1}{2}$, let us call the $W(m_1=+\frac{1}{2})$ initial states and the $W(m_1=-\frac{1}{2})$ final ones. Of the four possible transitions only two are allowed by selection rules in the unperturbed case where $H_2=0$. In our experiment, however, all four transitions may be observable because Θ changes during the transition, as indicated in Fig. 1; thus the final states of m_2 may not be orthogonal to the initial ones. The relative transition probability for a single nucleus is given by the square of the matrix element connecting initial and final states of nucleus 2, and for $I_2=\frac{1}{2}$ it is

$$P=\cos^2(\xi/2), \quad (7)$$

where ξ is the angle between initial and final states. However, the observed line intensity depends not only on P but also on the population distribution among the various energy levels, and the presence of H_2 changes the distribution from the usual Boltzmann distribution among the energy levels. The type of spin-spin interaction considered here generally does not enter into the thermal relaxation process to any significant extent, and the population distribution can then be calculated as if the two species of nuclei were completely separate and noninteracting. Thus, the total spin population for each value of m_1 is governed by the Boltzmann distribution, but at each value of m_1 the population difference between adjacent levels of m_2 is proportional, not to the Boltzmann distribution value M_0, but to M_s, where M_s is the "slow passage" population difference[8] and is a function of H_2 and Θ. An example of a calculation making use of this change in distribution is given at the end of Sec. IV.

Recently, Overhauser[9] has shown that the hyperfine coupling between electronic and nuclear spins in metals provides a means for greatly enhancing the net nuclear polarization in double resonance experiments, and Bloch[4] and Korringa[10] have predicted a similar effect in nonconducting paramagnetic substances. In order that the "Overhauser effect" take place it is necessary that the primary means of thermal relaxation available to the nucleus (here equivalent to our nucleus 1) be through the spin-spin coupling. However, in the experimental case considered here the thermal relaxation process for each species of nucleus is almost entirely through direct interaction with the lattice, as the J-coupling plays an insignificant role; thus it follows that an enhancement of polarization analogous to that predicted by Overhauser will *not* take place.

In the general case, including spins greater than $\frac{1}{2}$, the spin-spin multiplet in the absence of H_2 contains $(2I_2+1)$ lines. When H_2 is applied, the selection rule ($\Delta m_2=0$ in the laboratory frame) no longer holds strictly, as explained above, and in addition transitions starting from different m_1 levels may no longer be superimposed, since Eq. (6) is not a linear function of m_1. Thus there may be as many as $(2I_1)(2I_2+1)^2$ lines in the multiplet when H_2 is present. In addition, it appears possible that the selection rule ($\Delta m_1=\pm1$) is partially broken down by the effect of H_2, making possible the observation of multiple-quantum transitions.

III. CALCULATIONS

We present some calculated results for the simple case of two nuclei each of spin $\frac{1}{2}$, showing how the multiplet varies as a function of experimental conditions. For simplicity we define the four possible transitions by subscripts a, b, c, d, and the energies of transition in the laboratory frame as follows:

$$\Delta W_a=W(\tfrac{1}{2},\tfrac{1}{2})-W(-\tfrac{1}{2},\tfrac{1}{2})+\hbar\omega_2, \quad (8a)$$

[8] F. Bloch, Phys. Rev. **70**, 460 (1946).
[9] A. W. Overhauser, Phys. Rev. **92**, 411 (1953).
[10] J. Korringa, Phys. Rev. **94**, 1388 (1954).

$$\Delta W_b = W(\tfrac{1}{2}, -\tfrac{1}{2}) - W(-\tfrac{1}{2}, -\tfrac{1}{2}) + \hbar\omega_2, \quad (8b)$$

$$\Delta W_c = W(\tfrac{1}{2}, \tfrac{1}{2}) - W(-\tfrac{1}{2}, -\tfrac{1}{2}) + \hbar\omega_2, \quad (8c)$$

$$\Delta W_d = W(\tfrac{1}{2}, -\tfrac{1}{2}) - W(-\tfrac{1}{2}, \tfrac{1}{2}) + \hbar\omega_2. \quad (8d)$$

Case 1. $\omega_2 = \gamma_2 H_0$ (center of nucleus 2 doublet). ω_1 and amplitude of H_2 variable.

In this case $\Theta(-\frac{1}{2}) = -\Theta(\frac{1}{2})$. The transition angular frequencies become

$$\begin{aligned} \Delta W_a/\hbar &= \Delta W_b/\hbar = \gamma_1 H_0, \\ \Delta W_c/\hbar &= \gamma_1 H_0 + \tfrac{1}{2}J', \\ \Delta W_d/\hbar &= \gamma_1 H_0 - \tfrac{1}{2}J', \end{aligned} \quad (9)$$

where

$$J' = (J^2 + 4\gamma_2^2 H_2^2)^{\frac{1}{2}}. \quad (10)$$

The relative transition probabilities are

$$\begin{aligned} P_a = P_b &= 4\gamma_2^2 H_2^2/(J')^2, \\ P_c = P_d &= J^2/(J')^2. \end{aligned} \quad (11)$$

When $H_2 = 0$, $J' = J$ and transitions c and d form the doublet.[11] As the rf level H_2 is increased, the original doublet lines are spread apart and weakened; simultaneously a new line appears at the center frequency $\gamma_1 H_0$ and grows at the expense of the doublet. When $\gamma_2 H_2 \gg J$ there is only the single line due to transitions a and b, twice as intense as each of the original doublet lines. This result for strong H_2 agrees with the one obtained by using the concept of an "averaging out" of the spin-spin interaction due to rapid transitions in the laboratory frame.

Case 2. $\omega_2 = \gamma_2 H_0$, ω_1 fixed at $\gamma_1 H_0$, a sweep field ΔH is used to investigate the spectrum.

This case is generally more amenable to study in the laboratory than Case 1. By substituting $(H_0 + \Delta H)$ for H_0 in Eq. (6) and solving for transitions at $\Delta W = \hbar\omega_1$ in Eq. (8), we obtain lines at

$$\Delta H = 0, \quad (12a)$$

$$(\Delta H)^2 = \frac{J^2(\gamma_1^2 - \gamma_2^2) + 4\gamma_1^2\gamma_2^2 H_2^2}{4\gamma_1^2(\gamma_1^2 - \gamma_2^2)}. \quad (12b)$$

The intensity of the line at $\Delta H = 0$ is given by P_a in Eq. (11); for the other lines it must be determined with the aid of Eq. (7). If $\gamma_1 > \gamma_2$, the results are similar to those of Case 1. If $\gamma_1 < \gamma_2$, the line structure collapses with increasing H_2, giving only a single line for $4\gamma_2 H_2 \geq J$.

Case 3. $\gamma_2 H_2 \gg \frac{1}{2}J$, ω_1 and ω_2 variable.

By $\gamma_2 H_2 \gg \frac{1}{2}J$, we imply that to good approximation $\Theta(\frac{1}{2}) = \Theta(-\frac{1}{2}) = \Theta_0$, where Θ_0 is the effective field angle on nucleus 2 in the absence of any spin-spin interaction. In this case there are no more than two lines, located at

$$\Delta W/\hbar = \gamma_1 H_0 \pm \tfrac{1}{2}J\cos\Theta_0. \quad (13)$$

[11] Note that in the limit $H_2 = 0$ the effective field reverses direction during a transition, for $\omega_2 = \gamma_2 H_0$. Thus it requires a double transition (m_1 and m_2 both changing) in the rotating frame to agree with the selection rule ($\Delta m_2 = 0$) in the laboratory frame.

IV. EXPERIMENTAL RESULTS

To check the theory, an experiment was performed on the spin-spin interaction between F^{19} and P^{31}, with the former taken to be nucleus 1. Both nuclei have spin $\frac{1}{2}$ and their gyromagnetic ratios differ by more than a factor of two, thus the approximations used in the theory are valid to a high order of accuracy. The molecule studied was Na_2PO_3F in aqueous solution; since the Na atoms are ionically bonded or ionized in solution, they do not contribute to the spin interaction. The field-independent splitting of the fluorine resonance in this molecule has been reported previously by Gutowsky, McCall, and Slichter.[1]

The apparatus used was a Varian Associates V-4300 High Resolution Spectrometer and V-4012 Electromagnet operating at about 7500 gauss. The transmitter coil input circuit was modified so it was resonant at both the fluorine Larmor frequency of 30.00 Mc/sec and the phosphorous frequency of 12.91 Mc/sec. An auxiliary oscillator and power amplifier provided rf power for the H_2 field at the latter frequency. Both oscillators were crystal controlled; the one providing H_2 was tuneable over a range of several hundred cycles. The receiver coil and amplifiers were tuned only to the 30-Mc/sec fluorine signal. The V-4300 Spectrometer utilizes a slow linear magnetic field sweep and the signal intensity is displayed directly on the oscilloscope or recording meter.

Before the splitting could be studied as a function of H_2, the interaction factor J had to be determined. An audiofrequency sine wave modulation of the magnetic field was superimposed on the sawtooth sweep with the result that satellites were produced on each side of each doublet line. The satellites occur because a field modulation is in every way equivalent to a frequency modulation of the rf, insofar as the equations of motion of the nuclear ensemble are concerned.[8] The satellites thus have positions and intensities determined by the "sidebands" of the equivalent frequency modulation. The splitting $J/2\pi$ was thus determined as twice the value of the audiofrequency which superimposed the first satellites from each line in the center of the doublet. This measurement gave $J/2\pi = 860 \pm 4$ cps, which when converted to equivalent magnetic field difference gives a splitting of 0.214 gauss. The value obtained by Gutowsky *et al.*[1] by measurement of the field difference was 0.195 gauss. We have not explored the reasons for the discrepancy between our results and those of Gutowsky, but it should be pointed out that the accuracy of our method depends only on the calibration of the audio-oscillator and on the linewidth. In our measurements the audiofrequency was counted directly on a Hewlett-Packard 524-A frequency counter, and with sufficiently slow sweep the two satellites were clearly resolved if the frequency was varied by 5 cps on either side of its center value.

When the perturbing rf field was turned on at maxi-

mum amplitude, the doublet separation was found to be a function of ω_2, as expected. This is illustrated in Fig. 2. The angular frequency ω_2 was taken to be in the center of the phosphorous doublet when the two lines coalesced into one, and the deviations $\Delta\nu$ in Fig. 2 were measured from this value. The frequencies were determined by counting the crystal fundamental frequency with the 524-A counter. Owing to the existence of chemical shifts which are not known to sufficient accuracy, one cannot set ω_2 for $\Delta\nu=0$ in advance of actually seeing the spectrum.

Figure 3 shows the relative separation as a function of ω_2, compared with the theoretical separation calculated with the aid of Eq. (13). In this calculation $\gamma_2 H_2$ was taken to be 5000. However, it should be pointed out that H_2 was not strong enough to justify entirely the approximation $\Theta=\Theta_0$; this is evident in Fig. 2 from the fact that all four lines are visible instead of only the center two. A more exact calculation shows that the asymmetry of the intensities in some of the traces is a real effect and the direction of asymmetry can be reversed by changing the sign of $\Delta\nu$; this has been verified experimentally.

With $\Delta\nu$ set at zero, the amplitude of H_2 was varied and typical results were as shown in Fig. 4. At each setting of the H_2 attenuator, the alternating field $2H_2\cos(\omega_2 t)$ was investigated by means of a small search coil placed in the probe and connected to an electronic voltmeter. The search coil measurements were subject to large systematic errors owing to uncertainties in the effective area of the coil, and in addition were not very reproducible because it was difficult to place the coil in exactly the same spot each time, but the results indicate the order of magnitude of the field. Measurements were taken on the spectrometer traces of the relative separation of the outside lines (with the separation at $H_2=0$ taken as unity), and of the ratio of the center line peak amplitude to the average amplitude of the outside lines.

From the relative line splitting, we calculated H_2 with the aid of Eq. (12b) and compared it with the search coil measurements. Assuming the calculated H_2 to be correct, we calculated the relative intensity of the center line [Eq. (11)] and the outside lines, obtained by first calculating $\Theta(\frac{1}{2})$ and $\Theta(-\frac{1}{2})$. To these intensities a correction had to be made for changes in the population distribution. From the argument given in Sec. II it is easy to show that, for the line at $\Delta H>0$ the ratio of the true to the uncorrected line intensity is given by

$$1-(\gamma_2/2\gamma_1 M_0)[M_z(m_1=\tfrac{1}{2})-M_z(m_1=-\tfrac{1}{2})], \quad (14)$$

with an analogous expression for the other outside line (the center line requires no correction). An exact expression for M_z requires a knowledge of T_1 and T_2, which we did not have; however, under the circumstance that $\gamma_2^2 H_2^2 T_1 T_2 \gg 1$ we could use, to excellent approximation,

$$M_z = M_0 \cos^2\Theta. \quad (15)$$

The correction was relatively small, amounting at most to about 15 percent.

The results of the measurements and calculations are summarized in Table I. The line intensities are summarized as the ratios of the center to the average outside line amplitudes; uncertainties are based on the

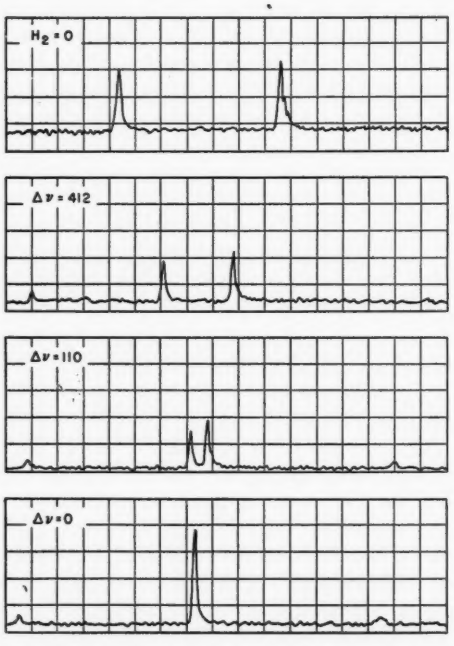

FIG. 2. Effect on the fluorine spectrum of varying the phosphorous rf frequency, with H_2 fixed at 0.464 gauss. The top trace shows the unperturbed spectrum ($H_2=0$) for comparison. We define $\Delta\nu=(\gamma_2 H_0-\omega_2)/2\pi$.

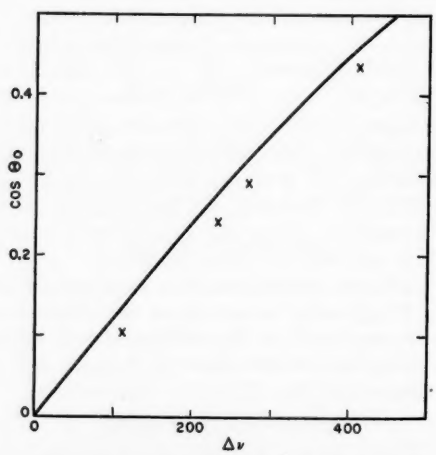

FIG. 3. Measured and calculated splitting as a function of the perturbing field frequency deviation, $\Delta\nu$, from the "center" frequency. In the calculation, we assume $\gamma_2 H_2=5000$.

TABLE I. Relative line splitting and intensity as a function of the perturbing field amplitude.

Relative splitting measured	H_2 (gauss) from search coil	H_2 (gauss) from splitting	Intensity ratio, measured	Intensity ratio from splitting
1.00	0	0	0	0
1.15	0.13	0.128	0.40±0.03	0.60
1.26	0.18	0.172	0.85±0.05	1.21
1.43	0.26	0.231	1.76±0.08	2.37
1.72	0.34	0.315	4.45±0.33	4.83
1.90	0.39	0.364	6.30±0.63	6.38
2.02	0.42	0.395	8.5 ±1.1	7.69
2.09	0.49	0.414	10.9 ±1.7	8.50
2.24	0.48	0.451	14.8 ±3.0	10.2
2.29	0.49	0.464	12.0 ±1.2	10.7
2.30	0.51	0.466	18.5 ±4.6	10.9

estimated rms noise level. In all calculations we used $\gamma_1=2.52\times10^4$, $\gamma_2=1.083\times10^4$, and $J=5400$.

V. DISCUSSION

A comparison of the experimental and calculated results in Fig. 3 and Table I seems to indicate that the concept of a Hamiltonian which is made stationary by transforming to a rotating coordinate system provides an adequate working model for prediction of the spectrum in magnetic double-resonance experiments. Since the lattice motions have about the same appearance in the rotating frame as in the laboratory frame, one would also predict that there should be no gross changes in linewidth due to the presence of the perturbing rf; this is also borne out by the experiment. Although it is probable that there are small changes in natural linewidth owing to changes in the matrix elements which affect the relaxation probability,[12] such changes would not be observable in our experiments because other work has shown that the observed linewidth is due almost entirely to instrumental effects, i.e., H_0 field inhomogeneity and rate of sweep.

The intensity measurements were based entirely on peak height, rather than on area, because it is much more difficult to measure the area accurately. It is therefore evident that any instrumental effects which preferentially broaden either the center or the outside lines will introduce systematic discrepancies between the observed and the calculated intensity ratios. Thus, if H_2 were not set exactly in the center of the phosphorous doublet, then the center line would in reality be a closely spaced doublet and an amplitude measurement would not give the full intensity. Such an effect, which is most important when H_2 is small, is noticeable in the traces of Fig. 4 and almost certainly accounts for the systematic discrepancies in Table I for values of H_2 less than 0.3 gauss. There is apparently a systematic discrepancy at large values of H_2 whose origin is not completely understood; however, it can be shown that an inhomogeneity in the H_2 field of the order of one percent would broaden the outside lines enough to account for the observed discrepancy. From the known geometry of the probe, one would expect inhomogeneities of this order of magnitude to be present.

[12] J. P. Lloyd and G. E. Pake, Phys. Rev. 94, 579 (1954).

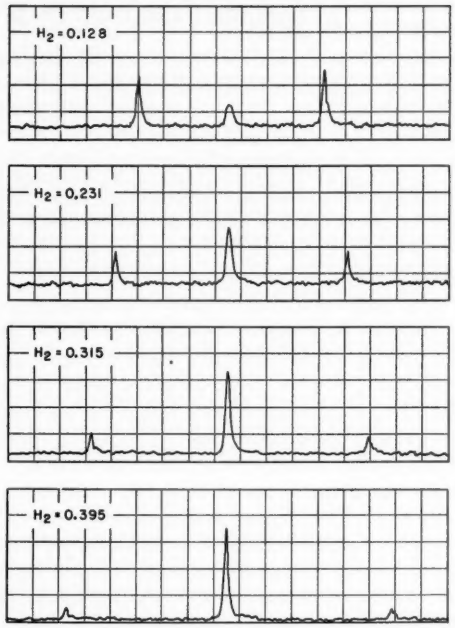

FIG. 4. Effect on the fluorine spectrum of varying the phosphorous rf amplitude H_2, with $\omega_2=\gamma_2 H_0$. The top and bottom traces of Fig. 2 are also part of this series.

The data of this experiment, and other data taken in H_2 fields as high as 0.7 gauss, show that in the limit of very large H_2 the intensity of the center line becomes exactly twice the height of the original doublet lines, within experimental error. Had an enhancement of the type predicted by Overhauser[9] been present, the center line intensity would have been increased still further by a factor $(1+|\gamma_2/\gamma_1|)$ or about 1.4. The absence of even a partial enhancement agrees with the statements made in Sec. II regarding the absence of the Overhauser effect in connection with the indirect nuclear spin-spin coupling.

We wish to thank Dr. M. E. Packard for advice and encouragement, and Virginia Royden for assistance in performing the experiment. The Na_2PO_3F was kindly lent by Ozark-Mahoning Company, Tulsa, Oklahoma. We are indebted to Professor F. Bloch for several stimulating discussions on this subject.

Gamma Rays from 14-Mev Neutron Bombardment of C^{12}†

M. E. Battat and E. R. Graves
University of California, Los Alamos Scientific Laboratory, Los Alamos, New Mexico
(Received November 15, 1954)

The gamma rays emitted by C^{12} under 14-Mev neutron bombardment have been investigated with a three-crystal pair spectrometer. In the energy range 1.5–5.5 Mev, the observed pulse-height distribution is consistent with the assignment of a single-energy line at 4.4 Mev. The calculated value for the production cross section of 4.4-Mev gamma radiation is 245±35 millibarns.

THE production of gamma rays by materials under 14-Mev neutron bombardment has been studied by a number of investigators using either a single scintillator crystal[1] or coincidence counter measurements.[2] In experiments of this type, the background from extraneous gamma rays and from neutrons incident on the detector is of prime importance. The present measurement of gamma rays resulting from the interaction of 14-Mev neutrons with carbon was made with a three-crystal pair spectrometer[3] which, under certain operating conditions, allows discrimination against background not attainable by the single-crystal or coincidence-counter measurements.

The pulses from each of the three NaI(Tl) crystals, after amplification, pass through a differential pulse-height discriminator to a threefold coincidence circuit with 0.2-microsecond resolving time. Pulses from the center crystal are also observed on an 18-channel analyzer gated by the coincidence output. Initial tests of the spectrometer with uncollimated sources resulted in pulse-height distributions with a prohibitively large continuum of pulses on the low-energy side of the pair peak. An explanation of this continuum of pulses, substantiated by further tests, is that there is a significant number of coincidences due to the random coincidence of a pulse from one side crystal with a true double coincidence between the pulses from the other two crystals caused by a Compton event. This background was removed by (a) delaying the side crystal pulses with respect to the center crystal pulses to decrease the effective resolving time and (b) accepting from the side crystals only those pulses which lay within a narrow band of 0.42 to 0.60 Mev. Other observers[4] have also found that this general type of operation improves the resolution of the spectrometer.

Calibration of the spectrometer, both as to energy scale and number of counts in the pair peak per incident gamma on the center crystal, was accomplished by counting gamma rays from a Pu-Be source whose neutron source strength was measured. Assumption of a branching ratio of 0.60±0.06 for the $Be^9(\alpha,n)C^{12*}$ reaction[5] allowed calculation of its 4.4-Mev gamma-ray strength. The inset of Fig. 1 shows the pulse-height distribution obtained for this source. The area under the portion of the pulse-height distribution below the pair peak is about 25 percent of that under the pair peak, or an energy loss, due to radiative loss and electron escape in the center crystal of approximately 9 percent. Because of the experimental error, a small contribution to this region from a cascade 3.2-Mev line[6] would not be detected. The response of the spectrometer to neutrons was also measured, response

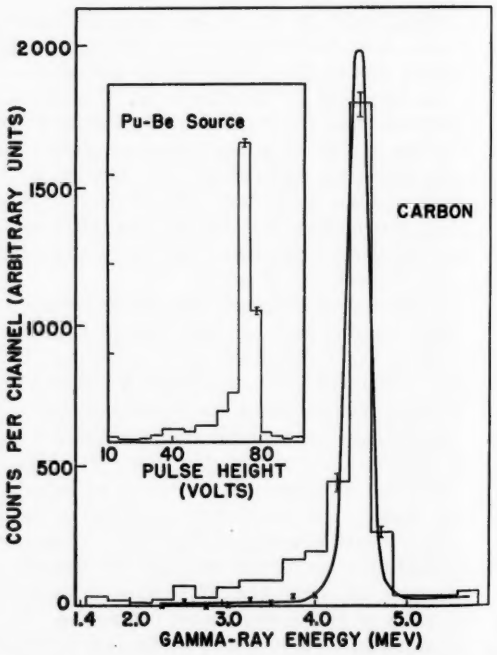

Fig. 1. Pulse-height distribution of gamma rays from carbon prior to adjustment for radiative loss and electron escape. Curve drawn shows the corrected pulse-height distribution. Inset: pulse-height distribution from Pu-Be source.

† Work done under the auspices of the U. S. Atomic Energy Commission.

[1] Scherrer, Theus, and Faust, Phys. Rev. **91**, 1476 (1953); L. C. Thompson and J. R. Risser, Phys. Rev. **94**, 941 (1954).

[2] M. E. Battat, Phys. Rev. **91**, 441 (1953).

[3] S. A. E. Johansson, Nature **166**, 794 (1950).

[4] H. I. West and L. G. Mann, Rev. Sci. Instr. **25**, 129 (1954); B. Hird and C. Whitehead, Proc. Phys. Soc. (London) **A67**, 644 (1954).

[5] D. E. Diller and M. F. Crouch, Phys. Rev. **93**, 362 (1954).

[6] Beghian, Halban, Husain, and Sanders, Phys. Rev. **90**, 1129 (1953).

being here defined as the number of coincidences in the pulse-height range corresponding to gamma-ray energies from 1.6 to 5.5 Mev in the center crystal per unit incident flux. Relative values for the response to 4.4-Mev gamma rays, to 14-Mev neutrons, and to 2.5-Mev neutrons were found to be 1.0, 0.08, and 0.008 respectively. From these measurements and available data on 14-Mev neutron elastic and inelastic scattering, it is estimated that the effect on the pulse-height distribution due to neutrons scattered by the sample into the detector is not more than a few percent for the geometries used.

A thick zirconium-tritium target bombarded by 130-kev deuterons from a Cockcroft-Walton accelerator provided the 14-Mev neutrons whose source strength was measured by a calibrated long counter. The long counter readings were corrected for the effect of neutron scattering by the graphite sample which was in the form of a ring and located so that the plane of the ring lay immediately behind the target. The spectrometer was placed 26 cm in front of the target, a tungsten bar providing shielding of the center crystal from the direct neutron beam.

Figure 1 shows the pulse-height distribution, scatterer in minus scatterer out, obtained for 14-Mev neutrons incident on carbon. The × points represent the net result after correction for radiative loss and electron escape obtained by normalization from the Pu-Be data, and the curve drawn shows the corrected pulse-height distribution. This distribution is consistent with the assignment of a single-energy line at 4.4 Mev in the 1.6–5.5 Mev region. The calculated value for the production of 4.4-Mev gamma rays from 14-Mev neutron bombardment of C^{12}, taking into account the attenuation of incident neutrons and resulting gamma rays in the scatterer, is 245±35 millibarns.

PHYSICAL REVIEW VOLUME 97, NUMBER 5 MARCH 1, 1955

Coincidence Studies of the Disintegration of Pm^{151} and Nd^{147}†

HARNAM SINGH HANS,* BABULAL SARAF,‡ AND C. E. MANDEVILLE
Bartol Research Foundation of The Franklin Institute, Swarthmore, Pennsylvania

(Received November 15, 1954)

Chemically pure Nd_2O_3 was irradiated by slow neutrons on five successive occasions in the Brookhaven pile. The 27.5-hour Pm^{151} was found to emit gamma rays of energies 64, 100, 163, 177, 240, 275, 340, 440, 650, and 700 kev. The 11-day Nd^{147} was shown to emit quanta of energies 92, 165, 280, 320, 410, 440, 530, and 690 kev. The relative intensities of the various quantum radiations have been determined, and coincidence measurements have been performed to ascertain the various sequential relationships between pairs of gamma rays. Partial decay schemes for both radionuclides have been indicated.

INTRODUCTION

IT was originally reported by Law, Pool, Kurbatov, and Quill[1] that 2.3-hr, 47-hr, and 11-day activities can be produced when neodymium is irradiated by certain nuclear particles. The mass number of the 11-day activity has been shown to be 147.[2,3] The 2.3-hr activity has been identified as the neodymium parent of the 47-hr promethium,[2,4] the mass numbers being 149.[5] Beta-gamma coincidence studies, and absorption measurements were carried out by Mandeville *et al.*[6] to establish the principal features and general pattern of the decay schemes of the 11-day neodymium and the 50-hr[7] Pm^{149}. Kondaiah[8] has reported in the decay of the 11-day activity gamma rays of energies 520, 391, 309, and 91 kev and three beta-ray spectra having end points at 350, 470, and 780 kev. This author found no gamma rays to be emitted in the decay of the 50-hr Pm^{149}. Emmerich and Kurbatov[9] have investigated the disintegration of the 11-day activity and report gamma rays at 91.5, 320, and 534 kev and beta-ray energies of 380, 600, and 825 kev. More recently, Cork *et al.*[7] have reported for Nd^{147} gamma rays of energies 91.2, 120.5, 168.1, 197.1, 231.2, 259.8, 273.3, 300.8, 318.1, 398.4, 441.4, and 532.3 kev. These latter authors have also reported the presence of Pm^{151} ($T_{1/2}$=27.5 hr) in samples of irradiated Nd which had been enriched in Nd^{150}. This activity is apparently grown from the 12-minute Nd^{151}. Pm^{151} was reported[7] to emit gamma rays of energies 64.7, 65.8, 69.6, 100.0, 105.2, 116.2, 144.0, 163.1, 168.0, 177.1, 208.3, 231.9, 239.9, 275.2, 340.2, and 715 kev.

† Assisted by the joint program of the U. S. Office of Naval Research and the U. S. Atomic Energy Commission.
* Fulbright Fellow from The Muslim University, Aligarh, India.
‡ On leave of absence from Agra College, Agra, India.
[1] Law, Pool, Kurbatov, and Quill, Phys. Rev. **59**, 936 (1941).
[2] Marinsky, Glendenin, and Coryell, J. Am. Chem. Soc. **69**, 2781 (1947).
[3] R. J. Hayden, Phys. Rev. **74**, 650 (1948).
[4] J. A. Marinsky and L. E. Glendenin, *Radiochemical Studies: The Fission Products* (McGraw-Hill Book Company, Inc., New York, 1951), Paper No. 7.543, National Nuclear Energy Series, Plutonium Project Record, Vol. 9, 1264 (1951).
[5] Ingram, Hess, and Hayden, Phys. Rev. **71**, 743 (1947).
[6] C. E. Mandeville and E. Shapiro, Phys. Rev. **79**, 391 (1950); Proc. Nat. Inst. Sci. India **17**, No. 1, 45 (1951); C. E. Mandeville and M. V. Scherb, Phys. Rev. **76**, 186 (1949).
[7] Rutledge, Cork, and Burson, Phys. Rev. **86**, 775 (1952).
[8] E. Kondaiah, Phys. Rev. **81**, 1056 (1951).
[9] W. S. Emmerich and J. D. Kurbatov, Phys. Rev. **83**, 40 (1951).

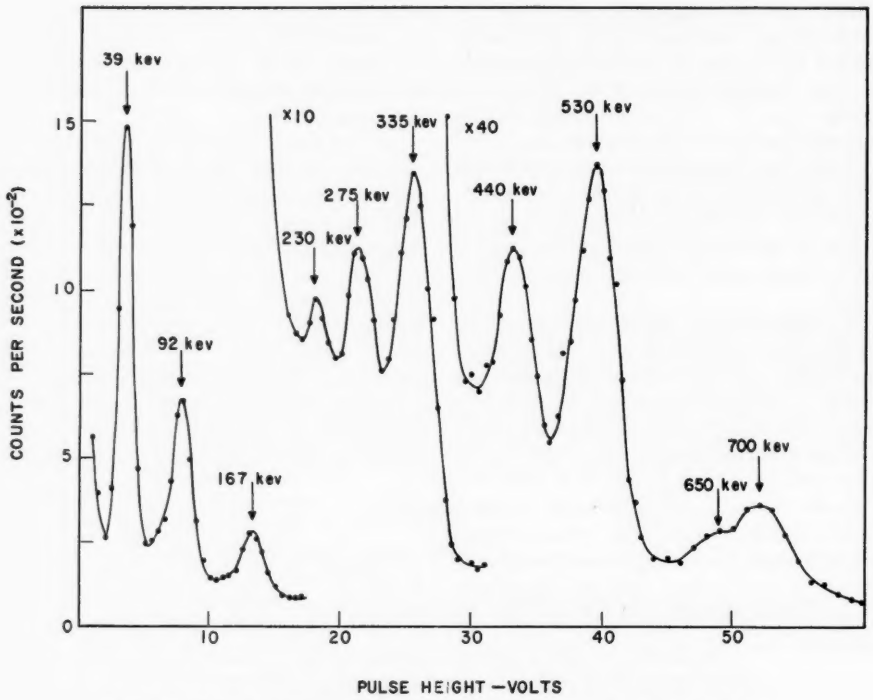

FIG. 1. Spectrum of gamma rays emitted in the decay of Nd^{147}, Pm^{149}, and Pm^{151} sixty hours after cessation of irradiation.

In none of the measurements described above were scintillation counting methods employed in coincidence studies of the decay of the several radionuclides of neodymium. Consequently, such investigations were undertaken for the purpose of obtaining additional information concerning the decay schemes in question. In all, five successive exposures of samples[10] of very pure Nd_2O_3 were carried out in the Brookhaven pile. The times of irradiation varied from two hours to two weeks in length, and measurements were usually commenced within a few hours after the target material had been removed from the reactor.

Pm^{151}

For the study of the radiations of the relatively short-lived activities of neodymium, exposure times of a few hours were employed so as to suppress any contributions of the 11-day period. The gamma-ray spectrum of $Pm^{149}-Pm^{151}$ is shown in Fig. 1. The spectrum was observed to decay for the most part with a half-life of 27.5 hours. Only in the vicinity of 280 kev were any contributions of an activity of half-period intermediate between 27.5-hr and 11-days in evidence. After four days of observations, it became apparent that in this spectral region, decay was proceeding at a somewhat slower rate than could be associated with a 27.5-hr period. Photopeaks are seen to occur which correspond to quantum energies of 39, 92, 167, 230, 275, 335, 440, 530, 650, 700, and ~1500 kev (not shown). From the measurements of Cork *et al.*[7] and from results to be subsequently discussed in this paper, it is clear that some of the above-listed peaks are composite ones corresponding to more than one gamma ray. In particular, observations about one week after cessation of irradiation showed that the radiations of the 11-day activity contributed appreciably only to the photopeaks at 92 kev and 530 kev. Of the full energy peaks observed in the spectrum of Fig. 1, the decay of the ordinate values related the following to the 27.5-hour period: 167, 230, 275, 335, 440, 650, and 700 kev with relative intensities of 70, 42, 55, 100, 40, 18, and 26.

In order to ascertain the complexity of the various peaks, coincidence measurements were undertaken. With the axes of two scintillation counters at 90°, a strong coincidence rate was observed when the channel of a differential pulse-height analyzer used in conjunction with either detector was placed at ~167 kev. Thus, at least two quanta in coincidence of energies about 167 kev are emitted in the decay of the 27.5-hour activity.

Coincidences between 230-kev quanta and the remainder of the spectrum are shown in Fig. 2 where photopeaks in the coincidence rate occur at 64 and 100 kev. Similarly, these two quanta were found to be

[10] Five grams of Nd_2O_3 were kindly supplied by Dr. F. H. Spedding of the Institute for Atomic Research, Iowa State College, Ames, Iowa.

coincident with the 275-kev gamma ray as shown in Fig. 3A. In Fig. 3B are shown photopeaks of the two gamma rays of energies 39 and 100 kev which are coincident with gamma rays of energies greater than 530 kev.

In addition to the data depicted in Figs. 2 and 3, several other coincidence measurements were performed. With the channel of one analyzer fixed at 100 kev, the other was moved through the region of 275 kev. No 275-kev gamma rays were found in coincidence with the 100-kev radiation. The coincidences at 100 kev shown in Fig 3A must then arise from Compton recoils of high-energy gamma rays coincident with the gamma ray at 100 kev. A curve of coincidences was also obtained by fixing the channel of one pulse height analyzer at 100 kev and moving the channel of the other through the energy interval about 167 kev. A pronounced peak appeared, but when the reverse procedure was followed of fixing at 167 kev and moving through 100 kev, no definite peak appeared. From these measurements it was concluded that the 100 kev–167 kev coincidences arose from coincidences between the 100-kev gamma ray and backscattered quanta deriving from the hard gamma rays of energies greater than 530 kev. Still another coincidence experiment was carried out when the channel of one analyzer was placed at 64 kev and the channel of the other moved through the region of 275 kev. In this case, genuine coincidences were distinctly observed. This peak of coincidences was so broad as to suggest the 64-kev radiation to be coincident with the interval of quantum energies extending from 230 kev to 280 kev. This conclusion is partially borne out by the data of Fig. 2. No two gamma rays of energies greater than 230 kev were found to be in coincidence.

The various coincidence studies of the preceding paragraphs combined with the spectrometric data of Cork *et al.*[7] suggest the decay scheme of Fig. 4. For example, the intense coincidence rate observed in the

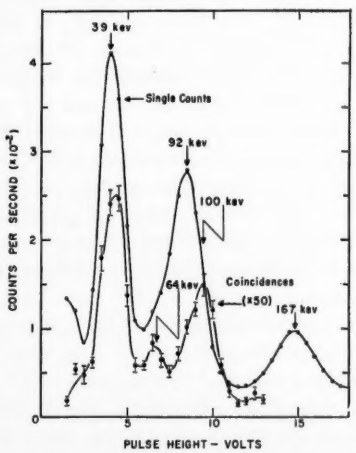

FIG. 2. Spectrum of gamma rays coincident with the 230-kev quanta of Pm^{151}.

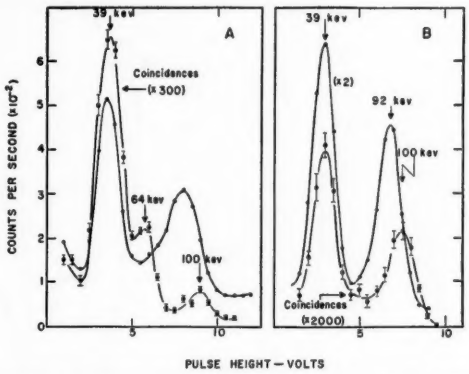

FIG. 3. A, spectrum of gamma rays coincident with the 275-kev gamma ray of Pm^{151}. B, spectrum of gamma rays coincident with quanta of energies greater than 530 kev.

present investigation between gamma rays of energies about 167 kev is assumed to arise from the quanta reported[7] at 163 and 177 kev. The 275 kev–65 kev cascade and the associated cross-over transition at 340 kev and the 240 kev–100 kev cascade are also consistent with the data of Cork *et al.*[7] Only in the case of the 240 kev–100 kev cascade is the order of emission of the gamma rays known. This particular sequence was established by a consideration of the fact that coincidences were found between the 100-kev radiation and the hard gamma rays of energies greater than 530 kev. The weak hard quanta at 1500 kev were previously assigned[7] to the 50-hr activity. In the present instance, this hard gamma ray was observed to decay with a half-life of 27.5 hours. After obtaining the data of Fig. 3B, the channel of the analyzer selecting pulses of higher energies was moved through the interval extending from 530 kev to 750 kev. Coincidences were detected for gamma-ray energies greater than 530 kev and less than 650 kev. Transitions from the 715- and 650-kev levels to the 100-kev level could account for them. These

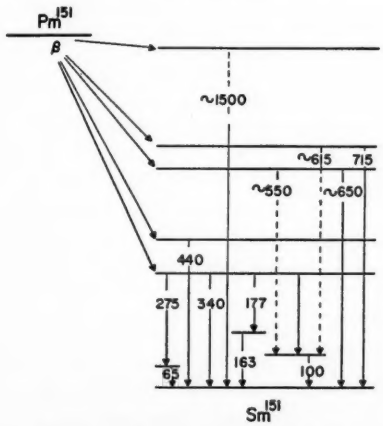

FIG. 4. Nuclear energy levels of Sm^{151}.

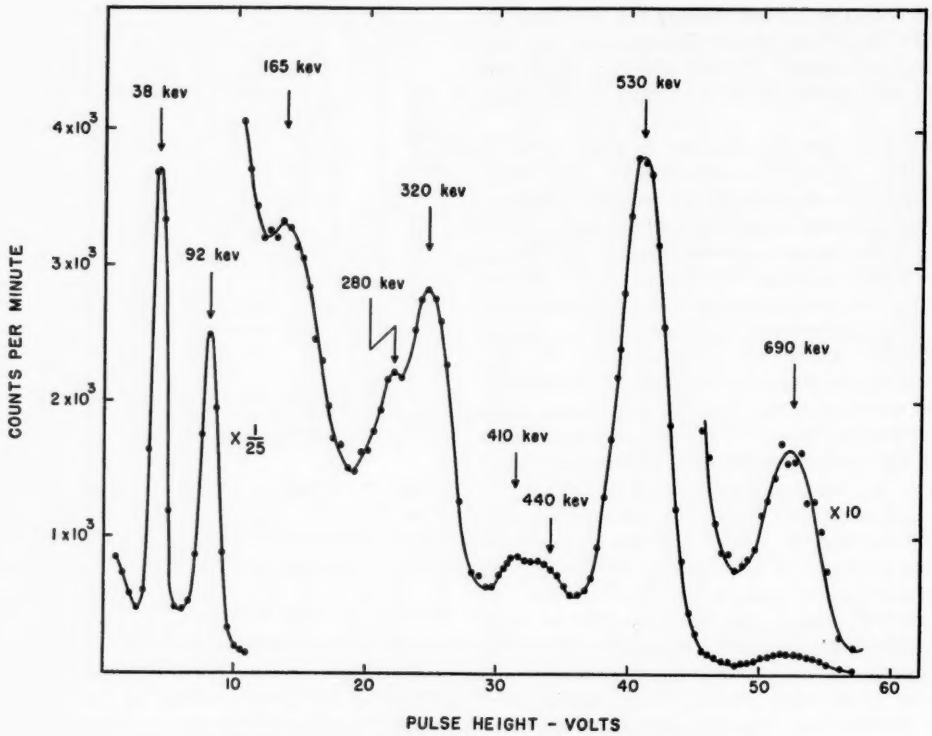

FIG. 5. Spectrum of gamma rays emitted in decay of Nd^{147}.

implied transitions are indicated by broken lines in Fig. 4.

Because of the poorer resolution of scintillation spectroscopy, it was not possible to account for all the gamma rays detected in the magnetic spectrometers.

Nd^{147}

The spectrum of the gamma rays emitted in the decay of the 11-day Nd^{147} is shown in Fig. 5 where peaks corresponding to quantum energies of 92, 165, 280, 320, 410, 440, 530, and 690 kev are indicated with relative intensities of 55, 1.5, 2.5, 4.5, 3.0, 3.5, 25, and 1.5. Earlier results[7–9] show that the regions of quantum energies about 165 kev and 320 kev contain contributions in either case from several gamma rays, more than indicated by the scintillation spectrometer. Cork *et al.*[7] report seven quanta in the entire energy interval extending from 165 kev to 320 kev.

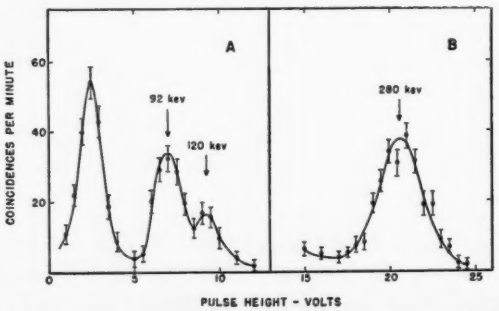

FIG. 6. Gamma rays coincident with 320-kev radiation of Nd^{147}

The presumably complex photopeak at 320 kev was found to be coincident with gamma rays at 92, 120, and 280 kev as shown in Fig. 6. The 120-kev radiation was evidently of too low an intensity to make an appreciable contribution to the curve of single counts shown in Fig. 5. To obtain the data of Fig. 6, the channel of one analyzer was fixed at 320 kev while that of the other was moved through the region of lower energies. Similarly, the 92-kev gamma ray was found to be in coincidence with quanta of energies of 120, 280, 320, 440, and 600 kev as shown in Fig. 7. The 120-kev and hardest coincident quantum were not of sufficient intensity to appear in the curve of single counts shown in Fig. 5. Not described in any figure is the additional fact that coincidences between the 280- and 410-kev gammas were also noted.

The disintegration scheme of Nd^{147} is shown in Fig. 8 where the coincidence studies of Figs. 6 and 7 have been combined with the information contained in the spectrum of single counts given in Fig. 5. The relative intensities of the 92-kev and 120-kev peaks of Fig. 6A show that in the triple cascade, the order of emission of the gamma rays is 120 kev→320 kev→92 kev. In

reaching this conclusion, it has been assumed that the conversion coefficient of the 120-kev radiation is not greater than that of the 92-kev line. Further confirmation of the suggested order of emission lies in the fact that the quantum energy of the 410-kev gamma ray is such as to indicate that it might be emitted in the cross-over transition of the 320 kev–92 kev cascade. Assuming little conversion of the 440-kev radiation, it can likewise be argued that because of its small intensity, it precedes the 92-kev radiation in the decay scheme. From energy considerations, it has been assumed that the 530-kev gamma ray is emitted in the cross-over transition of the 440 kev–92 kev cascade. The gamma ray of energy 690 kev has been taken as the cross-over quantum of the 280 kev–320 kev–92 kev cascade.

To obtain the K-shell conversion coefficient of the 92-kev gamma ray, the areas under the x-ray peak and

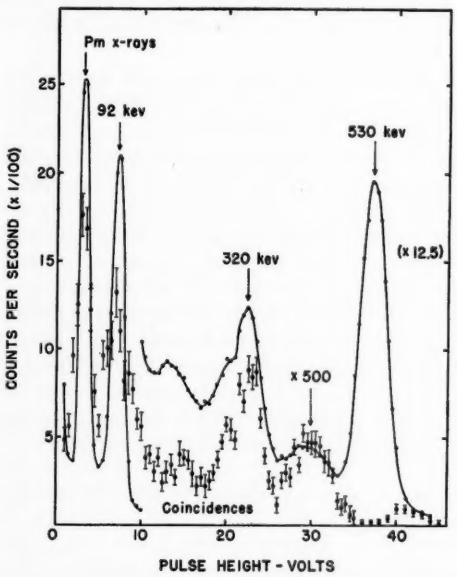

FIG. 7. Gamma rays coincident with 92-kev radiation of Nd^{147}.

under the full-energy peak of the 92-kev gamma ray were carefully determined in a crystal arrangement presenting practically no preabsorption to quanta of either energy. The counts in both peaks were properly corrected for escape from the crystal of the K-line of iodine. The K-shell conversion coefficient thus obtained was found to be 1.6 ± 0.2. In arriving at this result, it has been assumed that contributions to the x-ray peak arising from conversion of any other gamma rays are small. This assumption can be justified from a consideration of the data of Figs. 5 and 7.

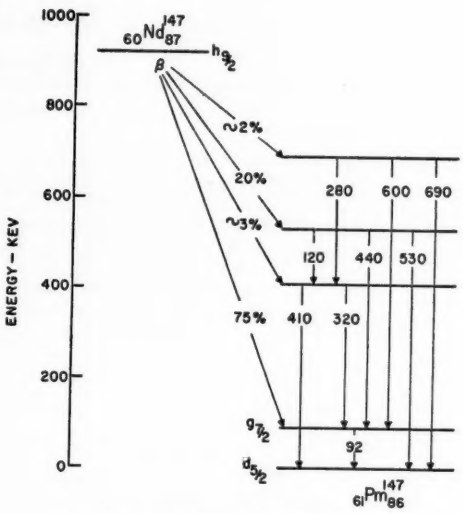

FIG. 8. Nuclear energy levels of Pm^{147}.

The measured[11] ground state spin of Sm^{147} is 7/2 in agreement with the orbital value of $f_{7/2}$ predicted by the nuclear shell model. The transition $Pm^{147}\rightarrow\beta\rightarrow Sm^{147}$ has been classified[12] as first forbidden, $d_{5/2}\rightarrow f_{7/2}$. All measured K/L ratios and K-shell conversion coefficients[7,8,13,14] favor identification of the 92-kev gamma transition as $M1$ so that the orbital of the first excited state of Pm^{147} may be reasonably taken as $g_{7/2}$. This latter assignment is furthermore consistent with an assignment of $h_{9/2}$ for the ground state of Nd^{147} and with the fact that the bulk of the beta rays are contained in a spectrum which terminates at the 92-kev level rather than at the ground state of orbital $d_{5/2}$. The values of $\log ft$ calculated for the various beta spectra shown in Fig. 8 are in the order of increasing end point energy 7.05, 7.00, 8.22, and 7.44. Thus, the ft value of the hardest spectrum is consistent with the orbital assignments. It seems inadvisable to attempt interpretation beyond this point, because gamma rays have been reported[7] which cannot be resolved by the methods employed in these measurements.

ACKNOWLEDGMENT

The writers wish to acknowledge the kind interest of Dr. W. F. G. Swann, Director of the Bartol Research Foundation. Two of them (H.S.H. and B.S.) are indebted to the Bartol Research Foundation for fellowships making possible their visits to the United States.

[11] C. S. Bogle and H. E. D. Scovil, Proc. Roy. Soc. (London) **A65**, 360 (1952); Kiyoshi Murakawa, Phys. Rev. **93**, 1232 (1954).
[12] Mayer, Moszkowski, and Nordheim, Revs. Modern Phys. **23**, 315 (1951).
[13] A. B. Smith and A. C. G. Mitchell, Phys. Rev. **87**, 1128 (1952).
[14] R. L. Graham and R. E. Bell, Can. J. Phys. **31**, 377 (1953).

Decay of Ti^{51} and Cr^{51}†

M. E. Bunker and J. W. Starner
University of California, Los Alamos Scientific Laboratory, Los Alamos, New Mexico
(Received November 22, 1954)

The radiations of Ti^{51} (5.8 min) and Cr^{51} (27 day) have been investigated with beta- and gamma-scintillation spectrometers. Gamma rays having energies of 0.323, 0.605, and 0.928 Mev and relative intensities of 95.8:1.4:4.2, respectively, were observed to accompany the decay of Ti^{51}. Two beta groups were observed of energy 2.13 and 1.5 Mev, having relative intensities of 94.4 and 5.6, respectively. The 2.13-Mev transition leads to the 0.323-Mev level of V^{51}. There is no evidence for a beta transition to the ground state of V^{51}. Cr^{51} decays by electron capture to both the ground state and the first excited state of V^{51}. The intensity of the capture branch to the 0.323-Mev level was measured to be 9.8 percent. A value of 3.25×10^{-3} was found for the total internal conversion coefficient of the 0.323-Mev gamma transition, indicating that the transition is $M1+E2$. The spin and parity assignments suggested by the experimental data are discussed.

I. INTRODUCTION

VANADIUM-51, daughter nucleus of both Ti^{51} and Cr^{51}, has 23 protons and a measured spin of 7/2. Its ground-state configuration can therefore be described as $(1f_{7/2}^3)_{7/2}$. In view of the relatively meager amount of information existing on the excited states of V^{51}, reinvestigation of the radiations of both Ti^{51} and Cr^{51} has been undertaken.[1] In particular, it was hoped that information would be gained regarding the theoretically predicted excited states of the $(1f_{7/2}^3)$ configuration.[2,3]

II. DECAY OF Ti^{51}

(a) Source Preparation

The Ti^{51} sources were prepared by neutron irradiation of titanium enriched in Ti^{50} (81.44 percent). The enriched titanium, obtained from Oak Ridge National Laboratory, was in the chemical form TiO_2. Since the spectrographic analysis indicated that none of the detectable impurities had an abundance of >0.1 percent, no further chemical purification of the irradiated titanium was made.

(b) Gamma-Ray Experiments

The gamma-ray spectrum of Ti^{51}, shown in Fig. 1, was obtained with a 2×2 inch NaI(Tl) crystal mounted on a DuMont 6292 photomultiplier. A ten-channel analyzer was used for the recording of data. The entire spectrum of Fig. 1 was found to decay with the half-life of Ti^{51}, which we have measured to be 5.80±0.03 minutes, in excellent agreement with the most recently reported value of 5.79±0.03 minutes.[4] Careful calibration with Au^{198} (411.8 kev), Sb^{124} (603 kev), Cs^{137} (661.6 kev), and Mn^{56} (845 kev) yielded energy values for the three observed Ti^{51} photopeaks of 323±2 kev, 605±4 kev, and 928±5 kev. The relative intensities of the three gammas, based on an empirical curve of photopeak sensitivity *vs* energy, were found to be 95.8:1.4:4.2.

On the basis of the above energies, it appeared likely that the 605- and 323-kev gammas are in coincidence and that the 928-kev gamma is the crossover transition. Therefore, a gamma-gamma coincidence experiment[5] was performed in which the 323-kev photopeak was used as the "gate" and the ten-channel analyzer was set to cover the 600-kev region of the coincidence spectrum. A strong peak was observed at 605-kev, only ~5 percent of which resulted from chance coincidences. The 605- and 323-kev gammas are therefore definitely in coincidence. No other photopeaks were found in the coincidence spectrum. Particular attention was given to the 160-kev region, where a weak photopeak could possibly be obscured in the ungated spectrum by the Compton peak of the 323-kev gamma.

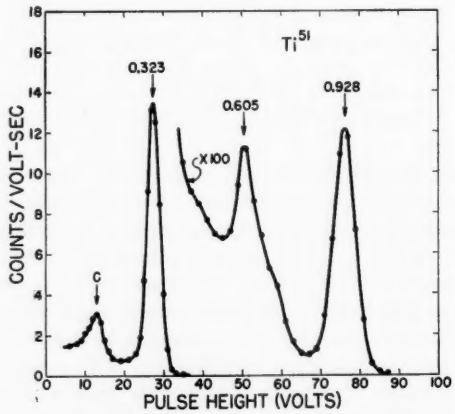

FIG. 1. γ-ray spectrum of Ti^{51}, obtained with a 2-inch NaI(Tl) crystal. The high-energy region is shown on an enlarged scale (100×).

† Work done under the auspices of the U. S. Atomic Energy Commission.

[1] Following completion of the experiments on Ti^{51} described below, accounts of studies of the Ti^{51} decay scheme were published by Jordan, Burson, and Le Blanc, Phys. Rev. **96**, 1582 (1954); R. H. Nussbaum, Thesis, Amsterdam (1954).

[2] D. Kurath, Phys. Rev. **91**, 1430 (1953).

[3] A. R. Edmonds and B. H. Flowers, Proc. Roy. Soc. (London) **A215**, 120 (1952); I. Talmi, Helv. Phys. Acta **25**, 185 (1952).

[4] Sargent, Yaffe, and Gray, Can. J. Phys. **31**, 235 (1953).

[5] For a description of the coincidence apparatus, see Bunker, Mize, and Starner, Phys. Rev. **94**, 1694 (1954).

(c) Beta-Ray Experiments

The beta spectrum of Ti^{51} was examined with a beta scintillation spectrometer consisting of a bare Pilot Plastic Scintillator-B[6] phosphor $1\frac{3}{4}$ inches in diameter and $\frac{3}{4}$-inch thick coupled directly to a DuMont 6292 photomultiplier with Dow Corning 200 fluid. The spectrometer was calibrated with the beta spectrum of P^{32}, whose end-point energy was taken to be 1.705 Mev. The Ti^{51} source consisted of an $\sim$1 mg/cm^2 deposit of irradiated TiO_2 on Scotch tape backing.

A Fermi analysis of the high-energy portion of the Ti^{51} spectrum is shown in Fig. 2 (upper curve). The end-point region has been corrected for resolution according to the method of Palmer and Laslett.[7] The Fermi plot appears to be straight from the end point of 2.13$\pm$0.03 Mev back to at least 1.5 Mev. The linearity of the Fermi plot was unexpected since previous studies[8,9] had indicated the presence of two high-energy beta groups differing in energy by $\sim$0.3 Mev.

Two beta-gamma coincidence experiments provided conclusive proof that the 2.13-Mev beta group goes to the 0.323-Mev level of V^{51}. In the first experiment, the beta spectrum in coincidence with the 323-kev gamma was examined. A Fermi plot of the observed data is shown in Fig. 2 (lower curve). The ungated and concidence spectra clearly have the same end-point energy. From the fact that there is no indication in the ungated spectrum of a beta group of energy $>$2.13 Mev, it is concluded that the intensity of the beta transition to the ground state of V^{51} must be less than 1 percent of the intensity of the 2.13-Mev transition.

The second beta-gamma coincidence experiment merely served to check the results just described. The gamma spectrum was gated with pulses from the beta spectrometer corresponding to energies $\geqslant$1.5 Mev. A calibrated geometry was used in which the photopeak sensitivity (ϵ_γ) of the gamma counter was known. By observing the number of coincidences in the 323-kev photopeak ($N_{\beta\gamma}$) per beta detected (N_β), the fraction (B) of the betas of energy $\geqslant$1.5 Mev which are followed by the 323-kev gamma can be determined from the relation $N_{\beta\gamma}/N_\beta = B\epsilon_\gamma$. The value found for B was 1.00. The probable error in the observed value of B is at least 5 percent since ϵ_γ is not known to better than 5 percent. However, this experiment provides additional proof that the ground-state beta transition, if detectable at all, is extremely weak.

The experiments described thus far suggest that there is an excited state of V^{51} at 928 kev which is

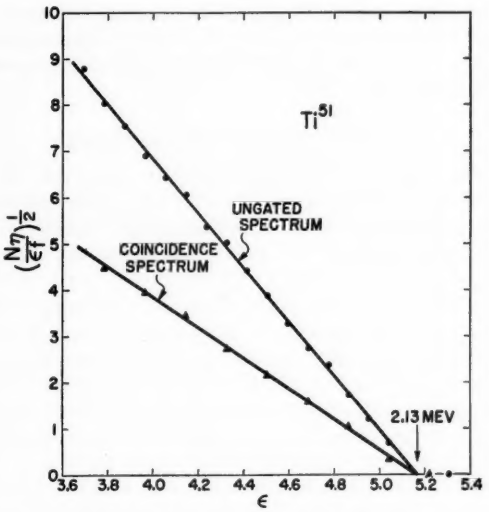

FIG. 2. High-energy portion of the Ti^{51} Fermi plots. "Ungated spectrum" refers to the normal beta spectrum; "coincidence spectrum" refers to the beta spectrum in coincidence with the 0.323-Mev gamma ray.

populated by a weak Ti^{51} beta group of end-point energy about 1.52 Mev. In order to verify this, an examination was made of the beta spectrum in coincidence with the 928-kev gamma. The coincidence spectrum was found to have an end-point energy of 1.50$\pm$0.05 Mev, in relatively good agreement with the energy predicted from the results of the preceding experiments.

III. DECAY OF Cr^{51}

(a) Previous Results

Previous studies[10–12] have established that Cr^{51} decays by K-capture to both the ground state and the 0.323-Mev level of V^{51}. The total disintegration energy is known to be 0.750 Mev from the threshold of the $V^{51}(p,n)Cr^{51}$ reaction.[13] The intensity of the capture branch to the excited state has been assigned values ranging from $\sim$3 percent[10] to 21 percent.[12] The internal conversion coefficient of the 0.323-Mev transition has recently been measured to be $\alpha_K = 1.5\times10^{-3}$.[12] Since the true value of α_K and the ft value of the capture branch to the excited state both provide valuable information about the 0.323-Mev level of V^{51}, these quantities have been redetermined.

(b) Source Material

The Cr^{51} source material was obtained from Oak Ridge National Laboratory. Since the radio-chemical

[6] Pilot Chemicals, Inc., 47 Felton Street, Waltham 54, Massachusetts.

[7] J. P. Palmer and L. J. Laslett, Atomic Energy Commission Report AECU-1220, March 14, 1951 (unpublished).

[8] Koester, Maier-Liebnitz, Mayer-Kuckuk, Schmeiser, and Schulze-Pillot, Z. Physik **133**, 319 (1952).

[9] E. der Mateosian, quoted in Hollander, Perlman, and Seaborg, Revs. Modern Phys. **25**, 469 (1953).

[10] Bradt, Gugelot, Huber, Medicus, Preiswerk, and Scherrer, Helv. Phys. Acta **18**, 259 (1945).

[11] W. S. Lyon, Phys. Rev. **87**, 1126 (1952).

[12] Maeder, Preiswerk, and Steinmann, Helv. Phys. Acta **25**, 461 (1952).

[13] Richards, Smith, and Browne, Phys. Rev. **80**, 524 (1950).

purity was known to be >99 percent, no further purification was deemed necessary. The specific activity at the time of the measurements described below was ~300 mc/g Cr.

(c) Branching Ratio Measurement

The intensity of the capture branch to the 0.323-Mev level was measured by means of an x-ray—gamma coincidence experiment. The vanadium K x-rays (~5 kev) were detected with a bare NaI(Tl) crystal $\frac{1}{8}$-inch thick coupled directly to a DuMont 6292 photomultiplier. With the Cr^{51} source in place, the background directly under the x-ray peak amounted to only ~1 percent of the gross counting rate. The gamma detector was a 2×2 inch NaI(Tl) crystal. A calibrated geometry was used in which the photopeak sensitivity (ϵ_γ) of the gamma counter was known. By observing the number of x-ray—gamma coincidences ($N_{x\gamma}$) per x-ray detected (N_x), one can determine the fraction of the Cr^{51} K-capture events (B) which are followed by the 0.323-Mev gamma from the relation $B=N_{x\gamma}/\epsilon_\gamma N_x$. A great advantage of this method is that it does not require knowledge of either the K fluorescent yield or the efficiency of x-ray detection. The value obtained for the branching ratio is $B=0.098$. The estimated probable error in this value is ±0.006, most of which results from lack of precise knowledge of ϵ_γ.

(d) Internal Conversion Measurement

The total internal conversion coefficient of the 323-kev gamma was measured by a comparison method. Thin sources (~1 mg/cm²) of Cr^{51} and Au^{198} were mounted on nylon backing (~0.5 mg/cm²), and the relative strengths of the 323-kev (Cr^{51}) and the 411.8-kev (Au^{198}) gammas were determined with the calibrated 2×2 inch NaI(Tl) crystal. The internal conversion spectra of these two sources were then examined in a magnetic lens spectrometer. Because of the inherent resolution of the spectrometer (~2.2 percent), the individual Cr^{51} conversion lines could not be resolved. Although both the Cr^{51} "line" and the Au^{198} K-line were slightly broadened because of source thickness, low-energy "tailing" was virtually absent, thus permitting an accurate comparison of the areas of these two lines. From the two comparison measurements just described and the theoretical[14,15] K conversion coefficient ($\alpha_K=0.0318$) of the 411.8-kev transition, one can calculate the total internal conversion coefficient (α_T) of the 323-kev gamma. The value thus obtained was $\alpha_T=3.25\times10^{-3}$, which is in reasonably good agreement with the results of Lyon,[11] who has reported that there are 3.0×10^{-4} e^-/x-ray disintegration. On the basis of published theoretical K and L conversion coefficients[14–16] and an assumed $L/(M+N+\cdots)$ ratio of 5, the $K/(L+M+\cdots)$ ratio for the 323-kev transition is calculated to be ~10 (for $M1$ or $E2$ transitions). This results in a value for the K conversion coefficient of $\alpha_K\approx2.95\times10^{-3}$. The experimental uncertainty in this value may be as high as ±10 percent. The two nearest theoretical conversion coefficients are $\beta_K{}^1=1.10\times10^{-3}$ and $\alpha_K{}^2=4.00\times10^{-3}$. The 323-kev transition therefore appears to be $M1+E2$, with the $E2$ component having an intensity of ~64 percent. The fact that the 323-kev level has been formed by Coulomb excitation[17] provides additional proof that the gamma transition is partially $E2$.

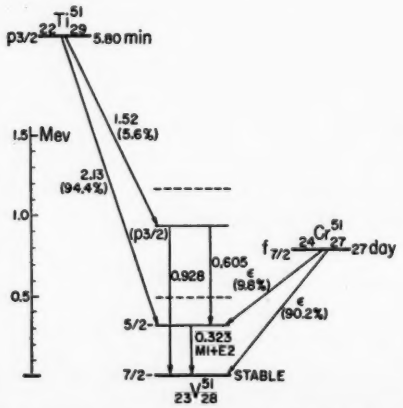

FIG. 3. Proposed decay scheme for Ti^{51} and Cr^{51}. Dotted lines at 0.48 and 1.16 Mev are levels found by inelastic proton scattering.

IV. DISCUSSION

The decay schemes suggested by the above measurements are shown in Fig. 3. The dotted lines at 0.48 Mev and 1.16 Mev are additional levels in V^{51} indicated by inelastic proton scattering experiments.[18]

The logft values associated with the various decay branches of Ti^{51} and Cr^{51} are given in Table I. It would appear that all of the transitions are of the allowed type. Therefore, since the ground state of V^{51} is a 7/2− state, the spin of Cr^{51} must be 5/2−, 7/2−, or 9/2−. It would seem that 7/2− is the only reasonable choice since the odd-particle configuration is $(1f_{7/2}{}^{-1})$, which should result in an $f_{7/2}$ state of relatively high purity.[19]

On the basis of the $M1+E2$ character of the 0.323-Mev gamma, the logft value of the 0.422-Mev K-capture transition, and the $f_{7/2}$ spin of Cr^{51}, a spin assignment of 5/2− or 7/2− is indicated for the 0.323-Mev level of V^{51}. The 7/2− possibility seems highly unlikely, however, since Ti^{51} decays very strongly to this level but does not decay to the 7/2−

[14] Rose, Goertzel, Spinrad, Harr, and Strong, Phys. Rev. 83, 79 (1951).
[15] Rose, Goertzel, and Swift (privately circulated tables).
[16] Gellman, Griffith, and Stanley, Phys. Rev. 85, 944 (1952).
[17] G. M. Temmer and N. P. Heydenburg, Phys. Rev. 96, 426 (1954).
[18] Hausman, Allen, Arthur, Bender, and McDole, Phys. Rev. 88, 1296 (1952).
[19] A. de-Shalit and M. Goldhaber, Phys. Rev. 92, 1211 (1953).

ground state of V^{51}. Therefore, the only spin assignment for the 0.323-Mev level which is consistent with all the experimental data is 5/2−. This level is very probably the $(1f_{7/2}^3)_{5/2}$ state predicted by *jj*-coupling theory.[2,3]

Ti^{51} has 29 neutrons, and from both the single-particle shell model[20] and the empirical data,[21,22] a spin assignment of $p_{3/2}$ would be expected for its ground-state. $f_{5/2}$ is the next most likely choice, but this possibility is excluded by the fact that there is no detectable beta transition to the ground state of V^{51}. Therefore, there would seem to be little doubt that the ground-state configuration of Ti^{51} is $(p_{3/2}^1)$. The problem which now arises is that the 2.13-Mev beta transition from Ti^{51} to the 5/2− state of V^{51} would appear to be ΔL-forbidden and would therefore not be expected to have a log*ft* value as low as 4.9.[22] The inference is that the 5/2− level is not a pure $(1f_{7/2}^3)_{5/2}$ configuration but has a sufficient admixture of *p*-state to result in the above anomaly.

On the basis of the level spacings predicted by Kurath,[2] which are in semiquantitative agreement with recent experimental results,[23,24] one would suspect that the level at 0.48 Mev (indicated by inelastic proton scattering) is a $(1f_{7/2}^3)_{3/2}$ state. There is no evidence that this level is populated in the decay of either Ti^{51} or Cr^{51}. Nussbaum *et al.*[25] have placed an upper limit on the intensity of the hypothetical 0.48-Mev gamma of 3 percent (relative to the intensity of the 0.323-Mev gamma). From the present experiments, this upper limit can safely be lowered to 0.4 percent. In addition, there is no evidence for the hypothetical ~0.16-Mev transition from the 0.48-Mev level to the 0.323-Mev level, as pointed out in Sec. II (b). It is easy to understand why the level at 0.48-Mev might not be involved in the decay of either Ti^{51} or Cr^{51}. The *K*-capture transition to this level from Cr^{51} would be second forbidden. The direct beta transition from Ti^{51} would be ΔL-forbidden, and the 0.928-Mev level would not necessarily be expected to exhibit detectable gamma branching to the 0.48-Mev level. On the other hand, the transition from the 0.48-Mev level to the ground state would be *E*2, and it is therefore difficult to understand why this level is not excited by Coulomb excitation with alpha particles.[17] A further investigation of the $V^{51}(p,p')$ reaction should probably be made in order to confirm the existence of the 0.48-Mev level.‡

TABLE I. Log*ft* values associated with the decay of Ti^{51} and Cr^{51}.

Parent nuclide	Transition energy (Mev)	Percent branch	log *ft*[a]
Ti^{51}	2.13	94.4	4.90
Ti^{51}	1.52	5.6	5.50
Cr^{51}	0.745	90.2	5.37
Cr^{51}	0.422	9.8	5.84

[a] Values for Ti^{51} were determined from the curves given by S. A. Moszkowski, Phys. Rev. **82**, 35 (1951); values for Cr^{51} were determined by the method outlined by J. K. Major and L. C. Biedenharn, Revs. Modern Phys. **26**, 321 (1954).

On the basis of the log*ft* value (5.5) of the 1.52-Mev beta transition and the proposed $p_{3/2}$ spin assignment for Ti^{51}, the level in V^{51} at 0.928 Mev must be a negative parity state of spin 1/2, 3/2, or 5/2. Since there is good evidence that the first single-particle level of odd-mass nuclides with 21, 23, 25, or 27 identical nucleons usually occurs somewhere between 1.0 and 1.5 Mev,[25] there is reason to believe that the 0.928-Mev level is the first single-particle excited state of V^{51}. From the shell model point of view, one would expect the first single-particle excited state to be either $p_{3/2}$ or $f_{5/2}$, with a tendency for the $p_{3/2}$ state to be lower. It thus seems reasonable to assign a spin of $p_{3/2}$ to the 0.928-Mev level, and a spin of $f_{5/2}$ to the 1.16-Mev level (observed by inelastic proton scattering[18]). The $p_{3/2}$ assignment is compatible with the relative transition probabilities of the 0.605- and 0.928-Mev gamma rays. The $f_{5/2}$ assignment makes the beta transition to the 1.16-Mev level ΔL-forbidden, thus providing a satisfactory explanation of why this beta transition is not observed.

The authors wish to thank Dr. M. Goldhaber for helpful discussions.

[20] M. G. Mayer, Phys. Rev. **75**, 1969 (1949); Haxel, Jensen, and Suess, Phys. Rev. **75**, 1766 (1949).

[21] P. F. A. Klinkenberg, Revs. Modern Phys. **24**, 63 (1952).

[22] Mayer, Moszkowski, and Nordheim, Revs. Modern Phys. **23**, 315 (1951); L. W. Nordheim, Revs. Modern Phys. **23**, 322 (1951).

[23] Nussbaum, Wapstra, Nijgh, Ornstein, and Verster, Physica **20**, 165 (1954).

[24] T. Lindqvist and A. C. G. Mitchell, Phys. Rev. **95**, 1535 (1954).

[25] Nussbaum, van Lieshout, and Wapstra, Phys. Rev. **92**, 207 (1953).

‡ *Note added in proof.*—Braams [C. M. Braams, private communication (October, 1954)], quoted by R. H. Nussbaum (see reference 1), has recently re-examined the $V^{51}(p,p')$ reaction and finds evidence for levels in Ti^{51} at 0.321, 0.925, 1.609, and 1.813 Mev. He finds no evidence for levels at 0.48 and 1.16 Mev.

High-Altitude Cosmic-Ray Neutron Density at the Geomagnetic Pole*

H. A. C. NEUBURG, R. K. SOBERMAN, M. J. SWETNICK,† AND S. A. KORFF
New York University, University Heights, New York, New York

(Received July 27, 1954)

Two successful balloon flights were launched near the geomagnetic North Pole, bearing low-energy cosmic-ray neutron detectors. The neutron maximum was found to occur at 75±5 mb. A value of 161 mb was found for the mean absorption depth, L.

INTRODUCTION

A MEASUREMENT of the neutron density as a function of altitude has been made by means of high-altitude balloon-borne equipment launched near the geomagnetic North Pole from a Coast Guard icebreaker. This is a continuation of the work of several investigators[1,2] to determine the latitude effect on cosmic-ray neutrons. The theory of the origin and vertical distribution of cosmic-ray neutrons has been developed by such investigators as Bethe, Korff, and Placzek,[3] Flügge,[4] and Davis.[2] Present results again indicate an exponential increase in neutron intensity as a function of altitude from sea level to about 200 millibars and a slower rise to a maximum somewhat above 100 millibars. Of major interest is the variation of the absorption coefficient and position of the maximum with geomagnetic latitude. Experiments are still in progress which, it is hoped, will yield a complete picture of the cosmic-ray neutron intensity dependence on altitude and latitude.

APPARATUS AND METHODS OF MEASUREMENT

The main features of the apparatus were the same as those used by Staker[1] and Davis.[2] A comprehensive description thereof is given by Pavalow, Davis, and Staker.[5] Essentially, two geometrically identical proportional BF_3 counters were employed. One was filled to an S.T. pressure of 23.3 cm Hg with B^{10}-enriched BF_3 gas,[6] the other to the same pressure with regular commercial unenriched BF_3. This arrangement afforded a means of determining the expected neutron counting rate for a counter containing 100 percent B^{10} isotope and also the background (due mainly to giant showers, stars, slow protons, and natural contamination alpha particles). The two brass-walled counters in each frame were carefully matched with respect to efficiencies and plateaus[7] and operated at approximately 2300 volts. Counter dimensions were: active length, 30 cm; inner diameter, 49.2 mm; diameter of central wire, 0.05 mm (0.002 in.); and wall thickness, 1 mm.

As in previous experiments, the counters, high-voltage batteries, and connecting cables were kept at atmospheric pressure to avoid spurious counts from corona discharge at altitudes above 40 000 ft. A 20-gauge galvanized iron stovepipe, with brass endcaps and brazed seams, served as a pressure chamber in which the counters were mounted with axes in line and separated by the high-voltage batteries. This geometrical arrangement afforded symmetry, provided a minimum contribution from neutrons produced in the batteries, and resulted in one counter subtending a negligibly small solid angle at the other. The counter pulses were fed into identical trains of circuitry com-

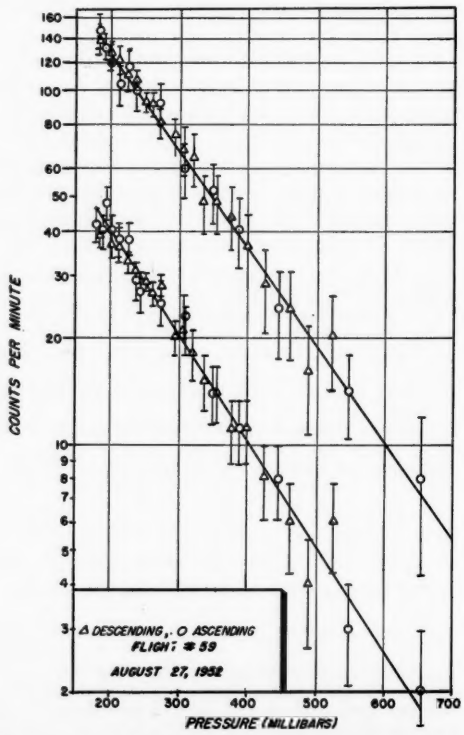

FIG. 1. Individual counting rates *vs* pressure. Flight No. 59. The upper curve represents the data for the enriched BF_3 counter, and the lower curve the data for the unenriched BF_3 counter.

* Assisted by the joint program of the U. S. Office of Naval Research and the U. S. Atomic Energy Commission.

† Now at Anton Laboratories, Brooklyn, New York.

[1] W. P. Staker, Phys. Rev. **80**, 52 (1950).

[2] W. O. Davis, Phys. Rev. **80**, 150 (1950).

[3] Bethe, Korff, and Placzek, Phys. Rev. **57**, 573 (1940).

[4] S. Flügge in *Cosmic Radiation*, edited by W. Heisenberg (Dover Publications, New York, 1946), Chap. 14.

[5] Pavalow, Davis, and Staker, Rev. Sci. Instr. **21**, 529 (1950).

[6] Obtained from the U. S. Atomic Energy Commission, Oak Ridge, Tennessee.

[7] Because of the difficulty in obtaining a source with a neutron energy spectrum comparable to that of neutrons in the atmosphere, an absolute calibration of the counters was not practicable.

posed of a preamplifier, amplifier, scalers, and a pulse lengthener. Both channels were continuously telemetered to the "ground" station. The pulses from the enriched counter, occurring between four and five times as frequently as those from the regular counter, were scaled down by a factor of 1:16 before being transmitted as a pulse of 0.2-second length. The pulses from the regular counter were scaled down by 1:4 and transmitted with a 0.4-second length. This different length permitted easy differentiation between enriched and regular counts, even in cases of overlapping.

A previously calibrated Olland cycle modulator sent data as to the atmospheric pressure at which the balloon floated, at one-minute intervals throughout each flight. The enriched and regular pulses as well as the pressure readings were broadcast at 3135 kilocycles by a three-watt AM crystal-controlled transmitter developed by Hillman.[8] Recording took place at the "ground" station on board the icebreaker by means of a shortwave receiver and a Brush oscillograph recorder system.

EXPERIMENTAL RESULTS

Two successful flights were completed in the vicinity of the geomagnetic North Pole from the rear flight deck of the U.S.C.G.C. Eastwind. Flight No. 59 was launched at 3:52 P.M. GMT on August 27, 1952. The ship's position was 77°45′ North and 72°47′ West in geographic coordinates. The balloon ascended at a decreasing rate of rise to an altitude of 40 800 feet, where it leveled off for about 30 minutes and then began a very gradual descent. This flight lasted a total of 4 hours and 33 minutes and came down at the approximate geographic position: latitude 78°00′ North, longitude 70°50′ West. Although this flight did not reach the altitude region of neutron maximum, the slow rise and descent gave counting rates with good statistical accuracy for the exponential portion of the curves described below.

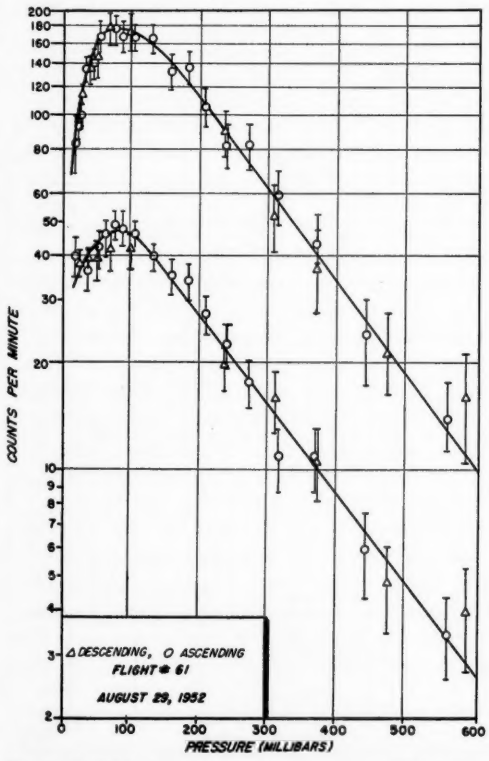

FIG. 2. Individual counting rates *vs* pressure. Flight No. 61. The upper curve represents the data for the enriched BF_3 counter, and the lower curve the data for the unenriched BF_3 counter.

[8] L. Hillman, Radio-Electronics (December, 1948).

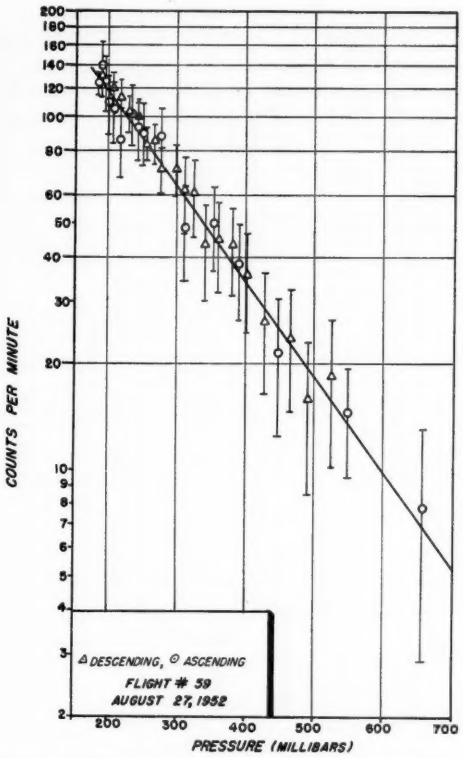

FIG. 3. Neutron counting rates *vs* pressure. Flight No. 59.

The second successful flight (No. 61) was launched at 11:42 A.M. GMT on August 29, 1952, from the geographic position of 77°28′ North and 73°37′ West. This flight ascended at a rate of 800 feet per minute to a maximum altitude of 92 000 feet and then slowly descended to an altitude of 72 500 feet. Here the gondola was released by clock-controlled explosive "squibs" and promptly descended by parachute to the ice-filled waters of upper Kane Basin. The approximate geographic position of descent was 77°51′ North and 74°45′ West, and the total horizontal distance traveled was 28 miles. The total elapsed time of the flight was 4 hours and 52 minutes. Good statistical results were

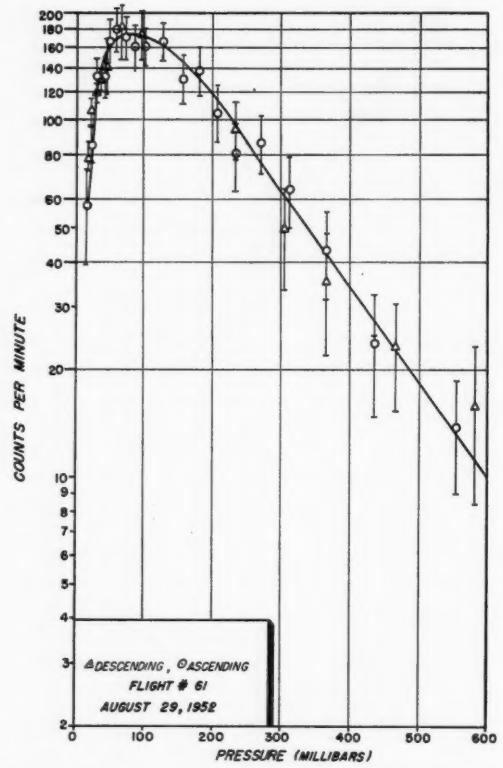

FIG. 4. Neutron counting rates *vs* pressure. Flight No. 61.

obtained from this flight both on the rise and in the vicinity of the maximum.

The curves for the individual counting rates on the two flights are shown in Figs. 1 and 2. The counting rate is plotted against atmospheric pressure in millibars. (1 millibar = 1.02 g/cm²). From the equations derived above, the calculation of N was carried out on the data of each one-minute interval and the curves of neutron counting rate *versus* pressure were plotted so that each point represents the average N over approximately equal pressure ranges. These curves are shown in Figs. 3 and 4. Finally a single composite curve of both flights was drawn. The result is shown in Fig. 5. For the sake of clarity, probable errors were not entered on this curve. It will be noted that there is very good agreement between the points of both flights. Information obtained from Simpson[10] indicated that the sea-level neutron counting rate varied an average of less than one percent during the period in which the two flights mentioned above were flown.

In their description of the neutron distribution in the atmosphere, Bethe, Korff, and Placzek[3] have given the relation $N = N_0 e^{-\mu p}$ for the region from sea level to an altitude corresponding to about 200 millibars. Applying this equation to the exponential portions of curves 2, 4, and 5 indicates a mean absorption coefficient μ of 6.2×10^{-3} millibar^{-1} (6.1×10^{-3} cm²/g). Taking the reciprocal of μ we find the mean absorption thickness L to be 161 millibars (164 g/cm²). Simpson[11] has reported a figure of 157 g/cm² for L at geomagnetic latitudes 53° and 65°. Yuan[12] has also reported an L of 156 g/cm² at 51°46′N. geomagnetic latitude. All three of the above positions are north of the knee of the neutron latitude curve. To within experimental accuracy, the present figure at 90° seems to agree with those of Simpson and Yuan despite the fact that Simpson was detecting only those neutrons with energies greater than the cadmium cutoff, and Yuan was interested in those neutrons with energies less than the cadmium cutoff. No discrimination was made in the present experiments.

Above 200 millibars the neutron counting rate curve departs from the exponential and reaches a maximum at 75±5 millibars. The counting rate at the maximum was 177 counts/min for the matched counters with dimensions and characteristics mentioned above. This would result in a neutron counting rate of 1.01 counts/min for a BF_3 counter, with a boron component of 100 percent B^{10} at S.T.P., and with a volume of one cubic centimeter. At the highest altitude reached by the balloon of flight 61 (15.5 millibars), the neutron

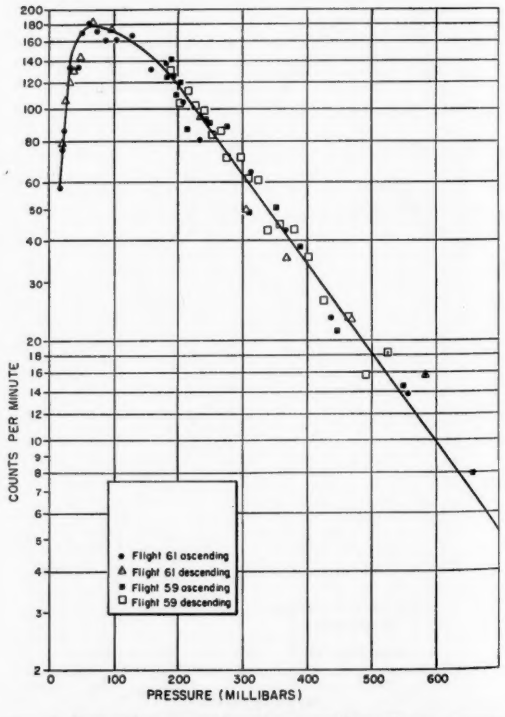

FIG. 5. Composite curve of neutron counting rates *vs* pressure at 90°N geomagnetic latitude.

[10] J. A. Simpson (private communication).

[11] J. A. Simpson, Phys. Rev. **83**, 1175 (1951).
[12] L. C. L. Yuan, Phys. Rev. **81**, 175 (1951).

counting rate dropped to about $\frac{1}{5}$ that found at the maximum.

ACKNOWLEDGMENTS

The authors wish to express their gratitude to various persons and agencies without whose valued assistance this work would not have been possible. Thanks are due the personnel of the U. S. Office of Naval Research, especially Lieutenant Malcolm Jones for his excellent liason work. We should like to voice our appreciation to Captain Peterson and the Officers and men of the U. S. Coast Guard Cutter Eastwind for their fine cooperation. We are indebted to J. R. Smith and "Bud" Froehlich of General Mills for their superb balloon-launching operations under very difficult conditions. Finally, we should like to thank our colleagues George Timmerman, Arie Borovitch, Israel Schlechter, and Roy Elkind.

PHYSICAL REVIEW VOLUME 97, NUMBER 5 MARCH 1, 1955

Photoproduction of Neutral Pions in Hydrogen: $p-\gamma$ Coincidences*

R. L. WALKER, D. C. OAKLEY,† AND A. V. TOLLESTRUP
California Institute of Technology, Pasadena, California
(Received November 17, 1954)

This paper reports measurements of the differential cross section for photoproduction of neutral pions in hydrogen at energies 300, 400, and 450 Mev, at center-of-momentum angles of 70° to 150°. One decay photon from the neutral pion is observed in coincidence with the recoil proton, whose energy and angle are measured to define the photon energy. The results obtained by this method are in good agreement with more accurate measurements obtained recently by the method of observing only the recoil proton.

INTRODUCTION

PROBABLY the most accurate method for measuring the photoproduction of neutral pions in hydrogen is to observe the recoil proton alone. Its energy and angle define uniquely the photon energy as is well known. This method has been used by Goldschmidt-Clermont, Osborne, and Scott[1] and recently in this laboratory by Oakley and Walker.[2] This method makes the assumption (for which there is good evidence) that recoil protons from hydrogen are not produced in competitive numbers by processes other than neutral pion production. In the method of Silverman and Stearns[3] the photoproduction process is identified a little more definitely, by requiring the recoil proton whose energy and angle are observed, to be in coincidence with one of the decay photons from the neutral pion. This method suffers from the disadvantages that the absolute efficiency of the photon counter enters into the cross section, and the counting rates are decreased by the photon coincidence requirement. It has an advantage if solid targets of polyethylene and carbon are used, in reducing considerably the relative background from the carbon. This reduction occurs partly because the angular correlation between neutral pion and recoil proton, which is definite for hydrogen, is destroyed to a significant extent for carbon.

The measurements here described are a continuation of earlier work[4] using the method of Silverman and Stearns. Angular distributions at 300, 400, and 450 Mev are obtained, and compared to the more recent and probably more accurate data of Oakely and Walker[2] which depend on counting the recoil proton only.

APPARATUS

The arrangement of target, counters, and absorbers is shown in Fig. 1. Recoil protons are counted by a counter telescope consisting of two scintillation counters (stilbene crystals $\frac{1}{4}$ inch thick) in coincidence followed by a third one in anticoincidence. The thickness of aluminum absorbers in the telescope determines the range, and thus the energy, of the protons, which are identified by their specific ionization, or pulse height, in the first counter.

The range, ΔT_p, of proton energies accepted by this counter is found from the range interval, ΔR, consisting of the aluminum absorber C plus a thickness of stilbene which depends on the effective biases of counters 2 and 3. This thickness is found by extrapolating the proton counting rate as a function of absorber C thickness to zero counting rate. During this measurement, when C is increased, absorber B is decreased half that amount, in order to keep the mean energy of the observed protons the same.

The photon counter consists of two liquid scintillators of dimensions 4×6×0.5 inches. The first is in

* This work was supported in part by the U. S. Atomic Energy Commission.
† Now at University of California, Radiation Laboratory, Livermore, California.
[1] Goldschmidt-Clermont, Osborne, and Scott, Phys. Rev. 89, 329 (1953).
[2] D. C. Oakley and R. L. Walker, following paper [Phys. Rev. 97, 1283 (1955)].
[3] A. Silverman and M. Stearns, Phys. Rev. 88, 1225 (1952).
[4] Walker, Oakley, and Tollestrup, Phys. Rev. 89, 1301 (1953).

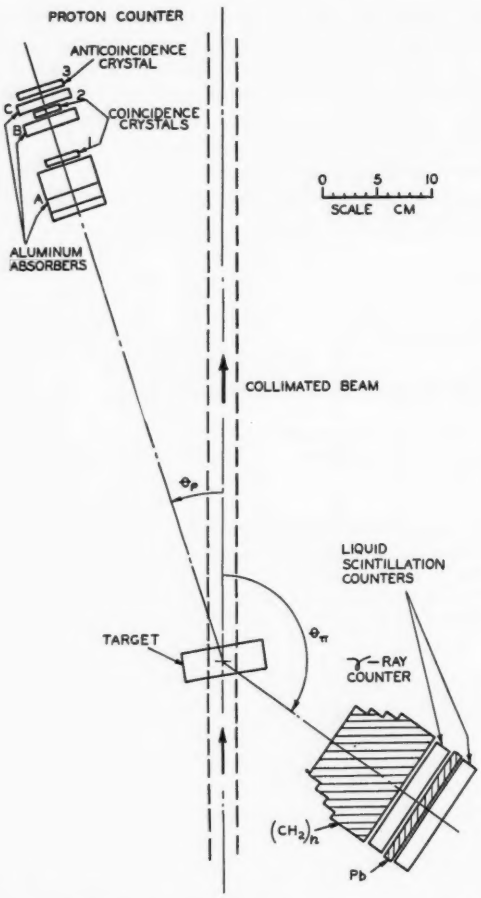

FIG. 1. Experimental apparatus. The synchrotron beam was monitored by a thick copper ionization chamber of the Cornell design, located behind the apparatus.

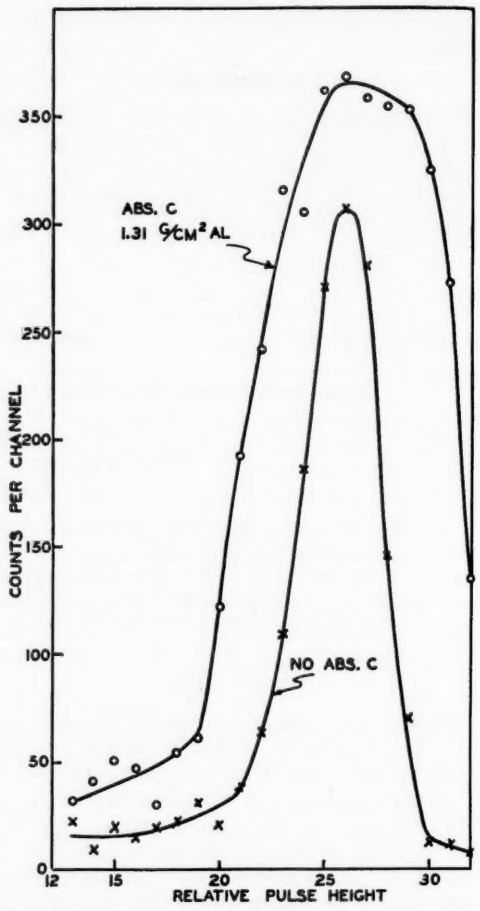

FIG. 3. Proton peaks in the pulse height spectra from proton counter number one, for two different range intervals ΔR. No photon coincidences were required in these measurements.

anticoincidence to eliminate detection of charged particles, and the second one in coincidence with the proton counter. A 0.64- or 0.95-cm lead converter between the counters gives an efficiency of 0.55 or 0.70, respectively, for counting a high-energy photon hitting it. A block of polyethylene was placed in front of these two counters in an attempt to reduce the large number of low-energy electrons without decreasing appreciably the photon counting efficiency.

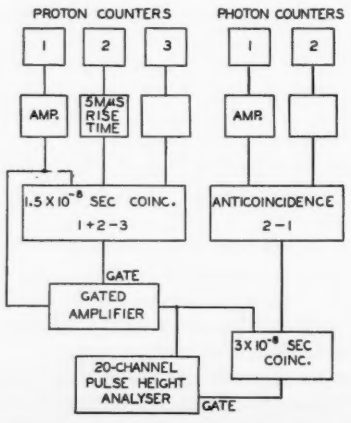

FIG. 2. Block diagram of the electronic circuits.

Targets of polyethylene and carbon of the same stopping power were used, and a subtraction made to obtain the cross section in hydrogen. The carbon background varied between 13 and 40 percent, depending on the proton energy and angle, but was typically 25 percent.

For each measurement, the target thickness, range interval ΔR, and proton angular resolution (determined by the distance between target and proton counter) were adjusted to maximize the counting rate for a given resolution. The energy resolution was about the same as that shown in Fig. 2 of reference 4, having a width at half-maximum of about 40 Mev.

The x-ray beam from the synchrotron was collimated by a primary lead collimator, followed by a secondary collimator, or "scraper". Some lead shielding which is not shown in Fig. 1 was placed near the counters to shield them as much as possible from the collimators and the beam path. Despite this shielding, the individual counting rates of the counters were large, and relatively fast electronic circuits were used. The electronic circuits and their resolving times are shown in the block diagram, Fig. 2.

THE PROTON COUNTER

The extent to which the proton counter telescope distinguishes protons from other particles is indicated in Fig. 3, which shows proton peaks in the pulse-height spectrum from the first counter. The two curves show the effect of changing the range interval ΔR by different thicknesses of absorber C. A second peak in the pulse-height spectrum due to mesons is off the scale to the left. The tail at small pulse heights is omitted in finding the proton counting rate.

THE PHOTON COUNTER

The photon counter, consisting essentially of a single counter, gives many pulses which do not originate from neutral pion decay photons. Its only duty is to eliminate all proton counts not accompanied by a decay photon, and to accept those which are with a known efficiency. The neutral pion detection efficiency depends on two factors: first, the probability that one decay photon from the pion strikes the photon counter, and second, the probability that the photon is converted in the lead converter and recorded.

Since the neutral pion is associated with a recoil proton of known energy and direction, its own energy and direction are known within limits set by the size

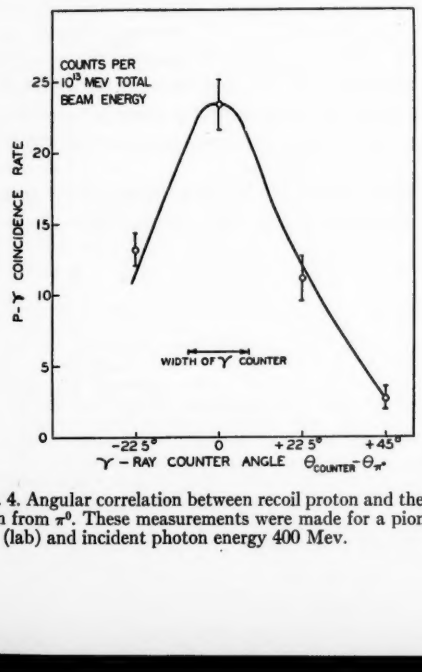

FIG. 4. Angular correlation between recoil proton and the decay photon from π^0. These measurements were made for a pion angle of 90° (lab) and incident photon energy 400 Mev.

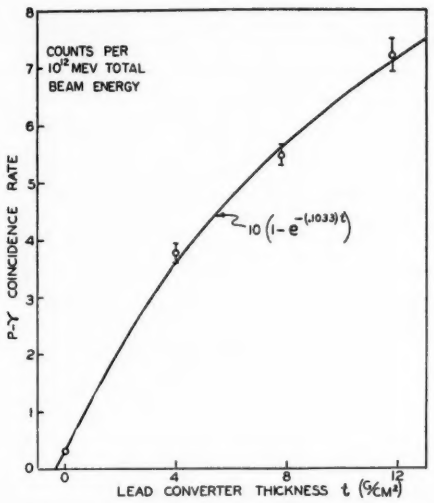

FIG. 5. Proton-γ coincidence rate as function of the lead converter thickness in the photon counter. The exponent used for the solid curve corresponds to the known absorption coefficient of lead for photons of about the average energy of the π^0 decay photons observed. These data were taken with a pion angle 90° (lab) and an incident photon energy 400 Mev.

of the proton counter and the range interval ΔR. Thus the angular and energy distributions of the decay photons are known, and the calculation of the probability of one hitting the photon counter is straightforward, although somewhat tedious. The angular correlation between proton and decay photons is illustrated in Fig. 4 which shows the proton-γ coincidences as a function of the angle of the photon counter from the direction of emission of the neutral pion.

The second factor in the pion detection efficiency, the photon conversion efficiency, is simplified by the high energy of the decay photons observed. By placing the lead converter very close to the coincidence counter to avoid scattering loss of the converted electrons, we may assume that the conversion efficiency is simply the probability of absorption of the photon in the lead. The absorption cross section, which is mainly that for pair production, is well known experimentally[5] and theoretically. The conversion efficiency is multiplied, of course, by the probability that the photon passes through the front polyethylene block and the anti-coincidence counter without absorption. This is 0.90.

The above procedure for obtaining the conversion efficiency is not valid for thick converters, of course, so a check was made to see if the 0.64- and 0.95-cm plates of lead used were so thick that absorption or scattering-out is important. Figure 5 shows the proton-γ coincidence rate as a function of lead converter thickness. This is compared to a (normalized) exponential growth curve with the proper exponent for lead, and shows that

[5] J. L. Lawson, Phys. Rev. **75**, 433 (1949); DeWire, Ashkin, and Beach, Phys. Rev. **83**, 505 (1951).

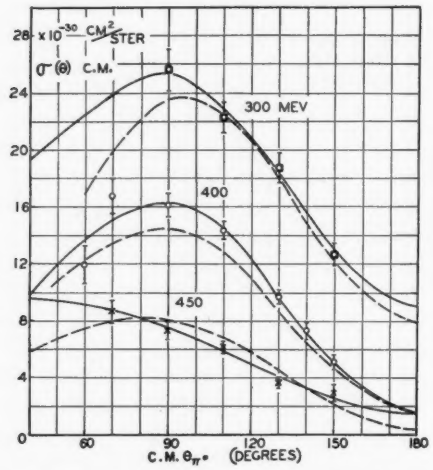

FIG. 6. Differential cross sections in the center of momentum system as a function of the c.m. pion angle. Errors are standard errors which include estimated systematic errors only to the extent that these affect the shape of the angular distribution. The solid curves are least-squares fits to the present data. The dashed curves are from the experiment of Oakley and Walker (see reference 2).

within the accuracy of the measurement, there is no correction for using too thick a converter.

THE SYNCHROTRON X-RAY BEAM

The synchrotron beam spectrum has been measured with a pair spectrometer[6] and its shape found to agree with theory within the experimental accuracy of about 3 percent. The absolute number of photons used in calculating the cross sections depends upon an absolute calibration of the beam monitor used. This was a Cornell type ionization chamber with 1-inch copper walls. The calibration used for the cross sections reported here was $Q=4.44\times10^{-18}$ Mev/coulomb. This is an average of two calibrations, one using a pair spectrometer[6] and the other the shower method of Blocher, Kenny, and Panofsky.[7] These differ unfortunately by 15 percent, and an error of about 8 percent is assigned to the beam calibration.

[6] D. H. Cooper, thesis California Institute of Technology (unpublished).
[7] Blocher, Kenny, and Panofsky, Phys. Rev. **79**, 419 (1950).

RESULTS

The differential cross sections obtained in the present experiment are shown in Fig. 6. The solid curves are least-squares fits to the form

$$\sigma(\theta)=A+B\cos\theta+C\cos^2\theta \quad \text{(c.m. system)}.$$

The values of the coefficients A, B, and C are given in Table I. The dashed curves in Fig. 6 are those obtained from the presumably more accurate values of A, B, and C reported by Oakley and Walker.[2] The present data are in reasonable agreement with these dashed curves.

The errors indicated in Fig. 6 include estimated systematic errors only to the extent that these influence the shape of the angular distributions. In addition the absolute cross sections are subject to the following errors: (1) beam calibration: 8 percent; (2) decay photon counting efficiencies: 8 percent; (3) other effects combined: 8 percent. The combined error in the absolute cross sections in thus about 14 percent.

TABLE I. Coefficients in the angular distributions, in units of 10^{-30} cm²/sterad (c.m. system).

k	300 Mev	400 Mev	450 Mev
A	25.3±1.4	16.2±0.5	7.5±0.4
B	1.6±6.1	1.4±1.2	4.2±1.2
C	−14.6±6.2	−13.4±1.7	−1.8±1.7

The absolute cross sections previously reported for 90° in the laboratory system[4] are 0 to 20 percent lower than the present values, after converting the previous cross sections to the c.m. system. The most likely source of this discrepancy is an error in the γ-ray counting efficiency assumed for the earlier experiment. The photon counter used in the present experiments is better than the earlier one in several respects, so the present cross sections are presumably the more reliable.

A comparison of the neutral pion photoproduction cross sections with the work of other laboratories and with theory is given in the accompanying paper[2] and will not be repeated here.

We are indebted to all the members of the Synchrotron Laboratory for contributions to this experiment.

Photoproduction of Neutral Pions in Hydrogen: Magnetic Analysis of Recoil Protons*

D. C. OAKLEY† AND R. L. WALKER
California Institute of Technology, Pasadena, California
(Received November 17, 1954)

The photoproduction of neutral pions from hydrogen has been studied by counting the recoil protons with a magnetic spectrometer and scintillation counters. The process has been studied between photon energies of 260 and 450 Mev and between center-of-momentum pion angles of 70° and 153°. The excitation functions show a resonance type shape with maxima at about 320 Mev. Angular distributions are analyzed in the form $A+B\cos\theta+C\cos^2\theta$ in the center-of-momentum system. The coefficient B, which gives the front-back asymmetry, is small at all energies; and the ratio $-A/C$ is 1.22 ± 0.10 at all energies between 295 and 450 Mev. The maximum cross section at 90° in the c.m. system is 26×10^{-30} cm²/steradian for 320-Mev photons. The total cross section divided by the square of the c.m. photon wavelength has a maximum near 340 Mev, and drops by nearly a factor of two at 450 Mev. These results are consistent with magnetic dipole and electric quadrupole absorption leading to a resonant state of the pion-nucleon system of angular momentum $\frac{3}{2}$ and isotopic spin $\frac{3}{2}$.

INTRODUCTION

THE photoproduction of neutral pions from hydrogen is one of the fundamental experiments to determine the nature of the pion-proton interaction. It is perhaps the least well known of the fundamental experiments, meson-proton scattering and photoproduction of pions from hydrogen. This work reports experimental work done at the California Institute of Technology's synchrotron on the photoproduction of neutral pions from hydrogen.

This reaction has shown[1–5] a marked difference from the positive pion photoproduction near threshold.[6] The positive pion photoproduction increases about as $(E_\gamma-E_T)^{\frac{1}{2}}$, where E_γ is the gamma-ray energy and E_T is the threshold of the reaction. The neutral production increases about as $(E_\gamma-E_T)^3$ near threshold and at 300 Mev is comparable with the positive production. Weak coupling theory predicts that neutral production should be much smaller than positive production. The energy dependence and nearly isotropic angular distribution of the positive pion photoproduction near threshold indicates a large S-state contribution to the cross section. The energy dependence and non-isotropic angular distribution of neutral pion photoproduction near threshold indicates very little S-state contribution and the large cross section near 300 Mev is suggestive of a resonance in the P-state contribution. Since strong coupling theory predicted a resonance, in pion-nucleon scattering, of the $P_{3/2}$ state with isotopic spin $\frac{3}{2}$, and experiments had shown an indication of this resonance, Brueckner and Case[7] suggested that this state might also be important in the photoproduction of pions. Brueckner and Watson[8] used this suggestion to calculate an excitation function.

Some general features of the possible angular distributions and energy dependence near threshold, based on angular momentum considerations, have been given by Feld[9] and by Watson[10] and Gell-Mann.[11] Watson[10] gives general relationships between photoproduction and meson-nucleon scattering. A "semi-phenomenological" theory relating photoproduction and scattering has been given by Ross,[12] which covers the energy range of the present experiment. Chew[13] has made calculations of meson scattering and photoproduction, using a cut-off theory.

Probably the most useful theory for the analysis of the experimental data is the phenomenological one of Gell-Mann and Watson,[11] as extended recently by Watson.[14] All such theories make an analysis in terms of matrix elements for photoproduction into states of definite angular momentum and isotopic spin. This means that a full comparison with experiment can only be made by combining data on charged and neutral pion production,—these involving different combinations of isotopic spin states. For this reason it is important to obtain cross sections for both positive and neutral pion production, whose absolute values may be compared. It is hoped that the present data, taken with the same magnetic spectrometer and same synchrotron beam as previous measurements of positive pion production[15] will fill this need, although the two sets of measurements were taken rather far apart in time.

* This work was supported in part by the U. S. Atomic Energy Commission.
† Now at University of California Radiation Laboratory, Livermore, California.
[1] Steinberger, Panofsky, and Steller, Phys. Rev. **78**, 802 (1950).
[2] Panofsky, Steinberger, and Steller, Phys. Rev. **86**, 180 (1952).
[3] A. Silverman and M. Stearns, Phys. Rev. **88**, 1225 (1952).
[4] Walker, Oakley, and Tollestrup, Phys. Rev. **89**, 1301 (1953).
[5] Goldschmidt-Clermont, Osborne, and Scott, Phys. Rev. **89**, 329 (1953); Phys. Rev. **97**, 188 (1955).
[6] See for example G. Bernardini and E. L. Goldwasser, Phys. Rev. **95**, 857 (1954).
[7] K. A. Brueckner and K. M. Case, Phys. Rev. **83**, 1141 (1951).
[8] K. A. Brueckner and K. M. Watson, Phys. Rev. **86**, 923 (1952).
[9] B. T. Feld, Phys. Rev. **89**, 330 (1953).
[10] K. M. Watson, Phys. Rev. **95**, 228 (1954).
[11] M. Gell-Mann and K. M. Watson, Ann. Rev. Nuc. Sci. (to be published).
[12] M. Ross, Phys. Rev. **94**, 454 (1954).
[13] Geoffrey F. Chew, Phys. Rev. **95**, 1669 (1954).
[14] K. M. Watson. Lectures at the California Institute of Technology during the summer, 1954.
[15] Walker, Teasdale, and Peterson, Phys. Rev. **92**, 1090 (1953). A complete report of these measurements will be published soon.

There have been four methods used to measure the reaction

$$\gamma+p\rightarrow p+\pi^0;\quad \pi^0\rightarrow 2\gamma.$$

(1) detect both gamma rays in coincidence,
(2) detect the proton and one gamma ray in coincidence,
(3) detect one gamma ray only,
(4) detect the proton only.

Steinberger, Panofsky, and Steller[1,2] used the first method in their work which pioneered the observation of this phenomenon and which demonstrated the existence of the neutral pion. This method had the advantage at that time of establishing the existence of the neutral pion and its mode of decay into two photons. Method 2 has been used by Silverman and Stearns[3] and later by Walker, Oakley, and Tollestrup.[4,16] This method suffers from counting rate difficulties and requires an accurate calibration of the efficiency of the gamma-ray counter for detecting at least one of the decay gamma rays from the neutral pion. Method 3 has been used by Cocconi and Silverman[17] for angular distributions and total cross section measurements even though the decay gamma rays are loosely correlated with the neutral pion. Method 4 has been used by Goldschmidt-Clermont, Osborne, and Scott[5] who counted the recoil protons by photographic plate techniques. Method 4 was also used in this experiment. The proton is identified at a laboratory angle by its momentum and its ionization loss in a scintillator. The experiment is capable of attaining good statistics, but requires proof that other processes are not contributing to the flux of protons.

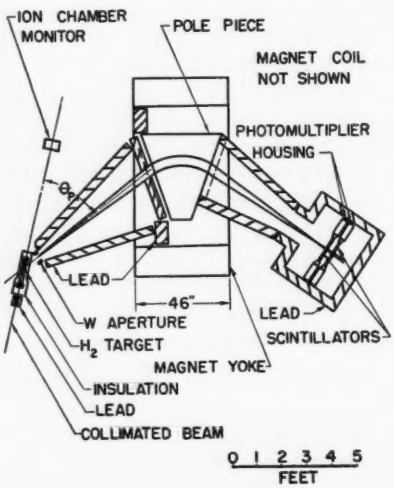

FIG. 1. Diagram of the magnetic spectrometer.

[16] Walker, Oakley, and Tollestrup, preceding paper [Phys. Rev. 97, 1279 (1955)].
[17] G. Cocconi and A. Silverman, Phys. Rev. 88, 1230 (1952).

APPARATUS

The apparatus used in this experiment is shown in Fig. 1. The 500-Mev bremsstrahlung beam of the CalTech synchrotron was collimated by a front lead collimator and two successive lead scrapers to eliminate the splatter from the walls of the front collimator. At the target, the beam was 3.8 cm in diameter.

The hydrogen target consisted of a steel flask of nominal thickness 0.030 inch, 2 inches in diameter, and 17 inches long, enclosed in a block of Styrafoam insulation 6×5 inches in cross section and most of the time further enclosed in a double polyethylene bag of 0.011-inch total thickness to keep water from condensing on the steel. Attached to the flask was a liquid nitrogen reservoir to cool the gas. The hydrogen was dried in a liquid nitrogen trap at each filling. The hydrogen was kept at a typical density of 0.032 gram/cm^3 by compressing the gas in the liquid nitrogen cooled flask to 2000 psi. The temperature was read periodically by comparing iron-constantan thermocouples attached to the flask with one immersed in boiling nitrogen. The Handbook of Chemistry and Physics was used for the calibration of the thermocouples. The density was found by interpolating the data of Johnson *et al.*[18] The density was read periodically and interpolated between readings.

There was considerable background counting rate at some of the settings. This rate was measured by taking runs with the hydrogen vented to the atmosphere or pumped below atmospheric pressure by a vacuum pump. Sufficient backgrounds were taken to give approximately the minimum statistical error in the hydrogen-background difference for a given total running time.

The wolfram slits define the volume of hydrogen used as a source. When looking at protons of momentum greater than could be directly measured by the spectrometer, carbon absorbers were placed at these slits to slow down the protons before they entered the magnet. By putting the absorber at the slits, the Coulomb multiple scattering out of the beam was cancelled by the scattering in. This was tested by using absorbers of larger atomic number and hence larger mean square scattering angle. These tests show that carbon is a safe absorber to use. Corrections have been made for the nuclear absorption by the absorbers, the target wall, and the air path, and for the nuclear scattering by the absorbers.

The counter house was placed 529 cm from the target for the "long focus" arrangement used at 12.5° and at 19.5°. It was placed 350 cm from the target for the "short focus" arrangement used at the other angles. The magnet was placed between the counter house and the target. The peak magnetic field of 15 kilogauss and the long-focus radius of curvature of 98 cm correspond

[18] Johnson, Bezman, Rubin, Swanson, Corak, and Rifkin, Atomic Energy Commission Report MDDC-850 (unpublished).

to protons of about 98 Mev and the short-focus radius of curvature of 72 cm to protons of about 54 Mev. The field of the magnet was calibrated by a proton moment apparatus, and the current was controlled by a current feedback system.

During the course of the experiment, it was found that the lead "bridges" used to shield the magnet aperture from stray particles were capable of scattering protons into the aperture that would not have gotten in otherwise. In the later portion of the experiment, the bridges were piled as shown in Fig. 1. The earlier portion had the bridges piled much closer to the particle trajectories. The effect of the position of these bridges will be discussed below under "Errors."

The counters were of two types. The thick counters used in the 12.5° setting were Lucite bottles of dimensions 1×6×9 inches, with $\frac{1}{16}$ inch walls, filled with a liquid scintillator. Thin counters made of plastic, kindly furnished by the Los Alamos laboratory, were used in all the other settings. The front thin counter was $\frac{1}{4}$×6×9 inches and the back one was $\frac{1}{2}$×6×9 inches. Both sets of counters were surrounded by 0.001-inch bright aluminum for a reflector and by a slightly thicker layer of aluminum for light shielding.

The scintillators were viewed by one RCA 5819 photomultiplier tube at each end. The outputs of the two tubes on each scintillator were connected in parallel.

A seven-channel analyzer recorded the pulse height from the phototubes in the front counter. For the lowest photon energies, the associated protons have too little energy to traverse the first counter and register a count in the second. For these energies, the pulse heights in the front counter were recorded, without requiring a coincidence with the second. For higher energies when the protons could traverse the first counter and get sufficiently far into the second counter to count reliably, coincidences were required between the two counters to trigger a gating circuit which then reproduces the pulse height in the front counter. Sample pulse-height histograms from the first counter under these two conditions are shown in Fig. 2. Accidental coincidences were monitored by counting the coincidences between the first counter and a signal from the second counter delayed 0.8 microsecond. The accidental rate was always negligible.

The total energy in the bremsstrahlung beam was monitored by a Cornell type ionization chamber with the output integrated by a current integrator. This chamber has copper walls one inch in thickness, which is very close to the peak of the shower curve for a wide range of energies. The output is nearly proportional to the total energy, independent of the maximum energy of the beam. This ion chamber and current integrator have been calibrated by a pair spectrometer[19] and also by J. C. Keck using the shower method of Blocker,

[19] D. H. Cooper, thesis, California Institute of Technology, 1954 (unpublished).

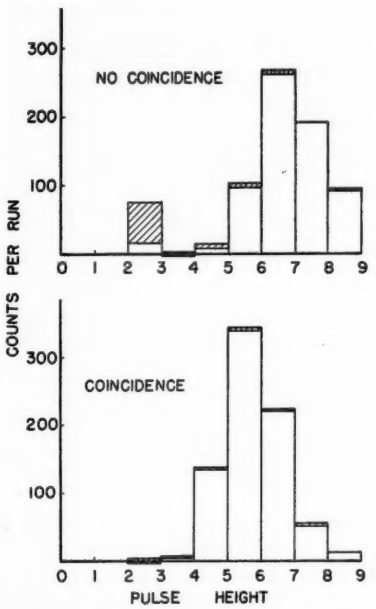

FIG. 2. Proton peaks in the pulse-height spectra from the first counter, with and without the requirement of a coincidence with the second counter. Cross-hatched areas represent backgrounds subtracted.

Kenny, and Panofsky.[20] The pair spectrometer measurement of the ion chamber calibration was (4.75±0.13) ×10[18] Mev/coulomb and the shower method measurement gave (4.12±0.20)×10[−18] Mev/coulomb. The mean value 4.44×10[18] Mev/coulomb, was used for this measurement.[21] The two calibrations are 3 standard deviations apart, but the discrepancy has not been found. An error of 7 percent is assigned to the beam calibration.

Room temperature and pressure and the peak energy of the synchrotron were monitored and corrections have been made for the effects of these on the number of ions collected from the ionization chamber.

RESULTS

Due to the size of the magnet and counter house and the need for restacking the lead bridges after each magnet moves, it was convenient to set the spectrometer in place and then make runs with different currents and absorbers, getting all runs, including backgrounds, before moving the magnet again. This procedure gives excitation functions for constant laboratory angles. The results are shown in Figs. 3 through 7 for 12.5°, 19.5°, 29°, 40.5°, and 50.3°, respectively. The cross sections are in the center of momentum system while the photon energies are in the laboratory system. Those

[20] Blocker, Kenny, and Panofsky, Phys. Rev. **79**, 419 (1950).
[21] Extrapolation of the mean value to 300-Mev bremsstrahlung gives 3.91×10[18] Mev/coulomb. The calibration at Cornell University is 3.68×10[18] Mev/coulomb.

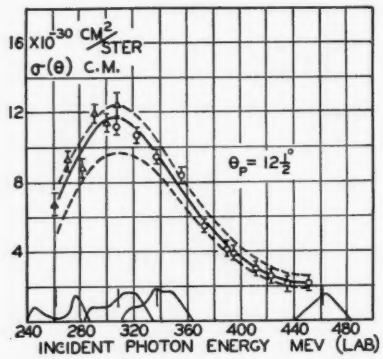

FIG. 3. Excitation function at 12.5° (lab). The differential cross section in the center-of-momentum system is shown as a function of the laboratory photon energy. Data shown by circles in this and the other excitation curves were obtained by requiring a coincidence between the two counters. Points indicated by triangles were obtained from counts in the first counter alone.

points having two errors have been obtained from the first set of experiments, with the lead bridges close to the proton trajectories; in which the protons were found to scatter from the bridges. A correction factor was determined from the ratio of the second set to the first set cross sections. The smaller errors are from the counting statistics, while the larger errors include the error in this correction factor. The entire 12.5° experiment, Fig. 3, is from the first set, with no correction factor, but large errors because of the uncertainty in this scattering effect. The points with only one error in the rest of the figures are from the second set. The triangles denote the points that could not make use of the coincidence technique of counting the protons, while the circles denote the use of coincidence between the two counters to trigger the gating circuit.

The energy resolution functions are shown at the bottom of each figure for various representative settings. These settings were chosen so that the shapes of the functions vary smoothly between the figures

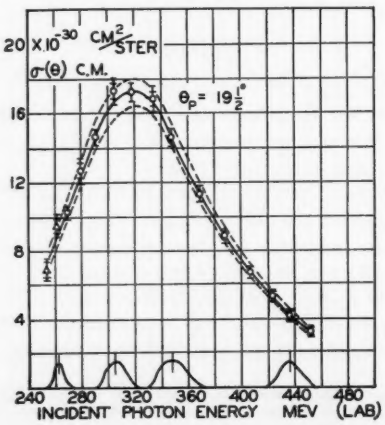

FIG. 4. Excitation function at 19.5° (lab).

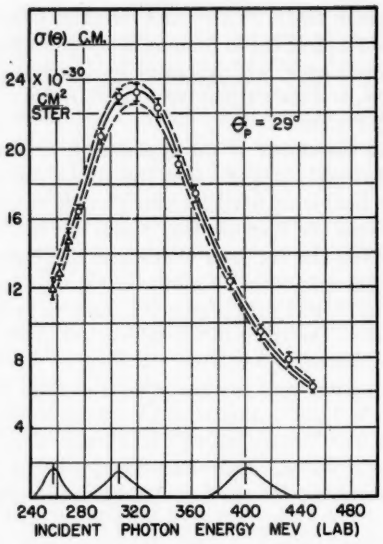

FIG. 5. Excitation function at 29° (lab).

shown. These resolution functions include the effects of the angular resolution as well as the momentum resolution. The unusual resolution functions in Fig. 3, 12.5°, are due to the target wall. At this angle, protons came through the cap of the target as well as the sides. The lower-energy peak is from those protons which came through the cap of the target, losing much less energy than those protons which came through the side wall, and which provide the higher-energy peak.

The errors on the points are standard deviations composed of statistical errors. The dotted curves

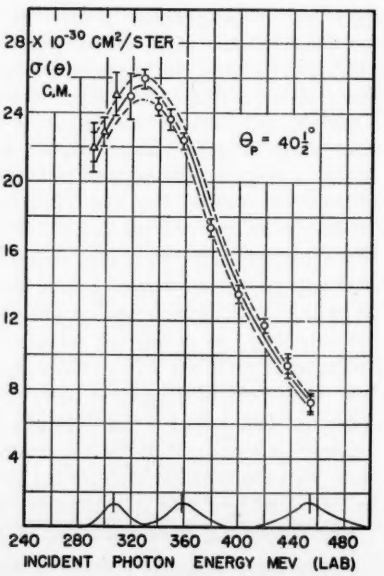

FIG. 6. Excitation function at 40.5° (lab).

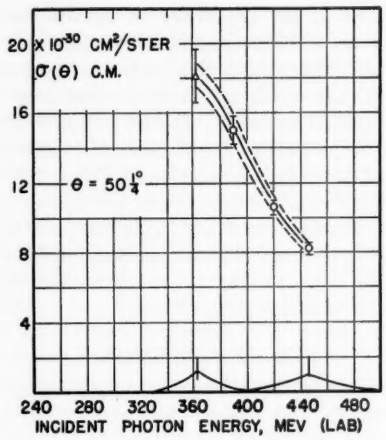

FIG. 7. Excitation function at 50.3° (lab).

indicate estimated systematic errors with the exception of systematic errors which affect only the overall absolute values of the cross sections. See the section on errors.

The angular distributions for constant photon energy can be found from the excitation functions by applying the relativistic angle transformation formulas. They are shown in Fig. 8 with a logarithmic ordinate and are tabulated in Table I. The center-of-mass angular resolutions are shown at the bottom of Fig. 8 with linear ordinate. The angular distributions have been fitted to the form $\sigma(\theta)=A+B\cos\theta+C\cos^2\theta$ by the method of least squares, and the resulting values of the coefficients A, B, and C are shown in Fig. 9.

Since the data do not extend forward of 70° at any energy, there is little experimental evidence that the cross section has the shape assumed, with only the three coefficients, A, B, and C. However, the assumption that only s- and p-wave mesons are produced appreciably in this energy region seems generally successful,

TABLE I. Angular distribution in c.m. system. $\sigma(\theta)$ is in units of 10^{-30} cm²/sterad.

		12.5° lab	19.5° lab	29° lab	40.5° lab	50.3° lab
270 Mev	$\sigma(\theta)$	8.1±1.3	10.5±0.6	15.1±0.5		
	θ_π	153°	136°	114°		
295 Mev	$\sigma(\theta)$	11.3±1.2	15.5±0.6	21.2±0.5	22.4±0.9	
	θ_π	153°	137°	115°	89°	
320 Mev	$\sigma(\theta)$	10.9±0.8	17.3±0.6	23.3±0.6	25.6±0.6	
	θ_π	153°	137°	115°	90°	
360 Mev	$\sigma(\theta)$	7.2±0.6	12.9±0.6	17.8±0.6	22.0±0.6	18.2±1.5
	θ_π	153°	138°	116°	91°	70°
400 Mev	$\sigma(\theta)$	3.6±0.4	7.6±0.4	10.9±0.5	14.1±0.5	13.6±0.6
	θ_π	153°	138°	117°	92°	71°
450 Mev	$\sigma(\theta)$	2.1±0.4	3.4±0.3	6.4±0.3	7.8±0.5	8.1±0.4
	θ_π	153°	138°	117°	93°	72°

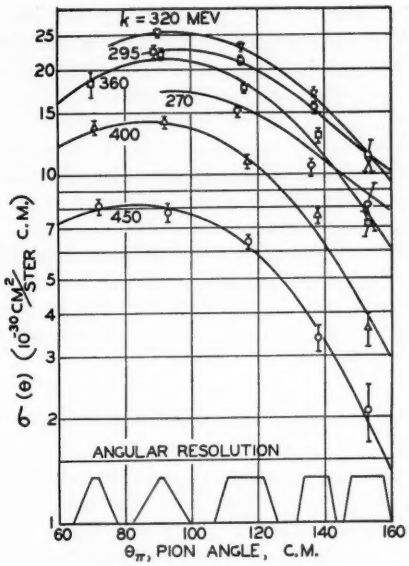

FIG. 8. Angular distributions for the reaction $\gamma+p\rightarrow p+\pi^0$. The differential cross section in the center-of-momentum system as a function of the c.m. pion angle for various laboratory photon energies.

and the more extensive data on positive pion production indicate no need for higher powers of $\cos\theta$ than the second. The values obtained for B and C depend, of course, on the form assumed for the cross section.

The simple least-squares analysis gives coefficients

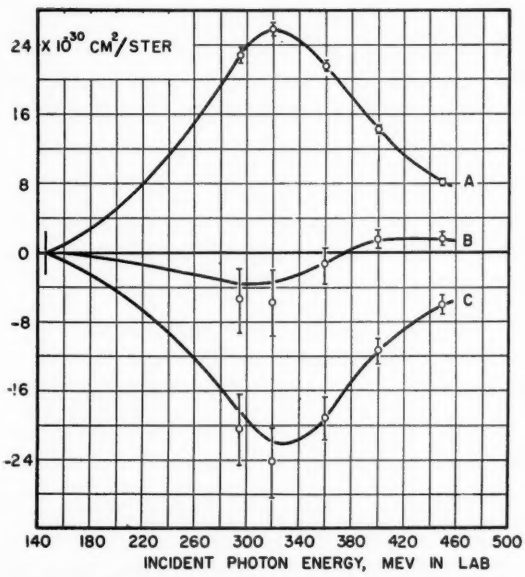

FIG. 9. Coefficients A, B, and C from a least-squares fit of the angular distributions to the form $\sigma(\theta)=A+B\cos\theta+C\cos^2\theta$ in the c.m. system. The solid curves have been drawn a little above the least-squares value at 295 and 320 Mev since the latter give negative cross sections at 0°.

B and C which at 295 and 320 Mev are impossible since they give negative cross sections at 0°. The solid curves in Fig. 9 have been drawn above the points (but within the indicated errors) so as to satisfy the requirement that the cross sections are nowhere negative. The curves have been extrapolated to threshold with a $(E_\gamma - E_T)^{\frac{1}{2}}$ energy dependence. The solid curves of Fig. 8 are computed from the coefficients A, B, and C corresponding to the solid curves of Fig. 9.

The total cross section, computed from the coefficients A and C given by the solid curves of Fig. 9, is given in Table II, and in Fig. 13. The total cross section divided by the square of the c.m. photon-wavelength is given in Fig. 10.

ELASTIC SCATTERING

Since only the recoil proton is observed in this experiment, the question arises whether protons may be produced from hydrogen by other processes than neutral pion production. One possible source of protons is, of course, elastic scattering of the photons in hydrogen. Since no mass is created in this process the relation between photon energy and proton angle and energy is different from the corresponding relation for photopion production, and this offers a possible means to distinguish between the two processes. Figure 11 shows data taken in an attempt to show that protons produced in elastic scattering are negligible. The insert in Fig. 11 shows a portion of the dynamics of the two reactions, i.e., values of the proton energy, T_p and lab angle θ_p, for incident photon energies of 250, 300, 350, and 400 Mev. The rectangle in this insert shows the regions of T_p and θ_p accepted by the spectrometer while taking these data. From the position of the photon energy lines, it is clear that the sensitivity of the spectrometer to elastic scattered protons from 310-Mev photons is the same as the sensitivity to neutral pion recoil protons from 350-Mev photons. Thus the ratio of the number of protons from elastically scattered 310-Mev photons to the number of recoil protons from neutral pion photoproduction at 350 Mev must be less than or equal to the ratio of the numbers of counts obtained with peak synchrotron energies of 310 and 350 Mev. This ratio is $\leq 0.04 \pm 0.03$. Thus, within the accuracy of a few percent, elastic scattering does not introduce any error in the neutral pion cross section. (The proton "Compton cross section" is much smaller than the upper limit obtained here.)

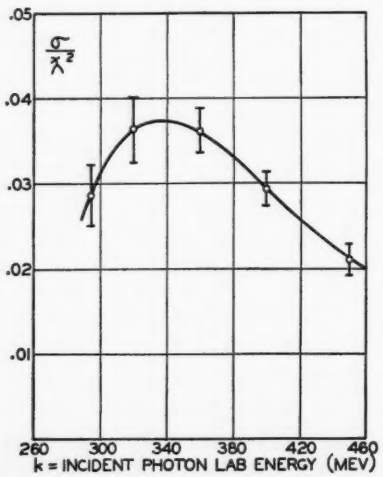

FIG. 10. Total cross section divided by λ^2. $2\pi\lambda$ is the c.m. photon wavelength.

DATA REDUCTION

The center-of-mass differential cross section $\sigma(\theta)$ is found from the counting rate by the following formula:

$$C = \sigma(\theta)\frac{d\Omega'}{d\Omega}\Delta\Omega N_H A N(k)\Delta K.$$

C is the counting rate per standard beam monitor reading, corrected for background. (Accidentals were always negligible.) This counting rate was found from pulse-height spectra such as shown in Fig. 2, in which the proton pulses are separable from pulses causes by mesons and electrons. $d\Omega'/d\Omega$ is the ratio of c.m. to laboratory solid angle at the given laboratory angle and energy; $\Delta\Omega$ is the laboratory solid angle accepted by the spectrometer; N_H is the number of hydrogen atoms per square centimeter normal to the photon beam, determined by the wolfram slits, and the hydrogen density; A is a correction for absorption and scattering in the target, absorbers, air path, and scintillators; $N(k)$ is the number of photons of energy k per Mev, per standard beam monitor reading; Δk is the range of photon energies corresponding to the range of proton energies defined by the counters.

TABLE II. Total cross sections. The errors are obtained from the least-squares analysis of the angular distributions. Errors of type C are not included.

k(Mev lab)	295	320	360	400	450
$\sigma(10^{-30}$ cm$^2)$	209±25	232±25	191±14	131±8	77±6

The energy k of the photons responsible for the counting rate is obtained from the measured momentum of the protons and the laboratory angle of observation by converting the momentum to its corresponding energy, converting the energy into a residual range for the protons as they traverse the magnetic analyzer, adding the range of the material in the proton path between the target and the magnet (including the target wall and the hydrogen inside the target), converting the total residual range back into an energy for the proton inside the target, and then using the relativistic kinetics of the two-body problem to obtain the laboratory photon kinetic energy.

The number of photons of this energy per Mev per standard beam monitor reading depends upon the absolute calibration of the ion chamber monitor mentioned under "Apparatus," and upon the shape of the bremsstrahlung spectrum. The spectrum of the synchroton beam has been measured with a pair spectrometer, and found to have the theoretical shape within the experimental accuracy of a few percent.[19]

To obtain the appropriate interval of photon energies, Δk, it is necessary to find the interval of proton energies at the point of production corresponding to the interval of momenta accepted by the spectrometer after the protons have passed through the target wall, any carbon absorbers, and air. This is done by converting the interval of momenta to an interval of proton energies at the spectrometer energy and then converting this to an interval of proton energies at the point of production by multiplying by the ratio of specific ionization at the production energy to that at the spectrometer energy.

The correction for absorption and scattering in the target, absorbers, air path, and scintillators used the theory of Fernbach, Serber, and Taylor[22] with the energy-dependent parameters determined by Taylor[23] for the nuclear absorption by the materials in the proton beam. The nuclear scattering cross sections were obtained by subtracting the absorption cross sections from the observed total cross sections reported in Rossi's book.[24] Coulomb multiple scattering was found to be negligible from the scintillators, air path, and carbon absorbers and the scattering-out from the target wall was assumed compensated by scattering-in.

The Coulomb multiple scattering in the carbon absorbers was checked by comparing cross sections obtained by using absorbers of aluminum, copper and lead. From the differences in these cross sections, the predicted loss from the carbon absorbers never exceeded 0.1 percent. This effect has been ignored and no error assigned to it.

ERRORS

The errors in the experiment may be classified into three types:

(A) *Random statistical errors*, indicated on the measured points in Figs. 3 to 7. These are mainly the counting statistics and an estimate of the error in separating the proton peak from the pion peak. However, they also include about 2 percent error from the reproducibility of reading the target density, the uncertainty in resetting the magnetic analyzer field, and fluctuations in the beam monitoring.

(B) *Systematic errors which vary smoothly* from point-to-point on an excitation curve or angular distribution. These errors are indicated by the dashed curves on either side of the excitation curves of Figs. 3 to 7.

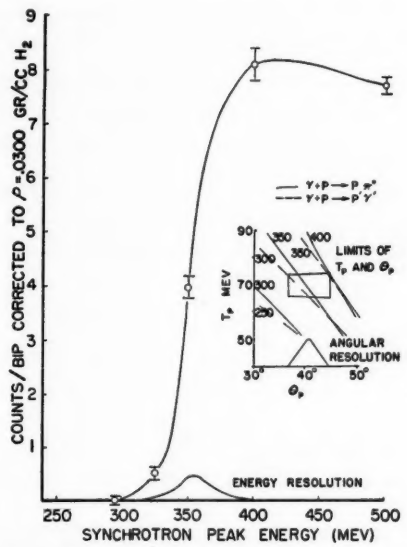

FIG. 11. Counting rate as a function of synchrotron energy, with the spectrometer set to count 70-Mev protons at 40.5°. See discussion in the section on Elastic Scattering.

They include the following: (1) Target wall thickness: 5 percent of thickness. (2) Absorber thickness: 1 percent of thickness. (3) Error in absorber scattering and absorption correction: 10 percent of the correction. (4) Slit penetration: 0 to 2 percent. (5) Error in proton angle setting: $\frac{1}{4}$ degree except at 12.5°, where it is 1 degree. (6) Beam monitor stability: 1.5 percent. (7) Uncertainty in the solid angle because the counters are not quite high enough to catch all the particles which get through the vertical aperture: 3 percent for long-focus measurements only.

A correction to the aperture solid angle was determined for the long-focus arrangement by comparing the counting rate with a 2-inch vertical aperture to that with the standard 3-inch aperture. The correction thus determined was 5.8 ± 2.9 percent. No correction is necessary for the short-focus measurements because of partial vertical focusing in the fringe field of the magnet.

(8) Scattering from the lead shielding: The first set of runs was made with the lead "bridges" in Fig. 1 in a position very close to the particle paths. These runs did not show good consistency in the lower energies and investigation indicated that protons were scattering from the lead bridges in such a manner that they contributed to the counting rate, increasing the apparent cross section. The second set of runs tried to correct this effect by moving the bridges as far from the proton beam as was practical, to the position shown in Fig. 1. The bridges could not be dispensed with, because of increased background. The 12.5° measurements used bridges stacked of 2-inch lead bricks alternating with 2-inch air spaces from the

[22] Fernbach, Serber, and Taylor, Phys. Rev. **75**, 1352 (1949).
[23] T. B. Taylor, Phys. Rev. **92**, 831 (1953).
[24] Bruno Rossi, *High Energy Particles* (Prentice-Hall, Inc., New York, 1952), p. 344.

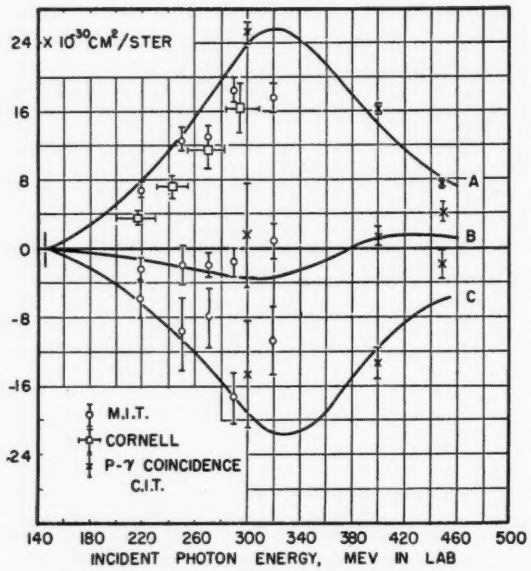

FIG. 12. Comparison with other experiments. The solid curves are the same as in Fig. 9 and represent the results of the present experiment. The data of Silverman and Stearns (see reference 3) at Cornell University are shown by the squares. Data from the Massachusetts Institute of Technology by Goldschmidt-Clermont, Osborne, and Scott (see reference 5) are shown by circles. The crosses are our older data obtained by measuring p-γ coincidences (see reference 16).

magnet to the target on one side and a solid wall of lead $\frac{2}{3}$ of the way from the magnet to the target on the other side. The other angles used solid bridges on both sides of the beam, so the corrections determined for these angles could not be applied directly to the 12.5° data, which were not repeated. Therefore, these data are reported as observed, but the correction factors are included in the estimate of the systematic errors shown by the dotted lines in Fig. 3.

(C) *Errors in the absolute cross sections*, independent of proton angle and energy. These amount to about 8 percent, and are not indicated in any of the figures. They include the following: (1) Error in the absolute beam calibration: 7 percent. (2) Error in the momentum range, Δp, accepted by the spectrometer: 2 percent. (3) Average target gas density: 2 percent.

COMPARISON WITH OTHER EXPERIMENTS

Data from other experiments are shown in Fig. 12, together with the same curves as in Fig. 9, obtained from this experiment. The old data of Silverman and Stearns[3] from Cornell University are considerably lower in value, but not by much more than the 30 percent quoted error in the absolute values.

The data from our older experiment using proton-γ coincidences[16] are indicated by the crosses in Fig. 12, and agree rather well with the present data.

The recently reported photographic plate results of Goldschmidt-Clermont, Osborne, and Scott[5] from the Massachusetts Institute of Technology are shown by the circles in Fig. 12. They agree fairly well with the solid curve which is extrapolated from our higher energy data by a $(E_\gamma - E_T)^{\frac{1}{2}}$ dependence. The Massachusetts Institute of Technology data give slightly lower values than this solid curve, but the worst discrepancy, at 320 Mev, is perhaps a result of the difficulties in obtaining data so near the upper end of the Massachusetts Institute of Technology bremsstrahlung spectrum.

Recent measurements in this laboratory[25] using a counter telescope to measure the recoil protons give preliminary results perhaps 10 percent lower than the present measurements in the region of the peak.

INTERPRETATION

As mentioned in the introduction, an analysis of photomeson production in terms of any theory is best done by considering charged and neutral production together. Such an analysis is being prepared in collaboration with K. M. Watson, based on his extension[14] of the phenomenological description of Gell-Mann and Watson.[11] For this reason only the most striking features of the data will be discussed here, namely the energy dependence of the cross section, and the angular distribution, which is rather independent of energy.

If one makes the assumption[8] that neutral pion photoproduction takes place mainly through a state of angular momentum $J=\frac{3}{2}$ and isotopic spin $T=\frac{3}{2}$ and that the production into s states is small, then the energy dependence near threshold[8,9] should be approximately like η^3, where η is the momentum of the pion in the c.m. system in units of the pion mass μ. At higher energies, the energy dependence of the matrix elements for production into the $J=\frac{3}{2}$, $T=\frac{3}{2}$ state becomes important. The approximate energy dependence of these "enhanced" matrix elements has been given by Watson,[10,26] and by Chew,[13] and may be expressed by a factor $\eta^{-2}\sin\alpha_{33}$, where α_{33} is the pion-nucleon scattering phase shift in the $J=\frac{3}{2}$, $T=\frac{3}{2}$ state. An estimate for the energy dependence of the c.m. cross section is obtained by multiplying the square of $\eta^{-2}\sin\alpha_{33}$ by a factor $\eta\omega E_f(\omega+E_f)^{-1}$ from the density of states, and dividing by the incident flux $c(1+\nu/E_i)$. $\omega=(\eta^2+1)^{\frac{1}{2}}$ is the pion energy, ν the photon momentum, and E_f the final nucleon energy, all in the c.m. system in units of the pion mass μ.

The resulting estimate is approximately (within one or two factors of ν or ω)

$$\sigma_{\text{est}} = N\left(1+\frac{\nu}{M}\right)^{-2}\eta^{-3}\sin^2\alpha_{33}.$$

[25] R. Smythe and R. M. Worlock, Bull. Am. Phys. Soc. 29, No. 8, 21 (1954).
[26] K. M. Watson, Phys. Rev. 88, 1163 (1952).

This function is shown in Fig. 13 for the scattering phase shift α_{33} chosen by Bethe and de Hoffman.[27] For comparison, the measured total cross section obtained from the coefficients A and C of Fig. 9 is also plotted in Fig. 13. The agreement at low energies is not very significant, of course, since the "measured" curve has also been given an energy dependence in this region expected from theory. However, the data of Silverman and Stearns,[3] and of Goldschmidt-Clermont, Osborn, and Scott[5] indicate that this energy dependence is about right.

At high energies, above 350 Mev, the estimated cross section falls off more rapidly than the measured one. This difference may be reduced by including in the analysis contributions from other $\not{p}$ state matrix elements than the enhanced $J=T=\frac{3}{2}$ ones.[14] However, even the simple analysis above shows that the rapid decrease in the cross section above 340 Mev, which is faster than the decrease in λ^2, as shown in Fig. 10, is explained quite simply by the idea of a resonance in the $J=T=\frac{3}{2}$ state. The resonance is indicated, of course, by the phase shift α_{33} going through 90° in the analysis of Bethe and de Hoffman.[27]

The angular distribution, Fig. 8, is rather independent of energy. The coefficient B is small, and the ratio $-A/C$ is 1.22 ± 0.10 at all energies from 295 to 450 Mev. If π^0 production took place solely by magnetic dipole absorption into the $J=\frac{3}{2}$, $T=\frac{3}{2}$ state, the ratio $-A/C$ would be 1.67 so experiment shows that other matrix elements are also involved, which is not surprising. Perhaps the most important is that for electric quadrupole absorption into the same pion-nucleon state.

[27] H. A. Bethe and F. de Hoffman, Phys. Rev. **95**, 1100 (1954).

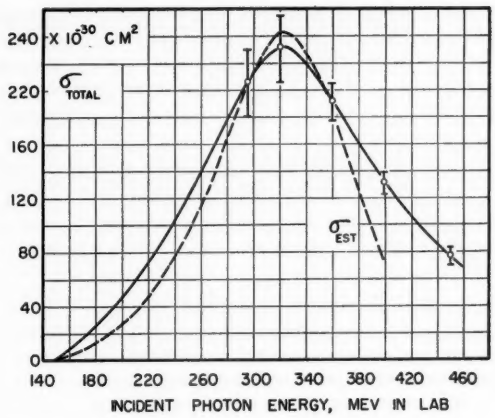

FIG. 13. The total cross section σ obtained from the present experiment, compared to an estimated energy dependence, σ_{est}, described under "Interpretation".

ACKNOWLEDGMENTS

We are considerably indebted to Michel Bloch, Paul Donoho, James Vette, and Dr. John G. Teasdale for helping to take some of the data, and to Professor R. F. Bacher for continued interest in the experiment, and many discussions about it.

Measurement of Multiply Charged Cosmic Rays by a New Technique*

JOHN LINSLEY†
University of Minnesota, Minneapolis, Minnesota
(Received August 4, 1954)

The Čerenkov effect has been applied to the problem of determining the charge of cosmic rays. Cloud chamber photographs have been obtained of the events that caused large signals from a thin Čerenkov counter during a balloon flight which carried the apparatus above most of the atmosphere. They show that the Čerenkov counter was notably effective at discriminating against the background effects that plague counter measurements on the charge spectrum of cosmic rays, for a relatively large proportion of the signals were caused by single heavily ionizing particles. The theory of the Čerenkov effect associates a lower velocity limit with the signal amplitude requirement that those particles met. Their ionization was determined well enough to classify particles of such velocity as having $Z=2$ or $Z>2$ with considerable certainty. The vertical flux of doubly charged particles with kinetic energy $>(610\pm100)$ Mev/nucleon beneath 17 g/cm² of atmosphere and 13 g/cm² of local matter is found to be (79 ± 11)/m² sec steradian. That result and currently accepted assumptions concerning absorption imply the value (135 ± 20)/m² sec steradian for the extrapolated vertical flux of primary alpha particles with energy above (670 ± 100) Mev/nucleon. Some of the alpha particles were seen to interact in copper plates within the cloud chamber. The observations indicate that the collision mean free path is (100 ± 25) g/cm². The problem of counter measurements on components heavier than helium is scrutinized.

I. INTRODUCTION

WHEN it was discovered that the primary cosmic-ray particles are nuclei not only of hydrogen but of many heavier elements it became plain that the cosmic radiation is a much richer source of information than there was reason to hope previously.

The fields that we suppose accelerate cosmic-ray particles act on the first power of their charge, while energy loss by ionization varies as the charge squared. Heavy nuclei that attain the energies observed can be degraded rapidly in mass if they suffer nuclear collisions, and the collision cross section varies somewhat more slowly than the charge. Therefore, the facts that heavy nuclei get accelerated in spite of competition from ionization loss and that they are delivered to the earth in spite of competition from nuclear collisions are very pertinent information concerning the processes that account for the phenomena. And the fact that they reach the earth at all means that the relation between the elemental composition of the cosmic radiation and that of the matter where its particles begin to acquire energy is not trivial, even though intervening processes may be supposed to affect it. Such matters have been discussed in some detail by Morrison, Olbert, and Rossi.[1]

The heavy nuclei were discovered simultaneously by means of two of the earliest techniques for detection of penetrating charged particles, the Wilson cloud chamber and the photographic emulsion.[2] Since then nearly all quantitative information that has been obtained about the relative abundances of the various nuclei heavier than helium has come from use of emulsions. Cloud chambers and counters of various types have been used mostly for measuring the abundance of helium and the total flux.

The experimental problem is to determine the charge of individual fast particles. A number of effects related to energy loss by ionization and proportional to Z^2 are available for that purpose. The dependence of the same effects on particle velocity presents a difficulty, for a sufficiently slow particle can lose energy by ionization at the same rate as a faster one with a greater charge, so commonly it is necessary to measure range or rate of change of ionization loss in order to establish with much accuracy the charge of individual particles. That difficulty is particularly troublesome in measuring the relative abundance of hydrogen and helium, for secondary protons that ionize the same as primary alpha-particles are as abundant as the latter in any attainable experimental environment, and such protons still have very appreciable range. The difficulty applies to the emulsion technique as well as to methods that exploit ionization counters.[3]

Charge-measuring counters suffer for their part from an inherent inability to distinguish the effect of an individual particle from that of a group of secondaries from a multiple event. The facts that multiple events are generated copiously by primary cosmic-ray particles and their immediate secondaries and that a nuclear interaction even at relatively low cosmic-ray energies is characterized by production of intense local ionization from evaporated secondaries mean that multiple events can be expected to compete effectively with primary heavy nuclei at producing large signals from ionization counters. Use of absorbers to impose a range requirement that will eliminate slow particle background tends to increase background from local interactions.

The Čerenkov effect provides an alternative principle

* The research was supported in part by the joint program of the U. S. Atomic Energy Commission and the Office of Naval Research.

† Present address: Department of Physics, Massachusetts Institute of Technology, Cambridge, Massachusetts.

[1] Morrison, Olbert, and Rossi, Phys. Rev. 94, 440 (1954).

[2] Frier, Lofgren, Ney, Oppenheimer, Bradt, and Peters, Phys. Rev. 74, 213 (1948).

[3] The term "ionization counter" is used here to designate any device that gives an electrical pulse proportional to ionization produced by an event within a certain volume; e.g., gas proportional counters, pulse ionization chambers, and scintillation counters.

for charge measurement, for the amount of Čerenkov radiation that is emitted by a fast particle in traversing a transparent medium varies with its charge as the square. The way in which the energy radiated varies with particle velocity indicates that the various events that go to make up background in an ionization counter will produce, in a Čerenkov counter, either no response whatever or a far smaller response, in terms of that produced by a single fast particle with unit charge.

II. ČERENKOV COUNTER MEASUREMENT OF CHARGE

According to classical electromagnetic theory the Čerenkov light is emitted in a forward cone of angle ϑ, where $\cos\vartheta=1/\beta n$, about the direction of motion of a sufficiently fast ($v>v_c\equiv c/n$) charged particle traversing a medium with refractive index n. The energy emitted (integrated over frequency, neglecting dispersion) is given by

$$E(Z,\gamma)=E_0Z^2\left[1-\frac{1}{(n^2-1)(\gamma^2-1)}\right]=E_0Z^2f_c(\gamma), \quad (1)$$

where $E_0\equiv E(1,\infty)$, Z is the charge in units of that of the electron, and $\gamma\equiv(1-\beta^2)^{-\frac{1}{2}}$, $\beta\equiv v/c$. The velocity dependence expressed by $f_c(\gamma)$ (Fig. 6) is distinctly unlike that of ionization loss.

Consider a detector consisting of a Lucite radiator viewed by a photomultiplier. Since the critical velocity in Lucite ($n=1.5$) corresponds to an ionization 1.6 times minimum the slow protons that are difficult to distinguish from fast alpha particles by use of emulsion or ionization counters will be completely ignored by the Čerenkov counter, and its response to an individual proton of any speed will be limited to one-fourth its response to a fast alpha particle. It is true that a Čerenkov counter can respond equally to a fast alpha particle and a slower heavier nucleus, but the heavier nuclei that can compete are rare and will not disturb a measurement of the flux of fast alpha particles.

As for background from multiple events, prediction again favors a Čerenkov counter over one that measures ionization. Studies with emulsion[4] show that most charged secondaries from multiple events at high altitude are low-energy evaporations (black tracks) or "knock-on" protons (gray tracks) with less than the critical velocity in Lucite, and that the great majority of nuclear interactions have less than two secondaries that are faster (thin tracks). Thus, only the less frequent interactions and only the least abundant of their secondaries can give Čerenkov light, whereas all the interactions give ionizing secondaries, and for ionization counters the most abundant secondaries are heavily weighted because ionization increases with diminishing velocity.

Bibliographies on experimental and theoretical investigations of the Čerenkov effect have been published elsewhere,[5,6] so only applications of the effect to detection and measurement of cosmic radiation will be referred to in this paper. Quantitative detection of cosmic rays by their Čerenkov radiation was first accomplished by Jelley.[7] In later experiments he and Galbraith[8] have succeeded in detecting the Čerenkov light produced in air by soft showers at sea level. Duerden and Hyams[9] have detected sea level cosmic-ray protons efficiently by using a Čerenkov counter in anticoincidence to set a velocity limit and an absorber to require penetration.

The possibility of using a Čerenkov detector for investigating the charge spectrum of primary cosmic rays was pointed out by Winckler and Anderson[10] in a letter describing the Čerenkov counters they have developed and used in a study of directional and albedo effects at high altitude.[11] In their design the directional properties of the Čerenkov radiation permit collection of light from 20 cm of path length in Lucite for traversals with one sense of direction and result in practically complete absorption of the light for traversals in the opposite sense. The pulse-height distribution they obtained at 25 g/cm² atmospheric depth (Fig. 10 of reference 11) has a tail toward large pulse heights which they attribute to nuclear interactions with relativistic secondaries, many of which must have originated in the relatively thick (29 g/cm²) Lucite radiator of their detector. The amplitude of their distribution near four and nine times the sea level meson pulse height seems to exceed significantly the background from collisions in those regions. They attribute the excess to individual fast doubly and triply charged nuclei.

It was decided to investigate the charge resolving capability of Čerenkov counters with "thin" radiators; that is, radiators of thickness a small fraction of an interaction mean free path. Promising results were obtained using a thickness of one inch. The radiator, a polished Lucite cylinder $1\frac{1}{2}$ in. in diameter, was coupled with Canada balsam to an EMI 6260 phototube ($1\frac{3}{4}$ in. diameter photosurface). Bright aluminum foil was sealed to the remaining Lucite surfaces with the same material. Figure 1(A) shows the distribution of pulse heights (multiplier gated by a Geiger counter telescope) from sea-level cosmic rays obtained with counter axis vertical and radiator uppermost. The smooth curve is the Poisson distribution for $\bar{n}=18$.

The differential expression corresponding to (1), integrated over the absolute spectral sensitivity characteristic of an S-9 photosurface, indicates that a very fast singly charged particle might give 40 photoelectrons per inch of path length in Lucite for a selected photo-

[4] Camerini, Fowler, Lock, and Muirhead, Phil. Mag. **41**, 413 (1950).

[5] R. L. Mather, Phys. Rev. **84**, 181 (1951).
[6] J. V. Jelley, Atomics **4**, 81 (1953).
[7] J. V. Jelley, Proc. Phys. Soc. (London) **A64**, 82 (1951).
[8] J. V. Jelley and W. Galbraith, Phil. Mag. **44**, 619 (1953).
[9] T. Duerden and B. D. Hyams, Phil. Mag. **43**, 717 (1952).
[10] J. Winckler and K. Anderson, Rev. Sci. Instr. **23**, 765 (1952).
[11] J. R. Winckler and K. Anderson, Phys. Rev. **93**, 596 (1954).

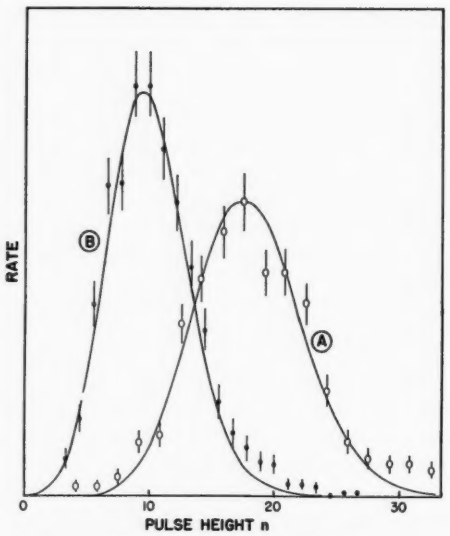

FIG. 1. Čerenkov counter pulse height distributions. The curves are Poisson distributions $P(18,n)$ (A) and $P(10,n)$ (B). Open circles are measured for normal counter sense; full circles for counter inverted. Total rate for each has been normalized to the area under the curve. The gain was the same during the two runs. Errors are statistical.

tube, with perfect light collection.[12] We think the assumption that the mean number of photoelectrons was about 18 in our case, i.e., that nearly all the spread in Fig. 1(A) comes from fluctuations in that number, is consistent with the prediction in view of its idealized hypotheses. More recent work at this laboratory shows that a width at half-maximum as small as 35 percent can be obtained for the sea-level flux with a similar radiator of the same thickness and a better phototube.

III. THE EXPERIMENT

It seemed then that by combining the counter with a cloud chamber in a high altitude experiment two results could be accomplished: the flux of fast alpha particles could be measured, and at the same time an insight into the general problem could be gained which might point out how to make more extensive and precise abundance measurements with simpler equipment.

The chamber was of the type that has been developed at the University of Minnesota for use in high altitude research.[13]

The particular model that was used had a sensitive region about 4 by 8 in. in plan and 8 in. in height. It was filled to a pressure of about 85 cm with argon and water-alcohol vapor and contained five transverse copper plates $\frac{1}{4}$ in. thick. The chamber walls were of $\frac{5}{16}$ in. Lucite. The control circuit imposed a dead time of about one minute following an expansion. Stereoscopic cameras photographed the events and an instrument panel showing time and temperature.

The Čerenkov counter was inverted so that the radiator could be directly above the top of the chamber (Fig. 2). The resultant change in sea-level pulse height distribution (to B, Fig. 1) is explained by imperfect reflection from the foil coating of the radiator. From symmetry it was believed that the 'inherent' resolution (the limit $Z\rightarrow\infty$) was not much changed.

The placing of the phototube coaxial with the Geiger counter telescope had obvious disadvantages: proton induced interactions in the phototube would add to the background, and the alpha particle flux would be attenuated. However, we have not been able to design a Čerenkov counter with good inherent resolution for particles that pass at right angles to the phototube axis. We chose for this experiment to accept the disadvantages of the coaxial arrangement for the sake of the better resolution it gives.

The beam defined by the telescope traversed the cloud chamber entirely within the chamber's illuminated region.

Figure 3 is a block diagram of the electronics. A Geiger counter tray of effective area 2 by 4 in. and a single counter of diameter 1 in. and nominal length 1 in. made up the telescope.

Usually the "geometric factor" of a counter telescope (the constant of proportionality between counting rate and flux of particles) is calculated from measured dimensions. In our case, however, the effective lengths of the counters were not known very precisely, so the

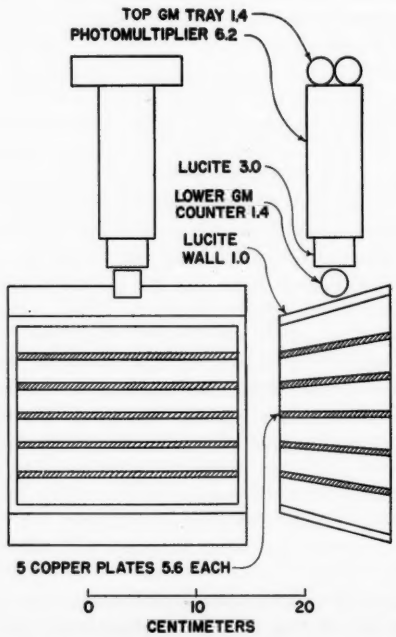

FIG. 2. Arrangement of apparatus. Numbers shown are thicknesses in g/cm².

[12] J. Marshall, Phys. Rev. **86**, 685 (1952).
[13] Lofgren, Ney, and Oppenheimer, Rev. Sci. Instr. **20**, 48 (1949). Extensive changes in design have been made since that article appeared.

geometric factor K was found by a substitution method. A second telescope of roughly similar size and shape was constructed using crossed counters to define its apertures so that its geometric factor could be calculated accurately. Counting rates of both telescopes were measured in the laboratory. The ratio of those rates times the calculated geometric factor gave, for the telescope to be used with the Čerenkov counter, $K=(0.78\pm0.04)$ cm² steradian. A small correction (3 percent) for difference in angular distribution between the flux used in calibration and that at high altitude was taken into account.

The position of the discriminator edge was adjustable and could be measured by counting trigger pulses delivered to the cloud chamber and referring to the absolute pulse height distribution at sea level. For the high altitude experiment it was set at about twice the mean pulse height for a fast singly charged particle.

It was necessary to stage the flight at 55° geomagnetic latitude, where the momentum cutoff for nuclei other than protons corresponds to a velocity less than v_c in Lucite. That fact influenced the results in two ways which will be mentioned now and discussed later: (1) the energy threshold for detection of particles was determined by a property of the detector and the discriminator bias rather than by geomagnetic effects, and (2) particles could trigger the cloud chamber and not be at their minimum ionization.

The equipment, housed in a pressurized insulated gondola with walls of thirty-mil aluminum, was flown October 12, 1953. The complete apparatus weighed 120 lb. The pressure-altitude was recorded by a separate unit in which a Wallace and Tiernan aneroid gauge, a clock and a thermometer were photographed at five minute intervals. Gauge calibrations before and after the flight showed no change. The flight reached 16.4 millibars and remained level within limits ±0.3 millibar for 345 minutes until the load was released. The gauge temperature did not leave the region in which tests at this laboratory have shown that the gauge is fully temperature compensated.

The temperature in the main gondola fell during the ascent, reaching its lowest value of 71°F slightly after the flight reached ceiling. Thereafter it rose slowly to an equilibrium value of 78°F. The cooling during ascent caused some condensation of vapor on the glass chamber-front, but that condition was never severe enough to cause uncertainty in interpreting events, and within less than an hour as the temperature rose the front had cleared.

The mean dead-time of the cloud chamber was determined from the set of trigger times recorded during the flight by photographing a sweep-second clock beside the cloud chamber. The total sensitive time during the 345 minutes at ceiling was $(1.013\pm0.017)\times10^4$ sec. One hundred fifty-seven events were photographed in that time, and tracks of good quality were produced at every expansion. The photographs show that the chamber condition stayed constant and that no change took place affecting its control cycle.

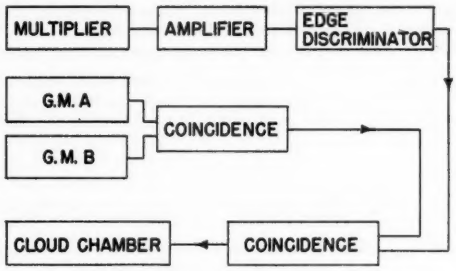

FIG. 3. Trigger circuit block diagram.

IV. ANALYSIS OF THE PHOTOGRAPHS

Classification of Events

Two kinds of event would be capable of triggering the cloud chamber: (I) an individual fast multiply charged particle could traverse the telescope and enter the chamber, or (II) the trigger requirements (Geiger counter coincidence plus a large enough Čerenkov counter signal) could be met by cooperation between secondaries from a multiplicative interaction or a primary and its fast secondaries. Which type of event triggered the chamber had to be determined in each case by examining the photographs. The events of type I measure the flux of multiply charged particles while those of type II provide information that may help in interpreting results of other experiments or in developing improved techniques for cosmic-ray measurement. It will be shown that although it was not always possible to establish the nature of the multiplicative events still there was hardly ever any doubt whether the chamber had been triggered by such an event or by one of the type described first. In most cases the decision could be made without ever estimating the ionization along a track.

The photographs were searched for counter-age tracks that projected through the telescope apertures in both stereoscopic views, penetrated the plates without scattering or else interacted, and—if they did not interact—remained visible in all spaces between plates except possibly the lowest one. The cases in which such a track was found include all events of type I; that is, in which a fast multiply charged particle traversed the telescope and entered the cloud chamber. (A track as dense as four times minimum is conspicuous and could not be overlooked.)

The events that satisfied the preceding necessary condition (criterion A) were subdivided in two ways: according to the density of the track (criterion B) and according to the number of other tracks in the photograph that appeared to be related to it (criterion C). Table I shows the result.

If more than one track satisfied criterion A, criterion B was applied to the densest of such tracks. Track

TABLE I. Breakdown of cases in which the photographs showed an "allowed" track (one that satisfied criterion A).

Density of allowed track	Number of additional related tracks 0	1	$\geqslant 2$
1	6	1	19
2	1	0	2
$\geqslant 4$	75	0	1

density in units of that corresponding to a fast singly charged particle was estimated visually by comparing the given track to others of the same age selected for some significant characteristic (for example, the electron tracks in a typical soft shower). We believe that relative ionization was estimated correctly within limits ± 50 percent.

Tracks of obvious knock-on electrons were not counted in applying criterion C, which was aimed at separating nuclear interactions from events in which a particle triggered the chamber all by itself. Tracks were considered related if they were of the same age and projection of the stereoscopic photographs showed that they came from a common point. The time resolution was good enough so that the background of counter-age tracks was small, about five reasonably long tracks per photograph.

In the following discussion of Table I a group of events will be designated by its coordinates in the table; for example, there were 75 "$(\geqslant 4, 0)$" events.

The $(j, \geqslant 2)$ events (all those in the third column) were surely multiplicative, nearly all of them nuclear interactions. However, they include only part of the multiple events that were photographed: only those that had an "allowed" track. In very few cases did an allowed track that was known to be secondary have greater than minimum density. The one event entered at $(\geqslant 4, \geqslant 2)$ showed two nearly parallel tracks of density four times minimum and a number of other related tracks. One of the heavily ionizing particles made a sizeable interaction in the fourth copper plate. The primary event was probably breakup of a heavy nucleus with production of two fast secondary alpha particles.

The small number of $(j, 1)$ events is understandable on two counts. In the first place only the more energetic nuclear interactions could satisfy the trigger requirement, so most of those that were detected show tracks of three or more secondaries. Second, there is less chance that a smaller interaction would happen to have a secondary whose track would be allowed.

The preceding observations permit a strong inference that none of the $(\geqslant 4, 0)$ events were local nuclear interactions which had a slow proton secondary whose track happened to satisfy criterion A and have 4 times minimum density but which had no other secondaries that made visible tracks. The argument follows: If we keep in mind that only rather large nuclear interactions could trigger the equipment, it is apparent that the condition $(j,0)$, "there shall be but one visible secondary, and it shall be allowed" is more restrictive than the condition $(j,1)$, "there shall be two visible secondaries, one of which shall be allowed." Consequently there should be fewer nuclear interactions of type $(j,0)$ than of type $(j,1)$, of which we find only one example. The clinching argument is that nuclear interactions of type $(\geqslant 4, 0)$ are a subset, and must be a rather small subset, of interactions with the properties $(j,0)$.

The (1,0) entry needs special comment. A singly charged particle can give a signal twice the average size for a fast mu meson by making a relativistic knock-on electron (see the 'tail' of the pulse height distribution, Fig. 1) though only with a small probability and only if the particle itself is at minimum ionization. It seems likely that the (1,0) events were not nuclear interactions but were multiplicative in the sense that a fast secondary electron provided part of the Čerenkov signal. It would be expected that in many cases the electron be absorbed or scattered so as not to produce a related track.

The only case in which doubt could not be resolved is entered at (2,0). The particle interacted in the topmost copper plate. Either it was a proton at minimum ionization whose track was abnormally bright in the one section where it was seen, or it was an alpha particle whose track was unusually faint.

This completes the argument for classifying the $(\geqslant 4, 0)$ events as type I and all others as type II. In what follows the latter will usually be called background events.

Tracks of Heavy Nuclei

Although the great majority of individual particles that triggered the chamber were helium nuclei, the term multiply charged particle has been used throughout the preceding discussion because in a number of type I events (13 of them in fact) the track of the particle that triggered the chamber was conspicuously denser than that of an alpha particle fast enough to generate a trigger. Moreover, several of the background events show a very dense counter-age track that penetrates a number of the quarter-inch copper plates. In such cases the particle that made the track must have been a nucleus heavier than an alpha particle.

Figure 5 shows examples of very heavy tracks, tracks of alpha particles and tracks of fast singly charged particles. In order to express quantitatively the difference in density between tracks of those different types the photographs were measured with an integrating photometer constructed for that purpose.

The tracks were projected full size on a slit 2.5 mm wide (the width of alpha-particle tracks being about 1 mm) and as long as the separation between cloud chamber plates. The light that fell on the slit was focused on the cathode of a vacuum phototube. The phototube current was measured for each section of a track, corrected for local background in the photograph,

and averaged. Figure 4 (ordinate) shows results for each track denser than that of an alpha particle, the average for the alpha particles, and the average for a selection of penetrating-shower secondaries. (The $Z=1$ tracks were necessarily favorable, not representative, examples. The photometer could not distinguish the faintest of such tracks from the background.)

The phototube measurements reflect the fact that a cloud chamber "saturates" for heavily ionizing particles. Fast alpha-particle tracks are not opaque and show occasional gaps. However, even the lightest of the very dense tracks has an opaque core and no gaps. Apparently, as the ionization increases the diameter of the completely opaque core increases, but it does so slowly.

Delta rays were counted for all tracks of multiply charged particles. The delta-ray range requirement, which cannot be considered precise, was about 1.5 mm (measured perpendicular to the track in projection). For the alpha particles, the mean count was (0.038 ± 0.008)/cm; for mesons (photographed in the laboratory, but with no other difference in conditions) it was (0.012 ± 0.002)/cm. Results for each heavier nucleus are shown in Fig. 4, where the quantity $(N/0.0105)^{\frac{1}{2}}$ is plotted as abscissa (N being the number of delta rays per cm).

It will be shown that the pulse height requirement implies that nearly all the alpha particles traversed the chamber with ionization within 20 percent of their minimum (Fig. 6). The same is not true for the heavier nuclei; they could enter the chamber with ionization up to 1.5 times their minimum and could be slowed down very appreciably (or even stopped, for $Z>6$) by the plates. Hence the "apparent charge" (Fig. 4, abscissa) is an upper limit to the real charge. Assuming that the heavy nuclei were primary and taking into account their energy spectrum, one would expect about half of the heavy nuclei to have traversed the chamber at minimum ionization and the remainder to have ionized more heavily.

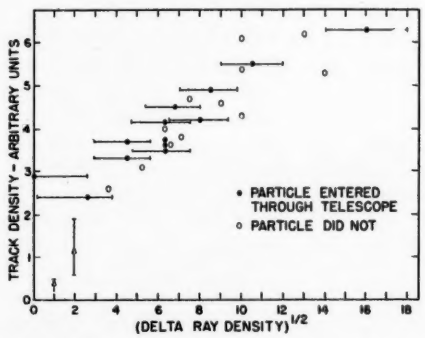

FIG. 4. Ionization measurements. Track densities were measured with a photometer. Delta-ray counts have been converted to a Z scale after being normalized to the mean density for alpha particles. Points represent individual tracks, and errors are statistical standard deviations, except for the triangles. The coordinates of the upper triangle are averages for alpha-particle tracks. The ordinate of the lower triangle is an average for selected tracks of singly charged particles. For those two cases limits of variation in density are shown.

TABLE II. Classification of all events that triggered the cloud chamber.

Description	Number
Type I. Chamber triggered by passage of an individual fast multiply charged particle through the telescope	
(A) Track density corresponds to $Z=2$	62
(B) Track density corresponds to $Z>2$	13
Type II. More than one fast particle contributed to triggering the chamber	
(A) Nature of multiplicative event is evident	
Hard shower above Čerenkov radiator	22
Hard shower in radiator	8
Hard shower below radiator	4
Soft shower	8
(B) Photographs show a single counter-age track, that of a particle at minimum ionization that traversed the telescope and penetrates or interacts	7
(C) The track of a penetrating particle with $Z=2$ (one instance) or $Z>2$ enters the chamber from above but does not project through both Geiger counter trays	11
(D) Photographs show little or nothing that would indicate what kind of event triggered the chamber	22
Total	157

Background

The many side-effects that commonly are lumped under the term "background" cause difficulty in most cosmic-ray experiments, but they depend to such an extent on details of method which may vary widely from one experiment to the next that an analysis of background in any particular case may have quite limited usefulness. Nevertheless in this instance there is perhaps more reason than usual for reporting what was learned about the unwanted events.

Only recently has the Čerenkov effect been put to use, and so far as the writer knows it was first deliberately employed to measure charge in this experiment. The reason for that step and for using a radiator many times thinner than has been used in a Čerenkov counter for cosmic-ray applications heretofore was to achieve the drastic reduction in background that it seemed might follow. Moreover, because a cloud chamber was used and because the photographs were of uniformly good quality it was possible to establish definitely the nature of a greater proportion of the unwanted events than in previous comparable experiments.

Contributions to the background would be expected from both of the mechanisms by which fast secondary charged particles can be generated, nuclear interaction and electromagnetic interaction. The latter could be either radiative (pair creation by a π^0 decay photon or by bremsstrahlung) or nonradiative (production of knock-on electrons). A phenomenological classification of the background events, which we will try to fit to the preceding framework, is given in Table II.

An event was called a hard shower if there were three or more counter-age tracks that extrapolate to a common point and there was evidence that some track was not that of an electron. If the event was clearly multiple but all the tracks seemed to be those of electrons it was called a soft shower. It must be substantially correct to equate "hard shower" to nuclear interaction and "soft shower" to radiative electromagnetic interaction.

The hard showers had definite origins whose location is interesting from an experimental design standpoint. The importance of reducing the radiator thickness and the amount of material above the radiator to the absolute minimum is evident. At the same time it is encouraging to learn that the counter was almost completely indifferent to interactions in matter beneath it. At most two of the multiple events that triggered the chamber occurred in the 6 kilograms of copper in the illuminated region of the cloud chamber (where they could be identified with nearly perfect efficiency) while at least 30 were contributed by the few hundred grams of material above or included in the radiator. Since the counter actually favored upward particles, that observation has to be explained by the counter's velocity bias and the tendency for the fast secondaries from nuclear interactions to preserve the primary direction.

Obviously any change in design that would reduce the hard shower background would do the same for soft showers.

It may be of interest that no event showed evidence of more than one charged particle incident from outside the gondola; that is, multiplication in the atmosphere had no effect, except of course to increase the total flux of background-producing particles.

The background events in group (II-B) show only one counter-age track, that of a fast singly charged particle which apparently went through both of the Geiger counter trays and the Čerenkov radiator before entering the chamber. Though the evidence is not conclusive we will assume that the mechanism was nonradiative electromagnetic interaction, that an unseen knock-on electron contributed enough additional Čerenkov light to satisfy the pulse height requirement.

The same mechanism, knock-on production, can operate in a different manner to cause background when the primary particle is multiply charged, for then the primary needs no help in satisfying the pulse-height requirement. The primary itself can miss either or both of the Geiger counter trays, so long as it goes through the radiator, and still satisfy the coincidence requirement by means of knock-on electrons. We use this model to account for the (II-C) events.

As for group (II-D), presumably the events were nuclear interactions whose secondaries all missed the illuminated region of the chamber or were similarly extreme manifestations of the other types of multiplicative interaction.

The number of events in each background group relative to the number of wanted events is of some interest, but the relative size of background pulses is probably more important from a design standpoint. Judging from the number of fast secondaries that seem to have passed through the Čerenkov radiator, the largest nuclear interaction might have produced as large a pulse as a fast boron nucleus, but it was exceptional. The next largest could have produced no larger a pulse than a beryllium nucleus, and most of the background pulses must have been much smaller than that.

However, one group is exceptional: the events in which a heavy nucleus went through the radiator, did not itself go through the telescope, but satisfied the trigger requirement with the aid of one or more long range delta rays. Background pulses produced in that way could be as large as any "legitimate" pulse. The numbers in Table II, which show that "background" heavies are practically as frequent as the legitimate events they compete with, are not surprising if one bears in mind that knock-on production increases as the square of the primary particle's charge. Figure 5 (D), which illustrates the abundant fast knock-on electrons associated with passage of a fast heavy nucleus through matter, may add emphasis to this discussion.

We think emphasis is justified, for those events point out potentially serious sources of uncertainty in measurements of the flux of heavy nuclei by means of counters alone. In the first place, one might rely solely on Geiger counters to define the trajectories of particles considered and thus underestimate the effective size of the telescope apertures. Or one might exclude events in which signals from guard counters resulted from knock-on electrons, mistaking the effect of the latter as indicating that the event in question was a nuclear interaction or an air shower rather than passage of a heavy nucleus. We will return to this matter again and suggest a method for solving the problem.

V. ENERGY THRESHOLDS

To meet the Čerenkov counter pulse-height requirement an individual particle not only had to be multiply charged but had to traverse the radiator with sufficient velocity. At the latitude of the experiment some multiply charged primaries would be too slow to meet that requirement; hence the measurements refer to primaries with energy above a threshold set by the counter and are to be compared with results obtained by conventional methods at certain latitudes lower than 55°.

Because the counter had limited resolution the effective threshold velocity for a given primary charge was a statistical average. We can assume as an approximation that the only significant fluctuation is in the number of photoelectrons that reach the first multiplier dynode. (Pulse heights will be expressed in units of the pulse from a single such electron.) Events for which the mean number of photoelectrons is $\bar{n}$ will give a normalized pulse height distribution $P(\bar{n},n)=\bar{n}^n$

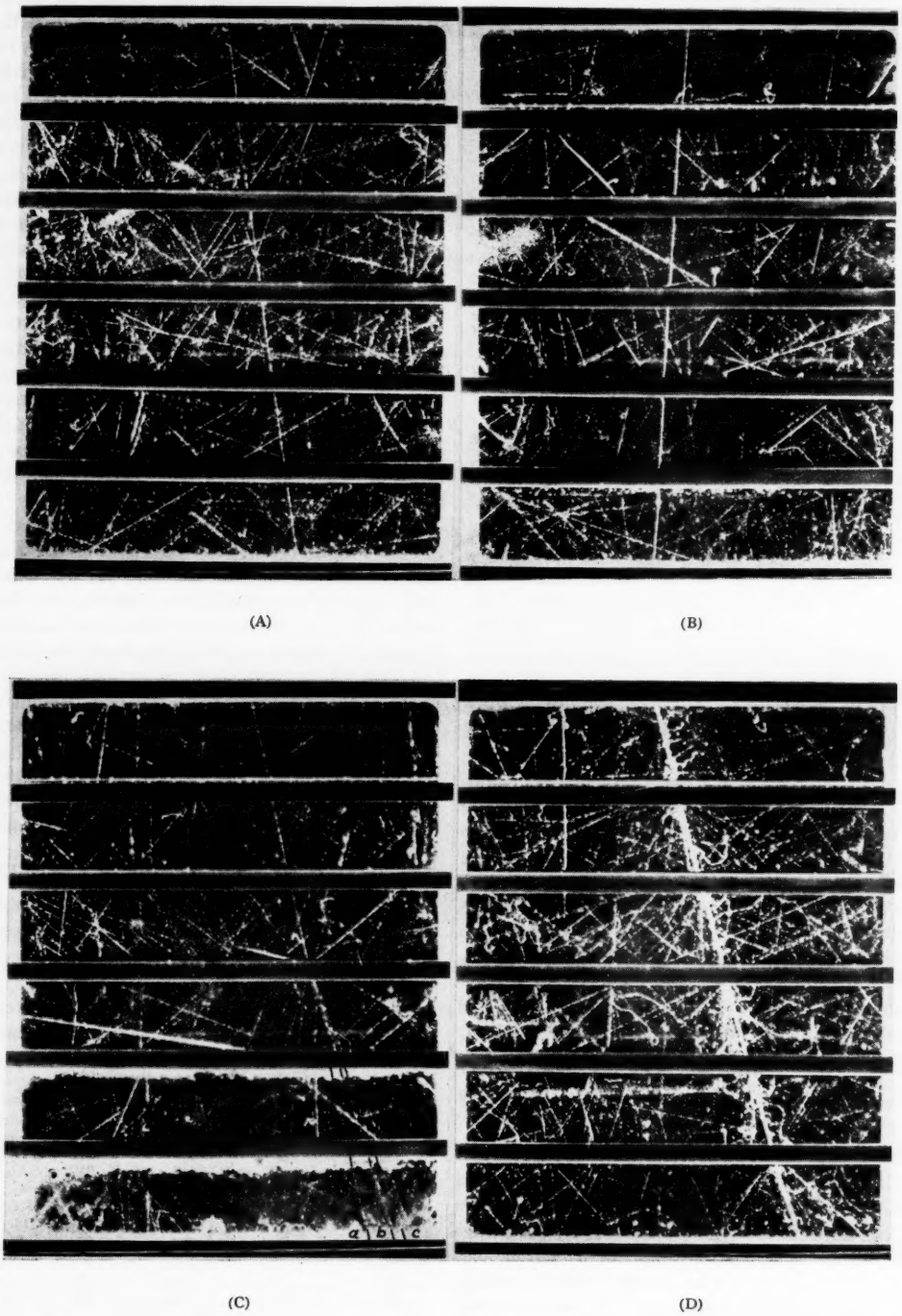

FIG. 5. Cloud chamber photographs. (A) An alpha-particle track of average density. (B) The least dense track classified $Z>2$ (probably that of a fast Li nucleus). (C) An alpha particle which interacted in the central plate. Tracks *a*, *b*, *c* of penetrating secondaries show clearly in the original although it is plain that they are much less dense than that of the primary. Condensation on the chamber front is illustrated. (D) The track of a nucleus with $Z\sim10$.

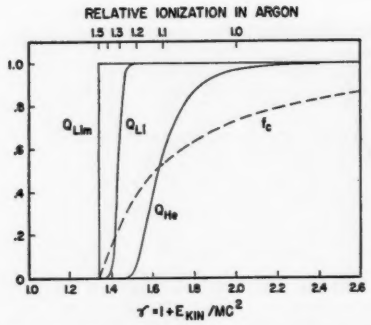

FIG. 6. Čerenkov radiation and detection characteristics. The solid curves give the probability of detection as a function of energy for helium and lithium, and the limiting curve for $Z\to\infty$. The dashed curve shows the energy dependence of Čerenkov radiation.

$\times\exp(-\bar{n})/n!$ (Poisson). If the pulses feed an edge discriminator set at n_1, the probability that such an event will trigger it is

$$R_{n_1}(\bar{n})=\sum_{n=n_1}^{\infty} P(\bar{n},n), \tag{2}$$

which is zero for $\bar{n}\ll n_1$, unity for $\bar{n}\gg n_1$, and assumes the value $\frac{1}{2}$ for $\bar{n}\sim n_1$. If the event is passage of a particle with charge Z and velocity parameter $\gamma=(1-v^2/c^2)^{-\frac{1}{2}}$ through a Čerenkov counter, $\bar{n}=Z^2\bar{n}_0 f_c(\gamma)$ where $\bar{n}_0$ is the mean pulse height for $Z=1$, $\gamma\to\infty$ (fast mu mesons) and $f_c(\gamma)$ expresses the velocity dependence of Čerenkov radiation [Eq. (1)]. Finally,

$$Q_{n_1}(Z,\gamma)=R_{n_1}[Z^2\bar{n}_0 f_c(\gamma)] \tag{3}$$

is the probability of detection (detection characteristic) for Z, γ (Fig. 6).

The differential energy spectrum of detected particles is the product of the detection characteristic and the energy spectrum of the incident particles, $D(E)dE$. The effective threshold energy E_b is defined so that the integral of the incident particles above that energy equals the integral of the detected particles over all energies. Since the detection characteristic is practically constant and equal to 1 for high energies ($>E_1$), the equation that defines E_b can be written

$$\int_0^{E_1} Q(E)D(E)dE=\int_{E_b}^{E_1} D(E)dE, \tag{4}$$

which shows that the form of the incident spectrum for $E>E_1$ does not influence the calculation. By assuming a reasonable analytical expression for $D(E)$ in the interval for which $Q(2,\gamma)$ is appreciably different from 0 or 1 and integrating (5) numerically the mean threshold γ for alpha particles was found to be $1.65_{-0.05}^{+0.07}$. Since not much of the total flux belongs to that energy interval, the result is relatively insensitive to what was assumed about the spectrum.

The quoted error arises instead from uncertainty in the measured parameters that determine $Q(2,\gamma)$. By substituting $\bar{n}_0 k$ for n_1 in (4) it can be seen that the mean threshold γ depends for its accuracy on the measurement of k. The threshold γ is essentially that for which the detection probability is $\frac{1}{2}$, and it has been pointed out that the detection probability attains that value when n_1 equals the argument of the function R, approximately; that is, when $f_c(\gamma)=k/Z^2$. $\bar{n}_0$ itself, which was obtained by fitting a Poisson distribution to the observed pulse-height distribution, plays a less important role in determining the energy threshold.

The value of k for the flight, 2.1 ± 0.2, was set by the ratio of over-all gain used for the flight to that needed in order to obtain the trigger rate from sea level cosmic rays that would correspond to $k=1$ according to the absolute pulse height distribution of Fig. 1. A calibrated linear attenuator was used to change the gain, and the value of k was found to be unchanged when checked after the flight. Detection characteristics for $k=2.1$ and $Z=2$, 3, ∞ are shown in Fig. 6, together with the function $f_c(\gamma)$.

For heavy enough nuclei the measured parameters k, $\bar{n}_0$ are unimportant; the threshold is determined by the critical velocity in Lucite. In this experiment $Q(Z,\gamma)$ could be considered a step function for $Z>2$, and error in the threshold is negligible for such nuclei. Results are shown in Table III, both for particles at the depth of the counter and primaries above the atmosphere. Taking into account the last column of that table, the fact that all of the 13 heavy nuclei that entered through the telescope penetrated all plates of the chamber (or else were seen to interact) confirms the ability of the Čerenkov counter to reject particles with less than critical velocity, regardless of their ionization.

VI. FLUX OF PRIMARY ALPHA PARTICLES

The flux of alpha particles that entered the cloud chamber was $(79\pm11)/\text{m}^2$ sec steradian. Both statistical and instrumental sources were taken into account in estimating the error.

The relation between the flux that entered the chamber and the cosmic radiation above the atmosphere

TABLE III. Energy thresholds.[a]

Nucleus	Z	E_b	E_a	E_a'
He	2	606	668	300
Li	3	442	519	370
Be	4	362	502	440
B	5	347	519	500
C	6	338	545	570
N	7	334	574	630
O	8	330	605	700
F	9	328	634	750
Ne	10	326	682	810

[a] E_b is the kinetic energy per nucleon in Mev corresponding to $2.1\bar{n}_0$ units of Čerenkov radiation in Lucite. E_a is the corresponding energy at entrance to the atmosphere. The depth of the center of the radiator was 26 g/cm² (16.9 g/cm² air, remainder telescope). E_a' is the kinetic energy per nucleon in Mev corresponding to range 60 g/cm². That figure is the thickness of material between the top of the atmosphere and the lowest space in the chamber.

depends on the effect of nuclear collisions, both in local matter and in the overlying atmosphere. Results published to date[14,15] agree with the following formula for collision cross sections:

$$\sigma=\pi R^2,$$
$$R=[1.45(A_1^{\frac{1}{3}}+A_2^{\frac{1}{3}})-2.0]\times 10^{-13}\text{ cm}. \quad (5)$$

(A_1, A_2 are mass numbers of incident and target nuclei, respectively), at least for incident nuclei with energy above 1 Bev/nucleon. There is evidence[14] that the cross section decreases somewhat for lower energies.

The experimental evidence is especially scanty for alpha particles. In the experiment we describe, traversal of 1.62×10^4 g/cm² of copper in the cloud chamber resulted in 16 interactions. The corresponding mean free path and the results of other investigators are shown in Table IV together with values given by Eq. (5).

From observing seven interactions of heavier nuclei in traversal of 560 g/cm² we obtain the mean free path (80 ± 30) g/cm², which agrees within its considerable statistical error with the prediction 65 g/cm² of Eq. (5).

Attenuation in local matter was taken into account using calculated collision cross sections. According to Eq. (6) the collision mean free path for alpha particles in air is about 50 g/cm². That value was reported by Davis *et al.*[16] for the absorption mean free path. Using it to take into account attenuation in the atmosphere, we find the value (135 ± 20)/m² sec steradian for the flux of primary alpha particles with energy above (670 ± 100) Mev/nucleon.[17]

For comparison with that result we have collected and show in Fig. 7 values of the primary alpha-particle flux obtained elsewhere by methods that discriminate strongly against at least one of the two types of background event discussed in the introduction, local multiplicative interactions and slow singly charged particles. Perlow *et al.*[18] and Davis *et al.*[19] measured ionization

TABLE IV. Alpha-particle collision mean free paths.

Material	Collision mean free path (g/cm²) Observed	Calculated [Eq. (6)]
Copper	100 ± 25	91
Brass	84 ± 17[a]	91
Glass	50 ± 11[a]	60

[a] See reference 15.

[14] Freier, Anderson, Naugle, and Ney, Phys. Rev. **84**, 322 (1951).
[15] Kaplon, Peters, Reynolds, and Ritson, Phys. Rev. **85**, 295 (1952).
[16] Davis, Caulk, and Johnson, Phys. Rev. **91**, 431 (1953).
[17] The difference between this result and that we reported earlier, Phys. Rev. **93**, 899 (1954), comes partly from adopting a greater value for the absorption mean free path in the present case and partly from correcting errors in values given in that letter for the geometry factor and the energy that corresponds to γ_0 in Lucite.
[18] Perlow, Davis, Kissinger, and Shipman, Phys. Rev. **88**, 321 (1952).
[19] Davis, Caulk, and Johnson, Phys. Rev. **91**, 431 (1953). Flux value corrected in communication to E. P. Ney.

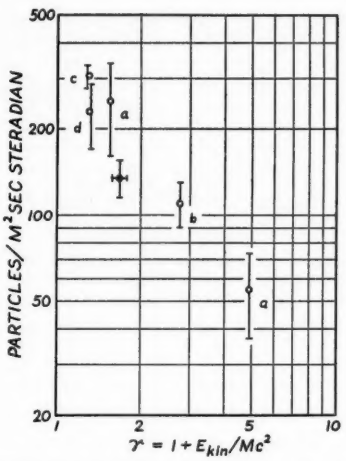

FIG. 7. Comparison of results. Filled circle is the result of this experiment. Open circles are previous measurements of the alpha-particle flux. Code: (a) Bradt and Peters (see reference 20), (b) Perlow *et al.* (see reference 18), (c) Davis *et al.* (see reference 19), (d) McDonald (see reference 22).

with proportional counters (2 and 3 of them, respectively) and eliminated individual slow particles by requiring penetration. Bradt and Peters[20] used photographic emulsions, so multiplicative events could not compete, and measured ionization of long tracks. The results we quote are a revision of those they reported originally,[21] and for the purpose of comparison we have adjusted them slightly to correspond to the absorption mean free path used in extrapolating other results shown. McDonald[22] used a scintillation counter to set upper and lower limits on ionization and a cloud chamber with absorber to eliminate both slow protons and interactions.

For protons our 670-Mev energy threshold would correspond to geomagnetic latitude 57°. Winckler and co-workers[23] found the value (0.23 ± 0.01)/cm² sec sterad for the total vertical flux under 1.9 cm Pb at 56°. Van Allen and Singer[24] found the value 0.29 ± 0.03 above the atmosphere at 58°. The relation between those measurements and the primary proton flux is still somewhat uncertain, however.

VII. PROBLEM OF FLUX MEASUREMENT BY MEANS OF COUNTERS IN THE REGION $Z>2$

The 13 heavy nuclei with allowed tracks observed in this experiment lead to the value (38 ± 12)/m² sec sterad for the extrapolated flux of nuclei with $Z>2$ and energy above 500 Mev/nucleon. That may be compared to the result 18.6 ± 2.0 reported by Kaplon *et al.*[15] for an insignificantly lower mean threshold, and the result 31 ± 3 reported by Dainton *et al.*[25] for a threshold 330

[20] H. L. Bradt and B. Peters, Phys. Rev. **77**, 54 (1950).
[21] G. Segrè, Nuovo cimento **9**, 116 (1952).
[22] F. B. McDonald (private communication to E. P. Ney).
[23] Winckler, Stroud, and Shanley, Phys. Rev. **76**, 1012 (1949).
[24] J. A. Van Allen and S. F. Singer, Phys. Rev. **78**, 819 (1950).
[25] Dainton, Fowler, and Kent, Phil. Mag. **43**, 729 (1952).

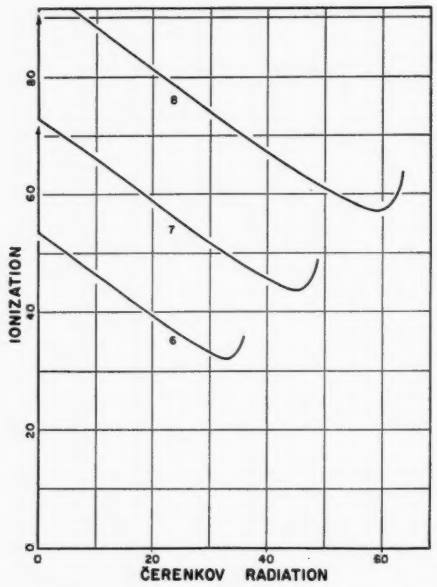

FIG. 8. Ionization *vs* Čerenkov radiation. Corresponding values of Čerenkov radiation and ionization for three values of charge: $Z=6$, 7, 8. Velocity is parameter for the curves. Scales have been normalized so that ionization plateau = Čerenkov plateau = 1 for $Z=1$.

Mev/nucleon. (For the purpose of comparison essentially the same value, 30 g/cm², was used for the air absorption mean free path in the present case as in the others.)

"Allowed" heavies and definite "background" heavies were observed in about equal numbers in this experiment. We believe that the measurements used in separating them were not capable of enough precision to avoid considerable uncertainty in the outcome. It is quite possible that in reality a third or even half of the allowed heavies narrowly missed one of the Geiger counter trays and triggered it by means of a knock-on electron. Consequently, the value 38 ± 12 we report above should not be considered a flux measurement but may be regarded as a measure of how far we have progressed toward solving the problem under discussion.

In a recent high-altitude experiment by Stix[26] a cloud chamber was triggered by sufficiently large pulses from each of three proportional counters in coincidence. He required that the cloud chamber show a single heavy track and that each of the pulses, which were recorded, be consistent with the density of the track. His result for the flux of heavy nuclei is in agreement with those obtained by use of emulsions. In the light of our observations, the fact that his geometry was defined entirely by proportional devices was important to that success. On the other hand the discrimination against background of the three proportional counters seems to have been poorer by orders of magnitude than might have been obtained using a single Čerenkov counter.

During the preparation of this report thin Čerenkov counters have been developed at this laboratory which have much better resolution and far greater useful area than the one we have described.[27] We suggest for consideration by others who are interested in this field that a Čerenkov counter might be combined with an ionization counter to great advantage, the geometry being defined by the two counter areas. There would be no knock-on electron problem as in the present experiment, and the Čerenkov counter would contribute its excellent discrimination against background. Furthermore, Fig. 8 shows that simultaneous measurements of Čerenkov radiation and ionization would serve to identify all primary nuclei as to charge up to the latitude at which the energy threshold determined by geomagnetic effects corresponds to the critical velocity in the material chosen for Čerenkov radiator.

VIII. ACKNOWLEDGMENTS

The writer wishes to express sincere gratitude to Prof. E. P. Ney, who not only provided him the opportunity to conduct this research, but played a prominent part in creating the technical background that was essential to its success. The active cooperation of R. Thorness, H. Carlson, and M. Weisman was invaluable during construction of the equipment. Special thanks are due Sam Brinda and Nahmin Horwitz for their generous and capable assistance during final preparation for the flight.

[26] T. H. Stix, Phys. Rev. **91**, 431 (1953); Phys. Rev. **95**, 782 (1954).

[27] J. Linsley and N. Horwitz, Rev. Sci. Instr. (to be published).

Tritium Production by 2.2-Bev Protons on Iron and Its Relation to Cosmic Radiation*

E. L. FIREMAN
Brookhaven National Laboratory, Upton, New York
(Received November 19, 1954)

The cross section for tritium production by 2.2-Bev protons on iron is measured to be 62±7 mb. This tritium cross section indicates that (1.4±0.4)×10⁻³ tritons/g sec would be produced in small iron meteorites (a few inches in radius) in space by cosmic rays of the intensity of those striking the earth's polar regions. In 4×10⁹ years, (6±2)×10⁻⁶ cc of He³ per gram of iron results from this cosmic-ray tritium. Mount Ayliff meteorite contains 11.5×10⁻⁶ cc of He³ per gram, indicating its bombardment by a cosmic-ray flux at least as intense as is presently striking the earth. The variation of tritium with target depth is also measured and indicates a decrease less rapid than an attenuation due to geometric cross section.

INTRODUCTION AND SUMMARY

THE proposal[1] that cosmic rays produce appreciable helium in meteorites has led to the discovery[2] of meteoritic He³ and the investigation of the variation of this helium with depth.[3]

The measurement of the tritium production by high-energy protons in meteoritic materials is a related problem.[4] The tritium cross section for 2.2-Bev protons on iron is measured to be 62±7 mb; the corresponding cross sections for oxygen and nitrogen[5] are 33±4 mb and 28±4 mb. For these three elements the tritium production cross sections are approximately 10 percent of the geometric cross sections. If meteorites in space are bombarded by an omnidirectional cosmic-ray flux of the character of the cosmic-ray primaries striking the earth above 55°N latitude[6] and if the tritium production cross section is the same for each bombarding nucleon, then (1.4±0.4)×10⁻³ tritons/g sec are produced in small iron meteorites. During the course of time, which is taken as 4×10⁹ years, (6±2)×10⁻⁶ cc of He³ per g iron would result. A smaller quantity[7] of additional He³ is produced directly.

The measurement[2] of He³ in iron meteorites gives 11.5×10⁻⁶ cc/g for the Mount Ayliff meteorite and lower values for four other iron meteorites. The Mount Ayliff He³ is just consistent with its bombardment for 4×10⁹ years by cosmic rays equivalent to those presently striking the earth's polar regions. Any loss of He³ from the meteorite or shielding by ablated material would require a more intense bombardment of this meteorite in the course of its travels. The smaller He³ content[2] in the four other meteorites can be explained in terms of either the shielding by ablated material, the loss of He³, a younger age, or their bombardment by less intense cosmic rays.

The stony meteorites[8] (chondrites) are composed primarily of oxygen (35 percent), iron (25 percent), silicon (18 percent), and magnesium (14.5 percent). If the measured tritium cross sections are used for oxygen and iron and tritium cross sections 10 percent of geometric are used for other elements, then the cosmic-ray tritium production in a gram of chondrite is 30 percent greater than in a gram of iron.

The variation of tritium yield with target depth in iron is given in Fig. 1. This yield appears to decrease less rapidly than an attenuation of the proton beam due to an interaction of geometric cross section. Since the total thickness of the target used is only 1.80 in., an extrapolation is necessary for the estimation of the shielding by larger thicknesses of iron. The measurement[3] of the variation of helium content with meteoritic depth has been done for several meteorites. It is difficult to say whether the results are in agreement because the reported measurements[3] are on the total helium content and because of our target size. A comparison of the variation with depth in iron with that in oxygen[5] indicates that the tritium yield decreases less rapidly with depth in iron than in oxygen.

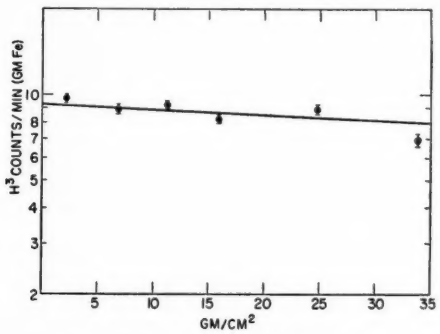

FIG. 1. Variation of tritium with target depth. The errors shown are standard deviations in the counting.

* Work performed under the auspices of the U. S. Atomic Energy Commission.

[1] C. A. Bauer, Phys. Rev. **72**, 354 (1947); **74**, 225 and 501 (1948); H. E. Huntley, Nature **161**, 356 (1948).

[2] Mayne, Reasbeck, and Paneth, Geochim. et Cosmochim. Acta **2**, 300 (1952).

[3] Chacketts, Reasbeck, and Wilson, Geochim. et Cosmochim. Acta **3**, 261 (1953).

[4] S. F. Singer, Nature **170**, 728 (1952); Phys. Rev. **90**, 168 (1953).

[5] E. L. Fireman and F. S. Rowland, Phys. Rev. **97**, 780 (1955).

[6] Data taken from Table II of Winkler, Stix, Dwight, and Salwin, Phys. Rev. **79**, 656 (1950).

[7] Martin, Thomson, and Wardle, Phil. Mag. **452**, 410 (1954).

[8] H. C. Urey and H. Craig, Geochim. et Cosmochim. Acta **2**, 36 (1953).

TABLE I. Summary of experimental data. The errors given are standard deviations in the counting.

Position No.	Average sample depth g/cm²	Sample[a] weight g	H^3 counts/min	No. Tritons $\times 10^{-8}$	(No. H^3/No. Fe) $\times 10^{15}$	σ(mb)[b]
1	2.24	4.38	42.4±1.2	5.2±0.5	11.0±1.1	69±7
2	6.72	8.09	71.7±1.5	8.7±0.8	10.1±0.9	64±6
3	11.20	8.09	74.6±1.5	9.1±0.8	10.5±0.9	66±6
4	15.68	8.00	65.5±1.5	8.0±0.8	9.3±0.9	59±6
6	24.64	7.91	70.5±1.5	8.6±0.8	10.1±0.9	64±6
8	33.60	7.99	56.0±1.5	6.9±0.7	8.0±0.9	50±5
Calibration		···	36.2±1.0	4.4±0.3		

[a] All samples 4.48 g/cm² thick.
[b] No. protons/cm² = 1.6×10^{11}.

Theoretical calculations[1,4,9] of a depth effect have been attempted; the most quantitative of these[9] does not appear to be in good agreement with our measurements.

EXPERIMENTAL DISCUSSION AND RESULTS

A. Target.—The target consists of a stack of 8 sheets of hot-rolled steel, 0.225 in. thick with 1 in.×4 in. faces, which are irradiated for 20 minutes in the internal beam of the Brookhaven Cosmotron. The beam strikes the 1 in.×4 in. face and passes through the 8 sheets of steel. A $\frac{1}{8}$ in. lip of Lucite projects $\frac{1}{4}$ in. from the target; this lip intercepts the beam and scatters it more uniformly over the face of the target on the next traversal.

B. Tritium Assay.—Samples of about 8 g are cut from the center of each steel sheet of target. Care is taken to prevent heating of the steel in cutting. The samples are heated to about 1800°C by an induction heater in an atmosphere (1.0-cm Hg pressure) of carrier hydrogen. In the first minutes of heating CO, N_2, and H_2 are released from the iron, raising the pressure in the furnace to about 15 cm Hg. During the next hour, the CO reacts with the molten iron and the pressure falls to 3 cm Hg. With the sample at 1800°C, the gas is pumped from the furnace. By three hours of pumping all the gas is extracted from the furnace; during the pumping about $\frac{1}{4}$ g of iron evaporates to the furnace walls. To test the completeness of the tritium extraction, several samples were subjected a second time to this procedure with negative results.

The hydrogen is removed from this gas by its passage through palladium. A 16-cc Geiger counter is filled to 10–18 cm pressure with this hydrogen; 2.5 cm of ethyl acetate is added to the counter for quenching. The counting is done in a low-level counting facility[10] which reduces the background of this counter to 1.20±0.10 counts/min. The data are given in Table I. The tritium yield is about 1.0×10^8 tritons/gram of iron with the front sample giving a somewhat higher yield and the rear sample a somewhat lower yield. Figure 1 shows the variation of tritium activity with target depth. The decrease appears to be somewhat less than would be given by an attenuation of the incident beam by an interaction of geometric cross section. The average value of the tritium production cross section in our target is 62±7 mb.

C. Proton Monitor.—The proton flux is measured by the Na^{24} production in 0.003-in. aluminum monitor foils on the front and back of the target. The cross section for this reaction[11] is 9.0 mb for 2.2-Bev protons. The errors given do not include any errors in this measurement, but represent errors relative to this cross section. A 20 percent correction to the front foil and 50 percent to the rear foil is necessary because of the Na^{24} produced by secondary neutrons from the target by the (n,α) reaction on aluminum. This monitor indicates that 1.6×10^{11} protons/cm² strike the center of the target during the 20-minute irradiation. The total number of protons striking the target is 1.5×10^{12}.

The author is indebted to Mr. Donald Schwarzer who assisted in all phases of the experiment and to the Cosmotron staff for the irradiation.

[9] G. R. Martin, Geochim. et Cosmochim. Acta 3, 288 (1953).

[10] The author wishes to thank Dr. R. Davis for the use of this facility.

[11] A. Turkevich, Phys. Rev. 94, 775 (1954).

Reaction $p+p\rightarrow\pi^{+}+d$*

FRANK S. CRAWFORD, JR. AND M. LYNN STEVENSON
Radiation Laboratory, Department of Physics, University of California, Berkeley, California
(Received November 1, 1954)

Absolute differential cross sections for the reaction $p+p\rightarrow\pi^{+}+d$ have been measured at incident proton energies (lab system) from 310 to 338 Mev and at meson angles (c.m.) from 30° to 90°. The two final particles were counted in coincidence. The data are well fitted by the phenomenological theoretical expression

$$4\pi\frac{d\sigma}{d\Omega}(\text{c.m.})=\alpha_{10}\eta+\beta_{10}\eta^{3}\frac{(x+\cos^{2}\theta)}{x+\frac{1}{3}},$$

with $x=0.082\pm0.034$, $\alpha_{10}=(0.138\pm0.015)\times10^{-27}$ cm², and $\beta_{10}=(1.01\pm0.08)\times10^{-27}$ cm²; θ=meson c.m. angle and $\eta=p_{\pi}$ (c.m.)$/m_{\pi}c$. By measuring α_{10} we have determined directly the amount of S-wave in this reaction.

Further measurements with polarized protons of ~315 Mev are presented. These confirm directly the presence of interfering S- and P-waves and give a result $|Q|=0.39\pm0.05$ for the asymmetry $(R-L)/(R+L)$ which would be obtained at 90° c.m. with 100 percent polarized protons. The polarized and unpolarized results are used together to determine the relative phases of the S- and P-wave mesons.

Using the recent Chicago measurement of the sign of the proton polarization, the sign we observe for meson production asymmetry shows that spin up protons produce more mesons to the right than to the left. The sign of this result, according to a theoretical prediction of B. T. Feld, provides strong evidence in favor of the Fermi type meson-nucleon interaction, and against the Yang type interaction.

I. INTRODUCTION

CARTWRIGHT *et al.*[1] were the first to observe positive mesons produced in proton-proton collisions. They used nuclear emulsions to detect the mesons. The presence of a pronounced peak at the high-energy end of the meson spectrum suggested that a large fraction of the production could be attributed to the reaction $p+p\rightarrow\pi^{+}+d$. That this was indeed the case was confirmed[2] by the detection of π-d coincidences in the early stages of the experiment here reported. We did not measure absolute cross sections at that time.

Since then we have reported[3–5] absolute differential cross sections at various angles and at proton energies from 324 to 338 Mev. The summary presented here includes new data extending to 310 Mev [(T_{π}) c.m. = 9.5 Mev]. These data show for the first time, through the excitation function and angular distribution, the presence of S-wave mesons in the above reaction. Using the same techniques, we have made further measurements[6] with a polarized proton beam of ~315 Mev. These measurements establish directly the simultaneous presence of S- and P-wave mesons and give additional information on their relative phases. This information can be used to set conditions on the p-p scattering phase shifts at these energies, for the states involved.

We have fitted all the data by the method of least squares to the phenomenological theory of Watson and Brueckner[7] as presented in the notation of Rosenfeld.[8]

II. EXPERIMENTAL TECHNIQUE

A. Unpolarized Protons

Figure 1 shows a nonrelativistic velocity vector diagram of $p+p\rightarrow\pi^{+}+d$ and displays the essential features of the particle dynamics for 342-Mev incident protons. The maximum angle that the deuterons can make with respect to the incident protons is ~6° and corresponds

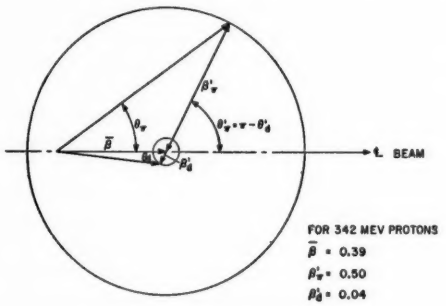
BEAM
FOR 342 MEV PROTONS
$\bar{\beta}$ = 0.39
β'_{π} = 0.50
β'_{d} = 0.04
$\bar{\beta}$ = VELOCITY OF THE C.M. SYSTEM
β'_{π} = VELOCITY OF THE MESON IN THE C.M. SYSTEM
β'_{d} = VELOCITY OF THE DEUTERON IN THE C.M. SYSTEM
θ'_{π} = ANGLE OF THE MESON IN THE C.M. SYSTEM
θ_{π} = ANGLE OF THE MESON IN THE LABORATORY SYSTEM
θ_{d} = ANGLE OF THE DEUTERON IN THE LABORATORY SYSTEM

FIG. 1. Velocity vector diagram for $p+p\rightarrow\pi^{+}+d$.

* This work was done under the auspices of the U. S. Atomic Energy Commission.

[1] Cartwright, Richman, Whitehead and Wilcox, Phys. Rev. **78**, 823 (1950).

[2] Crawford, Crowe, and Stevenson, Phys. Rev. **82**, 97 (1951).

[3] F. S. Crawford, Jr. and M. L. Stevenson, Phys. Rev. **91**, 468 (1953).

[4] Frank S. Crawford, Jr., University of California Radiation Laboratory Report UCRL-2187, April, 1953 (unpublished).

[5] M. Lynn Stevenson, University of California Radiation Laboratory Report UCRL-2188, April, 1953 (unpublished).

[6] F. S. Crawford, Jr. and M. L. Stevenson, Phys. Rev. **95**, 1112 (1954).

[7] K. M. Watson and K. A. Brueckner, Phys. Rev. **83**, 1 (1951).

[8] A. H. Rosenfeld, Phys. Rev. **96**, 139 (1954).

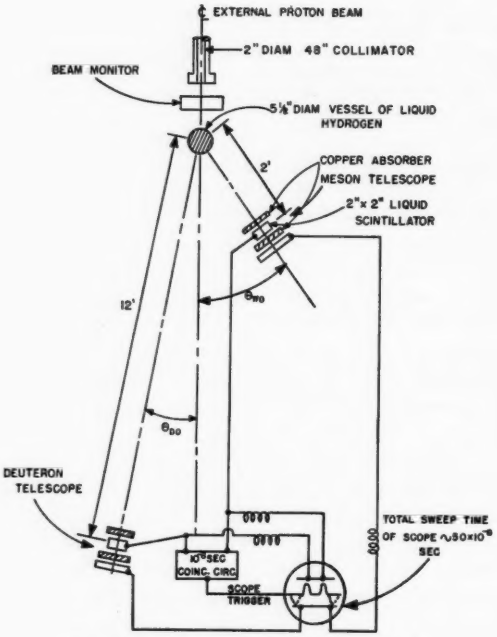

FIG. 2. Schematic diagram of $p+p\rightarrow\pi^{+}+d$ geometry and electronics.

to a c.m. angle of ~90°. The meson lab angle is always equal to about one-half of the c.m. angle. These over-all features of the particle dynamics persist in general, over the entire range of proton energies investigated.

Coincidence detection of the meson and deuteron was the most important feature of the experimental technique. For this purpose two scintillation counter telescopes were used, each of which consisted of two counters. (See Fig. 2.) Appropriate copper absorbers were placed between the two counters of each telescope so that the meson and deuteron could not enter the rear counters of their respective telescopes. The rear counters were used in anticoincidence to subtract penetrating background.

The sizes and positions of the counters varied from run to run. The most frequently used front meson counter was a liquid scintillator 2 by 2 by 1.5 inches, placed 24 inches from the target. This counter defined the solid angle. The deuteron counter was usually a liquid scintillator 3 by 3 by 0.5 inches, located ~140 inches from the target. The deuteron telescope was moved horizontally and vertically in increments of one counter width until almost all the deuterons were detected. It was impractical to count all the deuterons within the distribution; therefore, in practice, deuterons were usually detected only at the positions shown in Fig. 3. The number not counted in the "corners" of the distribution usually represented a correction of ~20 percent.

The fact that the deuteron counter was always at an angle less than ~6° made necessary the use of a liquid-hydrogen target. A CH_2 target would have caused too many diffraction-scattered protons from the carbon to enter the deuteron telescope. Most of the data were obtained with a 1.00-g cm^{-2} cylindrical liquid-hydrogen target.

A time-of-flight technique was used to eliminate most of the background from the deuteron counter by preventing high-energy protons from giving accidental coincidences. The rf fine structure of the proton beam made this technique possible. The duration of the external scattered beam produced in one frequency modulation cycle is $\sim 20\times10^{-6}$ sec. Within this time there are about 300 equally spaced bursts of protons, separated by the cyclotron rf period of 6.0×10^{-8} sec. Each burst lasts $\sim 5\times10^{-9}$ sec. At the deuteron telescope position, there was a time-of-flight separation of $\sim 2\times10^{-8}$ sec between the deuterons of ~120 Mev and full-energy protons scattered at small angles into the deuteron telescope. The 10^{-8}-sec coincidence circuit adequately resolved this time separation.

Figure 2 shows schematically the procedure by which the $p+p\rightarrow\pi^{+}+d$ event was identified. A coincidence between a pulse in the front meson counter and one in the front deuteron counter triggered a fast oscilloscope. The pulses from all four counters were displayed on the scope by means of appropriate delays in the counter cables, and were photographed on a continuously moving film. The presence of a pulse in the rear counter of either the meson or the deuteron telescope classified an event as "hard" and prevented it from being classi-

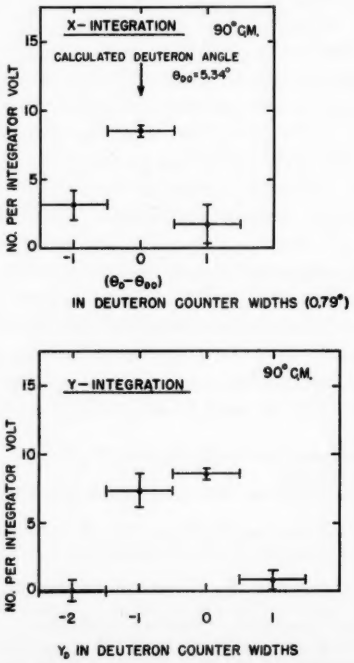

FIG. 3. Typical deuteron integration curves.

fied as a possible $p+p\rightarrow\pi^{+}+d$ event. In order to determine the fraction of accidental coincidences among the "soft" events, in a given run, we inserted into the meson telescope an amount of cable delay equal to the time separation of 6.0×10^{-8} sec between rf pulses, and repeated the run. The number of resulting "soft accidental" traces was then subtracted from the total number of soft events to obtain the number of real meson-deuteron coincidences. The soft accidentals were usually ~10 to 20 percent of the soft reals.

Not shown in Fig. 2 are the auxiliary electronics, which provided us with data during the run, corresponding to the information that was recorded on the film.

We identified the process as $p+p\rightarrow\pi^{+}+d$ essentially by determining the masses of the final products, after first showing, through the angular correlation, that a two-body process was involved. Identification was made by measuring the momenta and ranges of the final products. If the momentum of the incident proton is known, then a measurement of the angles of the final products determines their momenta uniquely. We determined the energy of the incident protons by measuring a Bragg curve, using the technique of Mather and Segrè.[9]

The experiment was performed at various beam energies from 310 to 340 Mev. To obtain a given energy the 340-Mev beam was degraded with appropriate beryllium absorbers. These were placed at Position *A* in Fig. 7 during the earlier runs and at Position *B* during the later runs.

Measurement of the meson and deuteron angles was accomplished by setting the meson telescope at the desired angle and then measuring the coincidence counting rate *vs* the deuteron telescope position, as is shown in Fig. 3. The width of the observed patterns agrees with that calculated from the finite meson counter width and the multiple Coulomb scattering of the meson and deuteron.

Typical range measurements of the particles in coincidence are shown in Fig. 4. Together with the angular correlation, the ranges determine the particle masses to be those of a meson and a deuteron. The absence of a step on the deuteron range curve shows that, within the errors, a single monoenergetic particle was detected. That is, the source of coincidences was the reaction $p+p\rightarrow\pi^{+}+d$, with no detectable contribution from $p+p\rightarrow\pi^{+}+n+p$. The shape of the deuteron range curve agrees with that calculated from the energy spread of the deuterons caused by the finite size of the target and the finite angular width of the defining meson counter. The arrows shown in Fig. 4 indicate the expected ranges of mesons and deuterons.

Further evidence that π mesons were detected came from the scope photographs taken during the running of meson range curves. When mesons were stopped in

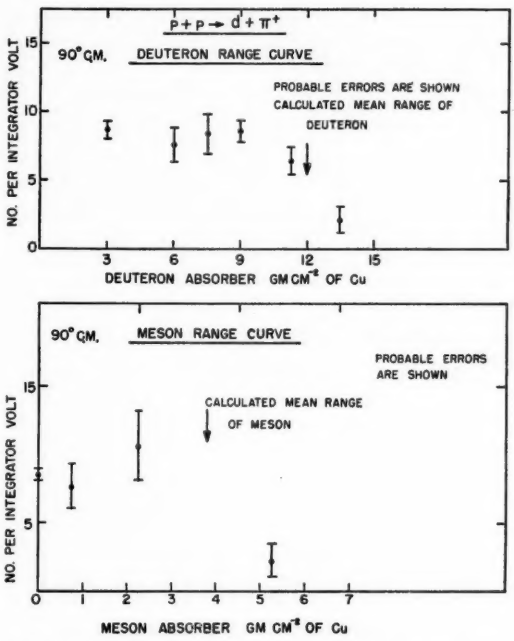

FIG. 4. Typical meson and deuteron range curves at 332 Mev.

the front counter, the expected number of $\pi-\mu$ decays was observed. A pulse from the recoiling muon was observed on the trailing edge of the pulse from the stopped pion.

At each angle, an absolute cross section was determined. Therefore, measurements were performed to insure that the reaction was detected with full efficiency. Pulse-height distributions for the meson and deuteron were obtained from the film data. A typical example is shown in Fig. 5. Only pulses larger than the "cutoff" value were accepted by the coincidence circuit. We estimate that less than 2 percent of the $\pi-d$ events were lost because of insufficient pulse height.

Time-delay measurements were made to insure that no events were lost because of misaligned cable delays. Figure 6 shows a typical time-of-flight plateau.

Apart from the deuteron integration correction, the $\pi-\mu$ decay in flight generally represented the largest correction made to the unpolarized beam data. This correction was usually approximately five percent. In Table I, the measurements at 312 and 325 Mev, which show relatively large correction factors, were made with a clearing magnetic field to eliminate background in part of a three-counter meson telescope. Because the path length of the mesons was longer than usual, a relatively large correction for $\pi-\mu$ decay in flight was necessary. These two are the only measurements in which a magnet was used, and which therefore differ from the general description given above.

Other small corrections made to the data include nuclear attenuation, Coulomb scattering in the walls of

[9] R. Mather and E. Segrè, Phys. Rev. 84, 191 (1951).

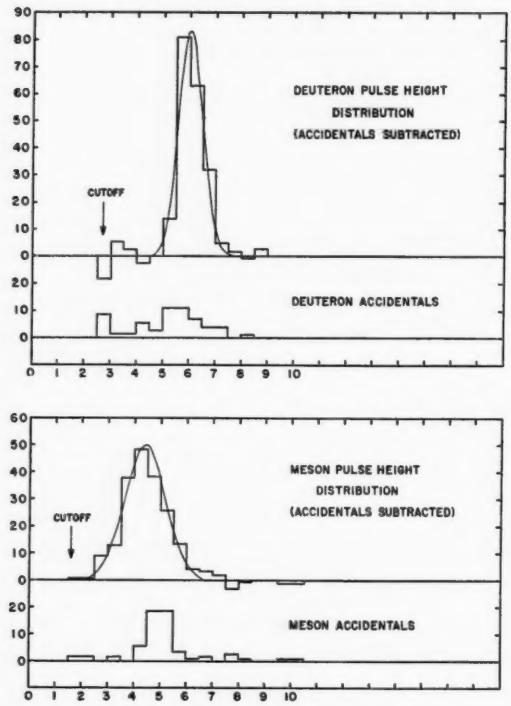

FIG. 5. Typical pulse-height distributions.

the liquid scintillators, finite aperture of the meson counter, finite beam and target, overlap error in the deuteron integration pattern, and loss of events by electronic dead time.

The statistical error of each cross section was compounded with an error of approximately three percent attributed to uncertainties in the systematic corrections. This was done in the usual manner by taking the square root of the sum of the squares of the errors. In all cases the compounding of this additional error resulted in a negligible increase in the error obtained from counting statistics alone. The last column of Table I tabulates all the over-all correction factors that were applied to the raw data.

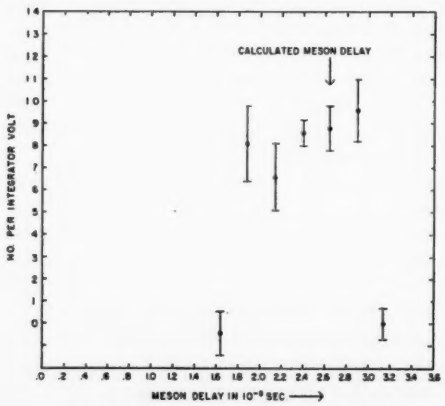

FIG. 6. Typical time-delay curve.

In order to search for large hidden systematic errors in the over-all detection scheme, a measurement was made of the elastic p-p scattering cross section at 90° c.m. The aforementioned apparatus and technique were used. A value of (3.3 ± 0.3) mb sterad^{-1} was obtained, in good agreement with the results of Chamberlain *et al.*[10]

A more detailed account of the experimental procedure and apparatus used in the $p+p\rightarrow\pi^{+}+d$ experiment with unpolarized protons is given in references 4 and 5.

B. Polarized Protons

With minor modifications, the techniques described in Sec. A were used with the 73 percent polarized proton beam[11] to measure the azimuthal asymmetry of $p+p\rightarrow\pi^{+}+d$. Because of the low intensity of the polarized beam, a large meson solid angle was necessary. The meson counter was a plastic scintillator 5.75 in. by 5.75 in. by 0.25 in. It was placed 20 in. from a 0.5-g cm^{-2} slab-shaped liquid-hydrogen target. The deuteron telescope was made large enough to detect all the deuterons at one counter position, with allowances for multiple scattering.

Accidental coincidences with the polarized beam were substantially fewer than with the unpolarized beam at the same beam intensity, primarily because the time spread of the polarized beam was approximately ten times that of the unpolarized beam. The polarized beam differed in another important respect from the unpolarized beam, in that its energy spread was much greater than that of the unpolarized beam. Therefore, since the measurements were made near meson threshold, precautions had to be taken to insure that no mesons were lost in the target because of insufficient energy. In order to obtain mesons with sufficient energy to avoid such losses, the meson telescope was placed at an angle corresponding to 69° in the c.m. system rather than at 90°, the expected angle of maximum asymmetry.

It was believed that there would be less likelihood of introducing false asymmetries if, throughout the measurement, the $p+p\rightarrow\pi^{+}+d$ reaction were detected with full efficiency. Meson-range plateaus, time-delay plateaus, and pulse-height plateaus were obtained to check this point.

In order to exclude the "unbound" reaction $p+p\rightarrow\pi^{+}+p+n$, an absorber, of two-thirds of the deuteron range in copper, was placed in front of the deuteron telescope. In addition, the deuteron counter was made only as large as was necessary to include all the deuterons, since protons from the unbound reaction, which

[10] Chamberlain, Segrè, and Wiegand, Phys. Rev. **83**, 923 (1951).
[11] Chamberlain, Segrè, Tripp, Wiegand, and Ypsilantis, Phys. Rev. **93**, 1430 (1954).

TABLE I. Cross-section data for $p+p\rightarrow\pi^{+}+d$ with unpolarized protons.

Date	T_p Mev	T_π (c.m.) Mev	$\eta=\frac{p_\pi \text{ (c.m.)}}{m_\pi c}$	θ (c.m.) degrees	$4\pi\frac{d\sigma}{d\Omega}$ (c.m.) experimental mb/steradian	$4\pi\frac{d\sigma}{d\Omega}$ (c.m.) least squares mb/steradian	Over-all correction factor
1-7-'53	338	21.5	0.577	30	0.449 ±0.052	0.470	1.12
5-23-'54	338.6	21.7	0.577	57	0.239 ±0.014	0.249	1.09
1-7, 2-10-'53	338	21.5	0.577	88	0.126 ±0.021	0.119	1.05
10-17, 11-19-'52	332	19.0	0.540	30	0.423 ±0.031	0.395	1.18
8-9, 10-15-'52	332	19.0	0.540	60	0.189 ±0.020	0.202	1.12
10-16, 17, 11-17-18-'52	332	19.0	0.540	89	0.125 ±0.0093	0.106	1.13
4-1-'54	325	16.0	0.493	79	0.1014±0.0045	0.103	1.27
1-8, 2-12-'53	324	15.5	0.484	89	0.0816±0.0126	0.090	1.20
4-1-'54	312	10.4	0.392	90	0.0597±0.0037	0.066	1.45
5-23-'54	310	9.52	0.377	55	0.151 ±0.028	0.107	1.16
5-21-'54	310	9.52	0.377	69	0.0819±0.0040	0.080	1.15
5-25-'54	310	9.51	0.377	69	0.0869±0.0044	0.080	1.15

might not be excluded by the copper absorber, are expected to have a larger angular spread than the deuterons.

We will use the terms "left" and "right" to refer to the left and right sides of the incident beam as viewed by an observer looking in the direction of motion of the beam. For instance, the polarized beam is produced by a "left" scatter, as is shown in Fig. 7. The details of production of the polarized beam can be found in reference 11.

Absolute differential cross sections were measured on the left and right sides of the beam. During each asymmetry measurement approximately 10 left-right cycles were made. On each side of the beam, measurements were made on hydrogen-plus-container and on the container alone. The approximate times required were 45 minutes and 15 minutes respectively. Thus, the time per left-right cycle was approximately two hours.

During the polarized beam experiments, real coincidences were observed from the empty container, although container effects had never been observed in previous $p+p\rightarrow\pi^{+}+d$ measurements with unpolarized protons. The effect was found to be characteristic of the target. This target was used for the first time during the asymmetry measurements. The coincidences from the "empty" styrofoam container were found to be $p+p\rightarrow\pi^{+}+d$ events produced when the beam passed through a long path of hydrogen vapor which was in equilibrium with the liquid hydrogen of the full container. There was a vapor effect as long as there was liquid hydrogen in the "full" target. The vapor effect disappeared when the targets were truly empty. The hydrogen vapor contribution was ~10 percent of that of the liquid hydrogen and gave the same asymmetry. This is an important point, because some of the asymmetry measurements did not include empty-container data.

A continuous monitor of the meson telescope was maintained by recording separately the coincidences between front and rear meson counters. These events were due mainly to protons from p-p collisions. In this way there was provided a high-counting-rate monitor of the meson detection efficiency, the reproducibility of the meson telescope angle, and the beam polarization. The same value was obtained for the p-p asymmetry as has been observed by Chamberlain *et al.*[11] A similar monitoring procedure was used with the deuteron telescope.

The following checks were made to search for instrumental sources of asymmetry. The counters were shown to be insensitive to stray magnetic fields, and to be uniform in sensitivity. Large intentional misalignments of the counter telescopes and of the liquid-hydrogen target were made. In this way it was demonstrated that only gross misalignments could have given a false asymmetry.

A final over-all check was made by replacing the polarized beam with the ordinary "scattered" beam, which has been shown[11] to be unpolarized. All other conditions, including beam energy, electronics, counter alignment, etc., remained the same. The result, in each case, was the vanishing of the asymmetry to within statistics. See Fig. 8.

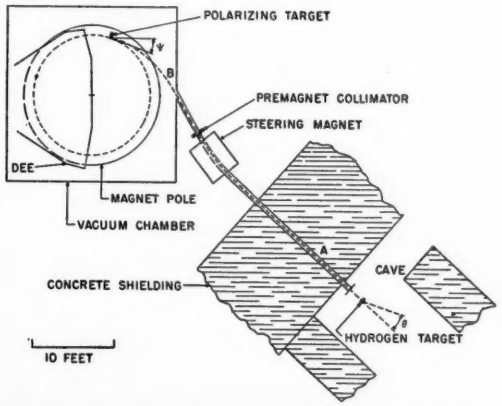

FIG. 7. Over-all geometry of the polarized proton beam.

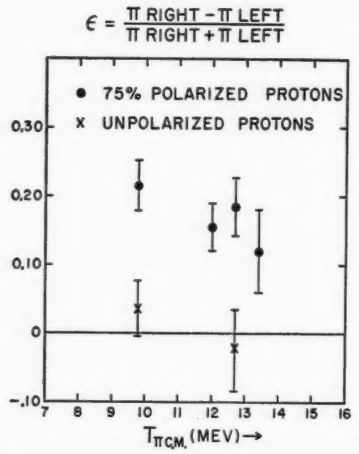
$\epsilon = \frac{\pi \text{ RIGHT} - \pi \text{ LEFT}}{\pi \text{ RIGHT} + \pi \text{ LEFT}}$
• 75% POLARIZED PROTONS
× UNPOLARIZED PROTONS
0.30
0.20
0.10
0
-.10
7 8 9 10 11 12 13 14 15 16
$T_{\pi CM.}$ (MEV)→

FIG. 8. $p+p\rightarrow\pi^+ +d$ asymmetries obtained with polarized and unpolarized protons.

Those polarized beam measurements for which a blank-target subtraction was performed were used to obtain differential cross sections for unpolarized protons. These cross sections were obtained from the average of the left and right yields. The corrections described in the previous section were applied. The statistical errors of these cross-section measurements were approximately three percent. An error of five percent was assigned to cover uncertainties in the systematic corrections. These runs are included in the unpolarized beam data of Table I.

III. RESULTS WITH UNPOLARIZED PROTONS

The twelve absolute differential cross sections which comprise all of our data are presented in the sixth column of Table I, together with their rms errors. These values were fitted by the method of least squares to the phenomenological theory of Watson and Brueckner,[7] which predicts that near meson threshold, in Rosenfeld's[8] notation,

$$4\pi\frac{d\sigma\ (\text{c.m.})}{d\Omega}=\alpha_{10}\eta+\beta_{10}\eta^3\frac{(x+\cos^2\theta)}{x+\frac{1}{3}}. \qquad (1)$$

Here $\eta=p_\pi$ (c.m.)$/m_\pi c$, and $\alpha_{10}\eta$ and $\beta_{10}\eta^3$ are S- and P-wave contributions, respectively, to the total cross section; $x+\cos^2\theta$ is the c.m. P-wave angular distribution.[12] In order to perform a least-squares analysis easily, one needs an expression linear in the parameters. We therefore rewrite the above as

$$4\pi\frac{d\sigma\ (\text{c.m.})}{d\Omega}=a_1\eta+a_2\eta^3+a_3\eta^3\cos^2\theta.^{13} \qquad (2)$$

Table II presents the least-squares results for the a_i, their rms errors δa_i, and the correlation errors $\delta a_i\delta a_j$.[14] Inserting these values for a_i into Eq. (2), we have calculated the least-squares value of $4\pi d\sigma/d\Omega$ corresponding to each of the twelve experimental cross sections, and have listed these in column 7 of Table I, for comparison with experimental values in column 6. In order to facilitate comparison of the goodness-of-fit of the data

TABLE II. The constants a_i in mb (10^{-27} cm^2), and correlation errors $\delta a_i\delta a_j$ in (mb)^2, resulting from a least-squares fit of the data in Table I to Eq. (2).

$a_1=0.138\pm0.015$	$\delta a_1\delta a_2=-11.2\times10^{-4}$
$a_2=0.200\pm0.078$	$\delta a_1\delta a_3=3.83\times10^{-4}$
$a_3=2.44\pm0.17$	$\delta a_2\delta a_3=-42.3\times10^{-4}$

to (2) [or (1)], we have divided (2) by η^3 and plotted the result against η^{-2} and $\cos^2\theta$, in Fig. 9, so as to exhibit a plane surface in three dimensions. The experimental points are plotted there for comparison.

We can rewrite the least-square results in Rosenfeld's

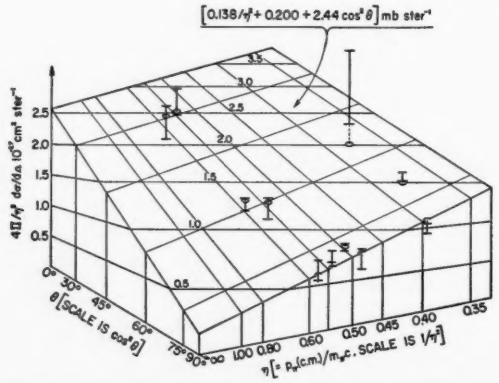

FIG. 9. Comparison of experimental points with the least-squares solution for the surface $4\pi d\sigma/d\Omega=a_1\eta+a_2\eta^3+a_3\eta^3\cos^2\theta$. [Eq. (2).]

[12] The first and second subscripts in α_{10} and β_{10} refer to the total isotopic spin of the two nucleons in the initial and final states, respectively.

[13] In all our previous cross section publications (see references 3 and 4) we believed that it was necessary to incorporate the relative excitation data at 0° of Schulz [A. G. Schulz, University of California Radiation Laboratory Report UCRL-1756, 1951 (unpublished)] in order to find the energy dependence of the angular distribution. If one inspects Eq. (2), however, he sees that a_1 and a_2 can be determined by two 90° (c.m.) points at different energies, after which a_3 can be determined by an angular distribution at any energy. Since Schulz measured only a relative excitation, then, in the spirit of Eq. (1) or (2), he measured essentially $a_1/(a_2+a_3)$. Analysis of his data gives $a_1/(a_2+a_3)=(4.8\pm4.6)\times10^{-2}$. Our data alone yield $a_1/(a_2+a_3)=(5.2\pm0.9)\times10^{-2}$, so that we no longer incorporate Schulz's data into ours. Our more accurate value is obtained mainly from our excitation points at 90° (c.m.), where the ratio of the S-wave term, a_1, to P-wave terms is greatly enhanced over that at 0°.

[14] The use of the correlation errors $\delta a_i\delta a_j$, $i\neq j$, may be illustrated by finding the least-squares rms error for $x=a_2/a_3$. Under the usual assumption of "small" errors so that differentials may be used, we differentiate, square, average, and take the square root to obtain

$$\delta x=\pm[a_3^{-2}(\delta a_2)^2+a_2^2a_3^{-4}(\delta a_3)^2-2a_2a_3^{-3}\delta a_2\delta a_3]^{\frac{1}{2}}=\pm0.034.$$

notation, Eq. (1), to obtain

$$\alpha_{10}=a_1 \quad =0.138\pm0.015 \text{ millibarns},$$
$$\beta_{10}=a_2+\tfrac{1}{3}a_3=1.01\pm0.08 \text{ millibarns},$$
$$x=a_2/a_3 \quad =0.082\pm0.034,$$
$$\eta_c=(a_1/a_2)^{\frac{1}{2}}=0.83\pm0.21.$$

IV. DISCUSSION OF UNPOLARIZED BEAM RESULTS

These experiments have exhibited directly for the first time, by measurement of α_{10}, the presence of S-wave mesons in $p+p\rightarrow\pi^+ +d$. It is interesting to note that a simple theoretical estimate,[15] which considers the S-wave mesons to be due to a nucleon recoil correction to dominant P-wave interaction, predicts that α_{10}/β_{10} should be of the order of the mass ratio $m_\pi/m_{(\text{nucleon})}$. Our experimental result of $\alpha_{10}/\beta_{10}=0.137\pm0.025$ substantiates this.

Another indirect predication of α_{10} has been made by Brueckner, Serber, and Watson.[16] They relate $\gamma+p\rightarrow\pi^+ +n$ near threshold through the π^- to π^+ photoproduction ratio in deuterium to $\gamma+n\rightarrow\pi^- +p$; through detailed balancing to $\pi^- +p\rightarrow\gamma+n$; via calculation to $\pi^- +d\rightarrow\gamma+2n$; through Panofsky's[17] branching ratio for π^- capture in deuterium to $\pi^- +d\rightarrow 2n$; through detailed balancing to $n+n\rightarrow\pi^- +d$, which finally, by the assumption of charge symmetry, may be replaced by $p+p\rightarrow\pi^+ +d$. Using the results of Bernardini *et al.*[18] for $\gamma+p\rightarrow\pi^+ +n$ near threshold, and for the π^- to π^+ photoproduction ratio in deuterium, one obtains $\alpha_{10}=(0.14\pm0.05)$ mb. This is in notably good agreement with our directly measured value of (0.138 ± 0.015) mb. Within the rather large error in the predicted value, which is presumed to cover the various uncertainties in the several steps, and provided that the assumption of charge symmetry is regarded as the least certain element in the above calculation, then we may regard the good agreement between our directly measured value and the predicted value as a confirmation of the assumption of charge symmetry.

TABLE III. $p+p\rightarrow\pi^+ +d$ transitions that conserve total angular momentum and parity, for meson angular momenta $l<2$. The indicated angular dependences hold if a single transition is present (no interference).

Initial p-p state	Relative transition amplitude	Final π state	Dependence on meson momentum and angle
$^1S_0$	$r_0=\lvert r_0\rvert \exp i\tau_0$	P	$\eta^3\times$const
$^3P_1$	$r_1=\lvert r_1\rvert \exp i\tau_1$	S	$\eta\times$const
$^1D_2$	$r_2=1$	P	$\eta^3\times(\frac{1}{3}+\cos^2\theta)$

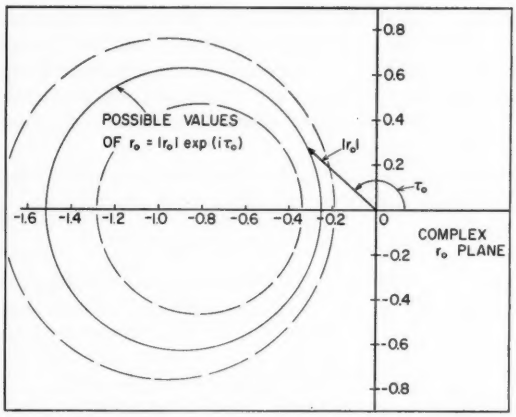

FIG. 10. Possible values of r_0 consistent with the experimental value of the P-wave angular distribution parameter, $x=0.082\pm0.034$. See Table III. The inner and outer dotted circles correspond to the errors ∓0.034, respectively.

The P-wave angular distribution is $x+\cos^2\theta$. If only the $^1D_2$ p-p states contributed to P-wave mesons, we would have $x=\frac{1}{3}$, as indicated in Table III. The measured value is $x=0.08\pm0.03$, which shows, therefore, that $^1S_0$ protons also contribute to P-wave meson production. The relative phase τ_0 between the $^1S_0$ and $^1D_2$ p-p contributions is unknown. Therefore the measurement of x serves only to put limits on the $^1S_0$ contribution. For the measured value of x these limits are given by $0.25<|r_0|<1.51$, as shown in Fig. 10. The value of τ_0 is 180° at both limits, and reaches a minimum of ~133° at $|r_0|\sim0.60$. Arguments have been given[19,20] which predict predominance of the $^1D_2$ over the $^1S_0$ p-p contributions. Roughly, these arguments

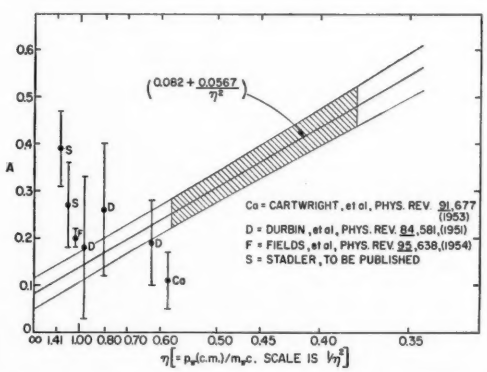

FIG. 11. Comparison of $p+p\rightarrow\pi^+ +d$ angular distribution parameter A obtained in this paper with results of other observers at higher energies. The curve and its rms error band were obtained from a least-squares fit of the data (not shown) of this paper alone. The cross hatching indicates the range of meson momenta covered in this paper.

[15] M. Gell-Mann and K. M. Watson, Ann. Rev. Nuclear Sci. 4, 219 (1954).
[16] Brueckner, Serber, and Watson, Phys. Rev. 81, 575 (1951).
[17] Panofsky, Aamodt, and Hadley, Phys. Rev. 89, 565 (1951).
[18] Goldwasser, Beneventano, Lee, Stoppini, Hanson, and Bernardini, Proceedings of the Fourth Annual Rochester Conference on High Energy Nuclear Physics (University of Rochester, Rochester, 1954).
[19] K. A. Brueckner and K. M. Watson, Phys. Rev. 81, 923 (1952).
[20] Aitken, Mahmoud, Henley, Ruderman, and Watson, Phys. Rev. 93, 1349 (1954).

point out that $^1D_2$ protons can produce the pion and one of the final nucleons of the deuteron in the strongly interacting state of total angular momentum $\frac{3}{2}$ and isotopic spin $\frac{3}{2}$, whereas the $^1S_0$ protons cannot. On the basis of this argument, one could take $|r_0| \sim 0.25$ and $\tau_0 \sim 180°$.

The c.m. angular distribution, including both S- and P-mesons, is given by $A+\cos^2\theta$. From Eq. (2),

$$A=(a_1\eta+a_2\eta^3)/a_3\eta^3=0.082+0.056\eta^{-2}.$$

This curve, with its rms least-square error band, is plotted in Fig. 11, and its extrapolation is compared there with results obtained at higher energies by other workers. We see that the experimental points for $\eta>1$ tend to lie above the extrapolated curve. This may represent the breakdown of Eq. (1), which is only assumed to hold "near threshold," where, approximately, $\eta<1$. For instance, meson momenta higher than P-states may no longer be negligible.

The total cross section obtained by integration of Eq. (1) is given by

$$\sigma_T=\alpha_{10}\eta+\beta_{10}\eta^3=(0.138\eta+1.01\eta^3)\text{ mb}.$$

This curve is plotted in Fig. 12, where it is compared with the experimental results of other observers. Except for the lowest energy result of Durbin *et al.* at $\eta=0.625$, and perhaps the result of Cartwright *et al.* at $\eta=0.585$, we see that there is very good agreement between the predictions of Eq. (1), as fitted by our data, and other measurements extending up to cross sections an order of magnitude larger than those we have measured. Thus, the phenomenological theory's assumption of negligible energy dependence of α_{10}, β_{10}, and $\varkappa$ is borne out by experiment, at least for β_{10}, the dominant term in the total cross section for $\eta\sim1$. We note that the experimental points, for $\eta>1$, tend to lie below the curve. This could indicate the beginning of the breakdown of applicability of Eq. (1). For instance, D-wave mesons may be not insignificant for $\eta>1$. In addition, it should be remembered that $\gamma+p\to\pi^0+p$,[21] $\gamma+p\to\pi^++n$,[22] and π-nucleon scattering[23] all go through maxima at T_π (c.m.)$\sim$125 Mev, or $\eta\sim1.6$, and we should presumably expect a similar behavior for $p+p\to\pi^++d$. Thus, the tendency noted could be due to an approaching maximum near $\eta\sim1.6$. Of course, the data shown in Fig. 12 barely suggest this as a possibility.

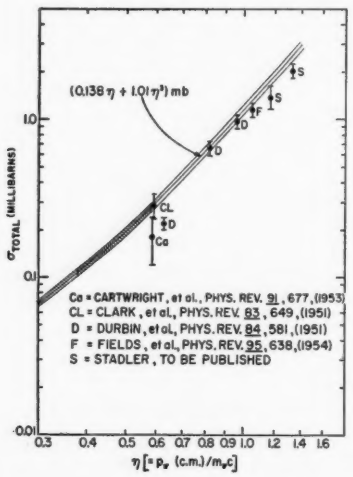

FIG. 12. Comparison of the total $p+p\to\pi^++d$ cross section obtained in this paper with results of other observers at higher energies. The curve and its rms error band were obtained from a least-squares fit of the data (not shown) of this paper alone. The cross hatching indicates the range of meson momenta covered in this paper. The experimental points shown for Clark *et al.*, Durbin *et al.*, and Stadler were obtained by detailed balancing from the inverse reaction $\pi^++d\to p+p$.

V. RESULTS WITH POLARIZED PROTONS

The raw data of the asymmetry measurements[6] on $p+p\to\pi^++d$ made with polarized protons near 315 Mev are shown in Fig. 8. Marshak and Messiah[24] have derived

$$\epsilon=(R-L)/(R+L)=PQA\sin\theta/(A+\cos^2\theta) \quad (3)$$

for the asymmetry produced by interference between the S- and P-wave mesons. Here P is the beam polarization, $A+\cos^2\theta$ is the c.m. angular distribution, and Q is the quantity of interest in the theory. In Rosenfeld's notation,

$$Q=\frac{\eta_c\eta\sqrt{2}}{\eta_c^2+\eta^2}\sin(\psi-\tau_1). \quad (4)$$

We note that Q, and therefore the asymmetry, disappears in the absence of S waves ($\eta_c=(a_1/a_2)^{\frac{1}{2}}=0$), or of P waves ($\eta_c=\infty$), and at certain values of the relative phase angle ψ and τ_1; $|Q|$ cannot exceed 0.70; ψ and τ_1 are given by $r_0+\sqrt{\frac{1}{2}}=|r_0+\sqrt{\frac{1}{2}}|\exp(i\psi)$ and $r_1=|r_1|\exp(i\tau_1)$. The terms r_0 and r_1 are the complex transition amplitudes for $\pi-d$ production from $^1S_0$ and $^3P_1$ p-p states, respectively, to P- and S-wave meson states, respectively, as is shown in Table III; r_0 and r_1 are defined relative to the amplitude r_2, which describes the transition from the $^1D_2$ p-p state to the P-wave meson state; r_2 is taken as unity; r_0 is written alternately as $r_0=|r_0|\exp(i\tau_0)$.

Taking $|P|=0.73$[25] (the sign of P is at present unknown), $A=(a_1\eta+a_2\eta^3)/a_3\eta^3$ from Eq. (2) and Table II, and averaging the angular dependence over the angular aperture centered at $\theta=69°$, we calculate from Eq. (3) a measured value of $|Q|$ for each of the experimental runs shown in Fig. 8. Because these values of $|Q|$ are all equal within the errors, we assume negligible varia-

[21] Walker, Oakley, and Tollestrup, Phys. Rev. **89**, 1301 (1953).
[22] Backer, Keck, Peterson, Teasdale, Tollestrup, Walker, and Worlock, Phys. Rev. **92**, 1090(A) (1953).
[23] Ashkin, Blaser, Feines, Gorwan, and Stern, Phys. Rev. 93, 1129 (1954).
[24] R. E. Marshak and A. M. L. Messiah, Nuovo cimento 11, 337 (1954).
[25] Chamberlain, Donaldson, Segrè, Tripp, Wiegand, and Ypsilantis, Phys. Rev. **95**, 850 (1954).

tion with energy in the region measured and average the results to obtain

$$|Q|=0.39\pm0.05$$

at an average $T_p=314$ Mev, $\eta=0.41$, (T_π) c.m.$=11.3$ Mev. Inserting $\eta_c=0.83$, $\eta=0.41$, and $|Q|=0.39\pm0.05$ into Eq. (4), we obtain

$$|\sin(\psi-\tau_1)|=0.70\pm0.14.^{26} \quad (5)$$

P and $\sin(\psi-\tau_1)$ have the same sign.

De Carvalho *et al.*[27] have looked for an asymmetry in meson production while examining sources of asymmetric background in elastic p-p scattering with 439-Mev polarized protons. Their measurement included about 78 percent of the "unbound" reaction $p+p\rightarrow\pi^{+}+p+n$, which is about equal in magnitude to $p+p\rightarrow\pi^{+}+d$ at Chicago energies.[8] They obtained essentially a null result of $2\epsilon=-0.07\pm0.085$.

Fields *et al.*[28] have measured the asymmetry in $p+p\rightarrow\pi^{+}+d$ using polarized protons of 415 Mev. They obtain $|Q|=0.45\pm0.08$, with (T_π) c.m.$=55$ Mev, $\eta=0.97$. The sign of Q agrees with our value. If we assume, as does the phenomenological theory, negligible energy variation in the parameters α_{10}, β_{10}, and x and in the relative phases τ_0 (or ψ) and τ_1, then we can use our results and Eq. (4) to calculate a predicted value of $|Q|$ at the Carnegie Tech. energy. Using $\eta_c=0.83\pm0.21$ from our unpolarized beam results, and our value of $|Q|=0.39\pm0.05$ at $\eta=0.41$, we would predict an increase in $|Q|$ by a factor 1.25 ± 0.24 in going to $\eta=0.97$, to yield $|Q|=0.49\pm0.10$. This value is clearly consistent with the result of Fields *et al.* The agreement would seem to indicate that the relative S- and P-wave phase angles, as well as the parameters of Eq. (1), are indeed energy-insensitive, as the phenomenological theory assumes.

Gell-Mann and Watson[15] have shown that, near meson threshold, τ_0 and τ_1 are related to the p-p scattering phase shifts for the corresponding states by the relations

$$\begin{aligned}\tau_0&=\alpha(^1S_0)-\alpha(^1D_2)+n\pi,\\ \tau_1&=\alpha(^3P_1)-\alpha(^1D_2)+(n'+\tfrac{1}{2})\pi\end{aligned}, \quad (6)$$

where the α's are the p-p scattering phase shifts in the indicated states, and n and n' are integers. Thus, the result, Eq. (5), of our polarized-beam experiment can be used to put conditions on p-p scattering phase shifts calculated near 315 Mev.

In addition, it should be possible to calculate $\sin(\psi-\tau_1)$ from meson theories. If the sign alone of $\sin(\psi-\tau_1)$ were to be calculated from meson theory, then one could predict the sign of the proton beam polarization P. Presumably, at present, such a prediction could not be considered to be conclusive. In the event, however, that the sign of P becomes determined through a more easily understood process, then the sign of $\sin(\psi-\tau_1)$ will be known and can be compared with a meson-theoretical calculation.†

ACKNOWLEDGMENTS

We are indebted to Dr. Kenneth M. Crowe and Prof. Herbert F. York for valuable discussions and suggestions. We wish to thank Vern G. Ogren for building the fast electronic circuits, and Richard L. Blumberg, Robert E. Donaldson, and Harrold B. Knowles for assistance during the runs.

[26] This supersedes our previously published (see reference 6) value, $|\sin(\psi-\tau_1)|=0.61\pm0.10$, which resulted from using the value $\eta_0=0.62\pm0.16$ instead of our present value, $\eta_0=0.83\pm0.21$.

[27] de Carvalho, Heiberg, Marshall, and Marshall, Phys. Rev. **94**, 1796 (1954).

[28] Fields, Fox, Kane, Stallwood, and Sutton, Phys. Rev. **96**, 812 (1954).

† *Note added in proof.*—J. Marshall and L. Marshall [Leona Marshall, Bull. Am. Phys. Soc. **29**, 18 (1954)] have measured the sign of the polarization P of the 440-Mev polarized proton beam of the Chicago cyclotron by degrading the energy of the protons to 10 Mev and scattering them from helium. Their result predicts that the Berkeley polarized protons (produced by a left scatter) have their spin up, i.e. $P>0$. The sign of our observed meson asymmetry, $(R-L)>0$, with Eqs. (3) and (4), then, says that $\sin(\psi-\tau_1)>0$.

B. T. Feld [Nuovo cimento, **12**, 425 (1954)] has discussed the polarization of the protons in $\pi^{+}+d\rightarrow p+p$. On the basis of reasonable assumptions derived from a resonance model of the meson-nucleon interaction, he has shown that the Fermi and Yang type meson-nucleon interactions predict opposite signs for the polarization. In particular, he shows that if the Fermi type interaction is the correct one, protons produced to the left (as seen by the incident meson) will be polarized with their spins down. (The complementary protons to the right are polarized spin up.) The Yang solution predicts the opposite sign of polarization, with a slightly different magnitude.

If we consider the time reversal of a $\pi^{+}+d\rightarrow p+p$ collision, first averaging over the polarization of (either) one of the protons so that it can represent an unpolarized target, we see that an excess of spin down protons produced to the left, in $\pi^{+}+d\rightarrow p+p$, corresponds to an excess of mesons produced to the right (as seen by the incident proton) by spin up protons in $p+p\rightarrow\pi^{+}+d$. (The proton spins, as well as velocities, are reversed when the time is reversed.) The fact that we do indeed observe an excess of mesons produced to the right by spin up protons provides strong evidence in favor of the Fermi type interaction.

We emphasize that, as shown by Fig. 10, the present $p+p\rightarrow\pi^{+}+d$ data alone, i.e., without additional arguments such as those of Feld, are relatively unbiased towards either the Fermi ($|r_0|\sim0.25$) or the Yang ($|r_0|\sim1.5$) type interactions. Preliminary indications are that combination of the $p+p\rightarrow\pi^{+}+d$ data with the elastic $p-p$ scattering phase shifts of Segrè, *et al.* (to be published), through the Gell-Mann and Watson relation, Eq. (6), will favor one or the other set of solutions, independent of meson theory. In addition, using Eq. (6), the Fermi and Yang interactions predict quite different magnitudes for the polarization of the deuteron in $p+p\rightarrow\pi^{+}+d$ production with unpolarized protons.

Polarization of Nucleons Elastically Scattered from Nuclei*

R. M. STERNHEIMER
Brookhaven National Laboratory, Upton, Long Island, New York
(Received November 15, 1954)

The polarization P of nucleons elastically scattered from nuclei has been calculated for the nuclear potential of Woods and Saxon which has the radial dependence $1/\{1+\exp[(r-r_0)/a]\}$, where r_0 is the nuclear radius and the parameter a determines the length of the exponential tail. The variation of P with the optical parameter k_1/K and the strength of the spin-orbit coupling was investigated for the case of Al. In general, P remains positive throughout the first diffraction minimum. For the Berkeley data for the polarization of 300-Mev protons scattered from Al, a reasonable fit has been obtained inside the first diffraction peak. The functions β and R introduced by Wolfenstein to describe the asymmetry in a triple scattering experiment are evaluated for several cases.

I. INTRODUCTION

IT has been shown by several authors[1–4] that the observed polarization[5–8] of protons of energy 200–400 Mev elastically scattered from nuclei can be accounted for by the assumption of a spin-orbit coupling of reasonable magnitude. If one uses a square well for the main spin-independent part of the potential,[3] one finds that the polarization is positive in the region of the first diffraction maximum, becomes negative around the first diffraction minimum, and oscillates back to positive values for larger scattering angles near the second diffraction peak. The experimental results[5–8] do not seem to give support to an oscillatory behavior of the polarization P. In agreement with this observation, it was found that if P is calculated using a potential well which is rounded near the nuclear surface,[9,10] P remains positive throughout the first diffraction minimum. This calculation was carried out using a harmonic oscillator form for the spin-independent part of the nuclear potential. Thus the potential was assumed to vary as $1-r^2/r_0^2$, where r_0 is the nuclear radius and r is the distance from the center of the nucleus. Since this radial dependence implies a large amount of rounding and since the potential does not have a tail for $r>r_0$, it was suggested by Weisskopf[11] that it would be of interest to calculate P with a more realistic nuclear potential, namely that used by Woods and Saxon[12] to fit the angular distributions of 22-Mev protons scattered from various nuclei.[13] This potential V has the radial dependence $V\propto 1/\{1+\exp[(r-r_0)/a]\}$, where a is a constant for which the value 0.49×10^{-13} cm was found to give the best fit for the experimental data[13] for Pt. This value of a was used in the present calculations which were carried out using the optical model of the transparent nucleus of Serber.[14] It will be shown that the potential V of Woods and Saxon[12] gives the same qualitative dependence of P on scattering angle θ as the harmonic oscillator potential, i.e., P remains positive throughout the region of the first diffraction minimum. This result was verified for a wide range of the ratio k_1/K, where the optical parameters k_1 and K measure the real and imaginary parts of V. A reasonable fit has been obtained for the experimental results obtained at Berkeley[6] for 300-Mev protons scattered from Al. The last section of this paper gives the results of a calculation of the functions β and R introduced by Wolfenstein[15] to describe polarization effects in triple scattering experiments.

II. CALCULATIONS OF THE POLARIZATION

The potential of Woods and Saxon[12] is given by

$$V=\frac{V_r+iV_i}{1+\exp[(r-r_0)/a]}, \tag{1}$$

where V_r and V_i are constants which determine the real and imaginary parts of V, respectively. In most of the calculations, the spin-orbit coupling was taken proportional to $(1/r)(dV/dr)$. Thus the term in the potential is $U(r)\mathbf{l}\cdot\boldsymbol{\sigma}$, where $\hbar\mathbf{l}$ and $\hbar\boldsymbol{\sigma}/2$ are the orbital and spin angular momentum of the incoming nucleon, respectively, and $U(r)$ is given by

$$U(r)=-\frac{b\exp[(r-r_0)/a]}{r\{1+\exp[(r-r_0)/a]\}^2}, \tag{2}$$

* Work done under the auspices of the U. S. Atomic Energy Commission.

[1] E. Fermi, Nuovo cimento **11**, 407 (1954).
[2] W. Heckrotte and J. Lepore, Phys. Rev. **94**, 500 (1954).
[3] Snow, Sternheimer, and Yang, Phys. Rev. **94**, 1073 (1954). This letter will be referred to as I.
[4] B. J. Malenka, Phys. Rev. **95**, 522 (1954).
[5] Oxley, Cartwright, and Rouvina, Phys. Rev. **93**, 806 (1954).
[6] Chamberlain, Segrè, Tripp, Wiegand, and Ypsilantis, Phys. Rev. **93**, 1430 (1954); **95**, 1105 (1954). I am very much indebted to Professors O. Chamberlain and C. Wiegand for sending me the experimental results for Al before publication.
[7] Marshall, Marshall, and de Carvalho, Phys. Rev. **93**, 1431 (1954).
[8] J. M. Dickson and D. C. Salter, Nature **173**, 946 (1954).
[9] R. M. Sternheimer, Phys. Rev. **95**, 587 (1954). This letter will be referred to as II.
[10] W. Heckrotte and J. Lepore, Phys. Rev. **95**, 1109 (1954).
[11] V. Weisskopf (private communication). I am very much indebted to Professor Weisskopf for informing me of the results of Woods and Saxon before the publication of their letter.
[12] R. D. Woods and D. S. Saxon, Phys. Rev. **95**, 577 (1954).
[13] B. I. Cohen and R. V. Neidigh, Phys. Rev. **93**, 282 (1954).
[14] Fernbach, Serber, and Taylor, Phys. Rev. **75**, 1352 (1949).
[15] L. Wolfenstein, Phys. Rev. **96**, 1654 (1954). I am very much indebted to Professor Wolfenstein for sending me a copy of this paper before publication.

where b is a constant. Concerning this choice of U, we note that the previous calculations for the square well[3] and harmonic oscillator potentials[9] showed that the behavior of P is not sensitive to the radial dependence of U. Thus the same qualitative behavior of P was obtained with the functions U_1 and U_2 where U_1 emphasizes the nuclear surface, whereas U_2 is strongly concentrated at the center of the nucleus. The radial dependence $U(r)$ used here is suggested by the form of the Thomas precession. Moreover, according to an argument due to Fermi,[16] the dependence $(1/r)(dV/dr)$ follows in a reasonable manner, if one considers that the polarization is a surface phenomenon, since a nucleon which is inside the nuclear matter will be completely surrounded by nucleons, so that there is no net force on its spin.

The potential V gives rise to the following phase shifts:

$$\delta_{l,0}=-\frac{k(V_r+iV_i)}{2T}\int_0^\infty \frac{dx}{1+\exp\{[(x^2+y^2)^{\frac{1}{2}}-r_0]/a\}}, \quad (3)$$

where k=wave number, T=kinetic energy of the incident nucleon,[17] x and y are coordinates with respect to the center of the nucleus, x is along the direction of incidence, and the value of y corresponding to l is $(l+\frac{1}{2})/k$. The integral of Eq. (3) is a function of y and will be called $A(y)$. The factor $-k(V_r+iV_i)/(2T)$ will be written as $k_1+iK/2$, where k_1 and K are the usual parameters of the optical model.[14] It may be noted that k_1 and K are here defined in terms of the potential at the center of the nucleus. The values of the optical parameters for a point on the nuclear surface would be correspondingly smaller.[18]

The contribution to the phase shift from $U(r)\mathbf{l}\cdot\boldsymbol{\sigma}$ is

$$\Delta_l=\pm\frac{kbl}{2T}\times\int_0^\infty \frac{\exp\{[(x^2+y^2)^{\frac{1}{2}}-r_0]/a\}dx}{(1+\exp\{[(x^2+y^2)^{\frac{1}{2}}-r_0]/a\})^2(x^2+y^2)^{\frac{1}{2}}}, \quad (4)$$

where $y=(l+\frac{1}{2})/k$. The integral of Eq. (4) will be called $B(y)$. From (3) and (4), one obtains for the complete phase shift

$$\delta_l^{\pm}=\left(\frac{iK}{2}+k_1\right)A[(l+\tfrac{1}{2})/k]\pm\frac{kbl}{2T}B[(l+\tfrac{1}{2})/k]. \quad (5)$$

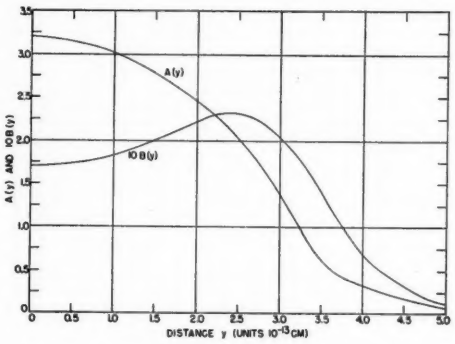

FIG. 1. Functions $A(y)$ and $B(y)$ which determine $\delta_l^{\pm}$. $A(y)$ is in units 10^{-13} cm.

The functions $A(y)$ and $B(y)$ were obtained by numerical integration. It was found sufficient to calculate A and B for about eight values of y. Figure 1 shows $A(y)$ and $B(y)$ for $r_0=3.2\times10^{-13}$ cm and $a=0.49\times10^{-13}$ cm, corresponding to the case of Al. This choice of r_0 will be discussed below. Near $y=0$, $A(y)$ is $\approx(r_0^2-y^2)^{\frac{1}{2}}$ in agreement with the result for a square well. Near $y=r_0$, A falls off slowly and does not become negligible until $y\gtrsim5\times10^{-13}$ cm, as expected from the exponential tail of V. $B(y)$ has a broad maximum near $y=2.4\times10^{-13}$ cm $(=0.75r_0)$ because for this region of y the integration path is mostly along the nuclear surface for which dV/dr is largest. Thus Bl, which enters into Δ_l, has a maximum for a value of l near kr_0. In the following the strength of the spin-orbit coupling will be characterized by the largest Δ_l rather than by the value of b. If $\Delta_{l,\max}$ denotes the largest Δ_l, the spin-orbit energy ϵ will be defined as follows[17]:

$$\frac{kr_0\epsilon}{2T}=|\Delta_{l,\max}|=\frac{kb(Bl)_{\max}}{2T}. \quad (6)$$

ϵ is analogous to the parameter ϵ_1 used in I and II.[19] As shown by Eq. (8) of I, if the spin-orbit coupling were equivalent to an extra potential ϵ, then $kr_0\epsilon/(2T)$ would be the maximum phase shift (attained for $l=0$) for a square well of radius r_0. Since $\Delta_{l,\max}$ occurs near $l=kr_0$, a given ϵ corresponds to an effective U of the order of ϵ/kr_0.

Using Eq. (5) for $\delta_l^{\pm}$, P is calculated from Eqs. (3)–(6) of I. Before proceeding to a comparison with the experimental data[6] for Al, we present the results obtained for $r_0=3.2\times10^{-13}$ cm with various values of k_1/K for 316-Mev neutrons. These calculations were

[16] Professor E. Fermi (private communication).

[17] At relativistic energies the factor $1/(2T)$ is replaced by $E/(\hbar^2c^2k^2)$, where E is the total energy of the particle (including rest mass). The curves of Figs. 2–5 were calculated from the values of ϵ listed in the figures by using the nonrelativistic Eq. (6) to obtain Δ_l from the ϵ. Thus the actual values of ϵ which correspond to these curves according to the relativistic expression are 0.874 times the values listed in the figures, where 0.874 is the value of $\hbar^2c^2k^2/(2TE)$ for 316-Mev neutrons. The same remark applies to the curves for $\epsilon=7.5$ Mev and $\epsilon_2=12$ Mev shown in Figs. 6 and 7.

[18] It was pointed out to the author by Dr. F. Chen that the values of the imaginary potential given in I and II which correspond to the K used in the calculations should be divided by 2. The potential for the square well used in I which corresponds to $k_1=0.86\times10^{13}$ cm^{-1}, $K=1.7\times10^{13}$ cm^{-1} should be $V=-(13+12.8i)$ Mev instead of $-(13+25.6i)$ Mev. The harmonic oscillator potential given in II should be $V_0=-(32.5+32i)$ Mev at the center of the nucleus, instead of $-(32.5+64i)$ Mev.

[19] In the present notation, the coupling U and ϵ correspond to U_1 and ϵ_1 as defined in I and II.

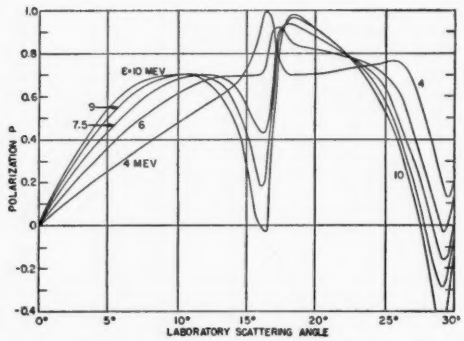

FIG. 2. Polarization P for 316-Mev neutrons scattered from Al, calculated for the Woods-Saxon potential with $k_1/K \approx 0.5$ ($k_1 = 0.86 \times 10^{12}$ cm^{-1}, $K = 1.7 \times 10^{12}$ cm^{-1}).

carried out in order to establish the behavior of P *vs* θ for the potential of Eq. (1) and to determine whether there is a strong dependence on k_1/K.

Figure 2 shows P *vs* θ for $k_1 = 0.86 \times 10^{12}$ cm^{-1}, $K = 1.7 \times 10^{12}$ cm^{-1}, and for $\epsilon = 4$, 6, 7.5, 9, and 10 Mev. These k_1 and K are the values given by Taylor[20] for 316 Mev. It is seen that for moderate values of ϵ (<9 Mev), P remains positive throughout the first diffraction minimum at 16°. For small ϵ (4 Mev), P has a maximum in this region. With increasing ϵ, P develops a minimum near 16°. The tendency for P to have a minimum with increasing spin-orbit coupling can also be noted in Fig. 1 of II which pertains to the coupling U_1 for the harmonic oscillator potential. A plausible explanation of this trend can be given as follows. Both the potential U_1 of II and the present potential U emphasize the nuclear surface in comparison to the main potential V, since they are proportional[19] to dV/dr. If U_1 or U are made large by increasing ϵ, the complete nuclear potential has therefore a rapid variation at the nuclear boundary, and the effect of the rounding of V is compensated by the large U_1 or U. Thus one expects that the behavior of P will be roughly the same as for a square well, in which case P has a (negative) minimum near the first diffraction minimum. Figure 2 shows that for $\epsilon \gtrsim 10$ Mev, the minimum of P is in fact negative.

Figure 3 shows the cross section $\langle d\sigma/d\Omega \rangle$ averaged over spin directions as obtained from Eq. (9) of I. It is seen that with increasing ϵ, the minimum of $\langle d\sigma/d\Omega \rangle$ at 16° becomes less pronounced. However, even for $\epsilon = 10$ Mev, this minimum is not filled in, contrary to the result for the spin-orbit coupling U_2 (see Fig. 3 of I and Fig. 3 of II). The reason for this difference is that the potential U of Eq. (2) emphasizes the nuclear boundary, whereas U_2 tends to wash out the boundary effects, since it falls off rapidly with increasing r throughout the nuclear volume [$U_2 \propto (r_0^2/r^2)$].

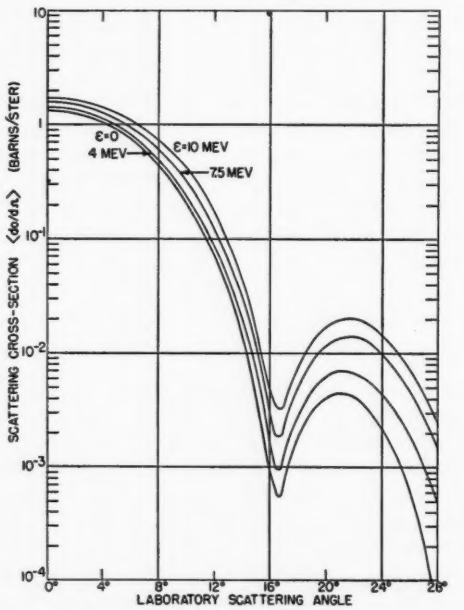

FIG. 3. Differential scattering cross section $\langle d\sigma/d\Omega \rangle$ averaged over spin directions for 316-Mev neutrons scattered from Al, calculated for $k_1/K \approx 0.5$ ($k_1 = 0.86 \times 10^{12}$ cm^{-1}, $K = 1.7 \times 10^{12}$ cm^{-1}).

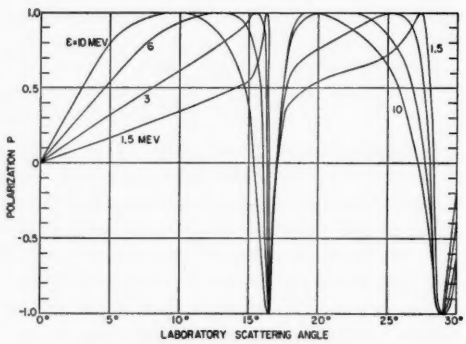

FIG. 4. Polarization P for 316-Mev neutrons scattered from Al, calculated for $k_1/K = 0$ ($K = 2.17 \times 10^{12}$ cm^{-1}).

In order to determine whether the behavior of P is strongly dependent on k_1/K, similar calculations were carried out for $k_1/K = 1$, 0.3, and 0. The results for $k_1/K = 1$ ($k_1 = K = 1.25 \times 10^{12}$ cm^{-1}) are not shown here. They are very similar to those for $k_1/K = 0.5$ as shown in Fig. 2. Thus the curves of P for small ϵ (4 and 6 Mev) have a maximum near 16°, while the curves for large ϵ have a minimum in this region. The results for $\langle d\sigma/d\Omega \rangle$ are qualitatively similar to those of Fig. 3 for $k_1/K = 0.5$. The value of $\langle d\sigma/d\Omega \rangle$ at the first diffraction minimum increases with increasing ϵ, but not enough (even for $\epsilon = 15$ Mev) to make the minimum disappear.

Figure 4 for $k_1 = 0$ ($K = 2.17 \times 10^{12}$ cm^{-1}) shows that all curves of P, even for small ϵ, become negative near 16° and, in fact, go through -1. The curves of P also go through $+1$ in the regions of the first and the second

[20] T. B. Taylor, Phys. Rev. **92**, 831 (1953).

diffraction peaks and through -1 near the second diffraction minimum. The reason for this behavior is that for $k_1=0$, the functions f and g defined in I become pure imaginary and real, respectively. Thus, if $f\equiv f_r+if_i$, $g\equiv g_r+ig_i$, where the subscripts r and i denote the real and imaginary parts, respectively, then P is given by

$$P=\frac{(f_i-g_r)^2-(f_i+g_r)^2}{(f_i-g_r)^2+(f_i+g_r)^2}. \quad (k_1=0) \qquad (7)$$

Hence $P=-1$ for $f_i=g_r$, and $P=+1$ for $f_i=-g_r$.

Since the experiments[5-8] do not seem to give support to a change of sign of P, it is of interest to obtain some information about the lowest ratio k_1/K for which the negative region of P is absent for reasonable values of ϵ. For this reason, the curves for $k_1/K=0.3$ ($k_1=0.59\times10^{13}$ cm^{-1}, $K=1.97\times10^{13}$ cm^{-1}) of Fig. 5 were calculated. It is seen from this figure that the same qualitative behavior obtains as for $k_1/K=0.5$ and 1, namely the existence of a maximum of P at 16° for small ϵ (1.5 and 3 Mev), and of a minimum for large ϵ ($\epsilon\gtrsim6$ Mev). However, this minimum does not become negative until $\epsilon\gtrsim8$ Mev. Hence the behavior of P for $k_1/K=0.3$ is qualitatively compatible with the experiments, and only the region of k_1/K appreciably smaller than 0.3 appears to be excluded.

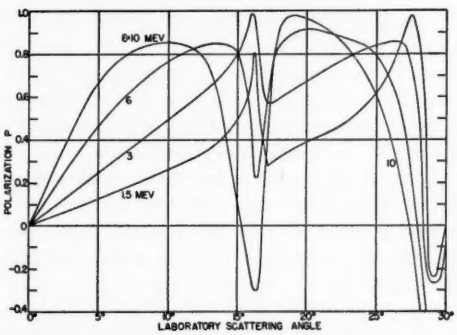

FIG. 5. Polarization P for 316-Mev neutrons scattered from Al, calculated for $k_1/K=0.3$ ($k_1=0.59\times10^{13}$ cm^{-1}, $K=1.97\times10^{13}$ cm^{-1}).

It may be noted that the maximum polarization P_{max} inside the first diffraction peak for $\epsilon=10$ Mev is 0.82 for $k_1/K=0.3$ and 1 for $k_1/K=0$, as compared to 0.70 for $k_1/K=0.5$. For $k_1/K=1$, P_{max} for $\epsilon=10$ Mev was found to be 0.46. Thus there is a tendency for P_{max} at a given ϵ to decrease with increasing k_1/K.

In order to obtain an approximate fit to the Berkeley data[6] for Al, it was noted that the observed P has a minimum at 16° and that the decrease of $\langle d\sigma/d\Omega\rangle$ with θ becomes less rapid at about the same angle. The experimental values of P were obtained by dividing the observed asymmetry by the polarization (0.64) of the scattered beam incident on the Al target. The experimental $\langle d\sigma/d\Omega\rangle$ was obtained by averaging over the

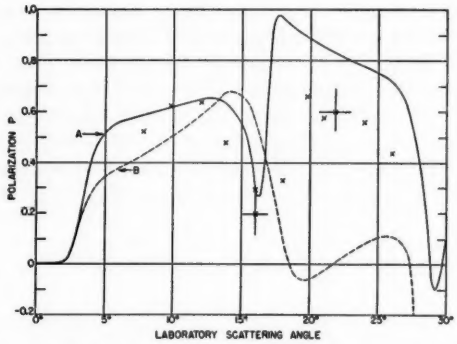

FIG. 6. Polarization P for 300-Mev protons scattered from Al. The crosses represent the experimental values.[6] The full curve (A) was calculated for the spin-orbit coupling U with $k_1=1.28\times10^{13}$ cm^{-1}, $K=2.56\times10^{13}$ cm^{-1}, and $\epsilon=7.5$ Mev. The broken curve (B) was obtained for the coupling U_2 with $k_1=1.28\times10^{13}$ cm^{-1}, $K=2.56\times10^{13}$ cm^{-1}, and $\epsilon_2=12$ Mev.

observed $d\sigma/d\Omega$ for scattering to the left and to the right of the beam incident on the Al target. The experimental values of P and $\langle d\sigma/d\Omega\rangle$ are shown in Figs. 6 and 7. Preliminary calculations were carried out with values of r_0 ranging from 2.44×10^{-13} cm to 4.49×10^{-13} cm. The angle θ_{min} for which the minimum of P occurs was found to decrease with increasing r_0. The product $(r_0+a)\sin\theta_{min}$ changes by only 7 percent between the two extreme radii given above, as would be expected from the equations for the optical model without spin-

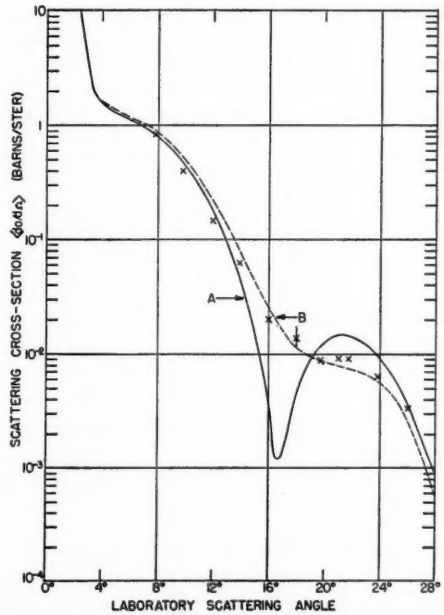

FIG. 7. Differential cross section $\langle d\sigma/d\Omega\rangle$ averaged over spin directions for 300-Mev protons scattered from Al. The crosses represent the experimental values.[6] The full curve (A) was obtained for the coupling U, and the broken curve (B) for the coupling U_2, with the same parameters as for Fig. 6.

orbit coupling.[14] As shown above, the value $r_0=3.2\times10^{-13}$ cm gives a minimum of P (for $\epsilon>6$ Mev) at $\sim16°$ so that this r_0 was used for Al. Note that this corresponds to $r_0=1.07\times10^{-13}A^{\frac{1}{3}}$ cm. The coefficient 1.07×10^{-13} is rather small, but since the potential has a large tail, the volume integral over V is larger than $(4\pi/3)r_0^3(V_r+iV_i)$. Thus for $r_0=3.2\times10^{-13}$ cm, $a=0.49\times10^{-13}$ cm, a numerical integration of Eq. (1) gives

$$4\pi\int_0^\infty Vr^2dr=(4\pi/3)(V_r+iV_i)(3.43\times10^{-13})^3. \quad (8)$$

Hence the coefficient of $A^{\frac{1}{3}}$ is effectively 1.14×10^{-13} cm.

In order to make a comparison with experiment, the Coulomb scattering must be included. The equations for the polarization including the Coulomb scattering can be obtained by a straightforward extension of the equations of I, using the method of Gatha and Riddell.[21] In their work, the amplitude of the scattered wave was written as the sum of the Coulomb amplitude f_c plus a term which represents the departure from the Coulomb amplitude for the scattered waves with small l. This procedure was previously described by Schiff.[22] Following Gatha and Riddell,[21] it will be assumed for simplicity that the nuclear charge is uniformly distributed over a sphere of radius r_1. The complete phase shifts $\delta_l^\pm$ (including Coulomb scattering) are given by

$$\delta_l^\pm=\delta_{l,n}^\pm+\delta_{l,c}, \quad (9)$$

where $\delta_{l,n}^\pm$ and $\delta_{l,c}$ are the phase shifts due to the nuclear potential and the Coulomb potential, respectively. Thus $\delta_{l,n}^\pm$ is the $\delta_l^\pm$ given by Eq. (5). Gatha and Riddell[21] have obtained $\delta_{l,c}$ using the WKB method, which gives

$$\delta_{l,c}=\operatorname*{Lim}_{r\to\infty}\left[-\frac{E}{c^2\hbar^2k}\int_0^{[r^2-(l+\frac{1}{2})^2/k^2]^{\frac{1}{2}}}V_c\,dx+\chi\ln(2kr)\right], \quad (10)$$

where $\chi=\alpha\gamma k_0/k$ with $\alpha=Z/137$, $E=$totale nergy, $\gamma=E/Mc^2$ ($M=$mass of proton), $k_0=Mc/\hbar$. The integration path is along $y=(l+\frac{1}{2})/k$. V_c is the Coulomb potential given by

$$V_c=(3r_1^2-r^2)Ze^2/(2r_1^3), \quad (r<r_1) \quad (11)$$

$$V_c=Ze^2/r_1. \quad (r>r_1) \quad (11a)$$

The term $\chi\ln(2kr)$, which represents the distortion of the waves at large distances, has been included in (10) following the usual procedure. Gatha and Riddell[21] have obtained

$$\delta_{l,c}=\chi\ln\{\eta+[\eta^2-(l+\tfrac{1}{2})^2]^{\frac{1}{2}}\}-[\eta^2-(l+\tfrac{1}{2})^2]^{\frac{1}{2}}\times\{u_c-v[\eta^2+2(l+\tfrac{1}{2})^2]\} \quad (l+\tfrac{1}{2}<\eta) \quad (12)$$

$$\delta_{l,c}=\chi\ln(l+\tfrac{1}{2})\equiv\eta_l, \quad (l+\tfrac{1}{2}>\eta) \quad (12a)$$

where $\eta=kr_1$, $v=\chi/(6\eta^3)$, and

$$u_c=(3\gamma k_0Ze^2)/(2r_1k^2\hbar c). \quad (13)$$

In the equations of I, f is proportional to the scattered amplitude without change of the spin component along the direction of incidence of the proton, while g is proportional to the scattered amplitude with spin flip along the incident direction. Thus the Coulomb amplitude f_c must be included in f, while g is affected by the Coulomb potential only through the fact that $\delta_l^\pm$ contains $\delta_{l,c}$. One thus obtains

$$f=\sum_{l=0}^{l_m}[(l+1)B_l^+ + lB_l^-]P_l^0(\cos\theta) - \frac{\chi}{2}\csc^2\frac{\theta}{2}\exp\{i[\chi\ln(\csc^2\tfrac{1}{2}\theta)+2\eta_0]\}, \quad (14)$$

$$g=-\sum_{l=0}^{l_m}[B_l^+-B_l^-]P_l^1(\cos\theta), \quad (15)$$

where

$$B_l^\pm\equiv[\exp(2i\delta_l^\pm)-\exp(2i\eta_l)]/(2i); \quad (16)$$

l_m is the maximum l for which $\delta_{l,n}^\pm$ is appreciably different from zero, and $\delta_l^\pm$ is given by Eq. (9). The η_l are the Coulomb phase shifts for a point charge, as given by (12a). The term $\exp(2i\eta_l)$ is subtracted in (16) since it is already included in the Coulomb part of f [term $\propto\csc^2(\frac{1}{2}\theta)$]. Note that g depends only on the $\delta_l^\pm$ since

$$B_l^+-B_l^-=[\exp(2i\delta_l^+)-\exp(2i\delta_l^-)]/(2i). \quad (17)$$

The polarization P and the average cross section $\langle d\sigma/d\Omega\rangle$ are again obtained from the equations of I:

$$P=\frac{|f-ig|^2-|f+ig|^2}{|f-ig|^2+|f+ig|^2}, \quad (18)$$

$$\langle d\sigma/d\Omega\rangle=\tfrac{1}{2}k^{-2}[|f-ig|^2+|f+ig|^2], \quad (19)$$

in which f and g are given by (14) and (15). If the charge distribution is assumed nonuniform with a charge density $\rho(r)$, the Coulomb phase shifts are given by Eq. (10) with the appropriate expression for V_c:

$$V_c=4\pi e\left[r^{-1}\int_0^r\rho r'^2dr'+\int_r^\infty\rho r'dr'\right]. \quad (20)$$

In the calculations the charge radius r_1 was taken as $r_1=3.43\times10^{-13}$ cm, which is the radius of the sphere having the same volume as the effective volume over which the potential V extends [Eq. (8)]. After some preliminary calculations, it was found that a reasonable fit to the Berkeley data[6] inside the first diffraction maximum can be obtained with the parameters: $k_1=1.28\times10^{12}$ cm^{-1}, $K=2.56\times10^{12}$ cm^{-1}, and $\epsilon=7.5$ Mev. These values of k_1 and K correspond to a complex potential $V_r+iV_i=-(16.5+i16.5)$ Mev at the center of the nucleus. The energy assumed in these calcula-

[21] K. M. Gatha and R. J. Riddell, Phys. Rev. **86**, 1035 (1952).
[22] L. I. Schiff, *Quantum Mechanics* (McGraw-Hill Book Company, Inc., New York, 1949), pp. 119–120.

tions is $T=300$ Mev, as given in reference 6. The potential of Eq. (1) was assumed with $r_0=3.2\times10^{-13}$ cm and $a=0.49\times10^{-13}$ cm, as mentioned above. Figures 6(A) and 7(A) show the resulting curves for P and $\langle d\sigma/d\Omega\rangle$. It is seen that the fit for P is reasonably good throughout the first diffraction maximum up to 16°. The minimum of P at 16° is ~0.25 in agreement with the observed result. In the region of the second diffraction maximum between 16° and 26°, the calculated P is higher by ~0.2 than the observed values. This result was also found for other values of k_1 and K (see Figs. 2, 4, 5) and is not believed to be due to the choice of the parameters k_1, K, and ϵ. However, this discrepancy is probably not serious for the following reasons. In the region of the second diffraction peak, the intensity of the elastic scattering from the nucleus is small compared to the "quasi-elastic" component which is due to collisions of the incident protons with a single nucleon (accompanied by an appreciable energy loss). It is likely that the polarization of the "quasi-elastic" scattering[5–8] is smaller than the value of P expected from the diffraction scattering. If an appreciable number of quasi-elastic protons are included in the measurements, this would decrease the observed values of P. It has also been suggested by Heckrotte and Lepore[10] that the transparent nucleus model using the WKB approximation may become less accurate at the large angles involved for the second diffraction peak.

Figure 7(A) shows that the calculated values of $\langle d\sigma/d\Omega\rangle$ are in reasonable agreement with experiment for $\theta\lesssim14°$. For larger angles, the theoretical curve has a diffraction minimum followed by the second diffraction peak, while the experimental points show a uniform decrease, except for a flat region between 20° and 22°. Three possible reasons for this discrepancy have been considered: (1) Ruderman[23] has made a calculation of the angular distribution of the protons which have lost only a few Mev leaving the nucleus in an excited state. The maximum of this distribution occurs in the region of the first diffraction minimum for the elastic scattering. Since the experiment[6] includes protons which have lost less than ~20 Mev to the nucleus, it can be concluded that if this effect is appreciable for Al, it tends to fill in the first diffraction minimum of $\langle d\sigma/d\Omega\rangle$ obtained with the spin-orbit coupling U. (2) It is possible that a should be increased above the value used here (0.49×10^{-13} cm), giving a smoother nuclear boundary which would tend to fill in the minimum. Calculations have been carried out for the potential of Eq. (1) with $a=0.85\times10^{-13}$ cm and $a=1.2\times10^{-13}$ cm, as well as exponential and Gaussian shapes for the potential V. The spin-orbit coupling $U\propto(1/r)(dV/dr)$ was used in these calculations which are reported below. The cases considered gave values of $\langle d\sigma/d\Omega\rangle$ which are generally too small at large angles ($\theta\gtrsim20°$) and did not give a minimum of P near 16°, as is observed. Moreover, both for the Gaussian and for Eq. (1) with $a=0.85\times10^{-13}$ cm, the minimum of $\langle d\sigma/d\Omega\rangle$ persists.[24] In order for this minimum to disappear a considerable rounding of V is required. The minimum disappears for the exponential and the potential of Eq. (1) with $a=1.2\times10^{-13}$ cm, but in these cases, $\langle d\sigma/d\Omega\rangle$ was found to be too small by a factor ~10 near 20°. Aside from these inadequacies, an extremely rounded potential like the exponential appears to be ruled out by the electron scattering experiments.[25] (3) As mentioned above, the spin-orbit coupling U_2 which has been defined in I and II fills in the first diffraction minimum for the square well and harmonic oscillator potentials. U_2 is so defined that the corresponding spin-orbit coupling $U_2\mathbf{l}\cdot\boldsymbol{\sigma}$ is equivalent to an extra potential with sign depending on the spin direction. For the potential V of Eq. (1), U_2 has the approximate form

$$U_2\sim u_2(r_0^2/r^2)\{1+\exp[(r-r_0)/a]\}^{-1}, \tag{21}$$

where u_2 = constant. The corresponding Δ_l is given by[17]

$$\Delta_l=(k\epsilon_2/2T)A[(l+\tfrac{1}{2})/k], \tag{22}$$

where ϵ_2 = constant. It was found that for $\epsilon_2=12$ Mev the calculated values of $\langle d\sigma/d\Omega\rangle$ show a smooth decrease without any minimum near 16°, and are in reasonable agreement with experiment throughout the range of θ. The parameters k_1, K, r_0, and a had the same values as used above for the coupling U: $k_1=1.28\times10^{12}$ cm^{-1}, $K=2.56\times10^{12}$ cm^{-1}, $r_0=3.2\times10^{-13}$ cm, and $a=0.49\times10^{-13}$ cm. The curves of P and $\langle d\sigma/d\Omega\rangle$ for U_2 are shown in Figs. 6(B) and 7(B). It is seen that the calculated values of P are in fair agreement with experiment inside 12°, although too low by ~0.1. Near 16°, P decreases to zero, passing between the experimental points at 16° and 18°. However, between 18° and 26°, P remains very small (<0.12) in contrast to the experimental values which rise to a second maximum near 21°. It would be possible to increase P inside the first diffraction peak by increasing ϵ_2. However, this would also increase the values of $\langle d\sigma/d\Omega\rangle$ which are already somewhat too high for $\epsilon_2=12$ Mev (see below). Moreover, calculations indicate that an increase of ϵ_2 within reasonable limits ($\epsilon_2\lesssim20$ Mev) would not increase substantially the values of P between 18° and 26°. As a measure of the average magnitude of $\langle d\sigma/d\Omega\rangle$ for the complete range of θ, it seems reasonable to consider the integrated cross section in the range in which it has been measured,[6] i.e., from 8° to 26°. Thus we define σ_d as

$$\sigma_d\equiv2\pi\int_{8°}^{26°}\langle d\sigma/d\Omega\rangle\sin\theta d\theta. \tag{23}$$

[23] M. A. Ruderman (private communication).

[24] This was also confirmed by calculations with the coupling U_1 for the harmonic oscillator potential considered in II. One finds that even with large ϵ_1 (15 Mev) the minimum of $\langle d\sigma/d\Omega\rangle$ persists for the choice of parameters given in II.

[25] D. G. Ravenhall and D. R. Yennie, Phys. Rev. **96**, 239 (1954). See also Yennie, Ravenhall, and Wilson, Phys. Rev. **95**, 500 (1954).

The experimental value is $\sigma_d=40$ mb. For comparison, the calculations with U and U_2 as shown in Fig. 7 give $\sigma_d=43$ mb and 47 mb, respectively. It may be noted that the value of σ_d is determined to a large extent by K, since even for $k_1=0$, σ_d is appreciable. As shown below, the value $K=2.56\times10^{12}$ cm^{-1} represents a minimum and is probably somewhat too low. The only way of decreasing σ_d would therefore be to decrease k_1 or ϵ. However, for the coupling U, a decrease of k_1 or of ϵ results in a deeper minimum of $\langle d\sigma/d\Omega\rangle$ at 16° and, in general, gives poorer agreement for the P *vs* θ curve. A decrease of ϵ_2 for the coupling U_2 would lead to a minimum of $\langle d\sigma/d\Omega\rangle$ at 16° since U_2 must be large enough to fill in this minimum. A decrease of k_1 for this coupling generally increases the magnitude of the negative values of P near 20° [see Fig. 7(B)].

The total absorption cross section is given by[14]

$$\sigma_a=\frac{2\pi}{k^2}\sum_{l=0}^{l_m}(l+\tfrac{1}{2})(1-\exp\{-2KA[(l+\tfrac{1}{2})/k]\}). \quad (24)$$

With the above parameters, one obtains $\sigma_a=290$ mb. On the other hand, the experiments of Millburn *et al.*[26] give for Al, $\sigma_a=410$ mb at 290 Mev, while the measurements of Kirschbaum and Hicks[27] give $\sigma_a=334$ mb at 305 Mev. Although there are appreciable uncertainties due to the difficulties of the experiment (multiple Coulomb scattering, charged secondaries), it appears that the experimental value is somewhat larger than the calculated result. In order to obtain better agreement for σ_a, K was increased to 4×10^{12} cm^{-1} (r_0 and a being kept constant). For this K, Eq. (24) gives $\sigma_a=360$ mb. It was found that a dip of P of the proper magnitude (~0.25) at 16° is obtained for $k_1=10^{12}$ cm^{-1} and $\epsilon=7.5$ Mev (coupling U). A smaller k_1 would give a negative minimum of P, consistent with the fact that for $k_1=0$ the minimum is -1 (see Fig. 4). On the other hand, a larger k_1, namely 1.6×10^{12} cm^{-1} (with $\epsilon=9$ Mev), was found to give no minimum at 16°, P remaining large (~0.8) throughout this region.

For $k_1=10^{12}$ cm^{-1}, $\epsilon=7.5$ Mev, with $K=4\times10^{12}$ cm^{-1}, the curve of P *vs* θ is practically the same as that shown in Fig. 6(A) for $K=2.56\times10^{12}$ cm^{-1}. The corresponding curve of $\langle d\sigma/d\Omega\rangle$ is also very close to that shown in Fig. 7(A) for the lower K. However, the values of $\langle d\sigma/d\Omega\rangle$ in the region of the first diffraction peak are slightly higher, and one obtains $\sigma_d=47$ mb, which is ~20 percent above the measured value.[28] We conclude that throughout the range of K from 2.56×10^{12} cm^{-1} to 4×10^{12} cm^{-1}, one can obtain fair agreement for P and $\langle d\sigma/d\Omega\rangle$, although with increasing K the calculated σ_d tends to increase above the experimental value.

The preceding considerations for $K=4\times10^{12}$ cm^{-1} pertain to the spin-orbit coupling U. Calculations have also been carried out for the coupling U_2 [Eqs. (21), (22)]. It was found that for $k_1=1.2\times10^{12}$ cm^{-1}, $\epsilon_2=15$ Mev, with $K=4\times10^{12}$ cm^{-1}, the calculated $\langle d\sigma/d\Omega\rangle$ has no minimum at 16°, but decreases uniformly with θ, in the same manner as shown in Fig. 7(B) for $K=2.56\times10^{12}$ cm^{-1}. However, the values of $\langle d\sigma/d\Omega\rangle$ are rather high, and lead to $\sigma_d=54$ mb, as compared to the experimental result of 40 mb. Inside the first diffraction peak, the curve of P *vs* θ is close to the corresponding curve for $K=2.56\times10^{12}$ cm^{-1} shown in Fig. 6(B). However, the minimum of P at 18° is -0.34 instead of -0.06, so that the negative region of P is more pronounced. From these calculations for U and U_2, one can conclude that the general behavior of P and $\langle d\sigma/d\Omega\rangle$ does not change as K is increased from 2.56×10^{12} cm^{-1} to 4×10^{12} cm^{-1}. The former choice of K gives somewhat better agreement for P and $\langle d\sigma/d\Omega\rangle$ while the latter agrees more closely with the measured values of[29] σ_a.

The root-mean-square radius for the potential of Eq. (1) with $r_0=3.2\times10^{-13}$ cm ($=1.07A^{\frac{1}{3}}\times10^{-13}$ cm) and $a=0.49\times10^{-13}$ cm is given by

$$\langle r^2\rangle^{\frac{1}{2}}=\left(\int_0^\infty Vr^4dr\Big/\int_0^\infty Vr^2dr\right)^{\frac{1}{2}}=3.09\times10^{-13}\,\text{cm}, \quad (25)$$

which corresponds to $1.03A^{\frac{1}{3}}\times10^{-13}$ cm. This agrees within 10 percent with the rms radius which is needed to fit the electron scattering[30] and mesonic x-ray[31] experiments which require $\langle r^2\rangle^{\frac{1}{2}}\approx0.95A^{\frac{1}{3}}\times10^{-13}$ cm. When the present calculations were near completion, a letter of Ravenhall and Yennie[25] appeared, in which a fit was obtained for the electron scattering data of Hofstadter *et al.*[30] for gold at 125 Mev. The calculations were carried out using the potential of Eq. (1), and satisfactory agreement was obtained with the following sets of parameters: (1) $r_0=6.63\times10^{-13}$ cm$=1.14A^{\frac{1}{3}}\times10^{-13}$ cm, $a=0.45\times10^{-13}$ cm; (2) $r_0=6.19\times10^{-13}$ cm$=1.06A^{\frac{1}{3}}\times10^{-13}$ cm, $a=0.54\times10^{-13}$ cm. It is seen that the parameters used here lie in the range of the values (1) and (2) which fit the electron scattering.

For the charge density a uniform distribution extending up to $r_1=3.43\times10^{-13}$ cm was used in all of the

[26] Millburn, Birnbaum, Crandall, and Schecter, Phys. Rev. **95**, 1268 (1954).

[27] A. J. Kirschbaum, thesis, University of California Radiation Laboratory Report UCRL-1967 (unpublished).

[28] We also note that the minimum at 16° is more pronounced, being 4×10^{-4} barn/sterad as compared to 1.2×10^{-3} barn/sterad for $K=2.56\times10^{12}$ cm^{-1}.

[29] These values of K correspond to a cross section per nucleon, $\sigma=K/\rho(0)$ where $\rho(0)$ is the density at the center of the nucleus: $\rho(0)=27/[(4\pi/3)(3.43\times10^{-13})^3]=1.6\times10^{38}$ cm^{-3}. $K=4\times10^{12}$ cm^{-1} gives $\sigma=25$ mb, which is close to the average $\bar\sigma$ of the p-p and n-p cross sections at 300 Mev, $\bar\sigma=27$ mb [B. Rossi, *High Energy Particles* (Prentice-Hall, Inc., New York, 1952) p. 347]. The value $\sigma=16$ mb obtained with $K=2.56\times10^{12}$ cm^{-1} is somewhat too low, even after taking into account the Pauli Principle [M. L. Goldberger, Phys. Rev. **74**, 1269 (1948); S. Fernbach, Ph.D. dissertation, University of California, 1951 (unpublished)].

[30] Hofstadter, Fechter, and McIntyre, Phys. Rev. **92**, 978 (1953); Hofstadter, Hahn, Knudsen, and McIntyre, Phys. Rev. **95**, 512 (1954).

[31] V. L. Fitch and J. Rainwater, Phys. Rev. **92**, 789 (1953); L. N. Cooper and E. M. Henley, Phys. Rev. **92**, 801 (1953).

calculations. In order to check whether the results for $\langle d\sigma/d\Omega\rangle$ and P are sensitive to the shape of the charge distribution, a density proportional to V (i.e., $\rho\propto 1/\{1+\exp[(r-r_0)/a]\}$) was assumed, and the Coulomb potential V_c was calculated by numerical integration using Eq. (20). $\delta_{l,c}$ was then obtained from Eq. (10). These $\delta_{l,c}$ were used to recalculate $\langle d\sigma/d\Omega\rangle$ and P for the case $k_1=1.28\times10^{12}$ cm^{-1}, $K=2.56\times10^{12}$ cm^{-1}, $\epsilon=7.5$ Mev. The resulting phase shifts $\delta_{l,c}$ differ by less than 1° from those obtained with the uniform charge distribution and the values of $\langle d\sigma/d\Omega\rangle$ and P differ by a negligible amount ($\lesssim 5$ percent) throughout the range of θ. Hence the results are not sensitive to the precise shape of the charge distribution for Al.

The calculations which were carried out with central potentials different from that used above will now be described. Unless otherwise indicated, the calculations were done with the spin-orbit coupling $U\propto(1/r)(dV/dr)$. (1) A Gaussian $V_g\propto\exp(-r^2/r_g^2)$ with $r_g=2.02\times10^{-13}$ cm was used. For three cases considered, $\langle d\sigma/d\Omega\rangle$ still showed a pronounced diffraction minimum, in spite of the fact that the potential V_g has no sharp edge. (2) The potential of Eq. (1) was used with larger values of a. Calculations were carried out for the following parameters: (a) $r_0=3\times10^{-13}$ cm, $a=0.85\times10^{-13}$ cm; (b) $r_0=2.8\times10^{-13}$ cm, $a=1.2\times10^{-13}$ cm. For these cases, it was found that the scattering at large angles ($\theta\gtrsim20°$) is too small. Case (a) still gives a minimum of $\langle d\sigma/d\Omega\rangle$ at 16° while for case (b) $\langle d\sigma/d\Omega\rangle$ is approximately flat beyond 16°, but with values of order 1.5×10^{-3} barn/sterad which are considerably too small (see Fig. 7). Moreover, for case (b), P has no pronounced minimum near 16°. (3) An exponential potential was used: $V_e\propto\exp(-r/r_e)$ where $r_e=0.87\times10^{-13}$ cm. This value of r_e leads to a rms radius $\langle r^2\rangle^{\frac{1}{2}}=12^{\frac{1}{2}}r_e=3.0\times10^{-13}$ cm. For two cases which were calculated with V_e, it was found that $\langle d\sigma/d\Omega\rangle$ decreases uniformly with θ, without any minimum. However, the values of $\langle d\sigma/d\Omega\rangle$ are considerably too small for $\theta\gtrsim18°$ (of order 5×10^{-4} to 10^{-3} barn/sterad) and the curves of P have no minimum at 16°. Besides these potentials, calculations were also carried out for a square well and a harmonic oscillator shape. In accordance with the results of I, it was found that the square well gives a region of negative P (with $P\sim-1$) near the expected first diffraction minimum. It also tends to give too much scattering at large angles (>20°). Calculations for the harmonic oscillator shape with couplings U and U_2 indicate that the situation is very similar to that for the potential of Eq. (1).

It can be concluded that the smoothed uniform shape of Eq. (1) appears to give the best overall agreement with the data for Al. The appropriate values of r_0 and a are: $r_0=3.2\times10^{-13}$ cm, $a\sim0.5\times10^{-13}$ cm. While r_0 directly determines the angle $\theta_{\min}$ of the minimum of P, the value of a is not so critical, but it is probably less than 0.7×10^{-13} cm. For the "best" values of K and k_1, one finds: $K\sim3\times10^{12}$ cm^{-1}, $k_1\sim1.2\times10^{12}$ cm^{-1}, corresponding to a potential $V_r+iV_i\approx-(15.5+19.3i)$ Mev at the center of the nucleus. For the spin-orbit coupling U, a value $\epsilon\sim7.5$ Mev is required. This corresponds to a potential U [Eq. (2)] whose maximum (near $r=r_0$) is ~0.7 Mev. With this coupling, one obtains good agreement for P, including the position and magnitude of the dip at 16°. The agreement for $\langle d\sigma/d\Omega\rangle$ is reasonably good inside the first diffraction peak, but the calculations predict a deep diffraction minimum at 16°, which is not observed. There are two possible explanations for this discrepancy. (1) As shown by Ruderman,[23] the angular distribution of the inelastic scattering in which the nucleus is excited has a maximum at the expected first diffraction minimum for the elastic scattering. If this effect is appreciable for Al, it would fill in the minimum of $\langle d\sigma/d\Omega\rangle$. (2) The spin-orbit coupling may be of the form U_2 which is strongly peaked at the center of the nucleus. A value of $\epsilon_2=12$ Mev gives a uniform decrease of $\langle d\sigma/d\Omega\rangle$ with θ, in agreement with experiment.

III. DEPENDENCE OF POLARIZATION ON ENERGY

In this section it will be shown that P depends on energy only through the parameter $kr_0\sin\theta$ for a range of energies where k_1, K, and $k\epsilon/(2T)$ remain constant. The derivation is based on the formulas given in I in which the WKB approximation was used. No assumptions are made about the radial dependence of the central potential and the spin-orbit coupling. However, the result is restricted for protons to angles which are not too small, so that the Coulomb scattering can be neglected.

The functions f and g which enter into P [Eq. (18)] are defined as follows in the absence of Coulomb scattering[3]:

$$f=\sum_{l=0}^{l_m}[(l+1)A_l^{+}+lA_l^{-}]P_l^0(\cos\theta), \tag{26}$$

$$g=-\sum_{l=0}^{l_m}[A_l^{+}-A_l^{-}]P_l^1(\cos\theta), \tag{27}$$

where

$$A_l^{\pm}\equiv[\exp(2i\delta_l^{\pm})-1]/(2i), \tag{28}$$

and l_m is defined after Eq. (16). Let r_0 be a nuclear radius suitably defined in terms of the shape of the central potential V, e.g., the radius r for which V has one-half the value at the center of the nucleus. Let L be the largest integer for which $L+\frac{1}{2}<kr_0$. For a square well, l_m equals L, while for a potential with a tail, $l_m>L$. Thus for the potential V for Al considered in Sec. II, $kr_0=13.5$ and $L=13$, but the sums in (26) and (27) [or (14) and (15)] were taken up to $l_m=20$. Since the values of l_m are large for the energies considered here ($\gtrsim300$ Mev), the sums in Eqs. (26) and (27) will be replaced by integrals.[14] We also approxi-

mate the P_l^0 and P_l^1 by Bessel functions, as follows,[14]

$$P_l^0(\cos\theta)\approx J_0[(l+\tfrac{1}{2})\sin\theta], \tag{29}$$

$$P_l^1(\cos\theta)\approx\cos\theta(l+\tfrac{1}{2})J_1[(l+\tfrac{1}{2})\sin\theta]. \tag{30}$$

Let $\zeta\equiv l/L$, $\zeta_m\equiv l_m/L$. We have

$$f\approx L^2\int_0^{\zeta_m}\zeta(A_l^+ + A_l^-)J_0(\zeta L\sin\theta)d\zeta, \tag{31}$$

$$g\approx -L^2\int_0^{\zeta_m}\zeta(A_l^+ - A_l^-)\cos\theta J_1(\zeta L\sin\theta)d\zeta, \tag{32}$$

where terms of order 1 have been neglected in comparison with l. Since we are interested mainly in small angles, $\cos\theta$ will be replaced by 1 in (32).

$\delta_l^{\pm}$ is given by

$$\delta_l^{\pm}=-(k/2T)\left[\int_0^{\infty}(V_R+iV_I\pm Ul)dx\right]_{y=lr_0/L}, \tag{33}$$

where V_R and V_I are respectively the real and imaginary parts of the central potential; U is the spin-orbit coupling; the subscript indicates that the integral is to be evaluated for $y=lr_0/L$. Let $\alpha\equiv x/r_0$, $\beta\equiv y/r_0$, $\xi\equiv r/r_0$, and let

$$V_R(r)=V_R(0)F(\xi), \tag{34}$$

where $F(\xi)$ describes the radial dependence of $V(r)$. The integral involving V_R can be written

$$-\frac{k}{2T}\left[\int_0^{\infty}V_R dx\right]_{y=lr_0/L} = -\frac{kV_R(0)r_0}{2T}\int_0^{\infty}F[(\alpha^2+\zeta^2)^{\frac{1}{2}}]d\alpha. \tag{35}$$

The quantity $-kV_R(0)/(2T)$ is the optical parameter k_1 for the center of the nucleus. The integral over F will be called $\bar{A}(\zeta)$. One obtains

$$-\frac{k}{2T}\left[\int_0^{\infty}V_R dx\right]_{y=lr_0/L}=k_1r_0\bar{A}(\zeta). \tag{36}$$

For the special case of the Woods-Saxon potential,[12] $V_R(0)\approx V_r$, where V_r is defined after Eq. (1). In this case, $\bar{A}(\zeta)$ equals $A(\zeta r_0)/r_0$, where $A(y)$ is the function defined after Eq. (3).

Similarly, we have

$$V_I(r)=V_I(0)F(\xi). \tag{37}$$

In view of $-kV_I(0)/(2T)=K/2$, where K is the optical parameter for the center of the nucleus, one obtains

$$-\frac{k}{2T}\left[\int_0^{\infty}V_I dx\right]_{y=lr_0/L}=(K/2)r_0\bar{A}(\zeta). \tag{38}$$

For the spin-orbit coupling, let

$$U(r)\equiv -cG(\xi), \tag{39}$$

where c is a constant and $G(\xi)$ determines the radial dependence. The contribution to $\delta_l^{\pm}$ is

$$\Delta_l=\mp\frac{kl}{2T}\left[\int_0^{\infty}U dx\right]_{y=\zeta r_0}=\pm\frac{kcr_0L\zeta\bar{B}(\zeta)}{2T}, \tag{40}$$

where

$$\bar{B}(\zeta)\equiv\int_0^{\infty}G[(\alpha^2+\zeta^2)^{\frac{1}{2}}]d\alpha. \tag{41}$$

Note that for the special case of the potential (1), $\bar{B}(\zeta)$ is proportional to $B(\zeta r_0)$ as defined by Eq. (4). The maximum of the function $\zeta\bar{B}(\zeta)$ will be denoted by M, and let $C(\zeta)\equiv\zeta\bar{B}(\zeta)/M$, $[C(\zeta)\leqq 1]$. The spin-orbit parameter ϵ will be defined as follows in terms of the largest Δ_l [see Eq. (6)]:

$$kr_0\epsilon/2T=|\Delta_{l,\max}|=kcr_0LM/2T. \tag{42}$$

Therefore Δ_l can be written

$$\Delta_l=kr_0\epsilon C(\zeta)/(2T). \tag{43}$$

Upon inserting (36), (38), and (43) into (33), one obtains

$$\delta_l^{\pm}=(k_1+iK/2)r_0\bar{A}(\zeta)\pm(k\epsilon/2T)r_0C(\zeta). \tag{44}$$

The factor $k\epsilon/(2T)$ for the spin-orbit coupling is analogous to k_1 and K, and will be called k_s.

In view of (44), $\delta_l^{\pm}$ and hence $A_l^{\pm}$ is a function of the following parameters,

$$A_l^{\pm}=A_l^{\pm}(k_1r_0,Kr_0,k_sr_0,\zeta), \tag{45}$$

where the functional form of $A_l^{\pm}$ depends on the shape functions $F(\xi)$ and $G(\xi)$. Upon inserting (45) into (31) and (32), one sees that f/L^2 and g/L^2 depend on the following parameters: k_1r_0, Kr_0, k_sr_0, and $kr_0\sin\theta$. In forming the ratio (18) for P, the factors L^2 in (31) and (32) cancel, so that P is a function of the same parameters as f/L^2 and g/L^2:

$$P=P(k_1r_0,Kr_0,k_sr_0,kr_0\sin\theta). \tag{46}$$

This expression depends explicitly on k only through $kr_0\sin\theta$, in the same manner as the angular distribution without spin-orbit coupling.[14] However, it should be remembered that K, k_1, and k_s depend on the energy since they contain a factor k/T. The potentials $V_R(0)$, $V_I(0)$ and the parameter ϵ are also expected to vary with energy. Nevertheless, over a small energy interval where K, k_1, and k_s are approximately constant, the main change of the P *vs* θ curve is expected to be a shift of the points of the same P to different angles related by $k^{(1)}\sin\theta^{(1)}=k^{(2)}\sin\theta^{(2)}$, where $k^{(1)}$ and $k^{(2)}$ are the two wave numbers at which P is compared and $\theta^{(1)}$, $\theta^{(2)}$ are corresponding angles.

The cross section $\langle d\sigma/d\Omega\rangle$ averaged over spin-directions is given by Eq. (19). In view of (31), (32), and (45), one obtains

$$\langle d\sigma/d\Omega\rangle = k^2 r_0^4 \varphi(k_1 r_0, K r_0, k_s r_0, k r_0 \sin\theta), \qquad (47)$$

where φ is a function of the same parameters as P. Assuming that the dependence on the first three parameters is weak, one can easily verify that (47) gives correctly the main dependence of the total diffraction cross section σ on r_0. The range of θ over which $\langle d\sigma/d\Omega\rangle$ is appreciable varies as $1/(kr_0)$, the corresponding solid angle goes as $1/(k^2 r_0^2)$. Upon multiplying this factor by $\langle d\sigma/d\Omega\rangle$ one obtains the expected result that $\sigma \propto r^2$.

IV. POLARIZATION EFFECTS IN TRIPLE SCATTERING EXPERIMENTS

It has been shown by Wolfenstein[15] that additional information about f and g can be obtained from a measurement of asymmetries in a triple-scattering experiment. The triple scattering yields additional information not obtained from the polarization observed in double scattering if the plane of the second scattering is not the same as the plane of the first scattering, and, in particular, if the two planes are at right angles to each other. As shown by Wolfenstein,[15] the asymmetry of the triple scattering involves the function R given by

$$R = (1-P^2)^{\frac{1}{2}} \cos(\theta-\beta), \qquad (48)$$

where θ is the angle of deflection of the nucleon in the second scattering, P is the corresponding polarization, and β is defined by[15]

$$\sin\beta = -\frac{4(f_r g_r + f_i g_i)}{(1-P^2)^{\frac{1}{2}}[|f+ig|^2+|f-ig|^2]}, \qquad (49)$$

$$\cos\beta = \frac{2[|f|^2-|g|^2]}{(1-P^2)^{\frac{1}{2}}[|f+ig|^2+|f-ig|^2]}. \qquad (50)$$

Equation (49) shows that β involves the real part of f^*g whereas P involves the imaginary part. The asymmetry of the triple scattering when the first and second scattering planes are at right angles is given by[15]

$$e = P_1 R P_3, \qquad (51)$$

where P_1 and P_3 are the polarizations for the first and third scattering, respectively.

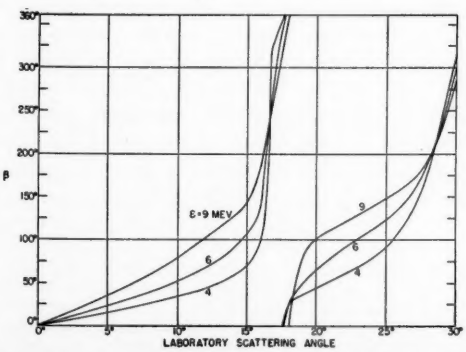

FIG. 8. β *vs* θ for 316-Mev neutrons scattered from Al, calculated for the Woods-Saxon potential with $k_1/K \approx 0.5$ ($k_1 = 0.86 \times 10^{12}$ cm^{-1}, $K = 1.7 \times 10^{12}$ cm^{-1}).

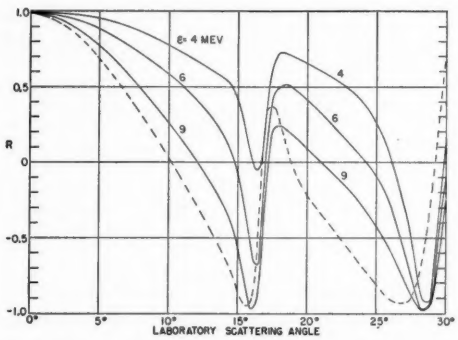

FIG. 9. R *vs* θ for 316-Mev neutrons scattered from Al, calculated for the Woods-Saxon potential with $k_1/K \approx 0.5$ ($k_1 = 0.86 \times 10^{12}$ cm^{-1}, $K = 1.7 \times 10^{12}$ cm^{-1}). The broken curve corresponds to $\epsilon = 9$ Mev, with the sign of β reversed [Eq. (48)].

The functions β and R were calculated for several cases for Al, using the functions f and g determined above from the Woods-Saxon potential. In addition, calculations were carried out for the square well[3] and harmonic oscillator potentials[9] for Be used in I and II. Figure 8 shows β *vs* θ for Al for the cases $\epsilon = 4$, 6, and 9 Mev with $k_1 = 0.86 \times 10^{12}$ cm^{-1} and $K = 1.7 \times 10^{12}$ cm^{-1}; the corresponding values of P are given in Fig. 2. It is seen that β increases from 0° at $\theta = 0°$ to 360° at the first diffraction minimum ($\theta \approx 18°$) and increases again by $\sim 300°$ between $\theta \approx 18°$ and 30° in the region of the second diffraction peak. This behavior was found in most of the cases where β was calculated. It may also be noted from Fig. 8 that inside the first diffraction peak, β is approximately proportional to ϵ; a similar proportionality is found for P (see Figs. 2, 4, and 5). Figure 9 shows R *vs* θ for the three cases for Al corresponding to Fig. 8. The negative regions of R are due to the fact that β goes through 360°. Inside the first diffraction peak R is appreciably smaller than 1. This should manifest itself in a reduction of the asymmetry $e = P_1 P_3$ which would be expected from the first and third scatterings alone [see Eq. (51)]. The broken curve of Fig. 9 corresponds to $\epsilon = 9$ Mev, but differs from the full curve for the same ϵ in that the sign of β has been reversed. This curve was calculated in accordance with the following suggestion of Wolfenstein.[15] Consider a situation in which the sign of the spin-orbit coupling would be reversed, while leaving its magnitude as a function of r [and also the potential $V(r)$] unchanged. This would interchange B_l^+ and B_l^- with the resulting transformation $g \rightarrow -g$, while f would remain

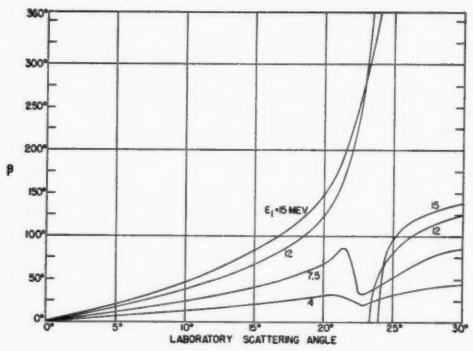

FIG. 10. β *vs* θ for 316-Mev neutrons scattered from Be, calculated for the harmonic oscillator potential with coupling U_1 (reference 9).

approximately unchanged.[32] As a result, $P \rightarrow -P$ and $\beta \rightarrow -\beta$. In a double scattering experiment only the product of two polarizations is measured, and there is, therefore, no way of determining the sign of the spin-orbit coupling. However, as pointed out by Wolfenstein,[15] the magnitude of R depends on the sign of β and can be used to determine the sign of the spin-orbit coupling. As shown by Fig. 9, the difference between the two curves of R is appreciable, so that it may be possible to use this method if sufficiently accurate triple-scattering experiments are carried out.

For the coupling U for Al, with the choice of constants used in Figs. 6(A) and 7(A), the functions β and R are qualitatively similar to those of Figs. 8 and 9 for $\epsilon=6$ and 9 Mev. Thus β passes through 360° at $\theta\approx 18°$. The corresponding R is negative between $\theta\approx 15.5°$ and 17.5° and for larger angles becomes positive again with values ~ 0.2. For the coupling U_2 used in Figs. 6(B) and 7(B), β passes through 90° at $\theta\approx 14°$ and slowly rises to 340° at $\theta=30°$. The corresponding R is negative between $\theta\approx 15°$ and 21°.

[32] In this transformation, f goes into

$$\hat{f}\equiv\sum_{l=0}^{l_m}[lB_l^{+}+(l+1)B_l^{-}]P_l^0(\cos\theta)$$

which is $\approx f$ if $l_m \gg 1$ so that $l \gg 1$ for most phase shifts.

For the square well potential for Be with the coupling U_1, considered in I, the behavior of β is similar to that shown in Fig. 8. β increases rapidly to 360° at $\theta\approx 20°$, resulting in a region of negative R. Figure 10 shows β for Be, as obtained from the harmonic oscillator potential with the coupling U_1, which was used in II. For small values of the parameter ϵ_1, β remains smaller than 90° throughout the first diffraction minimum, while for large ϵ_1 the behavior of β is the same as shown in Fig. 8. The corresponding curves of R are shown in Fig. 11. It is seen that for $\epsilon_1=4$ and 7.5 Mev, where

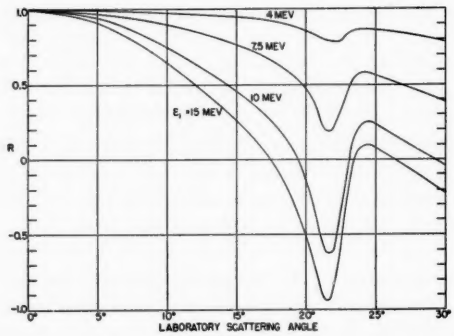

FIG. 11. R *vs* θ for 316-Mev neutrons scattered from Be, calculated for the harmonic oscillator potential with coupling U_1 (reference 9).

$\beta<90°$, R remains positive throughout the range of θ, while for large ϵ_1 (12 and 15 Mev), R has a negative region.

For the special case of a pure absorptive potential ($k_1=0$), β is zero since $f_r=g_i=0$. Hence R is given by

$$R=(1-P^2)^{\frac{1}{2}}\cos\theta. \quad (k_1=0) \qquad (48a)$$

In this case, R oscillates between 0 (for $P=\pm 1$) and $\cos\theta$ (for $P=0$).

I would like to thank Dr. George A. Snow for many stimulating discussions which helped greatly in completing this work. I am also indebted to Professor E. Fermi, Dr. R. Jastrow, and Dr. L. C. L. Yuan for valuable comments.

Yields of Photonuclear Reactions with 320-Mev X-Rays.* I. Experimental Results

R. J. Debs,† J. T. Eisinger,‡ A. W. Fairhall,§ I. Halpern,§ and H. G. Richter‖
Laboratory for Nuclear Science, Massachusetts Institute of Technology, Cambridge, Massachusetts
(Received September 20, 1954)

Several medium weight target elements were irradiated by 320-Mev bremsstrahlung. For each target, relative yields were determined for the production of a number of radioactive nuclides.

INTRODUCTION

HIGH-ENERGY photons are known to eject mesons, nucleons, and heavier nuclear fragments from nuclei. Some of these particles seem to be emitted as a result of the direct action of the photons and some seem to be emitted as evaporation fragments from an excited nucleus. The final unexcited nucleus remaining after all the emissions in a given interaction have taken place is often radioactive. When it is, one can determine its production rate by radiochemical techniques. A study of such production rates proves to be helpful in understanding the processes by which the particle emissions take place. In the experiment to be described, the relative production rates or yields of a large number of nuclides have been measured for several target elements of middle atomic weight exposed to 320-Mev bremsstrahlung radiation.

An examination of the distribution of the observed yields reveals strong similarities between the yield patterns observed in this experiment and in bombardments by high-energy particles. Indeed it appears that some of the chief features of observed yield distributions are to a surprising extent independent of both the nature of the incident particle and its energy. In the following paper these features are discussed in some detail and it is shown that they can be accounted for in a semiquantitative way by assuming that the emission of the last few nucleons by a highly excited nucleus is described by the "evaporation" theory of Weisskopf.

The results given here differ, in part, from the high-energy particle-induced reactions (so-called spallation reactions) in that for x-ray irradiation there occur relatively more reactions involving the emission of just one or two nucleons. These emissions are presumably due to those photons in the 320-Mev bremsstrahlung spectrum that have energies of about 20 Mev. This energy corresponds to the giant resonance for photon absorption.

* This work was supported in part by the joint program of the Office of Naval Research and the U. S. Atomic Energy Commission.
† Now at Stanford University.
‡ Now at Bell Telephone Laboratories.
§ Now at the University of Washington.
‖ Now at the U. S. Radiological Defense Laboratory, San Francisco, California.

EXPERIMENTAL PROCEDURES AND RESULTS

The targets used in this experiment were copper, zinc, gallium, germanium, and arsenic. These elements form a group having consecutive atomic numbers. It was decided to study such a group rather than a single element because a large fraction of the photoreactions were expected to lead to stable isotopes and it was felt that the study of just one target element might not provide enough significant information. This particular group of elements was chosen because the periods and radiations in this region of the isotope chart are exceptionally convenient for counting.

The targets consisted of a few grams of material and were exposed at about 2 feet from the x-ray target of the Massachusetts Institute of Technology synchrotron. A typical exposure lasted for several hours, and at its conclusion, quantitative chemical separations were made of the target element and of a number of elements having lower atomic numbers. The precipitates were counted on a set of end-window Geiger counters whose efficiencies had been determined as a function of source thickness and β energy. The counting was usually continued until the rate was very near that of the background. The initial rates of the various activities present were then determined from an analysis of the time-dependence of the counting rate. Corresponding saturation rates were computed and normalized for x-ray beam intensity, which was measured by the amount of 12.9-hr Cu^{64} activity in a standard copper foil irradiated together with the target. After correcting for chemical efficiencies, counting efficiencies and branching ratios, it is possible to express the data in the form of "yields." A yield is the production rate of a given radio-nuclide per g/cm^2 of target element when a standard amount of x-ray energy is being passed through the target per unit time.

The yields determined in this way are listed in Table I in arbitrary units. A number of remarks should be made about the interpretation of the data in this table.

All of the targets except arsenic have more than one isotope. This fact usually makes the assignment of parent isotopes for observed radio-nuclides uncertain. An exception to this ambiguity occurs when the radio-nuclide can be produced by a (γ,n) reaction. For example, the yield of Cu^{62} in a copper bombardment is due either to a (γ,n) reaction on Cu^{63} or a $(\gamma,3n)$

TABLE I. Relative production rates of observed radio-nuclides per g/cm² of target element through which a standard amount of x-ray energy is passed per unit time.

Target	Observed nuclide	Yield
Arsenic	As^{74}	1050
	As^{72}	100
	Ga^{73}	1.3
	Ga^{72}	3
	Ga^{68}	13
	Zn^{73}	0.1
	Zn^{69}	1.9
	Cu^{67}	0.3
	Cu^{64}	2.5
	Cu^{61}	0.75
	Ni^{66}	0.016
	Ni^{65}	0.11
	Co^{61}	0.17
	Co^{55}	0.01
Germanium	Ge^{75}	130
	Ge^{69}	310
	Ga^{73}	26
	Ga^{72}	18
	Ga^{68}	20
	Zn^{69}	3.8
	Cu^{67}	1.2
	Cu^{64}	3.6
	Cu^{62}	5.2
	Cu^{61}	2.3
Gallium	Ga^{68}	600
	Ga^{66}	18
Gallium	Zn^{69}	16
	Cu^{67}	1.7
	Cu^{64}	13
	Cu^{61}	3.2
	Ni^{66}	0.2
	Ni^{65}	0.8
	Co^{61}	0.4
	Co^{55}	0.09
	Mn^{56}	0.4
Zinc	Zn^{63}	540
	Zn^{62}	34
	Cu^{67}	13
	Cu^{64}	22
	Cu^{62}	73
	Cu^{61}	20
	Ni^{66}	0.16
	Ni^{65}	0.39
Copper	Cu^{64}	270
	Cu^{62}	470
	Cu^{61}	83
	Ni^{57}	0.83
	Co^{61}	3
	Co^{55}	0.4
	Mn^{56}	1.4
	Mn^{52}	0.6
	Cr^{49}	0.24

reaction on Cu^{65}. But measured (γ,n) yields are roughly twenty times larger than $(\gamma,3n)$ yields, so that it is quite certain that almost all of the Cu^{62} comes from the parent Cu^{63}. Assuming that all of the observed Cu^{62} does indeed come from Cu^{63}, it is possible, by taking the abundance of Cu^{63} into account, to convert the yield in the table into a more useful quantity. That is, one can obtain a yield per g/cm² of *parent* isotope instead of a yield per g/cm² of target element.

Unfortunately, for yields of reactions more complicated than the (γ,n) reaction, the proper assignment becomes less apparent and in fact rather uncertain. The general problem of yield assignments is connected with that of the interpretation of the yields and is discussed in the following paper.

It should be pointed out here that the yields in the table are not all necessarily primary yields because the observed radio-nuclides are not all "shielded" nuclides. In spite of this, most of the measured yields are probably predominantly primary because the experimental results indicate that the yields tend to decrease very rapidly for nuclides away from the stable valley of the nuclides. This would imply that the contributions of any "fed-in" yield are smaller than the original yield of any radio-nuclide being considered.

In addition to possible errors of the type just considered, that can come about from misinterpretations of the data, the experiment suffers from a number of more conventional sources of error. An observed yield of 0.1 corresponds, for reasonably short periods and reasonable decay schemes, to an initial counting rate of about ten counts a minute. For most of the data the yields are larger than 0.1 and the statistical errors on the observed counting rates are quite small. But the "initial rates" are not unambiguously determined except for samples decaying with only one period. The back-extrapolation of counting rate data to determine the initial rates is rather sensitive to the assumed periods and somewhat more sensitive to statistical errors than one might at first suspect. In every case the analysis of the decay curves was based on the half-lives compiled in *Nuclear Data*.[1] Most of the initial rates determined from the decay curves are probably good to ±20 percent although some of the lower rates are not known as well. The reliability of the initial rate determinations was tested empirically by having a number of people independently analyze some of the decay curves into component periods.

The "initial rate" data were converted into "saturation rates" without much additional error, but the corrections for Geiger counter efficiencies and the uncertainties in assumed branching ratios tend to increase the probable error of a typical yield datum to about ±50 percent. This would be a large error in some experiments, but in the present experiment the yields cover a range of over 10^5 and an error of even a factor of 2 represents only $\frac{1}{16}$ of this range on a logarithmic scale.

In certain cases, activities produced by either fast or slow neutrons in the synchrotron chamber could have contributed to the yields in the table. But measurements of the slow and fast neutron fluxes at the position of our targets showed that contributions to the observed yield by neutron-induced reactions were negligible. It should also be mentioned that the targets were kept thin enough so that there was no appreciable distortion of the x-ray spectrum as the x-ray beam passed through the target.

We are very grateful to Dr. J. S. Clark for his indispensable help in keeping the intensity of the synchrotron at the high level that was needed for most of the runs.

APPENDIX OF CHEMICAL PROCEDURES

The target material is dissolved, and a standard amount of carrier solution of each of the elements to be separated is added. The mixture is then processed according to one of the procedures outlined below, the final precipitates being weighed before being counted. The chemical yield of any given element is calculated by determining the weight of precipitate obtained from a known amount of the carrier solution.

Specific Separations

(*1*) *Chromium, Manganese, Cobalt, Nickel, and Copper from Copper*

Copper turnings are used as the target material. They are dissolved in HCl-H_2O_2 and carriers are added. The copper is then reduced to the metal with powdered iron, and centrifuged from the solution. After oxidation with H_2O_2 the iron is extracted from

[1] *Nuclear Data*, National Bureau of Standards Circular 499 (U. S. Government Printing Office, Washington, D. C., 1950).

the solution with dichloroethyl ether and discarded. A treatment with $NaOH$-Na_2O_2 precipitates nickel, cobalt, and manganese, and extracts the chromium in the form of chromate, which is precipitated with barium. The manganese is left in the form of MnO_2, and an extraction with concentrated HNO_3 separates it from nickel and cobalt. The MnO_2 is dissolved in HCl, reprecipitated with Na_2O_2, extracted with HNO_3, filtered and dried at 110°C. Nickel is precipitated with dimenthylglyoxime and then cobalt is precipitated with α-nitroso β-naphthol reagent.

(2) *Chromium, Manganese, Cobalt, Nickel, Copper, Zinc, and Gallium from Gallium*

Acid-soluable gallium oxide prepared by the decomposition of the nitrate at 250°C is used as the target. The target is dissolved in concentrated HNO_3 and carriers are added. Then the nitrates are converted to chlorides by fuming with HCl. Gallium is extracted with dicholoroethyl ether from 6*N* HCl solution and back extracted into water; an aliquot is precipitated with 8-hydroxyquinoline ("oxine") for counting.

Copper is reduced to metal with granulated tin. Zinc and chromium are separated by treatment with Na_2O_2. The chromium as chromate is precipitated with barium, and the zinc is precipitated with mercuric thiocyanate reagent. Manganese, cobalt, and nickel are separated as in Part (1).

(3) *Manganese, Cobalt, Nickel, Copper, Zinc, and Gallium from Germanium and Arsenic*

Germanium oxide or arsenious oxide are used as targets. The oxide is dissolved in a minimum of concentrated NaOH, after which the solution is made slightly acid with HCl. The carriers are added and precipitated with excess potassium ferrocyanide. An aliquot of the supernatant solution may be precipitated with H_2S to obtain germanium or arsenic activities.

The precipitated ferrocyanides are fumed with H_2SO_4 and the residue is dissolved in HCl. Copper is precipitated with granulated tin, which also reduces iron to the divalent state. Gallium is extracted with dichloroethyl ether, back extracted into water and precipitated with oxine.

Iron is then oxidized with H_2O_2, extracted with dichoroethyl ether and discarded. Zinc is separated by treatment with Na_2O_2, and precipitated for counting with mercuric thiocyanate. Manganese, cobalt, and nickel are separated as in Part (1).

PHYSICAL REVIEW VOLUME 97, NUMBER 5 MARCH 1, 1955

Yields of Photonuclear Reactions with 320-Mev X-Rays. II. Interpretation of Results*

I. HALPERN,† R. J. DEBS,‡ J. T. EISINGER,§ A. W. FAIRHALL,† AND H. G. RICHTER‖
Laboratory for Nuclear Science, Massachusetts Institute of Technology, Cambridge, Massachusetts

(Received September 20, 1954; revised manuscript received December 8, 1954)

It is convenient to separate the yields of radio-nuclides obtained in the work described in the preceding paper into two groups. The first group consists of the yields of nuclides which are only one or two mass units lighter than the target. All of the yields in this group, and especially those corresponding to (γ,n) reactions, are relatively large. They are due mainly to photons in the giant resonance region ($h\nu \sim 20$ Mev) of the x-ray spectrum, and account for most of the nuclear events produced in medium-weight targets by 320-Mev x-rays.

The yields of those radio-nuclides which are more than a few mass units lighter than the target are in many ways more interesting than the ones in the first group. They are found to exhibit a simple pattern very similar to those obtained in particle-induced high-energy reactions. It is shown that such patterns are at least qualitatively consistent with models of high-energy nuclear reactions in which the last few particles emitted from a struck nucleus, leave by "evaporation." Indeed the evaporation of these last particles exerts so strong an influence on the form of the observed yield pattern, that it becomes very difficult to say anything about either the nature of the original nuclear events or the emission of the first few particles on the basis of a study of yield patterns.

Finally, a rough quantitative comparison is made of the yields of radio-nuclides and the reported yields of neutrons and other particles emitted from medium-weight nuclei irradiated with 320-Mev x-rays.

IN the preceding paper, a number of relative yields are reported for the formation of radio-nuclides from the irradiation of medium weight elements by high-energy x-rays. In the following two sections, the yields for radio-nuclides which are more than a few mass units lighter than the target are shown to fall into simple patterns. These patterns are described quantitatively in Sec. 3 and it is shown that they are evidence for a major role of nuclear evaporation in high-energy photoreactions. It is found in Sec. 4 that the pattern described here is quantitatively very similar to patterns constructed from data of high-energy particle-induced reactions. An attempt is made in Sec. 5 to account for all of these patterns in a semiquantitative way by assuming that the last few particles ejected in a high-energy reaction are evaporated. Section 6 deals with those photoreaction yields in which the observed nuclide is only a few mass units lighter than the target. Finally, in Sec. 7, the data of this experiment are compared to data for neutron production and meson production by high-energy x-rays.

1. YIELDS FROM ARSENIC

When the work described in the preceding paper was undertaken, only a few measurements had been made of the distribution of the residual nuclides in high-

* This work was supported in part by the joint program of the Office of Naval Research and the U. S. Atomic Energy Commission.

† Now at the University of Washington.

‡ Now at Stanford University.

§ Now at Bell Telephone Laboratories.

‖ Now at the U. S. Naval Radiological Defense Laboratory, San Francisco, California.

energy nuclear reactions and none of these were for photoreactions. It was decided to observe photonuclear yields from a set of targets having consecutive atomic numbers in order to obtain a sufficient amount of data to establish any regularities of yield pattern.

Of the five elements used as targets, arsenic is the only one that is monoisotopic and its yields are therefore the easiest to interpret. The arsenic yields are plotted in Fig. 1 in a way designed to exhibit their regularity. It is seen that if the yields are expressed as a function of the atomic number and the atomic weight of the observed radio-nuclide, this function can be represented by a simple smooth surface. Lest it appear that the data of Fig. 1 seem rather meager for this conclusion, it should be mentioned that the data obtained from the other targets agree with the pattern for arsenic. Moreover, very similar surfaces have been reported for high-energy particle-induced reactions.[1,2]

Among the noteworthy features of the surface of Fig. 1 are the following: (1) The peak yields for any separated element occur near the stable valley of the nuclear energy surface (see Table I). (2) The yields of the various separated elements lie on very similar curves. (3) Corresponding points on these curves are separated by a constant factor of 2.3 in yield for each unit change in atomic number of the observed nuclide.

It should also be mentioned that the observed yields do not fit the pattern of Fig. 1 if the difference in atomic number between target and observed nuclide, ΔZ, is less than 2. These yields will be discussed separately (Sec. 6).

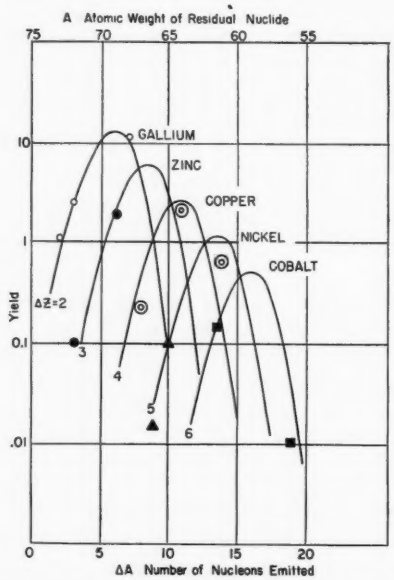

FIG. 1. The photonuclear yields from arsenic with 320-Mev x-rays, plotted as a function of ΔA, the number of nucleons emitted. Identical curves have been drawn through the data for each value of ΔZ, the change in nuclear charge in the reaction.

[1] E. Belmont and J. M. Miller, Phys. Rev. **95**, 1554 (1954).
[2] Rudstam, Stevenson, and Folger, Phys. Rev. **87**, 358 (1952).

TABLE I. The peaks of the yield surface in the photodisintegration of arsenic.

Separated element	Z	The atomic weight at the center of the stable valley[a]	The atomic weight at the peak of the yield surface
Gallium	31	69.4	69.0
Zinc	30	67.0	66.4
Copper	29	64.5	64.0
Nickel	28	61.4	61.3
Cobalt	27	58.9	58.8

[a] These numbers are based on characteristics of the nuclear energy surface described in reference 20.

2. YIELD SURFACES FOR THE TARGETS COPPER TO GERMANIUM

The comparison of yields from targets having more than one isotope to the yields from arsenic involves a certain amount of uncertainty. For multi-isotope targets each observed yield is a superposition of the yields from the various isotopes, and there is unfortunately no way of knowing how much each isotope contributes to the yield. In order to be able to see whether the yield patterns for such targets are consistent with the pattern for arsenic, it is necessary to assume some scheme for dividing up an observed yield among its possible parents.

The simplest such assumption, which will be called scheme 1, is that all target isotopes contribute to every yield in proportion to their abundance. Such an assumption would certainly not apply to yields which correspond to the emission of only one or two particles, but it might be reasonable for reactions in which $\Delta Z \geqslant 2$. In essence this assignment scheme assumes that the observed yield pattern is to a large measure independent of the exact mass of the target isotope.

The second procedure for dividing up yields, scheme 2, is also fairly easy to apply, but unlike scheme 1, it stresses the effect of the target mass on the observed distribution. In this scheme, one assumes that the relative probability of any two *reactions* is the same for all target isotopes.

Thus according to scheme 1, the yield of Co^{61}, for example, would be expected to be the same from a gram of Ga^{69} as from a gram of Ga^{71}. According to scheme 2, the yield of Co^{61} from Ga^{71} would be the same as the yield of Co^{59} from Ga^{69}.

In order to examine the consistency of the data under the assumption of scheme 1, the arsenic data of Fig. 1 were replotted to fall on a single curve in the following way. First each yield was multiplied by the factor $(2.3)^{\Delta Z}$. This brought all of the curves in Fig. 1, up to the same horizontal level. Then each modified yield point was replotted as a function of the "distance" of the corresponding radio-nuclide from the center of

the stable valley. By this distance we mean $(A-A_s)$, where A is the mass of a radio-nuclide and A_s is the mass at the center of the stable valley for the atomic number of the radio-nuclide. All of the arsenic data were made, in this way, to lie very nearly on the same simple curve. The next step was to treat the data for the other targets in exactly the same way. If it were now found that all of the data fell on a single curve, it would mean that all of the targets have an identical yield surface and the assumption underlying scheme 1 is correct. The data plotted in this way are shown in Fig. 2. This way of representing the data is very similar to the approach used by Belmont and Miller.[1]

In applying scheme 2, one begins again by replotting the arsenic data so that they lie on a single curve. The ordinate is once again the yield multiplied by $(2.3)^{\Delta Z}$ but the abscissa this time is related to ΔA, total number of nucleons emitted. In fact, it is $\Delta A-\Delta A_Z$ where ΔA_Z is the most probable number of nucleons emitted from arsenic when Z protons are lost. An example will show how data from targets other than arsenic are treated. Let Y represent the observed yield of Co^{61} in a copper bombardment. Some of Y is due to a $(\gamma,2p)$ reaction on Cu^{63} and some to $(\gamma,2p2n)$, possibly (γ,α), on Cu^{65}. According to the arsenic yield surface the second reaction is about eight times as probable as the first, but Cu^{63} is roughly twice as abundant as Cu^{65}. Hence $0.2Y$ is assigned to Cu^{63} and $0.8Y$ to Cu^{65}. These data can now be treated like the arsenic data and plotted on the same graph. (Fig. 3).

It is seen from Figs. 2 and 3 that either scheme, and especially scheme 1, serves to demonstrate a fairly consistent behavior of target nuclides in the copper-to-arsenic mass region. Scheme 1 does as well as one might expect considering only the experimental uncertainty in the data.

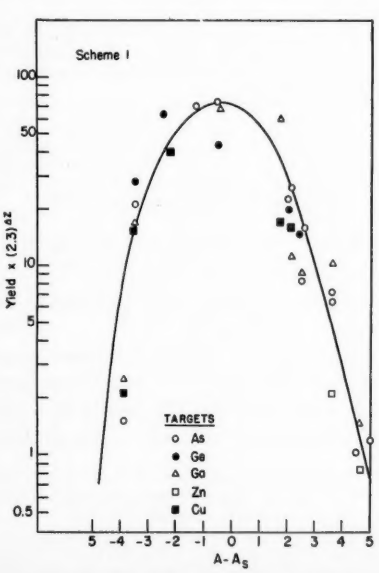

FIG. 2. Photonuclear yields with 320-Mev x-rays, plotted as a function of the distance (in units of atomic weight) of the observed nuclide from the center of the stable valley.

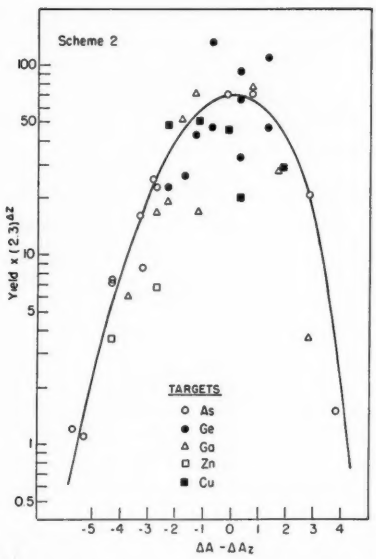

FIG. 3. Photonuclear yields with 320-Mev x-rays, plotted as a function of the number of nucleons emitted in the observed reaction. ΔA_Z is the most probable number of nucleons emitted for a given ΔZ according to the arsenic yield surface.

In a sense schemes 1 and 2 represent extreme assumptions about the nature of high-energy reactions. In general a given yield might be expected to depend on the nature of both the target and residual nuclides. According to scheme 1, there is practically no dependence on the target nuclide. Yields are determined by the location of the final nuclide with respect to the stable valley. According to scheme 2, any special properties of the residual nuclides have no bearing at all on the final distribution. The yield surface location depends only on the target nuclide location.

The fact that scheme 1 organizes the data somewhat more consistently than scheme 2 may indicate that the truth lies closer to the assumptions of scheme 1. That is, the shape of the yield surface depends more on the properties of the observed nuclides than on those near the starting point of the photoreaction. Such a conclusion is consistent with a strong role for evaporation processes in high-energy reactions. For according to an evaporation model, the probability of emitting a neutron or a proton from a given excited nucleus during a reaction does not depend on how many neutrons or protons have already been evaporated. The starting point of the reaction is easily forgotten. All that counts are the excitation energy and the binding energies of various particles to the intermediate nucleus. Since the relative neutron and proton binding energies are related to the position of the nuclide on the nuclear

energy surface, one might expect final yield patterns to be related to the nuclear energy surface.

In order to make more quantitative arguments for the role of nuclear evaporation in high-energy reactions, it is necessary to describe the photonuclear yield surfaces in somewhat more detail.

3. SHAPE OF THE YIELD SURFACE

The surface described in Figs. 1 and 2 is an inverted trough held at an angle to the plane of the isotope chart (see Fig. 4). It is possible to characterize this surface with three parameters: (1) The distance of the ridge from the stable valley. In the present experiment, the ridge stays fairly parallel to the valley at about half a mass unit to the neutron-deficient side. (2) The tilt of the ridge with respect to the N–Z plane. The ridge yield drops off by a factor of 2.3 for each unit change in Z. (3) The width of the trough. The width at half maximum seems to remain fairly constant and will be discussed in detail.

Although one might be tempted to interpret the closeness of the ridge to the stable valley as evidence for the role of evaporation in high-energy photoreactions, such an interpretation would not be entirely justifiable. If for any reason at all, proton emission happens to be on the average about $\frac{2}{3}$ as probable as neutron emission in this mass region, the peak yields would tend to occur near the stable valley.

It is the behavior of the third parameter, the yield surface width, that is the strongest evidence for the importance of nuclear evaporation in high-energy reactions. The particular value of the observed width as well as the fact that it stays nearly constant give evidence for the role of the nuclear energy surface in steering the particle emission process.

It is convenient to determine the numerical value of the width by passing a plane through the yield surface at constant A. The width at half maximum of the curves of intersection is found to be about 1.3 units of Z all along the surface. It is interesting to compare this to the result that one would expect for an uncorrelated sequence of nucleon emissions. Let us assume that only neutrons and protons can be emitted. (It can be shown that neglecting α particle emission does not seriously affect arguments about the surface width.) The expected width of the distribution resulting from the emission of $N+P=\Delta A$ nucleons, would be roughly $(\Delta A)^{\frac{1}{2}}$. That is, the width of the yield surface would increase noticeably as one leaves the neighborhood of the target. It would vary from about 2 to 4 for the range of ΔA covered in the present experiment. The observed width is definitely smaller than the widths estimated on this basis (see Fig. 5).

It must be concluded that the emissions of successive particles are not uncorrelated. The sequence of emissions is channeled by some confining "forces" and the final distribution of nuclides is therefore considerably tighter than one could otherwise expect. It is reasonable to suspect that these "forces" are associated with the nuclear energy surface. Before looking into this suggestion quantitatively, it would be useful to compare the yield surfaces observed in so-called spallation or high-energy particle-induced reactions to the photoreaction surface of the preceding sections.

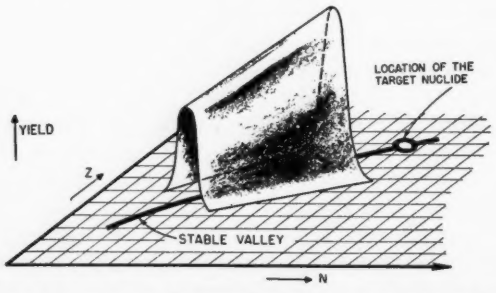

FIG. 4. A schematic representation of the portion of the photonuclear yield surface that has been examined in the present experiment.

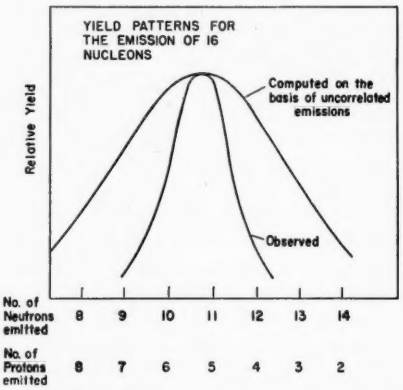
YIELD PATTERNS FOR THE EMISSION OF 16 NUCLEONS
Relative Yield
Computed on the basis of uncorrelated emissions
Observed
No. of Neutrons emitted 8 9 10 11 12 13 14
No. of Protons emitted 8 7 6 5 4 3 2

FIG. 5. A section taken through the yield surface at a constant atomic weight of the residual nucleus. The observed surface is much narrower than that to be expected on the basis of uncorrelated emission of nucleons.

4. YIELD SURFACES PRODUCED BY HIGH-ENERGY PARTICLE BOMBARDMENT

A considerable amount of information has been accumulated on the yields from nuclear reactions induced by high-energy particles. Bombardments have been made with high-energy protons,[1–5] neutrons,[6] deuterons,[3,7–9] and α particles.[3,9] Elements in a number of regions of the isotope chart have been investigated at

[3] Batzel, Miller, and Seaborg, Phys. Rev. **84**, 671 (1951).
[4] W. J. Worthington, Jr., University of California Radiation Laboratory Report 1627 (unpublished).
[5] W. E. Bennett, Phys. Rev. **94**, 997 (1954).
[6] L. Marquez, Phys. Rev. **88**, 225 (1952).
[7] M. Lindner and I. Perlman, Phys. Rev. **78**, 499 (1950).
[8] H. H. Hopkins, Jr., Phys. Rev. **77**, 717 (1950).
[9] Miller, Thompson, and Cunningham, Phys. Rev. **74**, 347 (1948).

energies up to 1.5 Bev.[10] Recently Templeton[11] has published a comprehensive review of this entire field. His interpretations of the role of nuclear evaporation in determining spallation patterns is similar to the one being developed here.

All of the yield surfaces observed in particle reactions have the general features of the photoreaction surface. Most of the data have been obtained for middle weight targets, and for such targets the yield surface widths are observed to be about 1.3 or 1.4 units of Z. The yield surface ridges for such targets lie roughly parallel to the stable valley at about a mass unit to the neutron deficient side. These features of the surfaces seem to be rather independent of the nature of the bombarding agent or its energy (provided that it is more than about 100 Mev). This independence is consistent with the notion that the shape of the yield surface depends mainly on the nature of the evaporation process (an aspect of the reactions that can easily be common to them all), rather than on any special features of the collisions initiating the reactions.

It has been somewhat more difficult to compare the remaining parameter, the slope of the ridge with respect to the N–Z plane, for the particle yield surfaces. This parameter is generally the one most poorly defined experimentally because the peak yields occur for nuclides near the center of the stable valley where most of the nuclides are stable and therefore unobservable. The widths and ridge locations can be determined fairly well nonetheless, because of the steepness of the sides of the yield surface. It is unfortunate that the ridge slope is so hard to determine, for it is the only parameter of the three that has to do with the nature of the original interaction. As Belmont and Miller[1] point out, it has to do with the distribution function for the energy made available in the nucleus by the original interaction. In some bombardments[1,2,12], it was possible to obtain yield data for radio-nuclides among the very light elements. These data indicate a leveling off of the ridge slope which is probably connected with the emission of α particles and other heavy fragments with relatively high probability.

5. EVAPORATION THEORY AND THE HIGH-ENERGY YIELD PATTERNS

A number of qualitative evidences have been discussed for the role of evaporation in high-energy nuclear reactions. It should be mentioned that there are experiments that show that not all the emitted particles are evaporated. The energy and angular distributions of particles observed in counter[13] and photographic plate[14–16] experiments seem to indicate that some particles are ejected from nuclei as a result of a succession of internal collisions started by an incoming fast particle. Bernardini[14] and others[17] have discussed such internal collision models in a fair amount of detail. Bernardini finds that after the collision part of the reaction is over, an average of 50 Mev of excitation energy is left behind in a nucleus of mass $A=100$. Presumably this energy is dissipated by the evaporation of some particles and some photons.

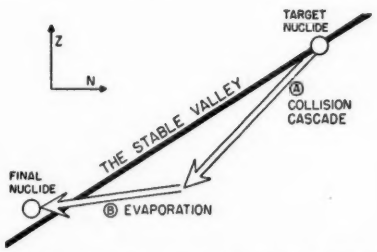

FIG. 6. A high-energy nuclear reaction can be imagined to take place in two steps. During the first step, particles are emitted more or less at random. During the second step they are evaporated.

We shall try to show that as long as enough energy remains on the average for the evaporation of four or five nucleons, the yield surfaces would be expected to have their observed features. The particle emission "trajectory" of a reaction, according to Bernardini's model, looks like the path A–B in Fig. 6. The starting point is a stable target nucleus and during the internal collision part of the reaction, along A, roughly equal numbers of neutrons and protons are emitted. It will be shown that during the final evaporation part of the reaction, B, the low average kinetic energy of emitted particles suppresses the emission of charged particles because of the Coulomb barrier. Mostly neutrons are emitted. The transition from A to B is probably less sharp than Fig. 6 would indicate.

The nature of the evaporation part of a high-energy reaction will be examined from the viewpoint of the statistical theory of Weisskopf.[18] A similar and more detailed treatment of this problem has been given by Le Couteur[19] in his explanation of prong distributions of cosmic ray stars. The main differences between the two treatments are that Le Couteur considers evaporations that start at rather higher energies than those involved here and that he is not specifically concerned with those implications of the evaporation process that have to do with the shapes of yield surfaces.

[10] Friedlander, Baker, Hudis, Miller, and Wolfgang, Phys. Rev. 94, 775 (1954).
[11] D. H. Templeton, Ann. Rev. Nuc. Sci. 2, 93 (1953).
[12] R. E. Batzel and G. T. Seaborg, Phys. Rev. 82, 607 (1951); D. H. Greenberg and J. M. Miller, Phys. Rev. 84, 845 (1951).
[13] J. Hadley and H. York, Phys. Rev. 80, 345 (1950).
[14] Bernardini, Booth, and Lindenbaum, Phys. Rev. 85, 826 (1952); 88, 1017 (1952).
[15] Harding, Lattimore, and Perkins, Proc. Roy. Soc. (London) A196, 325 (1949).
[16] H. Fishman and A. M. Perry, Jr., Phys. Rev. 86, 167 (1952).
[17] M. L. Goldberger, Phys. Rev. 74, 1269 (1948); R. Serber, Phys. Rev. 72, 1114 (1947).
[18] J. M. Blatt and V. F. Weisskopf, *Theoretical Nuclear Physics* (John Wiley and Sons, Inc., New York, 1952).
[19] K. J. Le Couteur, Proc. Phys. Soc. (London) A63, 259 (1950).

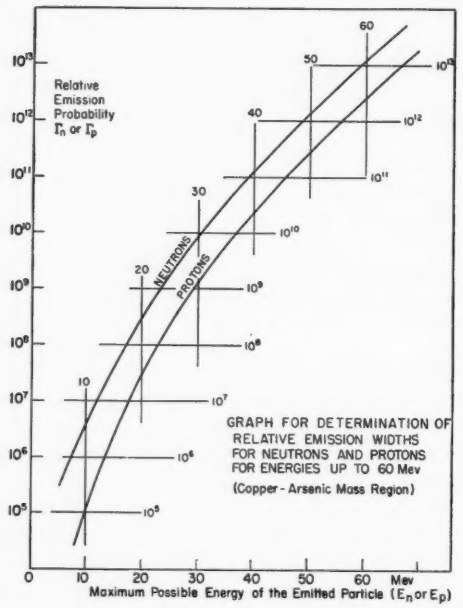
Relative Emission Probability Γ_n or Γ_p
NEUTRONS
PROTONS
GRAPH FOR DETERMINATION OF RELATIVE EMISSION WIDTHS FOR NEUTRONS AND PROTONS FOR ENERGIES UP TO 60 Mev
(Copper - Arsenic Mass Region)
Maximum Possible Energy of the Emitted Particle (E_n or E_p)
Mev

FIG. 7. These curves are based on the nuclear level densities given in Blatt and Weisskopf (see reference 18). They can be used to determine the ratio of protons to neutrons emitted from an excited nucleus if the excitation and binding energies are known.

It will be assumed to start with that only nucleons are evaporated from nuclei. Figure 7 shows a pair of curves from which relative probabilities for the evaporation of neutrons and protons can be determined for excited nuclei in the copper-arsenic region. These curves are essentially extensions of those given in Blatt and Weisskopf.[18] For a given excitation energy, one determines the ratio of ordinates for a pair of corresponding points, one on each curve. This number is the ratio of the emission probabilities for the two types of nucleons. The abscissa, E_n or E_p is the maximum energy with which the neutron or proton can be emitted. It is equal to the nuclear excitation energy, U, minus the binding energy, B_n or B_p, of the particular nucleon.

The curves of Fig. 7 are seen to be very nearly parallel with a slowly changing slope. To make the numerical arguments simpler, let us therefore replace them by a pair of parallel straight lines whose slope, S, is the average of the slope of the curves in Fig. 7. Then the probability ordinates are

$$\ln\Gamma_n = S(E_n - E_1),$$
$$\ln\Gamma_p = S(E_p - E_2),$$

where E_1 and E_2 are the energy axis intercepts. If the excitation energy of a particular nucleus is U, then $U = E_n + B_n = E_p + B_p$. It follows that

$$\ln(\Gamma_n/\Gamma_p) = S[(B_p - B_n) + (E_2 - E_1)]. \quad (1)$$

Thus, one finds that (to the extent that one may replace the curves of Fig. 7 by straight lines), the relative emission probabilities of neutrons and protons do not depend on the excitation energy, but only on the difference between neutron and proton binding energy. From the actual curves of Fig. 7, the best average values for S and $(E_2 - E_1)$ are 0.32 Mev^{-1} and 6 Mev, respectively. It remains to express $B_p - B_n$, the difference in binding energies, in terms of the position of the nucleus with respect to the stable valley. This can be done with the help of the mass formula as it is given by Coryell.[20] If local fluctuations such as odd-even effects are overlooked, then

$$M(A,Z) = M(A,Z_A) + \frac{B_A}{2}(Z - Z_A)^2.$$

Here Z_A is the value of the atomic number at the bottom of the stable valley for the mass number A. With the help of this formula, $(B_p - B_n)$ may be written $(M_p - M_n) - B_A[x - \frac{1}{2} + (\partial Z_A/\partial A)]$, where $(M_p - M_n)$ is the proton-neutron mass difference and x is the distance, $(Z - Z_A)$, of the excited nuclide from the stable valley. For the region of nuclear masses around $A = 70$, we find[20] that $B_A = 2.6$ Mev and $(\partial Z_A/\partial A) = 0.4$. Substituting for $(B_p - B_n)$ in (1),

$$\ln(\Gamma_n/\Gamma_p) = 1.60 - 0.83x. \quad (2)$$

From a graph of this equation (Fig. 8), one can determine average neutron and proton evaporation probabilities for any excited middle weight nuclide. These probabilities depend only on the distance of the nuclide from the stable valley. It can be seen that for nuclides lying along the stable valley, neutron evaporation is about five times more probable than proton evaporation. The two evaporation probabilities are equal at roughly two units of Z (measured along constant A), to the neutron-deficient side of the stable valley.

With the help of Eq. (2) or the corresponding graph, it is possible to follow the evaporation part of a spallation reaction. The average excitation energy left in a nucleus after the nucleon collision cascade part of a reaction, may be estimated[14] to be roughly 50 Mev.

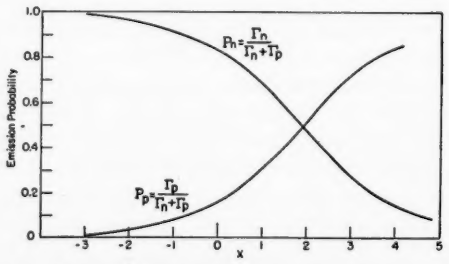

FIG. 8. The evaporation probability of neutrons and protons from medium weight nuclei (copper-arsenic mass region) as a function of x, the distance of the nucleus from the stable valley.

[20] C. D. Coryell, Ann. Rev. Nuc. Sci. 2, 305 (1953).

This is enough energy for the evaporation of four or five nucleons. According to the model of Fig. 6, the nuclides in which evaporation begins tend to lie to the proton-deficient side of the stable valley. It is possible to obtain a rough estimate of the most probable value of x at the start of the evaporation. Imagine, for example, that arsenic is the target and that ten nucleons are emitted during the nucleon-nucleon collision cascade. If equal numbers of neutrons and protons are emitted during this part of the reaction, the final nucleus is Ni^{65} for which x happens to be -1.2. Thus even for a fairly long collision cascade, the most probable final value of x is somewhere between -1 and -2. For shorter cascades, it is probably closer to -1. The distribution about this probable value is likely to be rather wide if the pre-evaporation emissions take place in a random uncorrelated way.

It turns out that the final distribution of nuclides after evaporation is not too sensitive to the distribution just before evaporation. In constructing Fig. 9, three different distributions were assumed to hold at the start of the evaporation. Final distributions were computed from these distributions by allowing 5 nucleons to evaporate one at a time. In order to construct a new distribution following an evaporation from a given distribution, one need only know the probabilities for neutron and proton emission from each nuclide in the given distribution. This information is given in Fig. 8.

In Fig. 9, the assumed starting distributions were centered at $x=-1$, 0 and 0 for the three distributions. The widths of these starting distributions were taken to be 3.7, 3.7, and 2.0, respectively. It is seen from the figure that the final distributions turn out to be very similar and therefore rather insensitive to the assumed starting distribution. The final distribution should, of course, correspond to the experimentally observed distribution and it is seen that the peaks occur at roughly half a unit of x to the neutron deficient side, just as one observes. The computed distribution widths are however about 50 percent wider than the observed widths.

Had the discrepancy been in the other direction, one could think of things that might tend to spread out the observed distribution. For example, not all nuclides are identical in their properties with respect to evaporation as we have here assumed. There are evidences for effects due to oddness or evenness of the numbers of neutrons and protons[1] in a nucleus. Any such deviations from an average behavior would tend to broaden the distribution.

Since the observed distributions are significantly narrower than the computed ones, it is worth looking hard at some of the assumptions made in the calculation.

(1) The length of the evaporation chain.—Distributions were computed for the evaporation of up to ten particles. Although the center of the distribution moves slowly toward $x=2$, the width doesn't change appreciably.

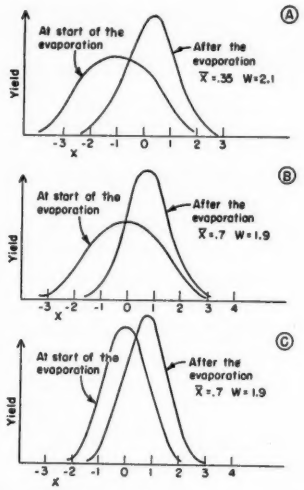

FIG. 9. The change in the distribution of nuclei, with respect to the center of the stable valley, that is brought about by the final evaporation of 5 nucleons. The locations of the centers of the final distributions and their widths are given. Three rather different starting distributions were assumed.

(2) Alpha-particle emission.—There is considerable evidence from photographic plate work[21,22] and other experiments that a fair number of α particles are emitted in spallation reactions. Their emission has been overlooked here in order to keep the calculations simple. Moreover it can be shown that α emission will not influence the width of a distribution curve unless α particles can be evaporated with high probability only from nuclides in a very limited range of x. Computations for α particles of the same sort as those leading to Fig. 8 indicate that an α particle has about a five percent chance of being evaporated at any stage of the evaporation and that this probability is hardly at all dependent on x. The only effect of α evaporation on the final distribution is to shift the peak slightly to the proton-deficient side. It does not change the width.

(3) Variation of level density with excitation energy.—The parameter S in Eq. (1) has to do with the way the nuclear level density depends on energy. In order to tighten up distribution curves, the slope, S, would have to have a larger value than the particular average value that has been assumed. It is seen that S actually increases toward the end of an evaporation (Fig. 8). Yet, it doesn't appear, on the basis of some trial calculations, that the final tightening up of yield surface due to this increase in S is sufficient to account for the narrow observed surfaces.

The calculations of this section indicate that the observed features of yield surfaces can be semiquantitatively accounted for by a model in which the last

[21] R. W. Deutsch, Phys. Rev. **90**, 499 (1953); **92**, 515 (1953).
[22] N. Page, Proc. Phys. Soc. (London) **463**, 250 (1950).

several nucleons are evaporated. The numerical discrepancies will perhaps be removed when more detailed information is available about nuclear level densities.

It should be emphasized at this point that the foregoing calculations apply only to targets of medium atomic weight. It is straightforward to carry out similar calculations for heavier targets. The most striking result of such calculations is the shift of the yield surface ridge to the neutron deficient side of the stable valley. For very heavy targets the ridge swings around until it is almost parallel to the N-axis of the isotope chart (Fig. 4). This shift is due in part to the suppression of charged particle evaporation because of the Coulomb barrier. This Coulomb effect is enhanced because the sides of the valley of the nuclear energy surface are less steep for heavy nuclei. The nuclear energy surface is therefore less able, than it is for lighter nuclei, to supply the restoring forces needed to keep a chain of evaporations confined to the neighborhood of the stable valley. Experimental results with heavy targets agree with these general conclusions. For example, Sugarman[23] found that the reaction $(\gamma,8n)$ is twice as probable as $(\gamma,p7n)$ in bismuth with 86-Mev bremsstrahlung.

6. PHOTONUCLEAR YIELDS FOR REACTIONS IN WHICH ONLY A FEW PARTICLES ARE EMITTED

The photonuclear yield data for reactions in which ΔZ is less than two do not fit the general patterns discussed in the preceding sections. It is not to be expected that such yields would fit, since yield distributions, where only a few particles are emitted, could hardly be sufficiently influenced by the nuclear energy surface. For these reactions, in which $\Delta Z \leqslant 1$, the observed yields can in most cases be assigned without ambiguity to specific isotopes in the target. They have been renormalized to a g/cm² of target isotope and are plotted as a function of the number of neutrons emitted. The data for reactions in which one proton (Fig. 10) and no protons (Fig. 11) are emitted are plotted separately. The dashed curve in each case is meant to represent a sort of back-extrapolation of the yield surface of the earlier sections to the region near the target. Some of the points plotted represent data obtained by other workers.[24,25]

It is seen that the yields in which two or more neutrons are emitted agree tolerably well with what one might expect on the basis of the extrapolated yield surface. But the yields for (γ,n), (γ,p), and (γ,pn) reactions are all much greater than one would expect from yield surface considerations. This fact is certainly due to the abnormally large absorption cross section for photons of about 20 Mev (the giant resonance). Indeed it can be argued that no more than 10 percent of the (γ,n) yield is due to photons in the bremsstrahlung spectrum with energies in excess of the resonance energy. From Sagane's work,[26] the ratio of the yield of the $(\gamma,2n)$ reaction to that of the (γ,n) reaction is about 0.1 for resonance photons. From the

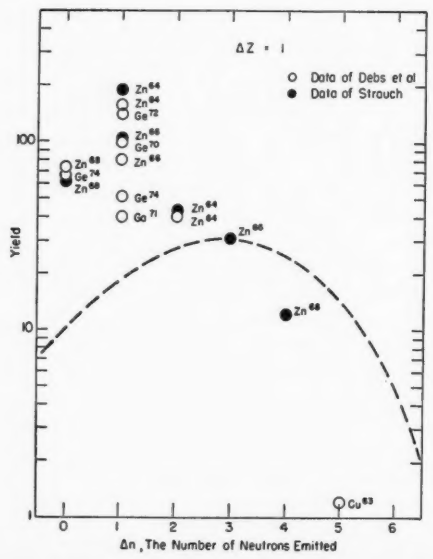

FIG. 10. A plot of the yield data for $\Delta Z=1$. The (γ,p) and (γ,pn) yields are seen to be larger than one would expect on the basis of the yield surface of Fig. 2.

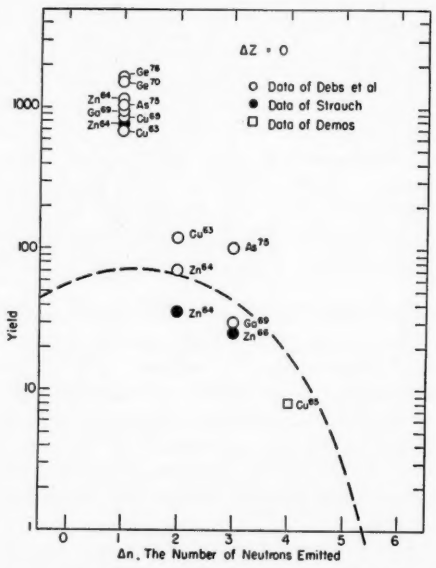

FIG. 11. A plot of the yield data for $\Delta Z=0$. The (γ,n) yields are larger than one would expect on the basis of the yield surface of Fig. 2.

[23] N. Sugarman and R. Peters, Phys. Rev. **81**, 951 (1951).

[24] K. Strauch, Phys. Rev. **81**, 973 (1951).

[25] P. T. Demos (unpublished).

[26] R. Sagane, Phys. Rev. **83**, 174 (1951).

TABLE II. Relative yields of separated elements in an irradiation of copper.

Element	ΔZ	Yield
Copper	0	900
Nickel	1	470
Cobalt	2	60
Iron	3	26
Manganese	4	11
Chromium	5	5
Vanadium and lighter elements	6	4
	Total	1476

present work, the similar ratio for 320 bremsstrahlung is less than 0.2. If one makes the reasonable assumption that the $(\gamma,2n)$ yield for post-resonance photons exceeds the (γ,n) yield for those photons, it follows that the (γ,n) yield for these photons is less than 10 percent of the resonance yield. Terwilliger[27] has been able to reduce this limit even lower.

Another noteworthy feature of the data in Figs. 10 and 11 is the spread of observed yields for (γ,n) and (γ,pn) reactions. In view of the dipole sum rule,[28] the integrated absorption cross section for resonance photons is presumably very nearly the same for all of the targets bombarded. Although part of the scatter in the data here is certainly due to experimental error, the major part is presumably due to varying degrees of competition with non-observed reactions. For example, the fact that the (γ,n) yield of Cu^{63} is 30 percent less than that of Cu^{65} has very likely to do with the fact that Cu^{63} has a lower binding energy for protons (compared to the neutron binding energy). The sum of the (γ,p) and (γ,n) yields from Cu^{63} may be very nearly equal to that from Cu^{65}. It is difficult to make very significant comparisons of observed (γ,n) yields with theoretical expectations, since neither the data nor the quantitative aspects of evaporation theory would, at present, warrant precise numerical comparison. This is especially true if one assumes that even in the resonance region, a fair fraction of the emitted neutrons and protons are directly ejected[29,30] rather than evaporated.

7. CROSS SECTIONS FOR NUCLEAR REACTIONS WITH HIGH-ENERGY X-RAYS

It is interesting to compare the yield data of the present experiment to estimates of yields for nuclear events measured in other ways. The following discussion will be restricted to a single representative medium weight target, namely, copper.

To begin with, it is possible to estimate the total number of nuclear events produced in copper by 320-Mev bremsstrahlung. One has only to supplement the yield data actually observed in copper irradiations

[27] L. W. Jones and K. M. Terwilliger, Phys. Rev. **91**, 699 (1953).
[28] J. S. Levinger and H. A. Bethe, Phys. Rev. **78**, 115 (1950); **85**, 577 (1952).
[29] E. D. Courant, Phys. Rev. **82**, 703 (1951).
[30] B. C. Diven and G. M. Almy, Phys. Rev. **80**, 407 (1950).

TABLE III. Measurements and estimates of photonuclear yields in copper for 320-Mev bremsstrahlung (given in units of mb/Q).

Total number of events	121[a]	107[b]	
Number of "post-resonance" events	32[a]	27[b]	20[c]
Number of events made by photons of more than 150 Mev	12[c]		
Total number of neutrons emitted	180[a]	158[b]	
Number of neutrons emitted in post-resonance reactions	94[a]	78[b]	
Number of protons emitted with energies greater than 10 Mev (non-evaporated protons)	26[e]	16[d]	
Number of mesons emitted	2.1[e]	2[e]	

[a] Present work normalized as described in Sec. 7.
[b] See reference 27
[c] S. Kikuchi, Phys. Rev. **86**, 41 (1952).
[d] J. C. Keck, Phys. Rev. **85**, 410 (1952).
[e] See references 32, 33, and 34.

with estimates based on interpolations of other data. One can use the yield surface, Fig. 2, and Figs. 10 and 11. In units of the preceding paper, the yields so estimated have been listed in Table II according to the separated element. To see how the listed numbers were arrived at, consider the first number, 900 units for the yield of copper isotopes. From Table I of the preceding paper the total (γ,n) yield is 740 units. The $(\gamma,2n)$ yield was measured only for Cu^{63} but assuming a comparable yield for Cu^{65}, the estimated combined yield is 120 units. The best estimate of the $(\gamma,3n)$ yield (Fig. 11) is 30 units and the yields for the production of lighter copper isotopes are smaller yet. In round numbers, the total yield of copper nuclides in a copper irradiation is 900 units. Similarly the yields of the other elements have been obtained.

It is possible to convert the arbitrary yield numbers of Table II into something more absolute by comparing our (γ,n) yield to the accurate measurements of Katz.[31] Although his measurements extend only to 25 Mev, we have seen that only a few percent of the (γ,n) yield is due to photons of higher energy. The excitation curves of Katz together with the shape of the 320-Mev x-ray spectrum lead to an estimate of 61 mb per equivalent quantum of 320-Mev x-rays for the (γ,n) yield in copper. Thus, since the (γ,n) yield of 740 units corresponds to 61 mb/Q (a Q, or equivalent quantum, contains 320 Mev of energy), the total yield (1476 units) is roughly 121 mb/Q. This number as well as estimates of some partial yields appear in Table III. One of the more interesting partial yields is that for events produced by just the resonance photons. To obtain an estimate for this yield, it is, of course, necessary to decide which of the observed yields are due to resonance photons and which are not. Because of the absence of good excitation curve data, such decisions must be somewhat arbitrary. It was assumed that all of the yield for reactions in which $\Delta A=1$, half the yield where $\Delta A=2$, and none of the yield where $\Delta A>2$, belong to the resonance. Under these assumptions only

[31] L. Katz and A. G. W. Cameron, Can. J. Phys. **29**, 518 (1951).

32 mb/Q or roughly a quarter of the total yield is due to post-resonance photons. The reason for the predominance of resonance reactions with 320-Mev x-rays is due not only to the large size of the cross section at those energies, but also to the shape of the bremsstrahlung spectrum.

Jones and Terwilliger[27] have recently determined neutron yields from copper irradiated by 320-Mev x-rays. Neutron yields can also be computed from our data by multiplying the mb/Q for each separate yield by the corresponding neutron multiplicity and adding the results. In carrying out this sum, the emission of composite particles (α particles, deuterons) was ignored. The resulting overestimate of the total neutron emission is, however, not very serious in view of the known relatively small yield of these heavier particles, the total neutron production yield comes out to be 180 mb/Q of which 94 mb/Q or roughly half is due to post resonance photons. Both these results are quite consistent with the more direct and precise measurements of Jones and Terwilliger.

For purposes of comparison, several other types of yields have been recorded in Table III. Some of these yields are due to fairly direct measurements but some are based on interpolations of data obtained for elements other than copper. For example, one of the listed meson production yields is based on the π^+ production yield in carbon,[32] the $A^{\frac{2}{3}}$ dependence of this yield,[33] on the observed ratio of π^- to π^+ production[33] and on estimates of the π^0 production rate.[34] A final estimate based on so many components is at best rather rough, but it was thought to be useful nevertheless to record a number of different types of yields in one place. If one believes all of the numbers in the table there are some disconcerting things about some of their relative sizes. For example, it is possible to estimate the yield for the production and recapture of mesons in a nucleus from the yield of those mesons that manage to get out, if one is willing to interpret the observed $A^{\frac{2}{3}}$ dependence of the meson-production cross sections in terms of a very short mean free path for mesons in nuclear matter. But such an estimate, together with a reasonable estimate for neutron multiplicity in meson-recapture events,[35] leads to an expected neutron production rate a few times larger than what is actually observed. In view of all the uncertainties involved in the determination in some of the yields quoted, it is hard to know how seriously to regard these discrepancies.

[32] J. Steinberger and A. S. Bishop, Phys. Rev. **86**, 171 (1952).
[33] R. M. Littauer and D. Walker, Phys. Rev. **82**, 746 (1951).
[34] Panofsky, Steinberger, and Steller, Phys. Rev. **86**, 180 (1952).
[35] V. Tongiorgi and D. A. Edwards, Phys. Rev. **88**, 145 (1952).

PHYSICAL REVIEW VOLUME 97, NUMBER 5 MARCH 1, 1955

Scattering of Fast Neutrons and Protons by Atomic Nuclei*

GYO TAKEDA† AND K. M. WATSON
Department of Physics, University of Wisconsin, Madison, Wisconsin
(Received November 18, 1954)

The effects of the Pauli principle on the analysis of the scattering of fast neutrons and protons by atomic nuclei are considered. This modifies the usual multiple scattering treatment of such problems in three ways: (1) It is necessary to agree on a convention for deciding which are "scattered" and which are "nuclear" nucleons. (2) The two-body scatterings obtained from the impulse approximation must be properly antisymmetrized. (3) Exchange corrections occur because of the non-orthogonality of the plane wave states for scattered particles and the states for bound particles. The latter corrections seem to be negligible for energies sufficiently high that the multiple-scattering approach is expected to be useful anyway. The present analysis is also applicable to other types of multiple-scattering problems.

I. INTRODUCTION

IN two previous publications[1,2] the theory of the scattering of fast particles by atomic nuclei was formulated as a multiple-scattering process. In the present work we wish to extend this to the scattering of fast neutrons and protons by atomic nuclei.[3] At first sight this might appear difficult, since the concept of a single particle passing through a medium and being scattered by particles of the medium does not lend itself conveniently to a description in which all the particles are treated as indistinguishable, as demanded by the Pauli principle.[4] Nevertheless, we shall be able to conclude that under such conditions that the multiple-scattering formulation is expected to be useful anyway, the Pauli principle adds no significant complication.

* Supported by grants from the National Science Foundation and from the Wisconsin Alumni Research Foundation.
† On leave from Kobe University, Kobe, Japan.
[1] K. M. Watson, Phys. Rev. **39**, 575 (1953). This paper will henceforth be referred to as I.
[2] N. C. Francis and K. M. Watson, Phys. Rev. **92**, 291 (1953). This paper will henceforth be referred to as II.
[3] G. Takeda and K. Watson, Phys. Rev. **94**, 1087 (1954), have given an application of the conclusions in the present paper.
[4] We use the generalized Pauli principle by which neutrons and protons are two states of the *nucleon*. The wave functions describing such systems are to be antisymmetrized with respect to all nucleons.

To see this, let us first suppose that the incident particle is distinguishable from the nucleons in the nucleus and review the physical basis for the multiple-scattering model.[5] The first and most significant step is the introduction of the *impulse approximation*,[6] by which the many-body dynamics of the problem is related to that of the two-body problem. This approximation permits one to describe the encounter of the incident particle with a nucleon in the nucleus as a scattering between two free particles. The criterion for the success of this approximation is essentially that the energy of the incident particle be much larger than the binding potential of the struck nucleon. Actually, this condition may be somewhat stronger than is needed, since it is the change, ΔU, in the binding potential during the scattering process which is important. Thus for a fairly uniform nuclear potential the impulse approximation might be valid for rather low-energy scatterings.[7] Indeed, when the ratio

$$\Delta U/E \tag{1}$$

is small (where E is the energy of the incoming particle),[8] we can consider the impulse approximation to be valid. (A more careful discussion is given in reference 6.) Since ΔU may be of the order of 10–20 Mev, we expect to find the impulse approximation useful for E larger than 50–100 Mev.

The formulation of the complete process in terms of such two-body scatterings has been given in reference 1. This involves expressions for such nuclear properties as the nucleon density in the nucleus, which are assumed to be known. After the first scattering, we expect the nucleus to be excited and thus these nuclear properties to be changed. As described in I, however, if the incident particle is fast, it should outrun the "storm" which it has created and is expected to encounter at each subsequent scattering a medium which is essentially in its ground state. For incident nucleon energies above 50–100 Mev,[8] we should expect this condition to obtain and the impulse approximation also to be valid (until, of course, the nucleon energy has been sufficiently degraded through successive scatterings).

A further requirement that a scattering between the incident particle and one in the nucleus be essentially the same as the scattering between free particles is that the distance between scatterings (mean free path) be sufficiently great that the energy of the scattered particle between collisions is fairly well restricted by energy conservation. This condition can be specified by the relation

$$\Delta E \Delta t \simeq \hbar,$$

where ΔE is the uncertainty in the energy of the scattered particle at the second scattering and Δt is the time between the two collisions. If the mean free path is λ, then

$$\Delta t \simeq \lambda/v$$

(where v is the velocity of the particle). For most problems of interest,

$$\lambda \simeq 4a_0,$$

where $a_0 \simeq \hbar/\mu c$ is the mean separation between nucleons in the nucleus. Thus

$$\Delta E/E \simeq \tfrac{1}{4}(v/c)(\mu c^2/E), \tag{2}$$

where E is the energy of the scattered particle. For $E > 100$ Mev, the uncertainty in the energy is small.[9]

We turn now to the point of major concern to us in this work—i.e., the consequences of the Pauli principle when the bombarding particle is a neutron or a proton. Perhaps the most obvious point to require clarification is the decision as to which is the "scattered particle" and which are the "nuclear particles" after the first and subsequent scatterings. The distinction implied here is evidently one of convenience only and also one which must be chosen appropriately for the problem at hand. Nevertheless, it appears useful for many cases to define the "scattered nucleon" as the one having the *greatest kinetic energy*. Since we are considering bombarding energies much larger than nuclear kinetic energies, this distinction seems meaningful and will be adopted, unless specified otherwise.[10] An alternate distinction which will be useful in studying the prong distribution of nuclear stars induced by high-energy nucleons will be to define as "scattered nucleons" all those whose kinetic energy exceeds a certain lower limit, which is presumably larger than that for the "bound nucleons."[11] In any case, it seems that the most convenient "labeling" of the fast nucleons will be in terms of their kinetic energy.

The above consideration involved only the choice of a useful convention. There are also other consequences of the Pauli principle which require more elaborate and detailed development. That there is a limit for which the multiple-scattering approximation is valid is apparent—to see this we need only consider the example of a proton being scattered in diffuse hydrogen gas. Here the only significant consequence of the Pauli principle is the proper antisymmetrization of the two-body wave function for each proton-proton scattering.[12] When the target is a nucleus, it is also necessary to antisymmetrize the two-body nucleon-nucleon wave

[5] R. Serber, Phys. Rev. **72**, 1114 (1947).

[6] G. F. Chew and G. C. Wick, Phys. Rev. **85**, 636 (1952); G. F. Chew and M. L. Goldberger, Phys. Rev. **87**, 778 (1952).

[7] See references 6 and Brueckner, Levinson, and Ahmoud, Phys. Rev. **95**, 217 (1954).

[8] The energy E should here be considered to be the energy of the incident particle *inside* rather than *outside* the nucleus. That is, we should add to the original energy the depth of the nuclear potential well. (See reference I for a justification of this statement.)

[9] The rapidity with which the cross section varies with energy is of some importance here. However, most cross sections in the energy range of a few hundred Mev do not seem to vary very rapidly with energy.

[10] This choice is evidently the proper one for studying the elastic scattering of fast nucleons by means of the optical method.

[11] This is essentially the point of view adopted by Goldberger for his semiclassical model of high-energy nuclear reactions [M. L. Goldberger, Phys. Rev. **74**, 1269 (1948)].

[12] This we shall call the "primary exchange" effect.

function for each two-body scattering. When the energy is sufficiently high that the impulse approximation is valid, this should adequately describe the scattering event. The reason for this is that the condition of validity of the impulse approximation is essentially just that the two scattering particles interact only with each other and not with other nuclear particles during a scattering event.

There is one final aspect of the Pauli principle which might appear to make the multiple-scattering formulation difficult at low energies. This is a process of the sort by which the incoming nucleon "2" strikes the bound nucleon "1," causing nucleons "1" and "0" to recoil (carrying off the energy of "2") and leaving "2" in "0"s position in the nucleus. Because of the Pauli principle which makes it impossible to distinguish between "0," "1," and "2," this type of process will interfere with that by which "0" strikes "1" and "0" and "1" recoil ("2" not being affected). This, we feel, will complicate the multiple-scattering analysis. However, the process described above can happen only because of the nonvanishing binding energy of the nucleus. When the kinetic energy of the colliding nucleon is large compared to that of a bound nucleon, this correction seems to be negligible (as will be described in more detail below).[13]

We may describe the conclusions of the last paragraph in another way. Exchange effects due to the Pauli principle for two (or more) particles are not important in general unless the wave functions of these particles overlap appreciably. Referring to the example above, we may then say that this process is not important unless a significant part of the *spectrum* of *kinetic energies* for particle "0" extends up to energies as high as that of the faster of the two nucleons. Instead of overlap of energies, we may think in terms of the overlap of wave functions in configuration space. Since particle "0" is just "any place in the nucleus," we can construct a wave packet for "2" which overlaps very little of "0's" wave function if the energy of "2" is high.

Our conclusion is thus that for energies sufficiently high that the impulse approximation is valid, the Pauli principle neither invalidates nor complicates the multiple-scattering description of high-energy nuclear reactions. This will be developed more precisely below, where we use the notation and techniques of references I and II.

II. FORMAL CONSEQUENCES OF THE PAULI PRINCIPLE

We shall use the notation of II. The nucleus is considered to have a complete set of eigenfunctions,

$$g_\nu(\xi_1,\xi_2,\cdots\xi_A),$$

of energy W_ν. Here ν is a set of variables used to denote the complete set of nuclear states ($\nu=0$ refers to the ground state) and the ξ's represent a complete set of nucleon variables for the A nucleons. The g's are supposed to be properly antisymmetrized as required by the Pauli principle. An incident nucleon in a plane wave state of momentum $\mathbf{p}$ and spin orientation ν has a wave function

$$\lambda_{\mathbf{p},\nu}(\xi_0).$$

The Hamiltonian describing the interaction of these $(A+1)$ nucleons is

$$H=K+V, \tag{3}$$

where K is the sum of the kinetic energies of the nucleons and

$$V=\sum_{\alpha>\beta}^{A} V_{\alpha\beta}. \tag{4}$$

$V_{\alpha\beta}$ is the interaction energy between the αth and βth nucleons.

Starting with the initial state,

$$g_0(\xi_1,\cdots,\xi_A)\lambda_{\mathbf{p},\nu}(\xi_0),$$

which describes nucleon "0" as incident on the nucleus in its lowest state, we suppose the Schrödinger equation to have a solution $\psi_a^{(0)}(\xi_0,\cdots,\xi_A)$:

$$H\psi_a^{(0)}=E\psi_a^{(0)}. \tag{5}$$

From $\psi_a^{(0)}$ we may construct an antisymmetrized[14] wave function:

$$\Psi_a=(A+1)^{-\frac{1}{2}}\Lambda_0\psi_a^{(0)}, \tag{6}$$

where

$$\Lambda_0=I-\sum_{\alpha=1}^{A} P_{\alpha 0}. \tag{7}$$

Here, $P_{\alpha 0}$ is the operator which interchanges ξ_0 and ξ_α and I is the identity permutation.

To evaluate the scattering cross section from Eq. (6), we write $\psi_a^{(0)}$ as

$$\psi_a^{(0)}=\psi_a^{(0)\text{in}}+\psi_a^{(0)\text{sc}}, \tag{8}$$

where the two terms contain, respectively, the incoming wave and outgoing scattered waves. The corresponding wave functions,

$$\psi_a^{(\alpha)}\equiv P_{\alpha 0}\psi_a^{(\alpha)}, \tag{9}$$

may be similarly decomposed. Letting

$$\mathbf{z}_0,\ \mathbf{z}_1,\ \cdots,\ \mathbf{z}_A$$

be the coordinates of the nucleons and

$$S_0^\nu,\ S_1^\nu,\ \cdots,\ S_A^\nu$$

[13] We shall henceforth use the term "target exchange" for this effect, which may also be described as a "non-orthogonality" correction.

[14] We recall that the g's are already antisymmetrized.

be their spin wave functions, we have

$$\lim_{z_0\to\infty}\psi_a^{(0)sc}=-\sum_f \frac{\exp(i\mathbf{p}_f\cdot\mathbf{z}_0)}{z_0}\times S_0^{\nu f} g_f(\xi_1,\cdots,\xi_A)[(2\pi)^2 M T_d],$$

$$\lim_{z_\alpha\to\infty}\psi_a^{(0)sc}=-\sum_f \frac{\exp(i\mathbf{p}_f\cdot\mathbf{z}_\alpha)}{z_\alpha}\times S_\alpha^{\nu f} g_f(\xi_1,\cdots,\xi_A)[(2\pi)^2 M T_e], \quad (10)$$

where M is the nucleon mass and T_d and T_e are the respective *direct* and *exchange* scattering amplitudes for scattering into a final momentum and spin state $(\mathbf{p}_f,\nu_f)$ with the nucleus in the state f.[15] Evidently,

$$(p^2/2M)+W_0=(p_f^2/2M)+W_f. \quad (11)$$

To calculate the cross section, we require the expectation value of the current operator ($\mathbf{p}_\rho$ is the momentum of the ρth nucleon):

$$\mathbf{J}(\mathbf{x})=\sum_{\rho=0}^{A}\mathrm{Re}\{\delta(\mathbf{x}-\mathbf{z}_\rho)(\mathbf{p}_\rho/M)\} \quad (12)$$

for large $|\mathbf{x}|$. This is

$$\langle\mathbf{J}\rangle_{sc}=\frac{1}{A+1}(\Lambda_0\psi_a^{(0)sc},\ \mathbf{J}(\mathbf{x})\Lambda_0\psi_a^{(0)sc})$$

$$=\frac{1}{A+1}\sum_{\rho=0}^{A}\left(\Lambda_0\psi_a^{(0)sc},\ \delta(\mathbf{x}-\mathbf{z}_\rho)\frac{\mathbf{p}_\rho}{M}\Lambda_0\psi_a^{(0)sc}\right). \quad (13)$$

Evaluation of Eq. (13) using Eqs. (10) is straightforward. We obtain

$$\langle J\rangle_{sc,f}=(1/x^2)(p_f/M)(2\pi)^4M^2S|T_d-AT_e|^2, \quad (14)$$

where S is the appropriate sum and average over final and initial spin substates. The differential cross section is

$$\frac{d\sigma}{d\Omega}(\mathbf{p}_f,f)=(p_f/p)(2\pi)^4M^2S|T_d-AT_e|^2. \quad (15)$$

For present purposes, it is important to note that one may calculate the cross section using any *one* term of the sum over ρ in Eq. (13), since the wave functions have been antisymmetrized. In particular, in the next section we shall calculate the flux of emitted "0" particles, multiplying by $(A+1)$ to obtain the cross section.

[15] Since the wave function $\psi_a^{(0)sc}$ is not properly symmetrized with respect to ξ_0, it might be felt that one should include in the sum over f nuclear states $g_f(\xi_1,\cdots,\xi_0,\cdots,\xi_A)$ which violate the Pauli principle. The reason for omitting these is that they cannot contribute to the cross section, since transitions into these states are forbidden, of course.

III. DEVELOPMENT OF THE MULTIPLE-SCATTERING PROBLEM

It is desirable to depart in certain trivial respects from the notation of I and II in order to treat the nucleons all on a equivalent basis. Referring to Eqs. (3), (4), and (5), we define

$$V_\alpha\equiv\sum_{\beta\neq\alpha}V_{\beta\alpha}\quad(\alpha=0,1,\cdots,A), \quad (16)$$

and

$$a\equiv E+i\eta-H. \quad (17)$$

(Here η is the infinitesimal positive parameter which is employed in scattering theory to define the contour of integration about the pole in such quantities as a^{-1}). We also define

$$a(\alpha)\equiv a+V_\alpha. \quad (18)$$

Evidently V_α represents the interaction of the αth nucleon with the remainder of the nucleons. Also, $a(\alpha)$ is diagonal when operating on the wave function

$$|\alpha)\equiv g_\nu(\xi_1\cdots\xi_{\alpha-1}\xi_0\xi_{\alpha+1}\cdots\xi_A)\lambda_{p,\nu}(\xi_\alpha). \quad (19)$$

Thus $[a(\alpha)]^{-1}$ is the "propagation function" for α in a plane wave state, the other nucleons being in one of their mutual eigenstates.

When the incident nucleon is α, the wave equation (5) has the formal Chew-Goldberger solution

$$\Omega(\alpha)=1_\alpha+\frac{1}{a}V_\alpha|\alpha)\quad(\alpha=0,1,\cdots,A). \quad (20)$$

for the Møller wave matrix. By 1_α we mean the result of letting the identity operator act on the state (19) when the nuclear state is $\nu=0$ (i.e., the nucleus is in its ground state). By $V_\alpha|\alpha)$ we mean the result of applying V_α to the state (19), again with $\nu=0$.

Equation (20) satisfies the Lippman-Schwinger integral equation,

$$\Omega(\alpha)=1_\alpha+\frac{1}{a(\alpha)}V_\alpha\Omega(\alpha). \quad (20')$$

Since the initial state is not antisymmetrized with respect to the coordinates of the nucleons, neither is the wave function $\Omega(\alpha)$. Using Eqs. (6) and (7), we may readily construct such a solution. This is

$$\bar{\Omega}\equiv\Omega(0)-\sum_{\alpha=1}^{A}\Omega(\alpha)$$

$$=\Lambda_0\Omega(0)$$

$$=\bar{I}+\frac{1}{a}\Lambda_0V_0|0)$$

$$\equiv\bar{I}+\frac{1}{a}\bar{V}. \quad (21)$$

Here

$$\bar{I}\equiv\Lambda_0 I_0=1_0-\sum_{\alpha=1}^{A}1_\alpha, \tag{22}$$

and

$$\bar{V}\equiv V_0|0)-\sum_{\alpha=1}^{A}V_\alpha|\alpha). \tag{23}$$

In obtaining the final form of Eq. (21) we have used Eq. (20) and the fact that Λ_0 commutes with a^{-1}.

Equation (21) is the final formal solution to the scattering problem. It remains to show how to calculate the cross section from it. By the conclusions of Sec. II, it is necessary to calculate the outgoing flux of only one nucleon, say nucleon "0," and properly normalize it. This we proceed to do. By using the Chew-Goldberger relation,

$$\frac{1}{a}=\frac{1}{a(0)}\left[1+V_0\frac{1}{a}\right],$$

Equation (21) can be written as

$$\bar{\Omega}=\bar{I}+\frac{1}{a(0)}\left[1+V_0\frac{1}{a}\right]\bar{V}. \tag{24}$$

Since $[a(0)]^{-1}$ describes the propagation of nucleon "0" as a free particle, the quantity

$$\left[1+V_0\frac{1}{a}\right]\bar{V}$$

is essentially the amplitude for emission of the "0" nucleon. By Eq. (21), we can write $a^{-1}\bar{V}=\bar{\Omega}-\bar{I}$ and convert Eq. (24) to an integral equation:

$$\bar{\Omega}=\bar{I}+\frac{1}{a(0)}[\bar{V}-V_0\bar{I}]+\frac{1}{a(0)}V_0\bar{\Omega}. \tag{25}$$

Except for the rather complex "source term,"

$$\bar{I}+\frac{1}{a(0)}[\bar{V}-V_0\bar{I}], \tag{26}$$

this is just the integral equation (20′) for "0" as the incident particle. It is easily seen that (26) satisfies the Schrödinger equation

$$a(0)\left[\bar{I}+\frac{1}{a(0)}(\bar{V}-V_0\bar{I})\right]=0,$$

just as does 1_0. Our argument will consist of showing that for high-energy collisions the expression (26) may essentially be replaced by 1_0 so that our problem is reduced to one for which nucleon "0" is treated as distinguishable. (We suspect that there may be more general conditions for this approximation to be valid than that the incident particle be fast, but we have not found them.) Returning to Eq. (25), the quantity $V_0\bar{I}$ is

$$V_0\bar{I}=V_0|0)-\sum_{\alpha=1}^{A}V_0|\alpha)$$

$$=\sum_{\beta\neq0}V_{\beta0}|0)-\sum_{\beta\neq0}\sum_{\alpha\neq0}V_{\beta0}|\alpha),$$

where $V_0|\alpha)$ is the result of letting V_0 operate on the state $|\alpha)$ of Eq. (19) with $\nu=0$, etc. The difference is

$$\bar{V}-V_0\bar{I}=\sum_{\beta\neq0}\sum_{\alpha\neq0,\beta}[V_{\alpha0}|\beta)-V_{\alpha\beta}|\beta)]. \tag{27}$$

When substituted into Eq. (25), the expression

$$\frac{1}{a(0)}[\bar{V}-V_0\bar{I}]$$

describes processes in which the fast particle "β" is incident on the nucleus and the fast particle "0" is emitted after a single scattering. From the structure of Eq. (27), it is seen that these processes are all of the "target exchange" type which we agreed in the introduction to neglect. (The magnitude of these terms is estimated in the next section.) Dropping this term then, Eq. (25) becomes

$$\bar{\Omega}=\bar{I}+\frac{1}{a(0)}V_0\bar{\Omega}. \tag{28}$$

Except for the antisymmetrized identity operator $\bar{I}$, this is just the integral equation for scattering if nucleon "0" were considered to be *distinguishable* from the other nucleons.

Let us introduce explicitly the variables $\xi_0, \xi_1, \cdots, \xi_A$ into Eq. (28) for the final state, leaving the initial state unspecified. Then, because of the antisymmetry of $\bar{\Omega}$ with respect to an exchange of two ξ's

$$\sum_{\beta,\xi_0',\xi_\beta'}(\xi_0\xi_\beta|V_{\beta0}|\xi_0'\xi_\beta')(\xi_0'\xi_1\cdots\xi_\beta'\cdots\xi_A|\bar{\Omega}$$

$$=\sum_{\beta,\xi_0',\xi_\beta'}\tfrac{1}{2}[(\xi_0\xi_\beta|V_{\beta0}|\xi_0'\xi_\beta')-(\xi_0\xi_\beta|V_{\beta0}|\xi_\beta'\xi_0')]$$

$$\times(\xi_0'\xi_1\cdots\xi_\beta'\cdots\xi_A|\bar{\Omega}. \tag{29}$$

We can write

$$\bar{V}_{\beta0}=(\xi_0\xi_\beta|V_{\beta0}|\xi_0'\xi_\beta')-(\xi_0\xi_\beta|V_{\beta0}|\xi_\beta'\xi_0')$$

and set

$$V_0\bar{\Omega}=\bar{V}_0\bar{\Omega}, \tag{30}$$

if we restrict the integration in the matrix product to $\xi_0'>\xi_\beta'$.[16]

From the expression (30), we note that the individual two-body scatterings are treated properly,[12] as required

[16] We suppose that we have established an ordering relation for the ξ's so that this inequality has meaning.

by the Pauli principle. That is,

$$\bar{\Omega}=\bar{I}+\frac{1}{a(0)}\bar{V}_0\bar{\Omega}. \tag{28'}$$

Our last step is to construct the submatrix of $\bar{\Omega}$ which refers to "0" as the *fast* outgoing particle.[17] For this purpose let us suppose that the set of quantum numbers, ξ_α, contains in some manner a description of the (average) kinetic energy of the nucleon. Let us also suppose that our ordering relation[16] is such that $\xi_\alpha > \xi_\beta$ if "α" has a higher (average) kinetic energy than "β." We then define the *submatrix* of $\bar{\Omega}$ which describes "0" as the fast outgoing particle in which we are interested to be $\bar{\Omega}(0)$. It is then $\bar{\Omega}(0)$ which we require to calculate the flux of outgoing nucleon "0." We shall write

$$\bar{\Omega}(0)\equiv\bar{\Omega}|_{\xi_0\gg\xi_\alpha}$$

(for most "α"), implying by the symbol on the right that "0" has a higher kinetic energy than *most* of the other nucleons and is also *the particle* which we are observing (distinguished by virtue of its momentum and direction, etc.). Then

$$\bar{\Omega}\equiv\bar{\Omega}(0)+\bar{\Omega}', \tag{31}$$

where Ω' is that submatrix of Ω for which "0" is *not* the particle of interest to us. Using the above notation, we have from Eq. (28'):

$$\bar{\Omega}(0)=\bar{I}|_{\xi_0\gg\xi_\alpha}+\frac{1}{a(0)}\bar{V}_0\bar{\Omega}|_{\xi_0\gg\xi_\alpha}. \tag{32}$$

Obviously,

$$\bar{I}|_{\xi_0\gg\xi_\alpha}=I_0 \tag{22'}$$

[see Eq. (22)], since only one particle is fast in the initial state.

Using Eq. (31), we have also

$$V_0\bar{\Omega}|_{\xi_0\gg\xi_\alpha}=\sum_{\beta,\xi_0',\xi_\beta'}(\xi_0\xi_\beta|\bar{V}_{\beta 0}|\xi_0'\xi_\beta')$$

$$\times(\xi_0'\xi_1\cdots\xi_\beta'\cdots\xi_A|\bar{\Omega}(0)+\textstyle\sum_\beta\bar{V}_{\beta 0}\bar{\Omega}'|_{\xi_0\gg\xi_\alpha}. \tag{33}$$

The last term refers to processes for which "0" becomes the particle of interest to us after the last scattering (represented by $\bar{V}_0$). We have already $\xi_0'>\xi_\beta'$ so this last kind of term is of the "target exchange" type. That is, these refer to processes for which "0" and "β" are both slow until a last scattering which gives them both (or at least "0") a large recoil energy, while other fast particles are "slowed down" without interaction with these (in order that energy be conserved). This process we have agreed to neglect (this will be discussed further in the next section).[18]

Combining our conclusions from Eq. (33) with Eq. (22'), we can write Eq. (32) as

$$\bar{\Omega}(0)=1_0+\frac{1}{a(0)}\bar{V}_0\bar{\Omega}(0). \tag{34}$$

This is an integral equation involving *only* the submatrix $\bar{\Omega}(0)$. Thus we can calculate $\bar{\Omega}(0)$ without knowing the complete matrix $\bar{\Omega}$. Except for the occurrence of the antisymmetrized two-body scattering interaction, $\bar{V}_0$, this is the same equation which we would have to solve if "0" were distinguishable from other nucleons.

In other words, Eq. (34) states that we may use the multiple-scattering analysis of references I and II *without* modification (other than in the use of antisymmetrized two-body amplitudes). This means that $\bar{\Omega}(0)$ is given by the equations of multiple scattering,

$$\bar{\Omega}(0)=1_0+\frac{1}{a(0)}\sum_{\alpha\neq 0}t_\alpha\bar{\Omega}(0)_\alpha,$$

$$\bar{\Omega}(0)\alpha=1_0+\frac{1}{a(0)}\sum_{\beta\neq\alpha,0}t_\beta\bar{\Omega}(0)_\beta, \tag{35}$$

with

$$t_\alpha=\bar{V}_{\alpha 0}+\bar{V}_{\alpha 0}\frac{1}{a(0)}t_\alpha. \tag{36}$$

On making the impulse approximation, t_α is just the properly antisymmetrized two-body scattering amplitude for nucleons "0" and "α." The development of the *optical model* or study of the inelastic scattering proceeds just as in I and II.

IV. ESTIMATED SIZE OF "TARGET EXCHANGE" TERMS

From Eqs. (27) and (33), we see that a "target exchange" term of typical magnitude can be described as follows:

Nucleon "2" is initially fast and has a momentum $\mathbf{p}_2$. Nucleons "0" and "1" are initially bound. "0" and "1" scatter and are ejected, "0" being fast. To conserve energy (see the introduction, in which it was assumed that the mean free paths are sufficiently long that energy is at least roughly conserved between scatterings), particle "2" must be very nearly stopped.

Let the wave function for the "stopped" "2" be $g_2(\mathbf{z}_2)$. Let "0" and "1" be initially in the state $g_0(\bar{\mathbf{z}},\mathbf{r})$,

[17] We do not of course mean to imply that "0" is necessarily the only fast—or even the fastest—nucleon emitted. "Target exchange" involving the exchange of "0" with a nucleon which has suffered a previous scattering is expected to be especially small, since in this case *both* nucleons can be rather well localized in space. Thus the presence of fast nucleons other than "0" will not be troublesome.

[18] There are also processes for which "0" is *fast*, but not the nucleon of interest to us. Such exchange processes, as discussed in footnote 17, are expected to be even less important than those for which "0" is slow.

where

$$\mathbf{r}=\mathbf{z}_0-\mathbf{z}_1,$$
$$\bar{\mathbf{z}}=\tfrac{1}{2}(\mathbf{z}_0+\mathbf{z}_1). \tag{37}$$

Here $\mathbf{z}_0$ and $\mathbf{z}_1$ are the space coordinates of "0" and "1."[19] Also let the final momenta of these nucleons be $\mathbf{p}_0$ and $\mathbf{p}_1$, respectively. Define

$$\mathbf{K}=\mathbf{p}_0+\mathbf{p}_1,$$
$$\mathbf{p}=\tfrac{1}{2}(\mathbf{p}_0-\mathbf{p}_1).$$

Then the amplitude for this process is roughly

$$I_z=(2\pi)^{-9/2}\int \exp(-i\mathbf{K}\cdot\bar{\mathbf{z}})e^{-i\mathbf{p}\cdot\mathbf{r}}g_2^*(\mathbf{z}_2)$$
$$\times V(\mathbf{r})\exp(i\mathbf{p}_2\cdot\mathbf{z}_2)g_0(\bar{\mathbf{z}},\mathbf{r})d^3\bar{z}d^3rd^3z_2. \tag{38}$$

$V(\mathbf{r})$ is the interaction potential between nucleons "0" and "1."

Since $g_0(\bar{\mathbf{z}},\mathbf{r})$ is expected to vary rather slowly with $\bar{\mathbf{z}}$ and $\mathbf{r}$ (in comparison with the exponentials), we take it outside the integral and set

$$g_0(\bar{\mathbf{z}},\mathbf{r})\simeq 1/V_A,$$

where $V_A(=4\pi R^3/3)$ is the nuclear volume. Let

$$V_T(\mathbf{p})=(2\pi)^{-3}\int d^3r e^{-i\mathbf{p}\cdot\mathbf{r}}V(\mathbf{r}), \tag{39}$$

and

$$g_T(\mathbf{p}_2)=(2\pi)^{-\frac{3}{2}}\int \exp(i\mathbf{p}_2\cdot\mathbf{z}_2)g_2^*(\mathbf{z}_2)d^3z_2$$
$$\simeq[(2\pi)^3V_A]^{-\frac{1}{2}}\int_{V_A}\exp(i\mathbf{p}_2\cdot\mathbf{z}_2)d^3z_2$$
$$\simeq(4\pi/3)[(2\pi)^3V_A]^{-\frac{1}{2}}[p_2]^{-3}. \tag{40}$$

Here we have made the reasonable assumption that $g_2(\mathbf{z}_2)$ extends over a region having the size of the nuclear volume.[20] We then have

$$I_z\simeq(2\pi)^{\frac{3}{2}}\delta(\mathbf{K})V_T(\mathbf{p})(4\pi/3)[V_A^{\frac{1}{2}}p_2]^{-3}. \tag{41}$$

We must compare this with the direct process by which "0" strikes "1" and recoils. If "1" is initially bound in the state $g_1(\mathbf{z}_1)$ and if the initial momentum of "0" is $\mathbf{p}_0$, we have for the amplitude of the direct process

$$I_d\simeq(2\pi)^{-9/2}\int \exp(-i\mathbf{K}\cdot\bar{\mathbf{z}})e^{-i\mathbf{p}\cdot\mathbf{r}}V(\mathbf{r})$$
$$\times g_1(\mathbf{z}_1)\exp(i\mathbf{p}_0\cdot\mathbf{z}_0)d^3\bar{z}d^3r. \tag{42}$$

Here $\mathbf{K}$ is the total recoil momentum of "0" and "1" and $\mathbf{p}$ is their relative momentum; $\bar{\mathbf{z}}$ and $\mathbf{r}$ are respectively their center-of-mass and relative coordinates. Again taking $g_1(\mathbf{z}_1)$ out of the integral and setting it equal to

$$g_1(\mathbf{z}_1)\simeq[V_A]^{-\frac{1}{2}},$$

we find

$$I_d\simeq(2\pi)^{-\frac{3}{2}}\delta(\mathbf{K}-\mathbf{p}_0)V_T(\mathbf{p}-\tfrac{1}{2}\mathbf{p}_0)V_A^{-\frac{1}{2}}. \tag{43}$$

Aside from the δ-functions and the factor of V_T, the ratio of Eqs. (41) and (43) is

$$I_z/I_d\simeq(4\pi/3)V_A^{-1}p_2^{-3}=[p_2R]^{-3}, \tag{44}$$

where R is the nuclear radius. This evidently decreases rapidly with increasing energy for the incoming particle. For a 100-Mev incoming nucleon, this ratio is

$$I_z/I_d\simeq 0.03/A, \tag{45}$$

where A is the mass number of the nucleus. It is clear that Eq. (45) predicts a very small contribution resulting from "target exchange" processes. (The other type of "target exchange" occurring in Eq. (27) has a comparable magnitude.) The factor of A^{-1} in Eq. (45) is removed when we sum over the $(A-1)$ nucleons, "2," "3," ... "A," as incident particles. The correction for "target exchange" is, however, small at $E=100$ Mev, as predicted by Eq. (45), and decreases rapidly with increasing energy.[21]

V. ELASTIC SCATTERING OF FAST NUCLEONS AND THE OPTICAL POTENTIAL

In Sec. III we have shown that the problem of the scattering of a high-energy nucleon by a target nucleon reduces essentially to solving Eq. (34), in which the incident nucleon can be "distinguished" from the others. This equation can be applied both to the elastic and the inelastic scatterings. When it is applied to the latter problem we have a transport equation which describes how the incident energy will be transferred to nucleons in the target nucleus by successive collisions between pairs of nucleons. On the other hand, the first problem can be reduced to the scattering of a nucleon in the optical potential where the form of the optical potential can be connected with more fundamental quantities in the two-body problem.[2]

Here, as an example of the application of our method, we shall construct the optical potential for the elastic scattering of a nucleon according to II.

If one assumes the invariance of the scattering amplitude for a collision between two particles under space rotation, reflection, and time reversal, its most general form has been given by Wolfenstein and Ashkin.[22] When two particles are both nucleons, the scattering amplitude is antisymmetric for an interchange of their coordinates before the scattering and for an interchange of those after the scattering. Furthermore, the scattering amplitude is assumed to have the charge invariance

[19] For simplicity we neglect the other nucleons and all spin variables.

[20] "2" is certainly not expected to be localized in a region much less than the size of the nuclear volume at the termination of the scattering event.

[21] Our estimate depends really on the assumption that the momentum of the incident particle is higher than the bulk of the momentum spectra of bound nucleons.

[22] L. Wolfenstein and J. Ashkin, Phys. Rev. 85, 947 (1952).

property, except for a small correction due to Coulomb forces.

Under these additional conditions the scattering amplitude in the center-of-mass system for a collision in which a nucleon "1" with a momentum $\mathbf{q}$ and a nucleon "2" with a momentum $(-\mathbf{q})$ scatter into states with momenta $\mathbf{q}'$ and $(-\mathbf{q}')$, respectively, is given by the following expression:

$$
\begin{aligned}
&(\mathbf{q}', -\mathbf{q}'|t_{12}|\mathbf{q}, -\mathbf{q}) \\
&=\frac{3+\boldsymbol{\tau}_1\cdot\boldsymbol{\tau}_2}{4}\Big\{A_{3,3}\frac{3+\boldsymbol{\sigma}_1\cdot\boldsymbol{\sigma}_2}{4}+A_{3,1}\frac{1-\boldsymbol{\sigma}_1\cdot\boldsymbol{\sigma}_2}{4} \\
&+B_3\frac{[(\boldsymbol{\sigma}_1+\boldsymbol{\sigma}_2)\cdot(\mathbf{q}\times\mathbf{q}')]}{qq'}+C_3\Big(\frac{(\boldsymbol{\sigma}_1\cdot\mathbf{Q})(\boldsymbol{\sigma}_2\cdot\mathbf{Q})}{Q^2}-\tfrac{1}{3}\boldsymbol{\sigma}_1\cdot\boldsymbol{\sigma}_2\Big) \\
&+D_3\Big(\frac{(\boldsymbol{\sigma}_1\cdot\mathbf{P})(\boldsymbol{\sigma}_2\cdot\mathbf{P})}{P^2}-\tfrac{1}{3}\boldsymbol{\sigma}_1\cdot\boldsymbol{\sigma}_2\Big)\Big\} \\
&+\frac{1-\boldsymbol{\tau}_1\cdot\boldsymbol{\tau}_2}{4}\Big\{A_{1,3}\frac{3+\boldsymbol{\sigma}_1\cdot\boldsymbol{\sigma}_2}{4}+A_{1,1}\frac{1-\boldsymbol{\sigma}_1\cdot\boldsymbol{\sigma}_2}{4} \\
&+B_1\frac{[(\boldsymbol{\sigma}_1+\boldsymbol{\sigma}_2)\cdot(\mathbf{q}\times\mathbf{q}')]}{qq'}+C_1\Big(\frac{(\boldsymbol{\sigma}_1\cdot\mathbf{Q})(\boldsymbol{\sigma}_2\cdot\mathbf{Q})}{Q^2}-\tfrac{1}{3}\boldsymbol{\sigma}_1\cdot\boldsymbol{\sigma}_2\Big) \\
&+D_1\Big(\frac{(\boldsymbol{\sigma}_1\cdot\mathbf{P})(\boldsymbol{\sigma}_2\cdot\mathbf{P})}{P^2}-\tfrac{1}{3}\boldsymbol{\sigma}_1\cdot\boldsymbol{\sigma}_2\Big)\Big\}, \qquad (46)
\end{aligned}
$$

where

$$
\begin{aligned}
&\mathbf{Q}=\mathbf{q}'-\mathbf{q}, \\
&\mathbf{P}=(\mathbf{q}'\times\mathbf{q})\times\mathbf{Q}. \qquad (47)
\end{aligned}
$$

A, B, C, and D are complex functions of $|q|$ and $\cos\theta$ where θ is the scattered angle in the center-of-mass system. Terms containing a factor $(3+\boldsymbol{\tau}_1\cdot\boldsymbol{\tau}_2)/4$ or a factor $(1-\boldsymbol{\tau}_1\cdot\boldsymbol{\tau}_2)/4$ correspond to the scattering in the state with the isotopic spin $T=1$ or $T=0$, respectively. $A_{3,1}$ and $A_{1,1}$ are the singlet state scattering amplitudes and the remaining terms are those for the triplet state. In principle, A, B, C, and D are obtainable from experimental results for p-p and p-n scattering.[23]

We have already shown that the scattering of fast nucleons by atomic nuclei can be treated according to the method of references I and II, with slight modifications due to the Pauli principle. The "optical potential" v_c for $\bar{\Omega}(0)$ (the part of the wave function with the nucleon "0" as the *fast* nucleon) can be obtained by averaging $\sum_{\alpha\neq 0}t_{0\alpha}$ over the wave function $g_0(\xi_1, \cdots, \xi_A)$ of the nucleon. $t_{0\alpha}$ is the scattering amplitude given by Eq. (46) when it is transformed to the laboratory system.

If we take, for simplicity, a self-conjugate $(N=Z)$ nucleus with the total angular momentum $J=0$, the matrix element of the optical potential v_c for an elastic scattering of the nucleon "0" from a state of relative momentum $\mathbf{p}$ to a state $\mathbf{p}'$ is given by

$$
\begin{aligned}
(\mathbf{p}'|v_c|\mathbf{p})&=\int d^3z\rho(\mathbf{z})\exp[i(\mathbf{p}'-\mathbf{p})\cdot\mathbf{z}] \\
&\times\Big\{\frac{9A_{3,3}+3A_{3,1}+3A_{1,3}+A_{1,1}}{16} \\
&+\frac{3B_3+B_1}{4}\frac{2[\boldsymbol{\sigma}_0\cdot(\mathbf{p}\times\mathbf{p}')]}{p^2}\Big\}. \qquad (48)
\end{aligned}
$$

Terms of $t_{0,\alpha}$ linear in $\boldsymbol{\tau}_\alpha$ and $\boldsymbol{\sigma}_\alpha$ average to zero because $Z=N$ and $J=0$. $\rho(\mathbf{z})$ is the density of nucleons in the nucleus. The term containing $\boldsymbol{\sigma}_0$ shows the presence of spin-orbit coupling in the optical potential.[24]

There are, of course, corrections to the optical potential because of successive inelastic scatterings which bring the nucleus into the initial state after the last inelastic scattering.[25] The magnitude of this correction depends on the strength of correlations among nucleons in the nucleus. For high-energy nuclear scattering this can be shown to be small. We should like to emphasize that a solution of the scattering equation for the potential thus obtained is in general quite different from and has a wider validity than solutions obtained in the ordinary Born approximation.[26]

If we limit our attention to the forward scattering, we obtain Eq. (3) of the reference 3 from Eq. (48) under the assumption that $A_{3,3}$, $A_{3,1}$, etc., can be considered to be constant in this small region of the scattering angle. When the scattering angle becomes large, the corresponding matrix element of v_c becomes rapidly small because the density $\rho(\mathbf{z})$ has only a small amount of high-momentum components comparable with $|\mathbf{p}'-\mathbf{p}|$. This indicates that the scattering is mostly inelastic for large angles.

In conclusion, the impulse and multiple-scattering approximations hold for scatterings of fast nucleons by nuclei even if we take into account the Pauli principle. Through these approximations, amplitudes for scattering fast nucleons by nuclei can be expressed in terms of those for p-p and p-n scattering together with the knowledge of nucleon density and correlation functions.

We should finally emphasize that our conclusions apply to a much wider class of multiple-scattering problems than just those involving atomic nuclei. A simple example is, for instance, provided by the double (or triple) scattering of a beam of protons by successive hydrogen targets.

[23] The D term in Eq. (9) of reference 22 vanishes because of the Pauli principle for two nucleons. Our A, B, C, and D are linear combinations of their A, B, C, E, and F.

[24] If a nucleus has J different from 0, there are other types of terms which will flip the spin of the incoming particle by changing the spin direction of the nucleus at the same time. This part of the optical potential might be quite sensitive to the value of J. The magnitude of this correction relative to the remainder of the potential is of the order of J/A.

[25] See the reference II, Eq. (75).

[26] S. Tamor, Phys. Rev. 93, 227 (1954).

Approximate Reduction of the Many-Body Problem for Strongly Interacting Particles to a Problem of Self-Consistent Fields

K. A. BRUECKNER AND C. A. LEVINSON
*Indiana University, Bloomington, Indiana**

(Received November 22, 1954)

It is shown for systems of strongly interacting particles that in the limit of very many particles a transformation exists leading to an alternative problem which can be solved by a self-consistent field method. The transformed wave function describes "particles" moving in a collectively determined uniform potential; the transformation relating the transformed and original wave functions determines the amount of incoherence and correlation in the original function. The method appears to be more useful for fermion systems and is illustrated by applications to some aspects of nuclear structure.

I. INTRODUCTION

A WELL known approximation method for dealing with particles with weak or long-range interactions is the self-consistent field method of Hartree[1] and the related methods of Slater[2] and Fock.[3] It has in the past, however, been difficult or impossible to apply this method to systems of particles which interact strongly through short-range potentials. The origin of the difficulty lies in the strong correlations which must exist in the wave functions of the many-particle system, and which are neglected in the Hartree method. The great power of this method in its region of validity, however, shows the advantage of being able to construct a transformation which will bring the problem for strongly interacting systems into a form where the Hartree method can be applied. We shall now show that such a transformation does exist if we consider systems of many particles. The methods we use are based on a generalization and re-interpretation of a transformation introduced in another context by Francis and Watson.[4]

Before proceeding to the explicit discussion of this problem, we mention some qualitative features of approximations to certain well-known physical phenomena which suggest that the transformation which we seek in fact may at least approximately exist. First, it is well known from the study of nuclear structure that it is possible to introduce a formal model which predicts correctly a variety of details of the nuclear structure. This "shell model"[5] is based on the assumption that in some sense the effect of the many nuclear particles on a specified one may be represented by a collectively determined uniform potential. In this case each particle moves in a medium, the properties of which are determined by the states of the remaining particles. Consequently, since the state of the particle considered must be simply related to the states of the others, a problem of self-consistency arises. This requirement is usually only qualitatively stated and not in fact satisfied in many formulations of the nuclear problem. Applications of the ideas of this paper have, however, been previously made in papers[6] by the authors and are extended more generally in the following paper.[7]

Another variety of problems to which some features of the Hartree method apply is provided by the well known applications of the "optical" model.[8] In these cases the effects of localized strong interactions are replaced by an equivalent uniform potential; in most problems the effects of this potential on the states of the scattering system are ignored although if properly taken into account a problem of self consistency would arise.

Finally, a well-known application of a transformation to an equivalent problem in which a uniform potential acts on the particles is that used for a periodic lattice.[9] In this case the modulating effect of the lattice structure on the wave function can be transformed away (by introducing a function which is a product of a modulating function and a plane wave) and its effect replaced by an equivalent potential. In this case, as in the optical model, the lattice structure is assumed to be given and the effects of interactions is in first approximation ignored. The inclusion of these effects, however, would again give rise to a self-consistency problem, the determination of the lattice structure in a field which is in turn affected by the lattice structure.

With these qualitative remarks as an introduction, we proceed to the development of the method. In Sec. II we shall develop the formal properties of the transformation; in Sec. III we examine in detail the conditions under which the transformation is exact; in Sec. IV we discuss the characteristics of the transformation

* Supported in part by a grant from the National Science Foundation. The work was also done in part while the authors were visiting associate physicists at Brookhaven National Laboratory.

[1] D. R. Hartree, Proc. Cambridge Phil. Soc. **24**, 111 (1928).
[2] J. C. Slater, Phys. Rev. **35**, 210 (1930).
[3] V. Fock, Z. Physik **61**, 126 (1930).
[4] N. C. Francis and K. M. Watson, Phys. Rev. **92**, 291 (1953).
[5] M. G. Mayer, Phys. Rev. **74**, 235 (1948); Haxel, Jensen, and Suess, Phys. Rev. **75**, 1766 (1949).
[6] Brueckner, Levinson, and Mahmond, Phys. Rev. **95**, 219 (1954); K. A. Brueckner, Phys. Rev. **96**, 508 (1954). These papers will be referred to henceforth as NS I and NS II, respectively.
[7] K. A. Brueckner, following paper [Phys. Rev. **97**, 1353 (1955)]. This paper will be referred to henceforth as NS III.
[8] M. Lax, Revs. Modern Phys. **23**, 287 (1951); L. Foldy, Phys Rev. **67**, 107 (1945).
[9] F. Bloch, Z. Physik **52**, 555 (1928).

to the coherent problem; in Sec. V we show that the solution may be formulated as a self-consistent problem; in Sec. VI we show to what extent this problem has the characteristics of a variational problem; in Sec. VII we discuss the physical interpretation of the transformed wave function and its relation to the physical wave function; finally in Sec. VIII we summarize our results and make some concluding remarks.

II. FORMALISM

In this section we shall examine in detail the nature of a transformation introduced by Francis and Watson[4] in their discussions of the many-body problem. We follow their notation and in much of this section we shall simply expand and comment on their derivation. In Appendix A we shall also give this derivation in an alternative form using the methods of second quantization. The necessary notation used there is less compact than that which we will use here; the more explicit representation of the operators, however, may give additional insight into the method.

The problem which we wish to solve is that of finding the eigenfunctions of the Hamiltonian

$$H=H_0+\sum_\alpha v_\alpha, \tag{1}$$

where H_0 is the sum of the kinetic energy operators and v_α is the potential energy of interaction for the αth pair. The sum over α is over all pairs, i.e.,

$$\sum_\alpha v_\alpha=\sum_{i<j}\sum v_{ij}=\tfrac{1}{2}\sum_i\sum_j v_{ij}. \tag{2}$$

We shall now show that we can replace the problem of solving for the eigenfunctions of H by an alternative simpler problem.

Following Watson, we introduce the functions t_α and V_C defined in the following way:

$$t_\alpha=v_\alpha+v_\alpha\frac{P}{E-H_0-V_C}t_\alpha, \tag{3}$$

and

$$V_C=\sum_\alpha t_{C\alpha}, \tag{4}$$

where $t_{C\alpha}$ is that part of the operator t_α which is diagonal with respect to the eigenstates of the operator $H_C=V_C+H_0$, i.e., the states defined by the equation

$$H_C\psi_C=(H_0+V_C)\psi_C=E\psi_C. \tag{4'}$$

In Eq. (3) for t_α, $P(E-H_0-V_C)^{-1}$ means that we take the principal value definition of the singularity. This is equivalent to omitting matrix elements to the ground state. The operator t_α is closely related to the scattering operator giving the scattering from the potential v_α, the only difference being the appearance of V_C in the energy denominator and the definition of the singularity.[10] The diagonal part of t_α is thus related to the forward scattering from the potential v_α.

[10] B. Lippmann and J. Schwinger, Phys. Rev. 79, 669 (1950).

To exhibit V_C in somewhat more compact form, we can combine Eqs. (3) and (4) for t_α and V_C into one equation by using first the result which follows from Eq. (1):

$$t_\alpha=v_\alpha+v_\alpha\frac{P}{E-H_0-V_C-v_\alpha}v_\alpha, \tag{5}$$

and inserting this into the definining equation for V_C. The result is

$$V_C=\sum_\alpha v_{C\alpha}+\left(v_\alpha\frac{P}{E-H_0-V_C-v_\alpha}v_\alpha\right)_C, \tag{6}$$

with the subscript C meaning diagonal with respect to the states ψ_C. This alternative defining equation for V_C is a nonlinear integral equation; we shall return to its implications and to a self-consistent method for solving it later. At present we shall proceed to evaluate the properties of the transformation operator which leads us to the potential.

We introduce the functions†

$$\begin{aligned} F&=1+\frac{1}{e}\sum_\alpha I_\alpha F_\alpha,\\ F_\alpha&=1+\frac{1}{e}\sum_{\alpha\neq\beta} I_\beta F_\beta, \end{aligned} \tag{7}$$

where

$$I_\alpha=t_\alpha-t_{C\alpha}. \tag{8}$$

The functions F and F_α thus depend only on the nondiagonal matrix elements of t_α except through the appearance of V_C in the energy denominators $e\equiv E-H_0-V_C$. We finally construct a function

$$\varphi=F\psi_C. \tag{9}$$

We wish to see to what extent the function φ is an eigenfunction of the original Hamiltonian. In the following we use the powerful symbolic methods of the operator algebra developed by Lippmann and Schwinger,[10] Chew and Goldberger,[11] and particularly by Watson.[12]

To carry out the desired proof, we consider first the product

$$\sum_\alpha v_\alpha F. \tag{10}$$

By using the defining equation for F, this can be written

$$\sum_\alpha v_\alpha\left(1+\frac{1}{e}\sum_\beta I_\beta F_\beta\right)=\sum_\alpha v_\alpha+\sum_\alpha v_\alpha\frac{1}{e}I_\alpha F_\alpha+\sum_{\alpha\neq\beta}\sum v_\alpha\frac{1}{e}I_\beta F_\beta. \tag{11}$$

† *Note added in proof.*—The specification of principal value for the singularity in e^{-1} will be omitted here and in the following but must be included in an explicit evaluation.

[11] G. F. Chew and M. L. Goldberger, Phys. Rev. 87, 778 (1952).

[12] K. M. Watson, Phys. Rev. 89, 575 (1953).

The second term may be broken into two parts, i.e., we replace I_α by $t_\alpha - t_{C\alpha}$ [Eq. (8)]. We also make use of the relation between t_α and v_α stated in Eq. (3). We then find

$$v_\alpha \frac{1}{e} I_\alpha = v_\alpha \frac{1}{e}(t_\alpha - t_{C\alpha}) = t_\alpha - v_\alpha \frac{1}{e} t_{C\alpha}. \quad (12)$$

We also use the identity

$$\sum_\alpha v_\alpha = \sum_\alpha v_\alpha \left(F_\alpha - \sum_{\beta\neq\alpha} \frac{1}{e} I_\beta F_\beta \right)$$

$$= \sum_\alpha v_\alpha F_\alpha - \sum_{\alpha\neq\beta} v_\alpha \frac{1}{e} I_\beta F_\beta. \quad (13)$$

Thus we can write Eq. (11), using Eq. (12), as

$$\sum_\alpha v_\alpha + \sum_\alpha \left(t_\alpha - v_\alpha - v_\alpha \frac{1}{e} t_{C\alpha} \right) F_\alpha + \sum_{\alpha\neq\beta} \sum v_\alpha \frac{1}{e} I_\beta F_\beta$$

$$= \sum_\alpha v_\alpha F. \quad (14)$$

The first, third, and last terms of this combine by Eq. (13) to give zero. We also transform the second term by making use of first Eq. (8),

$$\sum_\beta t_\beta F_\beta = \sum_\beta (I_\beta + t_{C\beta}) F_\beta$$

$$= \sum_\beta I_\beta F_\beta + \sum_\beta t_{C\beta} + \sum_\beta t_{C\beta}(F_\beta - 1), \quad (15)$$

and then Eq. (7) for F_β in the last term, to give

$$\sum_\beta t_\beta F_\beta = \sum_\beta I_\beta F_\beta + \sum_\beta t_{C\beta} + \sum_{\alpha\neq\beta} \sum t_{C\beta} \frac{1}{e} I_\alpha F_\alpha. \quad (16)$$

Combining this result with Eqs. (9), (10), and (14), we then find

$$\sum_\alpha v_\alpha \varphi = \left[\sum_\beta I_\beta F_\beta + \sum_\beta t_{C\beta} + \sum_{\alpha\neq\beta} t_{C\beta} \frac{1}{e} I_\alpha F_\alpha \right.$$

$$\left. - \sum_\beta V_\beta \frac{1}{e} t_{C\beta} F_\beta \right] \psi_C. \quad (17)$$

The second and third terms here can be combined by using Eq. (7):

$$\sum_\beta t_{C\beta} + \sum_{\alpha\neq\beta} \sum t_{C\beta} \frac{1}{e} I_\alpha F_\alpha$$

$$= \sum_\alpha \sum_\beta t_{C\beta} \left(1 + \frac{1}{e} I_\alpha F_\alpha \right) - \sum_\beta t_{C\beta} \frac{1}{e} I_\beta F_\beta$$

$$= \sum_\beta t_{C\beta} F - \sum_\beta t_{C\beta} \frac{1}{e} I_\beta F_\beta. \quad (18)$$

For the first term of Eq. (17) we use (inserting principal value explicitly)

$$(E - H_0 - V_C) F \psi_C = e \left(1 + \frac{P}{e} \sum_\alpha I_\alpha F_\alpha \right) \psi_C$$

$$= eP \frac{1}{e} \sum_\alpha I_\alpha F_\alpha \psi_C,$$

which follows from Eqs. (4′) and (7). Thus we obtain the final result:

$$\sum_\alpha v_\alpha F \psi_C = (E - H_0 - V_C) F \psi_C + \sum_\beta t_{C\beta} F \psi_C$$

$$+ \left[1 - (E - H_0 - V_C) P \frac{1}{e} \right] \sum_\beta I_\beta F_\beta \psi_C$$

$$- \sum_\beta \left(t_{C\beta} \frac{1}{e} I_\beta + v_\beta \frac{1}{e} t_{C\beta} \right) F_\beta \psi_C.$$

By using the defining equation for V_C [Eq. (4)], this can also be written

$$(E - H_0 - \sum_\alpha v_\alpha) F \psi_C = \sum_\beta \left(t_{C\beta} \frac{1}{e} I_\beta + v_\beta \frac{1}{e} t_{C\beta} \right) F_\beta \psi_C$$

$$+ \left[(E - H_0 - V_C) P \frac{1}{e} - 1 \right] \sum_\beta I_\beta F_\beta \psi_C. \quad (19)$$

This result is in no sense an approximation; it follows as an identity from the definitions of Eqs. (3), (4), (7), and (9).

The last term of Eq. (19) is zero everywhere except on the energy shell since $(E - H_0 - V_C)^{-1} P (E - H_0 - V_C)^{-1}$ is equal to one everywhere except at $E = H_0 + V_C$ where $P(E - H_0 - V_C)^{-1}$ is equal to zero.‡ The first two terms on the right side of Eq. (20) will be discussed in detail in the next section and shown to vanish as $1/N$ compared with the energy of the system. The only remaining correction to the energy which prevents $F\psi_i$ from being everywhere an exact solution in the limit $N \to \infty$ is the diagonal matrix element

$$\Delta E = \{ \psi_i, [1 - (E - H_0 - V_C) P (E - H_0 - V_C)^{-1}]$$

$$\times \sum_\beta I_\beta F_\beta \psi_C \} = (\psi_C, \sum_\beta I_\beta F_\beta \psi_C),$$

which gives in first nonvanishing order (inserting pair indices explicitly)

$$\Delta E = \sum_{i\neq j\neq k} \left(\psi_C, I_{ij} \frac{1}{e} I_{jk} \frac{1}{e} I_{kC} \psi_C \right). \quad (20)$$

The shift in the energy for a fermion system in a highly degenerate state which results from this correction has been evaluated in *NS I* and shown to give a very small

‡ The authors are indebted to R. J. Eden and N. C. Francis and to F. E. Low and J. Bardeen who independently pointed out an error in a previous treatment of these terms.

effect. Thus we shall take the provisional view that the net effect of these high order correlation terms is small and examine the interpretation of the transformation and wave function neglecting the effects of these corrections. This assumption corresponds to the treatment used in the nuclear problems considered in NS I, II, and III, and allows us to exhibit more easily the structure and physical content of the method.

III. "1/N" CORRECTION TERMS

Dropping the correlation terms, we rewrite Eq. (19) in the form

$$(E-H)F\psi_C=\sum_\beta\left(t_{C\beta}\underset{e}{1}I_\beta+v_\beta\underset{e}{1}t_{C\beta}\right)F_\beta\psi_C\equiv H_1F\psi_C. \quad (21)$$

We thus can consider H_1 as defined by Eq. (21) to be a perturbing term in the Hamiltonian and determine its first order effect on the energy by evaluating the diagonal matrix elements of the perturbing energy.

We first bring the correction terms to more symmetric form by using the equations relating t, v, t_C, and I. We have an expansion for v_α in terms of t_α which follows from Eq. (3):

$$v_\alpha=t_\alpha-t_\alpha\underset{e}{1}t_\alpha+t_\alpha\underset{e}{1}t_\alpha\underset{e}{1}t_\alpha-\cdots. \quad (22)$$

Upon using this result, the two terms on the right side of Eq. (21) become:

$$\sum_\alpha\left[t_{C\alpha}\underset{e}{1}I_\alpha+t_{C\alpha}\underset{e}{1}t_{C\alpha}+I_\alpha\underset{e}{1}t_{C\alpha}-t_\alpha\underset{e}{1}t_\alpha\underset{e}{1}t_{C\alpha}+\cdots\right], \quad (23)$$

where we keep at present only the leading terms in the expansion. To evaluate the energy perturbation we also expand the F function in a power series in the incoherent scattering operator I_α, i.e., we expand Eq. (7) for F and F_α to give

$$\begin{aligned}F&=1+\underset{e}{1}\sum_\alpha I_\alpha+\underset{e}{1}[\sum_{\alpha\neq\beta}\sum I_\alpha\underset{e}{1}I_\beta+\cdots,\\ F_\alpha&=1+\underset{e}{1}\sum_{\alpha\neq\beta}I_\beta+\underset{e}{1}\sum_{\alpha\neq\beta}\sum_{\neq\gamma}I_\beta\underset{e}{1}I_\gamma+\cdots.\end{aligned} \quad (24)$$

Using these expansions, we find to third order:

$$\begin{aligned}\Delta E_3&=(F\psi_C,H_1F\psi_C)\\ &=\sum_\alpha\Big(\psi_C,\Big[t_{C\alpha}\underset{e}{1}I_\alpha+t_{C\alpha}\underset{e}{1}t_{C\alpha}+I_\alpha\underset{e}{1}t_{C\alpha}-t_\alpha\underset{e}{1}t_\alpha\underset{e}{1}t_{C\alpha}\\ &\quad+\sum_\beta I_\beta\underset{e}{1}\Big(t_{C\alpha}\underset{e}{1}I_\alpha+t_{C\alpha}\underset{e}{1}t_{C\alpha}+I_\alpha\underset{e}{1}t_{C\alpha}\Big)\\ &\quad+\sum_{\beta\neq\alpha}\Big(t_{C\alpha}\underset{e}{1}I_\alpha+t_{C\alpha}\underset{e}{1}t_{C\alpha}+I_\alpha\underset{e}{1}t_{C\alpha}\Big)\underset{e}{1}I_\beta\Big]\psi_C\Big). \quad (25)\end{aligned}$$

In this result most of the terms give no contribution; terms in which the combination $e^{-1}t_{C\alpha}\psi_C$) or $(\psi_C,t_{C\alpha}e^{-1}$ appears vanish since $t_{C\alpha}$ is diagonal in energy and the principal value treatment of the singularity in $1/e$ is equivalent to omitting the energy conserving part of $1/e$. Further we get contributions from terms involving pairs of operators I_α only if these operators act twice in the same pair of particles, the remaining combinations having no diagonal matrix elements. Using these two results Eq. (25) for the energy shift reduces to:

$$\Delta E_3=\sum_\alpha\left(\psi_C,I_\alpha\underset{e}{1}t_{C\alpha}\underset{e}{1}I_\alpha\psi_C\right). \quad (26)$$

This term is easily interpreted; it is the result of a scattering of the pair of particles out of the ground state ψ_C, their propagation and coherent scattering, and the final rescattering of the pair to their original state.

We can immediately draw a conclusion about the dependence of this term on the total number of particles N. We note that the operators t_C and I_α each contain a factor of v^{-1} (v the total volume) from the normalization of the wave functions. Further, the sum over intermediate momentum states contains a factor of v, since $\sum_k\rightarrow[v/(2\pi)^3]\int d\mathbf{k}$. The sum over all pairs of particles gives a factor $N(N-1)/2$. The net result is that

$$\Delta E_3=\tfrac{1}{2}N(N-1)v^{-2}f, \quad (27)$$

where f is a function independent of N. Since the total volume itself depends on N as:

$$v=N\Delta, \quad (28)$$

where Δ is the volume per particle, the energy shift is (for $N\gg1$):

$$\Delta E_3=\tfrac{1}{2}\Delta^{-2}f, \quad (29)$$

and is consequently independent of N. This is to be compared with the total energy E of the system which is proportional to N. We therefore see that the correction term ΔE_3 is indeed of order $1/N$ compared with the total energy.

It is important to note that this result depends in detail on the separation of t_α into $t_{C\alpha}$ and I_α, since it is the absence of diagonal elements in I_α which suppresses the magnitude of the energy shift. For any other choice of I_α, the second order terms in the perturbing energy would not vanish and corrections of order N rather than of order unity would appear.

It is of interest to exhibit explicitly the magnitude of these "$1/N$" terms. We have done this in Appendix B in the case which is of particular interest to us, i.e., the nuclear structure problem. Using a simplified model we have found that the energy shift per particle resulting from the perturbing terms is approximately 10 Mev/N. This is quite negligible (for moderate values of N) compared with the unperturbed energy per particles of about -14 Mev.

It is easy to show by inspection of the next terms in the expansion of the perturbing energy that their matrix elements are also independent of N or depend on powers of $1/N$; they therefore also vanish compared with the unperturbed energy as $N\to\infty$. The only remaining question concerns the convergence of the expansion in $t_{C\alpha}$ and I_α which we have used. It is not easy to estimate the general term in this series which contains multiple combinations of incoherent and coherent scatterings. We have, however, examined the next term of fourth order, which can be shown to be:

$$\Delta E_4=\Big(\psi_C,\Big\{\sum_{\alpha\neq\beta\neq\gamma}\sum\sum\Big[\underset{e}{1}I_\alpha\underset{e}{1}t_{C\alpha}\underset{e}{1}I_\beta\underset{e}{1}I_\gamma+\underset{e}{1}I_\alpha\underset{e}{1}t_{C\beta}\underset{e}{1}I_\beta\underset{e}{1}I_\gamma+\underset{e}{1}I_\alpha\underset{e}{1}I_\beta\underset{e}{1}t_{C\gamma}\underset{e}{1}I_\gamma\Big]+\sum_\alpha\sum_\beta\Big[\underset{e}{1}I_\alpha\underset{e}{1}t_{C\beta}\underset{e}{1}t_{C\beta}\underset{e}{1}I_\alpha\Big]\Big\}\psi_C\Big). \quad (30)$$

Part of the last term here arises from the second order perturbation of H_1 [see Eq. (21)]; it is easily shown using the arguments used to evaluate the N dependence of ΔE_3 to be of order $1/N$ and hence to be negligible. We consider the remaining terms in more detail. They are closely related to the energy perturbation evaluated in the nuclear case in NS I[6] except for the presence of a term $t_{C\alpha}/e$. This we approximate rather roughly as being of the order $1/N$. The remaining sum over α, β, γ is identical with the expression evaluated in NS I which was found to give very approximately 0.15 Mev per particle. Thus we have, in order of magnitude,

$$\Delta E_4\approx(1/N)(0.15\text{ Mev}\times N)=0.15\text{ Mev}. \quad (31)$$

This is much smaller than the lowest order perturbation, $\Delta E_3\approx 10$ Mev; we therefore have some indication of a very rapid convergence of the expansion of Eq. (23) for the perturbing energy.

IV. INTERPRETATION OF THE TRANSFORMATION FUNCTION F

Restating the conclusion of the last section; we find (to the approximation discussed at the end of Sec. II) that

$$\varphi=F\psi_C\underset{N\to\infty}{=}\psi, \quad (32)$$

where ψ is an eigenfunction of H belonging to the energy E and ψ_C is an eigenfunction of H_C belonging to the same eigenvalue. We can easily derive an equivalent formal statement of this result. Let us introduce F^{-1}, the inverse of F. Then we have

$$E\psi_C=H_C\psi_C. \quad (33)$$

Multiplying by F, this becomes

$$FE\psi_C=EF\psi_C=FH_C\psi_C=FH_CF^{-1}F\psi_C. \quad (34)$$

Since $F\psi_C$ is the wave function ψ (in the limit as $N\to\infty$), this can be written as

$$E\psi=(FH_CF^{-1})\psi. \quad (35)$$

Thus we are led to identify FH_CF^{-1} with the Hamiltonian, i.e.,

$$FH_CF^{-1}=H \quad (36)$$

or

$$H_C=F^{-1}HF. \quad (37)$$

The function F therefore acts as a transformation on the wave function; the solution of the original problem for the eigenvalue is equivalent to the solution of the transformed problem with the transformed Hamiltonian H_C.

A difficulty not so far stated but implicit in these results arises from the specification of the boundary values in the transformed problem. We are interested in a bound system and it would perhaps seem sufficient to specify the vanishing of the wave functions on some boundary, thus approximating in the solution for H_C to the appearance of a surface in the actual solution for ψ. This cannot, however, be generally correct since the function F depends nonlocally on the coordinates of the particles and so can introduce a difference in the boundary conditions for ψ and ψ_C. It is thus important to show that the separation $t_\alpha=t_{C\alpha}+I_\alpha$ has been made in such a way as to minimize this boundary condition effect. That this is so is rather obvious in the nuclear problem in which we consider a highly degenerate Fermi gas. As a result of the action of the exclusion principle the incoherent operators I_α have matrix elements from the ground state only to excited states in which the excited particles occupy previously empty states. The associated large momentum transfers and large excitation energies can both be expected to reduce very considerably the effects of incoherence and thus to make F approximately an identity operator for states below the Fermi momentum.

Thus we see that in many ways the separation which we have made is an optimum one; not only is the transformed problem in H_C much more easily soluble than the original problem but also the effects of F in the fermion case are perhaps as small as the simpler choices of I_α will allow. We note that these remarks do not hold for a system of bosons where the exclusion principle cannot act to simplify the effects of F.

V. SELF-CONSISTENT APPROXIMATION METHOD

We restate the result of the preceding sections, which is that we can determine the energy eigenvalues by solution of the eigenvalue problem,

$$E\psi_C=(H_0+V_C)\psi_C, \quad (38)$$

with V_C defined by Eqs. (3) and (4). Let us examine the definition more closely; first, we note that the

definition[13] of t_α,

$$t_\alpha = v_\alpha + v_\alpha (E - H_0 - V_C)^{-1} t_\alpha, \tag{39}$$

involves V_C. Further, the definition of V_C involves evaluation of the diagonal matrix elements of t_α with respect to the unknown states ψ_C. Thus these definitions are obviously not fully specified, and a problem arises of choosing the states ψ_C and the potential V_C in such a way that the set of coupled equations for V_C and ψ_C are satisfied. A suitable self-consistent method is the following:

(1) Assume a set of states $\psi_C^{(0)}$ which are product functions of the variables of N particles, and a potential $V_C^{(0)}$ diagonal with respect to these states.

(2) Use Eq. (3) to calculate $t_\alpha^{(0)}$ and from this compute $t_{C\alpha}^{(0)}$ using the assumed definition of the states $\psi_C^{(0)}$.

(3) Construct $V_C^{(1)}$ from the computed $t_{C\alpha}^{(0)}$ and finally determine the eigenstates $\psi_C^{(1)}$.

(4) Compare the eigenstates $\psi_C^{(1)}$ with $\psi_C^{(0)}$ and the potential $V_C^{(1)}$ with $V_C^{(0)}$.

(5) Adjust the choices of states and V_C and recycle through steps 1–4.

This procedure is troubled by the same questions of convergency and stability that occur in the Hartree method. In the case of a semi-infinite medium, however, the procedure is greatly simplified since the states ψ_C are exactly known, namely, properly symmetrized product plane wave states. The potential V_C diagonal with respect to these states is simply diagonal in momentum space. An approximate solution to the self-consistency problem has been obtained for the nuclear structure case in NS III[7] and is discussed in detail there.

VI. VARIATIONAL ASPECTS OF THE PROBLEM

With the choice of the transformation function F which we have discussed in Secs. II, III, and IV, we see that ψ_C, describing as it does plane wave motion, can be written as a product of plane wave functions. The potential energy of the system can then be evaluated by carrying out the sum over the forward scattering amplitudes. This, however, is in some ways not closely related to the physical problem since the actual solution ψ for a bound system predicts a closed surface which cannot be given by the transformed Hamiltonian H_C. To approximate to the physical state, we thus are forced to specify boundary conditions for ψ_C which represent the effects of the surface. This can be done by requiring that the transformed wave function satisfy periodic boundary conditions or vanish on the surfaces of a normalization volume. For the nuclear case discussed in detail elsewhere, we have specified that the wave function vanish on the surface of a sphere. Further, since the energy of the system is a minimum when the physical system takes on its stable density, we regard the density a parameter to be varied until the energy is a minimum. In this way we assume that we approximate closely to the physical situation; one can also describe this procedure as a variational problem of standard form in which the trial function is $\varphi = F\psi_C$ and the density ρ is a variational parameter.

Let us consider the variational aspects of the problem more fully: We let ψ_0 be the true eigenfunction of the system with eigenvalue E. Introducing our approximate $\varphi = F\psi_C$ with a variational parameter ρ (the density) contained in the specification of ψ_C, we have

$$E_0 \leqq (\varphi, H\varphi)/(\varphi,\varphi) = E(\rho). \tag{40}$$

Making use of the transformation properties of F, this can be written as

$$E(\rho) = \frac{(F\psi_C, HF\psi_C)}{(F\psi_C, F\psi_C)} = \frac{(\psi_C, F^\dagger HF\psi_C)}{(\psi_C, F^\dagger F\psi_C)} \underset{N\to\infty}{=} \frac{(\psi_C, F^\dagger FH_C\psi_C)}{(\psi_C, F^\dagger F\psi_C)} = E_C = \frac{(\psi_C, H_C\psi_C)}{(\psi_C,\psi_C)}, \tag{41}$$

again neglecting the high order correlation terms and the correction terms which vanish for large N. The function F contains all the correlations in the system; the ψ_C is an uncorrelated product of plane wave functions. This is very similar to the form introduced by Bloch[9] and also to that used by Drell and Huang[14] in the nuclear problem; the particular form which we have chosen, however, allows us to make the transformation of Eq. (41) so that we are able to replace the problem of determining ψ by the simpler problem of determining ψ_C. We observe one very simple feature of these results, which is that we do not need an explicit form for F [other than the formal definition of Eq. (7)] to evaluate the energy $E_C(\rho)$, since we have an explicit form H_C for the transformed Hamiltonian $F^{-1}HF$.

VII. RELATION BETWEEN ψ_C AND ψ

It is important to remark that the relation between the actual wave function ψ and the "coherent" ψ_C is not simple since it involves the operator F which is known only formally through the defining equations [Eq. (7)]. We can, however, see several obvious features of ψ if we examine the lowest term in the incoherent scattering operators I_α in the expansion for F, which is

$$\psi = F\psi_C = \psi_C + \frac{1}{e}\sum_\alpha I_\alpha \psi_C + \cdots. \tag{42}$$

The leading term shows that the actual wave function contains an admixture of single-particle states, the predominance of this state depending on the matrix ele-

[13] See also Appendix A for the modification of this operator for the case of many fermions. The change discussed there is equivalent to the omission of certain intermediate states in the summation implied in Eq. (39).

[14] S. D. Drell and Kerson Huang, Phys. Rev. **91**, 1527 (1953).

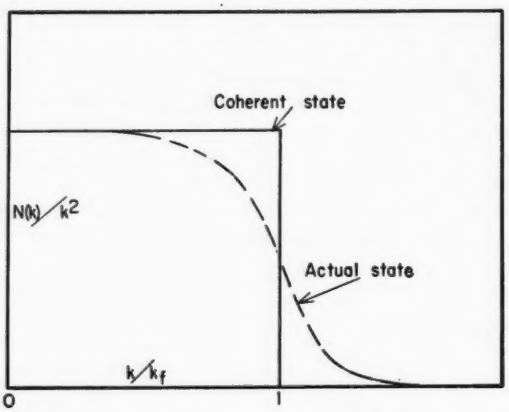

FIG. 1. Departure of lowest energy state ψ for a highly degenerate fermion gas from the state ψ_C.

ments of I_α for excitations of the nucleus. The effect of the term in the incoherent scattering operator I_α is to mix into the wave function excited states in which two particles at a time have been excited; if we fix our attention on a state ψ in which a given pair have been excited, then we find contributions to this state by evaluating the matrix elements of I_α between the desired state and all unexcited states. In a fermion gas we expect the effect to be largest on states just below the Fermi momentum since the matrix elements of I_α are then the largest. The energy denominator also varies rapidly with particle excitation, particularly because of the modified mass effect[7] which very considerably increases the kinetic energies. This is equivalent to including the effect of the rapid decrease of the potential (see NS II and III) felt by a particle as it goes into excited states. The higher terms in the expansion of F also have an obvious interpretation; they are associated with further incoherent scatterings which could lead to additional excitations of the system or to repopulation of the low-lying empty states.

Typically we might expect for a degenerate Fermi gas an effect of the sort shown in Fig. 1, the actual state ψ approximating fairly well to the state ψ_C for momenta below the Fermi momentum, but showing an admixture of higher-momentum states. Although the effect of these on, for example, the mean energy of the system is in our formulation zero, we would expect that under certain circumstances the appearance of very high Fourier components in the wave function would strongly manifest itself. This would be, for example, in high-energy processes depending critically on the high-momentum components, where the almost fully populated low-lying momentum states would have little effect and consequently a small admixture of high-momentum states would have great importance.

These results are not at all unexpected in the case of nuclear structure, since it is well known that the shell model is only a first approximation to a correct description of the nucleus, the perturbing effects on the surface states of two-body interactions being rather important. We see that the independent-particle model may give a good representation of certain properties of the nucleus (such as the ordering of states and mean energy, for example) but be quite inadequate for other properties dealing with finer details of the structure.

VIII. SUMMARY OF RESULTS AND CONCLUSIONS

In this paper we have examined the nature of the method which was introduced by Watson and Francis[1] in the study of the optical model and which we have generalized to apply to strongly correlated many-particle systems. This method is in essence the replacement of the original problem by an alternative simpler problem which arises from the original one by the transformation discussed in the preceding sections. This transformation is, as we have seen, exact as the number of particles become very large if the correlation terms discussed earlier are neglected. The transformed "coherent" problem is relatively easy to solve except for an uncertainty in the proper boundary conditions; its solution has been discussed in NS I, NS II, and NS III. The treatment of the boundary is difficult in the transformed problem; we have discussed the replacement of the physical surface by a boundary condition on the wave functions which lead to a variational problem for the energy. The "independent particle" wave function ψ_C, which arises naturally in the transformed problem, cannot be directly interpreted as the physical wave function since the latter is obtained from the former by a transformation which introduces correlations into the wave function. As a consequence, in the case of a nucleus the system departs from a Fermi gas in that, for example, higher-momentum components are present in the wave function. Reasons are discussed, however, which show that in considerations of certain general features of the nucleus, the actual wave function may be identified with the independent-particle function ψ_C. We expect, however, that the departures of the structure from a true independent-particle structure cannot be neglected for high-energy phenomena.

A dominant feature of the method we have described is that it has at present been shown to give only the correct lowest energy eigenvalue with good accuracy, this being the result of our obtaining an explicit (and simple) representation for the transformed Hamiltonian H_C. It is possible, however, that other quantum numbers of the transformed problem (such as parity and angular momentum) may also be simply related to the quantum numbers of the physical system, i.e., that it may be able to exhibit simply the transformed angular momentum and parity operators. These and similar questions are to be discussed in detail, together with the properties of more general transformations than we have considered, by Eden and Francis.[15]

[15] R. J. Eden and N. C. Francis, this issue [Phys. Rev. 97, 1366 (1955)].

APPENDIX A

Diagonalization of the Hamiltonian in Second-Quantized Form

We introduce a set of basis states φ_i and write the Hamiltonian as a second-quantized operator on the occupation numbers of these states, i.e., we have (with T_i the kinetic energy in the ith state):

$$H=\sum_i T_i\eta_i^*\eta_i+\tfrac{1}{2}\sum_{ijkl} v_{ij,k\eta_i}\eta_i^*\eta_j^*\eta_\eta\eta_k=H_0+V, \quad \text{(A1)}$$

where the η_i and η_i^* are annihilation and creation operators with commutation laws (for a system of fermions):

$$[\eta_i,\eta_j^*]_+=\delta_{ij}. \quad \text{(A2)}$$

The change for boson systems is of course made by replacing the anticommutator by the commutator.

We seek a transformation which will transform H into an operator with only diagonal matrix elements. In analogy with Sec. II, we introduce the scattering operator:

$$t_{ij,kl}=v_{ij,kl}+\sum_{mn}\frac{1}{e}v_{ij,mn}\eta_m\eta_n\eta_n^*\eta_m^* t_{mn,kl}. \quad \text{(A3)}$$

We also as before break this into a diagonal and nondiagonal part:

$$t_{ij,kl}=t_{ij,ij}\delta_{ik}\delta_{jl}+t_{ij,ji}\delta_{kj}\delta_{il}+I_{ij,kl}, \quad \text{(A4)}$$

and use this to define the diagonal operator:

$$e=E-\sum_i T_i\eta_i^*\eta_i-V_C, \quad \text{(A5)}$$

where E is the energy eigenvalue and

$$V_C=\tfrac{1}{2}\sum_{ij}(t_{ij,ij}\eta_i\eta_j\eta_j^*\eta_i^*+t_{ij,ji}\eta_i\eta_j\eta_i^*\eta_j^*). \quad \text{(A6)}$$

Finally, using the definition of $I_{ij,kl}$ given in Eq. (A4), we construct the operators F and F_{kl} by using the equations:

$$\begin{aligned} F&=1+\frac{1}{e}\sum_{ijkl} I_{ij,k\eta_i}\eta_j^*\eta_\eta\eta_k F_{kl}, \\ F_{kj}&=1+\frac{1}{e}\sum_{ij\neq kl}\sum_{mn} I_{ij,mn}\eta_i^*\eta_j^*\eta_n\eta_m F_{mn}. \end{aligned} \quad \text{(A7)}$$

We next proceed to the proof of the desired result. The development follows rather closely the more general technique used in Sec. II and consequently we shall somewhat condense our arguments. First we consider the sum:

$$\tfrac{1}{2}\sum_{ijkl} v_{ij,k\eta_i}\eta_j^*\eta_\eta\eta_k F=VF. \quad \text{(A8)}$$

By using the definitions of the various operators and proceeding in a way very similar to that used in Sec. II, this can easily be brought to the form

$$\begin{aligned} VF=&\tfrac{1}{2}\sum_{ijkl} t_{ij,k\eta_i}\eta_j^*\eta_\eta\eta_k F_{kl} \\ &-\tfrac{1}{2}\sum_{ijkl}\frac{1}{e}v_{ij,kl}\eta_k^*\eta_i^*(t_{kl,k\eta_\eta}\eta_k+t_{kl,u\eta_k}\eta_l)F_{kl}. \end{aligned} \quad \text{(A9)}$$

The last term here is of the type that has been shown to vanish for large numbers and will be dropped. The remaining term breaks into two parts:

$$\begin{aligned} VF=&\tfrac{1}{2}\sum_{ij}(t_{ij,i}\eta_i^*\eta_j^*\eta_j\eta_i+t_{ij,j}\eta_i^*\eta_j^*\eta_i\eta_j)F_{ij} \\ &+\tfrac{1}{2}\sum_{ijkl} I_{ij,k\eta_i}\eta_j^*\eta_\eta\eta_k F_{kl}. \end{aligned} \quad \text{(A10)}$$

To eliminate the second of these, we define a state function Ψ_0 such that $e=E-H_0-V_C$ operating on it vanishes. Using this and the defining equation for F [Eq. (A7)], we finally find

$$VF\Psi_0=(E-H_0)F\Psi_0, \quad \text{(A11)}$$

if we again drop a term which vanishes for a large number of particles. The state function $F\Psi_0$ thus satisfies the original eigenvalue equation for the energy if the auxuliary equation,

$$(H_0+V_C)\Psi_0=E\Psi_0, \quad \text{(A12)}$$

is satisfied. This equation for Ψ_0 replaces the original eigenvalue problem for E. The evaluation of the eigenvalue is now relatively easy if we know the operators $t_{ij,kl}$, since for the lowest eigenvalue of E we choose a Ψ_0 in which the states are all occupied, i.e., a degenerate gas.

Returning to the equation for $t_{ij,kl}$, a typical diagonal term is

$$t_{ij,ij}=v_{ij,ij}+v_{ij,mn}\eta_m\eta_n\frac{1}{e}\eta_n^*\eta_m^* t_{mn,ij}. \quad \text{(A13)}$$

When we operate on the initial state Ψ_0, the second term vanishes unless the particles m and n which are created occupy previously empty states. In this case, the matrix element of $\eta_m\eta_n\eta_n^*\eta_m^*$ is simply unity. The energy denominator then contains the difference between the energy E of the initial state and the energy of the excited state with the two particles m and n excited. Writing the energies in terms of H_0 and V_C, this difference may be written

$$\begin{aligned} \Delta E=&T_i+T_j-T_m-T_n+V_C(i) \\ &+V_C(j)-V_C(m)-V_C(n), \end{aligned} \quad \text{(A14)}$$

where

$$V_C(i)=\sum_{s\neq i}(t_{is,is}-t_{is,si}), \quad \text{(A15)}$$

again dropping terms which vanish for large numbers. Thus the energy denominator depends explicitly only on the coordinates of the initial and excited pairs of particles, although it depends implicitly on the states of the rest of the particles through the sum over the filled states of the rest of the system.

We also note the iterated form of F:

$$F=1+\frac{1}{e}\sum_{ij,kl} I_{ij,kl}\eta_i^*\eta_j^*\eta_l\eta_k + \frac{1}{e}\sum_{ij,kl} I_{ij,kl}\frac{1}{e}\eta_i^*\eta_j^*\eta_l\eta_k \sum_{mn\neq kl}\sum_{rs} I_{mn,rs} \times\eta_m^*\eta_n^*\eta_s\eta_r+\cdots. \quad \text{(A16)}$$

This has no diagonal elements in the state Ψ_0 until the fourth term of order I^3 is taken into account. This result has been already used in NS I.

We also consider in this notation a typical $1/N$ term discussed in Sec. III and also in Appendix B:

$$\left(\psi_C, \sum_{\alpha\beta} I_\alpha \frac{1}{e} t_{C\alpha} \frac{1}{e} I_\beta \psi_C\right).$$

In the second quantization notation, this is

$$\sum_{ijkl}\sum_{k'l'mn} (\Psi_0,\eta_i^*\eta_j^*\eta_l\eta_k\eta_k^*\eta_l^*\eta_l\eta_k\eta_{k'}^*\eta_{l'}^*\eta_n\eta_m\Psi_0) \times I_{ij,kl}\frac{1}{e}(t_{kl,kl}-t_{kl,lk})\frac{1}{e}I_{k'l',mn}.$$

In evaluating the matrix element of the annihilation and creation operators, the restriction on the sum over operators associated with the nondiagonal operators I shows that the only diagonal terms can come from pairing the annihilation and creation operators ($\eta_l\eta_k\eta_{k'}^*\eta_{l'}^*$) to give a diagonal contribution, i.e., the particles created by $\eta_{k'}^*\eta_{l'}^*$ must be annihilated by the pair $\eta_l\eta_k$. Thus the summation over k' and l' is restricted to the diagonal terms; a similar restriction occurs in the summation over i, j, m, n. A typical resulting term is

$$\sum_{ijkl}\left(I_{ij,kl}\frac{1}{e}t_{kl,kl}\frac{1}{e}I_{kl,ij}\right)$$

together with a variety of exchange terms. This term has the structure of the terms discussed in Sec. III and evaluated in Appendix B; thus the arguments showing the vanishing of these terms for large N go through as before.

APPENDIX B

Approximate Evaluation of ΔE_3

We wish to evaluate the first nonvanishing perturbation in the energy:

$$\Delta E_3=\sum_\alpha\left(\psi_C, I_\alpha\frac{1}{e}t_{C\alpha}\frac{1}{e}I_\alpha\psi_C\right). \quad \text{(B1)}$$

We consider as an explicit case the nuclear system. As discussed in Sec. III this term represents the incoherent scattering of a pair of particles to excited states, their coherent scattering, and final rescattering to the original state. We shall try to obtain only a qualitative result since, as we have shown, the effect on the energy is very small. Consequently we shall replace the exact expression by a simpler one in which we treat the pair as a single particle with mass equal to the reduced mass of the pair. We also consider the relative momentum as the momentum of a physical particle and require that it be above the Fermi momentum in the excited states. With these approximations we can write for a typical "particle" (i.e., pair):

$$\Delta E_3=\sum_{\mathbf{k}',|\mathbf{k}'|>k_F}(\mathbf{k}|I|\mathbf{k}')\frac{M^*}{k^2-k'^2}(\mathbf{k}'|t_C|\mathbf{k}') \times\frac{M^*}{k^2-k'^2}(\mathbf{k}'|I|\mathbf{k}), \quad \text{(B2)}$$

where we have approximated the effect of V_C in the denominator $1/e$ by a mass modification as discussed in NS III. For simplicity we choose for $(k'|t|k)$ the Born approximation scattering from a Yukawa well with Serber exchange mixture, i.e., we let

$$V(r)=V_0\frac{e^{-\mu r}}{\mu r}\tfrac{1}{2}(1+P_x), \quad \text{(B3)}$$

and consequently

$$(\mathbf{k}'|t|\mathbf{k})=\frac{2\pi V_0}{\mu v}[(\mu^2+(\mathbf{k}-\mathbf{k}')^2)^{-1}+(\mu^2+(\mathbf{k}+\mathbf{k}')^2)^{-1}], \quad \text{(B4)}$$

where v is the normalization volume for the wave functions. Using this and going over from the summation over $\mathbf{k}'$ to an integral by the relation

$$\sum_{\mathbf{k}'}\rightarrow\frac{v}{(2\pi)^3}\int d\mathbf{k}', \quad \text{(B5)}$$

we find

$$\Delta E_3=\left(\frac{2\pi V_0}{\mu v}\right)^3 v\frac{\mu^{*2}}{(2\pi)^3}\int_{k'>k_F} d\mathbf{k}'[(\mu^2+(\mathbf{k}-\mathbf{k}')^2)^{-1} +(\mu^2+(\mathbf{k}+\mathbf{k}')^2)^{-1}]^2[\mu^{-2}+(\mu^2+4k'^2)^{-1}] \times(k^2-k'^2)^{-2}. \quad \text{(B6)}$$

To exhibit the A dependence of this result, we make the rather crude approximation of replacing k by its average value for a Fermi gas, i.e., $k_{Av}=(\frac{3}{5})^{\frac{1}{2}}k_F$ and multiply by the number of pairs $A^2/2$ (for $A\gg1$). Also, writing $v=(4/3)\pi r_0^3A$, we find

$$\Delta E_3=\frac{1}{2}\left(\frac{V_0}{\mu}\right)^3\left(\frac{4}{3}\pi r_0^3\right)^{-2}f(k_F), \quad \text{(B7)}$$

with $f(k_F)$ independent of A. This integral has been evaluated and gives a value for ΔE_3 of about 10 Mev and thus of 10 Mev/A per particle.

Two-Body Forces and Nuclear Saturation. III. Details of the Structure of the Nucleus

K. A. BRUECKNER
*Indiana University, Bloomington, Indiana**
(Received November 22, 1954)

The characteristics of particle motion in the nuclear medium have been examined in detail. The origin of the strong dependence of the potential energy on the nucleon momentum is discussed and an equivalent formulation is exhibited in which a uniform and constant potential is assumed but the nucleon moves with markedly reduced mass. The determination of the potential is shown to lead to a self-consistency problem which is to some extent similar to that appearing in the Hartree method of self-consistent fields. Solution of this problem shows that the self-consistency requirements impose severe restrictions on the solution and have a strong stabilizing influence in the saturation problem. The volume energy of the nucleus has been evaluated by using two-body potentials closely equivalent to a combination of central and tensor forces which agree with the low-energy parameters and predict scattering correctly up to 90 Mev. The result agrees closely with the observed values of energy and density.

The collective character of the nucleon potential is described and shown to manifest itself markedly in the excitation energy of single-particle levels where a considerable fraction of the energy is taken up in small adiabatic shifts of the states of the remaining nucleons.

The origin of the surface and symmetry energy is discussed; an evaluation of these effects gives a result in good agreement with empirically derived values. The stability of the nucleus against distortion arising from the polarizing effects of the tensor force is also examined and it is found that the nucleus shows marked stability against such distortion.

I. INTRODUCTION

IN previous papers on the problem of nuclear saturation[1] (to be referred to as NS I and NS II), an approximation method was developed and applied to the determination of certain properties of the volume and surface energies of nuclear matter in the presence of central and tensor forces. It is the purpose of this paper to discuss a variety of additional structural details which considerably increase the completeness of this nuclear model. In Sec. II we shall consider various aspects of the motion of nuclear particles in nuclear matter and the problem of deriving the potential energy felt by such a particle. In this connection we shall develop some concepts of the dispersion law relating energy and wave number in nuclear matter and of the self-consistency requirements in the formulation of the problem. In Sec. III we shall discuss some of the collective aspects of the nuclear states which are implicit in the work of Sec. II; in Sec. IV we shall discuss the problems of the surface and symmetry energies of the nucleus and the stability of the nucleus against distortion arising from polarizing action of the tensor force. Finally in Sec. V we summarize our results and make some concluding remarks.

In this paper we shall not discuss the basic assumptions of the method as developed in NS I; a detailed discussion of these together with a physical interpretation of various aspects of the model will form the content of another paper now in preparation.

* Supported in part by a grant from the National Science Foundation. The work was also done in part while the author was a visiting Associate Physicist at Brookhaven National Laboratory.

[1] Brueckner, Levinson, and Mahmoud, Phys. Rev. **95**, 217 (1954); K. A. Brueckner, Phys. Rev. **96**, 908 (1954).

II. DISPERSION LAW IN NUCLEAR MATTER; SELF-CONSISTENCY PROBLEMS

A. Origin of Dispersion Effect and of Self-Consistency Requirement

In NS I and NS II it was shown that the potential energy of a particle moving in a plane wave state in uniform nuclear matter was in general a function of its momentum, so that the energy of a particle of momentum k was related to k by

$$E(k)=k^2/2M+V(k), \tag{1}$$

with $V(k)$ not a constant. This expression is a statement of a dispersion law relating E and k. In many typical applications such as those encountered in the development of the shell model, it is assumed that the potential is independent of the particle state. For example in the case of a square well the presence of the potential merely serves to define a boundary and a new zero point of energy without otherwise affecting the particle motion. It is, however, not in general possible to assume that the potential is independent of the state. We shall discuss qualitatively the origin of the dispersion effect stated in Eq. (1) before proceeding to an examination of its further implications.

The dependence of the potential energy on k arises from the origin of this energy in the interaction of the particle with its neighbors in the nuclear medium. In the model which we have developed, the potential energy is a manifestation of the effect of collisions on the wave function; since this effect drops off rapidly as the relative energy in collision increases (and the scattering decreases), one would expect to find a decrease in the potential strength as the momentum of the particle under consideration rises. The direction of the effect is of course intimately related to the satu-

rating character of the two-body interaction considered, since the amplitude for forward scattering arises from this interaction characteristically becomes small (or eventually changes sign) at high energy. Thus we expect a lessening of the potential strength for a rapidly moving particle.

Another interesting way of describing these effects has been suggested to the author by Wheeler.[2] He observes that near zero momentum the potential energy $V(k)$ can be expanded as

$$V(k)=V(0)+bk^2+\cdots, \tag{2}$$

where in some cases only these first two terms in the expansion need be considered. We expect the leading term $V(0)$ to be negative, while the quadratic correction term will in general be positive. Thus we can now write the dispersion law of Eq. (1) as

$$\begin{aligned} E(k)&=k^2/2M+V(0)+bk^2 \\ &=k^2/2M^*+V(0), \end{aligned} \tag{3}$$

where M^* as defined by this equation is related to the normal mass by

$$M^*=M/(1+2bM) \tag{4}$$

and consequently is less than the normal mass. Thus we are led to an equivalent description in which the nuclear potential is constant but the "nucleon" mass is modified. This effect can be expected to manifest itself in other ways to which we shall return later.

We have so far not discussed a consequence of this modification in nuclear matter of the propagation characteristics of a nucleon which, as we shall see, leads to a self-consistency requirement on the formulation of the problem. As developed in NS I, the potential energy of a nucleon could be expressed in terms of a summation over nuclear states of the two-body forward scattering amplitude *evaluated in the nuclear medium*. We shall express this requirement formally in the next section; we remark here only that already an obvious difficulty arises in that to evaluate the scattering *in the medium* it is necessary to know the dispersion law for propagation before carrying out this evaluation. Thus the dispersion law determined is a function of the dispersion law assumed and a self-consistency requirement arises. As we shall see, this presents a rather formidable mathematical problem which we shall discuss in the following sections.

B. Formal Statement of Self-Consistency Problem

The formal statement equivalent to the requirement that we determine the scattering amplitude "in the nuclear medium" is the following[3]: let v_{12} be the interaction between nucleons 1 and 2. We further define the two quantities t_{12} and V_C by the equations:

$$\begin{aligned} t_{12}=v_{12}+v_{12}[E_1+E_2-H_0(1)-H_0(2) \\ -V_C(1)-V_C(2)]^{-1}t_{12}, \end{aligned} \tag{5}$$

$$V_C(i)=\sum_{i\neq j} t_{Cij}, \tag{6}$$

where t_C is the part of the scattering operator t which is diagonal (or coherent) with respect to the nuclear states. We define the singularity in the energy denominator of Eq. (5) by taking the principal value[4]; this corresponds to the stationary character of the problem. The operator t defined this way is often called the reaction matrix. The potential $V_C(i)$ is the potential energy of the ith particle; the modification from the t defined for free-particle scattering arises from the presence of the potential energy V_C in the propagation function.[5] The complication of the problem arises from the appearance of V_C in the defining equation for t which must be solved to obtain V_C; the mathematical problem presented is the solution of a nonlinear integral equation for V_C.

The presence of the modified propagator in this problem represents the expected and quite reasonable many-body effect on the interaction of two nucleons in dense nuclear matter. We note that it does not arise from a change in the two-body potential v_{12}; this effect has been previously discussed in NS I and shown to be small.

This problem has some of the aspects of the self-consistent field problems encountered in atomic physics. In our case we know the wave functions (degenerate Fermi gas) but the interaction is not known, while in the Hartree method the interaction is specified but the wave function is unknown. The self-consistency requirement of our problem is to specify such an average potential, solve for the interactions and finally from the interactions determine the average potential. Thus the solution of this problem bears a certain resemblance to the atomic case but is fortunately somewhat easier to obtain.

In solving the pair of Eqs. (5) and (6) the simplest approximation method is that previously used in NS I and II. To exhibit this, we assume that the transformation to the center-of-mass system and relative coordinates is possible [as it is if $V_C(k_1)$ depends at most on a constant and a term quadratic in k_1] and write in momentum space, where k is the relative

[2] J. A. Wheeler (private communication).

[3] See N. C. Francis and K. M. Watson, Phys. Rev. **92**, 291 (1953).

[4] B. A. Lippmann and J. Schwinger, Phys. Rev. **79**, 469 (1950).

[5] The exclusion principle also acts to modify the scattering operators; it can be shown, however, that the most important class of intermediate states included in the construction of t which would appear to violate the exclusion principle are exactly cancelled when the expectation value in the many particle state is evaluated. In addition, most of the contribution to the integral over intermediate states comes from high excited states which are unaffected by the exclusion principle.

momentum,[6]

$$t_C(k)=(\mathbf{k}|t|\mathbf{k})=(\mathbf{k}|v|\mathbf{k})+(2\pi)^{-3}\int d\mathbf{k}'(\mathbf{k}|v|\mathbf{k}')$$
$$\times[E(k)-k'^2/M-V_C(k')]^{-1}(\mathbf{k}'|t|\mathbf{k}). \quad (7)$$

The pole in the denominator appears at the energy-conserving point,

$$E(k)=k^2/M+V_C(k), \quad (8)$$

which allows us to write

$$t_C(k)=(\mathbf{k}|v|\mathbf{k})+(2\pi)^{-3}\int d\mathbf{k}'(\mathbf{k}|v|\mathbf{k}')[k^2/M-k'^2/M$$
$$+V_C(k)-V_C(k')]^{-1}(\mathbf{k}'|t|\mathbf{k}). \quad (9)$$

Then, if $V_C(k)$ is independent of k or if the variation in $V_C(k)-V_C(k')$ is slow relative to the variation in $(k^2-k'^2)/M$, then the terms in V_C can be dropped and we have approximately:

$$t_C(k)=(\mathbf{k}|v|\mathbf{k})+M(2\pi)^{-3}$$
$$\times\int d\mathbf{k}'(\mathbf{k}|v|\mathbf{k}')(k^2-k'^2)^{-1}(\mathbf{k}'|t|\mathbf{k}). \quad (10)$$

In this case, which is now exactly analogous to the free scattering at momentum k, the effect of the potential has been merely to replace the (negative) energy E by k^2/M which is the kinetic energy in the nuclear medium. This approximation was used in NS I and II since it was assumed that an appreciable correction would not arise from this approximation to the properties of the medium; we shall now proceed, however, to develop a more rigorous method for solving Eqs. (5) and (6).

The defining equation for t_{12} of Eq. (5) can be rewritten

$$t_{12}=v_{12}\Omega, \quad (11)$$

where

$$\Omega=1+(E-H_0-V_C)^{-1}v_{12}\Omega. \quad (12)$$

Thus the construction of Ω is sufficient to determine t. This equation, however, is analogous to the usual scattering wave equation (except for the modified boundary condition); hence we know that the t can be expressed in terms of the phase shifts which we obtain by solving the wave equation

$$(E-H_0-V_C)\Omega=v_{12}\Omega. \quad (13)$$

Knowing V_C in momentum space allows us to make the transformation to coordinate space in a straight forward manner.

[6] In this and the rest of the paper we shall assume that the diagonal part of t is given only by the forward scattering. The inclusion of the exchange scattering has been discussed in NS I and shown there to give a trivial change to the formalism.

C. Approximation Methods for Solving the Self-Consistent Problem

We consider first the simple case in which only constant and quadratic terms in V_C are used. As we shall show, this is a quite good approximation over the range of momenta which enter in the ground state but breaks down somewhat in evaluating t since a considerably larger range of momenta enters (in virtual states) in solving the wave equation for t. Making this approximation, we can write the problem:

$$(E-2V_0+2b\nabla^2-H_0)\Omega=v\Omega. \quad (14)$$

Since the energy E is

$$E(k)=2V_0+2bk^2+k^2/M, \quad (15)$$

this is equivalent to

$$(k^2+\nabla^2)\Omega=M^*v\Omega, \quad (16)$$

with M^* defined by Eq. (4). The effect of the dispersion of the medium therefore (as was remarked earlier) is to introduce a mass modification. The solution of Eq. (16) for the phase shifts now follows standard methods; the usual scattering amplitude $a_k(\theta)$ is finally related to $t_C(k)$ by

$$t_C(k)=-\frac{4\pi}{M^*v}a_k(0). \quad (17)$$

It is interesting to note that t is independent of M^* in Born approximation since in such a case $a_k(0)$ is proportional to M^*.

The self-consistency requirement on $V_C(k)$ thus is reduced to a single-parameter problem, since it is now sufficient to find a value M^* (or b) in the dispersion law which will predict scattering amplitudes and hence a $V_C(k)$ which depends on k in the same way (i.e., is self-consistent). This procedure will be described in more detail in the following section.

Before proceeding, we make one further remark about a slightly more general choice of $V_C(k)$. Let

$$V_C(k)=V_0+bk^2+ck^4, \quad (18)$$

which is a somewhat better representation of the k dependence of the potential for k values rather larger than the Fermi momentum, although the term in k^4 is negligible for small values of k. According to Eq. (13) we now can write the Schrödinger equation:

$$[E-k_1^2/2M-k_2^2/2M-2V_0-b(k_1^2+k_2^2)$$
$$-c(k_1^4+k_2^4)]\Omega(1,2)=v_{12}\Omega(1,2), \quad (19)$$

where $\mathbf{k}_1$ and $\mathbf{k}_2$ are to be interpreted as operators on the coordinates of particles 1 and 2. Transforming to the center-of-momentum system and relative coordinates by the relations

$$\mathbf{k}_1=\mathbf{k}+\tfrac{1}{2}\mathbf{P}, \quad \mathbf{k}_2=-\mathbf{k}+\tfrac{1}{2}\mathbf{P}, \quad (20)$$

we are led to the transformed equation:

$$[E-(1/M+2b)(k^2+\tfrac{1}{4}P^2)-2V_0$$
$$-c(2k^4+3k^2P^2+\tfrac{1}{8}P^4)]\Omega=v\Omega. \quad (21)$$

Next, introducing the relation between energy, P, and k_0 (the asymptotic value of k),

$$E=(1/M+2b)(k_0^2+\tfrac{1}{4}P^2)+2V_0 +c(2k_0^4+3k_0^2P^2+\tfrac{1}{8}P^4), \quad (22)$$

we find

$$[(1/M+2b)(k_0^2-k^2) -2c(k^4-k_0^4+\tfrac{3}{2}k^2P^2-\tfrac{3}{2}k_0^2P^2)]\Omega=v\Omega. \quad (23)$$

This is of standard form (with modified mass) except for the term proportional to c. This we approximate in the following way; as we have remarked, the terms in c are unimportant except for large k values. Thus we expect only the term in k^4 to be appreciable for low values of k_0 and P. Treating this term as a perturbation, we make the replacement

$$ck^4\Omega\cong M^*ck^2[(1/M+2b)k_0^2-v]\Omega \approx -M^*ck^2v\Omega. \quad (24)$$

Next, introducing a new function

$$\phi=(1-2cM^{*2}v)\Omega, \quad (25)$$

Eq. (23) reduces to

$$(k_0^2+\nabla^2)\phi=\frac{M^*v}{1-2cM^{*2}v}\phi, \quad (26)$$

if we again drop some small terms in ck_0^2, with $M^*=M/(1+2bM)$ as before [Eq. (4)]. The asymptotic forms of Ω and ϕ are the same, and for nonsingular potentials the boundary condition at the origin is unchanged; thus a solution for the phase shifts using Eq. (26) is equivalent to a solution of the original problem.

Another way of expressing the result of Eq. (26) is that the "effective mass" M^{**} defined by

$$M^{**}=M^*/(1-2cM^{*2}v) \quad (27)$$

differs to some extent from the asymptotic value M^*. The direction of this correction depends on the size of c; as we shall see later the departure from the simple quadratic law for $V_C(k)$ given in Eq. (2) corresponds to a small negative c. Thus the "effective mass" used in solving Eq. (26) is somewhat larger than the asymptotic value or equivalently, the effective potential

$$v^*=v/(1-2cM^{*2}v) \quad (28)$$

is somewhat stronger. The effect is not very large; we shall, however, make at least qualitative use of this result in the next section.

These considerations have shown how the self-consistent problem may be reduced to a two-parameter problem, the self-consistent determination of the constants b and c in the expansion of the potential

$$V(k)=V_0+bk^2+ck^4. \quad (29)$$

The problem is however hardly a trivial one in that it is necessary to obtain a complete solution for all phase shifts over a large range of energies for each choice of the parameters b and c. Thus we must assume in practice a "zeroth order" form for $V_C(k)$ which we call

$$V_C^{(0)}(k)=V_0^{(0)}+b_0k^2+c_0k^4, \quad (30)$$

and for this choice construct the scattering amplitudes and finally a first iterate $V_C^{(1)}$ which will be a function of b_0 and c_0, i.e.,

$$V_C^{(1)}(k)=V_C^{(1)}(k,b_0,c_0). \quad (31)$$

Then, expanding the first iterate,

$$V_C^{(1)}(k,b_0,c_0)=V_0^{(1)}+b_1k^2+c_1k^4, \quad (32)$$

we expect the new constants b_1 and c_1 to be functions of b_0, c_0, i.e.,

$$b_1=b_1(b_0,c_0), \quad c_1=c_1(b_0,c_0). \quad (33)$$

The self-consistency requirement is finally

$$b_1=b_0, \quad c_1=c_0. \quad (34)$$

D. A Self-Consistent Solution

The method of the last section can in principle be applied to any two-body interaction; it is of course in the general case (in which tensor forces are included) extremely tedious since a considerable range of values of the parameters (particularly of the most important parameter b) must be studied to map out the dependence of V_C. We shall, however, in part avoid this difficulty by using simple potentials approximately equivalent to the ones considered in NS I and NS II. In these earlier works, a potential derived from meson theory was used which had a rather complicated exchange dependence and which contained a large tensor force. Since, however, the many-body potential energy derived depended primarily on the low-energy scattering characteristics of the potentials, it is possible to replace (at least at low energies) the original potentials used by any choice agreeing with the low-energy parameters. An important restriction on the potentials, however, is that the phase shifts at high energy show the rapid drop resulting from the presence of repulsive cores in the potentials. A further requirement is that the triplet even scattering approximate to the tensor scattering at high energies, which is rather smaller than the scattering from a central potential because of the first-order averaging to zero of the tensor force scattering.

Potentials which approximately satisfy these conditions and which allow relatively simple evaluation of the self-consistency problem are square wells of appro-

TABLE I. Equivalent square well parameters. The ranges are given in units of 1.40×10^{-13} cm.

	Singlet	Triplet
Range	1.53	0.93
Core radius	0.40	0.30
Depth (Mev)	40.6	148

priate range and strength, with a region of central repulsion. The parameters of these potentials are given in Table I; the s-wave scattering predicted by them is given in Fig. 1 in comparison with the s-wave scattering of NS II. The remaining partial waves have been omitted for the following reasons. (Since they can be treated in Born approximation and thus are only weakly affected by the modifications of the effective mass the following remarks based on the studies of NS II are valid.) (1) The investigations of the tensor scattering show that the effect of the higher waves is very small, considerable cancellation occurring among the D-waves of different J and m_J. (2) The D-wave singlet scattering is appreciable but is approximately cancelled by the scattering arising from the odd-state singlet repulsive potentials. (3) The magnitude of the energy is almost entirely determined by the interaction at low energy and thus is very well approximated by the s-wave scattering alone. These remarks have all been quantitatively verified by a comparison with the calculation in NS II of the energy as a function of density predicted by the equivalent square wells.

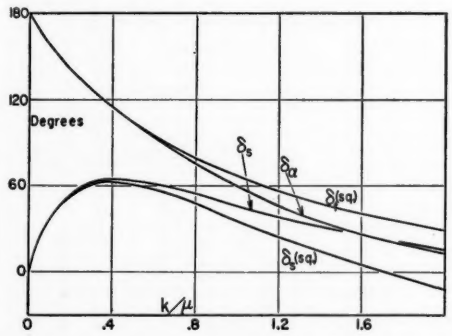

FIG. 1. S-wave scattering from square wells with parameters given in Table I, compared with S-wave scattering calculated for central and tensor wells of NS I and NS II. In the latter case for the tensor force, the δ_α eigen phase shift is given.

Thus we can proceed to an evaluation of the self-consistency problem using the simple equivalent square wells. We notice first that the equivalent Schrödinger equation is

$$(k_0^2+\nabla^2)\phi = M^{**}v\phi = -\frac{M^*V_0}{1+2cM^{*2}V_0}\phi, \quad r_c<r<R, \tag{35}$$

where r_c is the radius of repulsion and R is the range of the well. This equation determines phase shifts as a function of

$$M^{**}=M^*/(1+2cM^{*2}V_0), \tag{36}$$

and as a function of energy. The phase shifts predicted for the singlet and triplet states are shown as a function of the mass parameter in Fig. 2. The potential energy per particle is related to these phase shifts (see NS I and NS II) by the equations (for s states only):

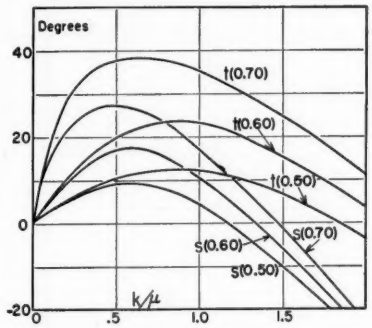

FIG. 2. Singlet (s) and triplet (t) phase shifts from equivalent square wells calculated as a function of mass parameter. The values of M^{**}/M are indicated.

$$V_C(k) = -\frac{6}{\pi M^*}\int P(k,k')[\tan\delta_s(k',M^{**}) + \tan\delta_t(k',M^{**})]k'dk', \tag{37}$$

where

$$P(k,k') = 2, \quad 0<k'<\tfrac{1}{2}(k_F-k)$$
$$= [\tfrac{1}{4}k_F^2-(\tfrac{1}{2}k-k')^2]/kk', \quad \tfrac{1}{2}|k_F-k|<k'<\tfrac{1}{2}(k_F+k). \tag{38}$$

Let us first consider the simple case for which $c=0$ and $M^*=M^{**}$ [see Eq. (36)]. In this case the self-consistency requirement is rather easy to satisfy since we have an additional parameter at our disposal, namely the adiabatic density parameter η. This parameter appears through the dependence of k_F on the density through the relation

$$k_F = 1.52\mu/\eta. \tag{39}$$

We thus proceed in the following way: for a given value of M_0^*, we compute

$$V_C(k,M_0^*,\eta) = V_0+b(M_0^*,\eta)k^2, \tag{40}$$

and adjust the density parameter η so that the value of M^*, predicted by the relation

$$M_1^* = M/[1+2b(M_0^*,\eta)M], \tag{41}$$

agrees with M_0^*. This requirement gives M^* as a function of the density (see Fig. 3) and thus also the potential energy V_C as a function of k and the density. We can then proceed to the mean potential energy per particle by evaluating the average

$$V_{Av} = \tfrac{1}{2}\int_0^{k_F} k^2V_C(k)dk \Big/ \int_0^{k_F} k^2dk, \tag{42}$$

the factor of $\frac{1}{2}$ compensating for the double summation over all particle coordinates. Finally, the mean energy per particle as a function of density is given by

$$E_{Av} = T_F+V_{Av}. \tag{43}$$

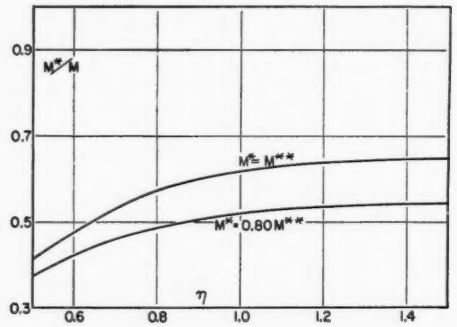

FIG. 3. Self-consistent values of mass parameter as a function of density parameter η [defined in Eq. (39)]. The two cases $M^*=M^{**}$ and $M^*=0.80M^{**}$ are given.

The self-consistency requirements having already been satisfied for each value of η, it is sufficient to determine the value of η for which the energy is a minimum, thus determining the equilibrium density and binding energy. This relation between E and η is given in Fig. 4, the minimum occurs at a density of $\eta=1.30$ or $R=1.82\times10^{-13}A^{\frac{1}{3}}$ and a binding energy of about 4.5 Mev per particle.

This rather unsatisfactory solution to the problem is not yet fully consistent since the k^4 dependence of the potential is not negligible. The function $V_C(k)$ as determined for the approximately self-consistent parameters $M^*/M=0.70$ and $\eta=0.9$ is given in Fig. 5 as a function of k up to a value of k considerably larger than the Fermi momentum k_F. A good approximation to this curve is:

$$V_C(k)=(-119+57.3k^2/k_F{}^2-7.18k^4/k_F{}^4)\text{ Mev}, \quad (44)$$

so that although the quadratic approximation is valid for $k<k_F$, the term in k^4 is not negligible for values of k/k_F appreciably larger than one. The sign of this term in V_C is negative; inserting this value in Eq. (36) for M^{**}, we find

$$M^*\simeq0.80M^{**}, \quad (45)$$

taking an average for the singlet and triplet states.

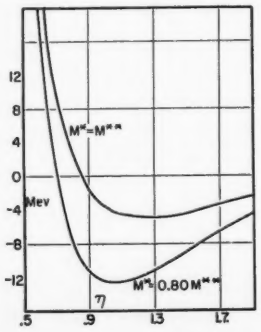

FIG. 4. Energy as a function of density for self-consistent potentials with $M^*=M^{**}$ and with $M^*=0.80M^{**}$.

This relation is of course not very well determined since it is a higher order correction to the dominant quadratic effect in the dispersion law. In addition its precise value depends rather sensitively on the high-momentum behavior of the scattering which is not given very reliably by these approximation methods. Nevertheless, it is probably correct to assume that the effective mass in the high-momentum region is somewhat greater than the effective mass at low-momentum values.

By using the ratio between M^{**} and M^* of Eq. (45), it is again possible to carry out a self-consistent evaluation of the effective mass M^* and consequently of the potential energy. These results are given in Figs. 3 and 4. For this case the binding energy per particle is now about 12.8 Mev at a density $\eta=1.00$ or $R=1.40\times10^{-13}A^{\frac{1}{3}}$. At this value of the density the effective low-momentum mass M^* is $0.54M$, and a check on the self-consistency at high momentum values shows that the ratio $M^*=0.8M^{**}$ is still approximately satisfied.

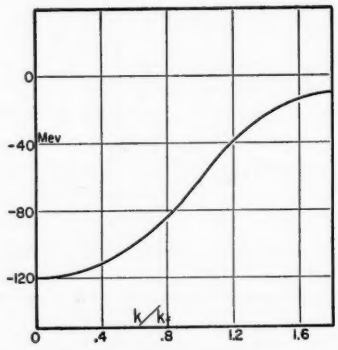

FIG. 5. Potential energy as a function of k for $M^*=0.70M$ and $\eta=0.90$.

Thus we have an approximately self-consistent solution to the two-parameter problem.

E. Discussion

Some rather striking features of these results are readily seen. The most evident effect of the self-consistent inclusion of the dispersion effects is the reduction in the mean potential energy and a simultaneous change in the position of the density minimum of the total energy curve (see Fig. 6). This modification arises from the impossibility of finding a self-consistent solution to the problem when the potential energy is too large or equivalently, when the "effective mass" is close to the nucleon mass. Thus a strong stabilizing influence on the nuclear density arises from the self-consistency requirement on the solution. The effect is intimately associated with the many-body character of the problem, arising as it does from the modification of the propagation characteristics of a nucleon in nuclear matter. As such it gives an interesting insight into the

interplay of effects which lead to the equilibrium configuration of the nucleus.

III. COLLECTIVE ASPECTS OF THE MOTION

As we have shown in the previous section, the motion of nucleons through nuclear matter is determined by a potential which varies rapidly with the nucleon momentum; it is also true in our treatment that the potential energy arises from two-body interactions. In this section we would like to discuss the significance of these results and how they may be related to the single-particle and collective aspects of the nuclear structure.

Let us consider first the relation of the energies of the nucleons to such quantities as mean binding energy and the binding energy of the last nucleon. The potential energy of a nucleus of momentum k we call $V_C(k)$ as

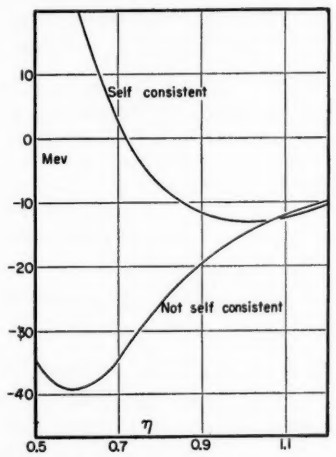

FIG. 6. Comparison of self-consistent energy E for $M^*=0.80M^{**}$ with the result obtained in NS II with no self-consistency requirement imposed. For the latter case $M^{**}=M$ and M^* is in the range 0.2 to 0.4.

before. This energy cannot, however, be unambiguously assigned to one nucleon, since it is the result of two-body interactions and thus is shared between the nucleon under consideration and the rest of the nucleus. Thus, in an obvious way, the potential energy is already a manifestation of a collective characteristic. The mean energy of the system we get by averaging (the kinetic energy and the potential energy) over the momentum distribution, i.e.,

$$E_{Av}=T_{Av}+V_{Av}$$

$$=\int k^2dk[k^2/2M+\tfrac{1}{2}V_C(k)]\Big/\int k^2dk, \quad (46)$$

as has been observed earlier.

We now proceed to the relation between the binding energy of a nucleon and the kinetic and potential

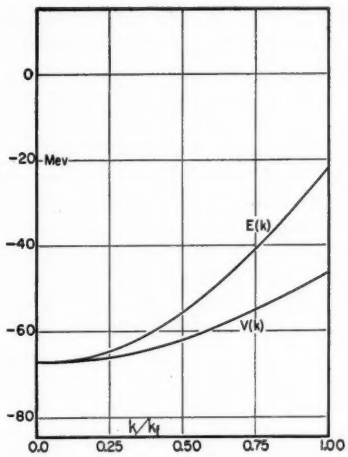

FIG. 7. Total energy and potential energy as a function of momentum at equilibrium density.

energies. At first we might expect to obtain this by simply evaluating $E(k)$; this, however, is obviously incorrect since we are not taking into account the "shared" character of the potential energy. A further complication arises from the possibility that the nuclear system will readjust its density to bring the energy to a minimum, which must also be taken into account in determining the binding energy. In spite of the complicated character of these questions, we can easily obtain an answer by considering the physical character of the binding energy, which is the difference between the energy of a nucleus of A nucleons in the ground state and the energy of a nucleus of $(A-1)$ nucleons in the ground state plus a removed nucleon. This difference is simply the mean binding energy as given in Eq. (46).

This simple result actually originates in a rather complicated interplay of effects which can be somewhat unphysically separated in the following way: we suppose that we formally consider the energy of removal of a nucleon as arising first from removal with the remaining nuclear configuration held fixed and second the energy of rearrangement of the remaining nucleus into its lowest state. The first of these is clearly $E(k)=T(k)+V_C(k)$; the rearrangement energy then makes up the difference between this value and the mean binding energy. The latter is a manifestation of the collective origin of the energy; in our example (see Fig. 7) the values of $E(k_F)$ is -22 Mev, of E_{Av} is -12.8 Mev; thus the rearrangement energy is 9.2 Mev. The origin of the rearrangement energy is fairly obvious; it arises in the adiabatic shift of all of the nuclear energy levels as one of the particles contributing to the binding is removed; it also arises from the reduction of the nuclear equilibrium volume as the particle is removed.

We can also express this result for the more general case of nuclear excitation. For simplicity let us consider a particle outside a core (for example a closed shell

+one nucleon). In this case the excitation of the outside particle to an excited state is also reflected in a change in the potential energy of each of the core particles, so that the energy of each level in the closed system shifts slightly as a consequence of the excitation of the outside particle. The excitation energy thus must be supplied not only to excite nonadiabatically the last nucleon but also to shift adiabatically the states of the core. Because of the related origin of these two effects in the two-body nature of the binding, they are of the same order of magnitude. We therefore see that in no sense are the "single-particle" excitation energies of the shell model single-particle in origin; they are rather of collective character and measure the sum of the changes in energy which take place in every state of the system upon excitation of any particle.

It might be remarked that the collective effect described here is rather different from the collective modes of excitation discussed by Bohr and Mottelson.[7] The effect we describe is present even in excitations which their theory would describe as of pure single-particle origin, since we find that a true single-particle picture has no zeroth order validity.

IV. SURFACE AND SYMMETRY ENERGIES: STABILITY AGAINST DISTORTION

A. Surface Energy

In this section we shall make a determination of the nuclear surface energy, i.e., that part of the energy of the nucleus which is associated with surface effects and hence has a different dependence on the total number of nucleons than does the volume energy. In this development we shall follow closely the procedure used in NS II with modifications, however, which lead to more reasonable results than those earlier obtained.

In NS II an approximate result of Hill and Wheeler[8] was used to represent the finite volume effect on the distribution of momentum states in the nucleus and was shown to lead to a surface energy. The result of Hill and Wheeler is that the effect of the finite volume is to modify the density of momentum states from the result valid for an infinite medium,

$$N_\infty(k)d\mathbf{k}=vd\mathbf{k}/(2\pi)^3, \tag{47}$$

to a result valid for a spherical nucleus of radius R,

$$\begin{aligned} N_R(k)d\mathbf{k}&=vd\mathbf{k}[1-3\pi/(4kR)]/(2\pi)^3 \\ &\equiv vd\mathbf{k}(1-k_0/k)/(2\pi)^3, \end{aligned} \tag{48}$$

with $k_0=3\pi/4R$. In this expression v is the volume on the surface of which the nuclear wave function is required to vanish. It is convenient to change the normalization of this density distribution in the following way: we notice first that the total number of states with momentum less than k_F is

$$n_R(k_F)=\int_{k<k_F} N_R(k)d\mathbf{k}=v\frac{4}{3}\frac{\pi k_F^3}{(2\pi)^3}(1-\tfrac{3}{2}k_0/k_F). \tag{49}$$

Defining a modified volume v_M by the relation

$$v_M=v(1-\tfrac{3}{2}k_0/k_F), \tag{50}$$

we can write

$$n_R(k_F)=v_M(4/3)\pi k_F^3/(2\pi)^3. \tag{51}$$

This modified volume thus is an equivalent volume in which the number of states with momenta less than k_F has the same form as in the case of an infinite medium. Let us consider the physical implication of this change in normalization volume. First we observe that the change in volume is equivalent to a change in radius:

$$\begin{aligned} R_M&=R(1-\tfrac{3}{2}k_0/k_F)^{\frac{1}{3}} \\ &\simeq R-\tfrac{3}{8}\pi\lambda\!\!\!^{-}_F, \end{aligned} \tag{52}$$

or that the effective radius R_M is less than the radius R of the original normalization volume by an amount

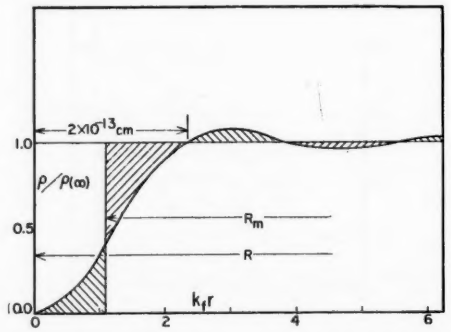

FIG. 8. Plot of the density of particles in a Fermi gas with the wave functions required to vanish on a plane boundary at $r=0$. The mean radius is indicated, as is also the scale in absolute units, showing that the nuclear edge in this case has a depth of the order of 2×10^{-13} cm.

very nearly equal to the wavelength $\lambda\!\!\!^{-}_F$ of the particles of maximum momentum. This, however, is a result previously pointed out by Swiatecki[9] and shown in Fig. 8. Physically the requirement that the wave function vanish on the surface of the volume has the effect of compressing the nuclear matter into a region of smaller mean radius, the compression being given by precisely the change from R to R_M. Thus the modified volume v_M represents more accurately the physical volume in which the nucleons are on the average confined. Using this result, we find for the relations between atomic number A and the Fermi momentum (with 2 neutrons and 2 protons per state):

$$A=4v_M(4/3)\pi k_F^2/(2\pi)^3, \tag{53}$$

[7] A. Bohr and B. Mottelson, Kgl. Danske Videnskab. Selskab, Mat.-fys. Medd. **27**, No. 16 (1953).

[8] D. Hill and J. Wheeler, Phys. Rev. **89**, 1102 (1953).

[9] W. J. Swiatecki, Proc. Phys. Soc (London) **A64**, 226 (1951).

and the average kinetic energy per particle:

$$T_F=\int\frac{k^2}{2M}(1-k_0/k)d\mathbf{k}\Big/\int(1-k_0/k)d\mathbf{k}$$
$$=\frac{3}{5}\frac{k_F^2}{2M}\left(1-\frac{5}{4}\frac{k_0}{k_F}\right)\Big/\left(1-\frac{3}{2}\frac{k_0}{k_F}\right). \quad (54)$$

To first order in k_0 (or to first order in $A^{-\frac{1}{3}}$), there is thus an increase in the kinetic energy per particle over that for an infinite medium:

$$T_F(R)-T_F(\infty)=\frac{3}{5}\frac{k_F^2}{2M}\times\frac{1}{4}\frac{k_0}{k_F}$$
$$=(5.69/\eta^2)A^{-\frac{1}{3}}\text{ Mev}. \quad (55)$$

We consider next the mean potential energy per particle. In this case we need evaluate a sum over states of the form:

$$V_{Nn}=\frac{1}{A}\sum_i\sum_j t_C(k_{ij}), \quad (56)$$

where t_C is the transition operator for forward scattering. Previously we have used the relation between $t_C(k)$ and the scattering amplitude $a_k(\theta)$

$$t_C(k)=\frac{4\pi}{M^*v}a_k(0), \quad (57)$$

where v is again the normalization volume for the nuclear states. The same effect, however, should be included here as we have just discussed, namely, the effective volume is more accurately represented by the modified (and reduced) volume v_M, the reason being precisely the same as that already discussed. Going over in Eq. (56) from the double sum to an integration and using the modified relation between t_C and a_k, we find

$$V_{Nn}(R)=\frac{-\frac{3}{8\pi^2M^*}\int d\mathbf{k}_1d\mathbf{k}_2\left[a_s\left(\frac{\mathbf{k}_1-\mathbf{k}_2}{2}\right)+a_t\left(\frac{\mathbf{k}_1-\mathbf{k}_2}{2}\right)\right]\left(1-\frac{k_0}{k_1}\right)\left(1-\frac{k_0}{k_2}\right)}{\int d\mathbf{k}_1(1-\frac{3}{2}k_0/k_F)^2}. \quad (58)$$

This expression is identical with that used previously in NS II except for one normalization factor $(1-\frac{3}{2}k_0/k_F)^{-1}$. This change is the result of the change in the normalization volume, which was not taken into account previously in a fully consistent way.

We again can separate this result into a term independent of R (or of k_0) and a correction term linear in k_0. The result is

$$V_{Nn}(R)-V_{Nn}(\infty)=\frac{9k_0}{32\pi^3M^*}k_F^{-3}\int d\mathbf{k}_1d\mathbf{k}_2$$
$$\times\left[a_s\left(\frac{\mathbf{k}_1-\mathbf{k}_2}{2}\right)+a_t\left(\frac{\mathbf{k}_1-\mathbf{k}_2}{2}\right)\right]\left(\frac{2}{k_1}-\frac{3}{k_F}\right). \quad (59)$$

In evaluating this correction we make use of the self-consistent results of Sec. II for M^* and the corresponding results for the scattering amplitudes. The result is a repulsive correction to the potential energy, of magnitude

$$V_{Nn}(R)-V_{Nn}(\infty)=\left(\frac{2.99}{\eta^2}+\frac{2.73}{\eta^4}\right)A^{-\frac{1}{3}}\text{ Mev}. \quad (60)$$

Combining these results with the kinetic energy effect of Eq. (55), we find

$$E=E_\infty+E_\sigma, \quad (61)$$

where the surface energy is

$$E_\sigma=\left(\frac{8.68}{\eta^2}+\frac{2.73}{\eta^4}\right)A^{-\frac{1}{3}}\text{ Mev}. \quad (62)$$

At the equilibrium density of $\eta=1.00$, $E_\sigma=11.4$ Mev $A^{-\frac{1}{3}}$ which is approximately equal to the usually accepted value.[10] It is interesting to note that the surface energy is almost exactly equally divided between effects on the potential and kinetic energies.

This result is considerably less than that previously obtained in NS II; the improvement is a consequence of the more nearly correct treatment of the effective nuclear volume. The great sensitivity of the surface energy to the precise details of the treatment shows that the results obtained are not completely quantitative; it is clear, however, that this model gives results which are quite compatible with the empirically derived surface energy.

B. Symmetry Energy

The symmetry energy of the nucleus arises from a departure of the nuclear state from the most symmetrical one, i.e., that with equal neutron and proton numbers. Observed displacements of the neutron-to-proton ratio from unity are the consequence of the Coulomb interaction which leads to a neutron excess. We wish to make a quantitative study of these effects. In this discussion we shall omit the surface effects since these have a different origin than the symmetry energy and can be omitted (in first approximations) in a discussion of the latter.

We shall assume the following nuclear model on which to base our considerations. We let the maximum Fermi momentum for the neutrons be k_N and for the protons k_P. We also introduce the numbers character-

[10] E. Feenberg, Revs. Modern Phys. **19**, 239 (1947).

izing the neutron excess:

$$N_N-N_P=I, \quad N_N+N_P=A, \tag{63}$$

or

$$N_N=\tfrac{1}{2}A(1+\epsilon), \quad N_P=\tfrac{1}{2}A(1-\epsilon), \tag{64}$$

where $\epsilon=I/A$. We further introduce the Fermi momentum k_F defined as before with $\epsilon=0$. As a function of ϵ, the maximum neutron and proton momenta are

$$k_N=k_F(1+\epsilon)^{\frac{1}{3}}, \quad k_P=k_F(1-\epsilon)^{\frac{1}{3}}, \tag{65}$$

and the mean kinetic energy is

$$T_\epsilon=\tfrac{3}{5}(k_F^2/2M)\tfrac{1}{2}[(1+\epsilon)^{5/3}+(1-\epsilon)^{5/3}]. \tag{66}$$

The linear term in ϵ vanishes; consideration of the quadratic term is sufficient for our purposes. Thus we find

$$T_\epsilon-T_F=(5/9)T_F\epsilon^2, \tag{67}$$

which is a repulsive term opposing departure of the neutron-proton ratio from unity.

We treat the potential energy similarly. First we define an integral

$$J(\epsilon)=(4\pi)^{-2}\Big\{\int_{kN}d\mathbf{k}_1\int_{kN}d\mathbf{k}_2 a_{NN} + \int_{kP}d\mathbf{k}_1\int_{kP}d\mathbf{k}_2 a_{PP}+\int_{kP}d\mathbf{k}_1\int_{kN}d\mathbf{k}_2 a_{NP}\Big\}, \tag{68}$$

where the three terms represent contributions from the neutron-neutron, proton-proton, and neutron-proton interactions, respectively. Restricting ourselves to consideration of the s-wave interaction alone, we can express this integral as a function of integrals over the amplitudes for scattering in the singlet and triplet spin states, i.e.,

$$\begin{aligned}J(\epsilon)=(4\pi)^{-2}\Big\{&\int_{kN}d\mathbf{k}_1\int_{kN}d\mathbf{k}_2 a_s\Big(\frac{\mathbf{k}_1-\mathbf{k}_2}{2}\Big)\\ &+\int_{kP}d\mathbf{k}_1\int_{kP}d\mathbf{k}_2 a_s\Big(\frac{\mathbf{k}_1-\mathbf{k}_2}{2}\Big)\\ &+\int_{kN}d\mathbf{k}_1\int_{kP}d\mathbf{k}_2\Big[a_s\Big(\frac{\mathbf{k}_1-\mathbf{k}_2}{2}\Big)\\ &+3a_t\Big(\frac{\mathbf{k}_1-\mathbf{k}_2}{2}\Big)\Big]\Big\}.\end{aligned} \tag{67'}$$

Let us denote the result of carrying out the angular integrals over $\mathbf{k}_1$ and $\mathbf{k}_2$ by

$$(4\pi)^{-2}\int d\Omega_1\int d\Omega_2 a\Big(\frac{\mathbf{k}_1-\mathbf{k}_2}{2}\Big)=\bar{a}(k_1,k_2). \tag{68}$$

Then we can write

$$\begin{aligned}J(\epsilon)=&\int_0^{k_N}dk_1\int_0^{k_N}dk_2 k_1^2k_2^2\bar{a}_s(k_1,k_2)\\ &+\int_0^{k_P}dk_1\int_0^{k_P}dk_2 k_1^2k_2^2\bar{a}_s(k_1,k_2)\\ &+\int_0^{k_N}dk_1\int_0^{k_P}dk_2 k_1^2k_2^2[\bar{a}_s(k_1,k_2)+3\bar{a}_t(k_1,k_2)].\end{aligned} \tag{69}$$

We now carry out an expansion of the integral $J(\epsilon)$ about the point $\epsilon=0$. The leading term $J(0)$ then corresponds to zero isotopic excess and therefore gives rise to the undisturbed potential energy. The linear term in ϵ is easily shown to vanish, if one makes use of the relations:

$$\partial k_N/\partial\epsilon=\tfrac{1}{3}k_F(1+\epsilon)^{-\frac{2}{3}}, \quad \partial k_P/\partial\epsilon=-\tfrac{1}{3}k_F(1-\epsilon)^{-\frac{2}{3}}. \tag{70}$$

Retaining only the quadratic term in ϵ, we find

$$J(\epsilon)-J(0)=\tfrac{1}{3}\epsilon^2k_F^6\Big\{\tfrac{1}{3}\bar{a}_s(k_F,k_F)-\bar{a}_t(k_F,k_F) +k_F^{-2}\int_0^{k_F}k^2dk\frac{\partial}{\partial k_F}[\bar{a}_s(k_F,k)+\bar{a}_t(k_F,k)]\Big\}. \tag{71}$$

The term depending on the difference in the scattering for singlet and triplet states represents the effect on the relative populations of the singlet and triplet spin states of increasing the isotopic excess. The second term is the result of the effect on the potential energy of the general shift to higher-momentum states. We finally can use the result expressed in Eq. (71) to find the effect on the potential energy, which is

$$[V(\epsilon)-V(0)]/V(0)=[J(\epsilon)-J(0)]/J(0),$$

or

$$\begin{aligned}[V(\epsilon)-V(0)]/V(0)=&\tfrac{1}{9}\epsilon^2k_F^6\Big\{\tfrac{1}{3}\bar{a}_s(k_F,k_F)-\bar{a}_t(k_F,k_F)\\ &+k_F^{-2}\int_0^{k_F}k^2dk\frac{\partial}{\partial k_F}[\bar{a}_s(k_F,k)+\bar{a}_t(k_F,k)]\Big\}\\ &\times\Big\{\int_0^{k_F}k_1^2dk_1\int_0^{k_F}k_2^2dk_2[\bar{a}_s(k_1,k_2)\\ &+\bar{a}_t(k_1,k_2)]\Big\}^{-1}.\end{aligned} \tag{72}$$

The evaluation of this integral is most easily effected if we choose an explicit dependence of the sum $a_s(\frac{1}{2}\mathbf{k}_1-\frac{1}{2}\mathbf{k}_2)+a_t(\frac{1}{2}\mathbf{k}_1-\frac{1}{2}\mathbf{k}_2)$ on the two vectors $\mathbf{k}_1$, $\mathbf{k}_2$. A good representation of these amplitudes for the self consistent mass $M^*=0.54M$ is

$$a_s+a_t=2a|\mathbf{k}_1-\mathbf{k}_2|^{-1}+b\mu^{-1}+\tfrac{1}{2}c|\mathbf{k}_1-\mathbf{k}_2|\mu^{-2}, \tag{73}$$

where $a=0.467$, $b=1.258$, $c=-0.885$. Inserting this expansion into the integrals of Eq. (72), we find

$$\frac{V(\epsilon)-V(0)}{V(0)}=\frac{1}{9}\epsilon^2\left(\frac{4a}{15}+\frac{bk_F}{9\mu}+\frac{ck_F^2}{9\mu^2}\right)^{-1}\left[\frac{k_F}{3}\bar{a}_s(k_F,k_F)-k_F\bar{a}_t(k_F,k_F)-\frac{2}{3}a+\frac{2}{15}c\frac{k_F^2}{\mu^2}\right]. \quad (74)$$

At equilibrium density, taking $\eta=1.00$ and inserting the values of the constants, we find

$$V(\epsilon)-V(0)=-0.62\epsilon^2V(0)=16.9\epsilon^2 \text{ Mev}. \quad (75)$$

Confirming this with the kinetic effect, we find for the symmetry energy:

$$E(\epsilon)-E(0)=25.1\epsilon^2 \text{ Mev}=25.1 \text{ Mev}\left(\frac{N-Z}{N+Z}\right)^2. \quad (76)$$

This is to be compared with the empirical value given by Feenberg[10] of $18.1\epsilon^2$ Mev. Thus the agreement between the observed and calculated symmetry energy is rather good. The result we have obtained depends, however, rather sensitively on the precise character of the scattering near the Fermi momentum through the first two terms on the right side of Eq. (74). While these contribute about $\frac{1}{3}$ of the total symmetry energy, their precise values (more exactly their difference) are not so critical elsewhere. Thus the agreement we have found is probably as good as we can expect considering the uncertainties of our methods on details such as this.

C. Stability of the Nucleus against Distortion

In this section, we shall examine the stability of the nucleus against spin polarization and shape distortion. In general we can expect that a repulsive symmetry energy of the type discussed in Sec. IV will arise in connection with polarization of the spin and thus that the most stable configuration of the nucleus will be that of greatest symmetry. This effect can be compensated to some extent, however, by the action of the tensor force which, coupling together the spin polarization and shape distribution of the nucleus, can possibly lead to a stable nonspherical configuration with spin polarization. In this effect the tensor force is somewhat analogous to the Coulomb force which polarizes the isotopic spin of the system.

We proceed in a manner similar to the previous section. We let k_+ be the maximum momentum of states with spin parallel to an axis (to be taken the axis of distortion) $\mathbf{n}$, and k_- the maximum for states with antiparallel spin. We further let

$$N_+-N_-=S, \quad N_++N_-=A, \quad (77)$$

or

$$N_+=\tfrac{1}{2}A(1+s), \quad N_-=\tfrac{1}{2}A(1-s), \quad (78)$$

where s is a parameter analogous to the isotopic spin polarization parameter ϵ of the last section. To allow for physical distortion of the nucleus, we introduce a distortion parameter ρ by the relation:

$$R=R_0[1+\rho P_2(\cos\theta)]. \quad (79)$$

This distortion of shape is the simplest possible for the nucleus, a distortion proportional to $P_1(\cos\theta)$ corresponding merely to a displacement of the surface. The density of momentum states is, following the method of Hill and Wheeler,[8]

$$N(k)d\mathbf{k}=\frac{vd\mathbf{k}}{(2\pi)^3}\left\{1-\frac{3\pi}{4R_0k}[1+\rho P_2(\cos\theta)]^{-1}\right\}, \quad (80)$$

where θ is now the angle between $\mathbf{k}$ and the axis of distortion $\mathbf{n}$. The determination of the kinetic energy gives to second order in ρ:

$$T=\frac{3}{5}\frac{1}{2M}\left\{k_+^5\left[1-\frac{5}{4}\frac{k_0}{k_+}\left(1+\frac{1}{5}\rho^2\right)\right]+k_-^5\left[1-\frac{5}{4}\frac{k_0}{k_-}\left(1+\frac{1}{5}\rho^2\right)\right]\right\}\times\left\{k_+^3\left[1-\frac{3}{2}\frac{k_0}{k_+}\left(1+\frac{1}{5}\rho^2\right)\right]+k_-^3\left[1-\frac{3}{2}\frac{k_0}{k_+}\left(1+\frac{1}{5}\rho^2\right)\right]\right\}^{-1}, \quad (81)$$

with k_0 defined as before in Eq. (48). Writing

$$k_+=(1+s)^{\frac{1}{3}}k_F, \quad k_-=(1-s)^{\frac{1}{3}}k_F, \quad (82)$$

and expanding the kinetic energy about ρ and s equal to zero, we find

$$T=T_F\left[1+\frac{1}{4}\frac{k_0}{k_F}+\frac{5}{9}s^2+\frac{1}{20}\frac{k_0}{k_F}\rho^2\right]. \quad (83)$$

In this result the second term is a surface correction, the third arises from spin polarization, and the fourth from shape distortion.

We consider next the potential energy. We define an integral related to the potential energy by the equation:

$$k(s,\rho)=(4\pi)^{-2}\sum_{\text{spins}}\int d\mathbf{k}_1d\mathbf{k}_2\left\{1-\frac{k_0}{k_1}[1+\rho P_2(1)]^{-1}\right\}\times\left\{1-\frac{k_0}{k_2}[1+\rho P_2(2)]^{-1}\right\}a\left(\frac{\mathbf{k}_1-\mathbf{k}_2}{2}\right), \quad (84)$$

where a is the scattering amplitude. For the case of tensor scattering which differs for the three substates of spin 1, it is convenient to introduce projection operators for the states in which the spin is parallel, perpendicular, or antiparallel to the relative momentum vector

$\mathbf{k}=\frac{1}{2}(\mathbf{k}_1-\mathbf{k}_2)$. Thus we write for the triplet states:

$$a_t(k)=\tfrac{2}{3}t_1(k)(1+\tfrac{1}{4}S_{12})+\tfrac{1}{3}t_0(1-\tfrac{1}{2}S_{12})$$
$$=\tfrac{1}{3}(2t_1+t_0)+\tfrac{1}{6}(t_1-t_0)S_{12}, \quad (85)$$

where

$$S_{12}=3\boldsymbol{\sigma}_1\cdot\mathbf{k}\boldsymbol{\sigma}_2\cdot\mathbf{k}/k^2-\boldsymbol{\sigma}_1\cdot\boldsymbol{\sigma}_2, \quad (86)$$

and t_1 (or t_0) is the amplitude for scattering with spin parallel or antiparallel (or perpendicular) to $\mathbf{k}$. The matrix elements of S_{12} for the three triplet substates are (relative to a direction of quantization at an angle θ with the relative momentum vector k):

$$(1|S_{12}|1)=(-1|S_{12}|-1)=3\cos^2\theta-1,$$
$$(0|S_{12}|0)=-2(3\cos^2\theta-1). \quad (87)$$

By using these results and separating the integration over momenta and summation over spins into integrations over the regions of spin up (+) and spin down (−), Eq. (84) can be written

$$k(s,\rho)=\tfrac{1}{3}(4\pi)^{-2}\Big\{\int_{k_+}d\mathbf{k}_1\int_{k_+}d\mathbf{k}_2N(k_1)N(k_2)$$
$$\times[2t_1+t_0+(t_1-t_0)P_2(\cos\theta)]$$
$$+\int_{k_-}d\mathbf{k}_1\int_{k_-}d\mathbf{k}_2N(k_1)N(k_2)$$
$$\times[2t_1+t_0+(t_1-t_0)P_2(\cos\theta)]$$
$$+\int_{k_-}d\mathbf{k}_1\int_{k_+}d\mathbf{k}_2N(k_1)N(k_2)[2t_1+t_0+9S$$
$$-2(t_1-t_0)P_2(\cos\theta)]\Big\}. \quad (88)$$

In calculating this integral we shall keep only the first nonvanishing terms in ρ and s^2; in so doing we omit terms in ρ^2 which are of the same magnitude as those kept in the kinetic energy and which are also repulsive. As we shall see, only a rough determination of the ρ^2 terms is sufficient to show that the system is stable against distortion so that we shall for simplicity make use of only the quadratic kinetic effect (and thus underestimate the set quadratic term in ρ). In expanding the integral $k(s,\rho)$, we find that as in the case of the symmetry energy the terms linear in s vanish. The result of this development is

$$k(s,\rho)=k(0,0)+s^2G+s^2\rho H, \quad (89)$$

where

$$k(0,0)=(4\pi)^{-2}\int_{k_F}d\mathbf{k}_1\int_{k_F}d\mathbf{k}_2\left(1-\frac{k_0}{k_1}\right)\left(1-\frac{k_0}{k_2}\right)$$
$$\times(2t_1+t_0+3S), \quad (90)$$

$$G=2\frac{\partial^2k(0,0)}{\partial s^2}=\frac{k_F^6}{27}\Big\{2\bar{t}_1(k_F,k_F)+\bar{t}_0(k_F,k_F)$$
$$-9\bar{S}(k_F,k_F)+3k_F^{-2}\int_0^{k_F}k^2dk\frac{\partial}{\partial k_F}[2\bar{t}_1(k_F,k)$$
$$+\bar{t}_0(k_F,k)+3\bar{S}(k_F,k)]\Big\}, \quad (91)$$

$$H=2\frac{\partial^3k(0,0)}{\partial s^2\partial\rho}=\frac{8}{9}k_0k_F^5\int\frac{d\Omega_1d\Omega_2}{(4\pi)^2}P_2(\cos\theta)$$
$$\times P_2(\cos\theta_1)\left[t_1\left(\frac{\mathbf{k}_1-\mathbf{k}_2}{2}\right)-t_0\left(\frac{\mathbf{k}_1-\mathbf{k}_2}{2}\right)\right] \quad (92)$$

with in the last integral the vectors $\mathbf{k}_1$ and $\mathbf{k}_2$ equal to k_F in magnitude. The term $k(0,0)$ is simply related to the potential energy without distortion, the repulsive "spin symmetry" energy arises from G, and the magnitude of H determines the amount of distortion. In the absence of tensor force, $t_1=t_0$ and no distortion will occur.

Before evaluating these integrals let us examine the general features of the change in kinetic and potential energy with distortion. After combining Eqs. (83) and (89) to give the total energy, the result is (dropping the $\frac{1}{4}k_0/k_F$ term in the kinetic energy):

$$E=T_0\left[1+\frac{5}{9}s^2+\frac{1}{20}\frac{k_0}{k_F}\rho^2\right]$$
$$+V_0\left[1+s^2\frac{G}{k(0,0)}+s^2\rho\frac{H}{k(0,0)}\right]. \quad (93)$$

Minimizing the energy with respect to ρ, we find

$$E=T_0+V_0+s^2\left[\frac{5}{9}T_0+V_0\frac{G}{k(0,0)}\right]$$
$$\times\left[1-\frac{s^2(V_0H/k(0,0))^2}{\frac{1}{5}\frac{k_0}{k_F}T_0\left(\frac{GV_0}{k(0,0)}+\frac{5}{9}T_0\right)}\right]. \quad (94)$$

The symmetry correction terms to the kinetic and potential energies are both repulsive and of the same order of magnitude; also T_0 and V_0 are nearly equal in magnitude. Thus let us write very roughly (for nuclei with $A\approx200$ that $\frac{1}{5}k_0/k_F\approx1/25$):

$$E-E_0\approx|V_0|s^2\left[1-s^2\frac{|V_0|}{T_0}\left(\frac{5H}{k(0,0)}\right)^2\right]. \quad (95)$$

For the energy of the nucleus to be lower for large distortions, it is necessary for the term proportional

to s^4 to dominate (with s^2 less than one). The ratio $H/k(0,0)$ is generally much less than unity since it involves a ratio of essentially a surface term to a volume term; this can be compensated for, however, by a sufficiently large ratio of V_0/T_0. This cannot occur in our problem because of the strong stabilization of the nuclear density near a normal density for which the kinetic and potential energies are of the same magnitude. Thus we can expect rather generally for saturating forces that the presence of an admixture of tensor force will not lead to polarization and distortion. Consistent with these remarks, we content ourselves with approximate evaluation of these integrals since only a qualitative result is needed.

In $k(0,0)$ and G we neglect the tensor force splitting of the spin substates since this affects the result only weakly. The integrals then may be evaluated following the methods used in evaluating the symmetry energy. In the integral for H we make the approximation of replacing the difference t_1-t_0 by its angular average leaving the integration over the product of the Legendre functions alone. We also get an approximate value for the tensor force splitting by examining the results of NS II which show that $(t_1-t_0)k_F$ is approximately equal to 0.30. Again the precise value of this quantity is not needed since we need only a very rough measure of the energy. The results of these approximations are

$$V(s,\rho)-V(0,0)=11.5 \text{ Mev } s^2+0.25 \text{ Mev } s^2\rho. \quad (96)$$

Combining this with the kinetic energy and minimizing with respect to the distortion parameter ρ, we find

$$E-E_0=21.5 \text{ Mev } s^2(1-0.0029s^2). \quad (97)$$

Thus, for possible values of s^2 (less than unity), the increment in the tensor force energy due to the distortion (the negative term in the bracket) is entirely negligible relative to the dominant repulsive energy associated with the spin polarization (the term in s^2). We therefore see that there is no tendency for the nucleus to depart from its spherical shape or to polarize its spin, the stability against such effects being marked.

V. SUMMARY OF RESULTS

In the preceding sections we have discussed some of the consequences of a treatment of the saturation and structure problems which is more general than the considerations of earlier papers (NS I and NS II). In considering the dispersive characteristics of the nuclear medium we have been led to a problem of self-consistency which we have formulated and approximately solved in Sec. II. The problems encountered there are mathematically difficult to solve and also depend on some features of the theory which are less certain than the central aspects of the formulation. In particular, the dispersive characteristics of the medium for very fast particles appear to be rather important; consequently a detailed knowledge of very high-energy scattering is necessary. Thus we can no longer claim that we have fully solved the problem originally formulated, although it is probable that the main features have been handled on the whole correctly. The quantitative results of this paper are, considering the approximations made, in very satisfactory and perhaps surprising agreement with the empirical values for density, binding energy, surface energy, and symmetry energy (see Table II). Since the theory has no free parameters this success is to some extent persuasive of the correctness of the main concepts involved.

TABLE II. Summary of results for volume, surface, and symmetry energy. For comparison the results of Feenberg[a] are also given. The energies are all in units of Mev.

	Radius	E_{volume}	E_{surface}	E_{symmetry}
Calculated	1.40×10^{-13}	12.8	11.4	25.2
Feenberg	1.46×10^{-13}	14.0	13.1	18.1

[a] See reference 10.

The picture of the nucleus which we have developed is one in which the nucleons move to a good approximation in the independent-particle states determined by a uniform potential. The properties of the highly dispersive nuclear medium are deduced from the two-body interactions and are a rapidly varying function of the density of the nuclear matter. The equilibrium density at the energy minimum occurs as the result of a rather complex balance between the kinetic and potential energy.

The properties of the nucleus are collective to a remarkable extent as a result of the codetermination by the nucleons of the potential in which they move. A striking consequence of this is shown in the collective character of the excitation energies of "single-particle" excited states, this energy being shared almost equally by the excited particle and by the remainder of the nucleus. The unique features of the nuclear structure are also expressed clearly in an equivalent formulation of the problem in which the potential is assumed constant but the nucleon mass reduced by a factor of approximately two. Thus the "nucleons" can be considered to move in a conventional uniform and constant potential but with a very different "effective mass."

The results of this work can of course immediately be extended to the shell model. A reasonable procedure in this case would be to assume that the potential energy appropriate to a shell-model state is for some mean value of the momentum in the state. The results of this paper could then be immediately applied to the case of spherical quantization. A simpler procedure would be to introduce the equivalent problem in which the nuclear mass is reduced and the appropriate constant potential used. In our case, for example, the mass reduction is by a factor 0.54 and the equivalent po-

tential has a depth of 67 Mev. One of the most obvious consequences of this change is that the spacing of shell-model energy states would be considerably increased. Other consequences of this change and their relevance to experiment will be discussed in a separate paper.

The author would like to acknowledge a number of helpful discussions of topics related to the contents of this paper with Dr. R. J. Eden, Dr. N. Francis, and Dr. C. A. Levinson. He is also indebted to Professor John A. Wheeler whose interest has been greatly stimulating to this work.

PHYSICAL REVIEW VOLUME 97, NUMBER 5 MARCH 1, 1955

Theory of Nuclear Models

R. J. EDEN* AND N. C. FRANCIS
Indiana University, Bloomington, Indiana†
(Received November 22, 1954)

The framework for a unified theory of nuclear structure is described in which the wave functions for different nuclear models are obtained by transformations on the actual nuclear wave function. This formulation provides a basis for explaining the success of weak-coupling models of the nucleus and showing that they are not in conflict with the assumption that nucleons have very strong mutual interactions. The explanation lies in the fact that only in certain circumstances can the "particles" in a nuclear model be interpreted as nucleons.

We investigate the properties which transformation operators must have to change the nuclear wave function into a model wave function and consider how far these properties are satisfied in practice. Self-consistent equations are set up for a model having a product wave function in the particle variables, and it is shown that these equations can be solved in an approximation relevant to the problem of nuclear saturation.

I. INTRODUCTION

IN recent years a number of nuclear models have been developed which successfully describe many aspects of nuclear structure. The most striking successes have been obtained by the Mayer-Jensen[1] shell model and by Weisskopf's[2] cloudy crystal-ball model, and it is clear that for low energies there must be a close correspondence between these models and the actual nucleus. On the other hand, these models are based on an assumption of weak interaction between the particles they describe and this assumption appears to be in direct contradiction with the strong nucleon interactions which are observed in scattering experiments. We shall show in this paper that this apparent contradiction is not a real one but is explained essentially by the fact that the "particles" in these nuclear models are not nucleons—that is to say they cannot in all circumstances be interpreted as nucleons.

Our program is firstly to set up and explain a formalism in which the wave functions of various models can be transformed by "model operators" into the real nuclear wave function. Next we consider how actual nuclear models fit into the framework of our theory, and finally we consider the problem of using these model operators in practical applications of the theory.

Since this theory shows that the particles, in the shell model, for example, are not nucleons, it is necessary to show that shell-model results can still be explained with this new interpretation. We do not attempt to derive the explicit assumptions of the shell model, although our formalism leads to self-consistent equations which if solved should lead to the well potential of the model. Our primary concern is to show how the following aspects of the shell model are consistent with our method: the particles in the model obey the exclusion principle as though they are neutrons and protons, energy levels are predicted with sufficient accuracy to indicate the order of filling single-particle states, angular momentum and parity are accurately predicted as though the model was the real nucleus, and selection rules are well predicted. This is not by any means a complete list but should serve to indicate the problems of interpretation which have to be considered. Also, we must consider the relation of our theory to the failures of the model such as the failure to predict transition rates with any accuracy.

Since our methods are quite general and apply to any nuclear model, a complete presentation of this theory would require detailed consideration of very many aspects of the relation of nuclear models to experiment. We have in this paper attempted to select sufficient of these aspects of the theory to indicate the power of the method, and hope in future papers to examine other aspects. In particular, we have limited ourselves to consideration of low-energy nuclear models although we believe that the methods are also applicable to high-energy problems. In addition to the shell model, we

* Smithson Research Fellow of the Royal Society, on leave of absence from Clare College, Cambridge, England.

† This work was supported by grants from the National Science Foundation, the Office of Naval Research, and the U. S. Atomic Energy Commission.

[1] Maria Goeppert Mayer, Phys. Rev. **75**, 1969 (1949); Haxel, Jensen, and Suess, Phys. Rev. **75**, 1766 (1949).

[2] Feshbach, Porter, and Weisskopf, Phys. Rev. **96**, 448 (1954).

consider the single-particle model and the related cloudy crystal-ball model. For the latter, we have to show how it is that the scattering of particles in the model has the same cross sections as elastic scattering of neutrons on the real nucleus.

We take as our starting point a representation in which the nuclear wave function is $\Psi(A)=\Psi(x_1,\cdots,x_A)$ where $x_1, \cdots, x_A$ are the coordinates of nucleons. The corresponding Schrödinger equation will have a Hamiltonian H which contains a potential energy $V(x_1,\cdots,x_A)$ which may include many-body potentials (it seems probable, however, that these can be neglected as a first approximation). It is known from nucleon-nucleon scattering data that there are very strong forces between two nucleons, and it seems unlikely that these forces will be much different when the nucleons are found in a nucleus. For strong nuclear forces the potential V is a rapidly varying function and the wave function $\Psi(A)$ will contain strong correlation effects; in particular, for short-distance repulsion between nucleons, $\Psi(A)$ will be small wherever $|x_i-x_j|$ is small. It is clear that the wave function $\Psi(A)$ will be very complicated and will not approximate (except in a very restricted sense) to the product wave functions used in nuclear models such as the independent-particle model of the shell model.

If the successes of these models are to be explained within the framework of present day quantum theory, it must be possible to make a transformation which will take the wave function $\Phi(A)$ for the model into the much more complicated wave function $\Psi(A)$ for the real nucleus. There will be different transformations corresponding to different nuclear models. We call the transformation operators "model operators" and much of this paper is devoted to considering their properties and uses. In general, observables will be represented in a model by different operators from those used for the actual nucleus, and it will be seen that the usefulness of a particular model depends on the behavior of observables under transformation by the appropriate model operator.

Our method is outlined as follows: (1) We consider the conditions on the transformed Hamiltonian $H^m=M^\dagger HM$ which are desirable in a useful model; (2) we deduce conditions on the model operator M; (3) we examine whether in general these conditions can be satisfied by a choice of M; (4) we consider how far these conditions enable us to regard the model as the real nucleus; (5) we consider whether these conditions are satisfied by existing nuclear models; (6) if the conditions are only satisfied approximately, we consider possible corrections which may allow for the resulting error; (7) we discuss the physical reasons why actual nuclear models satisfy the conditions mentioned above; (8) we develop the mathematical theory resulting from two particular forms of model operator relevant to the single-particle model and to the problem of nuclear saturation. We have not attempted to achieve completeness in the above program but have endeavored to carry it far enough to indicate the power and usefulness of the method.

The conditions (1) on H^m which are desirable cannot all be satisfied by any one model. They include the following: (*a*) H^m should be such that the transformed wave function $\Phi(A)$ is manageably simple, for example, a product wave function of some kind such as in the single-particle model or in the shell model. (*b*) H^m should be invariant for rotations and reflections of the coordinate axes and for rotations in isotopic spin space; when these conditions are satisfied, it is possible to define a new transformation which leaves the angular momentum, parity, and charge operators unchanged—then for these operators the model will appear to be the real nucleus. (*c*) H^m should give the same energy spectrum as the original Hamiltonian; this requires $\Psi(A)=M\Phi(A)$, where M is a unitary operator. (*d*) H^m should be the Hamiltonian for a system of particles which satisfy the exclusion principle in the same way as neutrons and protons; this condition sets certain symmetry requirements on M. (*e*) For a single-particle model of low-energy scattering the transformation operator must be chosen to commute with the elastic scattering part of the collision matrix. (*f*) for a single-particle model of a nucleus it may be desirable that $\Phi(A)=\psi(A)\Psi_0(A-1)$, where $\Psi_0(A-1)$ is the ground state of the $(A-1)$th nucleus. This list is far from a complete one but should be sufficient to indicate the conditions on H^m and M which we consider.

The basic point we wish to make about point (4) in our method arises because it is never in practice possible to satisfy all the above conditions simultaneously. It follows that no single nuclear model can be considered as the real nucleus; that is to say, the particles in a model cannot always be interpreted as nucleons without leading to incorrect results. Thus, for the shell model a "particle" in the model does not have the binding energy of a nucleon. For a single-particle model, we can choose the transformation so that the particle has the binding energy of the last nucleon added, but one can see that such a model cannot in general be expected to give the correct magnetic moment if the particle is interpreted as a nucleon in a definite state of angular momentum.

The nuclear models considered in point (5) have, of course, always been regarded as approximate, so our investigation is partly to the same degree of approximation. However, we are able also to show that some of these approximations are forced upon a particular model because one or more of its properties is not compatible with some of the desirable properties mentioned above. Some of these facts are well known, for example the use of a product wave function in the shell model precludes collective motion of a certain type, but the fact that limitations may be due to conflicting requirements does not appear to have been recognized before. We consider in step (6) some of the

corrections which have to be made because of the inherent limitations of a model, with particular reference to magnetic moments and deviations from the Schmidt lines.

The interpretation we given in step (7) is based essentially on the operation of the exclusion principle at low energies. This situation has been considered by Weisskopf[3] also with a view to justifying the shell model. His main point is that at low energies all nucleon states are occupied, so that because of the exclusion principle any one nucleon can only change its state by a transition in which high-energy states are involved; these transitions can be expected to occur with small probability, so a nucleon in a low-energy nuclear state will move with a long mean free path. One difficulty in interpreting this argument lies in giving a meaning to a "nucleon state" when the nucleon variables occur only in a strongly correlated wave function. In order to define a nucleon state, it is necessary to have some quantity like a single-nucleon wave function and this does not seem possible for a nucleon in a nucleus. We consider the problem from the viewpoint of transforming the shell-model wave function to the actual nucleus. It should be noted that the exclusion principle holds in the model because it holds in the actual nucleus. The arguments of Weisskopf can now be applied in considering the changes in observables under the transformation. Excited states of the model now occur as intermediate states, and it appears that for some operators the large energy differences in going to these excited states have a major simplifying effect, and in some cases make the operator commute with the transformation (approximately). However, it does not follow that there is always close resemblance between the actual nuclear wave function and the wave function for the model; in fact, consideration of the strong nucleon interactions shows that there cannot always be such a resemblance.

In the above sense, it seems that the arguments of Weisskopf provide some justification that a transformation exists which connects the real nucleus with a model consisting of particles moving in weak interaction and satisfying the other conditions of the shell model.

These physical ideas can be put in mathematical form to give an explicit model operator derived from two-body forces in a simplified problem connected with nuclear saturation. For this problem, the model operator is equivalent in a certain approximation to the transformation operator used by Brueckner, Levinson, and Mahmound[4] in their derivation of a nuclear radius in close agreement with observed values.

[3] V. F. Weisskopf, Helv. Phys. Acta **23**, 187 (1950).

[4] Brueckner, Levinson, and Mahmound, Phys. Rev. **95**, 217 (1954). See also K. A. Brueckner, Phys. Rev. **96**, 508 (1954), who notes that the "independent particle" of their coherent model does not refer to "independent nucleon" motion. It has also been noted by C. A. Levinson that the coherent model wave function is in a different space from the actual nuclear wave function.

In Sec. II of this paper, we illustrate our method by making a formal derivation of the single-particle model of a nucleus. In Sec. III, we consider the relation of this model to the elastic scattering of nucleons on a nucleus. In Sec. IV, we consider the general conditions on model operators which are related to the wave function of the model giving correctly eigenvalues of parity, angular momentum, and isotopic spin. In Sec. V, we deduce from conditions on model operators that the corresponding models will give selection rules correctly but will not in general give transition rates. In Sec. VI, we consider first the setting up of an "ideal" shell model and then examine how far it corresponds to the actual shell model. In Sec. VII, we consider in detail the development of a single-particle model having the same energy in one state as the actual nucleus; the energy condition is sufficient to determine the depth of the well in which the particle moves. In Sec. VIII, we derive a formula for the energy of a nucleus modified by extra boundary conditions; this is only approximately the formula used in reference 4, and our method appears to be of rather more general validity. Finally, in Sec. IX, we briefly state our conclusions and indicate further work which is proceeding.

II. FORMAL DERIVATION OF THE SINGLE-PARTICLE MODEL

We take as our starting point the many-body Schrödinger equation for A nucleons in a representation in which the kinetic energy is the sum of A single-nucleon kinetic energies and the potential energy is a function of the coordinates of the A nucleons:

$$(E-H_A)\Psi(x_1\cdots x_A)=0, \tag{1}$$

$$H_A=\sum_{i=1}^{A} T_i+V_A. \tag{2}$$

The potential V_A will depend on the mutual separations (x_i-x_j) of the nucleons and may include many-body potentials. It appears from scattering data that the two-nucleon parts of V are rapidly varying and non-monotonic functions of (x_i-x_j), and it is unlikely that the strong forces are compensated (i.e. smoothed out) by many-body interactions. It follows that in the representation defined by (1) and (2) the wave function $\Psi(A)[\equiv\Psi(x_1\cdots x_A)]$ contains strong correlations so that it is small when two nucleons are in a region of strong repulsion. It is, therefore, not possible to approximate to $\Psi(A)$ by product wave functions since these in general have considerable overlap between the positions of nucleons.

As an illustration of our method, we will consider a transformation which satisfies more rigid conditions than are necessary in practice. We will suppose the nucleons are distinguishable and assume that there

exists a unitary "model" operator M such that

$$\Psi(A)=M\Phi(A)$$

$$=\int dx_1'\cdots\int dx_A'(x_1\cdots x_A|M|x_1'\cdots x_A')\Phi(x_1'\cdots x_A'), \tag{3}$$

where

$$\Phi(A)=\psi(x_A)\Psi_0(A-1). \tag{4}$$

Then

$$(E-H_A{}^m)\Phi(A)=0, \quad H_A{}^m=M^{-1}H_AM. \tag{5}$$

In practice, it is often convenient to use non-unitary transformations. We have chosen M to be unitary here in order to obtain a model which has the same energy spectrum as the real nucleus. The wave function $\Psi_0(A-1)$ in (4) is defined to be the ground-state wave function of the $(A-1)$th nucleus with Hamiltonian H_{A-1}:

$$(E_{A-1}{}^0-H_{A-1})\Psi_0(A-1)=0. \tag{6}$$

From (4), (5), and (6),

$$\{E-E_{A-1}{}^0-H_A{}^m+H_{A-1}\}\Psi_0(A-1)\psi(x_A)=0. \tag{7}$$

Taking a scalar product with $\Psi_0(A-1)$ on the left, we get

$$\{E'-T_A'-W_c\}\psi(x_A)=0, \tag{8}$$

where $E'=E-E_{A-1}{}^0$ and

$$W_c=(\Psi_0(A-1), \{H_A{}^m-H_{A-1}-T_A'\}\Psi_0(A-1)). \tag{9}$$

Thus W_c is an operator depending only on the Ath particle's coordinates (or other variables associated with this particle). T_A' is the kinetic-energy operator of the Ath particle. Equation (8) is therefore a one-particle equation having eigenvalues of energy equal to the difference between the energy of different states of the Ath nucleus and the ground-state energy of the $(A-1)$th nucleus.

In practice, as a result of the very complicated energy spectrum of the nucleus, the potential W_c in (8) would be very complicated. It can be simplified if we relax the condition that M is unitary. Instead we replace M by an operator MP (to be called the new M), where P is a projection operator which selects only states corresponding to certain energy eigenvalues of the Ath nucleus. If this selection is made so that the new W is simple, we will have derived a model in which a one-particle equation predicts certain nuclear excited states of the nucleus. It is clear from the form of the transformation (3) that the particle in this model must not be identified with a nucleon. Such an identification would imply that other observables, which have not yet been considered, transform in a very special way under the transformation (3).

One freedom which may help to simplify W is worth noting here. The kinetic energy operator T_A' in (8) need not have the same mass as a nucleon, hence if there is a part of W which is proportional to $(\mathbf{k}_A)^2$ it can be incorporated in the nonrelativistic T_A' which is given by $(\mathbf{k}_A)^2/2m$ by introducing a modified mass m^* for the particle.[5]

It will become clear later that other operators will not take a simple form in a model as restrictive as indicated by (4). More generally, a transformation may be of use where a Φ is obtained which can be expanded as a sum of products of the eigenfunctions of Eqs. (6) and (10),

$$(E^r-T_A'-W_\alpha)\psi_r(x_A)=0. \tag{10}$$

$$\Phi(A)=\sum_{r,s}a_{r,s}\Psi_r(A-1)\psi_s(x_A). \tag{11}$$

In Eq. (10), W_α is assumed to be some potential for a single particle; it will approximate to the W_c in (8) if (4) is required to be the leading term in the expansion (11).

Another form of the single-particle equation which will be of use is obtained when a transformation M is such that the single-particle potential operator W has matrix elements:

$$W_{rs}=(\Psi_r(A-1), W\Psi_s(A-1)), \tag{12}$$

where W is the operator occurring in (9). Then the single-particle wave function will satisfy coupled equations:

$$(E_r-T_A'-W_{rr})a_{rr}\psi_r(x_A)=\sum_t\sum_{s\neq r}W_{rs}a_{st}\psi_t(x_A). \tag{13}$$

If the nondiagonal terms of W are small, this can be solved with zero-order equations:

$$(E_r-T_A'-W_{rr})\psi_r(x_A)=0, \tag{14}$$

and the coefficients are determined by perturbation methods.

It will be seen that in the approximation (14) the state of particle A depends on the state of the $(A-1)$ particles. The final approximation we wish to mention here is one in which the Ath particle satisfies equation (10), while the $(A-1)$th wave function $\Psi'(A-1)$ satisfies

$$(E-H_{A-1})a_{rr}\Psi_r'(A-1)=\sum_{r\neq s}\sum_t W_{rs}'a_{ts}\Psi_t'(A-1), \tag{15}$$

where

$$W_{rs}'=(\psi_r, \{H^m-H_{A-1}-T_A'-W_M\}\psi_s). \tag{16}$$

Again, for W_{rs} small when $r\neq s$, perturbation methods can be applied. In lowest approximation, the state of the $(A-1)$ particles depends on the state of the Ath particle. It will be seen later that the situation in the shell model resembles this approximation.

We have now considered formal transformations to the kind of approximate single-particle models which may be useful. The single particle may not have the same mass, and possibly the kinetic-energy operator T_A' will not be the operator for a Dirac particle, unless certain conditions are satisfied by the operator M; we will consider later whether these can be satisfied.

[5] J. A. Wheeler (private communication to K. A. Brueckner).

If we label the wave functions for the real nucleus and for the model in a suitable way, the model operator M will be formally equal to

$$M=\sum_r \Psi_r(A)\Phi_r^*(A). \tag{17}$$

If we are able to find a suitable operator W, the corresponding transformation will be obtained by solving the integral equation

$$M=1+[E-H^m+i\eta]^{-1}(V^{(A)}-W)M, \tag{18}$$

where $V^{(A)}$ is the part of the potential V which depends on the Ath nucleon. Equation (18) has boundary conditions appropriate to the scattering problem. (A different boundary condition is required for bound-state transformations.) The bound-state equation will be considered in Sec. VII where we make a more detailed investigation of the single-particle model.

It will be seen from (17) that since the wave function $\Psi(A)$ contains strong correlations, these correlations will be implicit in M. It is therefore not possible to use perturbation methods in solving Eq. (18) for M, and in general an approximate form of W may lead to a bad approximation to M. For these reasons, in considering explicitly the relation between models and the real nucleus—we will consider not the operator M but will investigate the expectation values of transformed operators $\langle O^m\rangle$. It will appear that in useful problems these operators are given by a rapidly convergent series although M may converge only very slowly.

The two most important extensions of the one-particle transformation are obtained by transforming $\Psi(A-1)$. When further transformations lead to single-particle equations, all of the form (10), one eventually obtains a complete product wave function analogous to the shell-model wave function. The other important transformation is to $\psi(x_{A-1})\Psi_0(A-2)$, when a model is obtained for two (or more) particles outside a core consisting of the ground state of the nucleus. The first of these transformations will be investigated in Secs. V, VI, and VIII.

III. ELASTIC SCATTERING

We have shown in the previous section that a transformation can be chosen to give some of the nuclear-energy levels by means of a single-particle model provided no restrictions are made on the complexity of the single-particle potential. In this section, we consider whether it is possible in general to choose a transformation which gives a single-particle model having the same elastic scattering matrix elements as a neutron on a nucleus.

The Schrödinger equation (4) can be written

$$(E-T_A-H_{A-1})\Psi_0(A-1)\psi(x_A)=W\Psi_0(A-1)\psi(x_A), \tag{19}$$

where

$$W=H_A{}^m-H_{A-1}-T_A. \tag{20}$$

We prove first that the elastic scattering matrix given by the potential W has an expectation value for the state $\Psi_0(A-1)$ which is equal to the elastic scattering matrix given for the one-particle problem by the potential W_c defined in (9).

Equation (19) has a solution corresponding to an initial plane wave state λ for the Ath particle, which can be written

$$\Psi_0(A-1)\psi(x_A)=\Omega\Psi_0(A-1)\lambda_A, \tag{21}$$

where

$$\Omega=1+(E-H_{A-1}-T_A+i\eta)^{-1}W\Omega. \tag{22}$$

Writing the scattering matrix $T=W\Omega$, we have

$$\begin{aligned}(\lambda_A'\Psi_0(A-1),\, T\Psi_0(A-1)\lambda_A)&\\ =(\lambda_A'\Psi_0(A-1),\, W\Omega\Psi_0(A-1)\lambda_A)&\\ =(\lambda_A'\Psi_0(A-1),\, W\Psi_0(A-1)\psi(x_A))&\\ =(\lambda_A',\, W_c\psi(x_A)).&\end{aligned} \tag{23}$$

Now $\psi(x_A)$ satisfies

$$(E_A-T_A)\psi(x_A)=W_c\psi(x_A), \tag{24}$$

which has a scattering solution for an initial plane wave state λ_A,

$$\psi(x_A)=\Omega_c\lambda_A, \tag{25}$$

where

$$\Omega_c=1+(E_A-T_A+i\eta)^{-1}W_c\Omega_c. \tag{26}$$

Upon writing

$$T_c=(\Psi_0(A-1),\, T\Psi_0(A-1)), \tag{27}$$

it follows from (23) and (25) that

$$T_c=W_c\Omega_c. \tag{28}$$

This completes the proof that the single-particle model gives the same elastic scattering as the many-particle model.

We next consider whether in general it is possible to choose the model operator M so that this single-particle scattering is the same as the elastic scattering of a neutron on a nucleus. We note first that M is by no means completely specified by the requirement that $\Phi(A)$ has the form given in (4). It is possible to vary it by any further transformation which acts only on $\psi(x_A)$. This should give enough freedom so that in principle a model operator M can be chosen so that it commutes with the elastic-scattering part of the collision matrix. It has already been noted that the purpose of the transformation M is to introduce correlations so that the model wave function $\Phi(A)$ goes in the real wave function $\Psi(A)$. Since the real wave function has no correlations between the Ath nucleon and the $(A-1)$ nucleons in the scattering limit, it will be possible to choose M so that it acts like a unit matrix in this limit. For this choice, M will not affect the boundary conditions of the problem and the model will give correctly the observed elastic scattering.

From the form of the wave function $\Phi(A)$ in (4), it is clear that the model only has end states for scattering which describes elastic scattering. The potential W_c cannot therefore give rise to excited states of the $(A-1)$ nucleus. It follows that W_c is a complex potential so the transformation operator M cannot be unitary. However, the lesser condition can be imposed on M, that it preserves the energy levels of single-particle excited states of the Ath nucleus. It appears that this condition is satisfied by the optical model of Watson, so we deduce that M can be chosen in practice so that W_c is equal to V_c, the optical model potential.

If we are not interested in resonances in the single-particle scattering, it will be sufficient to choose M only to preserve the lowest one-particle energy levels which do not lie in the continuous spectrum. It appears that these conditions on M are satisfied by the cloudy crystal-ball model of Weisskopf.[2] The approximate equality of the well depth in this model and the Mayer well depth indicates that single-particle energy levels are at least approximately preserved.

IV. PARITY, ANGULAR MOMENTUM, AND ISOTOPIC SPIN

In the previous two sections, we have considered conditions on the model operator M which are related to the correct prediction of energy levels and elastic scattering. In this section, we investigate the possibility of choosing M so that the parity, angular momentum, and isotopic spin operators take a simple form after they have been transformed.

In the representation used in our basic equation (1), the Hamiltonian H is invariant under reflections and rotations of the coordinate axes and under rotations in isotopic spin space if charge independence of nuclear forces is assumed. We will consider first the parity and angular momentum which, because of the invariance of H, can be used to label the energy eigenstates of (1). We denote a particular eigenfunction by $\Psi(E,P,j,m)$ where the eigenvalues of H, P, $\mathbf{J}^2$, J_z are E, P', $j(j+1)$, m.

If the transformation M leads to operators H^m, $P^m(\mathbf{J}^2)^m$, J_z^m, they will have the same eigenvalues E, P', $j(j+1)$, m, where

$$\Psi(E,P',j,m)=M\Phi(E,P',j,m). \tag{29}$$

We will now investigate the assumption that M can be chosen so that the Hamiltonian H^m of the model is invariant under rotations and reflections of the coordinate axes. From this assumption, it follows that H^m, P, $\mathbf{J}^2$, J_z form a commuting set so this set of operators can be used for labeling the wave functions of the model. Let these wave functions be $\Phi_1(E,P',j_1,m_1)$, where $j_1(j_1+1)$ and m_1 are the eigenvalues of $\mathbf{J}^2$ and $\mathbf{J}_z$. For a given value of energy, these wave functions can be expanded in terms of the wave functions $\Phi(E,P',j,m)$. If the degeneracy is the same, and this will in general be required for completeness of the two sets, we can deduce $(2j+1)=(2j_1+1)$. Hence, $j=j_1$ and the operators $\mathbf{J}^2$ and $(\mathbf{J}^2)^m$ have the same eigenvalues.

Now let

$$\Phi(E,P',j,m)=\sum_{m_1=-j}^{j} a_{mm_1}\Phi_1(E,P',j,m_1). \tag{30}$$

Then

$$\begin{aligned}\mathbf{J}^2\Phi(E,P',j,m)&=\sum a_{mm_1}\mathbf{J}^2\Phi_1(E,P',j,m_1)\\&=j(j+1)\Phi(E,P,j,m),\end{aligned} \tag{31}$$

since

$$\mathbf{J}^2\Phi_1(E,P',j,m_1)=j(j+1)\Phi_1(E,P',j,m_1). \tag{32}$$

Therefore $\Phi(E,P,j,m)$ is a common eigenfunction of both $\mathbf{J}^2$ and $(\mathbf{J}^2)^m$. This is true for every such wave function, and since these form a complete set,

$$\mathbf{J}^2=(\mathbf{J}^2)^m, \quad [\mathbf{J}^2,M]=0. \tag{33}$$

It will next be shown that M can be chosen so that J_z commutes with it. Let us assume that for an initial choice of M, $\Phi_1(E,P',j,m)$ is not the same as $\Phi(E,P',j,m)$. Define a unitary operator U whose components for fixed E, P', j are

$$U(E,P',j)=\sum_{m=-j}^{j}\Phi(E,P',j,m)\Phi_1^*(E,P',j,m). \tag{34}$$

Then U commutes with H, P, J^2, and

$$U\Phi_1(E,P',j,m)=\Phi(E,P',j,m). \tag{35}$$

Hence,

$$\begin{aligned}U^{-1}(J_z)^mU\Phi_1(E,P',j,m)&=U^{-1}(J_z)^m\Phi(E,P',j,m)\\&=m\Phi_1(E,P',j,m).\end{aligned} \tag{36}$$

But from the definition of $\Phi_1(E,P',j,m)$,

$$J_z\Phi_1(E,P',j,m)=m\Phi_1(E,P',j,m). \tag{37}$$

Since (36) and (37) hold for every eigenfunction in this complete set, it follows that

$$J_z=U^{-1}(J_z)^mU. \tag{38}$$

Hence, if we redefine M to be MU, for the new operator

$$[J_z,M]=0. \tag{39}$$

We now have

$$\Psi(E,P',j,m)=M\Phi(E,P',j,m). \tag{40}$$

Let $J_\pm=J_x\pm iJ_y$; then

$$J_\pm\Psi(E,P',j,m)=b_\pm(j,m)\Psi(E,P',j,m\pm1), \tag{41}$$

$$J_\pm\Phi(E,P',j,m)=b_\pm(j,m)\Phi(E,P',j,m\pm1). \tag{42}$$

Hence,

$$(J_\pm M-MJ_\pm)\Phi(E,P',j,m)=0. \tag{43}$$

Since this is true for each state in the complete set,

$$[J_\pm,M]=[J_x,M]=[J_y,M]=0. \tag{44}$$

From (39) and (44), we see that, provided that there

exists an M such that H^m is a scalar with respect to rotation, it is possible to choose a new M which is itself a scalar. The implications of this result will be considered after we have discussed parity and isotopic spin.

If the parity operator P as well as P^m commutes with H^m and there is no degeneracy of eigenstates with respect to parity,

$$P^m\Phi(E,P',j,m)=P'\Phi(E,P',j,m) \tag{45}$$

and

$$P\Phi(E,P',j,m)=P''\Phi(E,P',j,m), \tag{46}$$

for all eigenfunctions Φ in the transformed system. Hence,

$$[P^m,P]=0. \tag{47}$$

Using the fact that $P^2=1$, we get

$$[M^{-1},P]_+[M,P]_-=0. \tag{48}$$

Hence, either P always commutes with M or it always anticommutes with M. There is no loss of generality therefore in assuming the Φ state always has the same parity as the corresponding Ψ state.

The condition for the model to have the same charge as the real nucleus is much less stringent than the requirement of isotopic spin invariance. Provided it is possible to choose the model operator M so that it is symmetrical between neutrons and also symmetrical between protons, the total charge will be unaffected by the transformation. It appears that this can be achieved in practice for most useful models.

A much more valuable result can be achieved if complete charge independence of nuclear forces is assumed (i.e., neglect of Coulomb forces and neglect of neutron-proton mass difference). This assumption is approximately valid for light nuclei but not for heavy nuclei.

We consider a transformation for which H^m is invariant under rotations in isotopic spin space. Then (assuming similar invariance of H), the isotopic spin operators I^2 and I_3 can be considered in a manner exactly analogous to the angular momentum. It is then found that M can be chosen to be invariant under rotations in isotopic spin space:

$$[M,I_1]=[M,I_2]=[M,I_3]=0, \tag{49}$$

and also the corresponding wave functions Ψ and Φ of the real nucleus and the model have the same values for isotopic spin.

Up to now, we have considered the transformation properties of parity, angular momentum, and isotopic spin when the states Φ describing the model form a complete set. Since this is never satisfied by any of the nuclear models at present in use, it is useful to consider the situation when the states are not complete. We assume that the equation

$$\Psi(E,P,j,m)=M\Phi(E,P,j,m) \tag{50}$$

is satisfied for all Φ states but that it defines only a selection of the real nuclear states Ψ. In this case we can assume that M is unitary in the subspace based on the set of states given by the model. Provided that each state for which (49) is satisfied has the same degeneracy in the transformed system as in the real nucleus, the arguments already given about invariance go through except that Eqs. (33), (39), (44), and (49) hold only in the subspace defined by the model. It follows that departures from the invariance of M will be evident only as a result of transitions through states not in this subspace. If the model has been chosen so that these transitions have small probability, the concept of partial invariance of M will still be a useful one.

We will consider next how the results of this section can be used to justify the equivalence between the selection rules for a nuclear model and those for the real nucleus.

V. SELECTION RULES

The total Hamiltonian of the nuclear system and the radiation field can be written

$$H_{\text{total}}=H+H_{\text{int}}+H_{\text{rad}}. \tag{51}$$

Up to now we have considered only the part H which is the nuclear force Hamiltonian and primarily responsible for determining nuclear structure. The interaction H_{int} between the nuclear field and the radiation field has been assumed small so that to a good approximation H and H_{rad} can be treated independently. The model operator M is determined in this approximation by H only. Our discussion of the previous section has shown that when the transformed Hamiltonian H^m has certain invariance properties so does the operator M.

The interaction H_{int} will contain certain tensor operators A_i, B_{ij}, C_{ijk}, $\cdots$, which cause radiative transitions in the nucleus. Since M is a scalar with respect to rotations, the transformed operators $A_i{}^m$, $B_{ij}{}^m$, $C_{ijk}{}^m$, $\cdots$, will have the same tensor character as the untransformed operators. From the tensor character of one of these operators, it can be deduced that it will never cause transitions between states differing by certain values of angular momentum. Let us suppose that it is deduced that

$$(\Phi(E',P',j',m'),\ B_{ij}\Phi(E,P,j,m))=0. \tag{52}$$

Since this condition depends only on rotation properties of B_{ij} and the change in angular momentum specified by the matrix elements, it follows that when (52) is satisfied,

$$(\Phi(E',P',j',m'),\ M^{-1}B_{ij}M\Phi(E,P,j,m))=0. \tag{53}$$

Hence, using the results of Sec. IV,

$$(\Psi(E',P',j',m'),\ B_{ij}\Psi(E,P,j,m))=0. \tag{54}$$

This result shows that when a particular selection rule is obtained for a model forbidding transitions between

states of certain angular momenta, the same selection rule will be satisfied by the actual nucleus.

It will be noticed that in (54) we have assumed that M is unitary so that the energies E', E are the same as in (53). This assumption is not essential to the result provided that the invariance conditions on H^m are satisfied and the model gives the correct degeneracy of corresponding levels.

It is important to note that transition rates will not in general be given correctly by the model since nonzero matrix elements will not in general be equal to the matrix elements of the transformed operators:

$$(\Phi(E',P',j',m'), B_{ij}\Phi(E,P,j,m)) \neq (\Psi(E',P',j',m'), B_{ij}\Psi(E,P,j,m)). \quad (55)$$

Selection rules associated with changes in parity and isotopic spin can be shown to be the same for the model and the real nucleus in an analogous discussion to the above. It must be emphasized that the validity of the selection rules for isotopic spin depends on the assumption of complete charge independence. Thus, even an ideal model which satisfies all our other conditions cannot be expected to give correct isotopic spin selection rules except for light nuclei. When charge independence is not approximately true, it will not be possible in general to set up a model of the nucleus in which the transformed isotopic spin variables I^m resemble the untransformed variables I. It may be possible by considering explicit forms for M to estimate the difference $I_m{}^m - I$ and hence give a more precise meaning to isotopic spin of heavy nuclei.

When the states of a nuclear model form only a subspace of the complete set, the invariance of M holds only within the subspace. Then the selection rules predicted by the model will no longer be exact. However, they can only be violated by a process involving a transition with an intermediate state not in the subspace. If the coupling is small between states given by the model and other states, we can deduce that the selection rules will be satisfied approximately.

VI. THE SHELL MODEL

We consider first the setting up of an "ideal" shell model with a model operator M which satisfies as many desired conditions as possible; we will then consider how far this "ideal" model corresponds to the Mayer-Jensen shell model, and finally we will discuss the reasons why certain conditions on M are satisfied in practice.

The transformation corresponding to (3) is now required to give a complete product wave function:

$$\Psi(A) = M\Phi(A), \quad (56)$$

$$\Phi(A) = \prod_{i=1}^{A} \psi_i(x_i), \quad (57)$$

where each single-particle wave function satisfies the same Schrödinger equation:

$$(E_i - T_i - W^s)\psi_i(x_i) = 0, \quad (58)$$

$$H^m = M^\dagger H M = \sum_{i=1}^{A} \{T_i + W_s(x_i)\}. \quad (59)$$

If M is unitary, the energies E_i will satisfy

$$E = \sum_{i=1}^{A} E_i, \quad (60)$$

where E is an eigenvalue of the original Schrödinger equation,

$$(E - \sum_{i=1}^{A} T_i - V)\Psi(A) = 0. \quad (61)$$

The Φ equation, when (60) holds, is

$$(E - \sum_{i=1}^{A} T_i - \sum_{i=1}^{A} W^s(x_i))\Phi(A) = 0. \quad (62)$$

Provided that $\Psi(A)$ and $\Phi(A)$ satisfy suitable boundary conditions, it follows from (61) and (62) that the $W_s(x_i)$ must satisfy

$$(\Phi(A), \{V - \sum_{i=1}^{A} W^s(x_i)\}\Psi(A)) = 0. \quad (63)$$

In general, this will only be a necessary condition when $\Phi(A)$ and $\Psi(A)$ are bound states and tend to zero at infinity. Thus, a unitary M requires that the matrix elements (63) are zero between all states not in the continuous spectrum.

When (63) is satisfied, (61) and (62) have the same energy eigenvalues; then there is a solution to the equation:

$$(E - \sum_{i=1}^{A} T_i - \sum_{i=1}^{A} W^s(x_i))M = (V - \sum_{i=1}^{A} W^s(x_i))M, \quad (64)$$

given formally by

$$M = 1 + (E - \sum_{i=1}^{A} (T_i) - \sum_{i=1}^{A} W^s(x_i))^{-1}('V - \sum_{i=1}^{A} {}'W^s(x_i))M, \quad (65)$$

provided that

$$(\Phi(A), (V - \sum W^s)M\Phi(A)) = 0. \quad (66)$$

The primes to the left of V and a W^s in (65) indicate that when M acts on a particular $\Phi(A)$ this state is excluded to the left of these operators. This exclusion means that (65) automatically satisfies (64) for nondiagonal matrix elements of M on the left of (64). Equation (64) is satisfied for diagonal matrix elements because of the condition (66).

In principle, Eqs. (62), (65), and (66) provide a set of equations for W^s, $\Phi(A)$, and M which could be solved by a self-consistent method beginning with a trial potential W^s in (62). This would present a formidable problem unless a self-consistent solution exists for a simple form of W^s. The success of the Mayer-

Jensen shell model (although not for binding energies) suggests that in fact W^s may be simple to a good approximation, so the solution of this problem may not be beyond attainment. In Sec. VIII, we will define a similar but more restricted problem and show that this can be solved.

It is clear from (65) that M can be taken to be symmetrical between coordinates of protons and coordinates of neutrons, so the particles satisfying Eq. (58) will satisfy the exclusion principle. Hence, the wave function for the model will be the antisymmetrical sum of products of eigensolutions to (58). If charge independence is not assumed, there will be different potentials for positive and negative particles in the model. Hence, the ground state of the model is obtained by filling up the lowest one-particle energy levels exactly as though the particles were neutrons and protons.

The well W^s will depend on the number of nucleons, so it should be written $W^s(A)$. For $W^s(A+1)$ all the energies will change by a small amount, and there will be corresponding changes in the wave function. Hence the difference in total energy $[E(A+1)-E(A)]$ will be equal to the energy of the $(A+1)$th particle $E_{(A+1)}$ together with the small changes ΔE_i, $i=1, 2, \cdots, A$. This can be contrasted with the ideal single-particle model which had energy $E(A+1)-E(A)$.

We assume that the transformed Hamiltonian is invariant under rotation and reflection of the coordinate axes. Then the model operator M can be chosen so that the parity and angular momentum of the model can be calculated as though it were the real nucleus. This insures that when the single-particle levels are filled up in some particular way, the resulting parity and angular momentum of the model will be the same as for the corresponding states of the real nucleus. For the ground states of the model, successive filling of levels will lead to occupation of all angular momentum states at a given energy so one obtains the closed-shell phenomena. From the work of Sec. V, the model will predict selection rules but in general will not give transition rates.

We next consider how far the Mayer-Jensen shell model corresponds to the ideal model considered above. It leads to a product wave function like (57) with single-particle equations like (58). The potential W^s is simple but has a spin-orbit coupling term; our general considerations do not offer any evidence why W^s should have a particular form although in principle W^s can be derived from the self-consistent equations. The total energies in the shell model do not satisfy (60), although the different eigenvalues E_i are ordered so that shells fill up in the correct way. Not all energy levels (e.g., rotational energy levels) are described by the shell model. We deduce that the model operator is not unitary but that for the "noncollective" energy levels M only scales down the energies without affecting the order of levels. The transformed Hamiltonian is invariant under rotations and reflections in the coordinate axes and gives correct degeneracy, so the parity and angular momentum commute with M in the subspace defined by the model. Hence, the model predicts parity and angular momentum quantum numbers correctly to the approximation implied by this subspace; similarly selection rules will be valid to the same approximation.

It will be seen that the shell model corresponds to the approximation discussed in Sec. II given by Eqs. (10), (15), and (16). The well in which $(A+1)$ particles in the model move depends on the presence of the Ath particle, and more accurately even on the state of this particle. The filling of single-particle states in the model is insensitive to this interdependence, so for this, $W^s(A)$ can have its A dependence neglected. Other observables depend more sensitively on the well—for example, the magnetic moment. If it is known that the $(A-1)$th nucleus has zero magnetic moment, we do not know that $(A-1)$ particles in the Ath nucleus also have zero magnetic moment. Hence the Ath particle in the shell model cannot be regarded as moving in a nucleus with an inert care of $(A-1)$ particles. One can either attempt to represent the effect of this case in some collective way as for example in the theory of Bohr and Mottelson,[6] or one can transform to the single-particle model of Eq. (8) where the care is the $(A-1)$th nucleus. In the latter case, however it cannot be deduced that the potential W_c is invariant under rotations since W_c differs from W^s in the shell model.

It appears that in practice the transformation M to the single-particle picture with potential W_c does not commute with angular momentum except for certain light nuclei. This conclusion follows from the fact that the magnetic moment of nuclei does not lie on the Schmidt lines in general. Mathematically it means that the single-particle eigenfunction $\psi_r(x_A)$ does not correspond to an angular momentum quantum number. It can, of course, be expanded:

$$\psi_r(x_A)=\sum b_{rs}\psi_s'(x_s), \tag{67}$$

where $\psi_s'(x_s)$ are eigenstates for example of the shell-model Hamiltonian.

From our work up to this point it appears that there are two main errors involved in representing the shell model as the real nucleus when evaluating magnetic moments (or quadrupole moments). The first error arises if these operators do not commute with the model operator leading to the shell model. The second error arises from treating the shell-model potential as independent of the number (or state) of the individual particles.

Our final discussion of the shell model in this section is concerned with the reasons for the existence of a transformation M from a strongly interacting nucleus to a weakly interacting model. It has already been noted in the introduction that there is not much meaning to the term "state of a nucleon in a nucleus." Due to the strong interaction of nucleons Ψ cannot be expressed

[6] A. Bohr and B. Mottelson, Kgl. Danske Videnskab, Selskab, Mat.-fys. Medd. **27**, No. 16 (1953).

as a product, and only for product states has the concept of single-nucleon states any clear meaning. It does not therefore appear valid to use qualitative arguments based on the state of a nucleon and the exclusion principle.[3] Even if such arguments were valid and led for example to an expectation that nucleons had long mean-free paths,[2] it would be incorrect to assume that this implied weak interaction between nucleons. The form of Eq (1) is such that the energy will diverge if Ψ has the form implied by a weak interaction model. It seems impossible to interpret the shell-model wave function as an approximation to the real wave function.[4]

It has been one of the principle objects of this paper to show that such an interpretation is unnecessary. In Sec. VIII, we will construct a correlated wave function Ψ from a model wave function Φ. The model consists of particles satisfying the exclusion principle and occuping the lowest of a set of energy levels. In calculating operators in the model, it appears that they are simple largely because of the effect of the exclusion principle and the occupation of all neighboring states. This suggests that the validity of the shell model arises from the action of the exclusion principle in the model. This is of course related to the action of the exclusion principle in the real wave function Ψ but not in any simply described way.

VII. FURTHER CONSIDERATION OF THE SINGLE-PARTICLE MODEL

In this section we investigate a simplified single-particle model of the nucleus. The model will describe a single particle moving in a square well of depth V_0, and we choose the model operator M so that the energy of the particle is the binding energy of the Ath nucleon as defined in II, Eq. (8). We will see that this condition is sufficient to determine the well depth V_0.

The total nuclear wave function $\Psi(A)$ satisfies the Schrödinger equation:

$$(E-H_A)\Psi(A)=0. \tag{68}$$

We assume that H_A has the simplified form,

$$H_A=\sum_{i=1}^{A} T_i+\sum_{i<j} V_{ij}, \tag{69}$$

which corresponds to only two-body forces between nucleons. Define V and V_i by

$$V_i=V_{Ai}, \quad V=\sum_{i=1}^{A-1} V_i. \tag{70}$$

Then (68) can be written

$$(E_0-H_{A-1}-T_A-V_0)\Psi_0(A)=(V-V_0)\Psi_0(A), \tag{71}$$

where the suffix 0 serves to indicate we are considering a particular eigenstate. We require a model operator M_0 such that

$$\Psi_0(A)=M_0\Phi_0(A)=M_0\Psi_0(A-1)\psi_0(x_A), \tag{72}$$

where

$$(E_0-H_{A-1}-T_A-V_0)\Phi_0(A)=0. \tag{73}$$

Provided that $\Phi(A)$ and $\Psi(A)$ satisfy boundary conditions for a bound state of the A nucleons, the condition for (71) and (73) to have the same eigenvalue is

$$(\Phi_0(A),\ (V-V_0)\Psi_0(A))=0. \tag{74}$$

We take

$$M_0=1+\frac{1}{a}{}'(V-V_0)M_0, \tag{75}$$

where $a=(E_0-H_{A-1}-T_A-V_0)$ and the prime to the left of $(V-V_0)$ indicates that all matrix elements involving $\Phi_0(A)$ on the left are to be omitted. It is easily verified that (74) and (75) ensure that if $\Phi_0(A)$ satisfies Eq. (73), then $\Psi_0(A)$ satisfies (71) when it is defined by (72). From (72), (74), and (75) we deduce that since V_0 denotes a well of constant depth,

$$V_0=(\Phi_0(A),\ VM_0\Phi_0(A)). \tag{76}$$

From (75),

$$M_0=1+[E_0-H_{A-1}-T_A-V_0+{}'V_0-{}'V]^{-1}{}'(V-V_0) \tag{77}$$

$$=1+[E_0-H_{A-1}-T_A-{}^0V_0{}^0-{}'V]^{-1}{}'V, \tag{78}$$

provided that we only consider M_0 acting on the state $\Phi_0(A)$. In (78), ${}^0V_0{}^0$ is defined to be the matrix which has elements between $\Phi_0(A)$ states equal to V_0, and has all other matrix elements zero. Since in (78) it acts on $'V$, it has no effect in the equation; hence,

$$M_0=1+[E_0-H_{A-1}-T_A-{}'V]^{-1}{}'V=M \tag{79}$$

when acting on $\Phi_0(A)$ to the right, where

$$M=1+[E_0-H_{A-1}-T_A]^{-1}{}'VM. \tag{80}$$

Hence,

$$V_0=(\Phi_0(A),\ VM\Phi_0(A)). \tag{81}$$

We prove next that

$$M\Phi_0(A)=F\left(1+\frac{1}{e}t_c\right)\Phi_0(A), \tag{82}$$

where F, e, and t_c will be defined in the following discussion:

$$e=E_0-H_{A-1}-T_A-t_c. \tag{83}$$

Define ${}'t_i{}^\alpha$ to be a solution of the equation

$${}'t_i{}^\alpha={}'V_i+{}'V_{\frac{1}{e}}{}'t_i{}^\alpha, \tag{84}$$

where the prime indicates the ground state $\Phi_0(A)$ is excluded. Then t_c is defined as a diagonal matrix with respect to $\Psi'(A-1)$ having matrix elements

$$t_c=\sum_{i=1}^{A}(\Psi'(A-1),\ {}'t_i{}^\alpha\Psi'(A-1)), \tag{85}$$

$$C_i=(\Psi'(A-1),\ {}'t_i{}^\alpha\Psi'(A-1)). \tag{86}$$

C_i is defined to be diagonal in the nuclear states of the $(A-1)$ particles. Since $\Psi'(A-1)$ is antisymmetrical, C_i is independent of the subscript i and depends only on the energy of the state $\Psi'(A-1)$. Hence,

$$C_i=C=(\sum C_i)/A=t_c/A. \tag{87}$$

Define

$$'I_i='t_i^{\alpha}-C. \tag{88}$$

From its definition, $'I_i$ has no diagonal elements with respect to the state $\Psi'(A-1)$. F in (82) is defined by

$$F=1+\frac{1}{e}\sum_{i=1}^{A} 'I_iF_i, \tag{89}$$

$$F_i=1+\frac{1}{e}\sum_{i\neq j} 'I_jF_j=F-\frac{1}{e}'I_iF_i. \tag{90}$$

We now prove (82) by showing that the right hand side of (82) is a solution of Eq. (80) for M. Substituting from (82) in the right hand side of (80), we get

$$1+\frac{1}{b}'VF\left(1+\frac{1}{e}t_c\right), \tag{91}$$

where $b=E_0-H_{A-1}-T_A$. Upon using (89), (70), and then (88), Eq. (91) becomes

$$1+\left[\frac{1}{b}'V+\frac{1}{b}\sum_i 'V_i\frac{1}{e}'t_i^{\alpha}F_i+\frac{1}{b}\sum_{i,j,i\neq j} 'V_1\frac{1}{e}I_jF_j -\frac{1}{b}\sum_i 'V_i\frac{1}{e}CF_i\right]\left(1+\frac{1}{e}t_c\right). \tag{92}$$

Using (84) to remove the $'V_i(1/e)\,'t_i^{\alpha}$ term, we get

$$1+\left[\frac{1}{b}\sum_i 't_i^{\alpha}F_i-\frac{1}{b}\sum_i 'V_i\frac{1}{e}CF_i\right]\left(1+\frac{1}{e}t_c\right). \tag{93}$$

If we use (88), this gives

$$1+\left[\frac{1}{b}\sum_i 'I_iF_i-\frac{1}{b}\sum 'V_i\frac{1}{e}CF_i+\frac{1}{b}\sum_i CF_i\right]\left(1+\frac{1}{e}t_c\right). \tag{94}$$

Now from (87), (89), and (90),

$$\frac{1}{b}\sum_i CF_i=\frac{1}{b}\left(1-\frac{1}{A}\right)t_cF+\frac{1}{b}\frac{1}{A}t_c. \tag{95}$$

From the definitions of e, (83) and b, (91), we have

$$\frac{1}{b}=\left(1-\frac{1}{b}t_c\right)\frac{1}{e}. \tag{96}$$

Upon using (89), (95), and (96), Eq. (94) becomes

$$1+\left[\left(1-\frac{1}{b}t_c\right)(F-1)+\frac{1}{b}t_c-\frac{1}{b}\sum_i 'V_i\frac{1}{e}CF_i -\frac{1}{A}\frac{1}{b}t_cF+\frac{1}{A}\frac{1}{b}t_c\right]\left(1+\frac{1}{e}t_c\right). \tag{97}$$

If we use (87), this becomes

$$1+F\left(1+\frac{1}{e}t_c\right)-\left(1-\frac{1}{b}t_c\right)\left(1+\frac{1}{e}t_c\right) +\frac{1}{A}\left[\frac{1}{b}t_c-\frac{1}{b}\sum 'V_i\frac{1}{e}t_cF_i-\frac{1}{b}t_cF\right]\left(1+\frac{1}{e}t_c\right). \tag{98}$$

By (96), this becomes

$$F\left(1+\frac{1}{e}t_c\right)+\frac{1}{A}\left[\frac{1}{e}t_c-\left(\frac{1}{b}\sum 'V_i\frac{1}{e}t_cF_i+\frac{1}{b}t_cF\right) \times\left(1+\frac{1}{e}t_c\right)\right]. \tag{99}$$

Apart from the term involving A^{-1}, this completes the proof of Eq. (82). Terms involving A^{-1} of similar type to those in (99) have been considered by Watson[7] and are expected to be small.[8] We shall neglect these terms here but will discuss similar terms in greater detail in the next section.

We require V_0, which is given by (76), (79), and (82) as

$$V_0=\left[\Phi_0(A),\, VF\left(1+\frac{1}{e}t_c\right)\Phi_0(A)\right]. \tag{100}$$

We consider next the quantity VF. Using (70) and (89), we obtain

$$VF=V+\sum_i V_i\frac{1}{e}I_iF_i+\sum_{i,j,i\neq j} V_i\frac{1}{e}I_jF_j \tag{101}$$

$$=V+\sum_i V_i\frac{1}{e}'t_i^{\alpha}F_i+\sum_{i,j,i\neq j} V_i\frac{1}{e}I_jF_j-\sum_i V_i\frac{1}{e}CF_i. \tag{102}$$

We define a quantity t_i^{β} by the relation,

$$t_i^{\beta}=V_i+V_i\frac{1}{e}'t_i^{\alpha}. \tag{103}$$

Upon using (87), (90), and (103), Eq. (102) becomes

$$VF=\sum_i t_i^{\beta}F_i-\frac{1}{A}\sum_i V_i\frac{1}{e}t_cF_i. \tag{104}$$

We now obtain an equation for t_i^{β} which involves only scattering amplitudes. Define t_i to satisfy

$$t_i=V_i+V_i\frac{1}{e}t_i. \tag{105}$$

[7] K. M. Watson, Phys. Rev. **89**, 575 (1953).

[8] The neglect of these terms will not be valid at certain energies corresponding to resonances in single-particle scattering. For these energies the transformation leads to a series which at best would be slowly convergent and may diverge. If these terms are neglected, an "average" potential analagous to that of Weisskopf (reference 2) is obtained.

Then

$$V_i=t_i\left[1+\frac{1}{e}t_i\right]^{-1}, \tag{106}$$

$$'V_i='t_i\left[1+\frac{1}{e}t_i\right]^{-1}. \tag{107}$$

Also from (84),

$$'t_i{}^{\alpha}='V_i\left[1-\frac{1}{e}'V_i\right]^{-1}. \tag{108}$$

Substituting (106) and (108) into (103) and then using (107), we obtain

$$t_i{}^{\beta}=t_i\left[1+\frac{1}{e}{}^0t_i\right]^{-1}, \tag{109}$$

where

$${}^0t_i\doteq t_i-'t_i. \tag{110}$$

Neglecting the A^{-1} term in (104), the expression (100) for V_0 becomes, from (104) and (109),

$$V_0=\sum_{i=1}^{A}\left(\Phi_0(A),\, t_i\left[1+\frac{1}{e}{}^0t_i\right]F_i\left[1+\frac{1}{e}t_e\right]\Phi_0(A)\right). \tag{111}$$

The detailed consideration of this expression can be carried out by the methods given by Francis and Watson.[9] It is sufficient to illustrate the method to make the approximation $F_i=1$. The term $(1/e)\,{}^0t_i$ can be neglected. Then to lowest order, we get

$$V_0=\sum_{i=1}^{A}(\Phi_0(A),\, t_i\Phi_0(A)). \tag{112}$$

If the expression (111) is considered in more detail, it is found that V_0 is modified in a way which corresponds to dispersion in the nuclear medium.

VIII. APPLICATION TO NUCLEAR SATURATION

In this section we consider the evaluation of the energy of the nuclear wave function Ψ when it is subjected to additional boundary conditions, in the form of a potential well. The basis of the method has been described in Sec. VI where it was shown that a model could be chosen having the same energy as a particular state of the real nucleus.

We consider a model having wave function Φ_0 which is a complete product of A single-particle wave functions and satisfies a Schrödinger equation

$$(E_0-T-V_0)\Phi_0=0. \tag{113}$$

The corresponding equation for the modified nuclear wave function Ψ_0 is

$$(E_0-T-V_0)\Psi_0=(V-V_0)\Psi_0. \tag{114}$$

We assume that Φ_0 describes a system of particles moving in a square-well potential with depth V_0 (measured from zero energy), infinite walls, and radius r. This imposes a corresponding boundary condition on Ψ_0 which makes it differ from the actual nuclear wave function.

The well depth V_0 is determined by the condition that Eqs. (113) and (114) have the same energy eigenvalue. It is assumed that E_0 is the ground-state energy.

$$V_0=(\Phi_0,V\Psi_0)=(\Phi_0,VM_0\Phi_0), \tag{115}$$

where

$$\Psi_0=M_0\Phi_0, \tag{116}$$

$$M_0=1+(E_0-T-V_0)^{-1}{}'(V-V_0)M_0, \tag{117}$$

where the prime to the left of $(V-V_0)$ denotes omission of the ground state. It follows from (115) and (117) that if Φ_0 satisfies (113), then Ψ_0 given by (116) satisfies (114). From (115) and (117), we deduce that

$$V_0=(\Phi_0,\, V[1+(a-'V)^{-1}{}'V]\Phi_0) \tag{118}$$

$$=(\Phi_0,VM\Phi_0), \tag{119}$$

where

$$a=E_0-T-{}^0V_0{}^0, \tag{120}$$

$$M=1+(a-'V)^{-1}{}'V=1+a^{-1}{}'VM. \tag{121}$$

Since a always appears with $'V$ on the right, the term ${}^0V_0{}^0$ in a always gives zero, so we redefine

$$a=E_0-T. \tag{122}$$

Define

$$'t_{ij}{}^{\alpha}='V_{ij}+'V_{ij}\frac{1}{e}'t_{ij}{}^{\alpha}, \tag{123}$$

where

$$e=E_0-T-'t_e'=a-'t_e', \tag{124}$$

$$'t_e'=\sum{}'C_{ij}', \tag{125}$$

$$'C_{ij}'='t_{ij}{}^{\alpha}'. \tag{126}$$

The quantity $'C_{ij}'$ is a diagonal matrix element between excited states. Let

$$'I_{ij}{}^{\alpha}='t_{ij}{}^{\alpha}-'C_{ij}'; \tag{127}$$

this is the off-diagonal part of $'t_{ij}{}^{\alpha}$. Let

$$F=1+\frac{1}{e}\sum_{i<j}{}'I_{ij}{}^{\alpha}F_{ij}, \tag{128}$$

$$F_{ij}=1+\frac{1}{e}\sum_{i\neq l,\,j\neq m}{}'I_{lm}{}^{\alpha}F_{lm}, \tag{129}$$

$$=F-\frac{1}{e}{}'I_{ij}{}^{\alpha}F_{ij}. \tag{130}$$

We note that

$$\sum_{i<j}F_{ij}=\tfrac{1}{2}A(A-1)F-F+1. \tag{131}$$

We now prove that M in (119) can be replaced by F

[9] N. C. Francis and K. M. Watson, Phys. Rev. 92, 291 (1953).

with neglect of small terms. Consider $(1/a)\,'VF$,

$$\frac{1}{a}\,'VF=\frac{1}{a}\,'V+\frac{1}{a}\sum{}'V_{ij}\frac{1}{e}\,'I_{ij}{}^{\alpha}F_{ij}$$
$$+\frac{1}{a}\sum_{i\neq l,\,j\neq m}{}'V_{ij}\frac{1}{e}\,'I_{lm}{}^{\alpha}F_{lm} \quad (132)$$

$$=\frac{1}{a}\sum{}'t_{ij}{}^{\alpha}F_{ij}-\frac{1}{a}\sum{}'V_{ij}\frac{1}{e}\,'V_{ij}\,'F_{ij} \quad (133)$$

$$=\frac{1}{a}\sum{}'I_{ij}{}^{\alpha}F_{ij}+\frac{1}{a}\sum{}'C_{ij}\,'F_{ij}$$
$$-\frac{1}{a}\sum{}'V_{ij}\frac{1}{e}\,'C_{ij}\,'F_{ij} \quad (134)$$

$$=\frac{1}{e}\sum{}'I_{ij}{}^{\alpha}F_{ij}-\frac{1}{a}\,'t_{c}\,'\frac{1}{e}\sum{}'I_{ij}{}^{\alpha}F_{ij}$$
$$+\frac{1}{a}\sum{}'C_{ij}\,'F_{ij}-\frac{1}{a}\sum{}'V_{ij}\frac{1}{e}\,'C_{ij}\,'F_{ij} \quad (135)$$

$$=(F-1)-\left(\frac{1}{a}\sum{}'C_{ij}\,'\frac{1}{e}\,'I_{ij}{}^{\alpha}F_{ij}\right.$$
$$\left.+\frac{1}{a}\sum{}'V_{ij}\frac{1}{e}\,'C_{ij}\,'F_{ij}\right)+\frac{1}{a}\,'t_{c}\,'. \quad (136)$$

The last term in (136) gives zero when it acts on the the ground state Φ_0; the middle term is a correction term which will give a small contribution to the energy. Hence,

$$F\Phi_0\doteq M\Phi_0. \quad (137)$$

We next consider

$$V_0=(\Phi_0,VF\Phi_0), \quad (138)$$

where

$$VF=V+\sum_{i<j}V_{ij}\frac{1}{e}\,'t_{ij}{}^{\alpha}F_{ij}=\sum_{i<j,\,i\neq l,\,j\neq m}V_{ij}\frac{1}{e}\,'I_{lm}{}^{\alpha}F_{lm}$$
$$-\sum_{i<j}V_{ij}\frac{1}{e}\,'C_{ij}\,'F_{ij}. \quad (139)$$

Let

$$t_{ij}{}^{\beta}=V_{ij}+V_{ij}\frac{1}{e}\,'t_{ij}{}^{\alpha}. \quad (140)$$

Then, neglecting the last term in (141), we get

$$V_0=(\Phi_0,\sum t_{ij}{}^{\beta}F_{ij}\Phi_0). \quad (141)$$

$t_{ij}{}^{\beta}$ can be obtained in terms of other scattering amplitudes by using (125), (140) and defining

$$t_{ij}=V_{ij}+V_{ij}\frac{1}{e}\,t_{ij}. \quad (142)$$

From (123),

$$'t_{ij}{}^{\alpha}='V_{ij}\left(1-\frac{1}{e}\,V_{ij}\right)^{-1}. \quad (143)$$

Hence, by using (140) and (143),

$$t_{ij}{}^{\beta}\left(1-\frac{1}{e}\,'V_{ij}\right)=V_{ij}. \quad (144)$$

Solving (142) for V_{ij}, and hence obtaining $'V_{ij}$, we get after some simplification

$$t_{ij}{}^{\beta}=t_{ij}\left(1+\frac{1}{e}\,{}^{0}t_{ij}\right)^{-1}, \quad (145)$$

where

$${}^{0}t_{ij}=t_{ij}-'t_{ij}. \quad (146)$$

Hence, from (138) and (145),

$$V_0=\sum_{i<j}\left(\Phi_0,\,t_{ij}\left[1+\frac{1}{e}\,{}^{0}t_{ij}{}^{0}\right]^{-1}F_{ij}\Phi_0\right). \quad (147)$$

To lowest order this gives

$$V_0=\sum_{i<j}^{A}(\Phi_0,t_{ij}\Phi_0), \quad (148)$$

where Φ_0 is the antisymmetrized wave function for the ground state of the model.

The potential V_0 given by (148) is identical with that used by Brueckner, Levinson, and Mahmoud in their discussion of nuclear saturation.[10] It should be noted, however, that our assumptions about the relation between the model and the nuclear wave functions differ in some important respects from the assumptions of these authors. Probably the most important difference lies in our use of the consistency condition (63) and (115) to determine the potential well of the model and hence the energy of the system. This method not only gives a more rigorous derivation of the energy in the present approximation, but it can also be applied to the more general problem of obtaining a shell-model potential.

If we label the states of the model by the single particle momenta k, the wave function Φ can be written:

$$\Phi=(A\,!)^{-\frac{1}{2}}\begin{vmatrix}|k_1)_1 & |k_1)_2 & \cdots & |k_1)_A\\ |k_2)_1 & |k_2)_2 & \cdots & \\ \vdots & & & \\ |k_A)_1 & \cdots & & |k_A)_A\end{vmatrix}. \quad (149)$$

The chief drawback to the above method lies in the fact that the potential V has been split up in an unsymmetrical way so that the intermediate states which arise in calculation will not be antisymmetrized. This means that in considering the magnitude of the cor-

[10] Further details of the nuclear saturation problem have been considered by K. A. Brueckner, Phys. Rev. **96**, 508 (1954), and forthcoming papers.

rection terms in the series for V_0, one cannot restrict intermediate states to those above the Fermi gas. It seems probable therefore that the series will not converge as rapidly as it would if use could be made of antisymmetric intermediate states. If one uses a formulation with antisymmetrized intermediate states, new difficulties occur, however. As an illustration of these, we consider a formulation in which V is split into symmetric parts, each of which can only cause transitions to antisymmetric states provided that the initial state is antisymmetric. Let

$$V=\lambda v, \tag{150}$$

where $\lambda=A(A-1)/2$. Define

$$t=v+v\frac{1}{e}{}'t, \tag{151}$$

$$e=E_0-T-t_c, \tag{152}$$

$$t_c=\lambda\,'C'=\lambda\,'t', \tag{153}$$

$$I='t-\,'C', \tag{154}$$

$$F=1+\frac{1}{e}\lambda IF. \tag{155}$$

Neglecting terms of order A^{-1}, we get

$$F\Phi_0=M\Phi_0, \tag{156}$$

$$V_0\doteq(\Phi_0,\lambda tF\Phi_0) \tag{157}$$

$$=\lambda(\Phi_0,t\Phi_0)+\lambda^2\left(\Phi_0,t\frac{1}{e}F\Phi_0\right)+\cdots. \tag{158}$$

Although the intermediate states can now all be treated as antisymmetrical and the discussion of convergence is thereby simplified, it can be seen that there is now a difficulty at another point. This new difficulty lies in the solution to Eq. (151) for the new matrix t. It can be argued[11] that the two equations (151) and (105) have nearly the same solution if one is only interested in the coherent scattering part of t, provided that the interaction potential v is highly singular. The second term in (158) is not negligible (it is about one-quarter of the leading term at most) but does not appear in the work of Brueckner and Levinson,[11] due to their use of different equations for t and F. The other correction terms which we have neglected appear to be small; they are to be discussed in detail in a forthcoming paper by Brueckner and Levinson.[11]

[11] These questions are considered in an accompanying paper by Brueckner and Levinson, Phys. Rev. **97**, 1344 (1955), who are also developing a more detailed treatment of the use of antisymmetrization in the problem of nuclear saturation.

IX. CONCLUSION

The considerations of the present paper indicate that it is profitable to examine the theory of nuclear structure from a new viewpoint in which nuclear models are no longer to be interpreted as giving approximations to the actual nuclear wave function. The actual nuclear wave function can be obtained by acting on the wave function of the model with a suitable model operator. It appears that the success of actual nuclear models such as the shell model is due to a special choice of model operator which commutes with certain observables. It has been shown that a model operator can be used explicitly to define nuclear energy in a problem connected with nuclear saturation.

We have examined some of the simpler properties of model operators and investigated conditions which they must satisfy to ensure the "reality" of models with respect to certain observables such as angular momentum and parity. It is hoped in further work to consider in greater detail the special properties of model operators which are related to observables which are not accurately predicted by existing models. Preliminary work indicates that this study may give a clearer indication of the kind of correction terms which are needed in evaluating the magnetic moment for example.

The derivation of a formula for the energy of an "equivalent Fermi gas," although complicated, indicates that a derivation of the Mayer potential for the shell model may be possible by the method of this paper. Further work is proceeding on these aspects of the problem.

We wish to thank Professor Keith Brueckner and Dr. Carl Levinson for many helpful discussions.

One of us (R. J. E.) wishes to acknowledge hospitality from the Princeton Institute for Advanced Study and from the Canadian National Research Council.

Magnetic Moments of Conjugate Nuclei

J. G. BRENNAN, *The Catholic University of America, Washington, D. C.*

AND

A. B. VOLKOV, *University of Delaware, Newark, Delaware*

(Received September 27, 1954; revised manuscript received November 26, 1954)

Many experimentally-observed magnetic moments of conjugate (semi-mirror) nuclei deviate approximately the same amount from the Schmidt limits. It is shown that the theoretical magnetic moments provided by a simple form of the collective model are such that the difference between the deviations of a pair of conjugate nuclei is small. Those experimentally-observed exceptions to this rule where the difference between the deviations is quite large (such as $I^{127}-Mo^{97}$) can be explained by modifications of the collective model to include the effects of (a) shell model structure and (b) configuration admixing. In fact, the relative importance of the various dynamical features of the nucleus can be assessed, qualitatively at least, from the size and sign of the magnetic moment deviation difference of a pair of conjugate nuclei.

INTRODUCTION

THE symmetry properties, angular momentum and parity, of the ground states of most odd-even nuclei are correctly predicted by the independent-particle shell model of Mayer[1] and Haxel, Jensen, and Suess.[2] But this model seems less successful in determining the dynamical features of the nucleus as exemplified by the deviations of the experimental magnetic moments of odd-even nuclei from the predicted Schmidt values. The magnetic moment deviations indicate that either an incomplete magnetic moment operator is being used or that the independent-particle shell-model wave functions are a rather poor description of the complex nuclei.

Attempts to explain the magnetic moment deviations of the heavier nuclei by means of additional magnetic moments arising from meson effects have not been too successful. A detailed investigation by Ross[3] on meson exchange moments, normalized to explain the H^3 and He^3 magnetic moment anomalies, indicates that the experimentally observed magnetic moment deviations cannot be adequately accounted for on the basis of meson effects.

Recent attempts to explain the observed magnetic moment deviations have centered about the collective model approach of Bohr[4,5] and Mottelson and/or the modification of the Mayer-Jensen shell model due to configuration mixing. Both methods have resulted in a substantial improvement for $I=L+1/2$ nuclei. The pure collective model (without configuration mixing) contradicts observations by predicting no deviation for $I=1/2$ nuclei and by predicting deviations outside of the Schmidt line for many $I=L-1/2$ nuclei. The configuration mixing approach in an extreme form as suggested by Volkov[6] predicts deviations for $I=L-1/2$ nuclei too far *inside* the appropriate Schmidt line. The more fundamental configuration mixing calculations of Blin-Stoyle[7,8] gives excellent agreement for all $I=1/2$ nuclei ($I=L+1/2$ and $I=L-1/2$) as well as an unambiguous explanation for the anomalous closed shell plus one nucleus, Bi^{209}. However, it is difficult to believe that the many observed large quadrupole moments can be explained in terms of only mixed configurations which involve only a few particles.

Undoubtedly, complex nuclei must be described both in terms of collective phenomena and mixed configurations. In fact, Bohr and Mottelson considered the mixing of the configuration of the last odd particle due to interaction with the surface oscillations. However, if possible, it would be desirable to try to determine the relative importance to the magnetic moment of the collective motion of the nucleons as opposed to the admixing of different configurations.

CONJUGATE NUCLEI

Schawlow and Townes[9] observed that conjugate (semi-mirror) nuclei, i.e., an odd-even nuclear pair (one nucleus having Z odd protons while the other has Z odd neutrons), have nearly the same magnetic moment deviation from their respective Schmidt lines. This result can be explained by assuming that (a) the odd-particle wave functions are primarily responsible for the magnetic moment deviation, and (b) the odd-particle wave functions are the same in both nuclei.

In this connection, it is convenient to define the

[1] M. Goeppert-Mayer, Phys. Rev. **78**, 16 (1950).
[2] Haxel, Jensen, and Suess, Z. Physik **128**, 295 (1950).
[3] Marc Ross, Phys. Rev. **88**, 939 (1952). Additional references concerning meson effects and magnetic moments are to be found in this reference.
[4] A. Bohr, Kgl. Danske Videnskab. Selskab, Mat.-fys. Medd. **26**, No. 14 (1952).
[5] A. Bohr and B. R. Mottelson, Kgl. Danske Videnskab. Selskab, Mat.-fys. Medd. **27**, No. 16 (1953).
[6] A. B. Volkov, Phys. Rev. **94**, 1664 (1954). Additional references concerning configuration mixing are to be found in this reference.
[7] R. J. Blin-Stoyle, Proc. Phys. Soc. (London) **A66**, 11 (1953).
[8] R. J. Blin-Stoyle and M. A. Perke, Proc. Phys. Soc. (London) **A67**, 885 (1954).
[9] A. L. Schawlow and C. H. Townes, Phys. Rev. **82**, 268 (1951).

magnetic moment deviations in the following manner:

$$\Delta^P=\frac{\mu_S{}^P-\mu^P}{\mu_P-\frac{1}{2}},\quad \Delta^N=\frac{\mu_S{}^N-\mu^N}{\mu_N},\tag{1}$$

where μ_P and μ_N are the intrinsic magnetic moments of the proton and neutron, $\mu_S{}^P$ and $\mu_S{}^N$ are the respective Schmidt values of the magnetic moment, and μ^P and μ^N are the corresponding calculated or experimental magnetic moments. If the even particles are coupled to zero angular momentum, then regardless of the complexity of the odd-particle wave function,

$$\Delta^P=\Delta^N \quad \text{or} \quad \Delta^P-\Delta^N=0,\tag{2}$$

provided the odd-particle wave functions are the same for the nuclear pair (charge symmetry).[6]

The experimental deviations for sixteen cases of conjugate nuclei are listed in Table I.[10] The last column lists the quantity $\Delta^P-\Delta^N$ which is a measure of the validity of Eq. (2). It can be seen that with the exception of four cases $\Delta^P-\Delta^N$ is either quite small or else small compared to Δ^P and Δ^N themselves. Of these four cases, two ($Au^{197}-Ba^{135}$ and $Pr^{141}-Pd^{105}$) are poorly measured. In the worst case ($I^{127}-Mo^{97}$), I^{127} with a spin of 5/2 is in a region of very close competition with nuclei having a spin of 7/2 (the same competition is not evident among the corresponding odd-neutron nuclei). The competition between the $g_{7/2}$ and $d_{5/2}$ levels probably accounts for the extremely large magnetic moment deviation of I^{127} and the resulting large value for $\Delta^P-\Delta^N$. In the final case which is poor, the deviation of Nb^{93} appears to be too small when compared to other $g_{9/2}$ nuclei. The interpretation of this case in terms of shell-model structure is discussed later.

CONJUGATE NUCLEI AND THE COLLECTIVE MODEL

It has been suggested[6] that the mirror property of the magnetic deviations of the conjugate nuclei represents an argument against the collective model of the nucleus. The number of even particles in the nuclei of the conjugate pair are generally quite different because of the neutron excess. For this reason it would seem likely that the core contribution should be quite different for the two nuclei, leading to rather large values of $\Delta^P-\Delta^N$. However, it is found that the collective model of Bohr and Mottelson without configuration mixing also predicts small values (not zero as in the configuration case) for $\Delta^P-\Delta^N$.

The small values predicted for $\Delta^P-\Delta^N$ are a consequence of ignoring any possible shell structure in the core, e.g., by assuming a particular coupling (strong or weak) to be valid for both nuclei of the pair. The data for the magnetic moments of conjugate nuclei show for instance that the strong-coupling limit of the collective model without configuration mixing cannot be valid for several pairs. While this conclusion is not new, the approach may lead to some clarification as to the limitations which must be placed on the various forms of the collective model.

The magnetic moment operator for the odd-proton nucleus may be written as

$$\boldsymbol{\mu}^P=\mu_0[\mathbf{I}+(\mu_P-\tfrac{1}{2})\boldsymbol{\sigma}_P{}'+\textstyle\sum_P(\mu_P-\frac{1}{2})\boldsymbol{\sigma}_P +\sum_N(-\mathbf{j}_N+\mu_N\boldsymbol{\sigma}_N)],\tag{3}$$

where primes indicate the last odd particle and the summations extend over the core particles. μ_0 is the nuclear Bohr magneton, $\boldsymbol{\sigma}$ is the Pauli spin operator, and $\mathbf{I}$ is the total angular momentum of the nucleus.

The corresponding magnetic moment operator for the odd-neutron nucleus is

$$\boldsymbol{\mu}^N=\mu_0\{\mu_N\boldsymbol{\sigma}_N{}'+\textstyle\sum_P[\mathbf{j}_P+(\mu_P-\frac{1}{2})\boldsymbol{\sigma}_P]+\sum_N\mu_N\boldsymbol{\sigma}_N\}.\tag{4}$$

The wave function for the odd-proton nucleus is written as

$$\psi_I{}^M(P)=\sum_{\gamma,I,j}\alpha_{\gamma,\lambda,j}(A_P)\sum_\mu\langle j,\lambda,M-\mu,\mu|j,\lambda,I,M\rangle \times C_\lambda{}^\mu(A_P)\phi_j{}^{M-\mu}(P).\tag{5}$$

$C_\lambda{}^\mu(A_P)$ is the angular part of the core function of the odd-proton nucleus having angular momentum λ, a z component of angular momentum μ, and A_P particles in the core. $\langle j,\lambda,M-\mu,\mu|j,\lambda,I,M\rangle$ is the appropriate Clebsch-Gordon coefficient as defined in Condon and Shortley.[11] $\phi_j{}^m$ is the wave function of the odd particle having total angular momentum j. The summation over j thus includes the possibility of configuration admixing due to the interaction of the odd particle with the surface. γ includes all other required quantum numbers to specify the wave function such as the occupation numbers for the surfons (quantized surface vibrations), as well as all summations necessary to give the required symmetry properties of the wave function. $\alpha_{\gamma,\lambda,j}$ includes the remainder of the core wave function as well as the normalized probability amplitudes for the expansion. A similar wave function holds for the odd-neutron nucleus.

In most calculations involving low-lying states or ground states only the values $\lambda=0$, 2 ($\lambda=1$ represents a dipole vibration at much higher energy) are considered important. In the perturbation calculation of Milford[12] the values $\lambda=0$, 2, 4 are used since it can be shown that the odd particle interacts with the odd λ in the second order. In the following work it is assumed that λ assumes only even values.

With the use of these wave functions and the magnetic moment operators given by Eq. (3) and Eq. (4),

[10] All data are from P. F. A. Klinkenberg, Revs. Modern Phys. 24, 63 (1952) unless otherwise noted.

[11] E. U. Condon and G. H. Shortley, *The Theory of Atomic Spectra* (Cambridge University Press, New York, 1951), Chap. III.

[12] F. J. Milford, Phys. Rev. 93, 1297 (1954).

it is found that

$$\Delta^P-\Delta^N=\sum_{\gamma,\lambda,j,\mu}|\langle j,\lambda,I-\mu,\mu|j,\lambda,I,I\rangle|^2$$
$$\times\Big\{\alpha_{\gamma,\lambda,j}{}^2(A_N)\Big[\langle\phi_j{}^{I-\mu}|\sigma^z|\phi_j{}^{I-\mu}\rangle$$
$$+\Big\langle C_\lambda{}^\mu(A_N)\Big|\frac{\sum_P j_P{}^z}{\mu_N}+\sum_N\sigma_N{}^z$$
$$+\frac{\mu_P-\frac{1}{2}}{\mu_N}\sum_P\sigma_P{}^z\Big|C_\lambda{}^\mu(A_N)\Big\rangle\Big]-\alpha_{\gamma,\lambda,j}{}^2(A_P)$$
$$\times\Big[\langle\phi_j{}^{I-\mu}|\sigma^z|\phi_j{}^{I-\mu}\rangle+\Big\langle C_\lambda{}^\mu(A_P)\Big|\frac{-\sum_N j_N{}^z}{\mu_P-\frac{1}{2}}$$
$$+\sum_P\sigma_P{}^z+\frac{\mu_N}{\mu_P-\frac{1}{2}}\sum_N\sigma_N{}^z\Big|C_\lambda{}^\mu(A_P)\Big\rangle\Big]\Big\}$$
$$\sum_{\gamma,\lambda,j',j'',\mu}\langle j',\lambda,I-\mu,\mu|j',\lambda,I,I\rangle$$
$$\times\langle j'',\lambda,I,I|j'',\lambda,I-\mu,\mu\rangle$$
$$\times[\alpha_{\gamma,\lambda,j'}(A_N)\alpha_{\gamma,\lambda,j''}(A_N)-\alpha_{\gamma,\lambda,j'}(A_P)\alpha_{\gamma,\lambda,j''}(A_P)]$$
$$\times\langle\phi_{j''}{}^{I-\mu}|\sigma^z|\phi_{j'}{}^{I-\mu}\rangle. \quad (6)$$

No cross terms occur between core states since all values of λ are even.

It is now necessary to simplify Eq. (6) in a manner which is consistent with the usual assumptions of the various forms of the collective model. An especially simple case is the Bohr-Mottelson strong-coupling model without configuration mixing. In this case there is no admixture of different single particle j states. The only value of j is assumed to be that prescribed by the shell model, i.e., $j=I$. Furthermore, the core angular momentum is restricted to $\lambda=2$. With these conditions Eq. (6) becomes

$$\Delta^P-\Delta^N=\sum_\mu|\langle I,2,I-\mu,\mu|I,2,I,I\rangle|^2$$
$$\times\Big\{\Big\langle C_\lambda{}^\mu(A_N)\Big|\frac{\sum_P j_P{}^z}{\mu_N}+\sum_N\sigma_N{}^z$$
$$+\frac{\mu_P-\frac{1}{2}}{\mu_N}\sum_P\sigma_P{}^z\Big|C_\lambda{}^\mu(A_N)\Big\rangle$$
$$-\Big\langle C_\lambda{}^\mu(A_P)\Big|\frac{-\sum_N j_N{}^z}{\mu_P-\frac{1}{2}}+\sum_P\sigma_P{}^z$$
$$+\frac{\mu_N}{\mu_P-\frac{1}{2}}\sum_N\sigma_N{}^z\Big|C_\lambda{}^\mu(A_P)\Big\rangle\Big\}. \quad (7)$$

However, a more general simplification of Eq. (6) is desirable for the purposes of further study. The different numbers of even particles in the nuclei of the conjugate pair can affect $\Delta^P-\Delta^N$ in two ways. First, if the core shares in the total angular momentum of the nucleus, then the respective share of the even particles in the core angular momentum would be expected to be different for the two nuclei of the conjugate pair. Thus regardless of specific nuclear forces and the coupling of the core to the single odd particle, the neutron excess alone could possibly lead to large values of $\Delta^P-\Delta^N$.

The second effect of the unequal number of particles is related to the coupling of the single odd particle to

TABLE I. The magnetic moments and magnetic moment deviations of conjugate nuclei in order of ascending total angular momentum and mass.

Conjugate nuclei	Z	N	Single-particle state l_j	Magnetic moment	Δ^P or Δ^N	$\Delta^P-\Delta^N$
H^3	1	2	$s_{1/2}$	2.979	−0.081	+0.034
He^3	2	1	$s_{1/2}$	−2.127	−0.115	
P^{31}	15	16	$s_{1/2}$	+1.312	0.724	+0.014
Si^{29}	14	15	$s_{1/2}$	−0.555	0.710	
N^{15}	7	8	$p_{1/2}$	−0.283	−0.008	−0.041
C^{13}	6	7	$p_{1/2}$	+0.702	+0.033	
B^{11}	5	6	$p_{3/2}$	2.689	0.482	+0.098
Be^9	4	5	$p_{3/2}$	−1.177	0.384	
Cu^{63}	29	34	$p_{3/2}$	2.226	0.683	−0.058
Cu^{65}	29	36	$p_{3/2}$	2.385	0.614	−0.127
Cr^{53a}	24	29	$p_{3/2}$	−0.474	0.741	
Cl^{35}	17	18	$d_{3/2}$	2.226	−0.304	−0.036
Cl^{37}	17	20	$d_{3/2}$	2.385	−0.244	+0.024
S^{33}	16	17	$d_{3/2}$	+0.644	−0.268	
Au^{197b}	79	118	$d_{3/2}$	0.16	−0.02	+0.14
Ba^{135}	56	79	$d_{3/2}$	+0.835	−0.163	
Al^{27}	13	14	$d_{5/2}$	+3.641	0.502	−0.051
Mg^{25}	12	13	$d_{5/2}$	−0.855	0.553	
I^{127}	53	74	$d_{5/2}$	+2.809	0.865	0.353
Mo^{97}	42	53	$d_{5/2}$	−0.914	0.512	
Pr^{141c}	59	82	$d_{5/2}$	+3.58	0.53	−0.2
Pd^{105}	46	59	$d_{5/2}$	−0.6	0.68	
Rb^{85}	37	48	$f_{5/2}$	1.353	−0.214	+0.052
Zn^{67b}	30	37	$f_{5/2}$	+0.876	−0.256	
Mn^{55}	25	30	$(f_{7/2})^5$, $J=5/2$	3.468	0.291	0.004
Ti^{47d}	22	25	$(f_{7/2})^5$, $J=5/2$	−0.787	0.287	
V^{51}	23	28	$f_{7/2}$	5.148	0.281	−0.030
Ca^{43e}	20	23	$f_{7/2}$	−1.318	0.311	
Co^{59}	27	32	$f_{7/2}$	4.648	0.499	0.077
Ti^{49d}	22	27	$f_{7/2}$	−1.104	0.422	
Nb^{93}	41	52	$g_{9/2}$	6.166	0.273	−0.268
Ge^{73d}	32	41	$g_{9/2}$	−0.877	0.541	
In^{113b}	49	64	$g_{9/2}$	5.522	0.554	0.124
In^{115b}	49	66	$g_{9/2}$	5.534	0.545	0.115
Sr^{87f}	38	49	$g_{9/2}$	−1.089	0.430	

[a] F. Alder and K. Halbach, Helv. Phys. Acta **26**, 426 (1953).
[b] H. Walchli, Oak Ridge National Laboratory Report ORNL-1469, 1952 (unpublished).
[c] Hin Lew, Phys. Rev. **91**, 619 (1953).
[d] C. D. Jeffries, Phys. Rev. **92**, 1262 (1953).
[e] C. D. Jeffries, Phys. Rev. **90**, 1130 (1953).
[f] C. D. Jeffries and P. B. Sogo, Phys. Rev. **91**, 1286 (1953).

the nuclear core. The excitation energies of the nuclear core oscillations depend among other things on the nuclear radius and, therefore, on the number of particles in the core. Thus, even assuming the charge independence of nuclear forces, the coupling of the single odd particle to the surface oscillations would be different for the two nuclei of the conjugate pair due to the different polarizabilities of the nuclear cores. Formally, this means that in general, $\alpha_{\gamma,\lambda,j}(A_P) \neq \alpha_{\gamma,\lambda,j}(A_N)$ in Eq. (6) since $A_P \neq A_N$. However, the problem of calculating the correct excitation energies of the nuclear core oscillation is sufficiently complicated that most investigations involving calculations of magnetic moments assume an average excitation, i.e., an average polarizability of the nuclear core. These statements, of course, deal with a simple form of the collective model which ignores all shell structure.

In the light of the previous considerations, a general simplification of Eq. (6) which is consistent with the magnetic moment calculations of most investigators is to assume that

$$\alpha_{\gamma,\lambda,j}(A_P)=\alpha_{\gamma,\lambda,j}(A_N) \quad \text{for all } \gamma, \lambda, j. \tag{8}$$

Physically, Eq. (8) embodies the assumptions that (a) the nuclear forces are charge-independent and (b) the properties of the core are independent of the number of particles constituting it.

In the absence of shell effects, the two assumptions leading to Eq. (8) are at best approximate. As the number of protons in the core increases, the effect of Coulomb repulsions will tend to destroy the charge independence of the nuclear forces (as exemplified in the different ordering of the shell model states for protons and neutrons). However, the properties of the core tend to become more uniform with increasing numbers of core particles, which justifies to some extent the use of Eq. (8) as a first approximation. In a later section, Eq. (8) is modified to include the influence of shell structure, lack of charge symmetry, and the different polarizabilities of the nuclear cores.

Besides the simplification of Eq. (6) entailed by the assumption of Eq. (8), it is necessary to make some further assumptions to allow the evaluation of the matrix elements of Eq. (6). In treating the interaction of the odd particle with the core in terms of surface oscillations, the identities of the particles of the core are ignored. Thus it seems reasonable to assume that the angular momentum of the core is equally distributed among all the particles participating in the oscillation. For the liquid drop model the number of particles participating in the surface vibration can be shown[13] to be of the order of $(3/\lambda)A$, where A is the number of particles in the core and λ is the angular momentum of the oscillation. Since we shall assume that on the average $\lambda=2$, all the particles are assumed to participate in the oscillation. The work of Bohr and Mottelson indicates that this is probably an overestimate of the number of particles participating in the vibration.

If every particle has an equal share of the angular momentum, then

$$\langle C_\lambda{}^\mu(A)|\sigma^z|C_\lambda{}^\mu(A)\rangle = \frac{1}{A}\langle C_\lambda{}^\mu(A)|\sum_P \sigma_P{}^z+\sum_N \sigma_N{}^z|C_\lambda{}^\mu(A)\rangle = \frac{1}{A}\langle C_\lambda{}^\mu(A)|S^z|C_\lambda{}^\mu(A)\rangle$$

$$\langle C_\lambda{}^\mu(A)|j^z|C_\lambda{}^\mu(A)\rangle = \frac{1}{A}\langle C_\lambda{}^\mu(A)|\sum_P j_P{}^z+\sum_N j_N{}^z|C_\lambda{}^\mu(A)\rangle = \frac{1}{A}\langle C_\lambda{}^\mu(A)|J^z|C_\lambda{}^\mu(A)\rangle=\frac{\mu}{A}, \tag{9}$$

where A is the number of particles in the core, S^z is the z component of the total spin (in the spin-orbit sense) of the core, and J^z is the z component of the total angular momentum of the core (this is, of course, equivalent to λ^z).

The core wave functions can be expanded in an LS representation

$$C_\lambda{}^\mu(A)=\sum_{L,S}\beta_{LS}(A)\sum_{m_S}\langle L,S,\mu-m_S,m_S|L,S,\lambda,\mu\rangle \times \mathcal{L}_L{}^{\mu-m_S}\mathcal{S}_S{}^{m_S}, \tag{10}$$

where $\mathcal{L}_L{}^{m_L}$ and $\mathcal{S}_S{}^{m_S}$ are the orbital and spin wave functions, respectively. $\beta_{LS}(A)$ are the required probability amplitudes.

Implicit in the applications of the collective model (weak or strong coupled) is the assumption discussed in connection with Eq. (8), that the properties of the surface for sufficiently heavy nuclei are at most slightly dependent on the number of particles A_P or A_N of the core. This assumption leads to the simplification Eq. (8) and to the related simplifying assumption

$$\beta_{LS}(A_N)=\beta_{LS}(A_P)=\beta_{LS}. \tag{11}$$

Furthermore, the various forms of the collective model assume that the magnetic moment of the core is due to a gyromagnetic ratio

$$g_c=Z/A \tag{12}$$

associated with the angular momentum λ of the core. This is equivalent to the assumption that

$$S=0, \quad L=\lambda. \tag{13}$$

This assumption or the more general assumption that $S<L$ and small is probably justified if the nuclear forces are predominantly of the Wigner or Majorana

[13] J. M. Blatt and V. F. Weiskopf, *Theoretical Nuclear Physics* (John Wiley and Sons, Inc., New York, 1952), p. 302.

(space exchange) type.[14] The energetically most favored state of given λ would be that state with maximum space symmetry, which justifies the assumption Eq. (13). With these various assumptions, Eq. (7) becomes

$$\Delta^P-\Delta^N=\frac{3}{I+1}\left(0.436\frac{N_P}{A_P}-0.523\frac{Z_N}{A_N}\right), \quad (14)$$

while Eq. (6) becomes

$$\Delta^P-\Delta^N=\tfrac{1}{2}\sum_{\gamma,\lambda,j,L,S}\alpha_{\gamma,\lambda,j}{}^2\beta_{LS}{}^2 \times\left[\frac{I(I+1)+\lambda(\lambda+1)-j(j+1)}{I+1}\right] \times\left\{\left(0.436\frac{N_P}{A_P}-0.523\frac{Z_N}{A_N}\right) +\left[\frac{\lambda(\lambda+1)+S(S+1)-L(L+1)}{2\lambda(\lambda+1)}\right] \times\left[\frac{(N_N-1.195Z_N)}{A_N}-\frac{(Z_P-0.835N_P)}{A_P}\right]\right\}, \quad (15)$$

where the assumption Eq. (13) has not been used in this case. In these equations N_P, Z_P are the number of neutrons and the number of protons in the core of the odd-proton nucleus while N_N, Z_N are the same for the odd-neutron nucleus.

When calculating magnetic moments in the strong coupling limit of the simple collective model, Bohr and Mottelson make the approximation

$$g_c=Z/A\sim 0.45. \quad (16)$$

With this value, Eq. (14) becomes

$$\Delta^P-\Delta^N=0.012/(I+1), \quad (17)$$

TABLE II. The values of $\Delta^P-\Delta^N$ for the conjugate pairs $I^{127}-Mo^{97}$ and $Au^{197}-Ba^{135}$ for different values of S, L, and λ.

		$\Delta^P-\Delta^N$		
		$I^{127}-Mo^{97}$		$Au^{197}-Ba^{135}$
S	L	$\lambda=2$	$\lambda=4$	$\lambda=2$
0	2	0.023	0.095	0.052
1	3	−0.004	0.179	−0.024
1	2	0.037	0.227	0.090
1	1	0.064	0.262	0.166
2	4	0.032	0.143	−0.100
2	3	0.023	0.213	0.052
2	2	0.064	0.262	0.166
2	1	0.089	0.297	0.241
2	0	0.107	0.311	0.278
4	6	−0.087	0.070	−0.251
4	2	0.160	0.382	0.430
6	8	−0.165	0.011	−0.403
6	4	0.215	0.448	0.580

[14] R. G. Sachs, *Nuclear Theory* (Addison-Wesley Press, Cambridge, 1954), p. 190.

which is sufficiently small compared to the average magnitude of Δ^P or Δ^N to constitute a quasi-mirror theorem for the magnetic moments of conjugate nuclei as calculated by the assumptions of the Bohr-Mottelson strong-coupling collective model.

A result similar to Eq. (17) can be obtained by a direct calculation using the magnetic moment given by Bohr and Mottelson [their Eq. (IV-6)]. It is found that if the strength of the coupling of the odd particle to the surface oscillations is the same for both nuclei of the conjugate pair, then

$$-0.044<\Delta^P-\Delta^N<0.071 \quad (18)$$

in the range of experimental interest regardless of the coupling strength. In the strong-coupling limit, the same result holds regardless of the specific individual coupling strengths for the two nuclei.

An examination of the nineteen entries in the last column of Table I shows that ten cases, or more than half, fall outside the limits set by Eq. (18). Even more interesting is a consideration of those cases involving nuclei with more than 65 nucleons since the collective model should be most valid for heavier nuclei. Of the seven cases involving heavier nuclei, only one (an $I=L-1/2$ conjugate pair) satisfies the criterion of Eq. (18). Thus the mirror property of conjugate nuclei is most apparent for lighter nuclei where the conditions leading to Eq. (2) are more likely to hold.

CONJUGATE NUCLEI AND NUCLEAR MODELS

The various expressions obtained for the quantity $\Delta^P-\Delta^N$ are of considerable interest since any systematic error arising from the assumption made would probably tend to cancel. Thus a study of $\Delta^P-\Delta^N$ is a more sensitive means of investigating some aspects of the different nuclear models than a similar study of Δ^P or Δ^N alone. However, the very complicated nature of the nucleus as well as the extensive nature of the assumptions made to obtain Eq. (14) and Eq. (15) allow conclusions of only a qualitative nature. In this spirit the effect of modifying the various assumptions leading to the above equations will be studied.

Equation (15) is used to determine the effect of replacing $g_c=0.45$ by the appropriate values of Z_P, N_P, A_P and Z_N, N_N, A_N, as well as for different values of S, L, and λ for the core. Only $j=I$ is considered in the following discussion. For a comparatively light conjugate pair such as $V^{51}-Ca^{43}$, it is found that theoretically $|\Delta^P-\Delta^N|\leqslant 0.030$ for all values of S, L up to $S=6$ and $L=8$. Thus the observed small value of $\Delta^P-\Delta^N=-0.030$ is even compatible with Eq. (15) for the values of $S\neq 0$ and $S>L$. This observation is generally true for the lighter ($A<65$) conjugate nuclei because of the relatively small neutron excess and the consequent cancellations of terms in Eq. (15).

The application of Eq. (15) to a medium-heavy conjugate pair such as $I^{127}-Mo^{97}$ and a heavy conjugate

pair such as $Au^{197}-Ba^{135}$ is given in Table II. The importance of the increasing neutron excess is shown in the general increase in magnitude of $\Delta^P-\Delta^N$ for the same λ, S, and L. The core angular momentum $\lambda=4$ is not allowed for the $Au^{197}-Ba^{135}$ conjugate pair with the assumption that $j=I=3/2$. The application of Eq. (15) with $\lambda=4$ is given for the $I^{127}-Mo^{97}$ conjugate pair, and it is seen that there is a significant increase for given S and L of $\Delta^P-\Delta^N$ as λ increases. This may be of considerable importance for some conjugate pairs, since Milford[12] has shown that $\lambda=4$ occurs with significant probability in the straightforward perturbation calculation with the collective-model Hamiltonian. However, it is interesting to note that the values obtained for $\Delta^P-\Delta^N$ from Eq. (15) for $I^{127}-Mo^{97}$ are almost all smaller than the observed value of $\Delta^P-\Delta^N=0.353$. The results of Table II give further confirmation, for this conjugate pair, of the importance of configuration mixing mentioned earlier, i.e., the occurrence of $j\neq I$ and the breakdown of the assumption of Eq. (8).

For the conjugate pair $Au^{197}-Ba^{135}$ it is seen that the experimental value of $\Delta^P-\Delta^N=0.14$ can be obtained by many values of $0\leqslant S\leqslant 6$, $0\leqslant L\leqslant 8$ and $\lambda=2$. The majority of the calculated values of $\Delta^P-\Delta^N$ are positive, and the magnitude increases with increasing S, L, and λ. This general property leads to the expectation that $\Delta^P-\Delta^N$ if the collective model is valid. For the heavier conjugate nuclei ($A>65$ for both nuclei), it is found that $\Delta^P-\Delta^N>0$ for five out of seven cases. It is interesting to note that the remaining two cases which have $\Delta^P-\Delta^N<0$ have even neutron shells which are either closed or two more than closed.

It is now desirable to investigate qualitatively the possible effect of shell structure on the values of $\Delta^P-\Delta^N$. The occurrence of shell structure manifests itself by the increased stability (binding energy) associated with certain given (magic) numbers of either protons or neutrons in the nucleus. The collective model interprets this increased stability in terms of an increase of the surface tension of the core with a subsequent increase in the energy necessary to excite core oscillations. Simple perturbation considerations relate the probability amplitudes $\alpha_{\gamma,\lambda,j}$ to this excitation energy by the proportionality $\alpha_{\gamma,\lambda,j}\sim 1/(E_\lambda-E_0)$, where E_λ is the excitation energy of the λ core oscillation and E_0 is the energy of the zero-order state, in our case the shell-model wave function. In considering the influence of shell effects on the value of $\Delta^P-\Delta^N$, this perturbation approach will be assumed.

Equation (6) is simplified by assuming that only $j=I$ and $\lambda=0$, 2 occur, that $S=0$, and that Eq. (9) is valid. Furthermore, it is assumed as a consequence perturbation theory that

$$\alpha_{\gamma,2,I}(A)=\frac{C_I}{E_2(A)-E_0(A)}, \tag{19}$$

TABLE III. The values of $\Delta^P-\Delta^N$ taking into account the effects of shell structure on the collective model.

Conjugate nuclei	l_I	Z	N	$\Delta E(A)$ (Mev)	Exp. $\Delta^P-\Delta^N$	Theoretical $\Delta^P-\Delta^N$
Au^{197}	$d_{3/2}$	79	118	0.35	0.143	−0.227
Ba^{135}	$d_{3/2}$	56	79	0.79		
I^{127}	$d_{5/2}$	53	74	0.64	0.353	0.190
Mo^{97}	$d_{5/2}$	42	53	0.77		
Pr^{141}	$d_{5/2}$	59	82	1.6	−0.2	−0.472
Pd^{105}	$d_{5/2}$	46	59	0.56		
Rb^{85}	$f_{5/2}$	37	48	0.85	0.052	0.021
Zn^{67}	$f_{5/2}$	30	37	1.04		
Nb^{93}	$g_{9/2}$	41	52	0.93	−0.268	−0.099
Ge^{73}	$g_{9/2}$	32	41	0.68		
In^{113}	$g_{9/2}$	49	64	0.55	0.124	0.224
In^{115}	$g_{9/2}$	49	66	0.55	0.115	0.227
Sr^{87}	$g_{9/2}$	38	49	1.9		

where the constant C_I is taken to be independent of both A and the energy of excitation $\Delta E(A)$. Generally C_I will vary with these quantities, but this variation does not significantly alter the following considerations. With these assumptions, Eq. (6) becomes

$$\Delta^P-\Delta^N=\frac{3|C_I|^2}{I+1}\left\{\frac{1}{[\Delta E(A_P)]^2}\left[\frac{1}{\mu_P-\frac{1}{2}}\frac{N_P}{A_P}+\frac{1}{I}\right]+\frac{1}{[\Delta E(A_N)]^2}\left[\frac{1}{\mu_N}\frac{Z_N}{A_N}-\frac{1}{I}\right]\right\} \tag{20a}$$

for $I=L+1/2$ nuclei, and

$$\Delta^P-\Delta^N=\frac{3|C_I|^2}{I+1}\left\{\frac{1}{[\Delta E(A_P)]^2}\left[\frac{1}{\mu_P-\frac{1}{2}}\frac{N_P}{A_P}-\frac{2}{2I+1}\right]+\frac{1}{[\Delta E(A_N)]^2}\left[\frac{1}{\mu_N}\frac{Z_N}{A_N}+\frac{2}{2I+1}\right]\right\} \tag{20b}$$

for $I=L-1/2$ nuclei.

The above equations now include a contribution to $\Delta^P-\Delta^N$ from the single odd particle states which previously had vanished because of the assumption of Eq. (8). Equations (20) are applied to those heavier conjugate nuclei mentioned previously, i.e., conjugate nuclei both of whose members have $A>65$. The results of this application are given in Table III. The energy of excitation of the core $\Delta E(A_P)$ or $\Delta E(A_N)$ is assumed to be the experimentally-observed $\lambda=2$ first excited state for the appropriate even-even nucleus given by Scharff-Goldhaber.[15] For convenience, the coefficient C_I is chosen to make $\alpha_{\gamma,2,I^2}(A)=1$ for that nucleus of the conjugate pair having the lowest excitation energy. This last choice would lead to $|\Delta^P-\Delta^N|$ (theoretical) $\geqslant|\Delta^P-\Delta^N|$ (experimental), with the signs of both

[15] Gertrude Scharff-Goldhaber, Phys. Rev. **90**, 587 (1953).

TABLE IV. The values of $\Delta^P-\Delta^N$ when the single particle states are different for the nuclei of the conjugate pair.

$I=$	3/2	5/2	7/2	9/2
Conjugate pairs with $I=L+\frac{1}{2}$	0.34	1.01	1.27	1.41
Conjugate pairs with $I=L-\frac{1}{2}$	0.62	−0.92	−1.27	−1.43

being the same if the assumptions leading to Eq. (20) are valid.

It is seen in Table III that with the exception of the $Au^{197}-Ba^{135}$ conjugate pair, $\Delta^P-\Delta^N$(theoretical) agrees in sign with $\Delta^P-\Delta^N$(experimental), with shell effects leading to the negative signs of the $Pr^{141}-Pd^{105}$ and $Nb^{93}-Ge^{73}$ conjugate pairs. These shell effects appear in the increased value of $\Delta E(A)$ for that nucleus at or near a closed shell. All those conjugate pairs which either have different signs (one case) or which do not satisfy the condition $|\Delta^P-\Delta^N|$(theoretical) $\geqslant|\Delta^P-\Delta^N|$(experimental) are either (a) $I=L-1/2$ conjugate nuclei, or (b) conjugate nuclei in which one nucleus is in a region of very close competition between several single particle states. Nuclei with $I=L-1/2$ are not adequately explained by the simple collective model,[5,12] with the theoretical deviations tending in the opposite direction with increasing I compared to those observed. Therefore, it is not surprising that the conjugate pairs with $I=L-1/2$ do not display optimum behavior in Table III.

In all other cases where $|\Delta^P-\Delta^N|$(theoretical) $<|\Delta^P-\Delta^N|$(experimental), and in the case of $Au^{197}-Ba^{135}$, there are different degrees of close competition between single-particle states of different j for the odd-proton nuclei and odd-neutron nuclei. This competition can be seen by examining the observed ground state spins of nuclei in the region of the conjugate nuclei. For a nucleus in a region of close competition between different single particle states, it is no longer likely that $\alpha_{\gamma,2,j\neq I}$ is negligible, and it is, therefore, necessary to consider the case of configuration mixing. The term configuration mixing is used in the sense that different single-particle states (single-particle configurations) are admixed in the general odd-proton wave function, Eq. (5), or the odd-neutron equivalent.

In order to obtain an indication of the importance of configuration mixing, two simple but extreme cases are considered: for conjugate pairs with $I=L+1/2$,

$$\begin{aligned}&\alpha_{\gamma,2,j=I}{}^2(A_N)=1, \quad \alpha_{\gamma,\lambda,j\neq I}(A_N)=0,\\ &\alpha_{\gamma,2,j=I+1}{}^2(A_P)=1, \quad \alpha_{\gamma,\lambda,j\neq I+1}(A_P)=0,\end{aligned} \tag{21a}$$

while for conjugate pairs with $I=L-1/2$,

$$\begin{aligned}&\alpha_{\gamma,2,j=I}{}^2(A_N)=1, \quad \alpha_{\gamma,\lambda,j\neq I}(A_N)=0,\\ &\alpha_{\gamma,2,j=I-1}{}^2(A_P)=1, \quad \alpha_{\gamma,\lambda,j\neq I-1}(A_P)=0.\end{aligned} \tag{21b}$$

In either case the parities of the odd-particle states must be the same. These cases correspond to the Bohr-Mottelson strong-coupling collective model, where the final angular momentum I is obtained by coupling a different single-particle state to the surface oscillations for each of the two nuclei of the conjugate pair.

The values obtained for $\Delta^P-\Delta^N$ by using the conditions Eqs. (21) in Eq. (6) subject to the assumption Eqs. (9) are given in Table IV. It is immediately seen that the calculated values of $\Delta^P-\Delta^N$ are, for the appropriate I, larger than any experimentally observed $\Delta^P-\Delta^N$. The particular cases considered are appropriate for the $I^{127}-Mo^{97}$ ($I=L+1/2=5/2$) conjugate pair and the $Au^{197}-Ba^{135}$ ($I=L-1/2=3/2$) conjugate pair listed in Table III. I^{127} is in a region of very close competition between $d_{5/2}$ and $g_{7/2}$ single particle states, while Au^{197} is in a region of close competition between $d_{3/2}$ and $s_{1/2}$ single particle states. It is significant that the appropriate values of $\Delta^P-\Delta^N$ in Table IV have the correct sign to account for the observed values of $\Delta^P-\Delta^N$ for these two conjugate pairs. A more general calculation shows that the value of $\Delta^P-\Delta^N$ depends linearly, to a first approximation, on the probability (not probability amplitude) of occurrence of the admixed state. Therefore, if shell effects are not considered, the large $I^{127}-Mo^{97}$ value of $\Delta^P-\Delta^N$ can be explained by about a 30 percent probability for the $g_{7/2}$ state occurring in the I^{127} wave function. Similarly, about a 25 percent probability for the $s_{1/2}$ state in the Au^{197} wave function will account for the $Au^{197}-Ba^{135}$ experimental value of $\Delta^P-\Delta^N$.

CONCLUSIONS

The calculated magnetic moment deviations of conjugate nuclei are exactly equal (mirror property) according to the nuclear model of Volkov[6] and are nearly equal (quasi-mirror property) according to the strong-coupling Bohr-Mottelson[5] model. An analysis of the observed magnetic moment deviations shows that neither property (mirror or quasi mirror) holds for those heavier conjugate nuclei which should most closely approximate collective-model nuclei. However, it has been shown that the experimental results can be explained in terms of a simple form of the collective model, subject to modifications which incorporate shell structure in the core and/or the configuration mixing of different single-particle states.

Behavior of Neutral Particles under Charge Conjugation

M. GELL-MANN,* *Department of Physics, Columbia University, New York, New York*

AND

A. PAIS, *Institute for Advanced Study, Princeton, New Jersey*

(Received November 1, 1954)

Some properties are discussed of the θ^0, a heavy boson that is known to decay by the process $\theta^0 \to \pi^+ + \pi^-$. According to certain schemes proposed for the interpretation of hyperons and K particles, the θ^0 possesses an antiparticle $\bar{\theta}^0$ distinct from itself. Some theoretical implications of this situation are discussed with special reference to charge conjugation invariance. The application of such invariance in familiar instances is surveyed in Sec. I. It is then shown in Sec. II that, within the framework of the tentative schemes under consideration, the θ^0 must be considered as a "particle mixture" exhibiting two distinct lifetimes, that each lifetime is associated with a different set of decay modes, and that no more than half of all θ^0's undergo the familiar decay into two pions. Some experimental consequences of this picture are mentioned.

I

IT is generally accepted that the microscopic laws of physics are invariant to the operation of charge conjugation (CC); we shall take the rigorous validity of this postulate for granted. Under CC, every particle is carried into what we shall call its "antiparticle". The principle of invariance under CC implies, among other things, that a particle and its antiparticle must have exactly the same mass and intrinsic spin and must have equal and opposite electric and magnetic moments. A charged particle is thus carried into one of opposite charge. For example, the electron and positron are each other's antiparticles; the π^+ and π^- and the μ^+ and μ^- mesons are supposed to be pairs of antiparticles; and the proton must possess an antiparticle, the "antiproton".

Neutral particles fall into two classes, according to their behavior under CC:

(a) Particles that transform into themselves, and which are thus their own antiparticles. For instance the photon and the π^0 meson are bosons that behave in this fashion. It is conceivable that fermions, too, may belong to this class. An example is provided by the Majorana theory of the neutrino.

In a field theory, particles of class (a) are represented by "real" fields, i.e., Hermitian field operators. There is an important distinction to be made within this class, according to whether the field takes on a plus or a minus sign under CC. The operation of CC is performed by a unitary operator $\mathcal{C}$. The photon field operator $A_\mu(x)$ satisfies the relation

$$\mathcal{C}A_\mu(x)\mathcal{C}^{-1} = -A_\mu(x), \tag{1}$$

while for the π^0 field operator $\phi(x)$ we have

$$\mathcal{C}\phi(x)\mathcal{C}^{-1} = \phi(x). \tag{2}$$

Equation (1) expresses the obvious fact that the electromagnetic field changes sign when positive and negative charges are interchanged; that the π^0 field must not change sign can be inferred from the observed two-photon decay of the π^0.

We are effectively dealing here with the "charge conjugation quantum number" C, which is the eigenvalue of the operator $\mathcal{C}$, and which is rigorously conserved in the absence of external fields. If only an odd (even) number of photons is present, we have $C=-1(+1)$; if only π^0's are present, $C=+1$; etc. As a trivial example of the conservation of C, we may mention that the decay of the π^0 into an odd number of photons is forbidden.[1]

We may recall that a state of a neutral system composed of charged particles may be one with a definite value of C. For example, the $^1S_0$ state of positronium has $C=+1$; a state of a π^+ and a π^- meson with relative orbital angular momentum l has $C=(-1)^l$; etc.

For fermions, as for bosons, a distinction may be made between "odd" and "even" behavior of neutral fields of class (a) under CC. However, the distinction is then necessarily a relative rather than an absolute one.[2] In other words, it makes no sense to say that a single such fermion field is "odd" or "even", but it does make sense to say that two such fermion fields have the same behavior under CC or that they have opposite behavior.

(b) Neutral particles that behave like charged ones in that: (1) they have antiparticles distinct from themselves; (2) there exists a rigorous conservation law that prohibits virtual transitions between particle and antiparticle states.

A well-known member of this class is the neutron N, which can obviously be distinguished from the antineutron $\bar{N}$ by the sign of its magnetic moment. The law that forbids the virtual processes $N \rightleftarrows \bar{N}$ is the law

* On leave from Department of Physics and Institute for Nuclear Studies, University of Chicago, Chicago, Illinois.

[1] For other consequences of invariance under charge conjugation see A. Pais and R. Jost, Phys. Rev. **87**, 871 (1952); L. Wolfenstein and D. G. Ravenhall, Phys. Rev. **88**, 279 (1952); L. Michel, Nuovo cimento **10**, 319 (1953).

[2] This is due to the fact that fermion fields can interact only bilinearly. For example, one easily sees that the interactions responsible for $P \to N + e^+ + \nu$ would not lead to physically distinguishable results if ν were either an even or an odd Majorana neutrino.

of conservation of baryons,[3] which is, so far as we know, exact, and which states that n, the number of baryons minus the number of antibaryons, must remain unchanged. Clearly all neutral hyperons likewise belong to this class. Although we know of no "elementary" bosons in the same category, we have no *a priori* reason for excluding their existence. [Note that the H atom is an example of a "non-elementary" boson of class (b).]

Particles in this class are represented by "complex" fields, and the operation of charge conjugation transforms the field operators into their Hermitian conjugates.

It is the purpose of this note to discuss the possible existence of neutral particles that seem, at first sight, to belong neither to class (a) nor to class (b).

II

Recently, attempts have been made to interpret hyperon and K-particle phenomena by distinguishing sharply between strong interactions, to which essentially all production of these particles is attributed, and weak interactions, which are supposed to induce their decay. It is necessary to assume that the strong interactions give rise to "associated production "exclusively.[4]

Certain detailed schemes[5] which meet this requirement lead to further specific properties of particles and interactions. In particular, a suggestion has been made about the θ^0 particle, a heavy boson that is known to decay according to the scheme:

$$\theta^0 \rightarrow \pi^+ + \pi^- + (\sim 215 \text{ Mev}). \tag{3}$$

It has been proposed that the θ^0 possesses an antiparticle $\tilde{\theta}^0$ distinct from itself, and that in the absence of the weak decay interactions, there is a conservation law that prohibits the virtual transitions $\theta^0 \rightleftarrows \tilde{\theta}^0$. [In our present language, we would say that the θ^0 belongs to class (b) if the weak interactions are turned off.] This conservation law also leads to stability of the θ^0 and $\tilde{\theta}^0$; moreover, while it permits the reaction $\pi^- + P \rightarrow \Lambda^0 + \theta^0$ it forbids the analogous process $\pi^- + P \rightarrow \Lambda^0 + \tilde{\theta}^0$. In the schemes under consideration this is the same law that forbids the reaction: 2 neutrons$\rightarrow 2\Lambda^0$.

The weak interactions that must be invoked to account for the observed decay (3) evidently cause the conservation law to break down (a fact that is, of course, of little importance for production). This breakdown makes the forbiddenness of the processes $\theta^0 \rightleftarrows \tilde{\theta}^0$ no longer absolute, as can be seen from the following argument: In the decay (3) the pions are left in a state with a definite relative angular momentum and therefore with a definite value of the charge-conjugation quantum number C. The charge-conjugate process,

$$\tilde{\theta}^0 \rightarrow \pi^+ + \pi^-, \tag{4}$$

must also occur and must leave the pions in the same state; moreover the reverse of (4) must also be possible, at least as a virtual process. Therefore the virtual transition $\theta^0 \rightleftarrows \pi^+ + \pi^- \rightleftarrows \tilde{\theta}^0$ is induced by the weak interactions, and we are no longer dealing exactly with case (b).

In order to treat this novel situation, we shall find it convenient to introduce a change of representation. Since the θ^0 and $\tilde{\theta}^0$ are distinct, they are associated, in a field theory, with a "complex" field ψ (a non-Hermitian field operator), just as in case (b). Under charge conjugation ψ must transform according to the law:

$$\begin{aligned} \mathcal{C}\psi\mathcal{C}^{-1} &= \psi^+, \\ \mathcal{C}\psi^+\mathcal{C}^{-1} &= \psi, \end{aligned} \tag{5}$$

where ψ^+ is the Hermitian conjugate of ψ. Let us now define

$$\psi_1 \equiv (\psi + \psi^+)/\sqrt{2} \tag{6}$$

and

$$\psi_2 \equiv (\psi - \psi^+)/\sqrt{2}i, \tag{7}$$

so that ψ_1 and ψ_2 are Hermitian field operators satisfying

$$\mathcal{C}\psi_1\mathcal{C}^{-1} = \psi_1, \tag{8}$$

and

$$\mathcal{C}\psi_2\mathcal{C}^{-1} = -\psi_2. \tag{9}$$

The fields ψ_1 and ψ_2 evidently correspond to class (a); in fact ψ_1 is "even" like the π^0 field and ψ_2 is "odd" like the photon field. Corresponding to these real fields there are quanta, which we shall call θ_1^0 and θ_2^0 quanta. The relationship that these have to the quanta of the complex ψ field, which we have called θ^0 and $\tilde{\theta}^0$, may be seen from an example: Let Ψ_1 be the wave-functional representing a single θ_1 quantum in a given state, while Ψ_0 and Ψ_0' describe a θ^0 and a $\tilde{\theta}^0$, respectively, in the same state. Then we have

$$\Psi_1 = (\Psi_0 + \Psi_0')/\sqrt{2}.$$

Thus the creation of a θ_1 (or, for that matter, of a θ_2) corresponds physically to the creation, with equal probability and with prescribed relative phase, of either a θ^0 or a $\tilde{\theta}^0$. Conversely, the creation of a θ^0 (or of a $\tilde{\theta}^0$) corresponds to the creation, with equal probability and prescribed relative phase, of either a θ_1^0 or a θ_2^0.

The transformation (6), (7) to two real fields could equally well have been applied to a complex field of class (b), such as that associated with the neutron. However, this would not be particularly enlightening. It would lead us, for instance, to describe phenomena involving neutrons and antineutrons in terms of "N_1 and N_2 quanta". Now a state with an N_1 (or N_2) quantum is a mixture of states with different values of the quantum number n, the number of baryons minus the number of antibaryons. But the law of conservation of baryons requires this quantity to be a constant of the motion, and so a mixed state can never arise from a pure one. Since in our experience we deal exclusively

[3] Nucleons and hyperons are collectively referred to as baryons.
[4] A. Pais, Phys. Rev. **86**, 663 (1952).
[5] M. Gell-Mann, Phys. Rev. **92**, 833 (1953); A. Pais, Proc. Nat. Acad. Sci. U. S. **40**, 484, 835 (1954); M. Gell-Mann and A. Pais. *Proceedings of the International Conference Glasgow* (Pergamon Press, London, to be published).

with states that are pure with respect to n, the introduction of N_1 and N_2 quanta can only be a mathematical device that distracts our attention from the truly physical particles N and $\bar{N}$.

On the other hand, it can obviously not be argued in a similar way that the θ_1^0 and θ_2^0 quanta are completely unphysical, for the corresponding conservation law in that case is not a rigorous one. Always assuming the correctness of our model of the θ^0, we still have the θ^0 and $\bar{\theta}^0$ as the primary objects in production phenomena. But we shall now show that the decay process is best described in terms of θ_1^0 and θ_2^0.

The weak interactions, in fact, must lead to very different patterns of decay for the θ_1^0 and θ_2^0 into pions and (perhaps) γ rays; any state of pions and/or γ rays that is a possible decay mode for the θ_1^0 is not a possible one for the θ_2^0, and *vice versa*. This is because, according to the postulate of rigorous CC invariance, the quantum number C is conserved in the decay; the θ_1^0 must go into a state that is even under charge conjugation, while the θ_2^0 must go into one that is odd. Since the decay modes are different and even mutually exclusive for the θ_1^0 and θ_2^0, their rates of decay must be quite unrelated. There are thus two independent lifetimes, one for the θ_1^0, and one for the θ_2^0.

An important illustration of the difference in decay modes of the θ_1^0 and θ_2^0 is provided by the two-pion disintegration. We know that reaction (3) occurs; therefore at least one of the two quanta θ_1^0 and θ_2^0, say θ_1^0, must be capable of decay into two charged pions. The final state of the two pions in the θ_1^0 decay is then even under charge conjugation like the θ_1^0 state itself. These two pions are thus in a state of even relative angular momentum and therefore of even parity. So the θ_1^0 must have even spin and even parity. Now we assume that the θ^0 has a definite intrinsic parity, and therefore the parity and spin of the θ_2^0 must be the same as those of the θ_1^0, both even. If the θ_2^0 were to decay into two pions, these would again be in a state of even relative angular momentum and thus even with respect to charge conjugation. However, the θ_2^0 is itself odd under charge conjugation; its decay into two pions is therefore forbidden.

Alternatively, if the θ_2^0 is the one that actually goes into two pions, then the spin and parity of θ_1^0 and the θ_2^0 are both odd, and so the θ_1^0 cannot decay into two pions.

Of the θ_1^0 and the θ_2^0, that one for which the two-pion decay is forbidden may go instead into $\pi^+ + \pi^- + \gamma$ or possibly into three pions (unless the spin and parity of the θ^0 are 0^+), etc.

While we have seen that the θ_1^0 and θ_2^0 may each be assigned a lifetime, this is evidently not true of the θ^0 or $\bar{\theta}^0$. Since we should properly reserve the word "particle" for an object with a unique lifetime, it is the θ_1^0 and θ_2^0 quanta that are the true "particles". The θ^0 and the $\bar{\theta}^0$ must, strictly speaking, be considered as "particle mixtures."

It should be remarked that the θ_1^0 and the θ_2^0 differ not only in lifetime but also in mass, though the mass difference is surely tiny. The weak interactions responsible for decay cause the θ_1^0 and the θ_2^0 to have their respective small level widths and correspondingly must produce small level shifts which are different for the two particles.

To sum up, our picture of the θ^0 implies that it is a particle mixture exhibiting two distinct lifetimes, that each lifetime is associated with a different set of decay modes, and that *not more than half of all θ^0's* can undergo the familiar decay into two pions.[6]

We know experimentally that the lifetime τ for the decay mode (3) (and hence for all decay modes that may compete with this one) is about 1.5×10^{-10} sec. The present qualitative considerations, even if at all correct in their underlying assumptions, do not enable us to predict the value of the "second lifetime" τ' of the θ^0. Nevertheless, the examples given above of decays responsible for the second lifetime lead one to suspect that[7] $\tau' \gg \tau$. As an illustration of the experimental implications of this situation consider the study of the reaction $\pi^- + P \rightarrow \Lambda^0 + \theta^0$ in a cloud chamber. If the reaction occurs and subsequently $\Lambda^0 \rightarrow P + \pi^-$, $\theta^0 \rightarrow \pi^+ + \pi^-$, there should be a reasonable chance to observe this whole course of events in the chamber, as the lifetime for the Λ^0 decay ($\sim 3.5\times10^{-10}$ sec) is comparable to τ. However, if it is true that $\tau' \gg \tau$, it would be very difficult to detect the decay with the second lifetime in the cloud chamber with its characteristic bias for a limited region of lifetime values.[8] Clearly this also means an additional complication in the determination from cloud chamber data as to whether or not production always occurs in an associated fashion. In some such cases the analysis of the reaction $\pi^- + P \rightarrow \Lambda^0 + ?$ may still be pushed further, however, if one assumes that besides the Λ^0 only one other neutral object is formed.[9]

At any rate, the point to be emphasized is this: a neutral boson may exist which has the characteristic θ^0 mass but a lifetime $\neq \tau$ and which may find its natural place in the present picture as the second component of the θ^0 mixture.

One of us, (M. G.-M.), wishes to thank Professor E. Fermi for a stimulating discussion.

[6] Note that if the spin and parity of the θ^0 are even, then the θ_1^0 may decay into $2\pi^0$'s as well as into $\pi^+ + \pi^-$.

[7] The process $\theta^0 \rightarrow \pi^+ + \pi^- + \gamma$ may occur as a radiative correction to the allowed decay into $\pi^+ + \pi^-$ connected with the lifetime τ; see S. B. Treiman, Phys. Rev. **95**, 1360 (1954). The process may also occur as one of the principal decay modes associated with the second lifetime τ'. The latter case may be distinguished from the former not only by the distinct lifetime but also by a different energy spectrum which probably favors higher γ-ray energies; such a spectrum is to be expected in a case where the emission of the γ ray is not just part of the "infrared catastrophe", but is an integral part of the decay process.

[8] See, e.g., Leighton, Wanlass, and Anderson, Phys. Rev. **89**, 148 (1953), Sec. III.

[9] See Fowler, Shutt, Thorndike, and Whittemore, Phys. Rev. **91**, 1287 (1953).

Functional Analysis and Strong-Coupling Theory

J. HAMILTON
Christ's College, Cambridge, England
(Received November 19, 1954)

The relation of functional analysis to the Hamiltonian approach to strongly interacting quantized fields is examined. The propagation of fermions in an external unquantized boson field provides the basis for the solutions, as in the Green function method. The functional method may be useful in studying real nucleons and bound states.

FUNCTIONAL methods have recently been used by Edwards and Peierls[1] to derive an approximation to Green's function for the propagation of a nucleon including radiative corrections from Green's function for the propagation in an external field; their method is a development of the technique invented by Schwinger.[2] Matthews and Salam[3] have shown how the work of Edwards and Peierls may be extended; they derive the complete Green function for nucleon propagation by using functional integrations of the type first used in field theory by Feynman.[4] These functional techniques, which are deduced from the quantum-mechanical form of the action principle, have been developed in the hope that they will make possible approximation methods other than perturbation theory; however, the difficulties in using these methods are considerable, and there is no easy way of estimating the accuracy of any suggested approximate solution.

The functional methods of Schwinger and Feynman have all the advantages of covariant formulation, but they are necessarily difficult to apply to fields which interact strongly. The functional method can be introduced more easily in a simple single-time approach to the problem of strongly interacting fields; in fact the direct approach using the Hamiltonian appears to require the notion of propagation in an external field and a functional procedure. The form of the resulting equations suggests that they might be more suitable for approximations to strongly bound states and to real nucleon states.

As an example we use the theory of nucleons and charged pseudoscalar mesons with a charge independent pseudoscalar coupling. The Hamiltonian $\mathbf{H}$ is given by

$$\mathbf{H}=\mathbf{H}_M+\mathbf{H}_I+\mathbf{H}_N,$$

with

$$\mathbf{H}_M=\tfrac{1}{2}\int d^3\mathbf{x}\{\boldsymbol{\pi}\cdot\boldsymbol{\pi}+c^2(\mathrm{grad}\boldsymbol{\phi}\cdot\mathrm{grad}\boldsymbol{\phi})+c^2\mu^2(\boldsymbol{\phi}\cdot\boldsymbol{\phi})\},$$

$$\mathbf{H}_N=\hbar c\int d^3\mathbf{x}\{\bar{\psi}(\boldsymbol{\gamma}\cdot\mathrm{grad})\psi+\kappa\bar{\psi}\psi\}, \tag{1}$$

$$\mathbf{H}_I=\frac{ig}{\sqrt{2}}\int d^3\mathbf{x}\bar{\psi}(\boldsymbol{\tau}\cdot\boldsymbol{\phi})\gamma^5\psi,$$

$\boldsymbol{\phi}=(\phi_1,\phi_2,\phi_3)$, $\boldsymbol{\pi}=(\pi_1,\pi_2,\pi_3)$ are Hermitian vectors in isotopic space; $\boldsymbol{\tau}\times\boldsymbol{\tau}=2i\boldsymbol{\tau}$, $\tau_j^2=I$ $(j=1, 2, 3)$; and $\bar{\psi}, \psi$ are 8-component nucleon variables $(\bar{\psi}=\psi^\dagger\gamma^4)$. The commutation relations are given at one time t (and all manipulations are carried out at this time):

$$\begin{aligned}
&[\boldsymbol{\pi}(\mathbf{x},t), \boldsymbol{\pi}(\mathbf{x}',t)]_-=0=[\boldsymbol{\phi}(\mathbf{x},t), \boldsymbol{\phi}(\mathbf{x}',t)]_-,\\
&[\pi_j(\mathbf{x},t), \phi_k(\mathbf{x}',t)]_-=-i\hbar\delta_{jk}\delta^{(3)}(\mathbf{x}-\mathbf{x}');\\
&[\bar{\psi}(\mathbf{x},t), \bar{\psi}(\mathbf{x}',t)]_+=0=[\psi(\mathbf{x},t), \psi(\mathbf{x}',t)]_+,\\
&[\bar{\psi}_\sigma(\mathbf{x},t), \psi_\rho(\mathbf{x}',t)]_+=\delta_{\sigma\rho}\delta^{(3)}(\mathbf{x}-\mathbf{x}').
\end{aligned} \tag{2}$$

$\mathbf{H}_N$ and $\mathbf{H}_I$ could be written in a charge self-conjugate form, rather than (1), but that is not necessary for the discussion.

In perturbation theory the problem of finding the eigenstates Ψ of $\mathbf{H}$ is solved by first diagonalizing $\mathbf{H}_M+\mathbf{H}_N$, while in any strong-coupling theory it is essential to try first to solve the eigenstate problem either for $\mathbf{H}_M+\mathbf{H}_I$ or for $\mathbf{H}_N+\mathbf{H}_I$. The strong-coupling method of Wentzel[5,6] and the intermediate-coupling method of Tomonaga[6-8] start from $\mathbf{H}_M+\mathbf{H}_I$, so that the nucleon recoil has to be added as a perturbation. Apart from the difficulty of allowing for nucleon recoil, these theories become very complicated because of the nature of the nucleon source functions which appear in $\mathbf{H}_I$. Because the three components $\bar{\psi}\tau_j\gamma^5\psi$ do not commute, it is not possible in practice to diagonalize $\mathbf{H}_M+\mathbf{H}_I$ by a single canonical transformation; as a result, any effective manipulation is very difficult. (Scalar or pseudoscalar uncharged meson theory with the simplest coupling has only one component $\bar{\psi}\psi$ or $\bar{\psi}\gamma^5\psi$ occuring in $\mathbf{H}_I$, and a simple canonical transformation solves the problem[9]—apart from nucleon recoil.)

The advantage of first diagonalizing $\mathbf{H}_N+\mathbf{H}_I$ is that the meson variables $\boldsymbol{\phi}(\mathbf{x},t)$ which appear in $\mathbf{H}_I$ commute with each other and with all nucleon variables; the $\boldsymbol{\phi}(\mathbf{x},t)$ can therefore be treated as functions (not operators) in $\mathbf{H}_N+\mathbf{H}_I$, and they will be written $\boldsymbol{\phi}'(\mathbf{x})$ to indicate that they are eigenvalues. The nucleon eigenstates $\Psi_N[\boldsymbol{\phi}']$ and eigenvalues $E[\boldsymbol{\phi}']$ determined

[1] S. F. Edwards and R. E. Peierls, Proc. Roy. Soc. (London) A224, 24 (1954).
[2] J. Schwinger, Proc. Nat. Acad. Sci. U. S. 37, 452 (1951).
[3] P. T. Matthews and A. Salam, Nuovo cimento 12, 563 (1954).
[4] R. P. Feynman, Phys. Rev. 80, 440 (1950); see especially pages 449 and 450.
[5] G. Wentzel, Helv. Phys. Acta 13, 269 (1940).
[6] S. Tomonaga, Progr. Theoret. Phys. (Japan) 2, 6, 63 (1947).
[7] K. M. Watson and E. W. Hart, Phys. Rev. 79, 918 (1950).
[8] For a list of references see T. Tati, Progr. Theoret. Phys. (Japan) 10, 421 (1953).
[9] G. Wentzel, *Quantum Theory of Fields* (Interscience Publications, New York, 1949), Sec. 7.

by

$$(\mathbf{H}_N+\mathbf{H}_I[\boldsymbol{\phi}'])\Psi_N[\boldsymbol{\phi}']=E[\boldsymbol{\phi}']\Psi_N[\boldsymbol{\phi}'] \quad (3)$$

are functionals of $\boldsymbol{\phi}'(\mathbf{x})$. They obviously describe the behavior of the nucleon field in an external meson field $\boldsymbol{\phi}'(\mathbf{x})$.

The solutions of

$$\mathbf{H}\Psi=E\Psi \quad (4)$$

are directly related to the solutions of (3). We use a representation for Ψ specified by some complete set of eigenvalues for the nucleons, and by $\boldsymbol{\phi}'(\mathbf{x})$. $\mathbf{H}_M$ behaves like a number insofar as the nucleon components of Ψ are concerned, but it has nonzero matrix elements between states with different $\boldsymbol{\phi}'(\mathbf{x})$. The solution Ψ can therefore be written

$$\Psi=\sum_{S(\phi')} a[\boldsymbol{\phi}']\Psi_N[\boldsymbol{\phi}'], \quad (5)$$

where $\Psi_N[\boldsymbol{\phi}']$ is a normalized solution of (3). For the moment we relax the condition that $\Psi_N[\boldsymbol{\phi}']$ is normalized and write

$$\Psi=\sum_{S(\phi')} \Psi_N[\boldsymbol{\phi}']. \quad (6)$$

$S(\phi')$ is some set of functions $\boldsymbol{\phi}'(\mathbf{x})$ over which the summation is to be carried out. The set $S(\phi')$ need only be large enough to ensure that (8) below has a solution, or an approximate solution; one advantage of this method over that of Edwards and Peierls[1] is that nonenumerable sums need not appear.

The solution of (4) is thus

$$\sum_{S(\phi')} \mathbf{H}_M\Psi_N[\boldsymbol{\phi}']=\sum_{S(\phi')} (E-E[\boldsymbol{\phi}'])\Psi_N[\boldsymbol{\phi}']. \quad (7)$$

In this representation

$$\boldsymbol{\pi}(\mathbf{x})=\frac{\hbar}{i}\frac{\delta}{\delta\boldsymbol{\phi}(\mathbf{x})},$$

and (7) gives the eigenvalue equation

$$\sum_{S(\phi')} \tfrac{1}{2}\int d^3\mathbf{x}\left\{\left(\frac{\hbar}{i}\right)^2 \frac{\delta}{\delta\boldsymbol{\phi}'(\mathbf{x})}\cdot\frac{\delta}{\delta\boldsymbol{\phi}'(\mathbf{x})} + c^2(\operatorname{grad}\boldsymbol{\phi}'(\mathbf{x})\cdot\operatorname{grad}\boldsymbol{\phi}'(\mathbf{x}))+c^2\mu^2\boldsymbol{\phi}'(\mathbf{x})\cdot\boldsymbol{\phi}'(\mathbf{x})\right\}\Psi_N[\boldsymbol{\phi}'] = \sum_{S(\phi')} (E-E[\boldsymbol{\phi}'])\Psi_N[\boldsymbol{\phi}'], \quad (8)$$

with the eigenstate Ψ given by (6).

It is easy to derive equations equivalent to (8) for other representations; for example, with operators $\mathbf{q}_\mathbf{k}$, $\mathbf{p}_\mathbf{k}$ given by

$$\boldsymbol{\phi}(\mathbf{x})=\sum_\mathbf{k} \mathbf{q}_\mathbf{k}e^{i\mathbf{k}\cdot\mathbf{x}}, \quad \boldsymbol{\pi}(\mathbf{x})=\sum_\mathbf{k} \mathbf{p}_\mathbf{k}e^{-i\mathbf{k}\cdot\mathbf{x}},$$

the eigenvalues $\mathbf{q}_\mathbf{k}'$ can be used to label the boson component, and an equation similar to (8) with $\mathbf{p}_\mathbf{k}$ replaced by $(\hbar/i)(\delta/\delta\mathbf{q}_\mathbf{k})$ is obtained.

Some idea of the techniques which are required may be obtained by looking at the degenerate case in which g vanishes [see (1)]. The solution of (3) is $\Psi_N[\boldsymbol{\phi}']=\Psi_N$, $E[\boldsymbol{\phi}']=E_N$, and (5) becomes

$$\Psi=\sum_{S(\phi')} a[\boldsymbol{\phi}']\Psi_N.$$

In (8) the term $(\operatorname{grad}\boldsymbol{\phi}'(\mathbf{x})\cdot\operatorname{grad}\boldsymbol{\phi}'(\mathbf{x}))$ can be replaced by $-\boldsymbol{\phi}'(\mathbf{x})\cdot\nabla^2\boldsymbol{\phi}'(\mathbf{x})$, and the summation over $\boldsymbol{\phi}'$ can be limited to the set $S_k(\phi')$ of normalized functions $\boldsymbol{\phi}'(\mathbf{x})$ for which

$$\nabla^2\boldsymbol{\phi}'(\mathbf{x})+\mathbf{k}^2\boldsymbol{\phi}'(\mathbf{x})=0, \quad (\mathbf{k} \text{ real}).$$

Equation (8) reduces to

$$\sum_{S_k(\phi')} \tfrac{1}{2}\int d^3\mathbf{x}\left\{-\hbar^2\frac{\delta}{\delta\boldsymbol{\phi}'(\mathbf{x})}\cdot\frac{\delta}{\delta\boldsymbol{\phi}'(\mathbf{x})} +c^2(\mathbf{k}^2+\mu^2)\boldsymbol{\phi}'(\mathbf{x})\cdot\boldsymbol{\phi}'(\mathbf{x})\right\}a[\boldsymbol{\phi}']=E_M\sum_{S_k(\phi')} a[\boldsymbol{\phi}'],$$

where $E_M=E-E_N$. The set $S_k(\boldsymbol{\phi}')$ can be reduced to a single function:

$$a[\boldsymbol{\phi}']=\prod_{j=1}^{3} f(\phi_j'),$$

and a particular solution is

$$f(\phi_j)=\exp(-\tfrac{1}{2}y_j),$$

$$y_j=\left(\frac{c^2(\mathbf{k}^2+\mu^2)}{\hbar^2}\right)^{\frac{1}{2}}\int d^3\mathbf{x}\phi_j^2(\mathbf{x}).$$

In general the choice of the set $S(\phi')$ has to be varied according to the solution which is required; for example, to study real nucleons, functions $\boldsymbol{\phi}'(\mathbf{x})$ which are nonzero only near $\mathbf{x}=0$ are required. The interpretation of the eigenstates Ψ given by (6) and (8) is obtained by classifying the solutions by the eigenvalues of those operators which commute with $\mathbf{H}$. The vacuum state should be the eigenstate of least energy. Further details of the method will be given elsewhere.

Note added in proof.—Equation (9) is separable and its solutions can be studied by assigning $\phi'(\mathbf{x}_s)$ to the sth cell of space. If a cell is of volume $\delta\mathbf{x}$, a solution is $f[\phi_j']=\Pi_s f_s(\phi_j(\mathbf{x}_s))$ with $f_s(\phi_j)=H_N(Z)\ \exp(-\frac{1}{2}Z^2)$. $Z=(\delta\mathbf{x}\cdot c/\hbar)^{\frac{1}{2}}(\mathbf{k}^2+\mu^2)^{\frac{1}{4}}\phi_j(\mathbf{x}_s)$.

Boson-Fermion Scattering in the Heisenberg Representation*

F. E. Low
University of Illinois, Urbana, Illinois†
(Received October 27, 1954)

It is shown that the S-matrix for boson-fermion scattering can be simply expressed in the Heisenberg representation. By performing a time integration one obtains the S-matrix in the Schrödinger representation, which has the same form as the conventional perturbation theory sum over states. Suitably limiting the nature of the intermediate states entering into this sum leads to integral equations for certain matrix elements which are equal to the S-matrix elements on the energy shell. These equations appear in a completely renormalized form. For example, in the fixed source limit, the four pion-nucleon scattering states satisfy the same equation (with different numerical coefficients). The equations are nonlinear, but involve only the scattering phase shifts. The equivalent equation for photopion production is linear, and in the fixed source limit can be written down from a knowledge of the experimental scattering phase shifts. The zero-pion-mass theorems of Gell-Mann and Goldberger (concerning the isotopic spin independence of the zero-energy S-wave scattering) and of Kroll and Ruderman, [Phys. Rev. **93**, 233 (1954)] follow simply from the formalism.

1. EQUATION FOR THE S-MATRIX

WE shall for simplicity derive our results for only one process: the scattering of symmetric pseudoscalar mesons by a nucleon. The method is easily generalizable to other processes of interest: in Sec. II we state without proof the results for Compton scattering and photopion production.

We start from Dyson's definition[1] of the S-matrix for the scattering of an ith meson in momentum state q to a jth meson in state q', the scattering nucleon going from p to p'[2]:

$$S=\sum_{n=0}^{\infty}\frac{(-i)^n}{n!}\int dt_1\cdots dt_n(\Phi_{p'},a_j(q')\times P[H_I(t_1)\cdots H_I(t_n)]a_i^*(q)\Phi_p). \quad (1.1)$$

Here P is Dyson's time-ordering operator and a^* and a are, respectively, creation and annihilation operators for single mesons. Also

$$H_I=ig\int\bar{\psi}(x)\gamma_5\tau_i\psi(x)\phi_i(x)d\tau_x-\delta m\int\bar{\psi}(x)\psi(x)d\tau_x-\tfrac{1}{2}\delta\mu^2\int\phi_i(x)\phi_i(x)d\tau_x+\tfrac{1}{4}\lambda\int[\phi_i(x)\phi_i(x)]^2d\tau_x. \quad (1.2)$$

We proceed by commuting $a_i^*(q)$ through to the left and $a_j(q')$ through to the right in Eq. (1.1). Since

$$[\phi_k(x),a_i^*(q)]=\delta_{ki}e^{iqx}/(2q_0)^{\frac{1}{2}} \quad (1.3)$$

and

$$[a_j(q'),\phi_k(x)]=\delta_{kj}e^{-iq'x}/(2q_0)^{\frac{1}{2}}, \quad (1.4)$$

we obtain (for $q\neq q'$ and $p\neq p'$):

$$S=-i\int\frac{dxe^{iqx}}{(2q_0)^{\frac{1}{2}}}\Big(\Phi_{p'},a_j(q')\sum_{n=0}^{\infty}\frac{(-i)^n}{n!}\int dt_1\cdots dt_n\times P[H_I(t_1),\cdots H_I(t_n),O_i(x)]\Phi_p\Big), \quad (1.5)$$

$$S=(-i)^2\int\frac{dxdy}{(4q_0q_0')^{\frac{1}{2}}}e^{iqx}e^{-iq'y}\times\Big(\Phi_{p'},\sum_{n=0}^{\infty}\frac{(-i)^n}{n!}\int dt_1\cdots dt_n\times P[H_I(t_1),\cdots,H_I(t_n),O_j(y),O_i(x)]\Phi_p\Big)$$
$$-i\lambda\int\frac{dxe^{i(q-q')x}}{(4q_0q_0')^{\frac{1}{2}}}\Big(\Phi_{p'},\sum_{n=0}^{\infty}\frac{(-i)^n}{n!}\int dt_1\cdots dt_n\times P[H_I(t_1),\cdots H_I(t_n),\phi_k(x)\phi_k(x)\delta_{ij}+2\phi_i(x)\phi_j(x)]\Phi_p\Big), \quad (1.6)$$

where

$$O_i(x)=ig\bar{\psi}(x)\gamma_5\tau_i\psi(x)-\delta\mu^2\phi_i(x)+\lambda\phi_i(x)\phi_k(x)\phi_k(x).$$

Equation (1.6) can now be transformed by recognizing that an expression of the form

$$\Big(\Phi_{p'},\sum_{n=0}^{\infty}\frac{(-i)^n}{n!}\int dt_1\cdots dt_n\times P[H_I(t_1),\cdots,H_I(t_n),A_1(x),A_2(y),\cdots]\Phi_p\Big), \quad (1.7)$$

(where the A_α's are functions of the field variables at the

* Work supported in part by the joint program of the Office of Naval Research and the U. S. Atomic Energy Commission.

† Part of this work was done while the author was a visiting Associate Physicist at Brookhaven National Laboratory. The author would like to thank the Laboratory for hospitality.

[1] F. J. Dyson, Phys. Rev. **75**, 1737 (1949).

[2] Throughout this section we shall distinguish Heisenberg operators from interaction representation operators by using boldface type (A) for the former. State vectors are represented by capital Greek letters. Φ_p is an eigenstate of the unperturbed Hamiltonian of momentum p_i and energy $p_0=(p_i^2+m)^{\frac{1}{2}}$, where m is the observed Fermion mass. Ψ_p is an eigenstate of the total Hamiltonian with the same momentum and energy. A four-vector inner product is written $px=p_\mu x_\mu=p_ix_i-p_0x_0=\mathbf{p}\cdot\mathbf{x}-p_0x_0$. The subscripts i, j, k, etc., refer to the space-like components of a four-vector as well as to isotopic spin indices. Integrations over three-dimensional volumes are written $\int d\tau_x$, over four-dimensional volumes $\int dx$.

points x, y, etc., but not of their time derivatives) can be written equally well

$$(\Psi_{p'}, P[\mathbf{A}_1(x), \mathbf{A}_2(y)]\Psi_p), \tag{1.8}$$

where the operators $\mathbf{A}_\alpha(x)$ now have Heisenberg representation time dependence and the Ψ_p's are exact single-particle energy-momentum eigenstates of the entire Hamiltonian.

The identity of (1.7) and (1.8) may be proved in two ways. The first consists in calculating the scattering of a free nucleon by an arbitrary external symmetric pseudoscalar field, $\phi_i^{(e)}(x)$, both in the Heisenberg and interaction representations and equating the coefficients of $\phi_i^{(e)}(x)\phi_j^{(e)}(y)$ under the integral in the two forms of the S-matrix. The second is a direct calculation of the type used by Gell-Mann and the author.[3] Their proof was given for vacuum expectations of ordered products, but applies to other eigenstates provided the self-mass is properly subtracted from the interaction Hamiltonian so that there is no self-energy of these states.

We may therefore rewrite Eq. (1.6):

$$S=\int \frac{e^{iqx}e^{-iq'y}}{(4q_0q_0')^{\frac{1}{2}}}dxdy\{-(\Psi_{p'}, P[\mathbf{O}_j(y), \mathbf{O}_i(x)]\Psi_p) - i\delta(x-y)\lambda(\Psi_{p'}, [\delta_{ij}\phi_k(x)\phi_k(x) + 2\phi_i(x)\phi_j(x)]\Psi_p)\}. \tag{1.9}$$

If it were not for renormalization terms, the first-matrix element in Eq. (1.9) would be simply the time-ordered product of the interaction densities. With a $\delta\mu^2$ and a λ term, however, it is actually the combination that appears there that is simple, since the meson field satisfies the equation of motion:

$$(\Box^2-\mu_0^2)\phi_i(x)=ig\bar{\psi}(x)\gamma_5\tau_i\psi(x)+\lambda\phi_i(x)\phi_k(x)\phi_k(x),$$

or

$$(\Box^2-\mu^2)\phi_i(x)=ig\bar{\psi}(x)\gamma_5\tau_i\psi(x) + \lambda\phi_i(x)\phi_k(x)\phi_k(x)-\delta\mu^2\phi_i(x) \equiv \mathbf{O}_i(x), \tag{1.10}$$

where μ is the renormalized meson mass. Our final formula is thus

$$S=-\int \frac{e^{iqx}e^{-iq'y}}{(4q_0q_0')^{\frac{1}{2}}}dxdy \times(\Psi_{p'}, \{P[(\Box^2-\mu^2)\phi_j(y), (\Box^2-\mu^2)\phi_i(x)] + i\lambda\delta(x-y)[\delta_{ij}\phi_k(x)\phi_k(x) + 2\phi_i(x)\phi_j(x)]\}\Psi_p).^4 \tag{1.11}$$

[3] M. Gell-Mann and F. Low, Phys. Rev. 84, 350 (1951).

[4] The author has learned from Professor Goldberger and Professor Nambu that they have separately obtained results substantially equivalent to this equation.

The theorem of Gell-Mann and Goldgerger follows simply from Eq. (1.11). Ignoring the trivial normalization factor $(4q_0q_0')^{\frac{1}{2}}$, it is obvious that

$$\langle q', j|S|q, i\rangle=\langle -q, i|S|-q', j\rangle,$$

so that for $q'=-q=0$ (which is only possible for $\mu=0$) $\langle j|S|i\rangle=\langle i|S|j\rangle$ and the scattering is a symmetric function of i and j. It must therefore be a multiple of δ_{ij} and independent of isotopic spin to this approximation.

2. DISCUSSION OF THE RESULT

Before further discussion of our result we list similar formulas for two other scattering processes. Their derivation is completely analogous to that given in Sec. I for meson-nucleon scattering.

A. Compton scattering (by a nucleon interacting with pions)

$$S=\frac{e_i'e_j}{(4k_0k_0')^{\frac{1}{2}}}\Big[-2ie^2\delta_{ij}\int e^{i(k-k')x}(\Psi_{p'}, \phi^*(x)\phi(x)\Psi_p) - \int dxdye^{ikx}e^{-ik'y}(\Psi_{p'}, P[\mathbf{j}_i(y), \mathbf{j}_j(x)]\Psi_p)\Big]. \tag{2.1}$$

Here k_μ' and e_i' are the final photon four-momentum and polarization, k_μ and e_i the initial photon four-momentum and polarization. $\phi(x)$ and $\phi^*(x)$ are the charged meson field operators, and $\mathbf{j}_i(x)$ is the current density operator.

B. Photopion production (to lowest order in e)

$$S\begin{Bmatrix}0\\+\\-\end{Bmatrix}=\frac{ie_j}{(4q_0k_0)^{\frac{1}{2}}}\int dxe^{ikx} \times\Big[e^{-iqx}2eq_j\Big(\Psi_{p'}, \begin{Bmatrix}0\\ \phi(x)\\ -\phi^*(x)\end{Bmatrix}\Psi_p\Big) -i\int dye^{-iqy}\Big(\Psi_{p'}, P\Big[(\Box^2-\mu^2) \times\begin{Bmatrix}\phi_3(y)\\ \phi(y)\\ \phi^*(y)\end{Bmatrix}, \mathbf{j}_j(x)\Big]\Psi_p\Big)\Big]. \tag{2.2}$$

Here q_μ is the meson four-momentum, k_μ and e_j the photon four-momentum and polarization. The curly brackets represent the cases {neutral, positive, negative} production. Also $\mathbf{j}_j(x)$ and ϕ, ϕ^* have the same meaning as in Eq. (2.1).

As to renormalization: the two terms in Eq. (1.11) are not separately finite. Part of the λ term must be used to cancel a 4-meson divergence arising from the $[(\Box^2-\mu^2)\phi]^2$ term. Essentially the same is true of Eq. (2.1), where divergences in the two terms cancel against each other. To lowest order in e^2, however, each term of

Eq. (2.1) is finite as it stands if the matrix-elements are expressed in terms of the renormalized coupling constant g_c and the renormalized nucleon and meson masses. In Eq. (2.2) [as well as in Eq. (1.11)], a further renormalization is necessary, one which in any practical calculation can be done with no difficulty. That is, each meson operator $\phi_i(x)$ must be divided by the mesonic wave-function renormalization, $Z_3^{\frac{1}{2}}$. This extra factor is introduced because of the well-known ambiguous limit,

$$A=\lim_{q^2+\mu^2\to 0}(q^2+\mu^2)\Delta_F'(q),$$

which arises in calculating outgoing or incoming meson lines in the S-matrix. Our calculation is such that we first performed the multiplication and then took the limit as $\mu^2+q^2\to 0$. The result of this limiting order is $A=Z_3$. It is well known[2] that A must be set equal to $Z_3^{\frac{1}{2}}$ in order for the renormalization program to work, and plausible arguments can be given for this choice. This problem is not of immediate interest here, since it is already present in the conventional definition of the S-matrix [Eq. (1.1)]. The extra factor $Z_3^{\frac{1}{2}}$ is easily recognized and removed in any calculation.

In order to make practical use of the Eqs. (1.11), (2.1), and (2.2) it is convenient to transform them to the Schrödinger representation. This is accomplished by making explicit use of the Heisenberg representation time dependence

$$\mathbf{A}(x)=\mathbf{A}(x_i, x_0)=e^{iHx_0}\mathbf{A}(x_i, 0)e^{-iHx_0}$$
$$=e^{iHx_0}\mathbf{A}(\mathbf{x})e^{-iHx_0},$$

where $A(\mathbf{x})=\mathbf{A}(x_i, 0)$ is the Schrödinger representation operator function of the space coordinate $x_i=\mathbf{x}$.

Thus an expression of the form

$$\int e^{ikx}dx(\Psi_{p'}, \mathbf{A}(x)\Psi_p) \tag{2.3}$$

is given by

$$\int e^{ikx}dx(\Psi_{p'}, \mathbf{A}(x)\Psi_p)$$
$$=\int dx e^{ikx}(\Psi_{p'}, e^{iHx_0}A(\mathbf{x})e^{-iHx_0}\Psi_p)$$
$$=\int dx_0 e^{-ik_0x_0}e^{ip_0'x_0}e^{-ip_0x_0}\times\int d\tau_x(\Psi_{p'}, A(\mathbf{x})\Psi_p)e^{i\mathbf{k}\cdot\mathbf{x}}$$
$$=2\pi\delta(k_0+p_0-p_0')\int d\tau_x(\Psi_{p'}, A(\mathbf{x})\Psi_p)e^{i\mathbf{k}\cdot\mathbf{x}}, \tag{2.4}$$

whereas one of the form

$$\int dxdy e^{ikx}e^{-iqy}(\Psi_{p'}, P[\mathbf{A}(x), \mathbf{B}(y)]\Psi_p)$$

is given by

$$\int dxdy e^{ikx}e^{-iqy}(\Psi_{p'}, P[\mathbf{A}(x), \mathbf{B}(y)]\Psi_p)$$
$$=\frac{2\pi}{i}\delta(k_0-q_0+p_0-p_0')\Bigg(\Psi_{p'}, \Bigg[\int d\tau_x e^{i\mathbf{k}\cdot\mathbf{x}}A(\mathbf{x})\frac{1}{H-p_0+q_0-i\alpha}\int d\tau_y e^{-i\mathbf{q}\cdot\mathbf{y}}B(\mathbf{y})$$
$$+\int d\tau_y e^{-i\mathbf{q}\cdot\mathbf{y}}B(\mathbf{y})\frac{1}{H-p_0-k_0-i\alpha}\int d\tau_x e^{i\mathbf{k}\cdot\mathbf{x}}A(\mathbf{x})\Bigg]\Psi_p\Bigg)$$
$$=\frac{2\pi}{i}\delta(k_0-q_0+p_0-p_0')\sum_n\Bigg[\frac{\left(\Psi_{p'}, \int d\tau_x e^{i\mathbf{k}\cdot\mathbf{x}}A(\mathbf{x})\Psi_n\right)\left(\Psi_n, \int d\tau_y e^{-i\mathbf{q}\cdot\mathbf{y}}B(\mathbf{y})\Psi_p\right)}{E_n-p_0+q_0-i\alpha}$$
$$+\frac{\left(\Psi_{p'}, \int d\tau_y e^{-i\mathbf{q}\cdot\mathbf{y}}B(\mathbf{y})\Psi_n\right)\left(\Psi_n, \int d\tau_x e^{i\mathbf{k}\cdot\mathbf{x}}A(\mathbf{x})\Psi_p\right)}{E_n-p_0-k_0-i\alpha}\Bigg]. \tag{2.5}$$

The sum is over the complete set of stationary states Ψ_n of the Hamiltonian.

By means of Eqs. (2.4) and (2.5) we see immediately that the scattering matrix elements occurring in Eq. (1.11), Eq. (2.1), and Eq. (2.2) can be written as sums over states in a manner strongly reminiscent of old-fashioned first- and second-order perturbation theory. There are two essential but not independent differences:

(a) Every possible intermediate state Ψ_n which is allowed by the conservation laws will enter into the sums.

(b) The matrix elements must be calculated between

exact eigenstates of the Hamiltonian rather than between first approximations to these eigenstates (as is done in perturbation theory). Since the only property of the intermediate states which we have used is their completeness and orthogonality, they may be chosen in the most convenient way; that is, they may have incoming waves or outgoing waves or any other boundary conditions that leave them all orthogonal.

3. INTEGRAL EQUATIONS FOR PION-NUCLEON SCATTERING

We consider the expression

$$\begin{aligned}\langle p', q, j|O_i(x)|p\rangle &\equiv (\Psi_{p'}{}^{(-)}(q, j), \mathbf{O}_i(x)\Psi_p)\\ &\equiv (\Psi_{p'}{}^{(-)}(q, j), (\Box^2-\mu^2)\phi_i(x)\Psi_p), \quad (3.1)\end{aligned}$$

where $\Psi_{p'}{}^{(-)}(q, j)$ is an incoming wave scattering state whose plane wave part consists of a nucleon of momentum p' and a jth meson in momentum state q. The charge and spin quantum numbers of the nucleon are suppressed in this notation. Now

$$\Psi_{p'}{}^{(-)}(q, j)=U^\dagger(\infty, 0)a_j{}^*(q)\Phi_{p'} \quad (3.2)$$

and $\Psi_p=U(0, -\infty)\Phi_p$, where $U(t_1, t_2)$ is the unitary operator describing the time development of a state vector in the interaction representation.[5] Thus

$$\begin{aligned}&\langle p', q, j|O_i(x)|p\rangle\\ &=(\Phi_{p'}, a_j(q)U(\infty, 0)(\Box^2-\mu^2)\phi_i(x)U(0, -\infty)\Phi_p)\\ &=\Big(\Phi_{p'}, a_j(q)\sum_{n=0}^{\infty}\frac{(-i)^n}{n!}\int dt_1\cdots dt_n\\ &\qquad\times P[H_I(t_1), \cdots, H_I(t_n), O_i(x)]\Phi_p\Big), \quad (3.3)\end{aligned}$$

where, as in Sec. I,

$$O_i(x)=ig\bar\psi(x)\gamma_5\tau_i\psi(x)-\delta\mu^2\phi_i(x)+\lambda\phi_i(x)\phi_k(x)\phi_k(x).$$

Using the same technique as in Sec. I, we commute $a_j(q)$ through the P-bracket in Eq. (3.3). We find easily:

$$\begin{aligned}&\langle p', q, j|O_i(x)|p\rangle\\ &=\frac{\lambda e^{-iqx}}{(2q_0)^{\frac12}}\Big(\Phi_{p'}, \sum_{n=0}^{\infty}\frac{(-i)^n}{n!}\\ &\quad\times\int dt_1\cdots dt_n P[H_I(t_1), \cdots H_I(t_n),\\ &\quad\times\delta_{ij}\phi_k(x)\phi_k(x)+2\phi_i(x)\phi_j(x)]\Phi_p\Big)\\ &\quad-i\int\frac{dye^{-iqy}}{(2q_0)^{\frac12}}\Big(\Phi_{p'}, \sum_{n=0}^{\infty}\frac{(-i)^n}{n!}\int dt_1\cdots dt_n\\ &\quad\times P[H_I(t_1), \cdots, H_I(t_n), O_j(y), O_i(x)]\Phi_p\Big), \quad (3.4)\end{aligned}$$

$$\begin{aligned}&=\frac{\lambda e^{-iqx}}{(2q_0)^{\frac12}}(\Psi_{p'}, [\delta_{ij}\phi_k(x)\phi_k(x)+2\phi_i(x)\phi_j(x)]\Psi_p)\\ &\quad-i\int\frac{e^{-iqy}dy}{(2q_0)^{\frac12}}(\Psi_{p'}, P[\mathbf{O}_j(y), \mathbf{O}_i(x)]\Psi_p). \quad (3.5)\end{aligned}$$

Equation (3.5) follows from Eq. (3.4) by the same arguments as those given in Sec. I [Eqs. (1.7) and (1.8)].

Comparison of Eqs. (3.5) and (1.11) shows that

$$\langle p', q, j|S|p, k, i\rangle=\frac{i}{(2k_0)^{\frac12}}\int e^{ikx}dx\langle p', q, j|O_i(x)|p\rangle, \quad (3.6)$$

so that on the energy shell (i.e., when $p_\lambda'+q_\lambda-p_\lambda=k_\lambda$, where $k_\lambda{}^2+\mu^2=0$) the quantity $\langle p', q, j|O_i(x)|p\rangle$ is essentially the meson-nucleon S-matrix with the delta function of energy and momentum left out. It is not, however, the conventional T-matrix, since in the fixed source limit it depends primarily on the variable q and only trivially on the Fourier transform variable $p_\lambda'+q_\lambda-p_\lambda$, whereas the T-matrix depends nontrivially on both of its variables. It is this fact that makes our integral equation for $\langle p', q, j|O_i|p\rangle$ become, in the fixed source limit, an integral equation for the phase shifts.

We now transform Eq. (3.5) to the Schrödinger representation by performing the y_0 integration. We find, setting $x=0$:

$$\begin{aligned}&\langle p', q, j|O_i(0)|p\rangle\\ &=\frac{\lambda}{(2q_0)^{\frac12}}(\Psi_{p'}, [\delta_{ij}\phi_k(0)\phi_k(0)+2\phi_i(0)\phi_j(0)]\Psi_p)\\ &\quad-\frac{1}{(2q_0)^{\frac12}}\sum_{\substack{n\\ \mathbf{p}_n=\mathbf{p}'+\mathbf{q}}}(\Psi_{p'}, O_j(0)\Psi_n)\\ &\quad\times(\Psi_n, O_i(0)\Psi_p)/(E_n-p_0'-q_0-i\alpha)\\ &\quad-\frac{1}{(2q_0)^{\frac12}}\sum_{\substack{n\\ \mathbf{p}_n=\mathbf{p}-\mathbf{q}}}(\Psi_{p'}, O_i(0)\Psi_n)\\ &\qquad\times(\Psi_n, O_j(0)\Psi_p)/(E_n-p_0+q_0-i\alpha). \quad (3.7)\end{aligned}$$

In Eq. (3.7) the momentum $\mathbf{p}_n$ is the total momentum of the state Ψ_n. The sum is again over all the stationary states of the Hamiltonian.

Equation (3.7) is the first of a series of coupled integral equations which may be derived in a completely analogous manner to the derivation of Eq. (3.7). The iteration procedure is almost obvious for p-wave scattering. (As far as S-wave scattering is concerned this formalism does not appear particularly useful.) We retain, as a first approximation, only the single-nucleon and the single-nucleon plus single-meson intermediate states (and of course drop the λ term). The single-nucleon intermediate states provide an inhomogeneous term; the nucleon-plus-meson states involve the same

[5] M. Gell-Mann and M. Goldberger, Phys. Rev. 91, 398 (1953).

matrix element that appears on the left-hand side of Eq. (3.7).

Now

$$(\Psi_{p'}, O_i(0)\Psi_p)=(\Psi_{p'}, (\Box^2-\mu^2)\phi_i(x)\Psi_p)|_{x=0}$$
$$=-[(p_\lambda'-p_\lambda)^2+\mu^2]$$
$$\times\Delta_{Fc}(p'-p)ig_c\Gamma_{5c}(p', p)\tau_i Z_3^{\frac{1}{2}}, \quad (3.8)$$

where Δ_{Fc} and Γ_{5c} are the renormalized meson-propagation function and nucleon-meson vertex operator, respectively, and g_c is the renormalized coupling constant. In accordance with the discussion of Sec. I we may drop the factor $Z_3^{\frac{1}{2}}$. Furthermore, for $(\Delta p)^2/m^2\ll 1$, $[(\Delta p)^2+\mu^2]\Delta_{Fc}(\Delta p)\approx 1$, and $\Gamma_{5c}(p', p)\approx(\bar{u}(p'), \gamma_5 u(p))$ so that in the nonrelativistic region we will have

$$(\Psi_{p'}, O_i(0)\Psi_p)\approx -ig_c(\bar{u}(p'), \gamma_5\tau_i u(p))$$
$$\approx -\frac{ig_c}{2m}\tau_i\boldsymbol{\sigma}\cdot\Delta\mathbf{p}.$$

Also,

$$(\Psi_{p'}, O_i(0)\Psi_n)=(\Psi_n, O_i(0)\Psi_{p'})^*,$$

since O_i is a self-adjoint operator. Equation (3.7) thus becomes

$$\langle p', q, j|O_i(0)|p\rangle=-\frac{1}{(2q_0)^{\frac{1}{2}}}\sum_{\sigma,\tau}\left[\frac{(\Psi_{p'}, O_j(0)\Psi_{p'+\mathbf{q}}{}^{(\sigma,\tau)})(\Psi_{p'+\mathbf{q}}{}^{(\sigma,\tau)}O_i(0)\Psi_p)}{E(\mathbf{p}'+\mathbf{q})-E(\mathbf{p}')-q_0}\right.$$
$$\left.+\frac{(\Psi_{p'}, O_i(0)\Psi_{\mathbf{p}-\mathbf{q}}{}^{(\sigma,\tau)})(\Psi_{\mathbf{p}-\mathbf{q}}{}^{(\sigma,\tau)}, O_j(0)\Psi_p)}{E(\mathbf{p}-\mathbf{q})-E(\mathbf{p})+q_0}\right]$$
$$-\frac{1}{(2q_0)^{\frac{1}{2}}}\sum_{k=1}^{3}\int\frac{d\tau_{q'}d\tau_{p''}}{(2\pi)^3}\left[\frac{\langle p'', q', k|O_j(0)|p'\rangle^*\langle p'', q', k|O_i(0)|p\rangle\delta(\mathbf{p}''+\mathbf{q}'-\mathbf{p}'-\mathbf{q})}{p_0''+q_0'-p_0'-q_0-i\alpha}\right.$$
$$\left.+\frac{\langle p'', q', k|O_i(0)|p'\rangle^*\langle p'', q', k|O_j(0)|p\rangle\delta(\mathbf{p}''+\mathbf{q}'-\mathbf{p}+\mathbf{q})}{p_0''+q_0'-p_0+q_0}\right], \quad (3.9)$$

where the inhomogeneous term is essentially known, at least for small momenta.

The motivation for including only one-meson intermediate states is twofold. (1) It simplifies the problem. (2) Since the experimental P-wave scattering shows a low-energy resonant behavior, one might hope that the single-meson terms would dominate the sum in Eq. (3.7) for small external meson energy.

It must unfortunately be emphasized that in a theory with strong coupling there is no compelling reason for thinking that this approximation is a good one, as compared, say, with the Tamm-Dancoff scheme, where the successive approximations follow noninteracting states.

Higher approximations can be included in either of two ways: (1) Higher terms in the series (3.7) can be calculated in Born approximation and lumped with the inhomogeneous term in Eq. (3.9), or (2) An analogous calculation to the one leading to Eq. (3.7) can be performed for amplitudes of the form

$$(\Psi_{p'}{}^{(-)}(q_1, q_2, j, k), (\Box^2-\mu^2)\phi_i(x)\Psi_p)$$

and

$$(\Psi_{p'}{}^{(-)}(q_1, j), (\Box^2-\mu^2)\phi_i(x)\Psi_p{}^{(+)}(q_2, k)),$$

etc., leading to integral equations which will be coupled to Eq. (3.9). Arbitrary numbers of pions can be included in this way, although the complexity of the problem increases tremendously with each order. The point we would like to emphasize in favor of our scheme is that, as long as the meson-meson interaction is omitted, together with intermediate states involving pairs, these equations are automatically expressed in terms of the renormalized masses and coupling constant so that no new divergences will appear. This is the main advantage of the present method as contrasted with the Dancoff or Bethe-Salpeter approximation scheme.

In the fixed-source limit, Eq. (3.9) simplifies considerably. The appropriate matrix-element is $\langle q, j, \tau'|O_i(k)|\tau\rangle$, (where $O_i(k)=i(f/\mu)\boldsymbol{\sigma}\cdot\mathbf{k}\tau_i$ and $|\tau\rangle$ is a one-nucleon state), and satisfies the equation

$$\langle q, j, \tau'|O_i(k)|\tau\rangle$$
$$=\frac{1}{(2q_0)^{\frac{1}{2}}}\left[\left(\frac{f}{\mu}\right)^2(\tau_j\tau_i\boldsymbol{\sigma}\cdot\mathbf{q}\boldsymbol{\sigma}\cdot\mathbf{k}-\tau_i\tau_j\boldsymbol{\sigma}\cdot\mathbf{k}\boldsymbol{\sigma}\cdot\mathbf{q})\right]$$
$$-\sum_{l=1}^{3}\sum_{\tau''=1}^{2}\int\frac{d\tau_p}{(2\pi)^3}$$
$$\times\left\{\frac{\langle p, l, \tau''|O_j(q)|\tau'\rangle^*\langle p, l, \tau''|O_i(k)|\tau\rangle}{p_0-q_0-i\alpha}\right.$$
$$\left.+\frac{\langle p, l, \tau''|O_i(k)|\tau'\rangle^*\langle p, l, \tau''|O_j(q)|\tau\rangle}{p_0+q_0}\right\}. \quad (3.10)$$

Here f is the rationalized, renormalized, pseudovector coupling constant.

Equation (3.10) immediately yields an equation for the phase-shifts. We define $g_i(q)=e^{i\delta(q)}\sin\delta(q)$, where $i=1$ stands for the $(\frac{1}{2}, \frac{1}{2})$ state, $i=2$ for the $(\frac{1}{2}, \frac{3}{2})$ and

$(\frac{3}{2}, \frac{1}{2})$ states and $i=3$ for the $(\frac{3}{2}, \frac{3}{2})$ state. Then

$$g_1(q)=-\frac{8}{3}\frac{f^2}{4\pi}\frac{q^3}{\mu^2\omega_q}+\frac{q^3}{\pi}\int\frac{d\omega_p}{p^3}\Big[\frac{|g_1(p)|^2}{\omega_p-\omega_q-i\alpha}+\frac{|g_1(p)|^2-8|g_2(p)|^2+16|g_3(p)|^2}{9(\omega_p+\omega_q)}\Big],$$

$$g_2(q)=-\frac{2}{3}\frac{f^2}{4\pi}\frac{q^3}{\mu^2\omega_q}+\frac{q^3}{\pi}\int\frac{d\omega_p}{p^3}\Big[\frac{|g_2(p)|^2}{\omega_p-\omega_q-i\alpha}+\frac{7|g_2|^2-2|g_1|^2+4|g_3|^2}{9(\omega_p+\omega_q)}\Big], \quad (3.11)$$

$$g_3(q)=\frac{4}{3}\frac{f^2}{4\pi}\frac{q^3}{\mu^2\omega_q}+\frac{q^3}{\pi}\int\frac{d\omega_p}{p^3}\Big[\frac{|g_3(p)|^2}{\omega_p-\omega_q-i\alpha}+\frac{4|g_1|^2+4|g_2|^2+|g_3|^2}{9(\omega_p+\omega_q)}\Big].$$

Here $\omega_p=p_0=(p^2+\mu^2)^{\frac{1}{2}}$.

The coupling of the various amplitudes is not in contradiction with the over-all conservation laws; for example, the $|g_1|^2$ term in the g_3 equation takes into account a self-energy process modifying the $(\frac{3}{2}, \frac{3}{2})$ scattering.

We finally remark that a linear integral equation may be derived for the γ-π production matrix element by methods that are completely analogous to those we have used to obtain Eq. (3.9). In this case we must consider the matrix element $(\Psi_{p'}(q, j), \mathbf{j}(x)\Psi_p)$, where $\mathbf{j}(x)$ is the current density. The inhomogeneous term now consists not only of the contribution of single nucleon states to the sum over states but of the direct production term [essentially the first term in Eq. (2.2)]. The kernel of the equation (if the sum is restricted to single meson states) is just the matrix element $O_i(x)$ which turned up in the meson-scattering problem, and which for the fixed source P-wave theory is trivially related to the scattering phase shift.

The resulting equation for the fixed source theory follows:

$$\begin{aligned}&\langle q, j, \tau'|j_{k\lambda}|\tau\rangle(2q_0)^{\frac{1}{2}}\\&=\frac{ef}{\mu}\Big\langle\tau'\Big|(\delta_{j2}\tau_1-\delta_{j1}\tau_2)\Big(\boldsymbol{\sigma}\cdot\mathbf{e}_\lambda+\frac{2\mathbf{q}\cdot\mathbf{e}_\lambda\boldsymbol{\sigma}\cdot(\mathbf{k}-\mathbf{q})}{(\mathbf{q}-\mathbf{k})^2+\mu^2}\Big)\\&+\frac{f}{\mu q_0}\Big\{[\tau_j\boldsymbol{\sigma}\cdot\mathbf{q}, \boldsymbol{\mu}\times\mathbf{k}\cdot\mathbf{e}_\lambda]\\&-\frac{e(1+\tau_3)}{4m}\mathbf{q}\cdot\mathbf{e}_\lambda i\boldsymbol{\sigma}\cdot\mathbf{q}\tau_j\Big\}\Big|\tau\Big\rangle-\sum_{\tau'',l}\int\frac{d\tau_p}{(2\pi)^3}\\&\times\Big\{\frac{\langle p, l, \tau''|O_j(q)|\tau'\rangle^*\langle p, l, \tau''|j_{k\lambda}|\tau\rangle}{\omega_p-\omega_q-i\alpha}\\&+\frac{\langle p, l, \tau''|j_{k\lambda}|\tau'\rangle^*\langle p, l, \tau''|O_j(q)|\tau\rangle}{\omega_p+\omega_q}\Big\}, \quad (3.12)\end{aligned}$$

where $j_{k\lambda}=\int e^{i\mathbf{k}\cdot\mathbf{x}}\mathbf{j}(x)\cdot\mathbf{e}_\lambda$, $\boldsymbol{\mu}$ is the nucleon magnetic moment operator and $\langle p, l, \tau''|O_j(q)|\tau\rangle$ is the meson-nucleon scattering matrix element that satisfies Eq. (3.10).

4. KROLL-RUDERMAN THEOREM

We shall now show how Eq. (2.2) immediately leads to the Kroll-Ruderman[6] theorem on threshold photoproduction.

At threshold $\mathbf{q}=0$ so that the first term in Eq. (2.2) does not contribute. The S-matrix is thus given by

$$S\begin{Bmatrix}0\\+\\-\end{Bmatrix}=\frac{e_j}{(4q_0k_0)^{\frac{1}{2}}}\int dxdye^{ikx}e^{-iqy}\times\Big(\Psi_{p'}, P\Big[(\Box^2-\mu^2)\begin{Bmatrix}\phi_3(y)\\\phi(y)\\\phi^*(y)\end{Bmatrix}, \mathbf{j}_j(x)\Big]\Psi_p\Big), \quad (4.1)$$

with $q_i=0$, $q_0=\mu$, $k_0+E(k_i)=\mu+m$, $p_i'=0$, $p_0'=m$.

The coefficient of e_j in Eq. (4.1) is a pseudovector, and must be of the form $s_j=(4q_0k_0)^{-\frac{1}{2}}[A\sigma_j+B\boldsymbol{\sigma}\cdot\mathbf{k}k_j]$. Since we are going to let $k_i\to 0$, we neglect the second term, and attempt to calculate the coefficient A. We multiply s_i by k_i. Thus, if we call

$$(\Box^2-\mu^2)\begin{Bmatrix}\phi_3(y)\\\phi(y)\\\phi^*(y)\end{Bmatrix}=\mathbf{O}(y),$$

we find

$$\begin{aligned}A\sigma_ik_i&=\int dxdyk_ie^{ikx}e^{-iqy}(\Psi_{p'}, P[\mathbf{O}(y), \mathbf{j}_i(x)]\Psi_p)\\&=i\int dxdye^{ikx}e^{-iqy}\times\Big(\Psi_{p'}, P\Big[\mathbf{O}(y), \frac{\partial}{\partial x_i}\mathbf{j}_i(x)\Big]\Psi_p\Big)\\&=-i\int dxdye^{ikx}e^{-iqy}\times(\Psi_{p'}, P[\mathbf{O}(y), \partial\rho(x)/\partial x_0]\Psi_p)\\&=-i\int dxdye^{ikx}e^{-iqy}\Big(\Psi_{p'}, \Big\{\frac{\partial}{\partial x_0}P[\mathbf{O}(y), \rho(x)]\\&\qquad+\delta(x_0-y_0)[\rho(x), \mathbf{O}(y)]\Big\}\Psi_p\Big)\\&=k_0\int dxdye^{ikx}e^{-iqy}(\Psi_{p'}, P[\rho(x), \mathbf{O}(y)]\Psi_p)\\&\qquad-i\int dxdye^{ikx}e^{-iqy}\delta(x_0-y_0)\times(\Psi_{p'}, [\rho(x), \mathbf{O}(y)]\Psi_p). \quad (4.2)\end{aligned}$$

The first term in Eq. (4.2) vanishes with k like $k_0\cdot k_i$ and is thus a contribution to A of order $k_0/m\cong\mu/m$. This can

[6] N. M. Kroll and M. A. Ruderman, Phys. Rev. **93**, 233 (1954).

be seen most easily by expanding it into a sum over states such as the one in Eq. (2.5). Then the quantity $\rho(x)$ enters only in the form $\int e^{i\mathbf{k}\cdot\mathbf{x}}\rho(\mathbf{x})d\tau_x$ which, as $k_i\to 0$, is a c-number, the total charge, and hence has no off-diagonal matrix elements. That part of the sum having a free nucleon as intermediate state vanishes identically, since $\mathbf{q}=0$ and $(\Psi_p, \int \mathbf{O}(y)d\tau_y\Psi_p)=0$. Thus we need keep only the second term of (3.2) as $\mathbf{k}\to 0$, so that we may write

$$A\sigma_i k_i \cong -i\int dxdye^{ikx}e^{-iqy}\delta(x_0-y_0) \times(\Psi_{p'}, [\rho(x), \mathbf{O}(y)]\Psi_p). \quad (4.3)$$

The commutator in Eq. (4.3) can be explicitly calculated, since the two operators are to be taken at the same time.

Since

$$(\Box^2-\mu^2)\begin{Bmatrix}\phi_3(y)\\ \phi(y)\\ \phi^*(y)\end{Bmatrix}=ig\bar{\psi}(y)\begin{Bmatrix}\tau_3\\ \sqrt{2}\tau_-\\ \sqrt{2}\tau_+\end{Bmatrix}\gamma_5\psi(y) -\delta\mu^2\begin{Bmatrix}\phi_3(y)\\ \phi(y)\\ \phi^*(y)\end{Bmatrix}+\lambda\phi_k(y)\phi_k(y)\begin{Bmatrix}\phi_3(y)\\ \phi(y)\\ \phi^*(y)\end{Bmatrix}$$

and

$$\rho(x)=ie[\pi^*(x)\phi^*(x)-\pi(x)\phi(x)] +e\psi^*(x)\left(\frac{1+\tau_3}{2}\right)\psi(x),$$

we find, for $x_0=y_0$,

$$[\rho(x), \mathbf{O}(y)]=e\delta(\mathbf{x}-\mathbf{y})(\Box^2-\mu^2)\begin{Bmatrix}0\\ -\phi(x)\\ \phi^*(x)\end{Bmatrix}, \quad (4.4)$$

so that

$$A\sigma_i k_i=-ie\int dxe^{i(k-q)x} \times\left(\Psi_{p'}, (\Box^2-\mu^2)\begin{Bmatrix}0\\ -\phi(x)\\ \phi^*(x)\end{Bmatrix}\Psi_p\right). \quad (4.5)$$

The integrated matrix element on the right of Eq. (4.5) can be evaluated exactly. It is

$$-i(2\pi)^4\delta(k_\lambda-q_\lambda+p_\lambda-p_\lambda')[-(k-q)_\nu^2-\mu^2] \times\Delta_{Fc}((k-q)_\nu^2)ieg_c\Gamma_{5c}(p', p)\begin{Bmatrix}0\\ -\sqrt{2}\\ \sqrt{2}\end{Bmatrix}Z_3^{\frac{1}{2}}, \quad (4.6)$$

where the delta function is 4 dimensional and Δ_{Fc} and Γ_{5c} are, respectively, the renormalized meson propagation function and meson-nucleon 3-vertex operator. g_c is the renormalized mesonic coupling constant.

Now $\Gamma_{5c}(p', p)=\gamma_5 g((p'-p)_\lambda^2)$, so that, to order k^2, $\Gamma_{5c}(p', p)\approx\gamma_5 g(0)=\gamma_5$. Similarly $\Delta_{Fc}(\Delta p)=1/[(\Delta p)^2+\mu^2]+\sim 1/m^2$ so that $[\mu^2+(\Delta p)^2]\Delta_{Fc}(\Delta p)\approx 1+\sim\mu^2/m^2$. We find, therefore,

$$A\sigma_i k_i\cong(2\pi)^4 i\delta(k-q+p-p') \times\begin{Bmatrix}0\\ -\sqrt{2}\\ \sqrt{2}\end{Bmatrix}\bar{u}(p')ieg_c\gamma_5 u(p), \quad (4.7)$$

where we have dropped the factor $Z_3^{\frac{1}{2}}$ as discussed in Sec. I. In the c.m. system, $\mathbf{p}=-\mathbf{k}$, $\mathbf{p}'=0$. $\bar{u}(p')ig_c\gamma_5 u(p)$ is thus given by

$$(u(0), ig_c\beta\gamma_5 u(-\mathbf{k}))=ig_c\boldsymbol{\sigma}\cdot\mathbf{k}/2m(1+\sim k^2/m^2), \quad (4.8)$$

and

$$A=-(2\pi)^4\delta(k-q+p-p')\frac{eg_c}{2m}\begin{Bmatrix}0\\ -\sqrt{2}\\ \sqrt{2}\end{Bmatrix}. \quad (4.9)$$

The S-matrix is given by

$$S=-\frac{(2\pi)^4}{(4q_0k_0)^{\frac{1}{2}}}\delta(k-q+p-p')\mathbf{e}_\lambda\cdot\boldsymbol{\sigma}\frac{eg_c}{2m} \times\left[\begin{Bmatrix}0\\ -\sqrt{2}\\ \sqrt{2}\end{Bmatrix}+\sim\frac{\mu}{m}\right] \quad (4.10)$$

for neutral, positive, and negative threshold production, respectively. Equation (4.10) is equivalent to the result of Kroll and Ruderman.

Strong-Coupling Theory for the Case of Pseudoscalar Coupling

HIRONARI MIYAZAWA*
Institute for Nuclear Studies, University of Chicago, Chicago, Illinois
(Received November 22, 1954)

The pseudoscalar pion field in interaction with the nucleon field through the symmetric pseudoscalar coupling is quantized by using the lattice space method. A strong-coupling approximation is employed to diagonalize the Hamiltonian at each point. The vacuum is represented by a set of rotators, each having excited states. Propagation of this excitation through the lattice points has the character of particles, which are identified as pions and excited states of pions. Nucleons are found to have excited states, the lowest of which has isotopic spin $\frac{1}{2}$ and parity opposite to that of the ground state (one nucleon). In the pion-nucleon scattering, this state causes a strong attractive force for S-waves with $I=\frac{1}{2}$ and explains the qualitative behavior of S-phase shifts.

I. INTRODUCTION

ALTHOUGH the pion theory has proved successful for P-wave pions,[1] that is, in explaining the behavior of the P-phase shifts and other phenomena, it is not so successful for the treatment of the S-wave pions. Analysis of scattering experiments[2] of pions on hydrogen has revealed a remarkable τ-dependence of the two S-phase shifts. α_1, the S-phase shift for the state of total isotopic spin $\frac{1}{2}$, is probably positive; while α_3, that for $I=\frac{3}{2}$, is negative at small energy region. Theoretical treatments, however, yield almost the same value for both of them. This comes from the fact that if the Tani-Foldy-Wouthuysen transformation[3] is applied, the core term $\phi_\rho^2/2M$ is independent of τ and the τ-dependence appears only as a small correction.[4] It seems, therefore, that in order to obtain large τ-dependence, one must use a method which is entirely different from the usual ones. The usual treatments, which are more or less the weak-coupling approach, neglect effects of higher order processes, but the validity of this approximation is very questionable because of the somewhat large value of the pseudoscalar coupling constant.

In this paper an opposite approach, the strong-coupling treatment, is investigated. Although one has no reason to claim that the strong-coupling theory is a very good approximation, it is of theoretical interest to see what kind of conclusions we can obtain from this treatment; also, by approaching both from the weak- and strong-coupling limits, one can conjecture about the true situation with an intermediate value of the coupling constant. In the strong-coupling region we can in fact see the marked difference between the states of $I=\frac{1}{2}$ and $\frac{3}{2}$.

The difficulty in treating the pseudoscalar coupling case is that the γ_5 interaction easily creates nucleon-antinucleon pairs, thus forcing us to deal with vacuum fluctuations. Wentzel[5] treated the pseudoscalar coupling case by a strong-coupling method. In his treatment the second-order Dirac equation was used and the effect of pair creation was eliminated, at least in the first approximation. Here, however, we use the first-order Dirac equation and the effect of pair creation is very important. We shall be mainly concerned with S-wave pions, since in pseudoscalar coupling the interaction of the nucleon with P-wave pions appears in a higher stage of approximation. In this paper we use the lattice-space quantization method,[6] which consists of omitting the gradient term in zero order and replacing the resulting Hamiltonian by a set of systems defined at each lattice point. Each system has a finite number of degrees of freedom and can be handled easily. This allows us to make use of the strong-coupling approximation. The lattice-space quantization method can be applied only when the lattice constant is so large that the coupling between two systems is small. Actually this condition is not satisfied unless we assume the lattice constant to be larger than the pion Compton wavelength, which could hardly correspond to physical reality. Nevertheless, we can obtain much information from this method because, as we shall see in Sec. III, the largest part of the interaction between lattice points has the effect of merely changing the numerical value of the moment of isotopic inertia without altering the qualitative nature of each system.

In the next two sections we shall first deal with zero-nucleon states, by which we mean states in which the number of nucleons minus the number of antinucleons is zero. We shall see that these zero-nucleon states contain excited states, which are identified as pions and excited states of pions. This fact can be understood as follows. The vacuum is filled up with nucleons in negative-energy states. As can be seen from the second order perturbation theory, the interaction of pions with nucleons in negative-energy states is attractive, and some of the pion field is bound to the nucleon. This

* On leave of absence from the University of Tokyo, Tokyo, Japan.

[1] G. F. Chew, Phys. Rev. **89**, 591 (1953); K. Sawada, Progr. Theoret. Phys. (Japan) **9**, 455 (1953).

[2] Fermi, Metropolis, and Alei, Phys. Rev. **95**, 1581 (1954); J. Orear, Phys. Rev. **96**, 176 (1954).

[3] S. Tani, Progr. Theoret. Phys. (Japan) **6**, 267 (1950); L. L. Foldy and S. A. Wouthuysen, Phys. Rev. **78**, 29 (1950).

[4] However, see Fukuda, Goto, Okubo, and Sawada, Progr. Theoret. Phys. (Japan) **12**, 79 (1954) and T. Akiba and K. Sawada, Progr. Theoret. Phys. (Japan) **12**, 94 (1954).

[5] G. Wentzel, Phys. Rev. **92**, 173 (1953).

[6] G. Wentzel, Helv. Phys. Acta. **13**, 269 (1950); L. I. Schiff, Phys. Rev. **92**, 766 (1953).

nucleon now looks like a rigid body with a finite moment of isotopic inertia and has excited states corresponding to higher isotopic angular momenta. If all nucleons are in the ground states, this is the vacuum and nothing is observable. If one of them is excited, say to the state of $I=\frac{3}{2}$, the hole looks like a particle of $I=\frac{1}{2}$, which combined with $I=\frac{3}{2}$ gives particles of $I=1$ or 2. Particles with $I=1$ can be identified as pions and those of higher isotopic spins are excited states of pions. In Secs. IV and V, we shall treat the state of one nucleon and the scattering of pions by a nucleon.

II. STRONG-COUPLING THEORY OF THE VACUUM

First we consider the state in which no nucleon exists. The Hamiltonian with which we work is

$$H=\tfrac{1}{2}\int(\pi_\rho^2+(\nabla\varphi_\rho)^2+\mu^2\varphi_\rho^2)dx$$

$$+g\int\psi^*\tau_\rho\rho_2\psi\varphi_\rho dx+\int\psi^*(\alpha p+m\beta)\psi dx.$$

For simplicity the lattice space is introduced in simple cubic form with the lattice constant a. At each lattice point s there are pion variables $\varphi_{\rho s}$, $\pi_{\rho s}$ and variables describing nucleons and antinucleons. To describe nucleons and antinucleons, it is convenient to introduce at each lattice point four nucleons obeying the Pauli principle. This is because the vacuum is filled with nucleons in negative energy state and there are four states in negative energy corresponding to the 2×2 orientations of spin and isotopic spin. Thus any operator of the form

$$\int\psi^*O\psi dx$$

can be replaced by

$$\sum_s\sum_{i=1}^{4}O^{(is)},$$

where suffix s represents a lattice point and i denotes one of the four nucleons at point s. The Hamiltonian of this system, apart from an additional constant, is given by[7]

$$H=\sum_s[\tfrac{1}{2}\pi_{\rho s}^2+\tfrac{1}{2}(A+\mu^2)\varphi_{\rho s}^2+m\sum_i\rho_3^{(is)}$$

$$+f\varphi_{\rho s}\sum_i\tau_\rho^{(is)}\rho_2^{(is)}]+\tfrac{1}{2}\sum_s\sum_{s\neq t}A_{st}\varphi_{\rho s}\varphi_{\rho t},\quad(1)$$

where

$$\varphi_{\rho s}=a^{\frac{1}{2}}\int f(x-x_s)\varphi_\rho(x)dx,\quad\pi_{\rho s}=a^{\frac{1}{2}}\int f(x-x_s)\pi_\rho(x)dx,$$

$$f(x-x_s)=V^{-1}\sum e^{ik(x-x_s)},\quad A_{st}=(a^3/V)\sum k^2e^{ik(x_s-x_t)},$$

$$A=A_{ss}=(a^3/V)\sum k^2,\qquad f=ga^{-\frac{1}{2}},$$

and V is the normalization volume. The momentum of the nucleon is neglected since it turns out to give only a higher order correction. We assume that the lattice constant is so large that the last term in (1),

$$H'=\tfrac{1}{2}\sum_s\sum_{s\neq t}A_{st}\varphi_{\rho s}\varphi_\rho$$

can be treated as a small perturbation. It it then necessary to diagonalize the uncoupled Hamiltonian,

$$H_s=\tfrac{1}{2}(\pi_\rho^2+\mu'^2\varphi_\rho^2)+m\sum\rho_3^{(i)}+f\varphi_\rho\sum\tau_\rho^{(i)}\rho_2^{(i)},$$

where suffices s is omitted and $\mu'^2=\mu^2+A$. We assume that the coupling is strong and apply the strong-coupling approximation. This consists in finding a classical equilibrium position by ignoring the kinetic energy, and then introducing the harmonic oscillations about this point. So our first task is to find the minimum of the potential energy by the following equation:

$$\delta(\tfrac{1}{2}\mu'^2\varphi_\rho^2+m\sum\rho_3^{(i)}+f\varphi_\rho\sum\tau_\rho^{(i)}\rho_2^{(i)})=0.$$

In the first step, we diagonalize the ρ and τ matrices. The lowest eigenvalue of the last two terms, compatible with the exclusion principle, is $-4(m^2+f^2\varphi_\rho^2)^{\frac{1}{2}}$ and the solution is

(i) if $4f^2<m\mu'^2$: $\varphi_\rho^{02}=0$,

(ii) if $4f^2>m\mu'^2$: $\varphi_\rho^{02}=(16f^2/\mu'^4)-(m^2/f^2)\equiv C_0^2$.

There is another solution $\varphi_\rho^{02}=0$ in case (ii) but this corresponds to a maximum rather than a minimum and is therefore not stable. We assume that case (ii) holds. The nonvanishing value of the static field φ_ρ^0 means that this system has a finite moment of isotopic inertia. The absolute value of φ_ρ^0 is fixed by this equation but its direction is arbitrary. Thus this system has the character of a symmetrical rotator. The following is the mathematical representation of this situation.

We introduce polar coordinates for φ_ρ:

$$\varphi_\rho=\varphi e_\rho,\quad e_1+ie_2=\sin\alpha e^{i\beta},\quad e_3=\cos\alpha.$$

It is convenient to introduce an orthogonal unit system $\mathbf{n}^i$ in such a way that $\mathbf{n}^3$ is equal to $\mathbf{e}$[8]:

$$\left.\begin{matrix}\mathbf{n}^1=\{\cos\alpha\cos\beta,&\cos\alpha\sin\beta,&-\sin\alpha\\ \mathbf{n}^2=\{-\sin\beta,&\cos\beta,&0\\ \mathbf{e}=\mathbf{n}^3=\{\sin\alpha\cos\beta,&\sin\alpha\sin\beta,&\cos\alpha\end{matrix}\right\}.$$

It then follows that

$$\varphi_\rho=\varphi n_\rho^3,$$
$$\pi_\rho=\pi n_\rho^3+(p_\alpha n_\rho^1/\varphi)+(p_\beta n_\rho^2/\varphi\sin\alpha).\quad(2)$$

The canonical conjugate of α and β are p_α and p_β respectively. The isotopic angular momentum of the pion field is

$$\mathbf{L}=\boldsymbol{\varphi}\times\boldsymbol{\pi}=p_\alpha\mathbf{n}^2-(p_\beta\mathbf{n}^1/\sin\alpha).$$

[7] For the detail of the lattice-space method see reference 6.

[8] R. Serber and S. M. Dancoff, Phys. Rev. 63, 143 (1943).

With this L, π_ρ is given by

$$\pi_\rho=\pi e_\rho+(\mathbf{L}\times\mathbf{e})_\rho/\varphi.$$

To make π_ρ and φ_ρ pseudoscalar, we assume the following transformation of various quantities under space reflection:

$$(\varphi_\rho,\pi_\rho)\to(-\varphi_\rho,-\pi_\rho),$$
$$(\varphi,\pi)\to(\varphi,\pi),$$
$$(\alpha,\beta)\to(\pi-\alpha,\pi+\beta),$$
$$(\mathbf{n}^1,\mathbf{n}^2,\mathbf{e}=\mathbf{n}^3)\to(\mathbf{n}^1,-\mathbf{n}^2,-\mathbf{e}=-\mathbf{n}^3),$$
$$(p_\alpha,p_\beta)\to(-p_\alpha,p_\beta).$$

This transformation is compatible with (2). We note that in this transformation $\mathbf{e}$ behaves like a polar vector in ordinary space although it is defined in isotopic spin space. Thus states with even (odd) isotopic angular momentum have even (odd) parity under space reflection.

With these variables our Hamiltonian H_s can be written as

$$H_s=\tfrac{1}{2}(\pi^2+\mu'^2\varphi^2)+\frac{L^2}{2\varphi^2}+m\sum\rho_3^{(i)}+f\varphi e_\rho\sum\tau_\rho^{(i)}\rho_2^{(i)}.$$

Having seen that the potential energy has a minimum at $\varphi=C_0$, we shift the origin of φ to eliminate terms linear in φ';

$$\varphi=C_0+\varphi'.$$

Now it is necessary to diagonalize

$$m\sum\rho_3^{(i)}+C_0fe_\rho\sum\tau_\rho^{(i)}\rho_2^{(i)}.$$

This is done in two steps: first by the S-transformation,

$$A\to SAS^{-1},$$

where

$$S=\exp(\tfrac{1}{2}i\alpha\sum\tau_2^{(i)})\exp(\tfrac{1}{2}i\beta\sum\tau_3^{(i)}), \qquad (3)$$

$e_\rho\sum\tau_\rho^{(i)}\rho_2^{(i)}$ is brought to $\sum\tau_3^{(i)}\rho_2^{(i)}$. Then, by

$$U=\exp(-\tfrac{1}{2}i\theta\sum\tau_3^{(i)}\rho_1^{(i)}),\quad \tan\theta=C_0f/m,$$

the whole terms are transformed into

$$(m^2+f^2C_0^2)^{\frac{1}{2}}\sum\rho_3^{(i)}=\frac{4f^2}{\mu}\sum\rho_3^{(i)}.$$

In the ground state all ρ_3's have eigenvalues -1.

By these transformations, L is changed into L plus terms linear in $\sum\tau_\rho^{(i)}$ and $\sum\tau_\rho^{(i)}\rho_1^{(i)}$. However, in the ground state, namely the state in which four nucleons are occupying four negative energy states in the transformed system, the total isotopic angular momentum is zero, and also each component $\sum\tau_\rho^{(i)}$ is zero. $\sum\tau_\rho^{(i)}\rho_1^{(i)}$ itself is small, since ρ_1 has no diagonal element and couples between widely separated states $\pm 4f^2/\mu'^2$ and its square is a sum of small quantity and a constant. Thus L is not changed appreciably by these transformations.

Putting $\rho_1,\rho_2=0$, $\rho_3=-1$ in the transformed Hamiltonian, we have the reduced Hamiltonian:

$$H_s=-\frac{8f^2}{\mu'^2}-\frac{m^2\mu'^2}{2f^2}+\frac{L^2}{2C_0^2}+\tfrac{1}{2}(\pi^2+\mu'^2\varphi'^2), \qquad (4)$$

where terms higher order in $1/f^2$ are neglected. The part of the Hamiltonian described by φ' and π has excitation energy of μ' which is so large compared with $1/C_0^2$ [see (8) below] that we can neglect this term. Thus our whole Hamiltonian becomes

$$H=\sum_s\frac{L_s^2}{2C_0^2}+\frac{C_0^2}{2}\sum_s\sum_{s\neq t}A_{st}\mathbf{e}_s\mathbf{e}_t+\text{const.}$$

III. PIONS AND EXCITED STATES OF PIONS

The vacuum or zero-nucleon state is described as a set of rotators coupled to each other. Each rotator has possible eigenvalues

$$\frac{1}{2C_0^2}l(l+1),\quad l=0,1,\cdots,$$

and its eigenfunctions are spherical harmonics Y_l^m. Here l is the isotopic angular momentum of the state and this state has parity positive (negative) if l is even (odd). The lowest state of the unperturbed system is that in which all rotators are in S states. The first excited state of the uncoupled system is that in which only one rotator is in a P-state while all others remain in S-states. Because of the interaction between lattice points, this excitation is not located on one point but is propagated through the lattice points.[9] The eigenfunction and the eigenvalue of this state, up to the first order in H', are given by

$$\Psi=\sum_s e^{i\mathbf{k}\mathbf{x}_s}U(s), \qquad (5)$$

$$U(s)=Y_1(s)\prod_{t\neq s}Y_0(t), \qquad (6)$$

$$E-E_{\text{vac}}=\frac{1}{C_0^2}+\frac{C_0^2}{3}(k^2-A). \qquad (7)$$

This state has the character of one particle having a rest mass $1/C_0^2$ with a correction $-C_0^2A/3$. This state has isotopic spin 1, minus parity and no spin, since we are dealing with S-wave pions. Thus this particle can be identified as a pion. This solution is not Lorentz-invariant since (7) is not of the form $M+k^2/2M$. This lack of covariance is inherent in the Heisenberg and Pauli form of quantum field theory, and is caused by the nonvanishing value of the self-stress. It is not caused by the use of the lattice-space method or the strong-coupling method.

[9] T. Holstein and H. Primakoff, Phys. Rev. 58, 1098 (1940); L. I. Schiff, reference 6.

The second excited state with $I=2$ has rest mass $3/C_0^2$, which is three times the pion mass. This state also propagates through the lattice points. The energy of this particle with momentum k is given by

$$\frac{3}{C_0^2}+\frac{4C_0^6}{45}\frac{\pi^2}{a^2}k^2+O\left(\frac{C_0^6}{a^4}\right).$$

It can be seen that this state is not relativistically invariant either. This particle decays into a two-pion state with a lifetime given by

$$1/\tau\sim C_0^2a^3k^5,$$

where k is the momentum of one of the decaying pions.

In this way we have particles of higher isotopic spin which, together with the vacuum, can be called pion isobars.

We have to examine here the validity of the various approximations introduced. For the strong-coupling approximation to hold, that is, for the static field C_0 to be larger than the zero-point amplitude of φ', it is necessary that

$$C_0^2\gg\mu'^{-1}. \tag{8}$$

On the other hand, in order that H' can be treated as small, the isobar separation $1/C_0^2$ must be larger than H' which is of the order of C_0^2/a^2. Thus we are confined to the case

$$a\gg C_0^2.$$

This condition is quite severe since it means that the cutoff momentum K_0 must be smaller than the pion mass $1/C_0^2$.

In the opposite limit, in which H' is assumed to be very strong, we can also obtain a solution. Starting from (1), but retaining H', we obtain a minimum of the potential energy. The minimum occurs when all φ_s are equal and

$$\varphi_{ps}=\phi e_p,\quad e_p^2=1,$$

where ϕ is determined by

$$\delta\{\tfrac{1}{2}\mu^2\phi^2-4(m^2+f^2\phi^2)^{\frac{1}{2}}\}=0.$$

All the rotators of the vacuum rotate with approximately the same phase with small oscillations around a common phase. This means the freezing of the vacuum. The vacuum has an isotopic moment of inertia of the order of N, where N is the number of rotators in the vacuum, and has levels spaced by $1/N$. Such close level spacing is quite unreasonable and we need not carry this case further.

Except in these two cases, we cannot solve the problem but have to content ourselves with qualitative arguments. The situation should be intermediate between these two cases. A rotator, when it rotates, interacts with its neighbors and forces them to rotate. However, the interaction is not strong enough to affect all the rotators in the vacuum. If there are n rotators in this subunit, they can be described as one effective rotator with moment of inertia nI, if each has inertia I. Thus the vacuum may be thought of as a system of almost independent rotators with its effective inertia increased. This type of argument proved successful in the Feynman theory of liquid helium.[10]

Let the wave function of the ground state (vacuum) be Ψ_0, which is a real function. Following Feynman[11] we can argue that to a good approximation the first excited state is given by $\sum_s f(\omega_s)\Psi_0$ where $\omega_s=\alpha_s,\beta_s$ is the set of angular variables of the ith rotator and f is to be determined by the variational principle:

$$\delta E=\delta\{\mathcal{E}/\mathcal{I}\}=0,$$

$$\mathcal{E}=\frac{1}{2C_0^2}\sum_s\int\left(\left|\frac{\partial f}{\partial\alpha_s}\right|^2+\frac{1}{\sin\alpha_s}\left|\frac{\partial f}{\partial\beta_s}\right|^2\right)\Psi_0^2d^N\omega_s,$$

$$\mathcal{I}=\sum_{st}\int f^*(\omega_s)f(\omega_t)\Psi_0^2d^N\omega_s,$$

where $d\omega_s$ stands for $\sin\alpha_s d\alpha_s d\beta_s$. In $\mathcal{E}$, the integral of Ψ_0^2 over all rotators except s is the probability that the angular variable s is found in a unit solid angle around α_s,β_s. This is independent of α_s,β_s and is $1/4\pi$. In $\mathcal{I}$, integral of Ψ_0^2 over all rotators except s and t can be written $(1/4\pi)p_{st}(<(st))$, where p_{st} is the probability that the angle of the directions of two rotators s and t is $<(st)$. From the variational principle, we have the equation for f:

$$\frac{1}{2C_0^2}\left\{\frac{1}{\sin\alpha_s}\frac{\partial}{\partial\alpha_s}\left(\sin\alpha_s\frac{\partial f}{\partial\alpha_s}\right)+\frac{1}{\sin^2\alpha_s}\frac{\partial^2 f}{\partial\beta_s^2}\right\}$$

$$=-E\sum_t\int p_{st}(<(st))f(\omega_t)d\omega_t. \tag{9}$$

Since p_{st} is a function of the angle between ω_s and ω_t, it can be expanded in the following way

$$p_{st}(<(st))=\sum_{l,m}S_{st}(l)Y_l^m(\omega_s)Y_l^{m*}(\omega_t),$$

$$S_{st}(l)=\int p_{st}(<(st))Y_l^{m*}(\omega_s)Y_l^m(\omega_t)d\omega_s d\omega_t.$$

Thus (9) has the solutions

$$f(\omega)=Y_l^m(\omega),$$

with the energy values

$$E_l=\frac{l(l+1)}{2C_0^2S(l)},\quad S(l)=\sum_t S_{st}(l).$$

[10] R. P. Feynman, Phys. Rev. 91, 1291 (1953).
[11] R. P. Feynman, Phys. Rev. 94, 262 (1954).

If lattice points s and t are far apart, there is no correlation between ω_s and ω_t and the integral S_{st} vanishes. For adjacent s and t, there is a strong correlation between them and S_{st} is almost equal to one. $S(l)$ is a slowly decreasing function of l and is equal to the number n of the rotators which rotate as a subunit. Thus this system still has the character of rotators, although not rigid rotors because the moment of inertia depends on the angular momentum l. By assuming a trial function of the form $\sum f(\omega_s)f(\omega_t)\cdots\Psi_0$, we have a multiply excited state which corresponds to many pions. Although this state has no momentum, a more complicated trial function will give a state moving with momentum k. We do not attempt to do this, or to determine the value of $S(l)$. We note that even in the case of stronger H', the system has the character of a set of rotators. Results obtained by treating H' as a small perturbation may be good even in the case of a small lattice constant, under the proviso that the isotopic moment of inertia of each rotator is increased.

The presence of pion isobars leads to an interesting consequence. The first excited state of a pion has isotopic spin 2, a mass three times that of the pion mass, and decays into two pions. This state is very short-lived but plays a role as an intermediate state in some of the pion processes, especially in double pion production. In double pion production in the region of three to four hundred Mev, the most favorable process will be that in which an excited pion is emitted first, followed by its subsequent decay into two final pions. Furthermore, we know both from experiments and from theory that a nucleon isobar with isotopic spin $\frac{3}{2}$ could exist. Thus, for the double production by pions with energy 200–300 Mev, we can draw the diagram of Fig. 1 as the most favorable process. If this process is dominant in the reaction, we can predict the ratio of cross sections for the various possible reaction products. The ratios are given by

$$\pi^-+p\begin{cases} p+\pi^0+\pi^- & 9\\ p+\pi^-+\pi^0 & 9\\ n+\pi^++\pi^- & 2\\ n+\pi^-+\pi^+ & 2\\ n+\pi^0+\pi^0 & 8\end{cases}$$

$$\pi^++p\begin{cases} p+\pi^++\pi^0 & 9\\ p+\pi^0+\pi^+ & 9\\ n+\pi^++\pi^+. & 72\end{cases}$$

For double pion production by γ-rays the charge ratios cannot be determined, since in this case the dipole absorption by charged pions competes with the process through isobars and we cannot determine the ratio of these two processes in a simple way.

IV. ONE-NUCLEON STATE

Suppose that a single nucleon is present at the point $s=0$. The Hamiltonian at this point is different from those of other points and given by

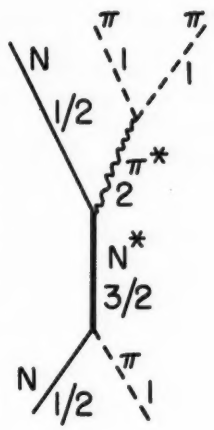

FIG. 1. Diagram of the dominant process for double pion production. The numbers attached to the lines indicate the isotopic spin and the asterisk indicates an isobaric state.

$$H_0=\tfrac{1}{2}(\pi_\rho^2+\mu'^2\varphi_\rho^2)+m\sum_{i=1}^{5}\rho_3^{(i)}+f\varphi_\rho\sum_{i=1}^{5}\tau_\rho^{(i)}\rho_2^{(i)},$$

where the summation now extends over five nucleons, since we now have one nucleon and the four which were present in the vacuum. The diagonalization of this Hamiltonian follows the same pattern as in Sec. II. The static field φ_ρ^0 is determined by

$$\delta\{\tfrac{1}{2}\mu'^2\varphi_\rho^2-3(m^2+f^2\varphi_\rho^2)^{\frac{1}{2}}\}=0,$$

where the -3 in front of the square root comes from the minimum value of $\sum\rho_3^{(i)}$ compatible with the exclusion principle. Thus we have

$$(\varphi_\rho^0)^2=9f^2/\mu'^2-m^2/f^2\equiv D^2.$$

A stronger condition than imposed in (ii), namely

$$3f^2>m\mu'^2$$

is necessary in order that the static field exist. We note that the isotopic moment of inertia D^2 is smaller than the C_0^2 of the zero-nucleon case. We introduce polar coordinates as in Sec. II, and make transformations in a similar manner except that now the summation over i is extended to $i=5$. Finally we get the reduced Hamiltonian corresponding to (4):

$$H_0=-\frac{9f^2}{2\mu'^2}-\frac{m^2\mu'^2}{2f^2}+\frac{L'^2}{2D^2}+\tfrac{1}{2}(\pi^2+\mu'^2\varphi'^2),$$

where

$$L'=L+\tfrac{1}{2}\cot\alpha\cdot n^1\sum\tau_3-\tfrac{1}{2}\cos\delta(n^1\sum\tau_1+n^2\sum\tau_2),$$

and

$$\tan\delta=Df/m.$$

Terms linear in ρ_1 are neglected in L' since they are small in themselves and give only an additive constant if squared in L'^2.

Our next task is to find the eigenvalues of L'^2. We first note that in the transformed system, four of the nucleons occupy the four negative energy states and only one of them is left in the positive energy state. The four in the negative energy states form a state of $I=0$ and do not contribute to the isotopic angular momentum. Thus $\sum\tau$ can be replaced by τ. Next we see that L'^2 is equal to

$$(L'-\tfrac{1}{2}\cos\delta\tau_3 n^3)^2,$$

except for an additive constant, since $(L'n^3)$ vanishes. We transform this by S^{-1}, where S is given by (3) with $\sum\tau$ replaced by τ and find

$$S^{-1}(L'-\tfrac{1}{2}\cos\delta\tau_3 n^3)^2 S=[L+\sin^2(\delta/2)\tau]^2.$$

Thus the eigenvalues of L'^2 are, apart from an additive constant, the same as the eigenvalues of

$$L^2+\lambda(L\cdot\tau),\quad \lambda=2\sin^2(\delta/2),$$

which are

$$l(l+1)+\lambda[I(I+1)-l(l+1)],$$

where $I=\frac{1}{2}, \frac{3}{2}, \cdots$ is the total isotopic angular momentum of the system and $l=0, 1, \cdots$ is the isotopic angular momentum of the pion field.

The isobar energy of the nucleon is given by $L'^2/2D^2$. If the coupling is not very strong, that is for small D, δ, and λ, the eigenvalues are given by $(1/2D^2)l(l+1)$ and do not depend on the total isotopic spin. This is in accord with the weak-coupling theory, which gave no distinction between $I=\frac{1}{2}$ and $\frac{3}{2}$ states for S-wave pions in interaction with a nucleon. However, in the case of stronger coupling, this difference is apparent. Because of the spin-orbit coupling, the two states with equal l but different I split into two levels, the lower level corresponding to smaller I as indicated in Fig. 2. For extreme strong-coupling, $D=\infty$, $\delta=\pi/2$, $\lambda=1$, two levels with the same I coincide. Thus in this case, besides the usual nucleon, we would have a pseudonucleon with the same mass but with opposite parity. In the intermediate region the first excited state has isotopic spin $\frac{1}{2}$ and opposite parity to the ground state. The next excited state has $I=\frac{3}{2}$ and the same parity as the first excited state. This splitting of two levels with different I is important in the theory of pion scattering since it produces a marked τ-dependence of the S-phase shifts. The eigenfunctions are given by the combination of the spherical harmonics Y_l^m representing the pion field and the spin functions α and β of the nucleon. They are

$$\alpha Y_0 \text{ and } \beta Y_0$$

for proton and neutron,

$$3^{-\frac{1}{2}}(\alpha Y_1^0-\sqrt{2}\beta Y_1^1) \text{ and } 3^{-\frac{1}{2}}(\beta Y_1^0-\sqrt{2}\alpha Y_1^{-1}) \quad (10)$$

for the first excited states,

$$\alpha Y_1^1,\ 3^{-\frac{1}{2}}(\beta Y_1^1+\sqrt{2}\alpha Y_1^0),$$
$$3^{-\frac{1}{2}}(\alpha Y_1^{-1}+\sqrt{2}\beta Y_1^0) \text{ and } \beta Y_1^{-1} \quad (11)$$

for the second excited states, etc.

The nucleon is coupled to other lattice points through the interaction

$$H_0'=C_0 D\sum_{s\neq 0} A_{s0}\mathbf{e}_s\mathbf{e}_0.$$

This causes the forced rotation of neighboring rotators and increases the moment of inertia of the nucleon. We will not treat this situation in the present paper.

This H_0' also induces the interaction of the nucleon with free pions. Except in the case of extremely strong coupling, the excitation energy is larger than the pion mass since $D^2<C_0^2$. Thus the excited state decays with the emission of a pion in such a short time that this state can hardly be said to be a metastable state. However, this state plays an important role in pion scattering.

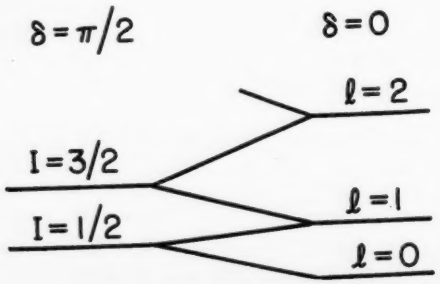

FIG. 2. Splitting of the nucleon isobaric levels.

V. SCATTERING OF S-WAVE PIONS

The Schrödinger equation is given by

$$\Big(\sum_{s\neq 0} H_s+H_0+\frac{C_0^2}{2}\sum_{s\neq t;\ s,t\neq 0}\sum A_{st}\mathbf{e}_s\mathbf{e}_t$$
$$+C_0 D\sum_{s\neq 0} A_{0s}\mathbf{e}_0\mathbf{e}_s-E_0\Big)\Psi=E\Psi,$$

where E_0 is the energy of the state in which the nucleon is in the ground state and no pion is present, and E is the energy of the incoming pion with momentum k_0:

$$E=\frac{1}{C_0^2}+\tfrac{1}{3}C_0^2(k_0^2-A). \quad (12)$$

In the presence of one nucleon at point $s=0$, the term corresponding to $s=0$ must be omitted from the expression (5) for the wave function of a pion:

$$\Psi'(k)=\sum_{s\neq 0} e^{ikx_s}U(s).$$

This is not the true wave function since the hole at $s=0$ causes diffraction scattering,[12] and another scattering is

[12] Maki, Sato, and Tomonaga, Progr. Theoret. Phys. (Japan) 9, 607 (1953) refer to this scattering as potential scattering, and R. G. Sachs, Phys. Rev. 95, 1065 (1954), calls it orthogonality scattering.

induced through the excited states of the nucleon. We adopt the following Tamm-Dancoff type wave function:

$$\Psi=\sum a(k)\Psi'(k)+b_1U_1(0)+b_3U_3(0),$$

where $U_1(0)$ and $U_3(0)$ are given by (6) for $s=0$ except that $Y_1(0)$ is replaced by (10) and (11) respectively. The equations for the amplitudes are simple to write for states with definite total isotopic angular momentum. For the states $I=i/2$, $i=1$ or 2, the equation is

$$(k^2-k_0^2)a(k)=-\frac{1}{N}\sum(A-k^2-k'^2+k_0^2)a(k')+\frac{1}{N}\frac{D}{C_0}b_i(A-k^2),$$

$$(\epsilon_i-E)b_i=\frac{DC_0}{3}\sum(A-k'^2)a(k').$$

ϵ_i is the excitation energy of the excited state with $I=i/2$. If we eliminate b_i from the equations, we have

$$(k^2-k_0^2)a(k)=-\frac{1}{N}\sum(A-k^2-k'^2+k_0^2)a(k')+\frac{D^2}{3N}\sum\frac{(A-k^2)(A-k'^2)}{\epsilon_i-E}a(k'). \quad (13)$$

The first term on the right hand side of this equation represents the repulsive potential due to the hole and independent of I. The second term is attractive and strongly I dependent. In a fairly strong coupling region, the second excited state lies high above the first excited state. For the wave of $I=\frac{1}{2}$, ϵ_1-E is small and the whole interaction may even become attractive, while for $I=\frac{3}{2}$, the interaction is repulsive. In this way the behavior of the two S-phase shifts found by experiments can be explained.

If we solve the Eq. (13) by Born approximation, we find that the scattering lengths are given by

$$\frac{\alpha_i}{k}=\frac{a^3}{4\pi}A\left(-1+\frac{D^2A}{3(\epsilon_i-\kappa)}\right), \quad i=1, 3,$$

where κ is the mass of the pion. They are to be equated to the experimental values[2]

$$\alpha_1/k=0.16/\kappa, \quad \alpha_3/k=-0.11/\kappa.$$

The Eq. (13) can be solved but the solution is quite complicated. However, we can get an approximate solution by replacing $(A-k^2-k'^2+k_0^2)$ by $(A-k^2)(A-k'^2)/A$. This solution has the form

$$a(k)=\delta(k,k_0)+C/(k^2-k_0^2-i\epsilon),$$

and the phase shifts are given by

$$\tan\alpha_i=-2\pi k_0(A-k_0^2)/(\lambda_i+\Lambda),$$

where

$$\Lambda=\mathrm{P}\int\frac{(A-k)^2}{k^2-k_0^2}dk,$$

$$\lambda_i^{-1}=\left(\frac{a}{2\pi}\right)^3\left(\frac{1}{A}-\frac{D^2/3}{\epsilon_i-E}\right),$$

and $\mathrm{P}\int\cdots$ means the principle part of the integral.

The general behavior of the α's is as follows. For the state $I=\frac{3}{2}$, λ_3 is positive at $E=\kappa$, since ϵ_3 is large. λ_3 increases with increasing E and becomes $+\infty$ at $E=E_3=\epsilon_3-AD^2/3$. The α_3 is negative at low energy and becomes zero at $E=E_3$ and is positive thereafter.

For $I=\frac{1}{2}$, λ_1 starts with negative value since ϵ_1 is small, and increases with E, while the integral Λ is a decreasing function of E. The sum $\lambda_1+\Lambda$ is negative at $E=\kappa$. If λ_1 increases rapidly, $\lambda_1+\Lambda$ becomes zero at some point $E=E_1$, where α_1 becomes $\pi/2$. However, if Λ decreases sufficiently fast, $\lambda_1+\Lambda$ stays negative. There is no resonance in this case but α_1 stays positive.

The above arguments only indicate the qualitative, not quantitative behavior of the phase shifts because the relation (12) is not valid for high energy. It should be remarked that Sachs,[13] in his rather phenomenological analysis of pion scattering, introduced an S-wave level with $I=\frac{1}{2}$ to fit the experimental data. The present calculation provides a theoretical foundation for his assumption.

VI. CONCLUSIONS

The strong-coupling theoretical treatment for the pion-nucleon system that has been described here seems to offer a clue for the explanation of the behavior of the S-phase shifts which was hard to understand by the weak-coupling theory. However, the use of the lattice-space method, which is not a good approximation when the lattice constant is small, does not allow a precise comparison of the theory with experiment. Nevertheless we can see that there is some hope of explaining the experimental facts within the framework of the Yukawa theory, without introducing any new interaction, by taking into account the strong interaction between pions and nucleons.

It is necessary to note that the excited states or isobars used in this paper have rather different meaning from what they are usually interpreted to mean. Here we separated the Hamiltonian into two parts, one part referring to the nucleon and the remaining part H_1 describing the unbound pions. The excited states we have found are the levels of the first part of the Hamiltonian. The scattering through this level, which might be called resonance scattering,[14] is masked by the diffraction scattering caused by the fact that H_1 has a hole at the point of the nucleon. The phase shift, therefore, does not necessarily reach $\pi/2$ even at the

[13] R. G. Sachs, Phys. Rev. 95, 1065 (1954).
[14] According to Maki *et al.* and Sachs, reference 12.

"resonant" energy. This indicates that our isobars are not even metastable.

A question remains about the P-wave interactions: Are they of the right order of magnitude? To answer this question we must introduce the momentum of the nucleons, which is omitted in this paper. Our formulation, however, is not suitable for this purpose and the problem of P-wave interactions as well as the quantitative comparison with experiment will be discussed in a following paper.

It is a pleasure to acknowledge several stimulating discussions with Professor G. Wentzel. Thanks are also due to Professor M. L. Goldberger, Professor R. Kikuchi, Dr. S. Cohen, and Dr. R. Oehme for helpful comments.

PHYSICAL REVIEW VOLUME 97, NUMBER 5 MARCH 1, 1955

Supplementary Conditions in Quantized Linear Systems

J. K. PERCUS*
200 West 86 Street, New York City, New York
(Received September 21, 1954)

A scalar product formalism is presented for the commutation relations and quadratic constants of the motion of a linear system. The modification of commutation relations necessitated by a supplementary operator condition is obtained by means of a projection operation, for which several computational methods are developed; some simple applications are discussed. The foregoing analysis is extended to a sequence of supplementary conditions; it is then applied to quantization of the integral-spin real-meson field.

INTRODUCTION

DURING a detailed investigation of the quantum mechanics of linear systems,[1] there was developed a systematic procedure for the inclusion of auxiliary conditions, which appears to be of wide applicability. To present this material most effectively, it will be convenient to review the quantization formalism employed by the writer, which, for the purposes of this discussion, may be stated as follows:

Suppose a linear system to be given by

$$\sum_s M_{rs}\psi_s(x)=0, \tag{1}$$

or $M\psi=0$, where $M=(M_{rs})$ is a real matric (square) differential operator and x stands for all n (generally 4) spatial coordinates. Further, let us assume that a coordinate-independent basis $\{F_\alpha\psi\}$, real or complex, has been chosen for quantities of the form $F\psi$, where F is a linear operator; by this we mean that if ψ is a general solution of $M\psi=0$, then "any" $F\psi$ can be expressed uniquely as[2]

$$(F\psi)_s=\sum_\alpha f_{\alpha s}(x)F_\alpha\psi, \tag{2}$$

$\sum_\alpha$ denoting both summation and integration, as required. Then the general rule of quantization may be expressed in the form

$$\mathcal{T}(\omega,\psi)\cdot F\psi=F\omega; \tag{3}$$

here ω is any c-number solution of $M\omega=0$,

$$A\cdot B=AB+JBA \tag{4}$$

for $J=\pm1$, and $\mathcal{T}(\omega,\psi)$ has the form of a scalar product

$$\mathcal{T}(\omega,\psi)=\sum F_\alpha\omega\tau_{\alpha\beta}F_\beta\psi, \tag{5}$$

where, assuming that there exists no c-number implicitly containing ψ, τ is an invertible coordinate-independent matrix.

PROPERTIES OF $\mathcal{T}(\omega,\psi)$

The meaning of $\mathcal{T}(\omega,\psi)$ may be elucidated by observing that if the commutation relations are given by

$$F_\alpha\psi\cdot F_\beta\psi=\mathfrak{F}_{\alpha\beta}, \tag{6}$$

a pure number, then (3) and (6) are completely equivalent providing that, matrixwise,

$$\mathfrak{F}=\tau^{-1}. \tag{7}$$

Explicit forms for $\mathcal{T}(\omega,\psi)$ may be obtained[1,3] and restrictions laid down due to the desired appearance of field quanta, and so forth, but we shall require only two general conditions, easily derivable from (6). First, applying (4), we see that $\mathfrak{F}$, and so τ, is symmetric or skew as $J=\pm1$:

$$\tau^T=J\tau, \tag{8}$$

where a^T denotes the transpose of the matrix a; second, predicating the existence of a Hermitian adjoint operation: $(\varphi\xi)^*=\xi^*\varphi^*$, under which ψ is real[4]: $\psi^*=\psi$, and applying this operation to (6) for a real basis $\{F_\alpha\psi\}$, we have

$$\tau_{\alpha\beta}{}^*=J\tau_{\alpha\beta}. \tag{9}$$

Equation (8), and Eq. (9) combined with (8), may be translated to read: the bilinear form or scalar product

* Now at New York University Institute of Mathematical Sciences, New York City, New York.

[1] J. K. Percus, Columbia University Dissertation, 1954 (unpublished).

[2] If in particular $\psi_s=\Sigma_\alpha C_{\alpha s}(x)F_\alpha\psi$, the $F_\alpha\psi$ are seen to be Fourier components of an expansion by the set of solutions C_α.

[3] J. K. Percus, Phys. Rev. **96**, 1147 (1954).

[4] This is no restriction, for a complex ψ may be regarded as a pair of reals.

$\mathcal{T}(\omega,\psi)$ obeys

$$\mathcal{T}(\sigma,\omega)=J\mathcal{T}(\omega,\sigma) \tag{10}$$

for c-numbers σ and ω, and

$$\mathcal{T}(\sigma,\omega)^*=\mathcal{T}(\omega^*,\sigma^*) \tag{11}$$

for any solutions σ and ω whatsoever.

At this point, it is expedient to introduce a little notation. Suppose that U is an invariant transformation in the sense that $M(U\psi)=0$ whenever $M\psi=0$. Then, if we define the matrix $U_{\alpha\beta}$ by

$$F_\alpha(U\psi)=\sum U_{\alpha\beta}F_\beta\psi, \tag{12}$$

$U_{\alpha\beta}$ is coordinate-independent and completely determines $U\psi$ according to $U\psi=\sum C_\alpha F_\alpha U\psi=\sum C_\alpha U_{\alpha\beta}F_\beta\psi$. (See footnote 2); in fact, from the evident $F_\alpha C_\beta=\delta_{\alpha\beta}$, we also have $U_{\alpha\beta}=F_\alpha UC_\beta$. Of crucial importance is that $U_{\alpha\beta}$ behaves like a matrix, obeying $(UV)_{\alpha\gamma}=\sum_\beta U_{\alpha\beta}V_{\beta\gamma}$ etc., which are readily verified. Now let us combine the concepts of invariant transformation U and scalar product $\mathcal{T}(\omega,\psi)$ based on the matrix τ to obtain the τ-transpose U^τ, defined by

$$\mathcal{T}(\sigma,U\omega)=\mathcal{T}(U^\tau\sigma,\omega), \tag{13}$$

which possesses the usual properties $(U^\tau)^\tau=U$ and $(UV)^\tau=V^\tau U^\tau$. If we write out (11): $\sum F_\alpha\sigma\tau_{\alpha\beta}U_{\beta\gamma}F_\gamma\omega=\sum(U^\tau)_{\beta\alpha}F_\alpha\sigma\tau_{\beta\gamma}F_\gamma\omega$, we find at once that the matrix $U^\tau=(U^\tau{}_{\alpha\beta})$ is determined by

$$U^\tau=\tau^{-1}U^T\tau. \tag{14}$$

The quadratic constants of the motion are now easily developed. If U is a real invariant transformation, we shall define

$$Q_U=\tfrac{1}{2}i\hbar\mathcal{T}(\psi,U\psi); \tag{15}$$

according to (11),

$$Q_U{}^*=-\tfrac{1}{2}i\hbar\mathcal{T}(U\psi,\psi)=\tfrac{1}{2}i\hbar\mathcal{T}(\psi,-U^\tau\psi),$$

or

$$Q_U{}^*=Q_{-U^\tau}, \tag{16}$$

so that Q_U will be Hermitian providing that U is τ-skew: $U^\tau=-U$. To show that when U is τ-skew, the coordinate-independent Q_U is the constant associated with the transformation U, we note first that Q_U transforms correctly under an infinitesimal τ-skew V: $V(Q_U)=\tfrac{1}{2}i\hbar\times\{\mathcal{T}(V\psi,U\psi)+\mathcal{T}(\psi,UV\psi)\}=\tfrac{1}{2}i\hbar\mathcal{T}(\psi,(UV-VU)\psi)$, or

$$V(Q_U)=Q_{[U,V]}. \tag{17}$$

More importantly for the investigation to be pursued, if one utilizes the obvious

$$[AB,C]=A(B\cdot C)-B(C\cdot A), \tag{18}$$

a simple calculation with (3) shows that

$$[F\psi,Q_U]=i\hbar FU\psi, \tag{19}$$

so that Q_U generates the transformation U on the quantized space.

EFFECT OF A SUPPLEMENTARY CONDITION

Let us now adjoin to $M\psi=0$ the auxiliary operator relation,

$$S\psi=0; \tag{20}$$

in the absence of incompatibility, the commutation relations will then change to

$$F_\alpha\psi\cdot F_\beta\psi=\mathfrak{F}'_{\alpha\beta}. \tag{21}$$

Our object is to relate $\mathfrak{F}'$ to $\mathfrak{F}$, and this requires specifying the properties of the original system which are to be preserved in the supplemented system. Of several possible starting points,[1] fortunately all equivalent, one of the most reasonable (although not the briefest) is to require that if U is invariant both for $M\psi=0$ and for $M\psi=S\psi=0$, then, defining Q_U as in (15), relation (19) is to be maintained; $\mathfrak{F}'$ will then be uniquely determined. If U is invariant for both systems and of course is τ-skew, then employing (21) rather than (6) and again making use of (18), a brief computation shows that

$$[F_\lambda\psi,Q_U]=i\hbar\sum(\mathfrak{F}'\tau U)_{\lambda\alpha}F_\alpha\psi, \tag{22}$$

rather than (19); thus our requirement is that

$$\sum(\mathfrak{F}'\tau U)_{\lambda\alpha}F_\alpha\psi=\sum U_{\lambda\alpha}F_\alpha\psi \tag{23}$$

when $M\psi=S\psi=0$.

In order to evaluate (23) properly, we must investigate more sharply the effect of the condition $S\psi=0$. To do this, define an operator ρ which projects the solutions of $M\psi=0$ onto those of $M\psi=S\psi=0$; thus,

$$\text{if } M\psi=0, \text{ then } M\rho\psi=S\rho\psi=0 \tag{24}$$

while

$$\text{if } M\psi=S\psi=0, \text{ then } \rho\psi=\psi. \tag{24'}$$

Clearly ρ is invariant on $M\psi=0$ and satisfies $\rho^2=\rho$. Now if U, invariant on $M\psi=0$, is to be invariant on $M\psi=S\psi=0$ as well, this means that $U\rho\psi$ satisfies $SU\rho\psi=0$, or that $\rho U\rho\psi=U\rho\psi$ for all solutions ψ of $M\psi=0$; thus, matrically,

$$\rho U\rho=U\rho, \tag{25}$$

and for such U, according to (23), we must have $\sum(\mathfrak{F}'\tau U)_{\lambda\alpha}F_\alpha\rho\psi=\sum U_{\lambda\alpha}F_\alpha\rho\psi$ or

$$(\mathfrak{F}'\tau-1)U\rho=0. \tag{26}$$

Since, utilizing $\rho^2=\rho$, the general solution of (25) is seen to be

$$U=\rho A\rho+\rho B(1-\rho)+(1-\rho)C(1-\rho), \tag{27}$$

we conclude from (26) that $(\mathfrak{F}'\tau-1)\rho A\rho=0$ for arbitrary A, whence

$$(\mathfrak{F}'\tau-1)\rho=0. \tag{28}$$

There remains the consistency condition for the commutation relations, stemming from the added relation $S\psi=0$, or equivalently, from (24'), $(1-\rho)\psi=0$; we thus require $0=\sum(1-\rho)_{\gamma\alpha}F_\alpha\psi\cdot F_\beta\psi=\sum(1-\rho)_{\gamma\alpha}\mathfrak{F}'_{\alpha\beta}$ (plus

an identical relation), or

$$(1-\rho)\mathfrak{F}'=0. \tag{29}$$

It is easy to characterize the solution, if one exists, of (28) and (29); writing (29) as $\mathfrak{F}'\tau=\rho\mathfrak{F}'\tau$, we have $(\mathfrak{F}'\tau)^2=\mathfrak{F}'\tau\rho\mathfrak{F}'\tau$, which by (28) is $\rho\mathfrak{F}'\tau=\mathfrak{F}'\tau$. Thus

$$(\mathfrak{F}'\tau)^2=\mathfrak{F}'\tau, \tag{30}$$

and $\mathfrak{F}'\tau$ has the aspect of a projection; in fact, if $M\psi=0$, then $S\mathfrak{F}'\tau\psi=S\rho\mathfrak{F}'\tau\psi=0$, while if $M\psi=S\psi=0$, then $\mathfrak{F}'\tau\psi=\mathfrak{F}'\tau\rho\psi=\rho\psi=\psi$, so that

$$\mathfrak{F}'\tau \text{ projects onto the solutions of } M\psi=S\psi=0. \tag{31}$$

Finally,

$$(\mathfrak{F}'\tau)^\tau=\tau^{-1}(\mathfrak{F}'\tau)^T\tau=\tau^{-1}(J\tau)(J\mathfrak{F}')\tau=\mathfrak{F}'\tau,$$

whence

$$\mathfrak{F}'\tau \text{ is } \tau\text{-symmetric.} \tag{32}$$

Now not only is the existence of a projection satisfying (31) and (32) necessary for the quantization of a supplemented system, but such a projection is also unique and directly determines the matrix $\mathfrak{F}'$. The uniqueness may be shown by solving (28) and (29) quite in general, but there is a simpler and more useful approach available for our purposes. If a τ-symmetric projection exists, we may take ρ to be this projection; then writing (29) as $\mathfrak{F}'\rho^\tau=\mathfrak{F}'$, we have from (28), $\rho=\mathfrak{F}'\tau\rho=\mathfrak{F}'\tau\rho^\tau=\mathfrak{F}'\rho^T\tau=\mathfrak{F}'\tau$, which establishes the uniqueness of ρ and $\mathfrak{F}'$, and more importantly, recalling $\tau^{-1}=\mathfrak{F}$, confirms that

$$\text{if } \rho^\tau=\rho, \text{ then } \mathfrak{F}'=\rho\mathfrak{F}. \tag{33}$$

CONSTRUCTION OF ρ

The major problem is now the determination of the τ-symmetric projection ρ, given S[5]; to this end, a number of reduction formulas are available, depending upon whether S may be expressed as a set, product, or sum of operators. For example, suppose that S consists of the set S_j, which commute, and that the projections ρ_j corresponding to the S_j commute as well. Then $S_j(\prod\rho_j)=0$, while if all $S_j\psi=0$, we have $(\prod\rho_j)\psi=\psi$; hence we may take

$$\rho=\prod\rho_j. \tag{34}$$

As another instance, if $S=\prod S_j$ is the product of commuting operators for which the ρ_j also commute, it is easy to verify that

$$\rho=1-\prod(1-\rho_j). \tag{35}$$

In a similar vein, if $S=\sum S_j$ is the sum of orthogonal operators: $S_jS_i=0$ if $j\neq i$, and if this orthogonality extends to the projections: $\rho_jS_i=S_j\rho_i=\rho_j\rho_i=0$ if $j\neq i$, then we have

$$\rho=\sum\rho_j. \tag{36}$$

[5] S is henceforth assumed to be written in the form of an invariant transformation, so that its functions have the same character.

An important realization occurs when the indices of S decompose so that $S_{\alpha\alpha'}=S_{\beta\gamma\beta'\gamma'}=S_{\gamma\gamma'}(\beta)\delta_{\beta\beta'}$; in such a case, if $\rho(\beta)$ is the projection for $S(\beta)$, we may certainly choose

$$\rho_{\beta\gamma\beta'\gamma'}=\rho_{\gamma\gamma'}(\beta)\delta_{\beta\beta'}. \tag{37}$$

It is clear that τ-symmetry of the ρ_j in (34)–(36) implies τ-symmetry of ρ. However, in the decomposition leading to (37), we may go even further, for if it so happens that $\tau_{\beta\gamma\beta'\gamma'}=\tau_{\gamma\gamma'}(\beta)\delta_{\beta\beta'}$ as well, then if we set $U^\tau{}_{\beta\gamma\beta'\gamma'}=U^\tau{}_{\gamma\gamma'}(\beta)\delta_{\beta\beta'}$ when the invariant U decomposes similarly, it follows at once that

$$U^\tau(\beta)=\tau(\beta)^{-1}U^T(\beta)\tau(\beta). \tag{38}$$

Thus $\tau(\beta)$ may be used to assess τ-symmetry of $\rho(\beta)$. On the other hand, a case of more frequent occurrence is that in which the various operators again have the form $U_{k\gamma k'\gamma'}=U_{\gamma\gamma'}(k)\delta(k-k')$, whereas $\tau_{k\gamma k'\gamma'}=\tau_{\gamma\gamma'}(k')\delta(k+k')$; k refers to a momentum 4-vector. Now, insertion into (14) yields the result[6]

$$U^\tau(k)=\tau(k)^{-1}U^T(-k)\tau(k); \tag{39}$$

$\tau(k)$ may be used to assess τ-symmetry of $\rho(k)$ provided that the modification (39) is used.

We have yet to indicate how a ρ may be secured when S has been reduced by (34)–(37) to relatively simple form. Of the numerous formulations available for obtaining ρ, most useful to us will be the fact that if $S\psi=0$ and $S^2\psi=0$ have the same solutions, equivalent to the minimal (=reduced characteristic) equation $f(S)=0$ possessing only simple roots (one of which must of course be 0), then

$$\rho=f(S)/Sf'(0) \tag{40}$$

will serve quite well. By this, we mean that $S\rho=0$, and $\rho\psi=\psi$ when $S\psi=0$, may be immediately verified. An equivalent expression which is sometimes of use is the following: if $S=S_{\lambda_0}$ is one of a continuous sequence of matrices S_λ, for which $S_\lambda\psi=0$ is solvable only for $\lambda=\lambda_0$, then since $f(S)/S=\lim[f_\lambda(S_\lambda)-f_\lambda(0)]/S_\lambda$ as $\lambda\to\lambda_0$, $=\lim[-f_\lambda(0)/S_\lambda]$, we may write

$$\rho=\lim[-f_\lambda(0)/S_\lambda f'(0)] \text{ as } \lambda\to\lambda_0. \tag{41}$$

One observes that the function $f(S)$ in the above need not be the minimal function, since any equation satisfied by S will do, if it has a simple zero; however, unless f is minimal, the result (40) is palpably of unnecessarily high degree in S.

A further modification of (41) may be convenient; we note that if the characteristic function of a matrix A is $c(A)$, then $\mathrm{Tr}(A^{-1})=\mathrm{coef}(-v^{n-1})$ in $|vI-A^{-1}|$ $=\mathrm{coef}(-v^{-1})$ in $|I-v^{-1}A^{-1}|=\mathrm{coef}(-v^{-1})$ in $(-1)^n\times|v^{-1}I-A|/|A|$, where I is the unit matrix, or

$$\mathrm{Tr}(A^{-1})=-c'(0)/c(0). \tag{42}$$

[6] The statement becomes trivial when scalar products $\mathcal{T}$ based on a complex space rather than a real one are employed; we shall not however enter into this in the present paper.

Now if $c(S)=S^d g(S)$, while $f(S)=Sh(S)$, where g and h do not have S as a factor, then $c_\lambda(y)f_\lambda(y)^{-d}$ remains finite in the vicinity of $y=0$ for a scalar y as $\lambda\to\lambda_0$, the same thus being true for its logarithmic derivative $c'_\lambda(y)/c_\lambda(y)-df'_\lambda(y)/f_\lambda(y)$. Hence the quantity $[f'_\lambda(y)/f_\lambda(y)]/[c'_\lambda(y)/dc_\lambda(y)]\to 1$ as $\lambda\to\lambda_0$, and we conclude that

$$\rho=\lim[dS_\lambda^{-1}/\mathrm{Tr}(S_\lambda^{-1})]. \tag{43}$$

The condition that ρ be τ-symmetric does not result automatically from (40); if S itself happens to be τ-symmetric, it is obvious that ρ of (40) is τ-symmetric. On the other hand, if S is τ-skew, its minimal equation $f(S)=0$ must be odd or even in S, for otherwise, noting that $f(S)^\tau=f(-S)=0$, one of $f(S)\pm f(-S)=0$ would be of lower degree than $f(S)=0$[7]; since $f(S)=0$ is to have the simple root $S=0$, $f(S)$ is then odd and $\rho(S)$ of (40) even, so that ρ is again τ-symmetric. Thus we should like to utilize a τ-symmetric or skew S' such that $S'\psi=0$ and $S\psi=0$ are equivalent[8]; if S is symmetric or skew, we need only choose

$$S'=\tau^{-1}S \text{ if } S^T=\pm S, \tag{44}$$

for then $(S')^\tau=\tau^{-1}(S')^T\tau=\tau^{-1}S^T(\tau^T)^{-1}\tau=\pm J\tau^{-1}S=\pm JS'$. If, as is often the case, there is a "pure imaginary" j (represented by a skew 2×2 matrix) which commutes with all operators being used, the τ-symmetry or skewness of S' may be reversed, if desired, by multiplication by j. Finally, working in a real basis so that the matrix S is real, a symmetric S' equivalent to S can in general be found, for $S\psi=0$ implies $S^TS\psi=0$, and (formally, and so for finite dimensional spaces, at least) if $S^TS\psi=0$, then $\psi^TS^TS\psi=|S\psi|^2=0$, whence $S\psi=0$:

$$S\psi=0 \text{ and } S^TS\psi=0 \text{ are equivalent.} \tag{45}$$

Combining (44) and (45), we have

$$S'=\tau^{-1}S^TS, \tag{46}$$

but it is also useful to note that

$$S'=\tau^{-1}S^T\tau S \tag{46'}$$

is always τ-symmetric, although the equivalence of S' and S must be verified in each case. If the matrix of S is not real, the equivalence attested to by (45) too may be invalid. The most important instance of this type is that in which a basis corresponding to a momentum representation is used; real operators which are diagonal in the k-component of this representation are characterized by $S_{\gamma\gamma'}(k)^*=S_{\gamma\gamma'}(-k)$. Now $\psi^{T*}S^{T*}S\psi=0$ does imply $S\psi=0$, so that $S(k)\psi=0$ and $S^T(-k)S(k)\psi=0$ are equivalent; further, if $\tau\infty\delta(k+k')$, then noting that $\tau^T(k)=-J\tau(-k)$, (39) tells us that $\tau(k)^{-1}S^T(-k)S(k)$ and $\tau(k)^{-1}S^T(-k)\tau(k)S(k)$ are τ-symmetric or skew. We can thus state the results of this discussion as well as (39) succinctly as:

$$\text{if } \tau\infty\delta(k+k'), \text{ then } S^T\to S^T(-k) \tag{47}$$

renders valid all equations which are diagonal in k.

SOME APPLICATIONS

Self-Adjoint Translation Invariant Field Equations

Consider the real linearly independent set of equations $\sum_s M_{rs}(\partial)\psi_s(x)=0$, where $M_{rs}(\partial)$ is a pure (coordinate-independent) differential operator; we shall assume that $M(\partial)$ is Hermitian or skew-Hermitian, as a differential operator, as $J=-1$ or $+1$. Now if $\mu(\partial)$ is the constant term (so-called reduced norm) of the minimal equation $f(M)=0$ with pure real differential operators as coefficients, then since $\mu(\partial)=[(\mu(\partial)-f(M))/M]M$, any solution ψ satisfies $\mu(\partial)\psi_s(x)=0$[9]; we may thus rewrite the system as

$$\mu(\partial)\psi_s(x)=0, \tag{48}$$

with subsidiary conditions:

$$\sum M_{rs}(\partial)\psi_s(x)=0. \tag{48'}$$

A comparison of $f(M)=0$ with the equally valid $(f(M))^\dagger=0$ shows that for f to be minimal, $\mu(\partial)$ must be Hermitian or skew Hermitian. Let us now introduce the plane wave expansion $\psi_s(x)=(2\pi)^{-n/2}\sum\psi_s(k)e^{ik\cdot x}$; if $\mu(\partial)$ has no repeated factor, a complete set of solutions is formally obtained by restriction to the surface $\mu(ik)=0$ which, according to the preceding remark, represents a real surface. At each point of $\mu(ik)=0$ we have, by (48'), the supplementary operator

$$S_{rs}(k)=M_{rs}(ik). \tag{49}$$

The general quantization methods of reference 1 show that the commutation relations for the simple expression (48) are determined by

$$\mathfrak{F}_{ksk's'}=\mathfrak{F}_{ss'}(k)\delta(\mu(ik))\delta(k+k') \tag{50}$$

or, formally, by

$$\tau_{ksk's'}=\tau_{ss'}(k')\delta(k+k')/\delta(\mu(ik)), \tag{50'}$$

in which, meaning is imparted by the fact that $\psi(k)$ contains the factor $\delta(\mu(ik))$. Since $M^T(ik)=\pm M(-ik)$, (47) tells us that we may apply (44):

$$S'(k)=\tau(k)^{-1}M(ik); \tag{51}$$

[7] In the case of S being τ-skew, it is thus necessary to employ the minimal equation and not any characteristic equation.

[8] Failure of the minimal equation of a τ-skew or τ-symmetric S' to have a simple zero makes (40) inappropriate, but need not prohibit the establishment of a suitable projection; note however that the Lorentz condition for the electromagnetic field does fail in this respect.

[9] If $M(\partial)$ is a polynomial in the ∂_j, and we tacitly assume this to be the case, then if $\mu(\partial)$ is the lowest common multiple of the $(M(\partial))^{-1}_{rs}$ when written in lowest terms, we may write $M(\partial)^{-1}=N(\partial)/\mu(\partial)$ where N is a polynomial, so that $N(\partial)M(\partial)\psi=\mu(\partial)\psi=0$; $\mu(\partial)$ differs from that in (48) by at most a constant factor.

$S'(k)$ is nonsingular except when $\mu(ik)=0$, so that if lim refers to this condition, we may, by (43) write

$$\rho(k)=\lim[dM(ik)^{-1}\tau(k)/\mathrm{Tr}(M(ik)^{-1}\tau(k))]. \quad (52)$$

Inserting (50) and (52) into (33), the factor $\delta(\mu(ik))$ renders the presence of lim unnecessary; we conclude that

$$\mathfrak{F}'_{ksk's'}=d(M(ik)^{-1})_{ss'}\delta(\mu(ik)) \times\delta(k+k')/\mathrm{Tr}(M(ik)^{-1}\tau(k)), \quad (53)$$

so that, setting

$$\mathfrak{D}(x,x')=(2\pi)^{-n}\int\cdots\int e^{ik\cdot(x-x')}\delta(\mu(ik))dk^n \quad (54)$$

we may write

$$\psi_s(x)\cdot\psi_{s'}(x')=[d(M(\partial))_{ss'}{}^{-1}/ \mathrm{Tr}(M(\partial)^{-1}\tau(-i\partial))]\mathfrak{D}(x,x'). \quad (55)$$

This generalizes a result of Takahashi and Umezawa.[10]

Nonlocal Real Vector Meson[11]

Here the equations of motion are, with umbral indices,

$$[(\partial/\partial X_\mu)(\partial/\partial X^\mu)-\kappa^2]\psi^\nu(X,\tau)=0, \quad (56)$$

and these are accompanied by the supplementary relations

$$\begin{aligned}&\tau^\mu(\partial/\partial X_\mu)\psi^\nu=0, \quad (\tau_\mu\tau^\mu-\lambda^2)\psi^\nu=0,\\ &(\partial/\partial X^\nu)\psi^\nu=0, \qquad\quad \tau_\nu\psi^\nu=0.\end{aligned} \quad (56')$$

Transforming to momentum space for the X_ν, the supplementary operators decompose according to $S^\mu{}_{k\tau\nu k'\tau'}=S^\mu{}_\nu(k,\tau)\delta(k-k')\delta(\tau-\tau')$, where

$$\begin{aligned}&{}^{(1)}S(k,\tau)=\tau^\mu k_\mu I,\\ &{}^{(2)}S(k,\tau)=(\tau^\mu\tau_\mu-\lambda^2)I,\\ &{}^{(3)}S(k,\tau)=\begin{pmatrix}k_0&k_1&k_2&k_3\\ \tau_0&\tau_1&\tau_2&\tau_3\\ 0&0&0&0\\ 0&0&0&0\end{pmatrix},\end{aligned} \quad (57)$$

while Eqs. (56) delimit solutions to the surface $k_\nu k^\nu+\kappa^2=0$; I again denotes the unit matrix. It may be shown[1] that we can with some generality choose

$$\tau_{\mu k\tau\nu k'\tau'}=\delta_{\mu\nu}\tau(k',\tau)\delta(k+k')\delta(\tau-\tau')/\delta(k_\sigma k^\sigma+\kappa^2). \quad (58)$$

Clearly, the projections

$${}^{(1)}\rho(k,\tau)=\delta[\tau^\mu k_\mu]I, \quad {}^{(2)}\rho(k,\tau)=\delta[\tau^\mu\tau_\mu-\lambda^2]I, \quad (59)$$

where the brackets indicate Kronecker, rather than Dirac δ's, formally suffice; for the third factor, application of (46) now yields, except for a factor in k alone,

$${}^{(3)}S'(k)=(-\delta_{\mu\nu})({}^{(3)}S(-k))^T\,{}^{(3)}S(k),$$

or

$${}^{(3)}S'^\mu{}_\nu(k,\tau)=k^\mu k_\nu-\tau^\mu\tau_\nu. \quad (60)$$

Employing $k_\mu k^\mu=-\kappa^2$, $\tau_\mu\tau^\mu=\lambda^2$, we obtain from (60), $(S')^3+(\kappa^2+\lambda^2)(S')^2+\kappa^2\lambda^2S'=0$ as minimal equation; it follows from (40) that ${}^{(3)}\rho=(S')^2+(\kappa^2+\lambda^2)S'+\kappa^2\lambda^2/(-\kappa^2\lambda^2)$, or

$${}^{(3)}\rho^\mu{}_\nu(k,\tau)=\delta^\mu{}_\nu+k_\nu k^\mu/\kappa^2-\tau_\nu\tau^\mu/\lambda^2. \quad (61)$$

Since the projections of (59) and (61) are seen to commute, the over-all projection is their product; thus the commutation relations may be written in the form

$$\psi^\mu(k,\tau)\cdot\psi^\nu(k',\tau')=(\delta^{\mu\nu}+k^\mu k^\nu/\kappa^2-\tau^\mu\tau^\nu/\lambda^2) \times\delta[\tau^\sigma k_\sigma]\delta[\tau^\sigma\tau_\sigma-\lambda^2]\delta(k+k')\delta(\tau-\tau')\mathfrak{F}(k,\tau). \quad (62)$$

SEVERAL SUPPLEMENTARY CONDITIONS

We now proceed to the case of a linear system augmented by a number of subsidiary relations ${}^{(j)}S\psi=0$. If the ${}^{(j)}S$ commute, then we know from (34) that the product of the individual projections, if also commutative, will serve as projection for the complete set; this approach was used in obtaining Eq. (62). On the other hand, even if the ${}^{(j)}S$ do not commute, we may form a rectangular matrix S by placing the ${}^{(j)}S$ one on top of another. Then, by (45), the set ${}^{(j)}S\psi=0$ is equivalent to the single $S'\psi=0$, where

$$S'=\sum{}^{(j)}S^T\,{}^{(j)}S; \quad (63)$$

the formation of (60) may be viewed in this light. Equation (63) may be regarded as a constructive proof of the fact that any set of linear equations in N unknowns is reducible, for N finite, to a set of at most N equations. The difficulty inherent in formulations such as (63) is that the further operations required to develop the desired projection tend to be excessively cumbersome; we shall therefore consider an indirect method which is generally more appropriate—that of applying the supplementary conditions one by one.

Suppose then that the operator ${}^{(1)}S$ alone has been treated, yielding the projection ${}^{(1)}\rho$ with

$${}^{(1)}\mathfrak{F}={}^{(1)}\rho\mathfrak{F}. \quad (64)$$

Consider the next supplementary operator ${}^{(2)}S$ and τ-symmetrize or τ-antisymmetrize it to obtain ${}^{(2)}S'$; now the various transformations required to convert ${}^{(2)}S'$ to a projection upon the system expressed by (64) cannot readily be performed unless ${}^{(2)}S'$ is invariant on the space of $M\psi={}^{(1)}S\psi=0$, i.e., unless it carries this space into itself. We must thus find a ${}^{(2)}S''$ which is a mapping on this space and whose value on it is the same as that of ${}^{(2)}S'$. The condition that ${}^{(2)}S'$ and ${}^{(2)}S''$ have identical values on this space is clearly that

$${}^{(1)}\rho({}^{(2)}S''-{}^{(2)}S')\,{}^{(1)}\rho=0, \quad (65)$$

while the condition that ${}^{(2)}S''$ carry this space into itself may be written, as in (25), as

$$(1-{}^{(1)}\rho)\,{}^{(2)}S''\,{}^{(1)}\rho=0. \quad (66)$$

[10] Y. Takahashi and H. Umezawa, Progr. Theoret. Phys. **9**, 15 (1953).

[11] H. Yukawa, Phys. Rev. **77**, 219 (1950).

From (65) and (66), ${}^{(2)}S''\,{}^{(1)}\rho={}^{(1)}\rho\,{}^{(2)}S''\,{}^{(1)}\rho={}^{(1)}\rho\,{}^{(2)}S'\,{}^{(1)}\rho$, and this result,

$$ {}^{(2)}S''\,{}^{(1)}\rho={}^{(1)}\rho\,{}^{(2)}S'\,{}^{(1)}\rho, \tag{67} $$

is seen to imply (65) and (66) as well; thus (67) alone is necessary and sufficient. There remains the task of checking the τ-symmetry or antisymmetry of ${}^{(2)}S''$ in the new basis; this however is trivial, for imposing the first supplementary condition on ψ and ω, the basic relation $\mathcal{T}(\omega, {}^{(2)}S'\psi)=\pm\mathcal{T}({}^{(2)}S'\omega, \psi)$ may be replaced by $\mathcal{T}(\omega, {}^{(2)}S''\psi)=\pm\mathcal{T}({}^{(2)}S''\omega, \psi)$.

One immediate solution of (67) is given by

$$ {}^{(2)}S''={}^{(1)}\rho\,{}^{(2)}S'\,{}^{(1)}\rho, \tag{68} $$

and this will be of primary importance. We note however that ${}^{(2)}S''$ defined by (68) is actually zero on a space complementary to that of ${}^{(2)}S'\psi=0$; this is of course not necessary, and in certain cases, we may take advantage of this fact to construct a more malleable solution. Suppose that ${}^{(1)}\rho$ may be decomposed as

$$ {}^{(1)}\rho=\sum\sigma_j, \text{ where } \sigma_j\,{}^{(1)}\rho=c_j\,{}^{(1)}\rho \tag{69} $$

for certain constants c_j (which due to $\rho^2=\rho$, must satisfy $\sum c_j=1$); then if (a_{ij}) is any matrix for which

$$ \sum a_{ij}c_j=1 \tag{70} $$

for each i, we may choose

$$ {}^{(2)}S''=\sum a_{ij}\,\sigma_i{}^{\tau}\,{}^{(2)}S'\,\sigma_j, \tag{71} $$

for it then follows that ${}^{(2)}S''\,{}^{(1)}\rho=\sum a_{ij}\,\sigma_i{}^{\tau}\,{}^{(2)}S'\,\sigma_j\,{}^{(1)}\rho=\sum a_{ij}\,\sigma_i{}^{\tau}\,{}^{(2)}S'\,c_j\,{}^{(1)}\rho=\sum\sigma_i{}^{\tau}\,{}^{(2)}S'\,{}^{(1)}\rho={}^{(1)}\rho\,{}^{(2)}S'\,{}^{(1)}\rho$, as desired. An important realization occurs when the σ_j form, except for a constant factor, a group of order N; then $\sigma_j\,{}^{(1)}\rho=N^{-1}\,{}^{(1)}\rho$, and we have, with $a_{ij}=N\delta_{ij}$,

$$ {}^{(2)}S''=N\sum\sigma_i{}^{\tau}\,{}^{(2)}S'\,\sigma_i. \tag{72} $$

Having found ${}^{(2)}S''$, ${}^{(2)}\rho$ may be obtained by methods previously discussed, so that ${}^{(2)}\mathfrak{F}={}^{(2)}\rho\,{}^{(1)}\rho\,\mathfrak{F}$, and the whole process may be repeated for additional supplementary conditions.

HIGHER SPIN MESON FIELD

As an illustration of the preceding discussion, we consider the quantization of the integral spin real meson, a problem first treated by Fierz.[12] The sth rank tensor $\psi^{\alpha\beta\gamma\cdots}(x)$ satisfies the Klein-Gordon equation

$$ [(\partial/\partial x^{\mu})(\partial/\partial x_{\mu})-\kappa^2]\psi^{\alpha\beta\gamma\cdots}(x)=0, \tag{73} $$

where $x_0=-ct$, together with the supplementary conditions

$$ \begin{aligned} &\psi^{\alpha\beta\gamma\cdots} \text{ symmetric in } \alpha, \beta, \gamma, \cdots, \\ &\psi_{\alpha}{}^{\alpha\gamma\cdots}=0, \text{ and } \psi_{,\alpha}{}^{\alpha\beta\gamma\cdots}(x)=0, \end{aligned} \tag{74} $$

which serve to restrict solution space to the $(2s+1)$-component subspace associated with spin s. If we switch to the momentum representation by means of

$$ \psi^{\alpha\beta\gamma\cdots}(x)=(2\pi)^{-2}\int\psi^{\alpha\beta\gamma\cdots}(k)\exp(ik_rx^r)(dk)^4, \tag{75} $$

the operators for the supplementary conditions on the kth subspace are then given by

$$ {}^{(1)}S^{\alpha\beta\cdots}{}_{\alpha'\beta'\ldots}=\delta_{\alpha'}{}^{\alpha}\delta_{\beta'}{}^{\beta}\cdots-1/s!\sum_Q\delta_{\alpha'}{}^{Q\alpha}\delta_{\beta'}{}^{Q\beta}\cdots, \tag{76} $$

where Q runs over all index permutations,

$$ {}^{(2)}S^{\alpha\beta\cdots}{}_{\alpha'\beta'\ldots}=k_{\alpha'}\delta_{\beta'}{}^{\beta}\delta_{\gamma'}{}^{\gamma}\cdots, \tag{77} $$

where $k_{\alpha}k^{\alpha}=-\kappa^2$, and

$$ {}^{(3)}S^{\alpha\beta\cdots}{}_{\alpha'\beta'\ldots}=\delta^{\alpha\beta}\delta_{\alpha'\beta'}\delta_{\gamma'}{}^{\gamma}\cdots. \tag{78} $$

Furthermore, if as usual we choose the Einstein-Bose commutation relations before application of the supplementary conditions as

$$ \psi^{\alpha\beta\gamma\cdots}(x)\cdot\psi^{\alpha'\beta'\gamma'\cdots}(x')=\delta^{\alpha\alpha'}\delta^{\beta\beta'}\cdots(\hbar/i)D(x-x'), \tag{79} $$

then except for factors in k which include $\delta(k+k')$, we have

$$ \tau_{\alpha\beta\cdots\alpha'\beta'\ldots}=\delta_{\alpha\alpha'}\delta_{\beta\beta'}\cdots. \tag{80} $$

We are now prepared to combine the supplementary conditions in sequence; the initial operation is to τ-symmetrize them, which we may do by means of (46′), modified by (47): $S'=\tau^{-1}S^{T}(-k)\tau S(k)$ or

$$ S'^{\alpha\beta\cdots}{}_{\alpha'\beta'\ldots}=S^{\alpha''\beta''\cdots\alpha\beta\cdots}(-k)S_{\alpha''\beta''\ldots\alpha'\beta'\ldots}(k). \tag{81} $$

This yields, except for sign,

$$ \begin{aligned} {}^{(1)}S'^{\alpha\beta\cdots}{}_{\alpha'\beta'\ldots}&=\delta_{\alpha'}{}^{\alpha}\delta_{\beta'}{}^{\beta}\cdots-(1/s!)\textstyle\sum_Q\delta_{\alpha'}{}^{Q\alpha}\delta_{\beta'}{}^{Q\beta}\cdots \\ {}^{(2)}S'^{\alpha\beta\cdots}{}_{\alpha'\beta'\ldots}&=k^{\alpha}k_{\alpha'}\delta_{\beta'}{}^{\beta}\delta_{\gamma'}{}^{\gamma}\cdots \\ {}^{(3)}S'^{\alpha\beta\cdots}{}_{\alpha'\beta'\ldots}&=\delta^{\alpha\beta}\delta_{\alpha'\beta'}\delta_{\gamma'}{}^{\gamma}\cdots, \end{aligned} \tag{82} $$

equivalent to the corresponding ${}^{(i)}S$.

Since $({}^{(1)}S')^2={}^{(1)}S'$, our first projection is given by ${}^{(1)}\rho=1-{}^{(1)}S'$, or

$$ {}^{(1)}\rho^{\alpha\beta\cdots}{}_{\alpha'\beta'\ldots}=(1/s!)\textstyle\sum_Q\delta_{\alpha'}{}^{Q\alpha}\delta_{\beta'}{}^{Q\beta}\cdots, \tag{83} $$

the index symmetrizing operator. Now (69) is satisfied by $\sigma_Q=(1/s!)\delta_{\alpha'}{}^{Q\alpha}\delta_{\beta'}{}^{Q\beta}\cdots$, so that reduction to the space of symmetric tensors is accomplished by $S''=s!\sum\sigma_Q{}^{\tau}S'\sigma_Q$, or

$$ S''^{\alpha\beta\cdots}{}_{\alpha'\beta'\ldots}=(1/s!)\textstyle\sum_Q S'^{Q\alpha Q\beta\cdots}{}_{Q\alpha'Q\beta'\ldots}, \tag{84} $$

just simultaneous symmetrization of both indices. Employing (84) yields

$$ \begin{aligned} {}^{(2)}S''^{\alpha\beta\cdots}{}_{\alpha'\beta'\ldots}&=(1/s!)\textstyle\sum k^{Q\alpha}k_{Q\alpha'}\delta_{Q\beta'}{}^{Q\beta}\delta_{Q\gamma'}{}^{Q\gamma}\cdots \\ &=(1/s)(k^{\alpha}k_{\alpha'}\delta_{\beta'}{}^{\beta}\delta_{\gamma'}{}^{\gamma}\cdots \\ &\qquad+\delta_{\alpha'}{}^{\alpha}k^{\beta}k_{\beta'}\delta_{\gamma'}{}^{\gamma}\cdots+\cdots), \end{aligned} \tag{85} $$

$$ \begin{aligned} {}^{(3)}S''^{\alpha\beta\cdots}{}_{\alpha'\beta'\ldots}&=(1/s!)\textstyle\sum\delta^{Q\alpha Q\beta}\delta_{Q\alpha'}{}^{Q\beta'}\delta_{Q\gamma'}{}^{Q\gamma}\cdots \\ &=2/s(s-1)(\delta^{\alpha\beta}\delta_{\alpha'\beta'}\delta_{\gamma'}{}^{\gamma}\cdots \\ &\qquad+\delta^{\alpha\gamma}\delta_{\beta'}{}^{\beta}\delta_{\alpha'\gamma'}\cdots+\cdots). \end{aligned} \tag{85′} $$

[12] M. Fierz, Helv. Phys. Acta 12, 3 (1939).

To obtain the projection corresponding to ${}^{(2)}S''$, we need only observe that ${}^{(2)}S''$ is the sum of commuting operators of the type $(k^\alpha k_{\alpha'}\delta_{\beta'}{}^\beta\delta_{\gamma'}{}^\gamma\cdots)/s$, so that, according to (34) its projection is the product of the subprojections. Since $(k^\alpha k_{\alpha'})^2=-\kappa^2(k^\alpha k_{\alpha'})$, these individual projections may be found from (40) and are thus given by

$$R_{\alpha'}{}^\alpha=\delta_{\alpha'}{}^\alpha+k^\alpha k_{\alpha'}/\kappa^2, \tag{86}$$

whence

$${}^{(2)}\rho^{\alpha\beta\cdots}{}_{\alpha'\beta'\ldots}=R_{\alpha'}{}^\alpha R_{\beta'}{}^\beta\cdots. \tag{87}$$

It is of interest to note that $R_{\alpha'}{}^\alpha$ itself is a divergenceless tensor which acts as Kronecker delta on the space of divergenceless tensors, as verified by

$$R_{\alpha'}{}^\alpha b_{\alpha'}=b_\alpha \text{ when } k^\alpha b_\alpha=0; \tag{88}$$

due to the vanishing of its divergence, $R_{\alpha'}{}^\alpha$ effectively acts on a three component space, consistent with $R_\alpha{}^\alpha=3$.

Having (86) and (87) at our disposal, we may now limit ${}^{(3)}S''$ to divergenceless symmetric tensors by choosing ${}^{(3)}S'''={}^{(2)}\rho\,{}^{(3)}S''\,{}^{(2)}\rho$; utilizing

$$R_\beta{}^\alpha R_\gamma{}^\beta=R_\gamma{}^\alpha, \tag{89}$$

a special case of (88), we obtain

$${}^{(3)}S'''{}^{\alpha\beta\cdots}{}_{\alpha'\beta'\ldots}=[2/s(s-1)](R^{\alpha\beta}R_{\alpha'\beta'}R_{\gamma'}{}^\gamma\cdots +R^{\alpha\gamma}R_{\alpha'\gamma'}R_{\beta'}{}^\beta\cdots+\cdots) \tag{90}$$

i.e., the $\delta^{\alpha\beta}$ have been replaced by the $R^{\alpha\beta}$. There remains only the problem of constructing the projection for ${}^{(3)}S'''$. For this purpose, it is helpful to remark that the space of symmetric tensors is generated by the Kronecker sth powers: $a^\alpha a^\beta a^\gamma\cdots a^\omega$, for clearly $\sum\delta_{\alpha'}{}^{Q\alpha}\delta_{\beta'}{}^{Q\beta}\cdots\delta_{\omega'}{}^{Q\omega}=\text{coef } t_1\cdots t_s \text{ in } a^\alpha a^\beta a^\gamma\cdots a^\omega$, where $a^\alpha=t_1\delta_{\alpha'}{}^\alpha+t_2\delta_{\beta'}{}^\alpha+t_3\delta_{\gamma'}{}^\alpha+\cdots$; to generate the symmetric divergenceless tensors, we need only require $k_\alpha a^\alpha=0$, an immediate consequence being that $R_{\alpha'}{}^\alpha a^{\alpha'}=a^\alpha$.

The construction of ${}^{(3)}\rho$ hinges on that of a characteristic equation for ${}^{(3)}S'''$ which, according to the preceding remark, need only be applied to $a^\alpha a^\beta\cdots$. It will be of aid to define

$$\Xi_f{}^{\alpha\beta\cdots\omega}=(1/s!)\sum R^{Q\alpha Q\beta}R^{Q\gamma Q\delta}\cdots a^{Q\eta}\cdots a^{Q\omega}(a_\lambda a^\lambda)^f, \tag{91}$$

for $f=0, 1, \cdots, [s/2]$ ($[s/2]$=largest integer $\leq s/2$), where f R-functions and $s-2f$ single a's are present; as a special case, we observe that

$$\Xi_0{}^{\alpha\beta\cdots\omega}=a^\alpha a^\beta\cdots a^\omega. \tag{92}$$

Now let us apply

$${}^{(3)}S'''{}^{\alpha\beta\cdots}{}_{\alpha'\beta'\ldots}=(1/s!)\sum(R^{Q\alpha Q\beta}R_{Q\alpha'Q\beta'}R_{Q\gamma'}{}^{Q\gamma}\cdots)$$

to Ξ_f; Ξ_f being symmetric, it suffices to apply $R^{\alpha\beta}R_{\alpha'\beta'}R_{\gamma'}{}^\gamma\cdots$ and then symmetrize. Since $R_{\gamma'}{}^\gamma R_\delta{}^\delta\cdots$ behaves as the identity on its associated indices in Ξ_f, we need only consider the effect of $R^{\alpha\beta}R_{\alpha'\beta'}$ upon the various classes of terms of Ξ_f; thus we require

$$\begin{aligned}(R^{\alpha\beta}R_{\alpha'\beta'})R^{\alpha'\beta'}&=3R^{\alpha\beta},\\ (R^{\alpha\beta}R_{\alpha'\beta'})R^{\alpha'\rho}R^{\beta'\sigma}&=R^{\alpha\beta}R^{\rho\sigma},\\ (R^{\alpha\beta}R_{\alpha'\beta'})R^{\alpha'\rho}a^{\beta'}&=R^{\alpha\beta}a^\rho,\\ (R^{\alpha\beta}R_{\alpha'\beta'})a^{\alpha'}a^{\beta'}&=R^{\alpha\beta}(a_\lambda a^\lambda),\end{aligned} \tag{93}$$

accounting (except for the distinction between such as $R^{\alpha'\rho}$ and $R^{\rho\alpha'}$) for all locations of α' and β' in Ξ_f.

Of the $s!$ terms of Ξ_f, the classes exhibited in (93), for a given pair such as α, β, encompass respectively $2f(s-2)!$, $2f(2f-2)(s-2)!$, $4f(s-2f)(s-2)!$, and $(s-2f)(s-2f-1)(s-2)!$ terms, and give rise to terms of type Ξ_f, Ξ_f, Ξ_f, and Ξ_{f+1}. Since any member of Ξ_f spreads on symmetrization into $\Xi_f/s!$, we conclude that

$${}^{(3)}S'''\,\Xi_f=[(s-2)!/s!](2f\cdot 3\Xi_f+2f(2f-2)\Xi_f +4f(s-2f)\Xi_f+(s-2f)(s-2f-1)\Xi_{f+1}),$$

or that

$$[{}^{(3)}S'''-2f(2s+1-2f)/s(s-1)]\Xi_f =(s-2f)(s-1-2f)/s(s-1)\Xi_{f+1}. \tag{94}$$

It follows from (94) that

$$\prod_{f=0}^{[s/2]}\left({}^{(3)}S'''-\frac{2f(2s+1-2f)}{s(s-1)}\right)\Xi_0=0,$$

whence

$$\prod_{f=0}^{[s/2]}\left({}^{(3)}S'''-\frac{2f(2s+1-2f)}{s(s-1)}\right)=0. \tag{95}$$

In the Appendix, it is shown that (95) is actually the minimal equation for ${}^{(3)}S'''$; thus, applying (40), the projection of lowest degree is readily found to be

$${}^{(3)}\rho=\prod_{f=1}^{[s/2]}\left[1-\frac{s(s-1)}{2f(2s+1-2f)}\,{}^{(3)}S'''\right]. \tag{96}$$

The modified commutation relations may now be written down in terms of $\mathfrak{F}'={}^{(3)}\rho\,{}^{(2)}\rho\,{}^{(1)}\rho\mathfrak{F}$, or, $[M_{\alpha'\beta'\ldots}{}^{\alpha\beta\cdots}]$ indicating the matrix of elements $M_{\alpha'\beta'\ldots}{}^{\alpha\beta\cdots}$,

$$\mathfrak{F}'=\prod[1-s(s-1)\,{}^{(3)}S'''/2f(2s+1-2f)] \times[R_{\alpha'}{}^\alpha R_{\beta'}{}^\beta\cdots][\textstyle\sum\delta_{\alpha'}{}^{Q\alpha}\delta_{\beta'}{}^{Q\beta}\cdots/s!]\mathfrak{F}.$$

Since $[R_{\alpha'}{}^\alpha R_{\beta'}{}^\beta\cdots]\,{}^{(3)}S'''={}^{(3)}S'''$, we have, on collecting equations (79), (83), (86), (87), and (96), the final result that if

$$P^{\alpha\beta\cdots}{}_{\alpha'\beta'\ldots}=(R^{\alpha\beta}R_{\alpha'\beta'}R_{\gamma'}{}^\gamma\cdots +R^{\alpha\gamma}R_{\beta'}{}^\beta R_{\alpha'\gamma'}\cdots+\cdots),$$

and

$$R^{\alpha\beta\cdots}{}_{\alpha'\beta'\ldots}=R_{\alpha'}{}^\alpha R_{\beta'}{}^\beta\cdots, \tag{97}$$

where

$$R_{\alpha'}{}^\alpha=\delta_{\alpha'}{}^\alpha-(1/\kappa^2)(\partial/\partial x^\alpha)(\partial/\partial x_{\alpha'}),$$

then

$$\psi^{\alpha\beta\cdots}(x)\cdot\psi_{\alpha'\beta'\ldots}(x')=(h/i)\sum^{Q}\prod_{f=1}^{[s/2]} \times[R-P/f(2s+1-2f)]_{Q\alpha'Q\beta'\ldots}{}^{\alpha\beta\cdots}D(x-x'). \tag{98}$$

Relation (98) differs from Fierz's result,[12] for in his attempt at proving the vanishing of the trace for the expression which he offers, he omits one type of term which is present for $s\geq 4$; indeed his results coincide with (98) for $s\leq 3$.

APPENDIX: MINIMAL EQUATION FOR ${}^{(3)}S'''$

To verify that (95) is the minimal equation for ${}^{(3)}S'''$, we shall first prove that the Ξ_f are linearly independent. To accomplish this, we must show that

$$\Upsilon_{(f,s)}{}^{\alpha\beta\cdots\omega}=(1/s!)\sum R^{\rho_\alpha\rho_\beta}R^{\rho_\gamma\rho_\delta}\cdots a^{\rho_\eta}\cdots a^{\rho_\omega}, \quad \text{(A1)}$$

containing f R's and $(s-2f)$ a's, does not vanish identically when $a_\lambda a^\lambda=0$. [The condition $k_\alpha a^\alpha=0$ is maintained from (91).] Now $a_\alpha\Upsilon_{(f,s)}{}^{\alpha\beta\cdots\omega}$ is clearly symmetric in β, $\cdots$, ω; since we now assume $a_\alpha a^\alpha=0$, while $R^{\alpha\sigma}a_\alpha=a^\sigma$, the latter possibility occurring in $2f(s-1)!$ of the $s!$ terms of $a_\alpha\Upsilon_{(f,s)}{}^{\alpha\beta\cdots\omega}$, we conclude at once that

$$a_\alpha\Upsilon_{(f,s)}{}^{\alpha\beta\cdots\omega}=2f\Upsilon_{(f-1,s-1)}{}^{\beta\cdots\omega}. \quad \text{(A2)}$$

Continuing this process, we see that $\Upsilon_{(f,s)}$ can be identically zero for $a_\lambda a^\lambda=0$ only if $\Upsilon_{(0,s-f)}=a^\alpha a^\beta\cdots a^\omega=0$ under the same conditions, which is clearly not true.

Suppose then that there exists a linear relation (an identity in the a^α for which $k_\alpha a^\alpha=0$) with constant coefficients:

$$\sum K_f\Xi_f=0; \quad \text{(A3)}$$

setting $a_\lambda a^\lambda=0$, we have $K_0\Upsilon_{(0,s)}=0$, whence $K_0=0$. Dividing (A3) by $a_\lambda a^\lambda$ and letting $a_\lambda a^\lambda\to 0$, $K_1\Upsilon_{(1,s)}=0$ or $K_1=0$; an inductive process leads to all $K_f=0$, so that the Ξ_f are linearly independent.

Now if $g({}^{(3)}S''')\Xi_0=0$ for g of degree $\leq[s/2]$, then according to (94), there is a linear relation among the Ξ_f, the coefficient of Ξ_f of highest index being nonvanishing, and this we have shown to be impossible. Thus the degree of g exceeds $[s/2]$, and (95), of degree $[s/2]+1$, must be the minimal equation for ${}^{(3)}S'''$.

Note added in proof.—The writer has been informed (private communication from Professor Fierz) that the error alluded to above, following Eq. (98), has previously been uncovered: M. Fierz, Helv. Phys. Acta **23**, 412 (1950). The corrected commutation relations were obtained as well in this publication, although in somewhat less explicit form than in the present paper.

PHYSICAL REVIEW VOLUME 97, NUMBER 5 MARCH 1, 1955

Sachs' Theorem on the Magnetic Moments of Nucleons

HIRONARI MIYAZAWA*
Institute for Nuclear Studies, University of Chicago, Chicago, Illinois
(Received September 20, 1954)

A correction due to nucleon-pair creation is given to Sachs' relationship between the sum of nucleon magnetic moments and the probability of virtual pions forming the state of angular momentum one. It is found that the probability determined by Sachs is considerably modified by this correction.

THE calculation of the magnetic moments of the proton and the neutron is one of the problems which the present pion theory cannot explain satisfactorily. Sachs[1] has shown that if P is the probability that the pions occur in the field with angular momentum one, the neutron and proton moments must satisfy the mirror condition:

$$\mu_p+\mu_n=1-(4/3)P,$$

from which he determined that $P=9$ percent. This is a very severe restriction on the construction of the wave function of the nucleon. In fact, with this small probability, the magnetic moment of the neutron turns out to be too small if the presence of two or more pions is neglected. To get the right value for the neutron moment, Sachs has to assume a special form for the pion cloud which is not easily derived from the usual interaction.

It is the purpose of this paper to see if we can alleviate this restriction. Sachs assumed that the magnetic moment of the bare proton is equal to one nuclear magneton. While this is true in the zeroth order approximation in $1/M$, where M is the nucleon mass, it is not necessarily a good approximation. Higher order approximations in $1/M$, in fact, give different results. Naively one would think that the magnetic moment of the bare proton is given by $e/2M_0$ instead of $e/2M$, where M_0 and M are the mechanical mass and experimental mass of the nucleon, respectively. Although it is in fact given by $e/2M_0$, other correction factors occur as a result of pair creation.

The sum of the proton and neutron moments is given by

$$\frac{e}{2M}(\mu_p+\mu_n)=\left\langle -ie\int\bar{\psi}(x)(x\times\gamma)_z\psi(x)dx\right\rangle, \quad (1)$$

where the expectation value is to be taken for the state of one nucleon with $J_z=\frac{1}{2}$. The pion current does not

* On leave of absence from the University of Tokyo, Tokyo, Japan.
[1] R. G. Sachs, Phys. Rev. **87**, 1100 (1952).

TABLE I. Values of the effective bare proton moment μ for various values of cutoff K_0 and coupling constant $g^2/4\pi$.

$g^2/4\pi$ \ K_0	$0.5M_0$	$1M_0$
5	1.025	1.12
10	1.03	1.15
20	1.06	1.2

contribute to this expression since it is opposite for proton and neutron. The integral on the right-hand side of (1) is indeterminate since the $\psi(x)$ has the character of a plane wave. This ambiguity can be settled by making use of the equation

$$\left(\gamma_\mu\frac{\partial}{\partial x_\mu}+M_0\right)\psi(x)=ig\gamma_5\tau_i\phi_i(x)\psi(x).$$

Substituting

$$\frac{1}{M_0}\left(-\gamma_\mu\frac{\partial}{\partial x_\mu}+ig\gamma_5\tau_i\phi_i(x)\right)\psi(x) \tag{2}$$

for $\psi(x)$ in (1) and then substituting the conjugate of (2) for $\bar{\psi}(x)$ and averaging, one obtains

$$\frac{e}{2M}(\mu_p+\mu_n)=\frac{e}{2M_0}\left\langle\int\bar{\psi}(x\times\dot{p})_z\psi dx+\int\bar{\psi}\sigma_z\psi dx\right\rangle. \tag{3}$$

This simple relationship can be obtained only in the case of pseudoscalar coupling. The first term in (3) is the orbital magnetic moment due to the motion of the proton caused by the emitted pions. This term can be neglected if recoil of the nucleon is small. This is the case if the cutoff momentum for the pion is smaller than the nucleon mass, which we assume to be true. However, this does not necessarily mean that nucleon-antinucleon pair creation does not occur, since it can be shown that the recoil correction is of higher order in $1/M$ than the pair creation. In order to evaluate

$$\frac{e}{2M_0}\left\langle\int\bar{\psi}\sigma_3\psi dx\right\rangle=\frac{e}{2M_0}\left\langle\int\psi^*\beta\sigma_z\psi dx\right\rangle, \tag{4}$$

we note that since the recoil of the nucleon is neglected, there is no correlation between S waves and P waves. Since β is coupled to S waves and σ_z to P waves, the average of the two quantities can be carried out separately. Thus, we may write (4) as

$$\frac{e}{2M}\frac{M}{M_0}\left\langle\int\psi^*\beta\psi dx\right\rangle\langle\sigma_z\rangle.$$

In this way, the evaluation of $\mu_p+\mu_n$ is divided into two independent problems, that is, first the calculation of

$$\mu=\frac{M}{M_0}\left\langle\int\psi^*\beta\psi dx\right\rangle, \tag{5}$$

which may be called the effective magnetic moment of the bare proton, and then the calculation of $\langle\sigma_z\rangle$. The latter has nothing to do with pair creation and was found by Sachs to be equal to $1-(4/3)P$. Thus one has a modified form of Sachs' theorem:

$$\mu_p+\mu_n=\mu[1-(4/3)P].$$

If μ is larger than one, then P can be larger than 9 percent and thus the restriction imposed by Sachs is no longer necessary. In the pseudoscalar coupling theory, M is larger than M_0 since the γ_5 interaction causes a large vacuum fluctuation and the subtraction of the vacuum energy gives a positive self-energy for the nucleon. Thus it is possible that μ becomes larger than one. However, the second factor in (5) gives an opposite contribution. For the self-energy to be positive, pair creation must occur and this means that $\langle\beta\rangle(=\langle\beta\rangle_{\text{nucl}}-\langle\beta\rangle_{\text{vac}})$ becomes smaller than one. In fact, up to the first order in g^2 and $1/M_0$, the two factors in μ cancel each other and one has $\mu=1$. However, in the next order μ is different from one.[2] We may obtain a rough idea of the value of μ by the Tamm-Dancoff approximation including up to one pion state. The Tamm-Dancoff approximation gives

$$M=M_0+\frac{g^2}{4\pi}\frac{3}{\pi}\int^{K_0}\frac{dk}{\omega_k(M_0+M+\omega_k)},$$

$$\left\langle\int\psi^*\beta\psi dx\right\rangle=\frac{\partial M}{\partial M_0}=\frac{1-\rho}{1+\rho},$$

$$\rho=\frac{g^2}{4\pi}\frac{3}{\pi}\int^{K_0}\frac{dk}{\omega_k(M_0+M+\omega_k)^2},$$

where $\omega_k=(k^2+\kappa^2)^{\frac{1}{2}}$. Numerical values of μ for various values of the cutoff momentum K_0 and coupling constant are given in Table I. In evaluating the integrals, ω_k has been set equal to $|k|$.

For $\mu=1.1$, one has $P=15$ percent. Although this is not large enough to explain the two nucleon moments in a simple way, one no longer has as severe a restriction as was imposed by Sachs. The construction of the wave function for the nucleon will be much easier and can be done with a more reasonable form of the pion cloud.

The author wishes to express his thanks to Dr. S. Cohen for helpful discussions.

[2] Since $M_0\langle\beta\rangle$ is equal to $-\langle T_{\mu\mu}\rangle$, one would have simple relations $\langle\beta\rangle=M/M_0$ and $\mu=(M/M_0)^2$ if the self-stress were zero. Actually the self-stress does not vanish and this argument fails.

Letters to the Editor

PUBLICATION of brief reports of important discoveries in physics may be secured by addressing them to this department. The closing date for this department is five weeks prior to the date of issue. No proof will be sent to the authors. The Board of Editors does not hold itself responsible for the opinions expressed by the correspondents. Communications should not exceed 600 words in length and should be submitted in duplicate.

Nuclear Absorption of a Fast Charged Hyperon

M. M. BLOCK* AND D. T. KING
Naval Research Laboratory, Washington, D. C.
(Received January 13, 1955)

EXPERIMENTAL evidence for the following reaction schemes involving heavy unstable particles has been obtained:

$$\pi+N\rightarrow Y+K,^{1} \quad (1)$$

$$K+N\rightarrow Y+\pi,^{2} \quad (2)$$

$$N+N\rightarrow Y+K+N,^{3} \quad (3)$$

where N, Y, and K represent nucleon, hyperon, and heavy boson, irrespective of charge. It is the purpose of this note to suggest the existence of a further reaction which is the absorption analog of (3):

$$Y+N\rightarrow N+N+K. \quad (4)$$

We have exposed Ilford $G5$ emulsions, 400 microns thick, to the cosmic radiation for 6 hours at an altitude of 95 000 feet and at geomagnetic latitude 55°N. A

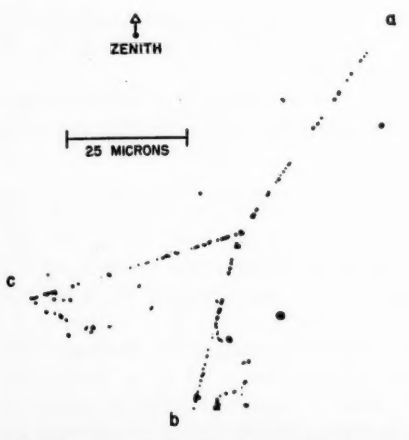

FIG. 1. Photomicrograph of a "fundamental" collision in which the target nucleon is a proton. Track a is taken to be the primary; b and c are assumed to be the tracks of a proton and K-meson, respectively.

TABLE I. Summary of the measurements.

Track	Polar angle θ (degrees)	Azimuthal angle ϕ (degrees)	Length (mm)	$p\beta$ (Mev/c)	Grain density (grains/100μ)	β	Measured mass (m_e)
a			12.2	550±100	40.4±1.6	0.58±0.06	2580±700
b	22.0	180	4.0	194± 40	63.5±2.0	0.44±0.04	1800±500
c	98.0	22.4	2.4	112± 30	58.1±2.4	0.47±0.04	900±350

systematic search for "fundamental" collisions, i.e., those stars which exhibit no evaporation phenomena, has been made. Some of these stars show a β-decay track and may be attributed to collisions with bound target nucleons possessing an internal momentum; the remainder often may be interpreted as collisions with free hydrogen nuclei. Among our collection of "fundamental" collisions we have found the star shown in Fig. 1. The observations on tracks a, b, and c are summarized in Table I. Track a, which is taken to be the primary, makes an angle of 37° with the zenith and lies close to the plane of the emulsion. The angles θ, ϕ in Table I are, respectively, the polar and azimuthal angles of b and c with respect to a as a polar axis. Track b is nearly parallel to the emulsion plane, while c rises to the surface at a 13.6° angle and is followed into a facing emulsion. No evidence of residual nuclear recoil or β decay was found at the origin of the event. The determination of the quantity $p\beta$ was obtained from a constant-cell measurement of multiple scattering. The value of the scattering constant and the necessary noise elimination appropriate to the cell length were employed; a suitable correction was made for large single deflections. The β-values were deduced from a theoretical ionization curve normalized to an experimental calibration of grain counts for singly charged particles. The errors indicated in β include both the statistical error in grain counting and an allowance for a systematic calibration error.

The measured masses of a, b, and c are found to be 2580±700 m_e, 1800±500 m_e and 900±350 m_e, respectively, where the indicated errors are standard deviations. The secondaries can reasonably be identified as proton and K-particle. The mass value for the primary is suggestive of a particle more massive than a proton, possibly a hyperon. The direct measurements do not exclude a proton or deuteron for a. However, it is not energetically possible for a proton or deuteron of this velocity to create a K-particle. The *a priori* probability that tracks a and c have been misidentified and that the event is indeed attributable to a collision of a proton with a bound proton, giving two outgoing protons, is estimated to be ~1 in 10^3. In the course of this work we have made 30 observations of quasi-elastic p-p scattering; thus the chance that this event is a p-p scatter is ~1 in 30. If the target nucleon were a free hydrogen nucleus, one or more neutral secondaries would have to be emitted, since a, b, and c are not coplanar. However, even if the target nucleon were a peripheral proton with

a small internal momentum, the principle of conservation of baryons would require at least one neutral secondary. For purposes of calculation, a single neutral secondary has been assumed and the masses of b and c have been taken to be 938 Mev and 499 Mev, respectively. From momentum and energy conservation, the mass of the neutral secondary can be derived in terms of the mass of the incident particle. If the primary is considered to be a charged hyperon of 2340 m_e,[4] and the neutral is assumed to be a neutron, the incident energy is below the threshold for reaction (4) if the target proton is at rest: a peripheral proton with internal momentum >400 Mev/c is required as the target, if the neutral mass is to be that of a neutron. We note that the probability of occurrence of an internal momentum exceeding 400 Mev/c is low.

However, if we assume a free proton target but now consider the primary to have the mass of the cascade hyperon,[5] namely 2590 m_e, it is found that the neutral secondary has mass 1820 ± 170 m_e, consistent with a neutron being the neutral secondary.

We propose that this observation is a possible example of the nucleonic absorption in flight of a charged hyperon, according to scheme IV, i.e., $Y^{\pm}+p\rightarrow p+K^{\pm}+n$, where p and n are, respectively, proton and neutron and $Y^{\pm}$ may represent either the hyperon or its heavier cascade counterpart. If the reaction has been correctly interpreted, the K-particle observed is a boson.

A recent observation of Eisenberg[6] was ascribed to the decay of a new hyperon, of mass (3200_{-500}^{+1200}) m_e, into a K^- meson. However, an alternate interpretation as a nuclear reaction of type (4), namely $Y^-+n\rightarrow K^-+n+n$, involving only known particles, might be made. The primary energy deduced from Eisenberg's data is well below threshold for the foregoing reaction if Y^- is the hyperon of mass 2340 m_e, whereas the energetics are satisfied if the incoming particle is a cascade hyperon that collides with a neutron with internal momentum ~150 Mev/c.

It is of interest to note that, according to the isotopic spin assignments of Gell-Mann and Pais,[7] if the hyperon in the foregoing reactions is a Σ^-, the reaction is allowed, but is forbidden for both Σ^+ and Ξ^- hyperons.

We are grateful to Dr. M. M. Shapiro for his support of this work, and to B. Stiller, N. Seeman, and F. O'Dell for their assistance.

* On military leave of absence from Duke University, Durham, North Carolina.

[1] Fowler, Shutt, Thorndike, and Whittemore, Phys. Rev. **93**, 861 (1954).

[2] H. DeStaebler, Phys. Rev. **95**, 1110 (1954).

[3] Block, Harth, Fowler, Shutt, Thorndike, and Whittemore, Bull. Am. Phys. Soc. **29**, No. 7, 33 (1954).

[4] Bonetti, Levi-Setti, Panetti, and Tomasini, Nuovo cimento **10**, 345 (1953).

[5] Armenteros, Barker, Butler, Cachon, and York, Phil. Mag. **43**, 597 (1952); E. W. Cowan, Phys. Rev. **94**, 161 (1954).

[6] Y. Eisenberg, Phys. Rev. **96**, 541 (1954).

[7] M. Gell-Mann and A. Pais, Proc. Glasgow Conference, July, 1954 (unpublished). In this paper the hyperon of mass 2340 m_e is denoted by Σ and the cascade hyperon by Ξ.

Deuteron Stripping and the Collective Nuclear Model

G. R. SATCHLER

Clarendon Laboratory, Oxford, England

(Received January 12, 1955)

EXPRESSIONS for the reduced widths for nucleon capture into low nuclear levels reached by deuteron stripping have been derived by using the nuclear shell model.[1] We now consider the effects of collective motion in nuclei.[2]

In the weak-coupling region the contribution to the capture probability is of first order in the surface coupling only for capture into vibrational states. For other states it is of second order and contributes, at most, a few percent of the reduced width. The surface coupling will allow capture of nucleons with angular momenta (j_nl_n) other than those expected on the simple shell model,[1] but interparticle forces have the same effect, and interpretation would be difficult.

With *strong* coupling, capture into rotational levels[2] becomes possible, but, owing to the orthogonality of the single-particle states, is only "allowed" when (j_nl_n) is the same as the (jl) of the orbit the captured nucleon enters. In practice, the surface coupling[2] (and also interparticle forces) will admix other spin-orbit states $(j'l')$. That is, the shell model (jl) will not be perfectly good quantum numbers, and captures that are otherwise "forbidden" will take place with reduced probability.

We may write the reduced width $\gamma^2(j_nl_n)$ for capture with total angular momentum j_n and orbital l_n to form a compound state with n like nucleons in an unfilled shell, (jl):

$$\gamma(j_nl_n)=[n\hbar^2/MR]^{\frac{1}{2}}u_{ln}(R)\beta(j_nl_n), \tag{1}$$

where $u_l(R)/R$ is the single-particle radial wave function evaluated at the nuclear surface, $r=R$, and M is the nucleon reduced mass.

With an even-even spin-zero target nucleus, $J_i=K_i=0$,[2] we must have $j_n=J_e$, the spin of the compound state. Then

$$\beta(j_nl_n)=\delta(j_nJ_e)\langle\tau_i|\tau\rangle[2/(2J_e+1)]^{\frac{1}{2}}\alpha(jj_n;\tau K_e). \tag{2}$$

When $j_n=j$, $\alpha(jj)\simeq1$, and $\tau=\tau_e$; but for $j_n\neq j$, $\alpha(jj_n)$ is the amplitude of the configuration $[(j)^{n-1}j_n]$ admixed to the "pure" state $[j^n]$ in the compound nucleus. As usual, K_e is the projection of J_e on the nuclear axis, and τ specifies the vibrational state of the nuclear surface. The $\langle\tau_i|\tau\rangle$ is an "unfavored" factor arising from the partial orthogonality of the vibrational wave functions, similar to that encountered in β and γ transitions.[2]

When the target nucleus is even-odd with spin J_i, projection $K_i=J_i$, and a rotational level of spin J_e in

the even-even compound nucleus ($K_e=0$) is formed,

$$\beta(j_n l_n)=\langle\tau_i|\tau\rangle[2(2J_i+1)/(2J_e+1)]^{\frac{1}{2}} \times C(J_i j_n J_e; J_i-J_i)\alpha(jj_n;\tau J_i). \quad (3)$$

α has the same interpretation, and $C(abc;\alpha\beta)$ is the Clebsch-Gordan coefficient.[3] In strong coupling, $J_i=j-\frac{1}{2}(n-2)$.

With $j_n=j$ we now have the possibility of forming several members of the rotational family with $|J_i-j|\leqslant J_e\leqslant J_i+j$, all, to first approximation, with the same vibrational character τ_e. We can then compare their reduced widths unambiguously:

$$\frac{\gamma(jl;J_e')}{\gamma(jl;J_e)}=\left[\frac{2J_e+1}{2J_e'+1}\right]^{\frac{1}{2}}\frac{C(J_i jJ_e';J_i-J_i)}{C(J_i jJ_e;J_i-J_i)}. \quad (4)$$

Taking into account only the surface coupling, we find for the admixture of $j_n\neq j$,

$$\alpha(jj_n;\tau K)=-k(ll_n)\Delta E^{-1}i^{l-l_n}(5/4\pi)^{\frac{1}{2}} \times\langle\tau|a_0|\tau_e\rangle C(2jj_n;0K)C(j_n{}^2j;\tfrac{1}{2}0). \quad (5)$$

$k(ll_n)$ is the coupling strength, $=V_0Ru_l(R)u_{l_n}(R)$ if V_0 is the depth of the shell-model potential well, and ΔE is the energy separation of the unperturbed states. $\langle\tau|a_0|\tau_e\rangle$ is an off-diagonal matrix element of the nuclear shape parameter $a_0=\beta\cos\gamma$. If the surface deformation is not greatly perturbed by the change in particle orbit, its order of magnitude should be given by the diagonal element. This is related to the intrinsic quadrupole moment, Q_0,

$$\langle\tau_e|a_0|\tau_e\rangle=(5\pi)^{\frac{1}{2}}Q_0/3ZR^2,$$

which may be estimated from measured quadrupole moments, isotope shifts, etc.[2]

The interpretation of deuteron-stripping data for medium-heavy nuclei, where rotational levels have mainly been found, is obscured because the Coulomb barrier is high. Even here, however, it should be possible to test the relation (4) with deuteron energies well over the barrier, without detailed knowledge of Coulomb effects. Rotational characteristics are also to be expected in the spectra of nuclei of the $1d$ shell (such as Mg^{24}) where the Coulomb barrier is not unduly high. Further investigation of these points is under way.

[1] A. M. Lane, Proc. Phys. Soc. (London) **A66**, 977 (1953); G. R. Satchler, Proc. Phys. Soc. (London) **A66**, 1081 (1953); **A67**, 471 (1954).

[2] A. Bohr and B. R. Mottelson, Kgl. Danske Videnskab. Selskab, Mat.-fys. Medd. **27**, No. 16 (1953).

[3] A. Simon, Oak Ridge National Laboratory Report 1718 (unpublished).

CONTENTS—Continued

Letters to the Editor:

Nuclear Absorption of a Fast Charged Hyperon . . . . . M. M. Block and D. T. King 1415

Deuteron Stripping and the Collective Nuclear Model . . . . . G. R. Satchler 1416

Editor's Note

As a trial in anticipation of a possible split of *The Physical Review*, the present issue contains papers on nuclear and high-energy physics only. The issue of March 15 will contain the other fields of physics. We shall continue this practice of alternating subjects for several months and would appreciate hearing your reaction.

CONTENTS

THE PHYSICAL REVIEW SECOND SERIES, VOLUME 97, NO. 5 MARCH 1, 1955

Electric Excitation of Heavy Nuclei by Protons . . Clyde McClelland, Hans Mark, and Clark Goodman 1535
Concept of Parentage of Nuclear States and Its Importance in Nuclear Reaction Phenomena . . . . . A. M. Lane and D. H. Wilkinson 1539
Cross Sections for Nonelastic Interactions of 14-Mev Neutrons with Various Elements . . . . . Elizabeth R. Graves and Roland W. Davis 1547
Alignment of Cerium-141 and Neodymium-147 Nuclei . . E. Ambler, R. P. Hudson, and G. M. Temmer 1550
Cross Section for Excitation of Pb^{207m} by Inelastic Scattering of Neutrons . . . . . P. H. Stelson and E. C. Campbell 1557
Gamma Radiation from the Inelastic Scattering of Protons by F^{19} . . . . . C. A. Barnes 1560
Search for Double Beta Decay in Ca^{48} . . . . . John A. McCarthy 1564
Nuclear Reactions in Stars. II. Protons on Light Nuclei . . . . . E. E. Salpeter 1568
Gamma Rays from Proton Bombardment of Li^7 . . . . . S. Hanshaw and R. R. Carlson 1576
Angular Distributions of Deuteron-Induced Reactions in Lithium . . . . . S. H. Levine, R. S. Bender, and J. N. McGruer 1580
Isomeric State of Y^{89} in the Decay of Zr^{89} . . . . . E. K. Hyde, M. G. Florence, and A. E. Larsh 1584
Angular Distribution of the Resonance Fluorescence Radiation from the 411-kev Excited State of Hg^{198} . . . . . Franz R. Metzger 1586
Effects of Perturbing Radiofrequency Fields on Nuclear Spin Coupling . . . . . Arnold L. Bloom and James N. Shoolery 1591
Gamma Rays from 14-Mev Neutron Bombardment of C^{13} . . . . . M. E. Battat and E. B. Graves 1595
Coincidence Studies of the Disintegration of Pm^{147} and Nd^{147} . . . . . Harnam Singh Hans, Babulal Saraf, and C. E. Mandeville 1599
Decay of Tl^{48} and Cr^{48} . . . . . M. R. Bunker and J. W. Starner 1603
High-Altitude Cosmic-Ray Neutron Density at the Geomagnetic Pole . . . . . H. A. C. Neuburg, R. K. Soberman, M. J. Swetnick, and S. A. Korff 1606
Photoproduction of Neutral Pions in Hydrogen: $p-\gamma$ Coincidences . . . . . R. L. Walker, D. C. Oakley, and A. V. Tollestrup 1609
Photoproduction of Neutral Pions in Hydrogen: Magnetic Analysis of Recoil Protons . . . . . D. C. Oakley and R. L. Walker 1613
Measurement of Multiply Charged Cosmic Rays by a New Technique . . . . . John Linsley 1618
Tritium Production by 2.2-Bev Protons on Iron and Its Relation to Cosmic Radiation . . E. L. Fireman 1622
Reaction $p+p \rightarrow \pi^+ + d$ . . . . . Frank S. Crawford, Jr. and M. Lynn Stevenson 1627
Polarization of Nucleons Elastically Scattered from Nuclei . . . . . R. M. Sternheimer 1630
Yields of Photonuclear Reactions with 320-Mev X-Rays. I. Experimental Results . . . . . R. J. Debs, J. T. Eisinger, A. W. Fairhall, I. Halpern, and H. G. Richter 1635
Yields of Photonuclear Reactions with 320-Mev X-Rays. II. Interpretation of Results . . . . . I. Halpern, R. J. Debs, J. T. Eisinger, A. W. Fairhall, and H. G. Richter 1643
Scattering of Fast Neutrons and Protons by Atomic Nuclei . . . . . Gyo Takeda and K. M. Watson 1658
Approximate Reduction of the Many-Body Problem for Strongly Interacting Particles to a Problem of Self-Consistent Fields . . . . . K. A. Brueckner and C. A. Levinson 1664
Two-Body Forces and Nuclear Saturation. III. Details of the Structure of the Nucleus . K. A. Brueckner 1653
Theory of Nuclear Models . . . . . R. J. Eden and N. C. Francis 1666
Magnetic Moments of Conjugate Nuclei . . . . . J. G. Rosenbaum and A. B. Volkow 1670
Behavior of Neutral Particles under Charge Conjugation . . . . . M. Gell-Mann and A. Pais 1387
Functional Analysis and Strong-Coupling Theory . . . . . J. Hamilton 1700
Boson-Fermion Scattering in the Heisenberg Representation . . . . . F. E. Low 1701
Strong-Coupling Theory for the Case of Pseudoscalar Coupling . . . . . Hironari Miyazawa 1708
Supplementary Conditions in Quantized Linear Systems . . . . . J. K. Perring 1712
Sach's Theorem on the Magnetic Moments of Nucleons . . . . . Hironari Miyazawa 1716

(Continued on cover three)

LANCASTER PRESS, INC., LANCASTER, PA.